## Universiteit Gent Faculteit van de Toegepaste Wetenschappen Vakgroep Civiele Techniek (TW15) Afdeling Weg- en Waterbouwkunde

# Golfoploop op stortsteengolfbrekers Wave run-up on rubble mound breakwaters

Björn Van de Walle



Proefschrift tot het verkrijgen van de graad van doctor in de toegepaste wetenschappen – optie bouwkunde  $Academiejaar\ 2002-2003$ 

Promotor: prof. dr. ir. Julien De Rouck

Afdeling Weg- en Waterbouwkunde Vakgroep Civiele Techniek (TW15) Faculteit van de Toegepaste Wetenschappen Universiteit Gent Technologiepark 904 B-9052 Gent (Zwijnaarde) Tel. nr. +32 9 264 54 89 Fax nr. +32 9 264 58 37

Doctoraatsbeurs gefinancieerd door: Bijzonder Onderzoeks Fonds (BOF – Universiteit Gent)

## **Speech of thanks**

A PhD is not a one man's job. A lot of persons contributed in one way or another to the completion of this thesis.

First of all, I would like to thank kindly my promotor, prof. dr. ir. Julien De Rouck to give me the opportunity to obtain a scholarship at Ghent University and to start working at a PhD. His numerous hints, indications,... were a great help throughout the creation of the presented work.

Also my colleagues of the Department of Civil Engineering (both Coastal Engineering and Roads and Bridges Unit) of Ghent University have been a big support throughout the years. The staff of the Department of Civil Engineering is very much acknowledged for their help and individual contributions. You all have been fantastic!

I am also grateful to ir. Luc Van Damme and ir. Bernard De Putter of the Coastal and Coastal Waterways Division of the Waterways and Marine Affairs Administration within the Environment and Infrastructure Department of the Ministry of the Flemish Community for putting at disposal the infrastructure at the Zeebrugge breakwater. Without this infrastructure, this thesis never would have existed.

I also would like to thank all partners of the OPTICREST project and the CLASH project for the help in finding an explanation for the – at first sight – impossible discrepancies and the nice co-operation, even after the project had finished, especially to Josep R. Medina, José Alberto Gonzalez Escribà, Joaquim Garrido for carrying out the small scale model tests at UPV, Hans F. Burcharth, Peter Frigaard, Flemming Schlütter, Liu Zhou, Morten Sand Jensen for performing the 3D tests at AAU. I also would like to thank dr. ir. Jentsje van der Meer very much for all the useful information, indications, hints and very valuable help.

The Magnel Laboratory for Concrete Research is very much acknowledged for putting the rock material for the small scale model tests at Ghent University at disposal. The author also would like to thank the department of Geotechnics within the Supporting Studies and Assignments Administration of the Environment and Infrastructure Department of the Ministry of the Flemish Community for putting at disposal the sieving machine many times.

A warm 'thank you' goes to prof. dr. Maria Ysebaert, ir. Katrien Audenaert and ir. Hendrik Blontroch for the help with statistical problems. I also would like to thank ir. Gaston de Saint-Aubain for all the hints and help.

The financial support of the European Community, the Ministry of the Flemish Community, the Fund for Scientific Research – Flanders and Ghent University is very much acknowledged, as well as the scientific and logistic support of the staff of the Forschungszentrum Küste in Hannover (Dipl.-Ing. Joachim Grüne, Dipl.-Ing. Reinold Schmidt-Koppenhagen, Dr.-Ing. Uwe Sparboom, Dr.-Ing. Dipl.-Phys. Jan Wienke, Dipl.-Ing. Günter Bergman, Dieter Junge und Wolfgang Malewski), Aalborg University (Einar Helgason, Jens Peter Kofoed, Michael Brorsen, Morten Kramer,...) and Flanders Hydraulics. The efforts of ir. Marc Willems and technical staff of Flanders Hydraulics to carry out the additional tests are very much appreciated.

Finally I would like to thank my parents Anny and Julien for the support throughout the years, as well as my brother Jarno, Ilse, my friends and all my 'best' friends: Tania, Sofie, Lennert and Britt. And last but not least, I would like to spotlight Han.

I certainly will have forgotten some persons. In case to your opinion you have contributed to this work in one way or another, at work or outside it, and your name has not been mentioned, please, accept my apologies not having mentioned your name and accept these sincere two words: 'Thank you!'

Björn Van de Walle March 2003

# Index

# SUMMARY (in Dutch)

# CHAPTER 1: GENERAL INTRODUCTION

1.1	Ratio		1-1		
1.2	Wave	1-2			
1.3	Wave overtopping Wave run-up or wave overtopping? Description of the investigated problem			1-4	
1.4	Wave	run-up o	r wave overtopping ?	1-5	
1.5	Descr	iption of 1	the investigated problem	1-5	
1.6	Objec	etives		1-8	
1.7	Activi	ities		1-9	
			CHAPTER 2:		
			STATE OF THE ART		
2.1	Intro	duction		2-1	
2.2	Wave	run-up		2-1	
	2.2.1	Iribarrer	n number	2-1	
	2.2.2	Hypothe	esis of equivalence	2-3	
	2.2.3	Paramet	ers	2-4	
		2.2.3.1	Wind	2-6	
		2.2.3.2	Spectral shape	2-6	
		2.2.3.3	Wave obliqueness	2-9	
		2.2.3.4	Water depth	2-10	
		2.2.3.5	Block size	2-11	
		2.2.3.6	Composite slope	2-12	
		2.2.3.7	Scale effects	2-12	
	2.2.4	Wave ru	ın-up formulae	2-14	
	2.2.5	Rough s	lopes	2-24	
	2.2.6	Permeat	ole structures	2-25	
	2.2.7	Other in	vestigations	2-32	

2.4	Wave run-up distribution Wave run-down Wave run-up measuring techniques Conclusions				
		CHAPTER 3: DETERMINATION OF $Ru_{2\%}$			
		DETERMINATION OF Ru2%			
3.1	Numb	per of wave run-up events N	3-1		
3.2		icant wave height	3-2		
	3.2.1		3-2		
	3.2.2	gauge(s) Distance between WG1 and WG2 (active wave absorption)	3-2		
	3.2.3	<u>-</u>	3-4		
3.3	Wave	run-up	3-7		
		Direct method	3-9		
	3.3.2	Using a fitted theoretical distribution	3-9		
		CHAPTER 4:			
	Fr	JLL SCALE MEASUREMENTS OF WAVE RUN-UP			
	rc	ON A RUBBLE MOUND BREAKWATER			
<b>4</b> 1	Introd	duction	4-1		
4.2		uring site	4-1		
4.3		ured storm events	4-5		
4.4		umentation	4-8		
7.7		Wave rider buoy (WR)	4-8		
		Pressure sensor (PR)	4-10		
	4.4.3	Infrared meter (IR)	4-10		
	4.4.4	Wave run-up measuring devices	4-10		
	7.7.7	4.4.4.1 'Spiderweb system' (SP)	4-12		
		4.4.4.2 Run-up gauge (RU)			
		4.4.4.3 Performance SP and RU			
	4.4.5	Anemometer	4-19		
	1. T.J		111		

	4.4.6	Video ca	amera	4-20
	4.4.7	Wave ov	vertopping and spray measurement	4-20
		devices		
4.5	Off lin	ne data pr	rocessing	4-23
	4.5.1	Wave ric	der data	4-24
	4.5.2	Spiderw	eb system data	4-26
	4.5.3	Run-up	gauge data	4-30
4.6	Analy	sis of data	a	4-30
4.7	Analy	sis results	S	4-32
	4.7.1	Wave ch	naracteristics	4-32
	4.7.2	Wave ru	n-up	4-35
4.8	Concl	usions		4-58
			Civi proper 5.	
			CHAPTER 5: SCALE MODEL TESTING	
			SCALE MODEL TESTING	
5.1	Intro	luction		5-1
<b>5.2</b>	Digita	l laborato	ory run-up gauge	5-2
5.3	Small	scale mo	del tests – OPTICREST	5-8
	5.3.1	Small sc	ale model tests – FCFH	5-13
		5.3.1.1	Introduction	
		5.3.1.2	Model setup	
		5.3.1.3	Instrumentation	
			5.3.1.3.1 Wave height meters	
			5.3.1.3.2 Wave run-up gauge	
		5.3.1.4	Results	
	5.3.2	Small sc	ale model tests – UPV	5-21
		5.3.2.1	Introduction	
		5.3.2.2	Model setup	
		5.3.2.3	Instrumentation	
		5.3.2.4	Results	
	5.3.3	Small sc	ale model tests – AAU	5-25
		5.3.3.1	Introduction	
		5.3.3.2	Model setup	
		5.3.3.3	Instrumentation	
		5.3.3.4	Results	
<b>5.4</b>	Small	scale mo	del tests – additional testing at FCFH	5-34

	5.4.1	Objective	es	5-34
		Model se		5-34
	5.4.3	Test mate	rix	5-35
	5.4.4	Results		5-38
		5.4.4.1	Wave data	
		5.4.4.2	Wave run-up	
5.5	Small	scale mod	el tests – additional testing at UGent	5-52
	5.5.1	Objective	es	5-52
	5.5.2	Model se	tup	5-52
	5.5.3	Instrume	ntation	5-54
	5.5.4	Test mate	rix	5-55
	5.5.5	Results		5-57
<b>5.6</b>	Large	scale mod	lel tests at GWK	5-66
	5.6.1	Introduct	ion	5-66
	5.6.2	Model se	tup	5-68
	5.6.3	Measurin	ng equipment	5-73
		5.6.3.1	Wave gauges	
		5.6.3.2	Run-up gauge	
	5.6.4	Test mate	rix	5-77
	5.6.5	Results		5-78
		5.6.5.1	Waves	
		5.6.5.2	Wave run-up	
		5.6.5.3	Wave run-down	
5.7	Concl	usions		5-90
			C	
			CHAPTER 6:	
			COMPARISON	
6.1	Introd	luction		6-1
6.2	Comp	arison of (	OPTICREST results	6-1
6.3	Model	l effects ar	nd scale effects	6-15
	6.3.1	Scale effe	ects	6-15
		6.3.12.1	Definitions	
		6.3.12.2	Wave run-up velocity	
		6.3.12.3	Estimation of influence of scale effects	
			6.3.12.3.1 Influence of surface	

				tension on wave run-up	
			6.3.12.3.2	Influence of surface	
			0.3.12.3.2	tension on wave	
				propagation	
			6.3.12.3.3		
				wave propagation	
			6.3.12.3.4	Influence of viscosity on	
	6.3.2	Model e	ffacts	wave run-up	6-26
	0.3.2	6.3.2.1		1/mataaralagigal	0-20
		0.3.2.1	6.3.2.1.1	l/meteorological	
				Spectral shape	
			6.3.2.1.2	C	
			6.3.2.1.3		
		6222	6.3.2.1.4	Longshore currents	
		6.3.2.2		A 1	
			6.3.2.2.1	Armour layer	
			6.3.2.2.2		
	~		6.3.2.2.3	Sand filling in core	
6.4	1		th literature		6-45
		Wave ru	•		6-45
		Wave ru			6-50
6.5		run-up fo	ormula		6-52
6.6	Concl	usions			6-54
			Снар	ΓER 7:	
GE	ENERAL	CONCLU	SIONS + REC	COMMENDATIONS FOR FUT	TURE
			RESE	ARCH	
7.1	Final (	conclusio	ns		7-1
7.2	Furth	er researc	ch areas		7-3

### **Annexes**

Annex A: Rayleigh and Weibull distribution

Annex B: Wave run-up distributions

Annex C: Results additional FCFH tests

Annex D: Test matrix additional UGent tests

Annex E: Results additional UGent tests

Annex F: Statistical tests

Annex G: GWK test matrix

Annex H: GWK test results

Annex I: GWK natural spectra

Annex J: FCFH wave spectra (OPTICREST tests)

Annex K: AAU wave spectra (OPTICREST tests)

Annex L: Scatter effect

## References

## List of symbols

The following symbols have been used in this thesis:

```
constant [-]
a
           constant [-]
\boldsymbol{A}
           slope angle [°], ratio between the number of run-up events
\alpha
           and the number of incident waves [-], constant [-]
b
           constant [-]
В
           constant [-]
           foreshore bottom slope [°]
β
           constant [-]
c
           wave celerity [m/s]
c_w
           variation coefficient [-]
δ
d
           water depth [m], constant [-]
           water depth at the toe of the structure [m]
d_t
           nominal diameter [m]
D_n
           diameter [m]
D
dof
           degrees of freedom [-]
           equivalent grain roughness [m]
           average value of variable X
E[X]
           kinetic energy [Nm]
E_{kin}
           potential energy [Nm]
E_{pot}
           spectral width parameter [-]
\varepsilon
f_p
           peak frequency [Hz]
f_s
           sample frequency [Hz]
           low cut off frequency [Hz]
f_{LC}
           high cut off frequency [Hz]
f_{HC}
           Froude number [-]
Fr
           gravitational acceleration [m/s<sup>2</sup>]
g
           peakedness parameter
γ
           reduction factor for a berm
\gamma_b
           reduction factor for a vertical wall
\gamma_{\nu}
           reduction factor for slope roughness
\gamma_f
           reduction factor for oblique wave incidence
\gamma_{\beta}
           layer thickness [m]
h
           alternative hypothesis
H_a
           design wave height [m]
H_{des}
H_0
           null hypothesis
           significant wave height (determined by analysis in time
H_s
           domain) [m]
```

```
significant wave height (determined by analysis in frequency
H_{m0}
          domain) [m]
k
          wave number [1/m], friction factor [-]
          stability factor [-]
K_D
          wave length [m]
L
          deep water wave length [m]
L_0
          i<sup>th</sup> order moment of the spectral density [m<sup>2</sup>/s<sup>i</sup>]
m_i
          dynamic viscosity [Pa.s], average value [-]
          Mean Sea Level [Z + ... m]
MSL
MWL
          Mean Water Level [Z + ... m]
          number of wave run-up events [-], number of waves [-]
N
          kinematic viscosity [m<sup>2</sup>/s]
\nu
          permeability [-], probability of occurrence of a Type I Error
P
          average wave overtopping discharge [m<sup>3</sup>/ms]
q
          peakedness parameter [-]
Q_p
          wave incident angle [°]
\theta
          wind direction [°]
\theta_{w}
          Still Water Level [Z + ... m]
SWL
          Reynolds number [-]
Re
R_c
          crest freeboard [m]
Ru
          wave run-up value [m]
          wave run-up value exceeded by x\% of the wave run-up
Ru_{x\%}
          events [m]
Rd
          wave run-down value [m]
          wave run down value exceeded by x\% of the run-down
Rd_{x\%}
          events [m]
          density [kg/m<sup>3</sup>]
\rho
          density of water [kg/m<sup>3</sup>]
\rho_{w}
          wave steepness [-]
          spectral density [m<sup>2</sup>s]
S(f)
          standard deviation
\sigma
          time interval
\Delta t
          time
t
          start of measurements [s]
t_0
          end of measurements [s]
t_f
          moment in time of high water
t_{HW}
          i^{th} hour before, resp. after t_{HW}
t_{HW} \pm i
          surface tension [N/m]
T
T_0
          length of analysed time series [s]
          peak wave period [s]
```

 $T_p$ 

 $T_{01}$ mean wave period (determined by analysis in frequency domain) [s]  $T_{02}$ wave period (determined by analysis in frequency domain) mean wave period (determined by analysis in time domain)  $T_m$ spectral wave period [s]  $T_{m-1,0}$ recording time [s]  $t_R$ wave run-up velocity [m/s] current velocity [m/s]  $v_c$ wind speed [m/s]  $v_s$ volume of water [m<sup>3</sup>] Vexceedance probability [%]  $\boldsymbol{x}$ distance between wave gauge i and wave gauge j [m]  $X_{i,j}$ Iribarren number [-] W

weight [kg]
Weber number [-]

We

# List of abbreviations

WG wave gauge
PR pressure sensor
RU run-up gauge
SP spiderweb system
WR wave rider buoy
IR infra red meter

GWK Großen Wellen Kanal (Hannover, Germany)

FCFH Ministry of the Flemish Community – Flanders Hydraulics

(Antwerp, Belgium)

UPV Universidad Politécnica de Valencia (Valencia, Spain)

AAU Aalborg University (Aalborg, Denmark)
UGent Ghent University (Ghent, Belgium)

NE north-east SW south-west

UCC University College Cork (Cork, Ireland)

## Golfoploop op stortsteengolfbrekers

Samenvatting doctoraatsproefschrift ir. Björn Van de Walle

## 1 Inleiding

Golfbrekers zijn kustwaterbouwkundige constructies die dienen om havens, offshore eilanden en kusten te beschermen tegen golfaanval van op zee. Kustwaterbouwkundige structuren zijn zeer dure constucties. Financiële overwegingen pleiten voor een zo laag mogelijke kruinhoogte daar het volume materiaal nodig om de structuur te belichamen evenredig is met het kwadraat van de hoogte van de constructie. Bovendien wordt een hoge structuur als visueel hinderlijk ervaren. Aan de andere kant mag de kruin van een zeewerende constructie niet té laag zijn om de veiligheid van de achterliggende gebieden te vrijwaren en om deze te beschermen tegen golfoverslag. Afhankelijk van de activiteit welke plaats vindt achter de constructie wordt steeds een zekere hoeveelheid golfoverslag toegelaten.

Golfbrekers worden ontworpen a.d.h.v. fysische modelproeven en/of numerieke modellering. De ontwerpcriteria voor het kruinpeil van een stortsteengolfbreker zijn golftransmissie en golfoverslag. Tijdens het ontwerpproces worden steeds de ontwerprandvoorwaarden getest. Er wordt echter zelden gekeken naar golfrandvoorwaarden welke een veel kleinere retourperiode hebben dan de ontwerpretourperiode (in de grootte orde van  $10^3$  à  $10^4$  jaar). Alhoewel monitoring van een bestaande constructie zeer belangrijk is om inzicht te krijgen in het gedrag van de structuur en de respons ervan op de golfbelasting, zijn metingen in situ zeer zeldzaam wegens het financiële prijskaartje dat aan dergelijke meetcampagnes vasthangt. De golfbreker van Zeebrugge werd uitgerust met apparatuur voor het meten van golven, golfoploop en golfoverslag. De metingen op de golfbreker in Zeebrugge en de stormsimulaties in de verschillende laboratoria gaven de unieke kans om randvoorwaarden met een retourperiode kleiner dan de ontwerpretourperiode te testen en alzo golfoploop in werkelijkheid en op schaalmodellen te meten.

Golfoploop gedefinieerd als de verticale afstand tussen het niveau welke door de oplopende golf bereikt wordt en het Stil Water Peil (*SWL*). Golfoverslag is gedefinieerd als de hoeveelheid water welke over de kruin van de golfbreker komt. Golfoverslag is nauw verwant

Summary-1

met golfoploop, maar wordt in dit proefschrift slechts zeer summier behandeld.

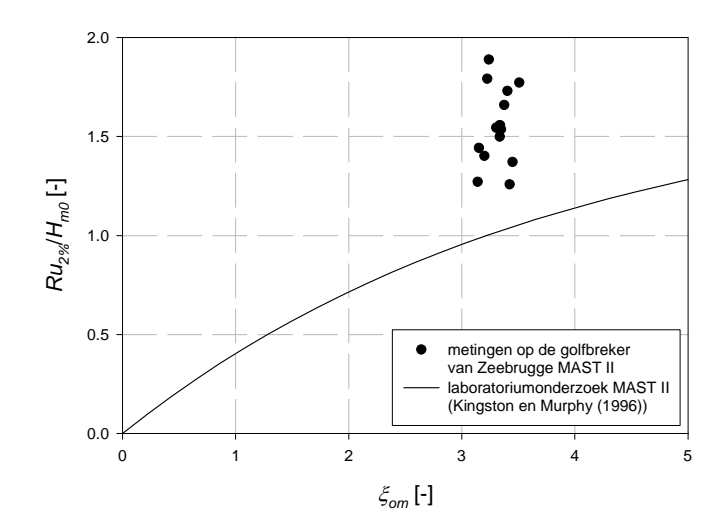
In het kader van het door de Europese Gemeenschap gefinancieerde MAST II project 'Full scale dynamic load monitoring of rubble mound breakwaters' (1994-1996) (contract nr. MAS2-CT92-0023) werden enkele jaren terug reeds golf-, golfoploop- en poriënwaterdrukdata verzameld op de golfbreker van Zeebrugge. Gedurende hetzelfde project werden laboratoriumproeven op drie verschillende schalen uitgevoerd. Golfoploop was één van de gemeten karakteristieken. Laboratoriumresultaten werden vergeleken met de resultaten van de metingen op ware grootte. Volgende conclusies werden getrokken (De Rouck et al. (1996)):

- metingen van golfoploop op ware grootte gaven duidelijk grotere waarden aan dan de experimentele resultaten (figuur 1).
- golfoploop in labo werd lichtjes onderschat door de golfoploopmeetmethode en de vorm van het golfoploopprofiel.
- golfoploopverdelingen in de labo's varieerden duidelijk van de golfoploopverdelingen gemeten op ware grootte.

Het eerste resultaat van het MAST II project initieerde verder golfoplooponderzoek in het kader van het door de Europese Gemeenschap gefinancierde MAST III OPTICREST project 'The optimisation of crest level design of sloping coastal structures through prototype monitoring and modelling' (1998-2001) (contract nr. MAS3–CT97–0116). Gedurende het OPTICREST project werd golfoploop op de golfbreker van Zeebrugge uitvoerig gemeten. De opgemeten stormen werden gesimuleerd in drie laboratoria. De resultaten van beide type metingen werden vervolgens met elkaar vergeleken.

In het kader van het MAST II project werd golfoploop in alle labo's gemeten m.b.v. een weerstandsdraad. Deze draad werd gespannen in een frame en zo dicht mogelijk boven de deklaag van het model geplaatst. Het meetprincipe is gebaseerd op een verandering in weerstand/geleidbaarheid of capaciteit door een verandering in waterniveau. Echter, een dun laagje water welke de helling van het golfbrekermodel opliep werd niet steeds gedetecteerd door de weerstandsdraad. Visuele observatie van de golfoploop en analyse van videobeelden bevestigden de onderschatting van de met de weerstandsdraad opgemeten golfoploop. Om de tweede conclusie van het MAST II project tegemoet te komen werd daarom een nieuw

golfoploopmeetinstrument ontwikkeld dat zowel in labo als in situ gebruikt werd.



Figuur 1: Vergelijking van golfoploopmeetgegevens verzameld op de golfbreker van Zeebrugge en de resultaten van laboproeven op een schaalmodel van de golfbreker van Zeebrugge (cfr. MAST II resultaten (De Rouck et al. (1996))).

Dit proefschrift concentreert zich op golfoploop op een doorlatende stortsteengolfbreker. De doelstellingen van dit proefschrift zijn:

- het uivoeren van een literatuurstudie van golfoploop
- het meten van golfoploop op een stortsteengolfbreker op ware grootte
- het vergelijken van de resultaten van de golfoploopmetingen op ware grootte en deze op schaalmodellen
- het identificeren van de drijvende kracht(en) achter de geobserveerde verschillen tussen metingen in situ en in labo en het onderzoeken van invloedrijke parameters op golfoploop door bijkomende laboratoriumproeven zowel op kleine als op grote schaal
- het opstellen van een formule om golfoploop op een doorlatende stortsteengolfbreker te evalueren.

Metingen van interacties van golven met kustwaterbouwkundige structuren op ware grootte zijn zeer zeldzaam, niet enkel omwille van de omvangrijke financiële middelen die nodig zijn om de metingen te kunnen uitvoeren, maar ook omwille van het feit dat deze dienen uitgevoerd in een zeer agressief zeeklimaat (stormcondities, zoute zeelucht,...). Bovendien hangt de mogelijkheid tot het uitvoeren van deze metingen volledig af van de weersomstandigheden. De metingen leveren slechts resultaten op voor een beperkte variatie van golfparameters. Het grote voordeel van metingen op ware grootte is dat schaaleffecten onbestaande zijn. Metingen op grote schaal zijn even waardevol als metingen op ware grootte, maar zijn ook zeer duur. Hoewel de zeetoestand bij proeven op grote schaal gedurende langere tijd constant kan gehouden worden dan op ware grootte, ontbreken er nog altijd een aantal parameters (wind, stroming, schuine golfinval (kortkammige golven),...) om de realiteit perfect te simuleren op grote schaal.

De activiteiten die ondernomen zijn in het kader van deze thesis worden hieronder kort besproken. Er is voor gezorgd dat het volledige bereik van groottes bestreken is: van metingen op ware grootte, over proeven op grote schaal tot kleine schaalmodellen op verschillende schalen. Naast een literatuuroverzicht (hoofdstuk 2) waarbij de meest relevante parameters, onderzoeken en inzichten i.v.m. golfoploop worden beschreven, worden in hoofdstuk 3 een aantal duidelijke definities gegeven. Hoofdstuk 4 omvat de metingen op ware grootte op de golfbreker van Zeebrugge. De labometingen komen aan bod in hoofdstuk 5. Deze omvatten o.a. de metingen welke uitgevoerd zijn in het kader van het OPTICREST project op drie schaalmodellen van de golfbreker van Zeebrugge in het Waterbouwkundig Laboratorium in Borgerhout (FCFH - België), de Universiteit van Valencia (UPV -Spanje) en de Universiteit van Aalborg (AAU – Denemarken), alsook de bijkomende testen op kleine schaal in FCFH en de Gentse Universiteit (UGent). Bovendien worden in hoofdstuk 5 de proeven op grote schaal in het Großen Wellen Kanal in Hannover (GWK -Duitsland) beschreven. In hoofdstuk 6 worden alle resultaten met elkaar vergeleken worden de oorzaken van mogelijke verschillen tussen golfoploopwaarden in situ en in labo opgespoord. Schaaleffecten en modeleffecten worden geïdentificeerd. De laboresultaten en de golfoploopmetingen op ware grootte worden vergeleken met de resultaten van golfoploopformules welke in de literatuur gevonden werden. Tevens wordt een golfoploopformule voorgesteld welke het resultaat weergeeft van alle uitgevoerde

golfoploopmetingen. Hoofdstuk 7 sluit dit proefschrift af met de conclusies en geeft enkele aanwijzingen voor verder onderzoek.

#### 2 Literatuuroverzicht

In de literatuur is golfoploop steeds terug te vinden als functie van het Iribarren getal  $\xi$ . Dit is niet zo verwonderlijk daar dimensieanalyse aantoont dat golfoploop in haar meest eenvoudige vorm functie is van de golfsteilheid (s = H/L) en de helling (tan  $\alpha$ ) van de structuur. Het Iribarren getal geeft niet enkel aan of een golf breekt of niet, het duidt ook aan hoe de golf breekt: schuimende ( $\xi < 1$ ), overstortende ( $1 < \xi < 3$ ) of oplopende ( $\xi > 3$ ) breker.

Veel golfoplooponderzoeken startten met de studie van golfoploop op een gladde ondoorlatende helling veroorzaakt door regelmatige golven. Door toepassing van de 'equivalentiehypothese' (Saville (1956), Battjes (1974)) werd overgegaan van regelmatige naar onregelmatige golven. De golfoploopverdeling welke het resultaat is van een onregelmatig invallende golftrein wordt bekomen door het samenstellen van alle golfoploophoogtes welke het resultaat zijn van het toepassen van de theorie geldig voor onregelmatige golven op elk der samenstellende (regelmatige) golven van een (onregelmatige) golftrein. Echter, het is niet altijd duidelijk uit de geraadpleegde literatuur welke karakteristieke waarden (voor golfoploop, golfhoogte, golfperiode,...) gebruikt dienen te worden om over te gaan van regelmatige naar onregelmatige golven.

De oudste formule is deze voorgesteld door Hunt (1957),

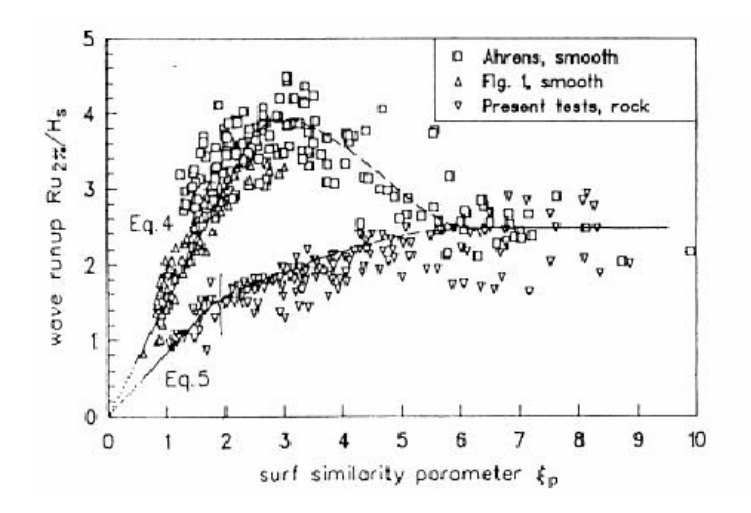
$$\frac{Ru}{H} = \xi \tag{1}$$

enkel geldig voor  $\xi < 2.3$ . Deze formule wordt vaak teruggevonden onder de gedaante:  $Ru/H = a\xi$ . Zoveel onderzoeken reeds uitgevoerd zijn, zoveel verschillende waarden voor a werden gevonden. De waarden van a variëren tussen 0.967 (Ahrens en Titus (1985)) en 2.88 (voor golfoploopmetingen in situ op dijken langsheen de Noord-Duitse kust (Grüne (1982)).

Voor oplopende brekers werden andere algemene formules voorgesteld (CIRIA/CUR (1991) and CIRIA/CUR (1995)):

$$\frac{Ru}{H} = a\xi_{op} + c \tag{2}$$

Vele onderzoekers (Battjes (1974), Ahrens (1981), Shore Protection Manual (1984), Sorensen (1997)) stelden voor om golfoploopformules geldig voor gladde hellingen tevens aan te wenden voor ruwe hellingen mits het toepassen van een reductiefactor welke de ruwheid en porositeit van de helling in rekening brengt. Echter, Losada en Giménez-Curto (1981), Pilarczyk (1990) en van der Meer en Stam (1992) (figuur 2) hebben aangetoond dat er een duidelijk wezenlijk verschil is tussen golfoploop op een gladde (ondoorlatende) helling en golfoploop op een ruwe (doorlatende) helling voor  $2 < \xi < 5$ . De toepassing van een reductiefactor is enkel geldig voor  $\xi < 2$ .



Figuur 2: Verschil tussen golfoploop op een gladde helling en golfoploop op een ruwe helling (van der Meer en Stam (1992)).

De belangrijkste formules voor het berekenen van golfoploop op stortsteengolfbrekers zijn deze voorgesteld door van der Meer en Stam (1992) en Losada en Giménez-Curto (1981). De formule van van der Meer en Stam (1992) luidt:

$$\frac{Ru_{x\%}}{H_s} = a\xi_{om} \qquad \text{voor } \xi_{om} \le 1.5$$
 (3a)

Summary-6

$$\frac{Ru_{x\%}}{H_s} = b\xi_{om}^c \qquad \text{voor } \xi_{om} > 1.5$$
 (3b)

$$\left(\frac{Ru_{x\%}}{H_s}\right)_{max} = d \qquad \text{voor doorlatende structuren}$$
 (3c)

De waarde van de parameters a, b, c en d hangt af van de beschouwde overschrijdingskans. Voor x = 2 bedragen deze respectievelijk 0.96, 1.17, 0.46 en 1.97.

De formule van Losada en Giménez-Curto (1981) luidt:

$$\frac{Ru}{H} = A(1 - \exp(B\xi)) \tag{4}$$

Deze formule is geldig voor regelmatige golven en een ruwe doorlatende helling. Echter, m.b.v. de equivalentiehypothese werd een aangepaste formule opgesteld voor onregelmatige golven. Verschillende bronnen geven waarden voor A en B voor gegroefde Antifer kubussen (Allsop et al. (1985), Silva et al. (1994), Kingston en Murphy (1996)) en voor andere types deklaagelementen.

Voor de golfoploopverdeling worden verschillende theoretische verdelingen voorgesteld: de Rayleigh verdeling, de Weibull verdeling, de Gamme distributie en de normale distributie.

Naast golfoploop werd ook golfterugloop bestudeerd. Golfterugloop is vooral belangrijk bij het bepalen tot op welke diepte de deklaag van de structuur dient aangebracht te worden om de invallende golfwerking te weerstaan.

Er bestaan verschillende golfoploopmeettoestellen. Het traditionele meetinstrument is de (analoge) weerstandsdraad die boven de deklaag van de structuur gespannen wordt. Een vergelijkende studie van golfoploopmeetapparatuur, uitgevoerd in het kader van het OPTICREST project, wees aan dat de weerstandsdraad niet het meest geschikte meetinstrument is om golfoploop te meten. Zelfs een meetsysteem met meerdere draden (drie, resp. vijf weerstandsdraden gespannen op verschillende hoogtes boven de helling van de

golfbreker) leidde niet tot het gewenste resultaat. Een lineaire extrapolatie van de wateroppervlakverheffingen opgemeten door de draden zorgde voor een betere schatting van de golfoploophoogte dan een enkelvoudige draad, doch de extrapolaties stemden nog steeds niet overeen met de visueel geobserveerde golfoploop. Een tweede type meettoestel is de digitale oploopbaak. Dit meettoestel meet golfoploop door het detecteren of een elektrode al dan niet door het water wordt kortgesloten. Een variant van dit type meettoestel werd in het kader van dit proefschrift ontwikkeld en werd gebruikt voor alle golfoploopmetingen. Daarnaast bestaan ook meer subjectieve meetmethoden: de visuele observatie en analyse m.b.v. video opnames.

## 3 Bepaling van Ru<sub>2%</sub>

In de literatuur worden verschillende methodes gebruikt om de karakteristieke relatieve golfoploopwaarde ( $Ru_2 \% H_{m0}$ ) te bepalen. In dit hoofdstuk wordt daarom beschreven hoe dit getal in het verdere verloop van dit proefschrift bepaald zal worden.

wordt uitgedrukt als de verhouding Golfoploop karakteristieke golfoploopwaarde tot de invallende significante golfhoogte. Veelal wordt voor de karakteristieke golfhoogte  $Ru_{2\%}$ gebruikt. Golfoploop wordt gerelateerd aan het aantal golfoplopen. Het aantal golfoplopen wordt gedefineerd als het aantal invallende golven N. Het aantal invallende golven is gedefinieerd als de duur van de geanalyseerde tijdreeks  $T_0$  gedeeld door de gemiddelde golfperiode  $T_{01}$  (bepaald in frequentie domein). Er bestaan verschillende methodes om  $Ru_{2\%}$  te berekenen. Vooreerst is er de directe methode. Hierbij worden de golfoplopen gerangschikt volgens dalende grootte en is de Bayesiaanse schatting van de overschrijdingskans van de  $p^{de}$ golfoploop in een reeks met N golfoploopwaarden gelijk aan p/(N+1)(Rice (1988)). Een tweede mogelijkheid is het fitten van een gekende theoretische distributie (twee parameter Weibull distributie, Rayleigh distributie,...) op de gemeten golfoploopwaarden. Hieruit kan dan gemakkelijk de  $Ru_{2\%}$  waarde bepaald worden. Het grote voordeel bij deze laatste werkwijze is dat ook het betrouwbaarheidsinterval van de schatting kan bepaald worden. Hoe langer de tijdreeks waaruit de schatting afgeleid wordt duurt. hoe smaller betrouwbaarheidsinterval wordt. Tevens leidt de Rayleighverdeling tot smallere 90% betrouwbaarheidsintervallen dan de twee parameter Weibull verdeling. Met de wetenschap dat langere tijdreeksen meer betrouwbare waarden voor  $Ru_{2\%}$  opleveren en wetende dat het bepalen

van  $Ru_{2\%}$  op een directe manier veel vlotter verloopt is geopteerd om tijdreeksen van 2 uur op hoog water te analyseren en daaruit de  $Ru_{2\%}$  rechtstreeks af te leiden m.b.v. de eerder vermelde Bayesiaanse schatting.

Om te vermijden dat op de structuur gereflecteerde golven opnieuw gereflecteerd zouden worden aan het golfschot werd in alle labo's (behalve in UPV) actieve golfabsorptie gebruikt. Hiervoor werd t.b.v. de additionele UGent proeven de tussenafstand van de twee golfhoogtemeters die voor dit doeleinde werden gebruikt berekend a.d.h.v. de aanbevelingen van Suzuki en Goda (1976).

Ter bepaling van de invallende significante golfhoogte zijn de aanbevelingen uit de literatuur gebruikt. Deze stellen dat de invallende significante golfhoogte aan de teen van de golfbreker moet gebruikt worden. Echter, in Zeebrugge, was er gedurende enkele stormen slechts één golfmeetboei aanwezig. In de gevallen dat er twee meetboeien aanwezig waren kon een reflectie analyse niet uitgevoerd worden om volgende reden. De plaats van de golfmeetboeien is niet vast bepaald vanwege de type verankering. De boeien dobberen rond, worden door de stromingen meegesleurd,... Dit had tot gevolg dat in de laboratoria waar de opgemeten stormen gereproduceerd werden ook totale golven (d.i. de som van de invallende en de gereflecteerde energie) opgemeten moesten worden. Voor de bijkomende proeven in het Waterbouwkundig Laboratorium werden tevens de totale golven gebruikt om vergelijking met eerder bekomen resultaten mogelijk te maken. De proeven uitgevoerd in de golfgoot van de Universiteit Gent maakten gebruik van invallende golven. Er is gebruik gemaakt van een drie puntsmethode om invallende golven van de gereflecteerde golven te onderscheiden (Mansard en Funke (1980)). Een optimale tussenafstand tussen deze drie golfhoogtemeters werd berekend voor verschillende golfperiodes en waterdieptes. De minimum afstand tussen de golfhoogtemeter welke zich het dichtst bij de structuur bevindt en de structuur zelf moet volgens verschillende auteurs (Klopman en van der Meer (1999), Pilarczyk en Zeidler (1996)) minstens  $L_p/4$  bedragen indien een meervoudige puntsmethode gebruikt wordt voor de reflectieanalyse. Indien de significante golfhoogte bepaald wordt door slechts één enkele golfhoogtemeter moet deze tussenafstand minstens twee keer de piekgolflengte bedragen. In Zeebrugge zelf is deze voorwaarde vervult voor WRII, maar niet voor WRI (voor  $T_p = 7.93$  s bedraagt de diep water golflengte  $L_p = 98.18 \text{ m}$ ).

### 4 Metingen op ware grootte

De doelstelling van de meetcampagnes was het uitvoeren van metingen op een echte stortsteengolfbreker met het oog op het vergaren van golf- en golfoploopgegevens teneinde meetresultaten van laboproeven hiermee te kunnen verifiëren. Hiertoe werd het noordelijke gedeelte van de westelijke strekdam die de buitenhaven van Zeebrugge (België) beschermt uitgekozen als meetsite. De ontwerpcondities voor de golfbreker van Zeebrugge, gebouwd in de jaren '80, zijn  $H_s = 6.20$  m,  $T_p = 9$  s en SWL = Z + 6.75. Het tijverschil in Zeebrugge varieert tussen 3.40 m bij doodtij en 4.30 m bij springtij. De topografie van de zeebodem is gekenmerkt door een zacht hellend voorland ( $\sim Z - 9.00$ ) met een erosieput (max. Z - 14.00) net voor de golfbreker. De kern van de golfbreker bestaat uit tout-venant (2-300 kg). Voor de filterlaag werd 1-3 ton breuksteen gebruikt. De teen van de golfbreker werd geconstrueerd met 3-6 ton breuksteen. De deklaag bestaat uit gegroefde kubussen (25 ton). Bovenop de golfbreker is een meetsteiger met een totale lengte van 60 m geplaatst. Deze steunt op een stalen paal ( $\phi = 1.80$  m) aan de teen van de golfbreker en op twee betonnen kolommen op de kruin van de golfbreker. De helling van de golfbreker t.p.v. de meetsteiger bedraagt tan  $\alpha = 1/1.3$ . In de sectie waarin de meetsteiger is geplaatst is meetapparatuur aangebracht ter bepaling van de golfkarakteristieken (golfhoogte en -periode, SWL,...), poriënwateroverdrukken in de kern van de golfbreker en golfoploop. In een meer noordelijke sectie van de golfbreker is apparatuur aangebracht welke golfoverslag detecteert en meet.

De analoge signalen van alle meetinstrumenten worden 24 uur op 24, 7 dagen op 7, het hele jaar rond gesampled aan  $f_s = 10$  Hz. De meetgegevens worden per kwartier weggeschreven op harde schijf. De inhoud van deze schijf wordt om de 4 tot 6 weken gekopieerd op een draagbare PC en wordt vervolgens op kantoor op een CD-rom geschreven. Alzo werd reeds een volledige datacatalogus gecreëerd.

Gebaseerd op stormverslagen toegezonden door het Oceanografisch Meteorologisch Station van de Afdeling Waterwegen Kust van de Administratie Waterwegen en Zeewezen binnen het Departement Leefmilieu en Infrastructuur van het Ministerie van de Vlaamse Gemeenschap werden dertien stormen geselecteerd uit een geheel aan stormobservaties en –metingen uitgevoerd tussen 1995 en 2000 voor de Vlaamse kust. Een storm is pas 'interessant' wanneer (1) de significante golfhoogte groter is dan 2.50 m, (2) het *SWL* voldoende hoog is (hoog water), (3) we te maken hebben met een volledig

ontwikkelde zeegang en (4) wanneer een sterke wind (bij voorkeur > 7 Beaufort) blaast vanuit het NW, zodat de golven zo goed als loodrecht op de as van de golfbreker invallen. Er zijn telkens periodes van twee uur rond hoog water geselecteerd gedurende dewelke het SWL als constant beschouwd wordt. Deze twee uur durende periodes worden aangeduid door [ $t_{HW}$  -1,  $t_{HW}$  +1] waarbij  $t_{HW}$  het tijdstip is van hoog water. Volgende stormen werden opgemeten:

- 28 augustus 1995 (02h45 04h45)
- 28 augustus 1995 (15h00 17h00)
- 19 januari 1998 (16h00 18h00)
- 20 januari 1998 (04h15 06h15)
- 7 februari 1999 (16h00 18h00)
- 17 februari 1999 (12h45 14h45)
- 22 februari 1999 (15h45 17h45)
- 6 november 1999 (11h30 13h30)
- 6-7 november 1999 (23h45 01h45)
- 3 december 1999 (21h00 23h00)
- 4 december 1999 (22h00 0h00)
- 22 januari 2000 (12h30 14h30)
- 23 januari 2000 (00h45 02h45)

Twee golfmeetboeien meten het golfklimaat voor de golfbreker (figuur 3). Een golfmeetboei meet in feite de verticale versnellingen van het wateroppervlak. Door dubbele integratie van deze versnellingen bekomt men de verplaatsingen. Uit de karakteristieken van de aangewende boeien wordt afgelezen dat deze boeien uitstekend werken voor golffrequenties tussen 0.065 Hz en 0.5 Hz.

In de kern van de golfbreker zitten dertien druksensoren welke golfgeïnduceerde poriënwaterdrukken doorheen de kern van de golfbreker opmeten. Bovendien werden twee druksensoren bevestigd aan de stalen paal welke de meetsteiger aan zeewaartse zijde ondersteunt. Deze druksensoren dienden voor de bepaling van het *SWL* voor de stormen tijdens dewelke de infrarood meter niet aanwezig was (1995 stormen) en ter controle van de metingen van de infraroodmeter.



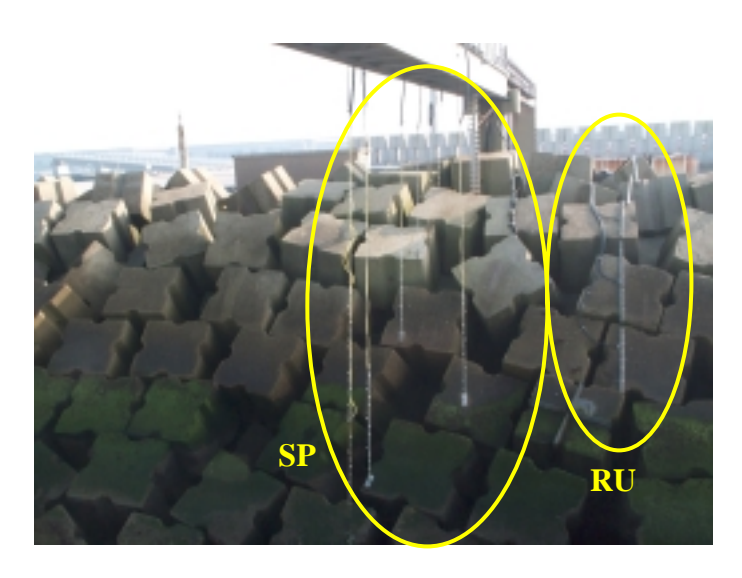
Figuur 3: Golfmeetboeien voor de stortsteengolfbreker van Zeebrugge.

Een infraroodmeter bevindt zich op de meetsteiger en dient ter bepaling van het *SWL* (figuur 4). Het principe van dit apparaat is eenvoudig. Het infraroodtoestel zendt een puls uit en meet de tijd die die puls nodig heeft om op het wateroppervlak te weerkaatsen en terug opgevangen te worden door het toestel. Deze tijd vermenigvuldigd met de lichtsnelheid geeft twee keer de afgelegde afstand tot het wateroppervlak.



Figuur 4: Infraroodmeter en anemometers geplaatst op de meetsteiger.

Golfoploop wordt gemeten m.b.v. twee verschillende meetsystemen (figuur 5). Er is het 'spiderweb systeem' (SP) en de golfoploopbaak (RU). Het 'spiderweb systeem' bestaat uit zeven verticaal geplaatste stappenbaken. Aan hun onderste uiteinde zijn deze vastgemaakt aan de deklaagelementen en aan hun bovenste uiteinde aan de meetsteiger. Elke stappenbaak meet de wateroppervlakverheffingen. M.b.v. een computeralgoritme wordt het golfoploopniveau bepaald d.m.v. lineaire extrapolatie, uitgaande van de stappenbaakmetingen.



Figuur 5: Het 'spiderweb systeem' (SP) en de golfoploopbaken (RU) op de stortsteengolfbreker van Zeebrugge.

De golfoploopbaak (RU) bestaat uit vijf stappenbaken welke bovenop de deklaagelementen geplaatst zijn (figuur 5). De golfoploopbaak laat een directe bepaling van het golfoploopniveau toe zonder tussenkomst van een computeralgoritme zoals het geval is bij het 'spiderweb systeem'. Hiervoor dient wel het niveau van elke individuele electrode gekend te zijn. Voor de stormen die zich hebben voorgedaan in het voorjaar van 1999 waren amper drie (onderste) van de vijf delen van de golfoploopbaak geïnstalleerd.

Windsnelheid en –richting worden gemeten m.b.v. een anemometer. Drie anemometers bevinden zich op de meetsteiger (figuur 4). Een windrichting  $\beta = 0^{\circ}$  correspondeert met een noordelijke wind. Een

positieve windrichting duidt op een meer westelijke windrichting, een negatieve windrichting op een meer oostelijke windrichting.

Een videocamera welke is opgehangen onder de meetsteiger visualiseert golfoploop en –overslag op een monitor in de meetcontainer. Deze beelden kunnen ook opgenomen worden en kunnen nadien gebruikt worden voor visuele analyse. Dit werd echter niet gedaan.

Een betonnen golfoverslagbak (2 m hoog, 2 m breed en 7.30 m lang) werd gebouwd achter de kruin van de golfbreker (figuur 6(a)). De bak vangt het over de kruin slaande water op. Een samengestelde overlaat, geplaatst in een zijwand van de golfoverslagbak, laat een gecontroleerde uitstroming van het water toe (figuur 6(b)). Het 'gemiddeld' waterpeil in de overslagbak wordt, gesteund op het principe van de communicerende vaten, opgemeten door twee druksensoren. Uit het opgemeten druksignaal werden de individuele golfoverslagvolumes [m³] en het gemiddeld golfoverslagdebiet [m³/ms] berekend.

Vier golfdetectoren zijn geplaatst op de kruinelementen. Deze laten toe om het aantal, de locatie en de omvang van de overslaande golven te bepalen.

Spray wordt gemeten m.b.v. zes pluviometers. Deze zijn geplaatst op een rechte lijn evenwijdig aan de as van de meetsteiger op afstanden van resp. 0 m, 20 m, 60 m, 90 m, 150 m en 1000 m achter de golfoverslagbak. De verst geplaatste pluviometer dient als referentiemeter. Deze wordt geacht enkel de regenintensiteit te meten en geen spray.

Alle meetgegevens worden op kantoor verwerkt. Hiervoor werd een deels bestaand deels zelfgeschreven analyseprogramma (in LabView $^{TM}$ ) aangewend.





Figuur 6: (a) Samengestelde overlaat in één van de zijwanden van de (b) golfoverslagbak geplaatst achter de kruin van de golfbreker van Zeebrugge.

Tabel 1: Relatieve golfoploopdata gemeten door de golfoploopbaak en gecorrigeerd met de zogenaamde 'Rayleigh equivalente golfoploop' waar nodig (cursief gedrukte waarden) (RU, 9 stormen, [ $t_{HW}$ -1,  $t_{HW}$ +1], tijdreeksen van 2 uur).

storm event n°	$Ru_{max}/H_{mo}$ [-]	$Ru_{1\%}/H_{m0}$ [-]	$Ru_{2\%}/H_{m0}$ [-]	$Ru_{5\%}/H_{mo}$ [-]	$Ru_{10\%}/H_{mo}$ [-]	$Ru_s/H_{mo}$ [-]	$Ru_{25\%}/H_{m0}$ [-]	$Ru_{so}/H_{mo}$ [-]
5	2.41	1.97	1.81	1.59	1.39	1.34	1.08	0.68
6	2.24	1.83	1.69	1.48	1.30	1.17	0.82	0.65
7	2.34	1.91	1.76	1.54	1.35	1.28	1.01	0.69
8	2.09	1.95	1.82	1.55	1.34	1.30	1.08	0.69
9	2.53	2.14	1.89	1.67	1.45	1.32	1.00	0.76
10	2.19	1.86	1.60	1.46	1.39	1.27	0.99	0.70
11	2.66	2.09	1.86	1.73	1.43	1.29	1.05	0.73
12	2.33	1.70	1.65	1.47	1.28	1.14	0.87	0.70
13	2.38	2.07	1.85	1.54	1.24	1.10	0.94	0.59
μ	2.35	1.95	1.77	1.56	1.35	1.25	0.98	0.69
δ	0.073	0.072	0.058	0.059	0.052	0.069	0.092	0.070

De golfoploopmeetresultaten voor de golfoploopbaken (RU) kunnen teruggevonden worden in tabel 1 en voor het 'spiderweb systeem' (SP) in tabel 2. Golfoploopniveaus welke het kruinniveau van de golfbreker overschrijden of golfoploopwaarden welke zich bij de analyse van de SP data voordoende platformen bevinden werden vervangen door hun equivalente golfoploopniveau  $Ru_{x\%,eq}$ . Uitgaande van de veronderstelling dat golfoploop op de golfbreker van Zeebrugge benaderd wordt door een Rayleighverdeling, kunnen deze bepaald worden op twee manieren. Enerzijds wordt een theoretische Rayleighverdeling gefit op de opgemeten golfoploopdata m.b.v. de kleinste kwadratenmethode en wordt a.d.h.v. de bekomen vergelijking de gewenste goloploopwaarde  $Ru_{x\%}$  bepaald. Anderzijds kan de  $Ru_{2\%}$  waarde geschat worden uitgaande van  $Ru_s$  voor zover deze gemeten

Tabel 2: Relatieve golfoploopdata gemeten door het 'spiderweb systeem' en gecorrigeerd met de zogenaamde 'Rayleigh equivalente golfoploop' waar nodig (*cursief* gedrukte waarden) (SP, 13 stormen, [t<sub>HW</sub>-1, t<sub>HW</sub>+1], tijdreeksen van 2 uur).

storm event	$Ru_{max}/H_{mo}$ [-]	Ru1%/Hmo [-]	$Ru_{2\%}/H_{mo}$ [-]	$Ru_{5\%}/H_{m0}$ [-]	Ru <sub>10%</sub> / H <sub>mo</sub> [-]	Rus/H <sub>mo</sub> [-]	Ru <sub>25%</sub> / H <sub>m0</sub> [-]	$Ru_{so}/H_{mo}$ [-]
1 <sup>a</sup>	2.07	1.71	1.56	1.37	1.20	1.12	0.93	0.66
<b>2</b> <sup>a</sup>	2.34	1.67	1.54	1.35	1.18	1.10	0.92	0.65
3 <sup>a</sup>	2.19	1.93	1.75	1.55	1.36	1.27	1.05	0.75
4	2.12	1.87	1.79	1.54	1.35	1.26	1.04	0.74
5	2.05	1.92	1.71	1.50	1.32	1.23	1.02	0.72
6	2.43	1.97	1.82	1.59	1.39	1.30	1.08	0.76
7	2.14	1.83	1.69	1.48	1.30	1.21	1.01	0.71
8	2.11	2.01	1.90	1.59	1.40	1.30	1.08	0.77
9	2.48	1.97	1.81	1.59	1.39	1.30	1.08	0.76
10	2.22	1.82	1.68	1.47	1.29	1.20	1.00	0.71
11	2.58	1.96	1.80	1.58	1.38	1.29	1.07	0.76
12	2.49	1.89	1.74	1.53	1.34	1.25	1.04	0.73
13	2.13	1.76	1.63	1.42	1.25	1.16	0.97	0.68
μ	2.26	1.87	1.73	1.50	1.32	1.23	1.02	0.72
δ	0.081	0.057	0.061	0.055	0.055	0.056	0.054	0.055

kon worden:  $Ru_{2\%} = 1.40Ru_s$ . Het nadeel aan deze laatste methode is dat wanneer  $Ru_s$  reeds behept is met meetfouten,  $Ru_{2\%}$  dit ook zal zijn.

Volgende conclusies werden getrokken:

- (1) Golfoploopdata verzameld door de golfoploopbaak (RU) gedurende negen stormen werd geanalyseerd. Tijdreeksen van twee uur op hoog water werden hiervoor geselecteerd. De gemiddelde waarde van de relatieve golfoploop  $Ru_{2\%}/H_{m0}$  bedraagt 1.77. Het Iribarren getal  $\xi_{om}$  is 3.63. Tijdens drie stormen waren slechts drie van de vijf delen van de golfoploopbaak op de golfbreker geïnstalleerd. Voor de bepaling van de golfoploop werd in deze gevallen gerekend met de zogenaamde 'Rayleigh equivalente' golfoploop  $Ru_{2\%,eq}$ . Wanneer de data verzameld door het 'spiderweb systeem' (SP) gedurende dertien stormen geanalyseerd wordt, bedraagt de gemiddelde waarde van de relatieve golfoploop  $Ru_{2\%}/H_{m0} = 1.73$  voor een Iribarren getal  $\xi_{om} = 3.64$ . Omwille van het meetprincipe van het SP moest vele malen met de 'Rayleigh equivalente' golfoploopwaarde gerekend worden.
- (2) De meetgegevens verzameld door de meest zeewaartse stappenbaak van het 'spiderweb systeem' gedurende een tijdsspanne van twee uur op hoog water werden gebruikt om golfterugloop Rd te bepalen. Golfterugloop heeft een waarde  $Rd_{2\%}H_{m0} = -0.87$ . Het Iribarren getal is  $\xi_{om} = 3.64$ .
- (3) Metingen op ware grootte van golfoploop zijn zeer zeldzaam. Deze data zijn onontbeerlijk om kleinschalige modellen te kalibreren en te verifiëren. Daarom moeten deze data zo betrouwbaar mogelijk zijn. Voor elk meettoestel on site was tevens een 'back up' toestel aanwezig. De metingen van de infraroodmeter werden gecontroleerd a.d.h.v. de metingen van de druksensor aan de paal. De twee golfmeetboeien WRI en WRII kunnen elkaar vervangen. Twee verschillende golfoploopmeetsystemen werden twee verschillende in dwarsdoorsnedes van de Zeebrugse golfbreker geplaatst. Voor beide meetsystemen werden gemiddeld gezien vergelijkbare waarden bekomen voor de relatieve golfoploop. Echter, de individuele meetresultaten van beide systemen verschillen soms sterk voor eenzelfde storm. Het plaatsingspatroon van de deklaagelementen en de verhouding  $D_{n50}/H_{m0}$  worden hiervoor verantwoordelijk geacht.

- (4) Wanneer tijdreeksen van een half uur gebruikt worden om de golfoploopbaakdata te analyseren, bedraagt de gemiddelde relatieve golfoploopwaarde  $Ru_2 \% H_{m0}$ , gedurende een twee uur durend tijdsinterval op hoog water (van  $t_{HW}$ -1 tot  $t_{HW}$ +1), 1.80. Ter bepaling van deze waarde werd het gemiddelde genomen van de vier  $Ru_2 \% H_{m0}$  waarden welke het resultaat zijn van de analyse van de vier opeenvolgende tijdreeksen van dertig minuten binnen het beschouwde tijdsinterval. Deze waarde is lichtjes hoger dan de waarde bekomen door de twee uur durende tijdreeks in één keer te analyseren (zie punt (1)). De lengte van de geanalyseerde tijdreeksen heeft weinig invloed op de resultaten (wanneer het SWL constant mag beschouwd worden).
- (5) Relatieve golfoploopwaarden zijn afhankelijk van het SWL:  $Ru_2\%/H_{m0}$  waarden stijgen wanneer de waterdiepte daalt. De absolute golfoploop Ru is minder afhankelijk van de waterdiepte dan de relatieve golfoploop  $Ru_2\%/H_{m0}$ . Echter, de lagere porositeit van de deklaag bij lagere peilen, onstaan door zettingen van de golfbreker, wordt hiervoor verantwoordelijk geacht. Relatieve golfoploopwaarden zijn ook groter tijdens vloed dan tijdens eb. De invloed van de langse stromingen en het asymmetrisch getijde zijn mogelijke oorzaken van dit fenomeen.
- (6) Des te lager de overschrijdingskans x, des te grotere variatie te zien is op de relatieve golfoploop in functie van de waterdiepte.

### 5 Metingen op schaalmodellen

#### 5.1 Inleiding

Modelproeven werden uitgevoerd in vijf Europese laboratoria, t.w.:

- Ministerie van de Vlaamse Gemeenschap, Waterbouwkundig Laboratorium (Borgerhout, België) *FCFH*
- Universidad Politécnica de Valencia (Valencia, Spanje) *UPV*
- Aalborg University (Aalborg, Denemarken) AAU
- Großen Wellen Kanal (Hannover, Duitsland) GWK
- Universiteit Gent (Gent, België) UGent

Alle geteste structuren waren modellen van stortsteengolfbrekers. Twee deklaagtypes werden getest: rip rap  $(D_{n50}/H_{m0} \le 0.50)$  en gegroefde kubussen  $(D_{n50}/H_{m0} \cong 1)$ . In het kader van het OPTICREST project werd de golfbreker van Zeebrugge gemodelleerd in drie

laboratoria: FCFH, AAU en UPV. In FCFH en UPV werd de golfbreker twee dimensionaal gemodelleerd op schaal 1:30. Het uitvoeren van dezelfde proeven in twee verschillende laboratoria heeft het grote voordeel dat resultaten met elkaar kunnen vergeleken worden. Een drie dimensionaal schaalmodel (schaal 1:40) werd gebouwd in AAU. De modellen werden verschaald volgens de wet van Froude. Het materiaal van de kern van de golfbreker werd verschaald op 1:20 voor de twee dimensionale modellen en op 1:24 voor het drie dimensionaal model (cfr. de verschalingsmethode van Burcharth et al. (1999)). De deklaagelementen in de buitenste laag van de schaalmodellen werden geplaatst overeenkomstig hun positie op de golfbreker van Zeebrugge. De lokaal steilere helling ter plaatse van de meetsteiger op de golfbreker (tan  $\alpha = 1:1.3$ ) werd gemodelleerd. In alle labo's zijn in Zeebrugge opgemeten spectra gereproduceerd. In AAU zijn bovendien testen uitgevoerd om de invloed van schuine golfinval, directionele spreiding, langse stromingen,... onderzoeken. Deze parametrische testen deden besluiten dat golfoploop stijgt voor stijgende snelheden van de langse stroming en dat golfoploop daalt voor schuinere golfinval en voor grotere golfspreiding. In de gecombineerde golfgoot en windtunnel van UPV werd de invloed van wind op golfoploop en golfoverslag onderzocht. Een lineair verband tussen de dimensieloze golfoverslag  $log(q/\sqrt{gH_s^3})$  en de dimensieloze de relatieve vrijboord  $R_c/H_s$  werd opgemerkt. Golfoverslag (en bijgevolg ook golfoploop) stijgt met stijgende windsnelheid.

Teneinde golfoploop op stortsteengolfbrekers nauwkeurig te kunnen opmeten werd in het kader van dit doctoraatsproefschrift een nieuw toestel ontwikkeld aan de Afdeling Weg- en Waterbouwkunde van de Gentse Universiteit. Deze nieuwe golfoploopbaak werd in alle labo's gebruikt en bestaat uit een kam met naalden (figuur 7). De afstand tussen het onderste uiteinde van een naald en het grillige talud van het golfbrekermodel kunnen voor elke naald afzonderlijk aangepast worden. Vooral voor golven met een kleine golfsteilheid is deze golfoploopbaak veel nauwkeuriger dan het traditionele meettoestel (d.i. een weerstandsdraad gespannen boven de helling van de golfbreker). Zulk een draad kan de individuele stenen van de deklaag van de golfbreker niet volgen waardoor golfoploop niet nauwkeurig kan opgemeten worden. Het verschil tussen de werkelijke oploophoogte en de met de weerstandsdraad opgemeten golfoplooghoogte is groter dan de 'gemiddelde' afstand tussen de

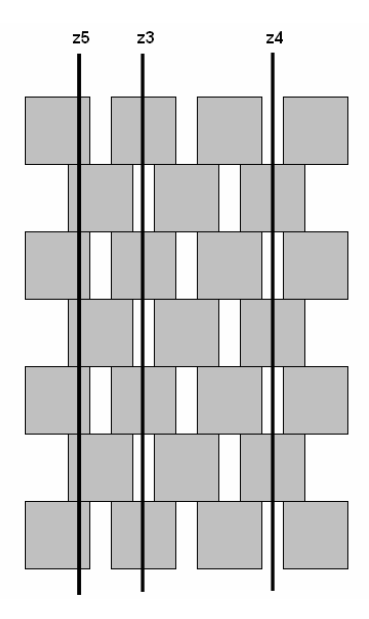
draad en de deklaag wanneer de golfsteilheid kleiner is dan 0.06. Dit verschil bedraagt vijf keer de afstand tussen de draad en de deklaag wanneer s < 0.02. In FCFH en in AAU werd een vergelijking gemaakt tussen het traditionele toestel en het nieuwe toestel. In FCFH werden gemiddeld 9% hogere golfoploophoogtes opgemeten met het digitale toestel dan met het traditionele toestel. In AAU waren de golfoploophoogtes 33% groter voor de digitale golfoploopbaak.



Figuur 7: De nieuwe digitale golfoploopbaak geïnstalleerd op het model van de Zeebrugge golfbreker in de golfgoot van het Waterbouwkundig Laboratorium van Borgerhout.

De calibratie van dit nieuwe toestel is zeer eenvoudig. Enkel het niveau van het onderste uiteinde van elk van de naalden dient opgemeten te worden. De golfoploopbaak heeft twee outputs: een 'sum' signaal welk aanduid hoeveel naalden contact maken met het water en een 'max' signaal dat aangeeft welke het rangnummer is van de hoogste elektrode die nog contact maakt met het water. Elke naald welke kortgesloten wordt door het water telt voor 0.1 Volt in het uitgangssignaal.

In alle laboratoria werden de in Zeebrugge opgemeten golfspectra zo goed mogelijk gereproduceerd. Dit gebeurde iteratief totdat beide spectra (het doelspectrum en het in het laboratorium opgemeten spectrum) zo goed als mogelijk met elkaar overeenstemden. Hierbij werd de spectrale vorm der beide spectra met elkaar vergeleken, alsook de spectrale parameters  $H_{m0}$  en  $T_{01}$ . De belangrijkste conclusie die getrokken wordt uit de storm reproducties in FCFH, AAU en UPV is dat golfoploop onderschat wordt door modelproeven, zélfs door gebruik te maken van het nieuwe digitale stappenbaak. De gemiddelde  $Ru_{2\%}/H_{m0}$  waarde voor FCFH bedraagt 1.46. In AAU werd een gemiddelde waarde  $Ru_{2\%}/H_{m0} = 1.63$  gemeten. De  $Ru_{2\%}/H_{m0}$  waarde voor UPV is gelijk aan de waarde voor  $Ru_{2\%}/H_{m0}$  opgemeten op de golfbreker van Zeebrugge (t.t.z.  $Ru_{2\%}/H_{m0} = 1.77$ ). Niettegenstaande de spectra visueel en de significante golfhoogte  $H_{m0}$  en de gemiddelde golfperiode  $T_{01}$  rekenkundig redelijk goed met elkaar overeenstemden, werd een duidelijk verschil opgemerkt tussen de spectrale breedte parameters van beide spectra.



Figuur 8: Drie verschillende posities van de kam van de golfoploopbaken t.o.v. het regelmatige plaatsingspatroon van de deklaagelementen.

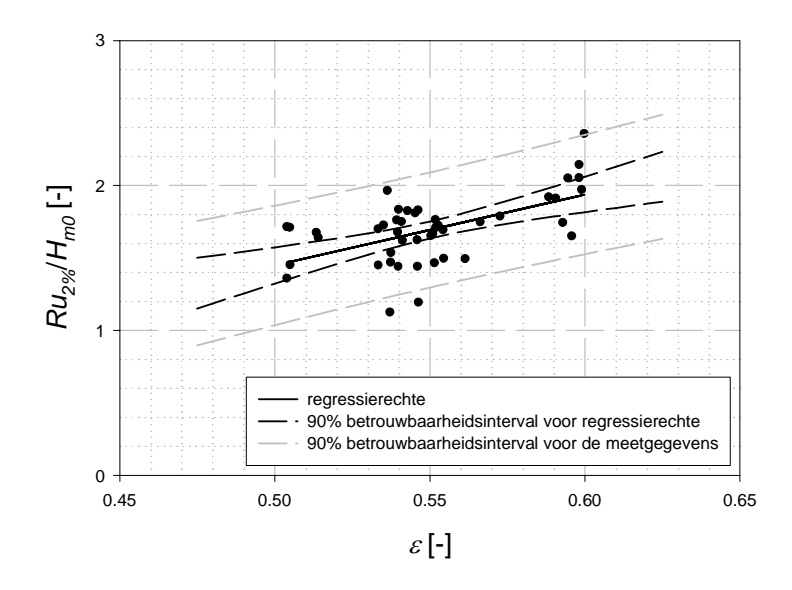
Bijkomende parametrische testen werden uitgevoerd in FCFH en in UGent. Het doel van deze proeven was het meer in detail onderzoeken van enkele tijdens het OPTICREST opgemerkte invloedrijke parameters zoals de spectrale vorm en de drie aan elkaar gekoppelde parameters (1) plaatsingspatroon van de deklaagelementen, (2) het

SWL en (3) de plaats van de kam van de oploopbaken t.o.v. de deklaagelementen. Hiertoe werden in FCFH twee verschillende plaatsingspatronen van de deklaagelementen onderzocht. De deklaagelementen in de buitenste laag werden vooreerst geplaatst in dezelfde positie als deze zich in werkelijkheid op de golfbreker van Zeebrugge bevinden (werfplaatsing). Vervolgens werden de deklaagelementen geplaatst in een regelmatig plaatsingspatroon. Bij dit laatste patroon werd de kam van de golfoploopbaak in drie verschillende posities t.o.v. de deklaagelementen geplaatst (figuur 8).

Alzo bekwam men vier reeksen proeven: z2 (onregelmatig patroon), z3, z4 en z5. Per testreeks werden twaalf proeven uitgevoerd waarbij steeds hetzelfde golfschotsignaal werd aangewend: drie verschillende golfperiodes ( $T_{p1}=1.39~\rm s$ ,  $T_{p2}=1.79~\rm s$ ,  $T_{p3}=2.12~\rm s$ ) en vier verschillende waterdieptes (Z+0.00, Z+2.00,  $Z+4.00~\rm en$  Z+6.00) werden gecombineerd. De target golfhoogte had dezelfde waarde ( $H_s=0.10~\rm m$ ) in alle testen. Negen proeven werden herhaald. Niettegenstaande het uitgestuurde golfschotsignaal en het opgemeten signaal hetzelfde was, werd een shift opgemerkt tussen de golfschotsignalen van de oorspronkelijke test en de herhaalde test. Deze shift bedroeg op het einde van de testen ongeveer 0.5 s. Een tekortkoming van het golfschotsturingsprogramma wordt hier als oorzaak aangeduid.

Tijdens golfterugloop stroomde het water van tussen de deklaagstenen uit de kern van de golfbreker, hierbij de elektrodes van de golfoploopbaken kortsluitend en aldus een verkeerdelijk golfterugloop niveau aanduidend. Het golfoploopsignaal dook in vele gevallen niet tot onder het SWL. Een klassieke golfoploopanalyse (d.i. zero down crossing) kon bijgevolg niet uitgevoerd worden. Dit euvel werd omzeild door het SWL kunstmatig te verhogen tot  $SWL + 0.5H_s$ . Een klassieke zero down crossing kon vervolgens zonder problemen uitgevoerd worden. Bij de uiteindelijk bekomen waarden voor  $Ru_{x\%}$  werd nadien terug een halve significante golfhoogte  $H_s$  bijgeteld. Deze werkwijze heeft voor de grootste golfoploopwaarden geen invloed.

Een duidelijke invloed van de spectrale breedte parameter  $\varepsilon$  werd opgemerkt (figuur 9): stijgende waarden van  $\varepsilon$  resulteren in stijgende dimensieloze golfoploopwaarden.



Figuur 9: Relatieve golfoploop  $Ru_{2\%}/H_{m\theta}$  [-] in functie van de spectrale breedte parameter  $\varepsilon$  [-] en de 90% betrouwbaarheidsgrenzen voor alle testen uitgezonderd deze met SWL = Z + 6.00.

Testen waarbij zowel de Iribarren getallen, de SWLs als de spectrale breedte parameters  $\varepsilon$  dezelfde waarde hadden vertoonden toch nog sterk verschillende waarden voor  $Ru_2 \% H_{m0}$ . De enige parameters welke verschillend waren voor deze testen waren (1) het SWL, (2) het plaatsingspatroon van de deklaagelementen en (3) de positie van de kam van de golfoploopbaken t.o.v. de deklaagelementen. De drie gerelateerde parameters (1) SWL, (2) plaatsingspatroon van de deklaagelementen en (3) relatieve positie van de kam van de golfoploopbaken t.o.v. de deklaagelementen bleken een grote invloed te hebben op de uiteindelijke golfoploopwaarde.

Om de invloed van de combinatie van bovenvermelde parameters te minimaliseren werden bijkomende proeven uitgevoerd in de kleine golfgoot van de Afdeling Weg- en Waterbouwkunde van de Universiteit Gent. Het doel van deze proeven was het onderzoeken van de invloed van de spectrale vorm. Aangezien de invloed van de spectrale vorm bij de additionele proeven in FCFH niet duidelijk naar voren kwam en verstoord werd door de parameter  $D_{n50}/H_s$ , werd deze parameter verkleind door stortsteen te gebruiken als deklaag in plaats gegroefde kubussen. Gedurende een test werd golfoploop gelijktijdig

opgemeten door twee golfoploopbakens. De kammen van deze toestellen werden in twee verschillende dwarsdoorsnedes geplaatst. Bovendien werden in FCFH de resultaten bij het hoogste onderzochte waterniveau beïnvloed door de vorm van de kruin van de golfbreker. Daarom werd de helling van de golfbreker zo hoog mogelijk opgetrokken teneinde deze invloed tevens te kunnen kortsluiten. Drie verschillende waterdieptes werden beproefd. Een tweede doelstelling van deze bijkomende proeven was het onderzoeken van de invloed van de kernverschaling. Hiertoe werd de golfbreker, welke een sterk vereenvoudigde versie van de golfbreker van Zeebrugge was, twee maal gebouwd. Eén maal met het kernmateriaal verschaald volgens Burcharth et al. (1999), t.t.z. op schaal 1:20 i.p.v. op schaal 1:30 zoals de rest van het model en één maal met het kernmateriaal verschaald volgens de wet van Froude (op schaal 1:30) zodat het Froude getal in het model dezelfde waarde had als in werkelijkheid.

Niettegenstaande de verhouding  $D_{n50}/H_{m0}$  stukken lager was voor dit model dan voor het FCFH model werden binnen éénzelfde test verschillen opgemerkt tussen de golfoploopwaarden van beide golfoploopbakens. Het gemiddeld (absoluut) verschil tussen de golfoploopwaarden opgemeten door de twee golfoploopbakens bedroeg 6.5%. M.b.v. een statistische t test kon aangetoond worden dat beide kammen – gemiddelde gezien – geen verschillende golfoploop maten ( $\alpha$  < 0.05).

Er wordt besloten dat golfoploop op stortsteengolfbrekers zeer gevoelig is aan minieme geometrische veranderingen in het deklaagpatroon en dit in het bijzonder voor testen met een zeer hoge waarde van  $D_{n50}/H_{m0}$ .

De porositeit van de deklaag werd in FCFH en AAU plaatselijk lichtjes gewijzigd. Door het opvullen van een holte tussen enkele deklaagelementen en onder de naalden van de kam van het golfoploopmeettoestel, werd de deklaag lokaal minder poreus. Een opmerkelijke stijging in absolute golfoploopwaarde (tot 18%) werd opgemeten.

Er werd tevens statistisch aangetoond dat de waterdiepte geen significante invloed ( $\alpha < 0.05$ ) heeft op golfoploop. M.a.w. golfoploop is onafhankelijk van het *SWL* of de waterdiepte *d*. Dit is de conclusie voor de reeks proeven op de eerste kern (op schaal 1:20), maar niet voor de tweede reeks proeven. De resultaten van de tweede reeks proeven (met kern op schaal 1:30) met d = 0.35 wijken af van de

resultaten van de proeven op dezelfde kern (op schaal 1:30) in combinatie met andere kleinere waterdieptes.

Tevens bestaat er een aanwijzing ( $\alpha$  < 0.05) dat op het model met kernmateriaal op schaal 1:20 andere golfoploopwaarden gemeten worden dan op het model met kernmateriaal op schaal 1:30. Er kon niet met duidelijkheid gesteld worden of op het ene model grotere of kleinere golfoploopwaarden gemeten werden.

De reflectiecoëfficiënt van de golfbreker getest in UGent bedroeg  $C_r$  = 0.20 voor  $T_{0I}$  = 0.8 s (t.t.z. 4.4 s op ware grootte) tot  $C_r$  = 0.40 voor  $T_{0I}$  = 1.5 s (t.t.z. 8.2 s op ware grootte).

Metingen van golfoploop op grote schaal zijn uitgevoerd in de Großen Wellen Kanal in Hannover (Duitsland). Het doel van deze proeven was tweeërlei: (1) het onderzoeken van de stabiliteit van de breuksteen met hoge dichtheid en (2) het vergaren van golfoploopgegevens op grote schaal. Een conventionele stortsteengolfbreker werd gebouwd. De golfbreker werd geplaatst op een twee meter dik zandpakket. Deze zandlaag werd onder een helling 1:50 aangelegd tot 100 m voor de golfbreker. Tussen de zandlaag en de golfbreker werd een geotextiel aangebracht. De hoogte van de golfbreker bedroeg 3.50 m zodat de totale hoogte van de constructie 5.50 m bedroeg. Twee types rots zijn achtereenvolgens als deklaag aangewend en in twee reeksen proeven getest. Het betrof breuksteen met hoge dichtheid ( $\rho = 3.05 \text{ t/m}^3$ ) en breuksteen met een normale dichtheid ( $\rho = 2.65 \text{ t/m}^3$ ). Golven werden tweeëntwintig capacitieve golfhoogtemeters. opgemeten met Golfoploop werd gemeten m.b.v. een driedelige golfoploopbaak. Gedurende het uitvoeren van de testen golfoploopmeetapparatuur niet naar behoren te werken. Daartoe werden enkele aanpassingen doorgevoerd. Zo werd de volledige golfoploopbaak waterdicht gemaakt met epoxy hars en werden de connectoren welke de verschillende delen van de golfoploopbaak met elkaar verbinden beschermd door afdekplaten. De golfoploopbaak werden vastgemaakt aan wapeningsstaven m.b.v. speciaal hiervoor ontworpen klemmen. De wapeningsstaven werden in de kern van de golfbreker gedreven met een voorhamer. De golfoploopbaak werd op een zulkdanige manier vastgemaakt dat de elektrodes zich in het (theoretische) bovenvlak van de deklaag van de golfbreker bevonden en er niet uitstaken zoals het geval is bij de elektrodes van de golfoploopbaken op de Zeebrugse golfbreker. Het niveau van elk van de elektrodes werd opgemeten m.b.v. een waterpastoestel. Alle druksensoren en golfhoogtemeters werden gekalibreerd door eerst de golfgoot volledig met water te vullen en nadien deze te laten leeglopen. Tijdens dit leeglopen werd op discrete tijdstippen het *SWL* opgemeten alsook de waarde van het uitgangssignaal van alle instrumenten. Ook de overslagbak en de daarin geïnstalleerde pomp werden zorgvuldig gekalibreerd.

In totaal werden er 93 testen uitgevoerd. Een statistische t test werd aangewend om te bewijzen dat breuksteen met hoge dichtheid dezelfde golfoploop heeft als breuksteen met normale dichtheid ( $\alpha$  < 0.05). Dit is nog maar eens het bewijs dat de verhouding  $D_{n50}/H_{m0}$  geen echte invloed uitoefent op golfoploop. De deklaag is enkel aansprakelijk voor de spreiding op de meetresultaten.

Golfoploop varieerde van  $Ru_{2\%}/H_{m0} = 1.64$  voor  $\xi_{om} = 2.14$  tot  $Ru_{2\%}/H_{m0} = 1.89$  voor  $\xi_{om} = 4.48$ . De absolute waarde van de relatieve golfterugloop  $Rd_{2\%}/H_{m0}$  stijgt met stijgende Iribarren getallen. Golfterugloop wordt gekenmerkt door  $Rd_{2\%}/H_{m0} = -0.24 \xi_{om}$ , geldig voor  $2.14 < \xi_{om} < 4.48$ .

Uit alle laboproeven is gebleken dat de invloed van de spectrale vorm (spectrale breedte parameter  $\varepsilon$ , gepiektheidsparameter  $Q_p$ ) zeer belangrijk is voor de uiteindelijke golfoploophoogte:  $Ru_{2\%}/H_{m0}$  is een monotoon stijgende functie van  $\varepsilon$ .

# 6 Vergelijking

De resultaten van de stormsimulaties op schaalmodellen van de golfbreker van Zeebrugge in de verschillende labo's (zie hoofdstuk 5) worden verder vergeleken met de waarden bekomen door meetcampagnes op de werkelijke golfbreker van Zeebrugge (zie hoofdstuk 4). Een vergelijking werd gemaakt tussen werkelijke en de gereproduceerde golfhoogtes, gemiddelde golfperiodes piekgolfperiodes. Het gemiddelde van de absolute waarde van het relatieve verschil tussen de laboratoriumwaarde en de werkelijke waarde t.o.v. de werkelijke waarde bedroeg voor de significante golfhoogte  $H_{m0}$  8.9%, resp. 2.0% en 12.7% voor de labo's FCFH, resp. AAU en UPV, voor de gemiddelde golfperiode  $T_{01}$  5.1%, resp. 4.0% en 4.9% en voor de piekgolfperiode  $T_p$  11.0%, resp.4.9% en 15.1%. Uit deze cijfers blijkt duidelijk dat voor het afstemmen van de laboratoriumspectra op de werkelijke spectra de parameters  $H_{m0}$  en  $T_{01}$ met elkaar vergeleken werden en niet zozeer gebruik gemaakt werd van  $T_p$ . Echter, de labowaarden van de piekgolfperiode werd niet

systematisch onder- of overschat. De golven in het 3D bassin (AAU) benaderden de werkelijkheid veel beter dan de golven in de golfgoten (FCFH en UPV). In figuur 10 werd de relatieve golfoploop (analyse van de tijdreeksen op hoog water ( $[t_{HW}-1, t_{HW}+1]$ )) uitgezet t.o.v. de spectrale breedte parameter  $\varepsilon$  en dit voor zowel de meetcampagnes in Zeebrugge als de laboproeven op de verschillende schaalmodellen van de golfbreker van Zeebrugge. Gemiddeld gezien levert een grote waarde van  $\varepsilon$  ( $\varepsilon \simeq 0.60$ ) een grote  $Ru_{2\%}/I_{m0}$  waarde op en vice versa.

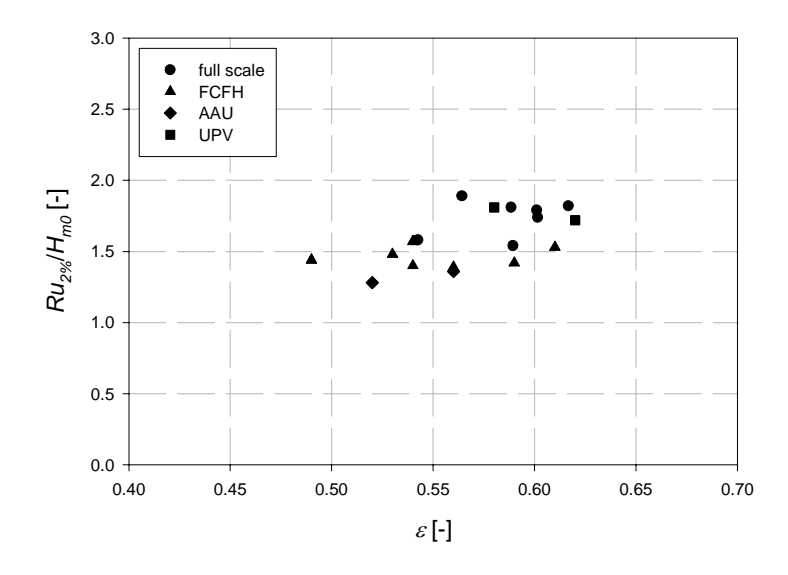


Figure 10: Relatieve golfoploop  $Ru_{2\%}/H_{m0}$  van de meetcampagnes in Zeebrugge en laboproeven op de verschillende modellen van de golfbreker van Zeebrugge t.o.v. de spectrale breedte parameter  $\varepsilon$ .

Voor testen met een veranderend waterpeil (tijdreeksen van een dertig minuten (op ware grootte)) werden volgende resultaten bekomen. Relatieve golfoploopwaarden stijgen bij afnemende waterdiepte voor zowel de metingen op ware grootte als de labometingen in AAU. Echter, de resultaten in AAU zijn steeds lager dan de resultaten van de meetcampagnes in Zeebrugge. Bij hoog water zijn de resultaten van UPV van dezelfde grootteorde als de metingen op ware grootte en nemen de  $Ru_2 \% H_{m0}$  waarden zelfs lichtjes af voor verminderende waterdiepte.  $Ru_5 \% H_{m0}$  lijkt in UPV onafhankelijk te zijn van de

waterdiepte en  $Ru_{10\%}/H_{m0}$  daalt voor afnemende waterdiepte. Bij hoog water zijn de FCFH resultaten een klein beetje groter dan deze van AAU, maar nemen bij dalende waterdiepte ook af. Dit is zo voor alle beschouwde overschrijdingsfrequenties (x = 2, 5 en 10).

De (schijnbare) invloed van de waterdiepte op golfoploop is dus niet éénduidig bepaald. Samen met de conclusies van hoofdstuk 5 (de waterdiepte heeft geen significante invloed op golfoploop) doet deze bevinding het verschil in porositeit tussen de deklaag in labo en in situ als mogelijke oorzaak voor de schijnbare invloed van de waterdiepte op relatieve golfoploop aanduiden.

In het algemeen komen de resultaten van de metingen in labo niet overeen met de resultaten van de metingen in werkelijkheid. De mogelijke invloedrijke parameters werden onderzocht. Schaal- en modeleffecten werden geïdentificeerd:

#### (i) schaaleffecten

- invloed van oppervlaktespanning op golfoploop
- invloed van viscositeit op golfvoortplanting, golfoploop en stroming in de kern van de golfbreker

### (ii) modeleffecten

- hydraulisch/meteorologisch
  - golven (spectrale vorm/golfhoogte)
  - wind
  - langse stromingen
- geometrisch
  - deklaag
  - voorland
  - zand in de kern van de golfbreker

Bij de studie van schaaleffecten blijkt de grootte van de getallen van Reynolds, Froude en Weber bepalend te zijn. Zowel de waarde van het getal van Reynolds als de waarde van het getal van Weber zijn in alle testen groter dan hun kritische waarden  $Re_{critical} = 10^4$ , resp.  $We_{critical} = 10$ . Bijgevolg is een verschaling van de werkelijkheid volgens de wet van Froude gerechtvaardigd. Viscositeit heeft geen invloed op golfvoortplanting. Viscositeit heeft geen rechtstreekse invloed op golfoploop, doch wel op een onrechtstreekse manier door de beïnvloeding van de stroming doorheen de golfbreker. De invloed van de viscositeit op de inwendige stroming in de kern van de

golfbreker werd onderzocht door tweemaal dezelfde proeven uit te voeren op eenzelfde model, zij het wel met twee verschillende kernen. Het materiaal van de eerste kern was verschaald volgens de methode van Burcharth et al. (1999) (op schaal 1:20) en het materiaal van de tweede kern volgens de wet van Froude (op schaal 1:30). De conclusie hieromtrent is dat beide modellen verschillende golfoploop hebben ( $\alpha$  < 0.05). De oppervlaktespanning heeft een invloed op golfoploopwaarden Ru < 2.2 cm. De golfoploopsnelheden gemeten in Zeebrugge waren hoger dan deze opgemeten in de modellen. Hierbij worden schaaleffecten als verklaring voor de verschillen aangegeven.

De *modeleffecten* worden onderverdeeld in hydraulische en meteorologische modeleffecten en de geometrische modeleffecten. De spectrale vorm, de golfhoogte, wind en stromingen worden ondergebracht onder de eerste groep modeleffecten. De deklaag, het voorland en het zand in de kern van de golfbreker worden bij de geometrische modeleffecten gerekend.

Alle onderzoeksresultaten (de relatieve golfoploopwaarden  $Ru_2\%/H_{m0}$  afkomstig van de metingen in Zeebrugge, de stormreproducties in de drie laboratoria, de bijkomende testen in FCFH (met zowel regelmatige als onregelmatige plaatsing van de deklaagelementen uitgezonderd de testen met SWL = Z + 6.00), de UGent testen (met twee verschillende schalen voor het kernmateriaal) en de GWK resultaten (proeven met JONSWAP golfspectra op grote schaal) werden uitgezet t.o.v. het getal van Iribarren  $\xi_{om}$  in figuur 11.

Dezelfde golfoploopwaarden werden tevens uitgezet t.o.v. de spectrale breedte parameter  $\varepsilon$  in figuur 12.

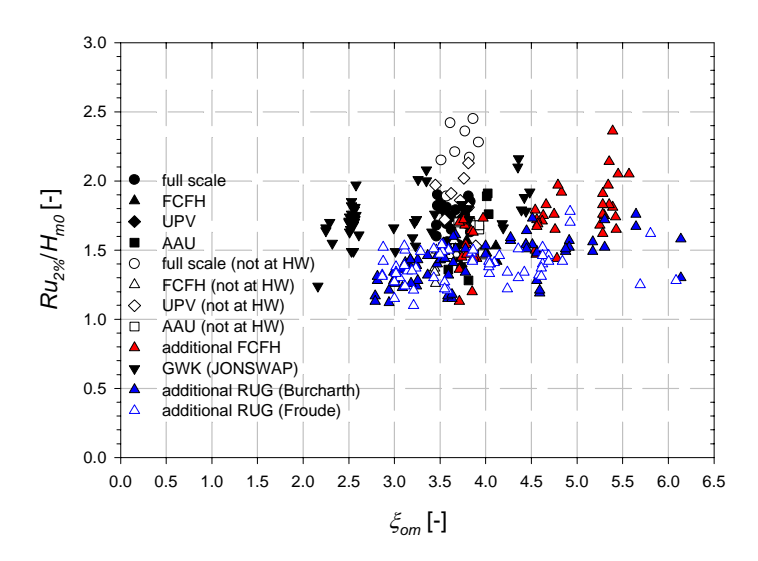


Figure 11:  $Ru_{2\%}/H_{m0}$  t.o.v. het Iribarrengetal  $\xi_{om}$  voor alle testen.

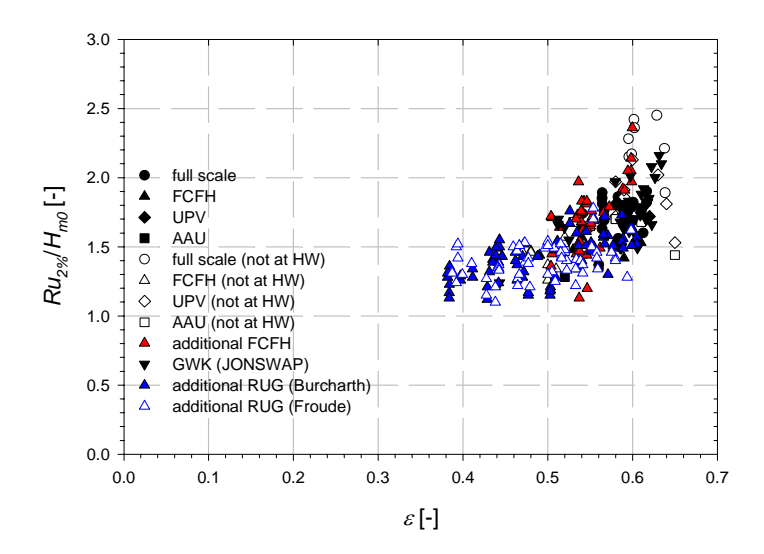
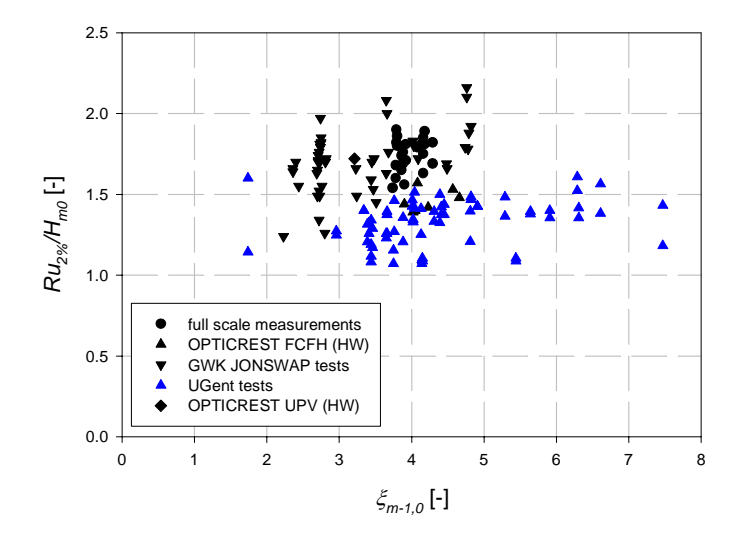


Figure 6.12:  $Ru_{2\%}/H_{m0}$  t.o.v. de spectrale breedte parameter  $\varepsilon$  voor alle testen.

Alhoewel bijna alle in de literatuur geraadpleegde bronnen de dimensieloze golfoploop  $Ru_{2\%}/H_{m0}$  uitdrukken als functie van het

Iribarrengetal  $\xi_{om}$ , toont figuur 11 een grote spreiding op de meetresultaten van de verschillende proefreeksen. De eerder opgemerkte trend in de vergelijking van de resultaten van de metingen in Zeebrugge en de resultaten van de stormsimulaties in de laboratoria (zie figuur 10) wordt bevestigd: dimensieloze golfoploop stijgt voor stijgende waarde van de spectrale breedte parameter  $\varepsilon$ .

Enkeltoppige golfspectra zijn relatief makkelijk te beschrijven met de spectrale periode  $T_p$  of  $T_{0I}$ . Dit is helaas niet het geval voor meertoppige en platgeslagen golfspectra. TAW (2002) en van Gent (1999) stelden daarom ook voor om de spectrale golfperiode  $T_{m-10}$ . te gebruiken i.p.v.  $T_p$  of  $T_{0I}$ . Figuur 13 en 14 tonen de resultaten van metingen in Zeebrugge ( $\bullet$ ), de stormsimulaties in FCFH ( $\blacktriangle$ ) en UPV ( $\bullet$ ), de GWK proeven met JONSWAP spectra ( $\blacktriangledown$ ) en de UGent testen met kern 1 ( $\blacktriangle$ ). Deze meetresultaten werden uitgezet t.o.v. het Iribarren getal  $\xi_{m-10}$  (berekend met  $T_{m-10}$ ) in figuur 13 en t.o.v. de spectrale breedte parameter  $\varepsilon$  in figuur 14.



Figuur 13:  $Ru_{2\%}/H_{m\theta}$  t.o.v. het Iribarren getal  $\xi_{m-1\theta}$  (berekend met de spectrale golfperiode  $T_{m-1\theta}$ ).

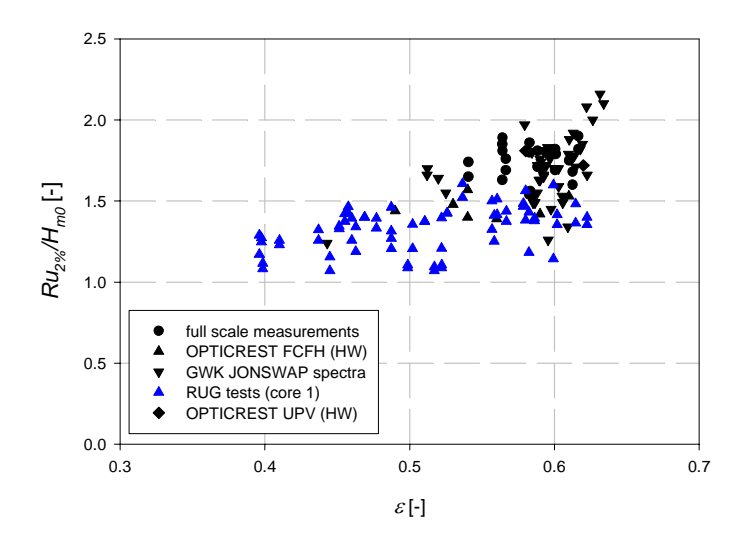
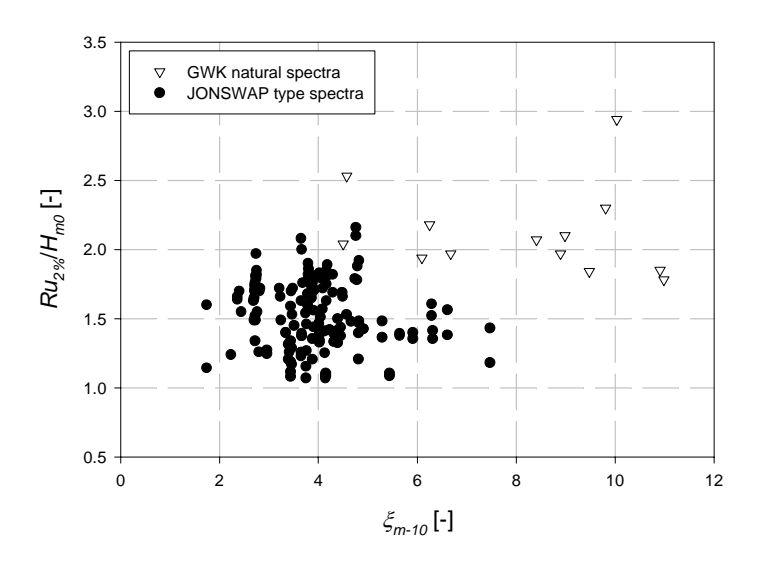


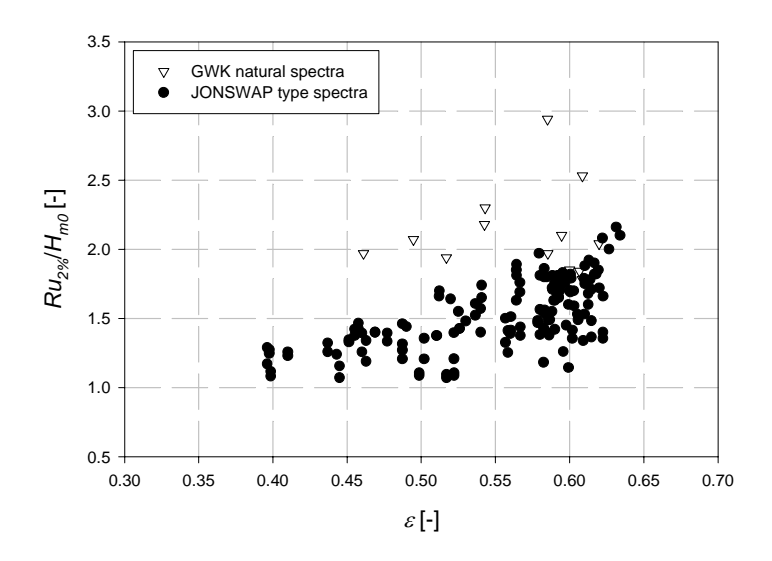
Figure 14:  $Ru_{2\%}/H_{m\theta}$  t.o.v. de spectrale breedte parameter  $\varepsilon$  (cfr. data van figuur 13).

In figuur 14 is een duidelijke trend merkbaar:  $Ru_{2\%}/H_{m0}$  waarden stijgen voor stijgende  $\varepsilon$  waarden. In figuur 13 stijgen de  $Ru_{2\%}/H_{m0}$  waarden ook met stijgende  $\xi$  waarden per testreeks maar de spreiding op de meetresultaten in figuur 13 is groter dan de spreiding op de meetresultaten in figuur 14. De UGent testen hebben in figuur 13 gemiddeld gezien een lagere relatieve golfoploopwaarde dan de GWK JONSWAP testen voor eenzelfde  $\xi$  waarde. Het verschil tussen deze resultaten wordt verklaard door de ligging van de resultaten t.o.v. elkaar in figuur 14 en bijgevolg de invloed van de spectrale breedte. Voor enkeltoppige golfspectra van het JONSWAP type is de spectrale breedte parameter een betere parameter dan  $T_{m-10}$  om golfoploop te beschrijven.

In het GWK werden naast standaard JONSWAP spectra ook natuurlijke spectra (opgemeten langsheen de Noord-Duitse kust) gegenereerd. Wanneer de GWK testen met een natuurlijk golfspectrum in beschouwing worden genomen, dan is voor zowel  $\xi_{m-10}$  (figuur 15) als voor  $\varepsilon$  (figuur 16) op de horizontale as een grote spreiding te zien op de meetresultaten. Noch  $T_{m-10}$ , noch  $\varepsilon$  geven een verklaring aan het verschil in  $Ru_{2\%}/H_{m0}$  waarde voor quasi dezelfde waarde van  $T_{m-10}$  of  $\varepsilon$ .



Figuur 15:  $Ru_{2\%}/H_{m0}$  waarden voor GWK testen met natuurlijke golfspectra t.o.v. het Iribarren getal  $\xi_{m-10}$ .



Figuur 16:  $Ru_{2}$ // $H_{m0}$  waarden voor GWK testen met natuurlijke golfspectra t.o.v. de spectrale breedte parameter  $\varepsilon$ .

De invloed van de spectrale vorm is één van de verklaringen waarom de labometingen (stormsimulaties) onderling en van de metingen op de golfbreker in Zeebrugge afwijken. Enkel de significante golfhoogte en de golfperiode van het werkelijke en het nagebootste golfspectrum op elkaar afstemmen is onvoldoende voor een nauwkeurige reproductie van de opgemeten golven.

Multiregressie analyse werd uitgevoerd op de meetresultaten. Het feit dat (1) in de literatuur golfoploop veelal voorgesteld wordt als functie van het getal van Iribarren (dat functie is van tan  $\alpha$ , H en T), (2) slechts een beperkte hellingsvariatie werd onderzocht (1:2 tot 1:1.3) en (3) de spectrale breedte parameter een invloedrijke parameter is, wordt volgend regressiemodel voorgesteld:

$$\frac{Ru_{2\%}}{H_{m0}} = a + b\varepsilon + cH_{m0} + dT_{m-10}$$
 (5)

Volgende waarden horen bij de parameters a, b, c en d:

- a = 0.546
- b = 1.623
- c = -0.120
- d = 0.072

De bijhorende  $R^2$  waarde is 0.581. Bovenstaande vergelijking is geldig voor enkeltoppige golfspectra van het JONSWAP type en niet voor natuurlijke spectra.

De individuele golfhoogtes opgemeten in Zeebrugge t.h.v. de infraroodmeter corresponderen niet met de opgemeten golfhoogtes in FCFH. De betrouwbaarheid van de infraroodmeter voor golfhoogtemetingen wordt in vraag gesteld. De golfhoogte opgemeten in de labo's ter plaatse van de golfmeetboei was de totale golfhoogte. Echter, in werkelijkheid meet de golfmeetboei de invallende en de op een (in planzicht) gebogen voorwerp gereflecteerde golfenergie. Door de bocht in de golfbreker van Zeebrugge wordt energie verstrooid. Echter, theoretisch gezien is de opgemeten golfhoogte in Zeebrugge slechts 4% kleiner dan de golfhoogte die zou opgemeten worden wanneer de golfbreker recht zou zijn. Deze daling in golfhoogte brengt wel een stijging van de relative golfhoogte met zich mee, maar

verklaart nog niet volledig de opgemerkte verschillen in relatieve golfoploop tussen labo en werkelijkheid.

In UPV werd de invloed van wind op golfoploop onderzocht. Stijgende windsnelheid zorgt voor stijgende relatieve golfoploopwaarden. Een schatting van deze stijging werd gemaakt. De stijging van de relatieve golfoploop bedraagt 1% (voor kleine waarden voor de relatieve vrijboord) tot 10% (voor grote waarden van  $R_c/H_{m0}$ ) voor een windsnelheid van  $v_s = 7$  m/s in vergelijking met een windstille situatie.

De resultaten bekomen in AAU betreffende testen met langse stromingen stroken niet met de metingen in Zeebrugge. Wanneer de stroming het grootst is in Zeebrugge, worden de laagste relatieve golfoploopwaarden opgemeten. In AAU merkte men een stijging van relatieve golfoploop voor stijgende stromingssnelheden op. De invloed van de porositeit van de deklaag wordt groter geacht dan het effect van de stromingen.

Individuele testresultaten laboproeven van waarbij golfoplooptoestellen werden aangewend om gelijktijdig golfoploop te meten, konden sterk van elkaar verschillen. Echter, gemiddeld (over een groot aantal testen) gezien komen de resultaten overeen. Eenzelfde effect werd opgemerkt bij de metingen op ware grootte. Twee verschillende meetsystemen meten gemiddeld gezien hetzelfde, maar de afzonderlijke waarden (opgemeten in verschillende dwarssecties van de golfbreker) kunnen van elkaar verschillen. De deklaag introduceert een spreiding op de meetresultaten. Het plaatsingspatroon is derhalve geen parameter welke in een formule verwerkt kan worden. Door het uitmiddelen van (voldoende) meetresultaten omzeilt men dit probleem.

In FCFH werd het voorland gemodelleerd tot 600 m vòòr de golfbreker. Hierdoor werd ook de kleine zandbank die zich voor de erosieput bevindt gemodelleerd. In UPV werd deze zandbank wegens de beperkte lengte van de golfgoot niet gemodelleerd. Ook in AAU werd de zandbank niet nagebouwd. De aanwezigheid van deze zandbank in FCFH bemoeilijkte het reproduceren van de golfspectra t.p.v. WRII.

### 7 Conclusies en indicaties voor verder onderzoek

De doelstellingen werden bereikt. Een literatuuroverzicht werd gemaakt om de meest belangrijke onderzoeken, fysische fenomenen en invloedrijke parameters te identificeren. Golfoploop werd gemeten op de golfbreker van Zeebrugge m.b.v. twee verschillende meetsystemen: het 'spiderweb systeem' en de golfoploopbaak. De resultaten van beide meetinstrumenten bevestigen Golfterugloop werd tevens opgemeten. Drie schaalmodellen van de golfbreker van Zeebrugge werden gebouwd. In Zeebrugge opgemeten spectra werden in de laboratoria gereproduceerd. Golfoploop werd gemeten met een golfoplooptoestel dat in het kader van dit proefschrift ontwikkeld werd. Met dit nieuwe toestel wordt golfoploop veel nauwkeuriger opgemeten. De golfoploopwaarden opgemeten op de golfbreker van Zeebrugge werden vergeleken met de waarden verkregen in de verschillende laboratoria door het reproduceren van opgemeten spectra. Een duidelijk verschil werd opgemerkt tussen de werkelijke waarden en de laboratoriumwaarden: laboratoriumwaarden waren opmerkelijk lager dan de waarden op ware grootte. De drijvende kracht achter de opgemeten verschillen in golfoploop werden onderzocht. Hiervoor werden bijkomende parametrische modelproeven uitgevoerd. De parameters welke verder werden onderzocht waren: de spectrale vorm (spectrale breedte parameter  $\varepsilon$  en gepiektheidsparameter  $Q_p$ ), het SWL, het plaatsingspatroon van de deklaagelementen, de positie van de kam van de golfoploopbaken t.o.v. de deklaag, de verhouding  $D_{n50}/H_{m0}$ .

In Zeebrugge werd een dimensieloos golfoploopgetal  $Ru_2 \% H_{m0} = 1.77$  gevonden voor  $\xi_{om} = 3.63$ . Deze waarde is veel groter dan de waarden gevonden in de literatuur en groter dan de golfoploopwaarden gevonden in de labo's welke stormen hebben gesimuleerd. Het feit dat golfbrekers ontworpen worden a.d.h.v. fysische schaalmodellen en/of numerieke modellering en het feit dat golfoploop in de labo's kleiner is dan in werkelijkheid doet het vermoeden rijzen dat golfoverslag in werkelijkheid veel hoger zal zijn bij de geteste (ontwerp)rand-voorwaarden van de golfbreker. Ook bij stormen met een kleine retourperiode zal de golfoploop en golfoverslag groter zijn dan geschat.

Het visueel en rekenkundig op elkaar afstemmen van de spectrale vorm mede a.d.h.v. de spectrale parameters  $H_{m0}$  en  $T_{01}$  van de laboratoria spectra op de werkelijke spectra blijkt helaas een onvolledige werkwijze te zijn. Niettegenstaande bovenvermelde

golfkarakteristieken in werkelijkheid en in labo met elkaar overeenstemden, was dit niet altijd het geval voor de spectrale vorm parameters. Een duidelijke afhankelijkheid van  $Ru_2 \% H_{m0}$  van de spectrale vorm (gekarakteriseerd door de spectrale breedte parameter ε) werd opgemerkt: dimensieloze golfoploopwaarden zijn een stijgende functie van de spectrale breedte parameter  $\varepsilon$ . In Zeebrugge werden grote waarden voor  $\varepsilon$  en  $Ru_2 \% H_{m0}$  opgemeten. In FCFH werden kleine waarden voor  $\varepsilon$  opgemeten en bijgevolg dus ook  $Ru_{2}$ // $H_{m0}$ . Een formule werd opgesteld die  $Ru_{2}$ // $H_{m0}$  geeft in functie van  $\varepsilon$  en die geldig is voor oplopende brekers op een doorlatende stortsteengolfbreker met een helling tan  $\alpha > 0.5$ . De positie van de kam van het golfoploopmeettoestel t.o.v. de deklaag is niet bepalend. Binnen eenzelfde test kunnen resultaten van twee verschillende meettoestellen van elkaar afwijken, maar gemiddeld gezien wordt de 'fout' die door het plaatsingspatroon van de deklaag wordt geïntroduceerd geminimaliseerd. Dit werd opgemerkt in Zeebrugge ('spiderweb systeem' en golfoploopbaak) en bij de bijkomende proeven in UGent (twee golfoplooptoestellen in verschillende dwarsdoorsnedes van de golfbreker). De afmeting van deklaagelementen en de verhouding  $D_{n50}/H_{m0}$  in het bijzonder hebben geen invloed op golfoploop. Dit werd bewezen door de testen op grote schaal in het GWK.

De waargenomen invloed van de waterdiepte op golfoploop in Zeebrugge en in de verschillende schaalmodellen van de golfbreker van Zeebrugge kan verklaard worden door twee geometrische factoren: de lokaal lagere porositeit van het onderste gedeelte van de deklaag als gevolg van zettingen van de golfbreker en de aanwezigheid van zand in de kern van de golfbreker.

Volgende aanbevelingen worden gegeven:

- Golfoploop dient zo nauwkeurig mogelijk opgemeten te worden. Er wordt daarom sterk aanbevolen om de nieuwe digitale golfoploopbaak te gebruiken. Tevens wordt aangeraden een voldoend aantal testen uit te voeren, de positie van de kam van de golfoploopbaak t.o.v. de deklaag te variëren (waarbij de testen dienen hernomen te worden met een identiek golfschotsignaal) of wordt het best gedurende één en dezelfde tests twee (of meerdere) golfoplooptoestellen gebruikt.
- Dezelfde laboratoriumtesten worden het best in twee afzonderlijke labo's uitgevoerd. Op die manier kunnen de resultaten met elkaar

- vergeleken worden en kunnen mogelijke verschillen opgespoord worden.
- Enkel het op elkaar afstemmen van  $H_{m0}$  en  $T_{01}$  (of  $T_p$ ) van zowel het doelspectrum (natuurlijk spectrum) en het gereproduceerde spectrum in het labo is onvoldoende. De spectrale breedte parameters van beide spectra dienen ook vergeleken te worden.

De auteur zou graag volgende items verder onderzocht zien:

- golfprofiel voor de golfbreker op het moment van maximale golfoploop en dit op ware grootte en in schaalmodel, rekening houdend met de bevindingen van voorliggend onderzoek
- numerieke modelling van golfoploop op stortsteengolfbrekers
- golfoverslag (vergelijking tussen metingen op ware grootte en laboratoriummetingen)
- optimisatie van golfgeneratietechnieken om gewenste spectra te genereren (niet enkel rekening houdend met het amplitudespectrum, maar ook met het fasespectrum)
- verdere uitdieping met fysische modelproeven van de kernverschalingsmethode voorgesteld door Burcharth et al. (1999).
- golfoploop- en golfoverslagssnelheden bij stortsteengolfbrekers

# **Chapter 1: General introduction**

#### 1.1 Rationale

Breakwaters are commonly used solutions to protect offshore harbours and harbours situated along the coast against severe wave attack. Three main types of breakwaters exist: (1) gravity structures, (2) caisson breakwaters and (3) floating breakwaters. A gravity structure borrows its stability from its weight and thus from 'gravity' as the name says. A well known breakwater type amongst gravity structures is the rubble mound breakwater. This structure consists of a core, one or more filter layers and an armour layer.

The design criteria for rubble mound breakwaters are wave overtopping and/or wave transmission. Structures for coastal protection are very expensive constructions. On the one hand, economical reasons force to keep the crest height as low as possible. The volume of materials (and thus the cost price) needed to embody the structure is proportional to the square of the height of the structure. Moreover, people spending their holidays at the sea side prefer a view at the sea without large visual obstructions. On the other hand, the crest height of a structure may not be too low either. When the crest level is too low, water could overtop the structure. Excessive wave overtopping will either increase the initial construction cost of coastal structures or the maintenance, repair and costs due to property lost during overtopping events. Wave overtopping and flooding require extremely expensive repair operations and very often insurance claims for injury and property damage are submitted. Harbours tend to be situated in areas with an open connection to the sea only within the shelter of a breakwater. Under bad weather conditions, harbour yard and dock activities are strongly affected by inadequate breakwater design: transhipment and storage of goods on the quays are disturbed and ships are unable to load or unload for long periods. This can have far-reaching consequences as companies fleeing to other harbours, loss of business and earnings, unemployment or even bankruptcy of firms. Moreover, for remediation works, at some places (e.g. cities near the sea) it is geometrically impossible to make the seawall higher and wider.

In practice, it is not likely to overdimension the structure, but to allow a certain (acceptable and not dangerous) amount of water. Depending on the activity behind the breakwater, a certain amount of water is allowed to overtop the crest of the breakwater. When wave overtopping occurs, waves rush down on the backward slope of the breakwater. These waves may gradually damage the backward armour layer. The backward slope is not protected as heavy as the seaward slope because in principle former is only intended to withstand diffracted waves and ship moving induced waves. Therefore, in case of a large amount of overtopping water, the rear side of the breakwater might be protected as heavy as the front side.

Breakwaters are designed by small scale model testing in the laboratory or by numerical modelling. Design sea state conditions are generated and structures are designed to withstand these conditions. Wave run-up is hardly considered as for design sea state conditions, heavy (but still) admissible wave overtopping will occur and wave run-up is absolutely out of the question. In reality, however, design conditions for sea defences are not very likely to occur and are estimated to occur only once in a thousand or ten thousand years. Although monitoring of the structure is important to have an idea about the actual behaviour of the construction under less severe sea state conditions than the design sea state conditions, full scale measurements of wave-structure interaction are very scarce. This is not only because of the expensive character of the measuring campaigns and the dependency of the feasibility on weather conditions but also because of the harsh marine environment in which sensitive instrumentation needs to be installed and measurements have to be performed. Full scale measurements are indispensable to validate small scale model test results and results of numerical models. However, full scale measurements only yield data within a limited range of sea state parameters and structural parameters. In Zeebrugge, it was possible to measure wave run-up during less severe sea state conditions than the design sea state conditions. Only during a limited number of storms waves overtopped the structure. These 'normal' sea state conditions have hardly been investigated in the laboratory. This investigation was a unique opportunity to compare wave run-up at full scale under 'normal' sea state conditions and wave run-up in the laboratory. The outcome of the investigation allows to get insight in the frequency of overtopping waves.

## 1.2 Wave run-up and wave run-down

Wave run-up Ru [m] is defined as the vertical distance between the still water level (SWL) and the level to which the leading edge of the water tongue running up the seaward slope of the breakwater extends (figure 1.1). Likewise wave heights are characterised by  $H_s$  (the

average of the one third highest waves determined by a zero down crossing method or zero up crossing method) or another meaningful parameter (which are all linked together if and only if wave heights are Rayleigh distributed), wave run-up can be characterised by one single number. For the design of the crest level of sea dikes, the wave run-up level with a 2% exceedance probability,  $Ru_{2\%}$ , is a widely used parameter (van der Meer and Stam (1992), Shore Protection Manual (1984),...).  $Ru_{x\%}$  is the run-up level which is exceeded by x% of the run-up events. The number of run-up events is defined as the number of incident waves within the analysed time series. The origin of the use of the  $Ru_{2\%}$  value has to be found in Dutch dike design and is nothing more than a historical transfer. According to van der Meer et al. (1998), the 2% wave run-up criterion, i.e. a crest level exceeded by 2% of the incoming waves, yields an overtopping discharge of the order of 1 l/s per m crest for relatively heavy seas and wave heights up to a few meters and 0.1 l/s per m crest for lower waves (e.g. on a river). In this thesis, the habit of using  $Ru_{2\%}$  for characterisation of wave run-up on smooth impermeable dikes has been adopted for the characterisation of wave run-up on permeable rubble mound breakwaters.

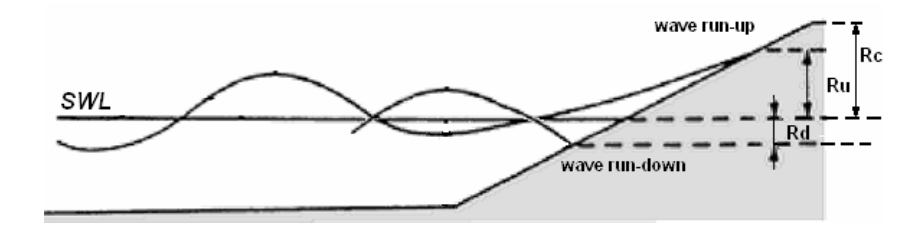


Figure 1.1: Definition sketch for wave run-up on the slope of a coastal structure (dike, breakwater,...).

The degree of protection by a breakwater against wave overtopping is primarily determined by the ratio  $Ru_2 \% R_c$ .  $R_c$  is the freeboard parameter and is the vertical distance between SWL and the crest. The design criterion states that the ratio  $Ru_2 \% R_c$  should be equal or smaller than unity.

Wave run-down  $R_d$  is defined as the vertical distance between the *SWL* and the level to which a wave retains on a structure slope. Alike wave run-up is characterised by a value  $Ru_{2\%}$ , wave run-down can also be

characterised by the value which is exceeded by 2% of the wave rundown events,  $Rd_{2\%}$  or by its maximum value  $Rd_{max}$  which is interesting for slope protection.

# 1.3 Wave overtopping

Wave overtopping is closely related to wave run-up. Wave overtopping is defined as the amount of green water which exceeds the crest of a coastal structure (figure 1.2). Wave overtopping will only be discussed very briefly. Wave overtopping is the subject of the European Community supported Fifth Framework Programme project 'CLASH' ('Crest Level Assessment of coastal Structures by full scale monitoring, neural network prediction and Hazard analysis on permissible wave overtopping' (2002–2004) – contract nr. EVK3–CT–2001–00058).

Wave overtopping can be expressed in two different ways. Firstly, wave overtopping can be expressed in terms of individual volumes of water V [m³] comprising the overtopping waves. A second way is to express wave overtopping by its mean wave overtopping discharge q [m³/sm], i.e. the volume of water that overtops the structure per second and per meter crest width. The second quantity is an average value of the investigated time series and is useful for drainage design. The knowledge of the distribution of individual wave overtopping volumes is practical for the design of certain parts of the coastal structure which have to withstand the impact of large masses of water.

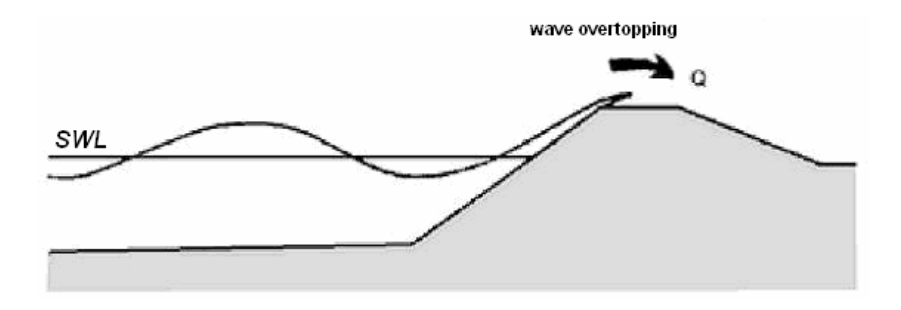


Figure 1.2: Definition sketch for wave overtopping over the crest of a coastal structure (dike, breakwater,...).

## 1.4 Wave run-up or wave overtopping?

The waves which overtop the structure have a wave run-up level which exceeds the crest level of the structure. Whether wave run-up measurements are useful or not, one has to check the wave run-up distribution curve for wave run-up values which exceed the freeboard of the breakwater. When wave overtopping occurs, the highest wave run-up heights are truncated at the crest level. It becomes very difficult to determine the  $Ru_{2\%}$  level once more than 2% of the waves overtop the structure. In this case, wave run-up is no longer the investigated variable. Nevertheless, wave run-up levels higher than the crest level can be estimated using a known and fitted theoretical distribution. Wave run-up levels lower than the crest level of the structure are measured correctly. From these wave run-up measurements, the  $Ru_{2\%}$  value still can be determined if and only if wave run-up values obeys the assumed theoretical distribution.

# 1.5 Description of the investigated problem

Within the MAST II programme of the European Community the project 'Full scale dynamic load monitoring of rubble mound breakwaters' (1994–1996) (contract nr. MAS2–CT92–0023) started the acquisition of full scale wave and pore pressure data on the Zeebrugge rubble mound breakwater. In the same project, the Zeebrugge breakwater was modelled at three different scales and tested. Wave run-up was one of the investigated parameters. Model test results have been compared with full scale data. Several conclusions were drawn (De Rouck et al. (1996)):

- full scale measurements of wave run-up tended to be clearly higher than experimental results (figure 1.3).
- wave run-up as measured in scale model studies tended to be slightly underestimated due to the method of wave run-up measurement and the shape of the wave run-up profile.
- wave run-up distributions for all models varied significantly from these measured at full scale.

In the MAST II project, wave run-up in the model tests was measured using a resistance probe placed along the surface of the armour layer. The thin leading edge of the waves running up the slope of the breakwater was not detected by the probe being slightly above the armour layer surface. Visual observation and later analysis of video footage confirmed the underestimation of wave run-up measured by a single wave probe stretched along the slope of the breakwater.

The first outcome of the MAST II project initiated further research on wave run-up within the European funded MAST III OPTICREST project ('The optimisation of crest level design of sloping coastal structures through prototype monitoring and modelling' (1998–2001) – contract nr. MAS3–CT97–0116). Wave run-up has been measured extensively on a full scale rubble mound breakwater and measured storms have been simulated in different laboratories. Results have been compared. To meet the second outcome of the MAST II project, a new measuring device was developed for full scale wave run-up measurements, as well as for use in laboratory environments. With the new measuring device wave run-up could be measured more accurately. The results of the measurements on the full scale Zeebrugge rubble mound breakwater and the measurements on several small scale versions of this breakwater will be described and discussed in this thesis.

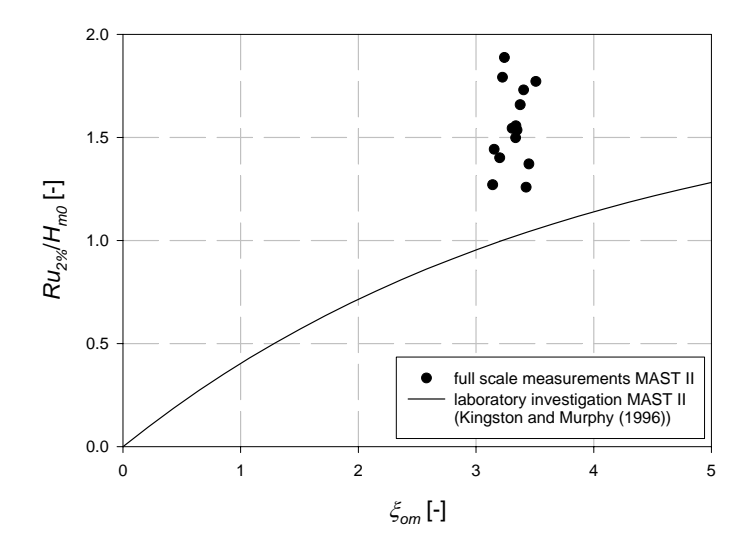


Figure 1.3: Comparison of full scale wave run-up data and results of small scale model tests on the Zeebrugge rubble mound breakwater (De Rouck et al. (1996), Troch et al. (1996)).

Besides the finding that wave run-up on a rubble mound breakwater in reality reaches much higher levels than observed in scale model tests, the sea level rise is a world-wide known phenomenon (Führböter (1990)) which affects wave run-up adversely. An indication of the expected sea level rise could be 40 to 65 cm by the year 2100, due to predicted greenhouse gas induced climate warming (http://www.giss.nasa.gov/research/intro/gornitz\_01/). Increasing sea level rise indicates that existing structures will become less 'safe' in the future as the freeboard decreases. Research also revealed that storm intensity and storm frequency are increasing (Führböter (1990) and Carter et al. (1988)). The probability that the design conditions will occur during the lifetime of the structure increases.

During the last decades, a lot of rubble mound breakwaters have been built around the world, both for harbour protection as well as for coastal protection purposes. Four examples of rubble mound breakwaters have been highlighted.

Burns Waterway Harbour is located in northwest Indiana on the southern shore of Lake Michigan in Porter County, 28 miles southeast of Chicago Harbour. The design conditions for this breakwater were: SWL = +1.07 low water datum (LWD), crest level LWD +4.27 and  $H_{des} = 3.35$  m. The dimensionless freeboard parameter  $R_c/H$  was 0.96. Severe damage occurred to the breakwater since 1973, resulting in excessive operation and maintenance costs. Damages to vessels, cargo, and the harbour infrastructure were experienced, as well as shipping delays. Results of a study which provided hindcast data over a 32-year period on the Great Lakes indicated that the original design conditions had been underestimated. The design wave height should have been  $H_{des} = 4.88$  m. With this, the dimensionless freeboard parameter  $R_c/H$  equalled only 0.66 in stead of 0.96. One of the alternative solutions was to heighten the crest level to +5.79. By this, the dimensionless freeboard parameter increased to  $R_c/H = 0.97$ . Finally, the plan selected for construction was the placement of a segmented reef breakwater on the lakeside of the existing breakwater. (http://bigfoot.wes.army.mil/6539.html).

The western rubble mound breakwater at the port of Sines (Portugal) failed during a storm on February 26<sup>th</sup>, 1978. For wave overtopping investigations, a design water level of +4.00 m Chart Datum (*CD*) was taken. The crest level of the original breakwater was +19.00 m *CD*. A deep water design wave height with a hundred years return period was established:  $H_s = 13.9$  m. Wave periods ranged from 16 to 22 seconds. The dimensionless freeboard  $R_c/H$  equals 1.08. (*Edge B.L. et al.* (1982))

The design conditions of the rubble mound breakwater of Zeebrugge are: SWL = Z + 6.75 m, crest level Z + 12.40 m and  $H_s = 6.20$  m. The dimensionless freeboard  $R_c/H$  equals 0.91. (Van Damme et al. (1982))

Near Madras (India) a new breakwater has been built (1997-2001). The southern breakwater (1040 m long) and the northern breakwater (3070 m long and herewith the longest breakwater in India) protect the coal quay for a power station supply. The armour layer consists of acropodes. The crest level is +4.75 *CD* (Chart Datum). The high tide level is +1.50 *CD*. The significant design wave height is 6.50 m and the design wave period is 10 s (Khattar (2001)). So, the freeboard  $R_c$  of the breakwater is 3.25 m, yielding a value 0.5 for the dimensionless freeboard  $R_c/H$ .

Concluding, all examples show a rather small value for the dimensionless freeboard parameter  $R_c/H$  with H= the design wave height ( $R_c/H \le 1$ ). The observation of higher wave run-up in Zeebrugge than indicated by small scale laboratory tests and the aforementioned examples suggest less safe constructions as envisaged as much more water will overtop the structure during design storm conditions than expected by laboratory testing. Also during normal storm conditions, corresponding to smaller return periods, wave transmission will be higher than expected.

For (smooth, impermeable) dikes, a lot of investigation has already been carried out. Not all researchers came to the same conclusions. van Gent et al. (2001) found a good agreement between full scale data and small scale test results of wave run-up measurements on the Petten Sea Defence (the Netherlands). Field measurements of wave run-up on dikes along the German coastline indicated higher wave run-up than predicted by common used formulae (Grüne (1982)). Small scale model tests have shown considerable discrepancies from large scale tests in terms of slope stability and wave run-up behaviour (Gadd (1984)). Permeable and rough slopes have also been subjected to extensive testing, but most slopes were protected by rip rap ( $D_{n50} < < H_s$ ). For the Zeebrugge breakwater the ratio  $D_{n50}/H_s$  approximates unity.

# 1.6 Objectives

This doctoral thesis focuses on wave run-up on permeable rubble mound breakwaters. The objectives of this dissertation are formulated:

- (1) to carry out a study of the existing literature to investigate the governing physical processes, influential parameters and points of special interest concerning wave run-up on coastal structures and the existing wave run-up formulae.
- (2) to collect full scale data on waves and wave run-up on a rubble mound breakwater.
- (3) to verify small scale models by comparison of full scale measurement results to results of small scale model testing in which storm events measured at full scale are reproduced.
- (4) to identify the driving forces (scale effects and model effects) behind the observed discrepancies in case results of full scale measurements do not agree with small scale model test results and to investigate the influencing (spectral) parameters on wave run-up by small scale and large scale model testing.
- (5) to provide a formula to estimate wave run-up on a permeable rubble mound breakwater.

#### 1.7 Activities

To meet the aforementioned objectives, following activities have been undertaken.

- (1) Wave run-up and its influencing parameters and governing physical processes are studied by means of a **literature overview**.
- (2) Wave run-up on a rubble mound breakwater has been measured at **full scale**. The outer harbour of Zeebrugge (Belgium) has been chosen for this purpose. The harbour is protected by two rubble mound breakwaters built in the eighties and armoured with flattened grooved cubes. Wave run-up has been measured on the northern part of the western breakwater by two different measuring systems: a 'spiderweb system' and a run-up gauge.

- (3) Small scale model tests have been carried out on the Zeebrugge rubble mound breakwater in three selected laboratories spread over Europe. The models have been tested extensively. Parametric tests have been carried out, as well as reproductions of storm events measured at the Zeebrugge breakwater. A two dimensional model has been built in Flanders Hydraulics (FCFH - Belgium) and in Universidad Politécnica de Valencia (UPV - Spain) on scale 1:30. A three dimensional model has been built in Aalborg University (AAU - Denmark) on scale 1:40. The distorted scale of the core material of these models was 1:20 for the 2D models and 1:24 for the 3D models. Results of full scale measurement campaigns and small scale model tests have been compared. Anticipating the comparison, it can already been mentioned that results of full scale measurements and small scale model tests do not agree. Wave run-up in scale models is smaller than wave run-up measured at full scale. The difference is due to scale effects and model effects. Scale effects are very difficult and not very likely to be estimated. Therefore, emphasis is put on the identification of model effects. So, additional parametric tests have been carried out on the original (Zeebrugge breakwater with an irregular outer armour unit pattern) and on a slightly modified model (Zeebrugge breakwater with a regular outer armour unit pattern) at Flanders Hydraulics to gain a better insight in the main influential parameters on wave run-up on a rubble mound breakwater.
- (4) The results of the additional small scale testing at FCFH initiated **further additional testing** on a **simplified model** of the Zeebrugge breakwater (without the armour layer) which has been built in the small wave flume of the Coastal Engineering Unit of the Department of Civil Engineering of the Faculty of Applied Sciences of Ghent University (UGent Belgium) to evaluate the influence of the spectral shape (by means of the spectral width parameter  $\varepsilon$  and the peakedness parameter  $Q_p$  (Goda (1985))), the location of the comb of the run-up gauge and the SWL and to investigate the influence of the core scaling. The influence of parameters such as  $D_{n50}/H_{m0}$  have been minimised. The same breakwater has been built twice to investigate the

influence of the scaling of the core material (either Froude scaling or scaling according to Burcharth et al. (1999)).

(5) Large scale measurements have been carried out on a didactical example of a rubble mound breakwater in the Large Wave Flume in Hannover (Germany) in autumn 2001. This breakwater was a conventional breakwater covered with quarry rock. The main objectives of these large scale tests was to investigate the stability of high density rock ( $\rho = 3.05 \text{ t/m}^3$ ) and to collect large scale wave run-up data on a rubble mound breakwater. Thus, the influence of the dimensions of the armour unit on wave run-up has been investigated.

The whole range covering full scale, large scale and small scale has been investigated.

Full scale measurements data are unique. Large scale data are a good alternative for full scale measurements. Large scale data are a lot more valuable than small scale model data as scale effects are minimised in large scale tests. The smaller the scale of the model, the more important become scale effects. Although large scale approximates full scale, large scale tests cannot fully imitate reality (3D effects, tides, currents, wind,...).

Small scale model tests have the big advantage of being easy to perform. Also a lot of combinations of different input parameters (hydraulical/geometrical/meteorological/...) can be investigated in limited time whereas this is not the case for large scale tests and certainly not for full scale measurements. On the other hand, scale effects may have an adverse influence on test results.

An overview of the tested models is given in table 1.1. It must also be mentioned that numerical modelling has not been the subject of this thesis at any time.

		overall scale	slope	armour layer	
FULL SCALE	Zeebrugge rubble mound breakwater (Belgium)	1:1	~ 1:1.3	grooved cubes	measurements of storm events
LARGE SCALE	rubble mound breakwater (GWK - Germany)	1:1	1:2	rock (high/normal density)	parametric tests
SMALL SCALE	2D model (FCFH - Belgium)	1:30 <sup>(1)</sup>	1:1.3	grooved cubes	storm event reproductions and parametric tests
	2D model (UPV - Spain)	1:30 <sup>(1)</sup>	1:1.3	grooved cubes	storm event reproductions and parametric tests
	2D model (UGent - Belgium)	1:30 <sup>(2)</sup>	1:1.5	rock (normal density)	parametric tests
	3D model (AAU - Denmark)	1:40 <sup>(3)</sup>	~ 1:1.3	grooved cubes	storm event reproductions and parametric tests

<sup>(1):</sup> core materialscaled to 1:20

<sup>(2):</sup> core material scaled to 1:20, resp. 1:30

<sup>(3):</sup> core material scaled to 1:24

# **Chapter 2: State of the art**

#### 2.1 Introduction

This chapter provides an overview of the existing knowledge on wave run-up. The author has tried to present the most important formulae, insights and investigations. The overview is not complete as numerous investigations have been performed in the past. A lot of these investigations had their own specific restricted research topic. An enumeration of all existing wave run-up investigations would have gone too far. Though, important formulae and their range of application have been highlighted. An extensive description of wave run-up research is found in Allsop et al. (1985) and Verdonck et al. (1998).

### 2.2 Wave run-up

### 2.2.1 Iribarren number

A lot of phenomena in the surf zone are described by means of the Iribarren number  $\xi$  (Iribarren and Nogales (1949) (cfr. Battjes (1974a))). The Iribarren number, or also called the surf similarity parameter (due to the fact that  $\xi$  has the same value in the model as at full scale, provided the small scale model is dynamically similar) is defined as

$$\xi = \frac{\tan \alpha}{\sqrt{s}} \tag{2.1}$$

in which  $\bullet$  tan  $\alpha$  = slope of the coastal structure

• 
$$s =$$
 wave steepness, defined by  $s = \frac{H}{L}$ 

Different definitions of the Iribarren number are suggested, depending on the wave parameters (H and L and thus T) used to calculate  $\xi$ . For irregular waves, mostly the incident significant wave height  $H_{m0}$  (or  $H_s$ ) at the toe of the structure and the deep water wave length  $L_0$  are used to calculate a 'fictive' wave steepness. The significant wave height  $H_{m0}$  is calculated as  $4\sqrt{m_0}$  in which  $m_i$  is the i<sup>th</sup> order moment of the energy in the wave spectrum between  $f_{min}$  and  $f_{max}$ :

$$m_{i} = \int_{f_{\min}}^{f_{\max}} f^{i} S(f) df \tag{2.2}$$

The IAHR recommends the lower frequency boundary  $f_{min}$  to be the minimum of  $f_p/3$  and 0.05 Hz and the upper frequency boundary  $f_{max}$  to be  $3f_p$ . The spectral peak period  $T_p$  corresponds to the peak frequency  $f_p$ . The peak frequency  $f_p$  is the frequency at which the spectrum S(f) has a maximum.  $H_s$  is the significant wave height calculated in time domain and is defined as the average of the one third highest waves within the considered wave record detected by a zero (down or up) crossing method. Mostly, a zero down crossing method is used.

The deep water wave length  $L_0$  can be calculated using either the mean wave period  $T_{01}$  (or  $T_m$ ) or the peak wave period  $T_p$ :

$$L_{0m} = \frac{gT_{01}^2}{2\pi} \tag{2.3}$$

$$L_{0p} = \frac{gT_p^2}{2\pi} \tag{2.4}$$

In frequency domain, all periods are defined by

$$T_{ij} = \left(\frac{m_i}{m_j}\right)^{\frac{1}{j-i}}, i < j \tag{2.5}$$

According to (2.5), the mean wave period  $T_{0I}$  is given by  $m_0/m_I$ .  $m_0$  is the surface bounded by the S(f) curve, the horizontal axis, the vertical line at  $f_{min}$  and the vertical line at  $f_{max}$ .  $m_I$  is the static moment around the vertical axis of the surface bounded by the S(f) curve, the horizontal axis and the aforementioned vertical lines. Both  $T_{0I}$  and  $T_p$  are determined in frequency domain.  $T_m$  is the mean wave period in time domain and is the average of all wave periods detected by a zero down crossing method.

The index '0' in (2.3) and (2.4) indicates that the wave period is taken in deep water. Whether the mean wave period  $T_{01}$  (or  $T_m$ ) or the peak wave period  $T_p$  should be used to calculate the Iribarren number and to

relate to wave run-up is not always clear. However, van der Meer and Stam (1992) and Grüne (2000) advise to use the mean wave period. TAW (2002) recommends the use of  $T_{.10}$ .

The Iribarren number not only indicates whether a wave is breaking or not, it also characterises the breaker type (figure 2.1):

- spilling ( $\xi$  < 0.5)
- plunging  $(0.5 < \xi < 3)$
- collapsing  $(3 < \xi < 3.5)$
- surging  $(\xi > 3.5)$

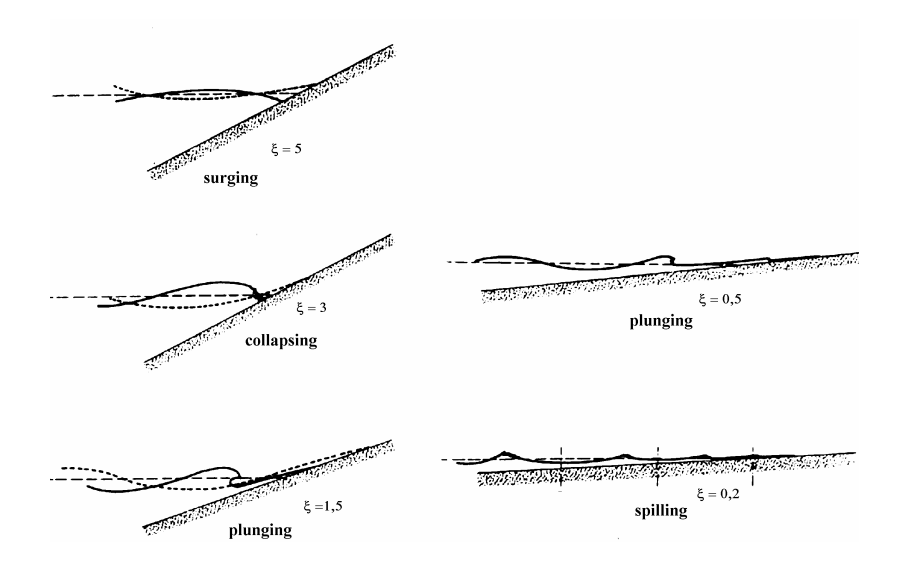


Figure 2.1: Iribarren numbers related to the type of breaker (taken from van der Meer (1988)).

# 2.2.2 Hypothesis of equivalence

The very first wave run-up tests have been performed with monochromatic waves attacking a gentle smooth slope. Afterwards, a lot of equations, basically meant for the estimation of wave run-up induced by regular waves, have been expanded to irregular waves by the 'hypothesis of equivalence' (Battjes (1974)) which was introduced by Saville (1956). This hypothesis considers all composing waves in a wave train as individual (regular) waves and applies the theory for regular waves on each of these. The wave run-up distribution which is

the result of an irregular wave train incident on a coastal structure is found by composing all wave run-up heights which are the result of each individual regular wave within the irregular wave train with its corresponding wave height and wave period.

It is not always clear which wave height  $(H_{rms}, H_s, H_{mean},...)$ , wave run-up value  $(Ru_{2\%}, Ru_s, Ru_{mean},...)$  and wave period  $(T_p, T_{mean}, T_{01}, T_{02},...)$  have to be used when wave run-up formulae, primarily conceived for regular wave attack, are applied for irregular wave attack. Silva et al. (1994) proposed to use the mean wave period and the  $H_{rms}$  value to link wave parameters to the  $Ru_{rms}$  value. Mase et al. (1984) proposed to use  $H_s$  and  $L_s$  (calculated starting from  $H_s$ ) to calculate the Iribarren number.

#### 2.2.3 Parameters

Wave run-up Ru is function of the following parameters:

- (i) hydraulic/meteorological parameters
  - water density  $\rho_w$
  - dynamic or kinematic viscosity of the fluid  $\mu$ , resp.  $\nu$
  - $\bullet$  compressibility of the fluid K
  - $\bullet$  surface tension  $\sigma$
  - for regular waves: wave height H and wave period T
  - for irregular waves: characterised either by parameters calculated in time domain  $(H_s, T_m,...)$  or by the incident wave spectrum S(f) and its spectral parameters calculated in frequency domain  $(H_{m0}, T_{01}, T_p$ , spectral shape parameters (spectral width parameter  $\varepsilon$ , peakedness parameter  $Q_p$ , groupiness parameter GF,...)
  - wave incident angle  $\theta$
  - wind velocity  $v_s$  and wind blowing direction  $\theta_w$
- (ii) geometry/characteristics of the structure:
  - water depth at the toe of the structure d
  - bottom slope angle  $\beta$
  - slope angle of the structure  $\alpha$  (presence of a berm and its elevation relative to SWL)
  - armour unit type and pattern
  - porosity of the armour layer
  - roughness of the armour layer  $(D_{n50}/H_{m0})$
  - armour unit density  $\rho_r$

- gravitational acceleration g
- permeability of the structure *P*

In general, wave run-up is function of all these parameters. Retaining the most important parameters (cfr. Losada and Giménez-Curto (1981) and Stam (1989)),

$$\frac{Ru}{H} = f(H, T, \varepsilon, g, d, \alpha, \beta, \theta, D_{n50}, v, \rho_r, \rho_w, K, \sigma, v_s, P)$$
 (2.6),

assuming the spectral width parameter  $\varepsilon$  (see paragraph 2.2.3.2) to describe the spectral shape. Introducing a number of dimensionless parameters (according to Buckingham's Pi Theorem, thirteen dimensionless parameters are needed to describe the phenomenon with sixteen parameters), wave run-up is described as

$$\frac{Ru}{H} = f\left(\frac{H^2}{vT}, \frac{d}{H}, \frac{H}{gT^2}, \frac{v_s T}{H}, \frac{\rho H^2}{KT^2}, \frac{\rho H^3}{\sigma T^2}, \alpha, \beta, \theta, \varepsilon, \frac{D_{n50}}{H}, P, \frac{\rho_r}{\rho_w}\right)$$
(2.7)

Simplifying (2.7) by neglecting oblique wave incidence ( $\theta = 0^{\circ}$ ), no foreshore slope ( $\beta << \alpha$ , assume  $\beta \cong 0^{\circ}$ ), assuming incompressible water and regular non-breaking waves, a high Reynolds number and a high Weber number (Re and We) threshold value (see paragraph 6.3) by which viscosity and surface tension of the water have no longer influence on wave propagation and wave run-up), dimensionless wave run-up (relative to the wave height) on a smooth slope becomes function of only two parameters:

$$\frac{Ru}{H} = f_1 \left( \alpha, \frac{H}{L} \right) \tag{2.8}$$

or

$$\frac{Ru}{H} = f_2(\xi) \tag{2.9}$$

The wave run-up height, relative to the incident wave height is function of the Iribarren number  $\xi$ . Many researchers have found an expression for  $f_2(\xi)$  (see paragraph 2.4).

Some of the enumerated and other parameters are further discussed in the next paragraphs.

### 2.2.3.1 Wind

Ward et al. (1994, 1996, 1997) mention the influence of wind. Strong winds increase wave run-up, especially on steep slopes. The influence of wind may results in

- an increase in incident wave energy due to shear forces on the water surface and the transfer of energy between air and water by which the incident wave spectrum is affected
- wind induced water set-up additional to SWL
- change in wave kinematics by introduction of a horizontal force which has its strongest influence at the point of breaking of the waves

# 2.2.3.2 Spectral shape

The shape of a spectrum is described by many parameters. One of these is the spectral width parameter  $\varepsilon$ . Two different definitions (in frequency domain) of the spectral width parameter  $\varepsilon$  exist. On the one hand, there is the bandwidth parameter  $\varepsilon$  (Cartwright and Longuet-Higgins (1956)), defined as

$$\varepsilon = \sqrt{I - \frac{m_2^2}{m_0 m_4}} \tag{2.10}$$

where  $0 \le \varepsilon \le 1$ . Calculating  $\varepsilon$ , van Oorschot and d'Angremond (1968) ignored the high frequencies with an energy content of less than 5% of the peak energy component. The found values of  $\varepsilon$  varied in the interval [0.22, 0.59].

On the other hand, Longuet-Higgins (1983) proposed the spectral width parameter defined by

$$v = \sqrt{\frac{m_2 m_0}{m_1^2} - 1} \tag{2.11}$$

where  $0 \le v \le 1$ . This definition has not been used further on.

In general, the smaller the value of the spectral width parameters  $\varepsilon$  and  $\nu$ , the more narrow banded the spectrum, the less energy content of the spectrum and the smaller the induced wave run-up is. Conversely, the larger spectral width parameter values, the more broad banded the spectrum, the more energy is comprised in the spectrum and the larger the wave run-up is. The more energy is given to the low frequency waves, the larger the values of  $\varepsilon$  and  $\nu$ .

Theoretically, it is impossible to change the spectral width parameter  $\varepsilon$  for an arbitrary spectrum whilst the significant wave height (determined by spectral analysis)  $H_{mo}$  and the mean wave period  $T_{01}$  are kept constant simultaneously. With this  $H_{m0} \cong 4 \sqrt{m_0}$ . Indeed, it is not possible to keep  $m_0$  and  $m_1$  simultaneously constant whilst the shape of the spectrum is varied. The spectral width parameter has been calculated for theoretical extreme wave spectra:  $\varepsilon = 0$  for an impulse function and  $\varepsilon = 0.67$  for white noise.

The magnitude of the wave height does not affect  $\varepsilon$  when a parameterised JONSWAP or a parameterised Pierson-Moskowitz (PM) spectrum is considered. The effect of  $\varepsilon$  on wave run-up is reduced to an effect of the wave period. For standard spectra it does not matter which period is considered (peak wave period  $T_p$  or the mean wave period  $T_{0l}$ ) as both wave periods are related. The spectral width parameter is more sensitive to changes of the wave period when small wave periods are considered. Changing the peak enhancement factor  $\gamma$  (in the JONSWAP spectrum) only has a very slight influence on the spectral width parameter:  $\varepsilon$  decreases for increasing values of  $\gamma$ . The influence of  $\gamma$  on  $\nu$  is larger than the influence of  $\gamma$  on  $\varepsilon$ . All this does not apply for natural spectra.

The definition of the spectral width parameter  $\varepsilon$  in time domain is (Van Torre (2001)):

$$\sqrt{1-\varepsilon^2} = \frac{N_0}{N_1} = \frac{T_c}{T_z} \tag{2.12}$$

with  $N_0$  = the number of zero crossings of the wave diagram,  $N_I$  = the number of crests and troughs in the wave diagram,  $T_c$  = the average

period between the wave crests and  $T_z$  = the average period between two zero upcrossings. This definition has neither been used further on.

Ward et al. (1997) made the remark on the influence of the peakedness parameter  $Q_p$  as defined by Goda (1985) on wave run-up. The peakedness parameter  $Q_p$  (Goda (1970)) is defined as

$$Q_p = \frac{2}{m_0^2} \int_0^2 f[S(f)]^2 df$$
 (2.13)

and describes the peakedness of the spectral peak. The peakedness parameter  $Q_p$  is rather insensitive to the cut off frequency in the spectral analysis and is less affected by wave non linearity than the spectral width parameter.  $Q_p$  equals unity for white noise, around 2 for wind generated waves and higher values for swell.

Stam (1989) and van der Meer and Stam (1992) use another parameter to characterise the spectral shape: the parameter  $\kappa$ , defined by

$$\kappa = \sqrt{\frac{\left[\int_{0}^{\infty} S(f)\cos(2\pi f\tau)df\right]^{2} + \left[\int_{0}^{\infty} S(f)\sin(2\pi f\tau)df\right]^{2}}{m_{0}^{2}}}$$
(2.14)

with

$$\tau = T_{02} = \sqrt{\frac{m_0}{m_2}} \tag{2.15}$$

However, this parameter has not been used further on.

On the one hand, Van Oorschot and d'Angremond (1968), Battjes (1974), Grüne (1982), the TACPI report (cfr. paper of Allsop et al. (1985)), Stam (1989) and Pilarckzyk et al. (1996) all mention the influence of the spectral shape. On the other hand, a number of researchers claimed the opposite and found no significant influence of the spectral shape on wave run-up. van der Meer and Stam (1992) found that data of broad banded spectra are lower than data of PM

spectra and narrow banded spectra. However, van der Meer and Stam (1992) tested a breakwater with an impermeable core and a slope 1:3 with PM spectra, broad and narrow banded spectra and concluded that the spectral width has no real influence on wave run-up. van der Meer and Stam (1992) also admit that too little investigation was done to draw firm conclusions on the spectral width parameter. No effects on wave run-up have been observed from the changes in spectral width by Ward et al. (1997) too.

# 2.2.3.3 Wave obliqueness

In general, wave run-up induced by oblique waves is not the same as wave run-up induced by head-on waves. Wave obliqueness is taken into account in wave run-up formulae by means of the reduction factor  $\gamma_{\beta}$ . Several expressions of this reduction factor have been suggested. Pilarczyk et al. (1996) mentions

$$\gamma_{\beta} = \cos(\beta - 10^{\circ})$$
 for  $\beta \le 65^{\circ}$  (2.16)

In any case,  $Ru_{x\%}$  is always larger than  $H_s$  for  $\beta > 65^{\circ}$ .

Losada and Giménez-Curto (1982) conclude that wave run-up and wave run-down on rough slopes under oblique wave incidence are lower than under perpendicular wave incidence and used therefore a modified Iribarren number  $\xi_{\theta} = \xi . \cos \theta$  in stead of  $\xi$ .

Tautenhaim et al. (1982) suggested

$$\gamma_{\beta} = \cos \beta (2 - \cos^3 2\beta)^{\frac{1}{3}}$$
 (2.17)

This equation has a local maximum for  $\beta=22^\circ~(\gamma_\beta\cong1.09)$ . Tautenhain et al. (1996) reported an increase of wave run-up heights for wave directions in the range of approximately  $0<\beta<35^\circ$  in comparison with perpendicular wave attack. Pilarczyk et al. (1996) concludes that wave run-up does not change much for incident wave angles between  $0^\circ$  and  $40^\circ$ , with even a slight increase for angels about  $15^\circ$  to  $20^\circ$ . Losada and Giménez-Curto (1981) and Hosoi and Shuto (1964) conclude that wave run-up and wave run-down on rough slopes under oblique wave incidence are lower than under perpendicular wave incidence.

## 2.2.3.4 Water depth

The water depth is often referred to by means of the relative water depth d/H. Waves either break by a too large wave steepness or when the water becomes too shallow. Miche (1944) (cfr. De Rouck (1998)) formulated the breaking criterion as

$$s_b = a \tanh \frac{2\pi d}{L} \tag{2.18}$$

with a = 0.14, valid for regular waves (the subscript 'b' indicates the breaking condition). Equation (2.18) has been fitted to measurement data of irregular seas by Vrijling et al. (1980) and Smith (1999):  $H_s = 0.093 L \tanh(kd)$ , resp.  $H_{m0} = 0.10 L \tanh(kd)$ . In shallow water these equations become  $H_s = 0.584 d$ , resp.  $H_s = 0.628 d$ .

According to the rule of thumb, found in Hardy et al. (1990), waves break when

$$H_s/d > 0.40 \text{ (to 0.50)}$$
 (2.19)

(2.19) is valid for waves broken on a broad sandy foreshore (cfr. Flemish and Dutch foreshores).

Thornton and Guza (1982) concluded that random waves are induced to break in shallow water when

$$H_{rms} \cong 0.42d \tag{2.20}$$

Assuming that wave height are Rayleigh distributed, is:

$$H_{m0} = \sqrt{2}H_{ms} \tag{2.21}$$

The above limit thus corresponds to

$$H_{m0} = 0.42\sqrt{2}d \cong 0.6d \tag{2.22}$$

or  $H_{m0}/d = 0.6$ , which is close to equation (2.18) with the values of a found by Vrijling et al. (1980) and Smith (1999).

In case waves do not break, d/H has a slight influence on Ru/H: relative wave run-up increases with decreasing d/H, provided that  $d/H < \sim 3$  (Schijf (1972)). When the ratio d/H > 3, tests by Saville (1956) revealed that wave run-up is independent on the water depth d in front of the structure. Stam (1989) came to the same conclusion for irregular waves, characterised by the significant wave height  $H_s$ . Hunt (1957) states that if the water depth has an influence on wave run-up it should be very little, and only through the affection of the wave characteristics. Wave run-up distributions are strongly dependent on the wave distributions (Stam (1989)). When the ratio water depth to wave height d/H is smaller than 2 to 3, waves will no longer be Rayleigh distributed (due to shoaling and refraction) and this will have its repercussion on wave run-up which also will no longer be distributed according to a distribution valid for deep water conditions.

### **2.2.3.5 Block size**

The 50% passing nominal diameter of a stone  $D_{n50}$  (i.e. the length of the side of the cube with the same volume of the stone) is defined as:

$$D_{n50} = \sqrt[3]{\frac{W_{50}}{\rho_s}} \tag{2.23}$$

in which •  $W_{50}$  is the block mass for which 50% of the total sample mass is of lighter blocks (i.e. the median mass) [kg]

•  $\rho_s = \text{rock density [kg/m}^3]$ 

Losada and Gimenez-Curto (1981) conclude that when the incident wave height is considerably larger than the nominal diameter of the rock, the magnitudes of the physical phenomena which take place on the slope of the structure are independent on the size of the blocks. Also Stam (1989) did not find any influence of the block size on wave run-up.

When the nominal diameter of the rocks becomes very small in comparison to the wave height, rip rap is not longer the object of testing, but sand is. The ratio  $D_{n50}/H_s$  gains influence (Stam (1989)). van der Meer and Stam (1992) emphasises the importance of the  $D_{n50}/H_s$  parameter as this ratio is a measure for the relative roughness of the slope.

Thompson and Shutter (1975) concluded that the diameter of the rock does not have any influence on wave run-up. For all tests  $d/H_s$  was larger than 5 and the investigated range of  $D_{n50}/H_s$  was 0.17 to 0.33. Stam (1989) investigated the grading  $D_{85}/D_{15}$  of the rock and found no influence.

#### 2.2.3.6 Composite slope

For wave run-up on a composite slope (e.g. a slope with a berm), different solutions have been investigated. All methods (Saville (1958) and referred to in the Shore Protection Manual (1984), Wang et al. (1995), Grüne et al. (1999), van der Meer and de Waal (1992),...) define a 'mean slope'. No further details are given as the geometry of the rubble mound breakwaters investigated in the framework of this dissertation did not include a berm.

#### 2.2.3.7 Scale effects

An estimation of scale effects is given in Stoa (1979) (cfr. Ahrens 1981)). The Shore Protection Manual (1984) presents a correction factor to take into account the inability to scale roughness effects in small scale laboratory tests. The U.S. CERC (1975) (cfr. Günbak (1979)) gives wave run-up correction curves for scale effects on smooth slopes. These predict a maximum underestimation of 20% by small scale model tests for steep slopes (cot  $\alpha \leq 2$ ). This underestimation decreases with decreasing slope angle  $\alpha$ .

The Reynolds number is defined as

$$Re = \frac{VD}{V} \tag{2.24}$$

with  $\bullet V =$  a characteristic velocity

- D = a characteristic length
- $v = \text{kinematic viscosity of the fluid } [\text{m}^2/\text{s}], \text{ given by}$

$$v = \frac{\mu}{\rho} \tag{2.25}$$

in which  $\mu$  is the dynamic viscosity [Pa.s] and  $\rho$  is the density [kg/m³]. The viscosity of the water is  $\nu=1.00.10^{-6}$  m²/s at  $20^{\circ}$ C and  $\nu=1.79.10^{-6}$  m²/s at  $0^{\circ}$ C.

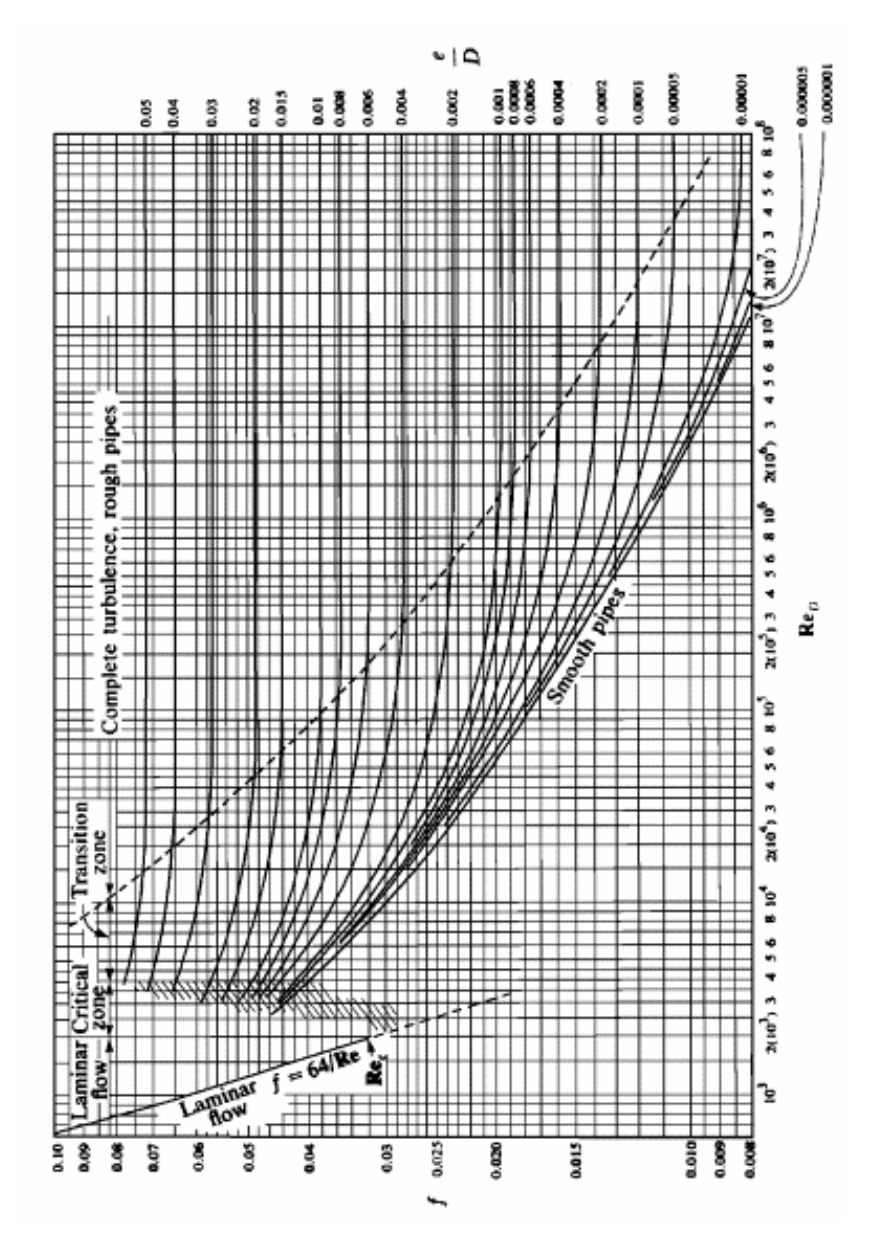


Figure 2.2: MOODY diagram.

The Reynolds number is a measure for the ratio of inertia forces to friction forces. V is taken equal to the velocity of the uprushing water

and D as the thickness of the uprushing water layer. As the Reynolds number will be smaller in small scale than at full scale, the friction factor will have a larger value in the model than at full scale. However, as the slope of a rubble mound breakwater is very rough (e/D) (with e the equivalent grain roughness) is quite large), the friction factor f will not be much smaller in small scale than at full scale. This is seen in the Moody diagram (figure 2.2 which is not only valid for flow in tubes but also for flow in open channels (Verhoeven (1996)). The very rough surface at full scale will probably lead to a hydraulic rough surface in small scale models as well, so little influence of scale effects is expected. Führböter (1986) concluded after having performed model tests on scale 1:10 with regular waves and having compared small scale results with large scale test results that with respect to wave run-up scale effects are negligible.

# 2.2.4 Wave run-up formulae

A large variety of empirical and/or experimentally determined formulae have been developed. Each formula has its (dis)advantages and range of applicability. Some authors started from theoretical considerations to derive a wave run-up formula. Others have fit a parametric equation to laboratory data.

Although this Ph.D. thesis deals primarily with wave run-up on conventional rubble mound breakwaters, i.e. permeable structures with a rough slope, wave run-up on smooth impermeable dikes cannot be overlooked. The link with smooth impermeable slopes is inevitable.

In most consulted literature, a clear distinction has been made between regular waves and irregular waves, breaking waves and non breaking waves, smooth and rough slopes, permeable and impermeable slopes. Firstly, wave run-up on smooth impermeable slopes is discussed. Next, wave run-up on rough slopes is treated. Distinction is made between permeable and impermeable slopes.

The most simple formulae to predict wave run-up is the Wassing (1957) formula (or the so-called 'Old Delft Formula')

$$Ru_{2\%} = 8H_s \tan \alpha \tag{2.26}$$

valid for a wave steepness s = 0.05 and slopes not steeper than  $16^{\circ}$  (tan  $\alpha \approx 1.3.5$ ).

The mother formula, i.e. the Hunt (1959) formula, reads as

$$Ru = \sqrt{HL} \tan \alpha \tag{2.27}$$

or, as found in Battjes (1974),

$$\frac{Ru}{H} = \xi \tag{2.28}$$

Equation (2.28) is only valid for impermeable smooth slopes attacked by monochromatic waves. The application range of the Hunt formula is limited to  $\xi \le 2.3$  (plunging waves). For surging waves, wave runup is limited by Ru/H = 3. The formula predicts wave run-up well for natural beaches, but is inaccurate for seawalls and breakwaters. Formula (2.28) is clearly dependent on the Iribarren number.

The Hunt-formula (2.28) is often found in literature as

$$\frac{Ru}{H} = a\xi \tag{2.29}$$

or in a more general form (cfr. CIRIA/CUR (1991) and CIRIA/CUR (1995)) as

$$\frac{Ru_{2\%}}{H_s} = a\xi_{op} + c \tag{2.30}$$

with the value of a given in table 2.1 for different investigations. All values are discussed further on. In case of plunging waves, the parameter c in (2.30) equals 0.

Table 2.1: Coefficient *a* in equation (2.29) (for regular waves) or (2.30) (for irregular waves) according to various investigations (only plunging waves have been considered).

(only plunging waves have been considered).			
reference	а		
Hunt (1959) (1)	1.00		
Losada and Giménez-Curto (1981) (2)	1.00		
Tautenhain (1982) (3)	$1.29(1 - \chi_r)$		
Hunt (1959) (4)	1.84		
Ahrens and Titus (1985) (5)	0.967		
SPM (1984) <sup>(6)</sup>	0.82 to 1.02		
Pilarczyk (1990)	$\sqrt{2\pi} C_x = 2.5C_x$		
Pilarczyk (1996) (7)	$\sqrt{2\pi} C_x - 2.3C_x$		
CUR/CIRIA (1995) (8)	1.6		
van Oorschot and d'Angremond (1968) <sup>(9)</sup>	$C_{2\%}(arepsilon)\!\sqrt{2\pi}$		
van der Meer (1993) (10)	$1.5 \gamma_b \gamma_f \gamma_\beta (1.6 \gamma_b \gamma_f \gamma_\beta)$		
TAW (1974) (cfr. van der Meer (1998)) (11)	1.61		
van der Meer and Stam (1992) (12)	1.49 to 1.87		
Ahrens (1981) (13)	1.61		
Grüne (1982) (14)	1.33 to 2.88		
Alloop (1004) <sup>(15)</sup>	1.89 (smooth slopes)		
Allsop (1994) <sup>(15)</sup>	1.01 (armoured slopes)		

<sup>(1):</sup> valid for regular waves on impermeable smooth slopes

$$\frac{Ru}{H} = \xi \qquad \text{for } \xi \le 2.5$$

$$\frac{Ru}{H} = 2.5 - \frac{\xi - 2.5}{3} \qquad \text{for } 2.5 < \xi \le 4.0$$
 (2.32)

$$\frac{Ru}{H} = 2 \qquad \text{for } \xi > 4.0 \tag{2.33}$$

<sup>&</sup>lt;sup>(2)</sup>: for wave run-up on smooth impermeable slopes attacked by regular waves, Losada & Giménez-Curto (1981) found:

These formulae are based on data from tests carried out in the seventies and are valid for regular wave attack on a smooth impermeable slope.

<sup>(3)</sup>: Tautenhain (1982) proposes an expression including the reflection coefficient  $\chi_r$  to describe wave run-up on uniform smooth slopes for normal wave approach (regular waves):

$$\frac{Ru}{\sin\alpha} = 1.29\sqrt{HL_0} \left(\frac{1-\chi_r}{\cos\alpha}\right) \tag{2.34}$$

so that

$$Ru = 1.29\sqrt{HL_0} \left(1 - \chi_r\right) \tan \alpha \tag{2.35}$$

or

$$\frac{Ru}{H} = 1.29(1 - \chi_r) \frac{\tan \alpha}{\sqrt{\frac{H}{L_0}}} = 1.29(1 - \chi_r) \xi_0$$
 (2.36)

<sup>(4)</sup>: valid for regular waves and  $\xi < \sim 1.25$ 

(5): Ahrens and Titus (1985) found

$$\frac{Ru}{H_0'} = 0.967\xi$$
 for  $\xi \le 2$  (2.37)

$$\frac{Ru}{H_0'} = \left(\frac{3.5 - \xi}{1.5}\right) 0.967 \xi + \left(\frac{\xi - 2.0}{1.5}\right) c_0 \left(\frac{\pi}{2\alpha}\right)^{c_1} exp \left[c_2 \left(\frac{R_c}{H} - 0.5\right)^2\right]$$
for  $2 < \xi < 3.5$  (2.38)

$$\frac{Ru}{H_0'} = c_0 \left(\frac{\pi}{2\alpha}\right)^{c_1} exp \left[c_2 \left(\frac{R_c}{H} - 0.5\right)^2\right] \text{ for } \xi > 3.5 \qquad (2.39)$$

in which  $\bullet Ru =$  wave run-up height

- $H_0$ ' = deep water wave height
- H = wave height at the toe of the structure
- $R_c$  = crest freeboard
- $c_0 = 1.093$ ,  $c_1 = 0.449$ ,  $c_2 = 6.354$
- $\alpha$  = slope angle

for monochromatic waves on a plane smooth slope.

<sup>(6)</sup> In the Shore Protection Manual (1984) graphs are given for the estimation of wave run-up  $R/H_o$  (with  $H_o$  = unrefracted deep water wave height) on smooth impermeable vertical, stepped and curved seawalls. These graphs are all based small scale laboratory tests with regular waves carried out by Saville (1956). Figure 2.3 shows two examples of these graphs, valid for smooth impermeable slopes with d/H < 3 (figure 2.3(a)) and  $d/H \ge 3$  (figure 2.3(b)). For a constant slope, steeper waves have a lower relative wave run-up (on the vertical axis).

From these graphs it is seen that for steep slopes, wave run-up becomes almost independent on the wave steepness. As already mentioned in paragraph 2.2.3.4, the water depth has an influence on wave run-up when d/H < 3 through the affection of wave characteristics. This is seen by comparing figure 2.3(a) with figure 2.3(b) and especially for steep slopes.

For plunging waves, the value of a in (2.27) is found by calculating the Iribarren numbers for cot  $\alpha = 10$  and cot  $\alpha = 30$  for all displayed curves. The value of a varies between 0.79 (for the steepest waves) and 1.05 (for small values of s).

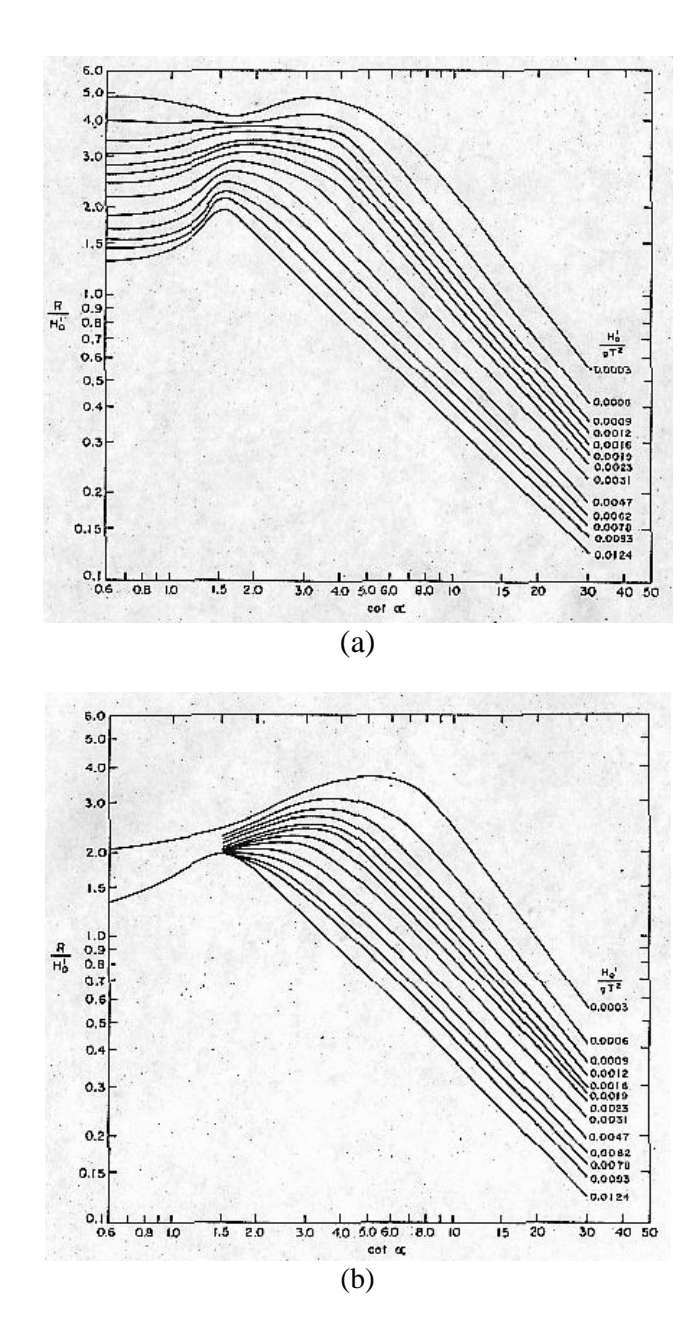


Figure 2.3: Relative wave run-up  $R/H_{o}$  according to the Shore Protection Manual (1984) for (a) d/H < 3 and (b) d/H > 3.

- valid for  $\xi_p < 2$  and  $\tan \alpha < 1/3$ . The TACPI report (cfr. paper of Allsop et al. (1985)), Pilarczyk (1990) and Pilarckzyk et al. (1996) suggest the use of a correction factor  $C_{x\%}$  for the influence of spectral shape.  $C_{x\%}$  is a constant depending on the type of the wave spectum and the considered exceedance probability x:  $C_{2\%} = 0.55$  to 0.60 for narrow banded spectra and  $C_{2\%} = 0.70$  to 0.80 for a broad banded spectrum so that dimensionless wave run-up values  $Ru_{2\%}/H_s$  vary between 1.38 and 1.50 for narrow banded spectra and between 1.75 and 2.00 for broad banded wave spectra. The equation applies for random (irregular) waves and smooth plane slopes (slopes flatter than 1:3). Using  $C_{2\%} = 0.70$  and a wave steepness of 0.05, equation (2.26) is obtained. More general,  $C_{2\%} = 0.70$  (fully developed wind induced sea state) implies (2.30) to become  $Ru_{2\%}/H_s = 1.75 \xi_p$  (valid for  $\xi_p < 2$  to 2.5). For  $\xi_p > 2.5$ ,  $Ru_{2\%}/H_s$  equals 3.5, or more commonly adopted 3.0.
- <sup>(8)</sup>: valid for  $\xi_p < 2$  for plane smooth slopes.  $Ru_{2\%}/H_s$  is limited to 3.2. The equation is valid for smooth, non-bermed slope profiles attacked by Rayleigh distributed head on waves. CUR/CIRIA (1995) fitted (2.30) to the data of Ahrens (1981), van Oorschot and d'Angremond (1968) and Allsop et al. (1985). Ahrens (1981) tested slopes of 1:1 to 1:4. van Oorschot and d'Angremond (1968) tested slopes 1:4 and 1:6 and Allsop et al. (1985) tested slopes between 1:4/3 and 1:2. It must been said that data of Ahrens (1981) are not very reliable because of the limited length of the time series (CUR/CIRIA (1995), Burcharth (1998)). Only 200 to 300 waves have been measured. A lot of spreading was seen on the  $Ru_{x\%}$  values. The results of Allsop et al. (1985) were lower than the results of Ahrens (1981). A different definition of wave run-up and different test methods are believed to be responsible for these differences. The data of van Oorschot and d'Angremond (1968) accounts for tests with narrow banded wave spectra and structures with a slope tan  $\alpha$  < 1/3. For the data of Ahrens (1981), a = 1.6 and c = 0 for  $\xi_p < 2.5$ . For  $\xi_p > 2.5$  is a = -0.2 and c = 4.5. Fitting (2.30) to the data of van Oorschot and d'Angremond (1968) yields a = 1.75 and c = 0. For the data of Allsop et al. (1985), CUR/CIRIA (1995) obtained a = -0.21 and c = 3.39 for  $2.8 < \xi_p < 6$ . CUR/CIRIA (1995) not only gives recommendations for a and c in (2.30), thus for  $Ru_2 /\!\!/ H_s$ , but also for  $Ru_s /\!\!/ H_s$ . In latter case is a = 1.35 for  $\xi_p < 2$  and is a = -0.25 and c = 3 for  $\xi_p > 2$  in case Ahrens' (1981) data are used. Allsop et al.'s (1985) data

yields a = -0.09 and c = 2.11 for  $2.8 < \xi_p < 6$ . In general, a varies between 1.3 and 2 for  $\xi_p < 2$  and between -0.25 and -0.1 for  $\xi_p > 2$ .

- (9):  $C_{x\%}(\varepsilon)$  is a factor depending on the spectral width parameter  $\varepsilon$  (see paragraph 2.2.3.2).  $C_{x\%}(\varepsilon)$  increases with increasing  $\varepsilon$  value. Schijf (1974) summarises the values of the coefficient  $C_{2\%}(\varepsilon)$ :  $C_{2\%}(\varepsilon)$  ranges from 0.55 to 0.73 for 0.34  $\leq \varepsilon \leq$  0.59. All this is valid for impermeable slopes (cot  $\alpha = 4$  to 6).
- <sup>(10)</sup>: valid in the range  $0.5 < \gamma_b \xi_{op} < 4$  to 5. The general design formula (for probabilistic design) for wave run-up on dikes (plane smooth slopes with perpendicular wave attack) is given by van der Meer (1998):

$$\frac{Ru_{2\%}}{H_s} = 1.5\gamma_b \gamma_f \gamma_\beta \xi_{op} \tag{2.40a}$$

$$\frac{Ru_{2\%}}{H_s} \le 3\gamma_f \gamma_\beta \tag{2.40b}$$

with a variation coefficient c = 0.085 on the factor 1.5 in (2.40a) and with  $\gamma_b$ ,  $\gamma_f$  and  $\gamma_{\beta}$  = reduction factors for a berm, resp. slope roughness and oblique wave attack. These equations are based on both small scale and large scale model tests. For deterministic design (i.e. a more conservative approach) the values 1.5 and 3 in (2.40a) and (2.40b) have to be replaced by 1.6 and 3.2.

- <sup>(11)</sup>: valid for smooth straight slopes with tan  $\alpha$  < 1/2.5.
- (12):  $Ru_{2\%}/H_s = 1.49$  is valid for fully developed seas and  $Ru_{2\%}/H_s = 1.87$  applies for very young seas.
- (13): applies for plunging waves (  $\frac{H_s}{gT_p^2}$  > 0.003 or  $\xi_{op}$  < 1.82). This

value is based on wave run-up tests on a plane, smooth slope of 1:4 with  $d_s/H_s \ge 3$ .

(14): Remarkable are the results of the full scale measurement campaigns of Grüne (1982). Grüne (1982) carried out full scale

wave run-up measurements at two locations along the coast of the German Bight: (1) at WANGEROOGE, i.e. a dike with a sand core and a cover layer from asphalt concrete on a 1:4 slope and (2) at the EIDER river storm surge barrier, i.e. a dike with a sand core and concrete joined stone revetment. Full scale wave run-up measurements indicate higher values of a than the laboratory investigations and the commonly used formulae do. Wave run-up in small scale models did not correspond with wave run-up in large scale tests, mainly due to scale effects, but also did not correspond at all with field measurements. Grüne (1982), Wang et al. (1995), Grüne et al. (1999) claim that realistic wave spectra (natural spectra) give rise to higher wave run-up than standard wave spectra do. Latter is because standard spectra (JONSWAP, Pierson-Moskowitz, Brettschneider, Ochi,...) hardly occur along coastlines. Most standard spectra are the result of fully developed seas in deep water. Close to the coast waves undergo a transformation due to the foreshore topography. Double peaked spectra, flattened spectra,... have a complete other outcome than a smooth one peaked spectrum.

Allsop (1994) found for smooth slopes and armoured slopes the equations for  $Ru_s/H_s$  given in table 2.2.

Table 2.2: Formulae for smooth and armoured slopes for  $Ru_s/H_s$  (according to Allsop (1994)).

smoo	smooth slopes armoured slopes		oured slopes
$\xi_p < 2.0$	$\xi_p > 2.0$	$\xi_p < 1.5$	$\xi_p > 1.5$
$1.35\xi_p$	$3 - 0.25 \xi_p$	$0.72\xi_p$	$0.88\xi_p^{0.41} < 1.35$

Assuming wave run-up heights to follow a Rayleigh distribution, the values for  $Ru_s$  are transformed to  $Ru_{2\%}$  by

$$Ru_{2\%} = Ru_s \sqrt{-\frac{1}{2} \ln(0.02)}$$
 (2.41)

i.e.  $Ru_{2\%} = 1.40 Ru_s$ , so that table 2.2 is transformed into table 2.3.

Table 2.3: Formulae for smooth and armoured slopes for  $Ru_{2\%}/H_s$  (according to Allsop (1994)).

smooth slopes		slopes armoured slopes	
$\xi_p < 2.0$	$\xi_p > 2.0$	$\xi_p < 1.5$	$\xi_p > 1.5$
$1.89\xi_{p}$	$4.20 - 0.35\xi_p$	$1.01\xi_p$	$1.23\xi_p^{0.41} < 1.89$

Chue (1980) proposed:

$$\frac{Ru}{H_0} = 1.8 \left( 1 - 3.111 \frac{H_0}{L_0} \right) \xi_0 \left[ 1 - \exp\left( -\frac{1}{\xi_0} \sqrt{\frac{\pi}{2\alpha}} \right) \right]$$
 (2.42)

in which

$$\xi_0 = \frac{\tan \alpha}{\left(\frac{H}{L}\right)^{0.4}} \tag{2.43}$$

Notice the exponent 0.4 in (2.43) in stead of the normal square root in the definition of the Iribarren number. Both Chue (1980) and Ahrens and Titus (1985) used data of Saville (1956) and Savage (1958).

For wave run-up on gentle (1:30 to 1:5) smooth slopes, Mase and Iwagaki (1984) found

$$\frac{R}{H_s} = a \left( \frac{\tan \alpha}{\sqrt{H_s/L_s}} \right)^b \tag{2.44}$$

with R the wave run-up value and the corresponding values of a and b given in table 2.4.  $L_s$  has been calculated from the significant wave.

Table 2.4: Values of parameters a and b in equation (2.44).

R	а	b
$Ru_{max}$ (based on 650 to 900 waves)	2.319	0.771
$Ru_s$	1.497	0.695
$Ru_{50\%}$	1.085	0.678

Ahrens (1981) investigated wave run-up induced by irregular waves on plane smooth structures in relatively deep water ( $3 \le d/H_s \le 12$ ). The deep water conditions guaranteed Rayleigh distributed waves (Shore Protection Manual (1977) and Ahrens (1977)). Test results indicated

$$\frac{Ru_{x\%}}{H_s} = C_1 + C_2 \frac{Hs}{gT_p^2} + C_3 \left(\frac{Hs}{gT_p^2}\right)^2$$
 (2.45)

 $C_1$ ,  $C_2$  and  $C_3$  are dimensionless regression coefficients depending on the slope tan  $\alpha$  and given in table 2.5. x is either 2, 13.5 (significant wave run-up) or 50 (mean wave run-up).

Table 2.5: Regression coefficients  $C_1$ ,  $C_2$  and  $C_3$  (Ahrens (1981)).

ton a -	Ru₂ <sub>%</sub> /H₅			
tan $\alpha$	$C_1$	$C_2$	<b>C</b> <sub>3</sub>	
1:1	2.32	7.15.10 <sup>1</sup>	0	
1:1.5	2.52	$1.95.10^2$	0	
1:2	3.21	7.19.10 <sup>1</sup>	0	
1:2.5	3.39	$1.29.10^2$	-1.61.10 <sup>4</sup>	
1:3	3.70	0	-1.70.10 <sup>4</sup>	
1:4	3.60	$-2.22.10^2$	0	

#### 2.2.5 Rough slopes

Some authors (Battjes (1974), Ahrens (1981), Shore Protection Manual (1984), Sorensen (1997), ...) suggest to apply a correction factor to take into account the roughness of the slope to calculate wave run-up on a rough slope starting from the equation for the estimation of wave run-up on a smooth sloping dike. The correction factor is the ratio between relative wave run-up on a rough slope and the relative wave run-up on a smooth slope. For most cases, the reduction factor is determined by laboratory investigation with monochromatic waves. It has been shown that the factors valid for irregular waves may also be applied for irregular waves (Battjes (1974)). Hunt (1959) and the Shore Protection Manual (1984) suggested the use of a combined porosity and roughness factor. An 'average' slope roughness factor may be calculated in case the slope consists of different parts with

different roughnesses. Schijf (1974) mentions that the influence of the roughness elements increases with the ratio of their dimensions to the wave height H. For rubble mounds, both the roughness and the permeability co-operate in a wave run-up reducing effect. A rubble slope has a water retaining effect. However, both effects cannot be isolated. Therefore is it advisable not to use a combined 'roughness' factor depending on the armour type as this 'roughness' factor also depends on the permeability of the slope.

However, research on wave run-up on permeable slopes indicated that the application of a single roughness factor does not correspond with reality for the whole range of structure slopes and wave steepnesses. van der Meer & Stam (1992), Losada and Giménez-Curto (1981) and Pilarczyk (1990) clearly demonstrated the difference between wave run-up on a smooth slope and wave run-up on a rough slope (figure 2.4, 2.5 and 2.6). Only for breaking waves, i.e.  $\xi \leq \sim 2.5$ , the application of a reduction factor might be correct as dimensionless wave run-up increases linearly with increasing Iribarren numbers. The difference between smooth and rough slopes is the most clear for  $2 < \xi_p < 5$ . The application of a roughness factor in this range has no physical meaning at all. Wave run-up on a smooth slope can be up to twice as high as wave run-up on a rough slope. For large Iribarren numbers ( $\xi > 5$ ), wave run-up becomes independent on the slope roughness.

Allsop et al. (1985) agrees as well: wave run-up on rough permeable slopes cannot be calculated on the basis of wave run-up on smooth impermeable slopes by application of a reduction coefficient depending on the type of armour unit (rock or artificial).

## 2.2.6 Permeable structures

It is not always clear in the consulted studies whether slopes are 'permeable' or 'impermeable' when it concerns a rough slope.

The behaviour of wave run-up on permeable slopes is completely different from wave run-up on impermeable slopes. The notional permeability factor P, introduced by van der Meer (1988) plays an important role. P may be estimated from figure 2.7 or can be calculated. A rough estimation of P is sufficient (Pilarckzyk and Zeidler (1996)).

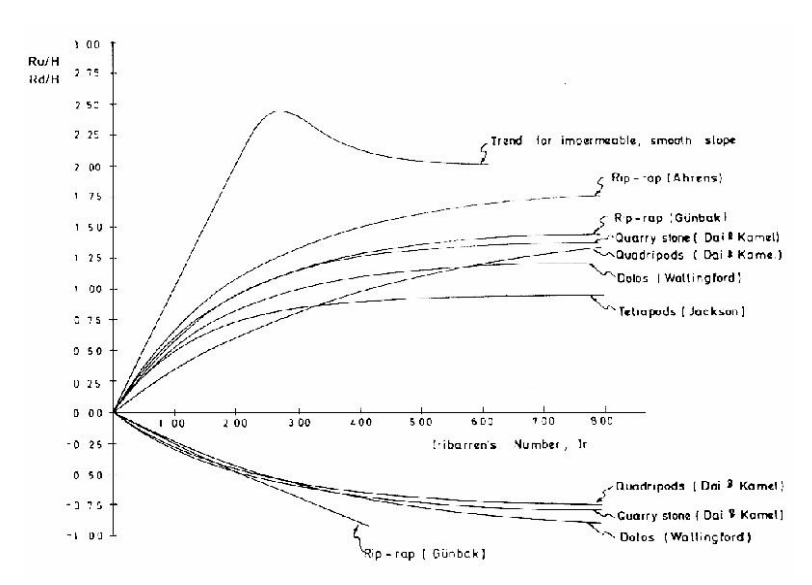


Figure 2.4: Difference between wave run-up on smooth slopes and wave run-up on rough slopes (Losada and Giménez-Curto (1981)).

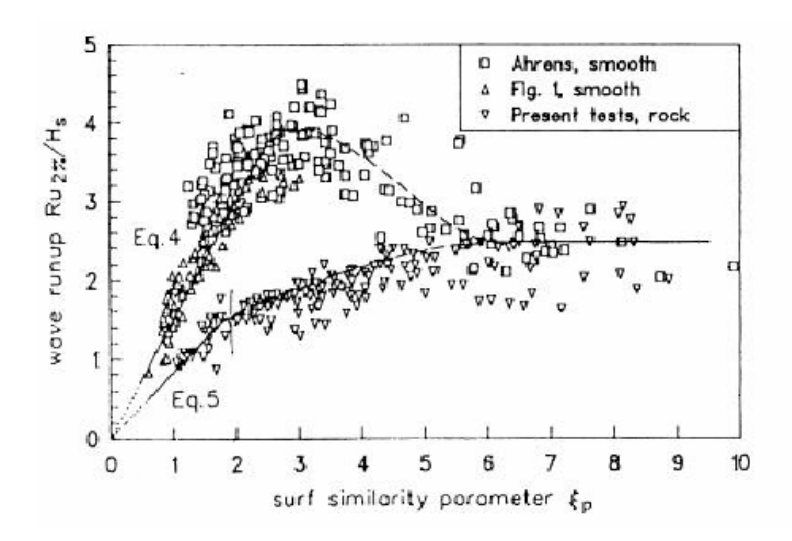


Figure 2.5: Difference between wave run-up on smooth slopes and wave run-up on rough slopes (van der Meer and Stam (1992)).

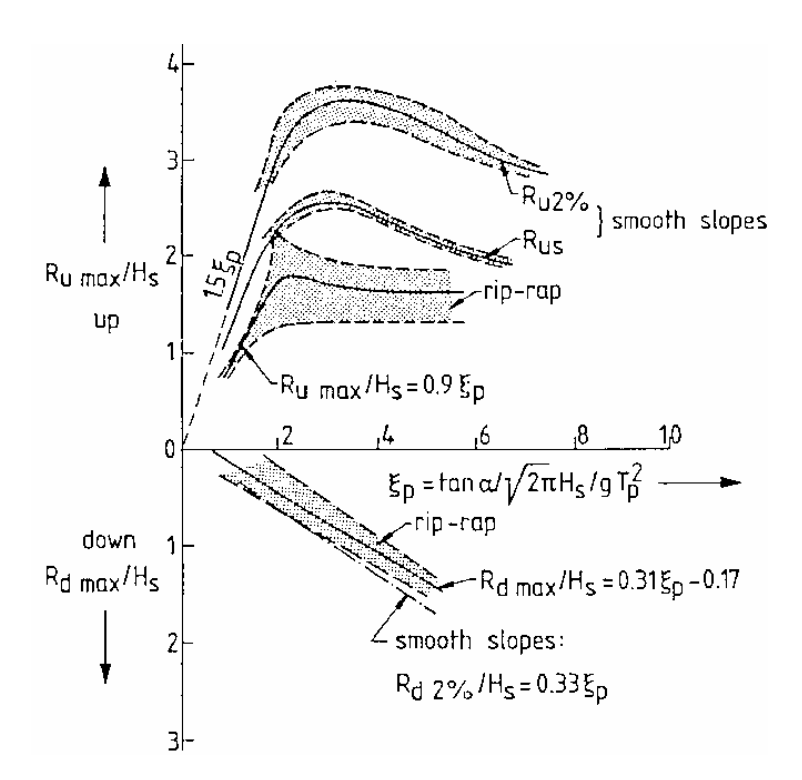


Figure 2.6: Difference between wave run-up on smooth slopes and wave run-up on rough slopes (Pilarczyk (1990)).

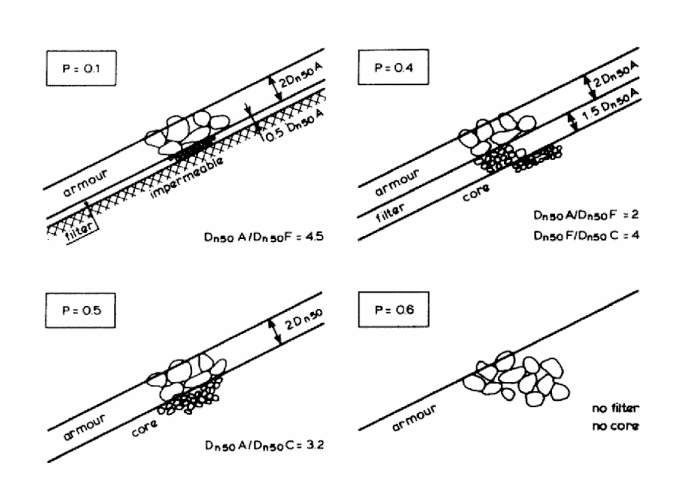


Figure 2.7: The notional permeability parameter P introduced by van der Meer (1988).

Wave run-up on permeable rubble slopes is presented in the Shore Protection Manual (1984), but information is very limited: only one graph in which  $Ru/H_0$  is plotted versus the deepwater wave steepness  $H_0/gT^2$  for different slope angles is provided. The graph shows that wave run-up on a rubble mound slope is smaller than on a smooth slope.

Losada and Giménez-Curto (1981) presented an exponential model for the analysis of flow characteristics (e.g. wave run-up, wave run-down, reflection, transmission) on rough, permeable slopes under regular wave action. The model only depends on the Iribarren number:

$$\frac{Ru}{H} = A(1 - \exp(B\xi)) \tag{2.46}$$

Losada and Giménez-Curto (1981) fit their equation (2.46) to test results obtained by various researchers for various armour types (rip rap, quarry stone, tetrapods, doloses and quadripods) by the least squares method. The results are displayed in figure 2.4. It is clear that wave run-up on rip rap slopes is higher than wave run-up on slopes covered with artificial armour units.

Silva et al. (1994) applied (2.46) for different permeabilities of a rubble mound breakwater and obtained different values of *A* and *B* for different armour layer types.

In the MAST II project, Murphy and Kingston (1996) applied the formula of Losada and Giménez-Curto (1981), originally intended only for regular waves, to results of small scale model tests with irregular waves and obtained the coefficients A=1.76 and B=-0.28. In the formulation (2.46), the significant wave height  $H_{m0}$ , the  $Ru_{2\%}$  value and the mean wave period  $T_{02}$  (see definition (2.5)) have been used instead of the regular wave characteristics H and T and the wave run-up height Ru (cfr. figure 1.1).

Small scale model tests carried out by Allsop et al. (1985) with Antifer cubes, stabits, tetrapods and diodes as tested armour units. These have been placed on an underlayer of quarry rock placed on a perforated and suspended steel sheet which could be moved into different slopes (1:1.33, 1:1.5 and 1:2). Tests with a smooth slope have been performed as well. Wave run-up measurements were based

on two different measuring principles. The first measuring technique was analysis of video recordings of wave run-up on the slope. The second technique was similar to the traditional wire gauge stretched along the slope surface. The measured wave run-up on the tetrapod armoured slopes is (based on the equation of Losada and Giménez-Curto (1981)):

$$\frac{Ru_{2\%}}{H_{c}} = 1.94 \left(1 - \exp(-0.3\xi_{op})\right)$$
 (2.47)

and for the antifer cube armoured slope:

$$\frac{Ru_{2\%}}{H_s} = 1.68 \left(1 - \exp(-0.35\xi_{op})\right)$$
 (2.48)

Günbak's formula (Günbak (1979)) is a Hunt-type formula:

$$\frac{Ru}{H} = 0.4\xi$$
 for  $\xi < 3.0$  (2.49a)

$$\frac{Ru}{H} = 1.2$$
 for  $\xi \ge 3.0$  (2.49b)

and is valid for permeable rubble mound breakwaters and regular waves. By transferring regular wave run-up results to irregular seas by means of the hypothesis of equivalence (see paragraph 2.2.2), the wave run-up corresponding to each single wave of the irregular wave train was calculated using (2.49a) and (2.49b) and the assumption tan  $\alpha = 1/1.5$ . Günbak (1979) also used a theoretical joint distribution (as presented by Longuet Higgins) by which

$$\frac{Ru}{H} = \frac{a\xi}{1 + b\xi} \tag{2.50}$$

with a=0.8 and b=0.5 has been used to calculated the predicted wave run-up. These formulae have been obtained by wave run-up measurements made by a wire gauge stretched along the slope of the breakwater.

Equation (2.50 also been adopted by Seelig (1980) (cfr. Pilarczyk and Zeidler (1996)) to estimate wave run-up on a rough slope: a = 0.692 and b = 0.504. The Iribarren number has been calculated using  $H_s$  and the deep water wave length. It is not clear which Ru value has to be used.

The most important formula which describes wave run-up on a permeable rubble mound breakwater attacked by irregular waves is the formula of van der Meer and Stam (1992):

$$\frac{Ru_{x\%}}{H_s} = a\xi_{om} \qquad \text{for } \xi_{om} \le 1.5$$
 (2.51a)

$$\frac{Ru_{x\%}}{H_s} = b\xi_{om}^c \qquad \text{for } \xi_{om} > 1.5 \qquad (2.51b)$$

In case of a permeable slope, the equations (2.51a) and (2.51b) are supplemented with

$$\frac{Ru_x}{H_s} = d ag{2.51c}$$

The addition of the last equation indicates that the permeability of the breakwater is only accounted for in case of high Iribarren numbers. The equations are valid for relatively deep water in front of the structure and for a Rayleigh distributed wave height distribution. The values of a, b, c and d are dependent on the exceedance probability x and are given in table 2.6.

The latest version of the Shore Protection Manual, the 'Coastal Engineering Manual' (http://bigfoot.wes.army.mil/cem026.html (2002)), as well as the 'Manual on the use of rock in hydraulic engineering' (CUR/CIRIA (1995)) and Pilarckzyk et al. (1996) recommend the use of the formula of van der Meer and Stam (1992).

Table 2.6: Coefficients a, b, c and d in equations (2.51a), (2.51b) and (2.51c).

exceedance probability x [%]	а	b	С	d
$\max (x = 0.13)$	1.12	1.34	0.55	2.58
1	1.01	1.24	0.48	2.15
2	0.96	1.17	0.46	1.97
5	0.86	1.05	0.44	1.68
10	0.77	0.94	0.42	1.45
significant ( $x \approx 13.5$ )	0.72	0.88	0.41	1.35
mean $(x = 50)$	0.47	0.60	0.34	0.82

For rough permeable slopes, Stam (1989) gives following formula:

$$\frac{\overline{Ru_{\text{max}}}}{H_s} = 1.0\xi_m \tag{2.52}$$

for  $\xi_m \le 1.5$ .  $\overline{Ru_{\max}}$  is the average maximum wave run-up. The spreading of the test results on which (2.52) is based was less for gentle slopes (cot  $\alpha = 4$  and 6) than for steeper slopes (cot  $\alpha = 2$  and 3). In general,  $Ru_{max}$  is subjected to a lot of spreading. Therefore it is more appropriate to use  $Ru_{2\%}$  or  $Ru_s$ .

Ahrens and Heimbaugh (1988) recommend the upper limit of wave run-up  $Ru_{max}$  on rip rap revetments under irregular wave attack to be calculated as:

$$\frac{Ru_{\text{max}}}{H_{m0}} = \frac{a\xi}{1 + b\xi} \tag{2.53}$$

in which • the pair of coefficients a=1.022 and b=0.247 when the deep water wave length  $L_0$  is used to calculate  $\xi$  and a=1.154 and b=0.202 when  $\xi$  is calculated using the local peak wave length  $L_p$  (latter is the 'alternative' method to predict the upper limit of wave uprush)

- $H_{m0}$  = zero moment wave height at the toe of the structure
- $Ru_{max}$  = the maximal wave run-up

In Schijf (1974) and Stam (1989), the recommendation is given to investigate wave run-up on steeper slopes than the thus far investigated slopes which all had a slope less than 1:1.5.

## 2.2.7 Other investigations

Wave run-up can also be related to time instead of being related to the number of wave run-up events. With the introduction of the 'residence time', wave run-up is treated as a time dependent variable (Schüttrumpf et al. (1994)). The level which is submerged during x % of the total time (instead of the level which is exceeded by x % of the wave run-up events) of the test is taken as the  $Ru_{x\%}$  value. The equation describing the time dependent wave run-up yield lower relative wave run-up heights and lower relative run-down heights than the standard formulae (e.g. van der Meer and Janssen (1994)) predict.

By using the Fourier transformation technique, wave run-up can also be described by its spectrum (Mase (1988)). Comparing the incident wave energy spectrum and the wave run-up spectrum, it is concluded that the energy density for high frequent wave run-up is independent on the incident wave energy (saturated energy) and the energy density for low frequent wave run-up increases with increasing incident wave energy.

# 2.3 Wave run-up distribution

Some authors state that wave run-up is Weibull distributed (Verdonck et al. (1999), van der Meer and Stam (1992),...). The Weibull cumulative distribution function has two or three parameters:

$$F(x) = 1 - \exp\left(-\left(\frac{x - c}{b}\right)^{a}\right)$$
 (2.54)

with  $x \ge 0$ , a > 0, b > 0. The parameter a is the shape parameter and b is the scale parameter. When c = 0, the three parameter Weibull distribution becomes the two parameter Weibull distribution. The Rayleigh distribution is a special case of the Weibull distribution:

$$F(x) = 1 - \exp\left(-\frac{x^2}{2a^2}\right)$$
 (2.55)

with  $x \ge 0$ . The Rayleigh distribution has only one parameter. Other suggestions are the Gamma distribution (Stam (1989)) or a normal distribution (cfr. Carlson (1984)).

The statement that wave run-up is Rayleigh distributed when waves are Rayleigh distributed is based on the hypothesis of equivalence which holds that every single component in an irregular wave train is treated as a regular wave which gives rise to a wave run-up event. Provided that (1) wave heights and wave periods are strongly correlated in deep water, (2) wave heights are Rayleigh distributed and (3) wave heights are not depth limited, wave run-up heights are also Rayleigh distributed.

### 2.4 Wave run-down

Wave run-down is important in the design of the revetment of a structure slope. Most damage to revetments occurs at and under the *SWL*. It is important to know how far the wave withdraws on the slope in order to design the slope revetment in this zone adequately. The downrushing velocities are larger than the uprushing velocities as in former case, gravity forces co-operate. Unfortunately, wave run-down is ill defined experimentally (Battjes and Roos (1974)) and has been examined less extensive than wave run-up.

Ahrens (1981) found for smooth plane slopes:

$$\frac{Rd_{2\%}}{H_s} = -2.32 \exp\left(-\frac{2.46}{\xi_{op}}\right)$$
 (2.56)

Another formula to calculate wave run-down is:

$$\frac{Rd_{2\%}}{H_s} = 0.33\xi_{op}$$
 for  $\xi_{op} \le 4$  (2.57a)

$$\frac{Rd_{2\%}}{H_s} = 1.5$$
 for  $\xi_{op} > 4$  (2.57b)

valid for smooth plane slopes and irregular wave attack (CIRIA/CUR (1991)). Both the formula of Ahrens (1981) and the formula of

CIRIA/CUR (1991) are plotted in figure 2.8. Both formulae have almost the same solution.

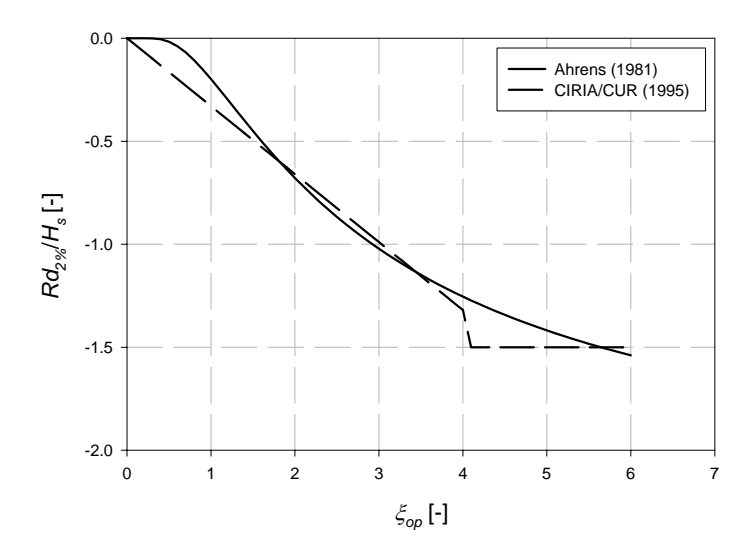


Figure 2.8: Comparison of wave run-down formulae for  $Rd_{2\%}/H_s$ .

CIRIA/CUR (1991) and Pilarckzyk et al. (1996) report a double effect of the structure slope on wave run-down. Next to the presence of the slope (tan  $\alpha$ ) in the equation for the Iribarren number, tests have demonstrated that wave run-down is less on steeper slopes. Therefore, wave run-down on rock slopes is expressed as:

$$\frac{Rd_{2\%}}{H_s} = 2.1\sqrt{\tan\alpha} + 1.5\exp(-60s_m) - 1.3P^{0.15}$$
 (2.58)

in which  $s_m = H_s / (gT_m^2)$ . The factor 1.3 in (2.58) is 1.2 in van der Meer (1993).

Kingston and Murphy (1996) investigated wave run-down on a rubble mound breakwater armoured with grooved cubes. Wave run-down was measured with a wire gauge stretched just above the slope of the breakwater. Following equation has been derived from a least squares fit of the experimental data:

$$\frac{Rd_{2\%}}{H} = -1.05(1 - \exp(-0.43\xi)) \tag{2.59}$$

The CUR/CIRIA (1995) manual also suggests the use of the equation by Thompson and Shuttler (1977):

$$\frac{Rd_{1\%}}{H_s} = 0.34\xi_p - 0.17\tag{2.60}$$

for maximal (~ 1%) wave run-down estimation on an impermeable slope protected by riprap (of wide graded rock).

The lower limit of slope protection ( $Rd_{max}$ ) against wave attack is given by Pilarczyk (1996):

$$\frac{Rd}{H_s} = 0.8\xi_{op} + 0.5$$
 for  $\xi_{op} < 2.5$  (2.61a)

$$\frac{Rd}{H_s} = 2.5$$
 for  $\xi_{op} \ge 2.5$  (2.61b)

Battjes and Roos (1974) found

$$\frac{Rd}{Ru} \cong 1 - 0.4\xi \tag{2.62}$$

for  $0.02 < H/L_0 < 0.09$  and  $0.3 < \xi < 1.9$  for smooth slopes. Pilarckzyk et al. (1996) also states that much less difference in wave run-down is observed between rock slopes and smooth slopes than the difference in wave run-up on both types of slopes.

#### 2.5 Wave run-up measuring techniques

The difficulties encountered when wave run-up has to be measured are

(i) the foamy nature of wave run-up which makes it rather difficult or impossible for a measuring probe to make distinction between (entrained) air and water. Especially broken waves and waves which break against the sloping structure show a lot of mixture of water and air.

- (ii) the thin water layer of the water tongue rushing up the slope of the structure. A wave run-up measuring device should be installed as close as possible to the structure slope. If not, a thin water layer may pass the gauge without being detected.
- (iii) position of measuring gauges. Geometrical limitations may force to resort to another type of wave run-up measuring device. 'Big' devices are not easy to apply in 'small' scale models. In the field, one has to keep in mind the harsh and aggressive sea environment which force to use solid and strong instrumentation.

Different types of wave run-up measuring devices exist:

### • conductivity/resistance probe

The measuring principle of this probe is based on the difference in conductivity between water and air. The depth of immersion of the gauge is – mostly linear – proportional to the voltage recorded by the data acquisition system. This measuring system is easy to use and is very cheap. Disadvantages are the necessary proper and frequent calibration as salinity, temperature,... might influence the characteristics of the gauges. van der Meer and Stam (1992) and Ward et al. (1997) used a traditional wire gauge to measure wave run-up.

## • capacitance probe

The gauge is an insulated conductor. The insulated conductor and the tank containing the water in which the probe is installed are the two plates of a capacitor. Any change in water level changes the dielectric effect between the plates. Any change in water level, changes the measured output voltage.

# • digital wave run-up probe

Different versions have been developed during the last two decades. Grüne (1982) used a step gauge with non equidistant electrodes for field measurements of wave run-up on smooth slopes along the German coastline. Also at Delft Hydraulics a step gauge has been used to measure wave run-up. Both instruments consist of a frame with a number of conductivity probes on it. A digital wave run-up probe does not require any calibration but the knowledge of the elevation of each single electrode. Attention must be paid to the

installation of the gauge on the slope. The frame holding the probes or electrodes must be sunk down in the revetment of the structure in order to have the probes or electrodes in the theoretical upper surface of the armour layer. This is an easy task to perform when an impermeable smooth slope has to be instrumented. There is no need to say this is a very hard task to do when a rubble mound breakwater is subjected to wave run-up measurements.

#### • visual observation

This is not an objective measuring method, but can help to verify measured data.

## • video recordings

Wave run-up events are recorded with a video camera and are taped. Offline data processing is difficult.

A study concerning the optimisation of wave run-up measuring devices has been carried out in the framework of the OPTICREST project by the Hydraulics and Marine Research Centre (HMRC) within the Department of Civil and Environmental Engineering of the Engineering Faculty of University College in Cork (UCC). A number of wave run-up tests has been performed on a smooth impermeable slope and on three slopes covered with different types of armour units (SHED, DIAHITIS, Antifer cubes). Regular waves have been generated by which it was possible to determine visually the wave run-up height on all of the four types of slopes quite accurately by means of a pointer gauge. A run-up measurement frame containing five gauges at distances from the slope surface of 2 mm, 5 mm, 10 mm, 15 mm and 20 mm has been installed on each of the slopes. By means of linear extrapolation of the water level data from each of the gauges on to the slope surface, wave run-up has been estimated. The extrapolated values have been obtained by considering the maxima of the gauge closest to the slope and the simultaneous values of the other probes. It was found that wave run-up becomes more non-linear as the value of  $\xi$  decreases. The use of only two gauges for extrapolation of data did not yield reliable results. The difference between the visually observed wave run-up height and the run-up height measured by the gauge closest to the structure slope was in several cases not significant. This finding would plead in favour of the use of a single gauge measuring technique. However, it was also recognised that the magnitude of errors was dependent on the distance between the first gauge and the slope. In case of a rubble mound breakwater, the gauges

cannot be placed closer than some millimetres from the slope. In these cases, linear extrapolation could offer a solution to the problem. Therefore, an attempt to measure wave run-up more accurately was to use three conductivity gauges in stead of five. The first gauge was placed as close as possible to the breakwater surface (approximately 2.7 mm where possible). The other two have been fixed 4.0 mm, respectively 10.6 mm above the first one. The gauges have been placed next to each other with the lowest gauge in the middle. Two wave run-up signals were produced: the middle gauge measurements and an extrapolation of all three run-up gauges towards the slope of the breakwater. This extrapolation was done by polynomial fitting in stead of linear extrapolation through the measurements of each run-up gauge. Comparison of the extrapolated signal with the first mentioned run-up signal has demonstrated that latter run-up signal was not reliable due to the changing distance between the gauge and every single armour unit. This measuring device gave unsatisfying results. At the Civil Engineering Department of Ghent University, a novel digital wave run-up gauge for laboratory use has been designed, developed and built (see paragraph 5.2).

For full scale wave run-up measurements, the 'spiderweb system' (see paragraph 4.4.5) and a five part run-up gauge (see paragraph 4.4.6) have been used. The run-up gauge employed at full scale is very similar to the laboratory run-up gauge.

#### 2.6 Conclusions

All wave run-up formulae show a dependency of wave run-up on the Iribarren number. The Iribarren number is either calculated using the mean wave period or the peak wave period.

A large number of equations exist to estimate wave run-up on a coastal structure. Wave run-up research was initiated with the investigation of wave run-up on a smooth sloping dike attacked by regular waves. By means of the 'hypothesis of equivalence', workable formulae for estimation of wave run-up induced by irregular waves are obtained. To take into account the roughness of the slope, some researchers suggested the application of a reduction factor. It is proven that wave run-up on a rough permeable structure cannot be estimated by applying a roughness reduction factor to wave run-up formulae valid for smooth impermeable slopes. The application of a roughness factor may apply for  $\xi < \sim 2$  and for  $\xi > 5$  but certainly not for the intermediate range of  $\xi$ .

As long as wave heights are Rayleigh distributed, not depth limited and strongly correlated with wave periods, wave run-up is Rayleigh distributed as well. A good alternative to approximate wave run-up distribution is the Weibull, Gamma or log normal distribution.

The most important formulae for estimation of wave run-up on a permeable rubble mound breakwater are these of Losada and Giménez-Curto (1981) (2.46), Ahrens and Heimbaugh (1988) (2.53) and van der Meer and Stam (1992) (2.51).

From this literature study, following points of attention have been identified:

- the influence of the spectral shape, the ratio between the nominal diameter  $D_{n50}$  and the wave height, the permeability of the breakwater and the effect of wind on wave run-up
- to exclude the influence of the water depth on wave run-up, the ratio between the water depth and the applied wave heights should be larger than three
- scale effects in tests on a model with a very rough surface are small

The structures investigated in the framework of this thesis are all permeable rubble mound breakwaters armoured with either rip rap other artificial armour units (grooved cubes). The behaviour of wave run-up on these structures is investigated for  $\xi > \sim 3$  (surging waves). Taking into account the findings of the wave run-up instrumentation survey, the wire gauge is not the appropriate measuring device for wave run-up measurements.

# Chapter 3: Determination of $Ru_{2\%}$

As to avoid any ambiguity and discussion, clear definitions of the number of wave run-up events *N*, incident significant wave height and a characteristic wave run-up value are given in this chapter.

## 3.1 Number of wave run-up events N

The total number of waves running up the slope is equal or less than the number of incident waves (Zeidler et al. (1992)). The ratio between the number of wave run-up events and the number of waves decreases with increasing relative water depth  $d/H_s$  in the range of 0.95 to 0.50 (Grüne (1982)). Smaller wave run-ups are 'eaten' by bigger wave run-ups and disappear in these. Mase et al. (1984) found a dependency of the ratio between the number of wave run-up events and the number of incident waves on the Iribarren number (figure 3.1). The smaller the  $\xi$  value, the smaller the ratio. According to the discussion of Zeidler et al. (1992) on the paper of van der Meer and Stam (1992) and the recommendation in Frigaard and Schlütter (1999), the reference number of wave run-up events N is equal to the number of incident waves. The number of incident waves is defined as the length of the analysed time series  $T_0$  divided by the mean wave period  $T_{0I}$  determined by analysis in frequency domain (Schlütter and Frigaard (1999)):

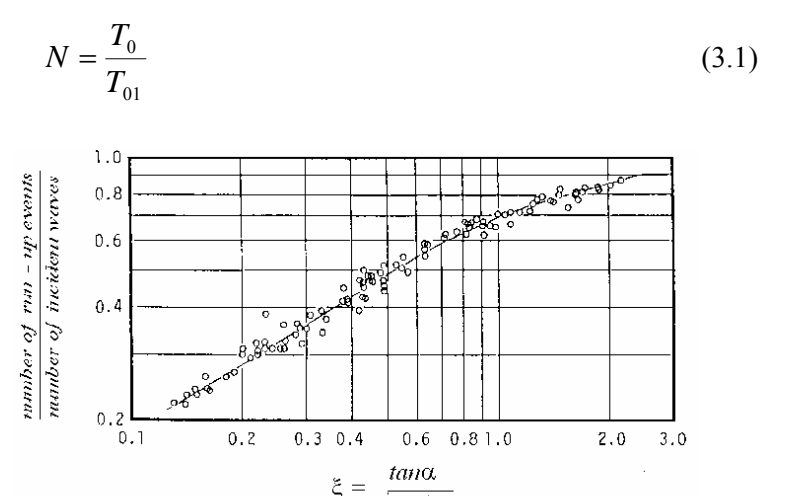


Figure 3.1: Dependency of the ratio between the number of runup events and the number of incident waves on the Iribarren number (cfr. Mase et al. (1984)).

For full scale measurements, no reflection analysis could be performed. This was due to the presence of only one wave measuring device during some storm events. Even with two wave riders reflection analysis could not be performed because the wave rider buoys do not have fixed positions due to currents. So, the number of wave run-up events has been taken equal to the number determined by (3.1), but with  $T_{0I}$  equal to the mean wave period determined by analysis in frequency domain of the wave buoy (measures total waves, i.e. incident and reflected waves) time series.

#### 3.2 Significant wave height

#### 3.2.1 Distance between wave paddle and first wave gauge(s)

To avoid the evanescent wave modes to disturb the measurements of the wave gauge(s) closest to the wave paddle, the distance between the wave paddle and these wave gauge(s) has to be at least two or three times the water depth (Frigaard et al. (1997)).

## 3.2.2 Distance between WG1 and WG2 (active wave absorption)

Günbak (1976) identified the re-reflection of waves on the wave paddle as a parameter with an important influence on wave run-up. Therefore, active wave absorption has been used for all small scale model tests, except for those carried out at UPV (see paragraph 5.3.2). Only for the additional small scale model tests carried out at UGent (paragraph 5.5), following method has been applied to determine the distance between the two wave gauges used for active wave absorption purposes (WG1 and WG2). The distance between the first two wave gauges, i.e. the two gauges closest to the wave paddle,  $x_{1,2}$  is determined following the recommendations of Suzuki and Goda (1976) described in Frigaard et al. (1997). As singularities exist for  $x_{1,2}/L = n/2$  (n = 0, 1, 2,...), it is suggested to avoid values of  $x_{1,2}/L$  in the range  $\pm 0.05$   $x_{1,2}/L$  at the singularity points, or

$$0.05L \le x_{1,2} \le 0.45L \tag{3.2}$$

has to be fulfilled for every single wave length (wave period) in the wave train. To obtain the optimal distance  $x_{I,2}$ , the following method has been applied.

A JONSWAP spectrum is defined by three parameters: a peak wave period  $T_p$ , a significant wave height  $H_s$  and a peakedness parameter  $\gamma$  (Frigaard et al. (1997)):

$$S(f) = \frac{1.4}{\gamma} \frac{5}{16} H_s^2 f_p^4 f^{-5} \gamma^{\alpha} \exp\left(-\frac{5}{4} \left(\frac{f_p}{f}\right)^4\right)$$
(3.3)

where

$$\alpha = \exp\left(-\frac{\left(f - f_p\right)^2}{2\sigma_f^2 f_p^2}\right) \tag{3.4}$$

and  $\sigma_f = 0.10$  for  $f \le f_p$ 

$$\sigma_f = 0.50 \text{ for } f > f_p$$

Varying the peak wave period  $T_p$  within the interval [0.5 s, 2 s] and keeping the other two parameters constant at  $H_s = 0.10$  m and  $\gamma = 3.3$ , a number of JONSWAP spectra have been generated. For each spectrum, three different frequencies have been determined: the peak frequency  $f_p = 1/T_p$  and the frequencies  $f_{LC}$  and  $f_{HC}$  for which the corresponding energies  $S(f_{LC})$  and  $S(f_{HC})$  have about 10% of the peak energy  $S(f_p)$  (figure 3.2).

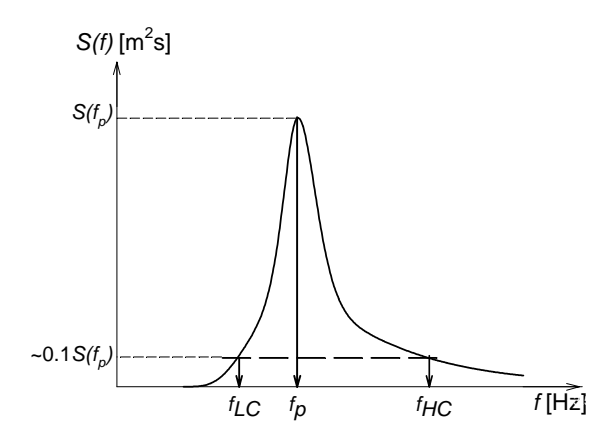


Figure 3.2: Wave spectrum with indication of  $f_{LC}$ ,  $f_p$  and  $f_{HC}$ .

For each of these three frequencies  $f_{LC}$ ,  $f_p$  and  $f_{HC}$ , the corresponding wave lengths  $L_{LC}$ , resp.  $L_p$  and  $L_{HC}$ , have been determined by

$$L = \frac{g\left(\frac{1}{f}\right)^2}{2\pi} \tanh \frac{2\pi d}{L} \tag{3.5}$$

Equation (3.5) requires a number of iterations starting with the deep water wave length given by (2.4). For  $L_{LC}$ ,  $L_p$  and  $L_{HC}$ , the lower and upper boundary values for  $x_{1,2}$  have been calculated by means of (3.2). Thus, for one single peak wave period, three lower boundary values and three upper boundary values of  $x_{1,2}$  have been calculated. Figure 3.3 shows six boundary lines, obtained by applying the aforementioned method for a number of peak wave periods within the interval [0.5 s, 2 s] for a water depth d = 0.40 m. The black lines indicate the upper and lower boundaries of  $x_{1,2}$  for  $f_{LC}$ . The gray lines show the upper and lower boundaries of  $x_{1,2}$  when taking  $f_p$  into account and the blue lines indicate the boundaries of  $x_{1,2}$  for  $f_{HC}$ . The red lines correspond to deep water conditions. As the wave with the peak wave period  $T_p$  has the largest energy content, this wave period has been used to draw the green dashed line in figure 3.3 indicating the 'best choice' for  $x_{1,2}$  (i.e. the average value of the boundary values  $0.05L_{LC}$  and  $0.45L_{HC}$ ).

The same calculations have been performed for different water depths (d = 0.20 m to d = 0.60 m) with discrete steps of 5 cm). The 'best choices' for all considered cases have been plotted in figure 3.4. Also the deep water solution has been plotted.

# 3.2.3 Distance between toe of structure and group of wave gauges measuring the incident wave field

The wave height in the denominator of the dimensionless wave run-up  $Ru_{xy}/H_{m0}$  is the significant incident wave height at the toe of the structure determined by analysis of wave data in frequency domain. The incident wave height is determined by reflection analysis by a three wave gauge method (Funke and Mansard (1980)). The three wave gauges placed in the vicinity of the toe of the breakwater have been placed according to the recommendations of Klopman and van der Meer (1999), Pilarczyk and Zeidler (1996) and Mansard and Funke (1980). Because of the nodal and anti-nodal pattern of the wave field, the significant wave height changes close to the reflecting

structure. When a single-gauge significant wave height measurement is envisaged, the gauge has to be placed further than two spectral peak wave lengths away from the reflective structure. When a multi gauge wave analysis of incident and reflected waves is carried out, the multi gauge technique can be used up to a distance  $x \ge 0.4L$  from the toe of the structure (Klopman and van der Meer (1999)). This means that the distance between the last gauge (the furthest away from the wave paddle) and the toe of the structure may not be smaller than the values mentioned in table 3.1.

Table 3.1: Minimum distance x between the toe of the structure and the wave gauge closest to the structure  $(x > L_p/4)$ .

$T_p[s]$	x [m]
0.8	0.25
1.0	0.39
1.2	0.56
1.5	0.88
1.8	1.26

The incident wave height at the toe of the structure has been determined by reflection analysis. The computer programme Refcross (Andersen et al. (1995)) has been used for this purpose. The method of Mansard and Funke (1980), i.e. a three points method has been applied. This method is an extension of the most simple method for reflection analysis of Suzuki and Goda (1976) which uses only two wave height meters. The applied method takes an additional probe into use which makes it possible to add an error to the measurements and hence to minimise this error in a least squares sense. Thus, the reflection coefficient is determined more accurate. Mansard and Funke (1980) suggest that

$$x_{1,2} = \frac{L}{10} \tag{3.6a}$$

$$\frac{L}{6} < x_{1,3} < \frac{L}{3} \tag{3.6b}$$

$$x_{1,3} \neq \frac{L}{5} \tag{3.6c}$$

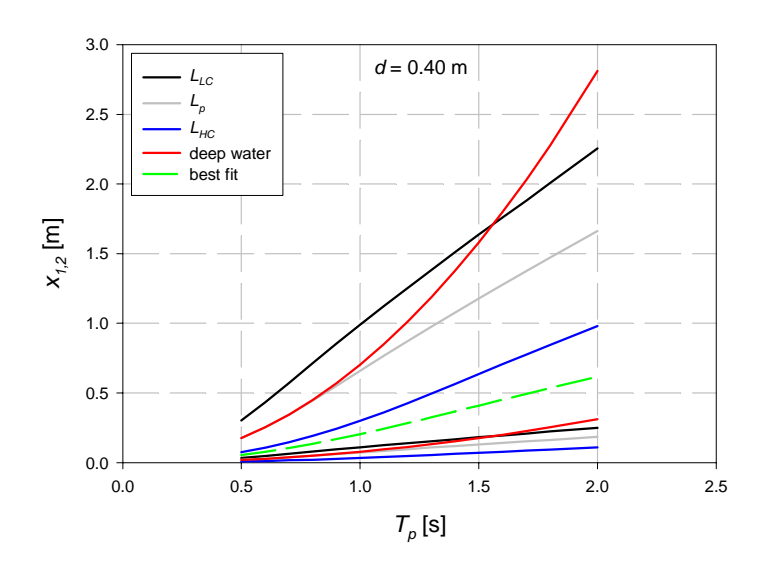


Figure 3.3: Upper an lower boundary lines for the distance  $x_{1,2}$  [m] for  $f_{LC}$ ,  $f_p$ ,  $f_{HC}$  for different peak wave periods  $T_p$  between 0.5 s and s for d = 0.40 m according to the method of Suzuki and Goda (1976).

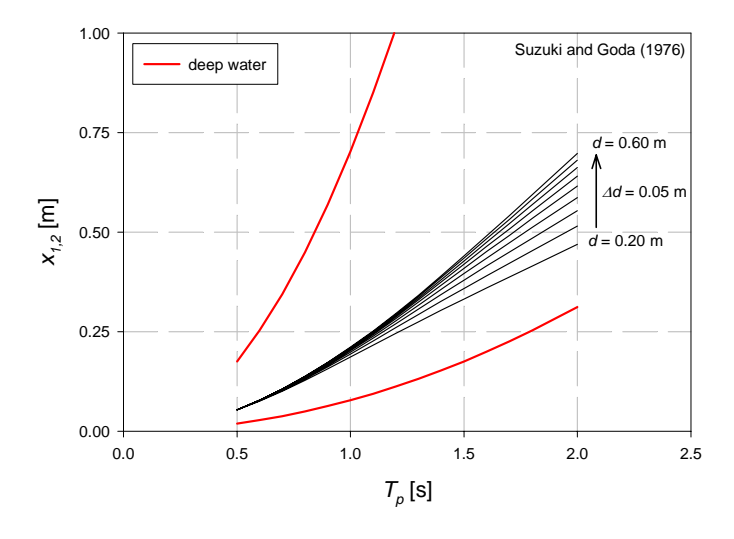


Figure 3.4: 'Best choice' for  $x_{1,2}$  for different water depths d between 0.20 m and 0.60 m and peak wave periods  $T_p$  between 0.5 s and 2 s according to the method of Suzuki and Goda (1976).

$$x_{1,3} \neq \frac{3L}{10} \tag{3.6d}$$

in which  $x_{I,2}$  is the distance between the first and the second wave gauge and  $x_{I,3}$  is the distance between the first and the third wave gauge.

In figure 3.5, the best 'choices' for the distances  $x_{I,2}$  and  $x_{I,3}$  for a three gauge method for peak wave periods varying between 0.5 s and 2s and for water depths d = 0.20 m, d = 0.25 m, d = 0.30 m, d = 0.35 m, d = 0.40 m and d = 0.45 m have been displayed. The red line is the deep water solution.

Because of the presence of only one wave measuring device for full scale measurements, the total significant wave height has been used. Also in the laboratories which simulated full scale storm events, the total wave height has been measured at the same location as in full scale in order to make possible the comparison between full scale and small scale.

## 3.3 Wave run-up

The definition of wave run-up has already been given in paragraph 1.2. Many researchers have published formulae to calculate the 2% wave run-up level (cfr. paragraph 2.2.4). All these formulae are based on laboratory tests. Wave run-up investigations have been performed both in small scale model tests and in large scale tests (e.g. Delta flume (Delft), Large Wave Flume (Hannover),...). In such laboratory tests, the sea state (wave height, wave period, wind, SWL,...) can be kept constant for a long time and tests can be performed with a very high number of waves, leading to very accurate estimations of the 2% wave run-up level. In the field, on the contrary, the sea state is hardly constant and varies continuously. The sea state can be considered approximately constant only during relatively short periods of time. During this limited period of time, only a very limited number of waves is measured, leading to rather inaccurate estimations of  $Ru_{2\%}$ . Assuming the sea state to be constant during a larger period of time and thus, neglecting small (acceptable) variations of the sea state, a reliable estimation of the  $Ru_{2\%}$  value can be made. Two methods have been used to estimate  $Ru_{2\%}$ : (1) a direct method and (2) by fitting a theoretical distribution to the data.

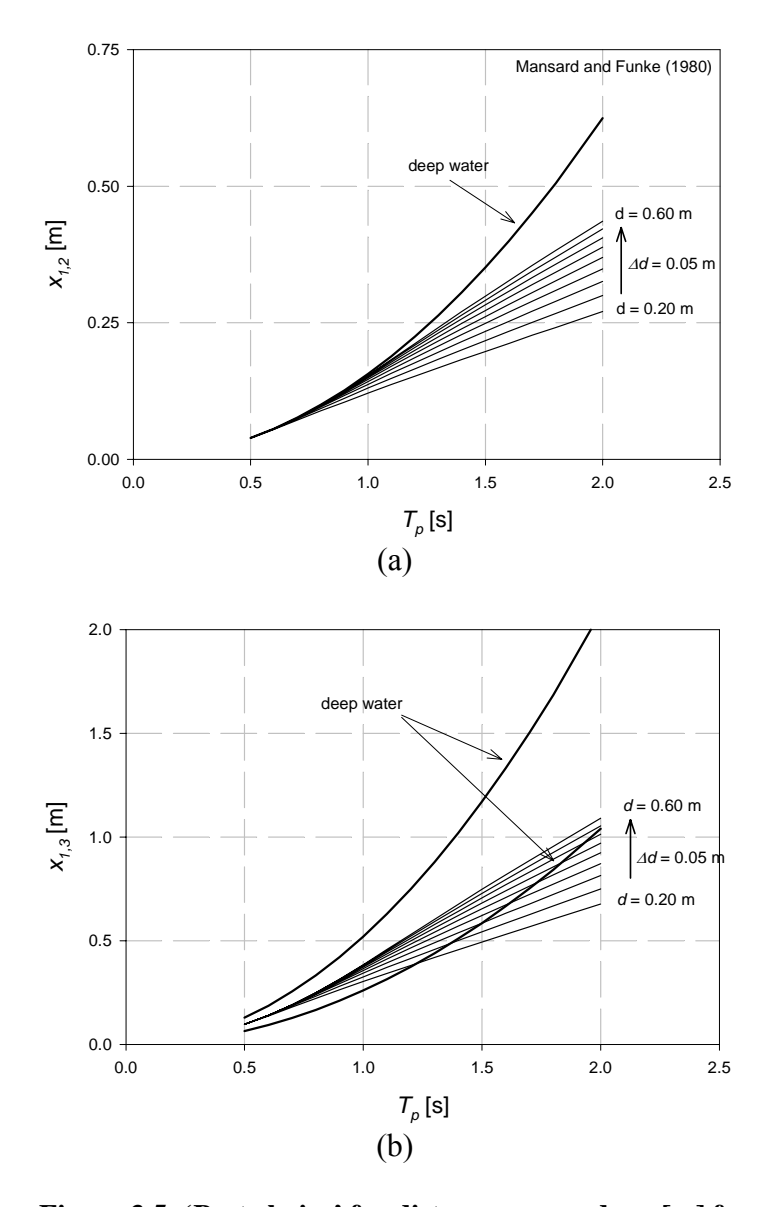


Figure 3.5: 'Best choice' for distances  $x_{1,2}$  and  $x_{1,3}$  [m] for different water depths d between 0.20 m and 0.60 m and peak wave periods  $T_p$  between 0.5 s and 2 s according to the method of Mansard and Funke (1980).

#### 3.3.1 Direct method

The first method to estimate  $Ru_{2\%}$  is very simple and straightforward. When wave run-up levels are put in descending order, the Bayesian estimator of the exceedance probability of the  $p^{th}$  wave run-up value in a series of N wave run-up values is p/(N+1) (Rice (1988)). Therefore, the wave run-up level for which p/(N+1) equals x/100 is  $Ru_{x\%}$ . If necessary, some interpolation method (e.g. linear interpolation) has to be used.

This method has the advantage of being very simple to use. Moreover, no assumptions have to be made about the wave run-up distribution. The disadvantage is that no information on its accuracy is available.

## 3.3.2 Using a fitted theoretical distribution

Another method to obtain an estimation of  $Ru_{2\%}$  is to approximate the wave run-up distribution by a theoretical distribution. Assume wave run-up follows a *two parameter Weibull distribution*, with a and b as the two parameters (see also Annex A). By definition is

$$P[Ru > Ru_{x\%}] = exp\left(-\left(\frac{Ru_{x\%}}{b}\right)^{a}\right) = \frac{x}{100}$$
 (3.7)

The major disadvantage of this method is that an assumption has to be made about the wave run-up distribution. The advantage is that a confidence interval of the estimation can be calculated.

The wave run-up values can be considered as random realisations of a distribution. Therefore, the parameters a and b are also random variables. It can be shown (Rice (1988)) that a is approximately normally distributed with the true value  $a_t$  as its mean value and with a standard deviation  $\sigma_a$ . Also b is approximately normally distributed with the true value  $b_t$  as its mean value and with a standard deviation  $\sigma_b$ . The standard deviations are given by the following equations (Rice (1988)):

$$\sigma_a = \frac{1}{\sqrt{N.I(a_t)}} \tag{3.8}$$

$$\sigma_b = \frac{1}{\sqrt{N.I(b_t)}} \tag{3.9}$$

with N = the number of wave run-up events. The exact standard deviations  $\sigma_a$  and  $\sigma_b$  cannot be computed when the true values  $a_t$  and  $b_t$  are unknown. A good approximation of  $a_t$  and  $b_t$  is obtained by using the estimations of  $a_t$  and  $b_t$ , i.e.  $\hat{a}$  and  $\hat{b}$  instead.

The function I in (3.8) and (3.9) is defined as

$$I(a) = E \left[ \frac{\partial}{\partial a} \ln \left( f_{Ru} \left( Ru | a, b \right) \right) \right]^{2}$$
 (3.10)

$$I(b) = E \left[ \frac{\partial}{\partial b} \ln \left( f_{Ru} \left( Ru | a, b \right) \right) \right]^{2}$$
(3.11)

for a and b respectively. Assuming the function f to be smooth, the functions I(a) and I(b) may be replaced by

$$I(a) = -E \left[ \frac{\partial^2}{\partial a^2} \log (f_{Ru}(Ru|a,b)) \right]$$
 (3.12)

$$I(b) = -E \left[ \frac{\partial^2}{\partial b^2} \log \left( f_{Ru} \left( Ru | a, b \right) \right) \right]$$
 (3.13)

The function  $f_{Ru}(Ru|a,b)$  is the two parameter Weibull probability density function, which is expressed as:

$$f_{Ru}(Ru|a,b) = \frac{d}{dRu} F_{Ru}(Ru|a,b)$$
(3.14)

$$f_{Ru}(Ru|a,b) = \frac{a}{b} \left(\frac{Ru}{b}\right)^{a-1} \exp\left(-\left(\frac{Ru}{b}\right)^{a}\right)$$
(3.15)

Using the Rayleigh distribution, defined by

$$P[Ru > Ru_{x\%}] = exp\left(-\frac{Ru_{x\%}}{2a^2}\right) = \frac{x}{100}$$
 (3.16)

to fit the measurement data in stead of a two parameter Weibull distribution, the function I(a) is defined as

$$I(a) = E \left[ \frac{d}{da} \log f_{Ru} (Ru|a) \right]^2$$
 (3.17)

Under appropriate smoothness conditions of f, I(a) may also be expressed as

$$I(a) = -E \left[ \frac{d^2}{da^2} \log f_{Ru} (Ru|a) \right]$$
 (3.18)

Applied to the Rayleigh distribution, (3.18) contains

$$\frac{d}{da}\log f_{Ru}(Ru|a) = -\frac{2}{a\ln 10} + \frac{Ru^2}{a^3\ln 10}$$
 (3.19)

$$\frac{d^2}{da^2}\log f_{Ru}(Ru|a) = \frac{2}{a^2\ln 10} - \frac{3Ru^2}{a^4\ln 10}$$
 (3.20)

The mean value and the standard deviation of parameter *a* are:

$$\mu = \hat{a} \tag{3.21}$$

$$\sigma = \frac{1}{\sqrt{NI(a)}}\tag{3.22}$$

Both methods (direct method and the method by fitting a theoretical distribution) have been applied to the full scale measurement data of one storm event and have been compared. Reference is made to paragraph 4.7.2.

# Chapter 4: Full scale measurements of wave run-up on a rubble mound breakwater

# 4.1 Objectives

A rubble mound breakwater has been instrumented for measurements of attacking waves, pore water pressure variations inside the breakwater core, wave run-up and wave overtopping.

The objective of this chapter is to collect full scale data on wave characteristics and wave run-up on a rubble mound breakwater and to analyse these data.

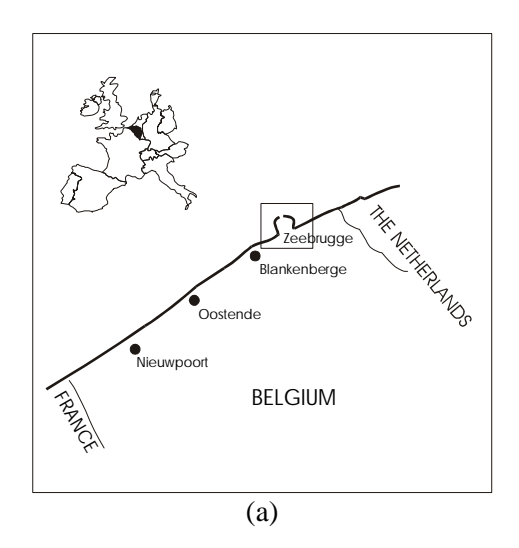
The measuring site and the measured storm events are presented in paragraph 4.2, resp. paragraph 4.3. The measuring instrumentation and the off line data processing are described in paragraph 4.4. The data analysis is discussed in paragraph 4.5. The analysis results are presented in paragraph 4.6. Paragraph 4.7 contains the conclusions of the full scale measurements.

## 4.2 Measuring site

At the northern part of the western breakwater sheltering the outer harbour of Zeebrugge (Belgium) (figure 4.1), full scale wave run-up measurements have been carried out on a conventional rubble mound breakwater. The breakwater has been built in the eighties. The design wave height at the breakwater is 6.20 m. The design wave period is 9.0 s and the design water level is Z + 6.75 (Z = TAW - 0.11). One tide cycle lasts for 12 hours and 25 minutes. The tidal range varies between 3.40 m at neap tide to 4.30 m at spring tide. The breakwater has a total height of 20 m with a crest level at Z + 12.40. An aerial photograph of the Zeebrugge outer harbour with indication of the measuring site is given in figure 4.2.

The armour layer consists of 25 ton grooved cubes. In section 2861 of the breakwater, a jetty with a total length of 60 m is constructed on the breakwater. Figure 4.3 shows the cross section of the breakwater at the position of the measuring jetty. At the seaward side, a steel pile ( $\phi = 1.80$  m) supports the measuring jetty. At the landward side, the jetty is supported by two concrete columns. The cross section of the breakwater is instrumented to measure wave characteristics in front of the breakwater, pore pressures in the core of the breakwater and wave run-up. In the direct vicinity of section 3000 of the breakwater,

instrumentation for wave overtopping and spray measurements has been installed.



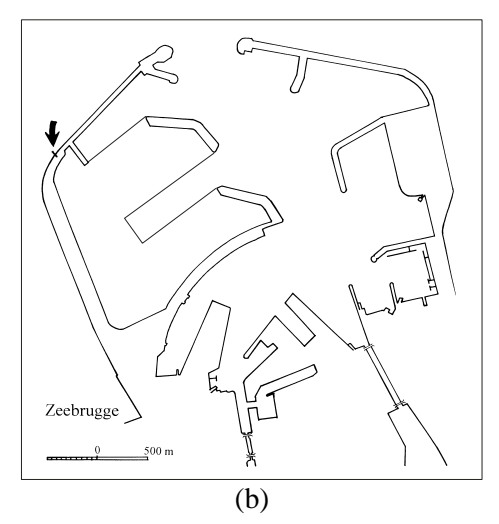


Figure 4.1: Location of (a) Zeebrugge Harbour (Belgium) and (b) the measuring site at the NW breakwater.



Figure 4.2: Aerial view on Zeebrugge outer harbour with indication of the measuring site (photo: MBZ).

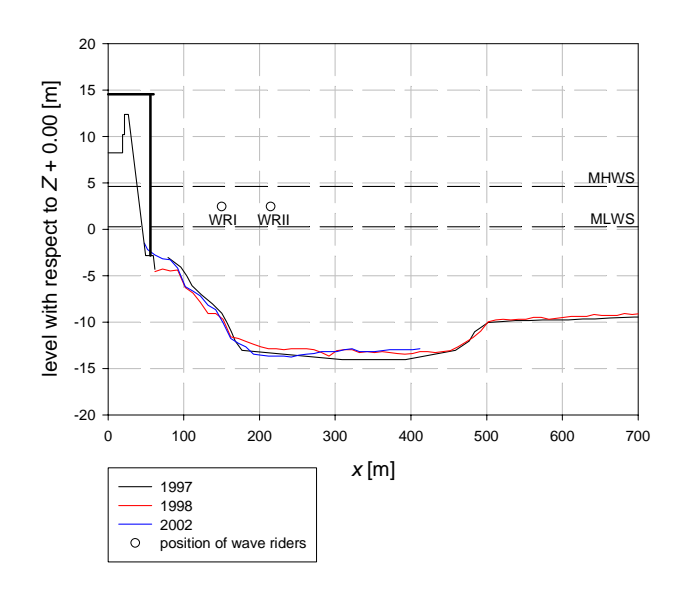


Figure 4.4: Foreshore slope at the Zeebrugge rubble mound breakwater with indication of the breakwater.

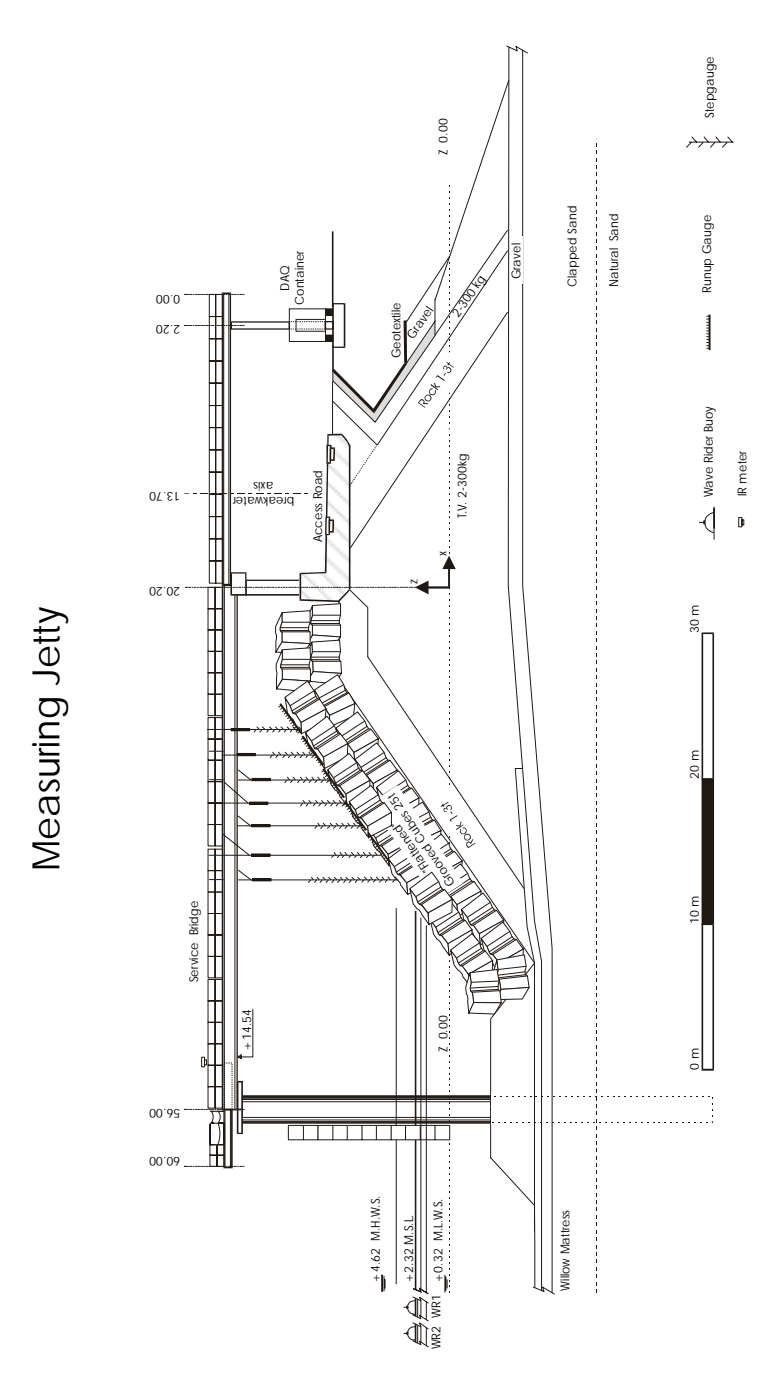


Figure 4.3: Cross section of the Zeebrugge rubble mound breakwater at the measuring jetty.

The bathymetry of the foreshore slope is characterised by a relatively flat slope at approximately Z-9.00. Near the breakwater, an erosion pit is present (figure 4.4). The data of figure 4.4 have been taken from a sounding map dating from May  $12^{th}$ , 1997 (plan  $n^{\circ}$  202-01-eroswdam-n-187-97), resp. November  $23^{rd}$ , 1998 (plan  $n^{\circ}$  373-03-eroswdam-b-643-98) and July  $4^{th}$ , 2002 (plan  $n^{\circ}$  009dc-2002)). The breakwater and the measuring jetty have been drawn on the left side of the figure. The maximal depth is Z-14.00. The foreshore changes only very slowly.

#### **4.3** Measured storm events

In front of the Belgian coast many measuring poles and buoys have been placed (figure 4.5). These poles and wave buoys are part of the Monitoring Network Flemish Banks which was set up for the acquisition of real-time oceanographical and meteorological data along the Belgian coast and on the Belgian continental shelf. Data of these measuring poles and buoys together with the most recent marine weather forecast can be found online on http://www.lin.vlaanderen.be/awz/weerberichtkust/interoms.html.

Next to online data presentation, two times a day the Oceanographic Meteorological Station of the Coastal Division of the Waterways and Marine Affairs Administration within the Environment and Infrastructure Department of the Ministry of the Flemish Community in close co-operation with the Royal Meteorological Institute of Belgium (KMI) provides data on weather forecast and sea state predictions as observations of these of the past 12 hours by fax.

Based on the observation data of these reports, thirteen storm events have been selected amongst all observed heavy weather conditions measured during the period from 1995 to 2000 along the Belgian coast (table 4.1). A 'storm event' is defined as the period of time at high tide of two hours during which the water level is quasi constant and the wind is blowing strongly and quasi parallel to the axis of the measuring jetty. The moment of high water is noted as  $t_{HW}$ .  $t_{HW}$  - i and  $t_{HW}$  + i are the i<sup>th</sup> hour before, respectively after the point in time of high water. The storm selection criteria are:

- a strong wind, preferably stronger than 7 Beaufort (wind speed > 14 m/s), blowing from north west, so that wind generated waves incidence perpendicular to the breakwater
- a significant wave height  $H_s > 2.5$  m
- a high SWL (preferably spring tide)
- a long storm period so that a fully developed sea is obtained.

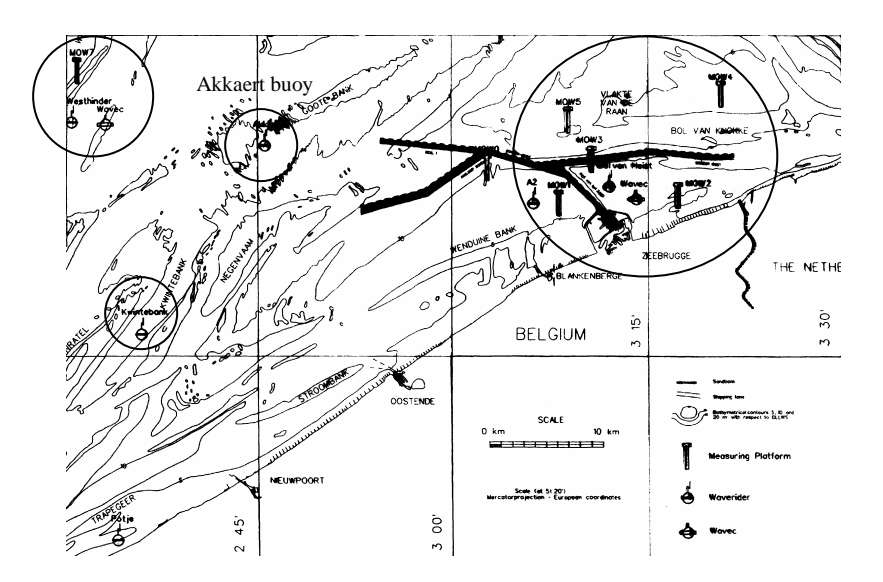


Figure 4.5: Wave measuring poles and buoys in front of the Belgian coast.

Table 4.1: Full scale storm events analysed for wave run-up.

storm event n°	date	hour	
1 <sup>a</sup>	August 28, 1995	02h45 - 04h45	
$2^{a}$	August 28, 1995	15h00 - 17h00	
3 <sup>a</sup>	January 19, 1998	16h00 - 18h00	
4	January 20, 1998	04h15 - 06h15	
5	February 7, 1999	16h00 - 18h00	
6	February 17, 1999	12h45 - 14h45	
7	February 22, 1999	15h45 - 17h45	
8	November 6, 1999	11h30 - 13h30	
9	November 6-7, 1999	23h45 - 01h45	
10	December 3, 1999	21h00 - 23h00	
11	December 4, 1999	22h00 - 0h00	
12	January 22, 2000	12h30 - 14h30	
13	January 23, 2000	00h45 - 02h45	

<sup>&</sup>lt;sup>a</sup>: time series slightly different than these of chapter 5

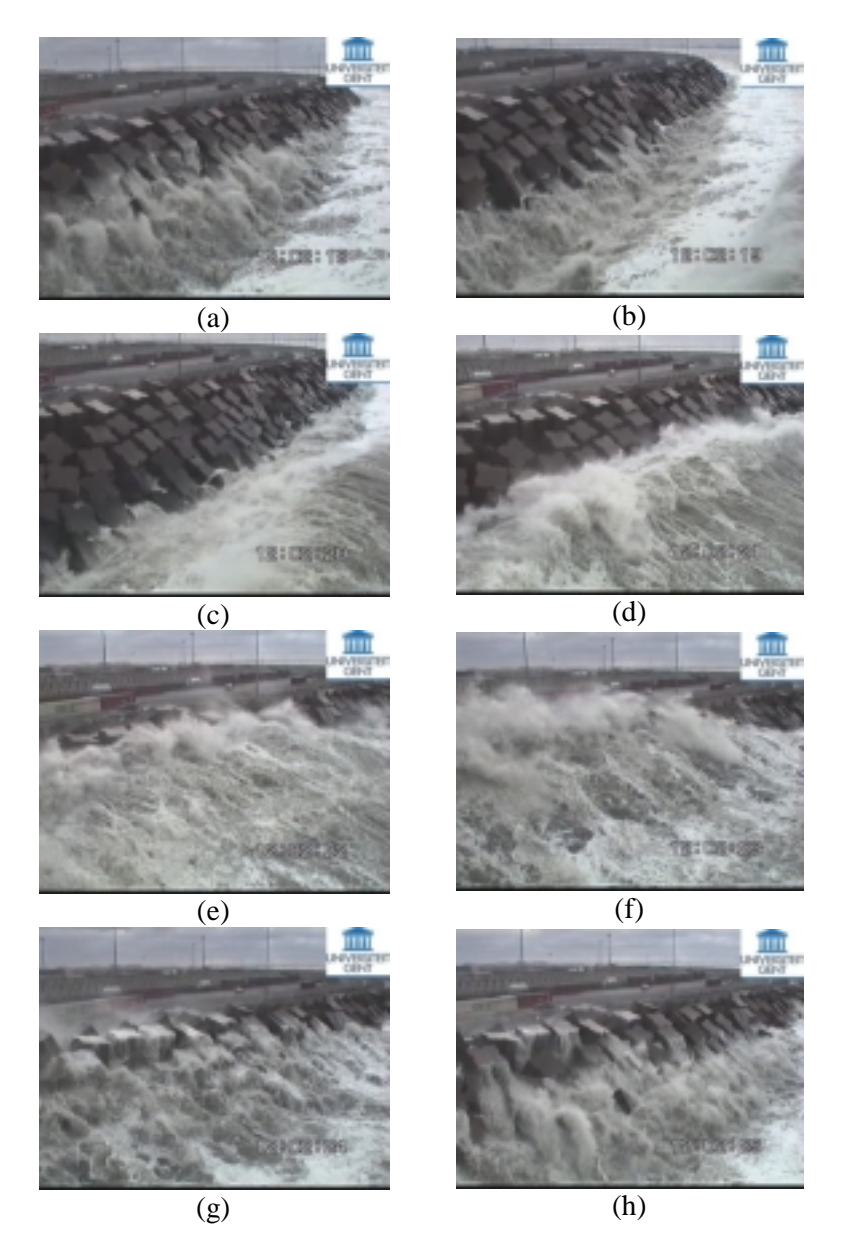


Figure 4.6: Wave run-up event (film frames taken each one second).

The wave climate during these thirteen selected storm events was characterised by a significant wave height  $H_{mo}$  varying between 2.40

m and 3.13 m, a mean wave period  $T_{01}$  of approximately 6.24 s, a peak wave period  $T_p$  of 7.93 s on average, a wind force of at least 7 Beaufort and a wind blowing direction almost perpendicular to the breakwater.

Figure 4.6 shows a sequence of eight frames ( $\Delta t = 1$  s) cut out of a record on video of a wave run-up event of storm event n° 8 ( $H_{m0} = 3.04$ ;  $T_{01} = 6.29$  s).

## 4.4 Instrumentation

Analogue signals of all connected measuring devices are sampled at a sample frequency rate of  $f_s = 10$  Hz, 24 hours a day, 7 days a week, the whole year round. Data are stored each 15 minutes in a RAW file in binary format. Each RAW file contains 9000 values per connected channel. At short or long intervals (depending on weather conditions), data files are copied from the hard disk of the data acquisition computer to a portable hard disc by a parallel connection. After having checked whether data are copied correctly, the data stored on the hard disc of the data acquisition computer are deleted. The portable hard disc is transported to the office and data files are copied on a CD-rom for storage in the data catalogue and for off-line data processing.

The various measuring devices installed at the Zeebrugge breakwater have been described below. Emphasis is put on the instrumentation for measurements of wave run-up: the 'spiderweb system' (SP) and the wave run-up gauge (RU) (paragraph 4.4.4). For more detailed information on the wave rider buoys, the pressure sensors and the infra red meter, reference is made to Troch (2000).

## 4.4.1 Wave rider buoy (WR)

Two wave riders measure the wave climate in front of the Zeebrugge breakwater (figure 4.7). A wave rider is a buoy which measures waves by measuring and by double integration of the vertical accelerations of the buoy. By their mooring, measuring errors of maximum 1.5% can occur. Due to the harsh sea environment, geometrical and legal restrictions, wave buoys cannot be placed in the field at any arbitrary position. The wave riders are located at a distance of approximately 150 m (wave rider 1 (WRI)) and 215 m (wave rider 2 (WRII)) from the breakwater axis.

The wave rider transfer function given in figure 4.8 shows how the wave rider buoy responds to waves with a certain wave period. One can see a perfect agreement between buoy motion amplitude and wave motion amplitude in the frequency range 0.065 Hz to 0.5 Hz (only 0.3 dB). Wave periods measured in Zeebrugge are found within this range. The phase shift between buoy motion and wave motion increases with increasing wave period.



Figure 4.7: Wave rider buoy in front of the Zeebrugge breakwater.

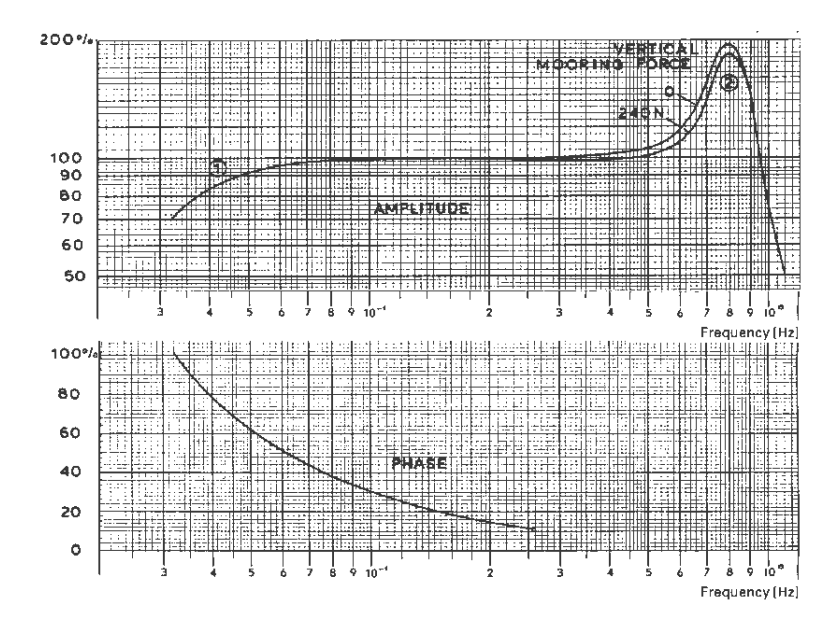


Figure 4.8: Wave rider amplitude and phase transfer function.

## 4.4.2 Pressure sensor (PR)

Inside the core of the breakwater, thirteen pressure sensors have been installed. These measure the wave induced pore pressure field through the breakwater.

Two pressure sensors PR383 and PR137 at the steel pile supporting the measuring jetty (figure 4.9) at level Z-0.39, resp. Z+1.11 have a two folded function. Firstly, these pressure sensors allow a check on the infrared meter measurements (see paragraph 4.4.3). Secondly, the pressure sensors have been used to measure the *SWL* when the infrared meter was absent.





Figure 4.9: Pressure sensors at the pile supporting the measuring jetty on the Zeebrugge breakwater.

A Druck PTX 161/D type has been installed, a type specially recommended for salt water applications. The pressure range is -0.5 bar to 1.5 bar. The operating (compensated) temperature range is -2°C to +30°C with only 0.3% measuring error. The pressure sensors have been calibrated in the laboratory.

# 4.4.3 Infra red meter (IR)

A THORN infra red wave height sensor is placed on the jetty near the pile supporting the jetty (figure 4.10). The IR measures water surface

elevations (waves) at the toe of the breakwater. This type of infra red meter is very suitable for use in offshore and marine environments. The measuring device is protected against sun and rain by a plastic washing basin. The working range of the infra red meter is between 6 m and 50 m. The accuracy is  $\pm$  1% over the range 10 to 50 m. The operational temperature range is -15°C to 40°C. Due to its age (more than 15 years use in marine environments), the good working of the infra red meter has to be checked regularly.

The infra red meter has been used to measure the *SWL*. The *SWL* is determined by averaging the water surface elevation measurements made by the infra red meter over the investigated period.

The working principle of this measuring device is quite simple. The infra red meter transmits an infra red light pulse and measures the transit time of this pulse to be reflected back to the sensor. The transit time is converted into an analogue linear voltage output between 0 and 5 V. The time divided by the propagation velocity of light equals twice the unknown distance x between the sensor and the water level.



Figure 4.10: Infra red meter installed on the measuring jetty.

Several factors affect the infra red meter measurements adversely:

- reflections from spray water and foamy water
- the salty and moist environment changes the characteristics of the medium the infrared light has to travel through

• the infra red light has to reflect on a moving water surface in stead of to be reflected on a static metal sheet as used during calibration in the laboratory

The good working of the infra red meter has been checked in the field upon the measurements of the pressure sensor at the steel pile supporting the measuring jetty. Both instruments are thought to measure the same *SWL* during a 'calm weather' period.

# 4.4.4 Wave run-up measuring devices

## 4.4.4.1 Spiderweb system (SP)

The 'spiderweb system' (SP) has been used for wave run-up measurements. The 'spiderweb system' (SP) consists of seven vertical step gauges placed between the measuring jetty and the breakwater slope (figure 4.11). At their lower end the step gauges are attached to the armour units. At their upper end the gauges are fixed to the jetty by means of a cable and a heavy spring (figure 4.12). The spring allows some flexibility, necessary to withstand wave impact during storm conditions. Each step gauge has 16 electrodes (the two most seaward step gauges have each 32 electrodes). The vertical distance between two electrodes is 200 mm. The water surface elevations at the location of each of the step gauges are measured by the electronics circuit which counts the number of submerged electrodes of each step gauge. Therefore, the output voltage of a step gauge is increased by 0.5 Volt for each electrode submerged by sea water. Based on the measurements of these water surface elevations, the wave run-up level is determined through an algorithm (see paragraph 4.5.2).

Figure 4.13 shows the vertical elevation of the basis of each step gauge. The co-ordinates are given in table 4.2. The basis is the location where the step gauge is attached to an armour unit. As years passed by, the step gauges have been removed occasionally to be repaired and to be cleaned. The lowest almost continuously submerged electrodes are the favourite place for a mollusc to attach itself. Some gauges have been fixed to other armour units after having been removed. The level of the bases of the step gauges are displayed with respect to the Z 0.00 level (Z 0.00 = TAW 0.00 – 0.108 m) and to the axis of the breakwater (x = 0). The levels of the base of each step gauge have been measured by a land surveyor. The level of mean high water spring (MHWS) Z + 4.61 is indicated, as well as the level of mean low water spring (MLWS) Z + 0.27.

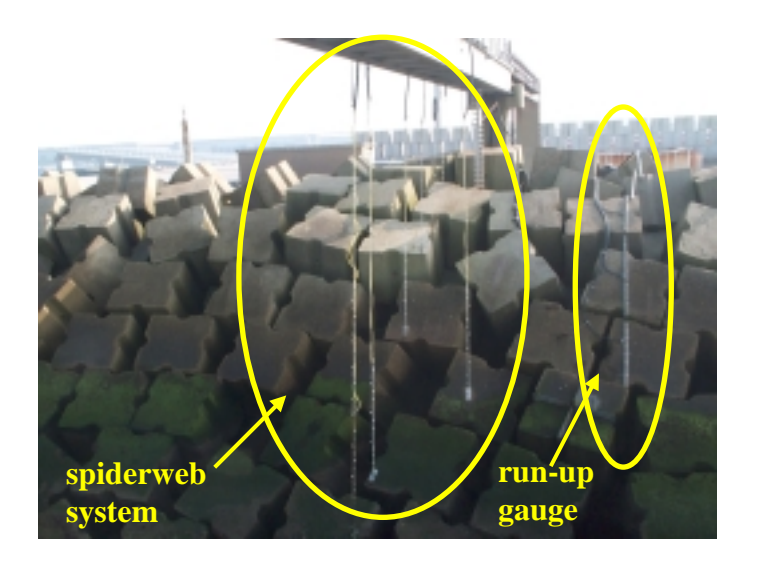


Figure 4.11: The spiderweb system (SP) for wave run-up measurements on the Zeebrugge rubble mound breakwater.

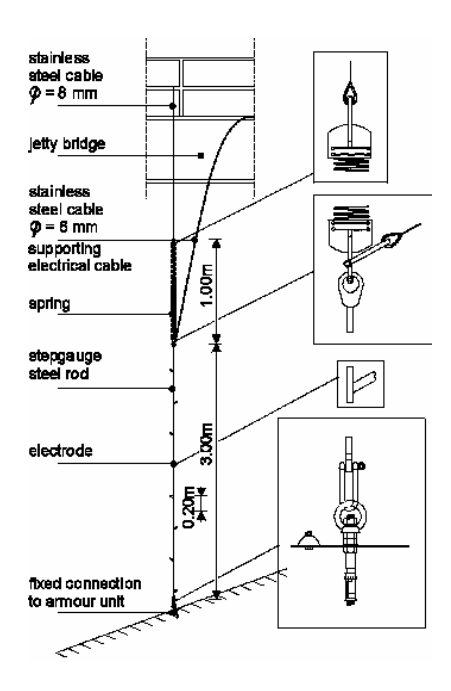


Figure 4.12: Sketch of a step gauge of the 'spiderweb system' fixed to the armour units at its lower end and attached to the measuring jetty at its upper end (Troch et al. (1998)).

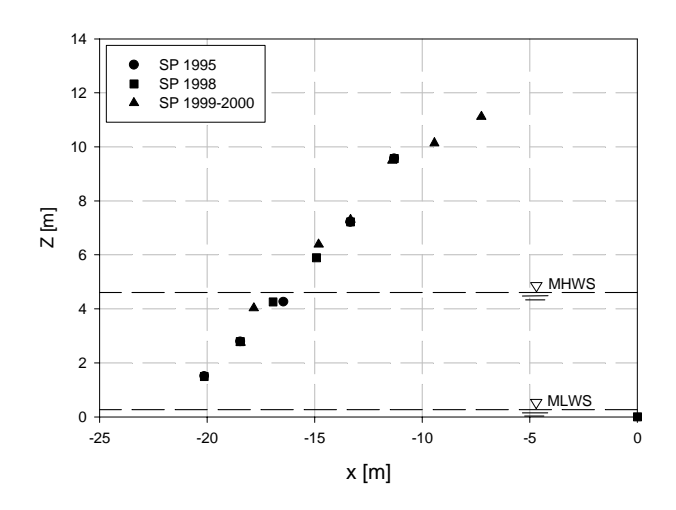


Figure 4.13: Position of the bases of the step gauges of the spiderweb system at which these are fixed to the armour units.

Table 4.2: Position of the fixing points of the step gauges of the 'spiderweb system' to the armour units throughout the years 1995 to 2000.

	1999/2000		1998		1995	
	<i>x</i> [m]	<i>Z</i> + [m]	x [m]	<i>Z</i> + [m]	<i>x</i> [m]	<i>Z</i> + [m]
SP1	-18.45	2.75	-20.14	1.5	-20.14	1.51
SP2	-17.84	4.03	-18.46	2.79	-18.46	2.79
SP3	-14.82	6.39	-16.94	4.26	-16.46	4.26
SP4	-13.34	7.3	-14.92	5.89	-13.35	7.22
SP5	-11.4	9.5	-13.34	7.22	-11.31	9.57
SP6	-9.44	10.14	-11.31	9.57		
SP7	-7.26	11.12				

For more detailed background information on the 'spiderweb system', Troch et al. (1998) is referred to.

## **4.4.4.2** Run-up gauge (RU)

A more conventional run-up gauge (RU) has been mounted along the slope of the breakwater for the measurement of wave run-up. Five individual parts have been been mounted in one line on top of the

armour units (figure 4.11 and 4.14). These gauges allow a direct determination of the run-up level. The gauges are made of glass fiber reinforced polyester profiles with protruding electrodes made of stainless steel (figure 4.15 and 4.16). A heat shrunk tube isolates the electrodes from the profiles. These tubes stick 6 mm out of the profiles so thin water layers are obstructed to make contact with the electrodes. The gauges are filled up with epoxy resin. Thus, the run-up gauges are completely watertight. The dimensions of the run-up gauges have been kept as small as possible. Reasons of strength could not avoid that only water layers thicker than 5 cm can be detected because of the thickness of the gauge.



Figure 4.14: The five part run-up gauge mounted along the slope of the breakwater on top of the armour units.

Not every gauge has an equal number of electrodes. The lowest gauge is gauge  $n^{\circ}$  1. The upper gauge is gauge  $n^{\circ}$  5. Gauges  $n^{\circ}$  1 and 2 have each 18 electrodes. The other gauges have 16 electrodes each. The two lowest electrodes of gauge  $n^{\circ}$  1 are the ground of the run-up gauge. The vertical spacing of the electrodes is approximately 9 cm,

11 cm, 6 cm, 4 cm and 5 cm for parts  $n^{\circ}$  1, 2, 3, 4 and 5 of the run-up gauge. During winter season 1998-1999, only three parts (gauges  $n^{\circ}$  1, 2 and 3) of the run-up gauge were present. After that winter season, the five parts of the run-up gauge were available for wave run-up measurements.

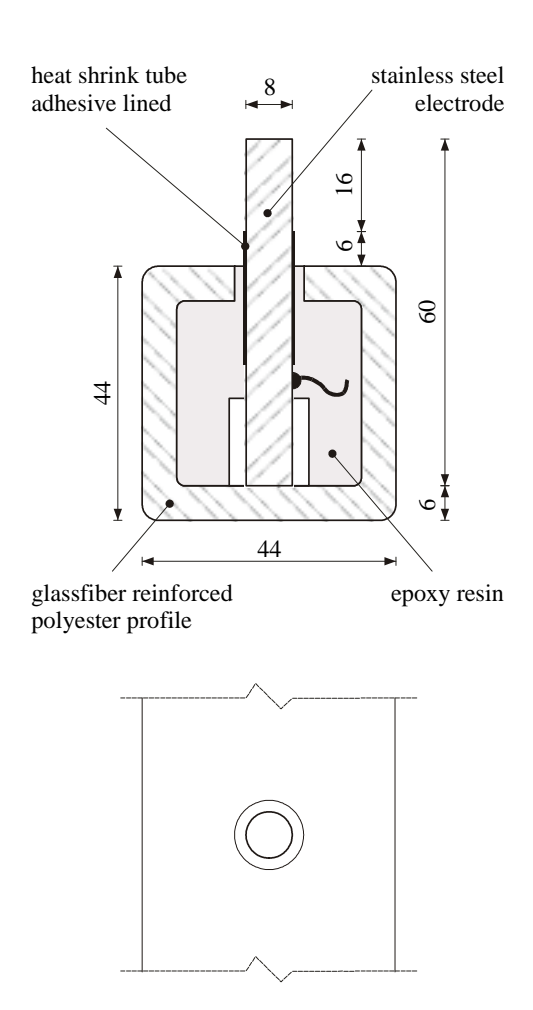


Figure 4.15: Design drawing of the wave run-up gauge used for full scale wave run-up measurements (dimensions in [mm]).

The measuring principle of the run-up gauge is similar to the measuring principle of each single step gauges of the spiderweb

system: each submerged electrode counts for an output voltage of 0.1 V which is added to the total output signal (see also the discussion about the laboratory run-up gauge in paragraph 5.2). Each of the five gauges is connected to an electrical cable led over the armour units. The cables are protected by a HDPE tube, firmly attached to the armour units at regular distances.

Each voltage level of the output signal is related to a wave run-up level. Therefore, the exact co-ordinates of each electrode have been measured by a surveyor.

Figure 4.17 shows the elevation of each single electrode of the run-up gauge with respect to the Z+0.00 level and to the axis of the breakwater (x=0). The level of mean high water spring (MHWS) Z+4.61 and the level of mean low water spring (MLWS) Z+0.27 are again indicated. It is seen that the lowest electrode of the run-up gauge is situated above MHWS. Design SWL is 6.75 m. However, the maximal measured SWL during the measuring campaigns was Z+5.46, i.e. lower than the lowest electrode of the run-up gauge (Z+6.12). This was also the reason why wave run-down could not be measured with this measuring device.

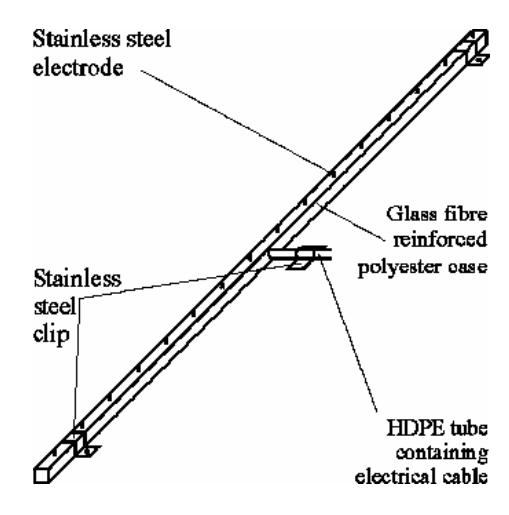


Figure 4.16: Sketch of run-up gauge for wave run-up measurements on Zeebrugge rubble mound breakwater (Verdonck et al. (1999)).

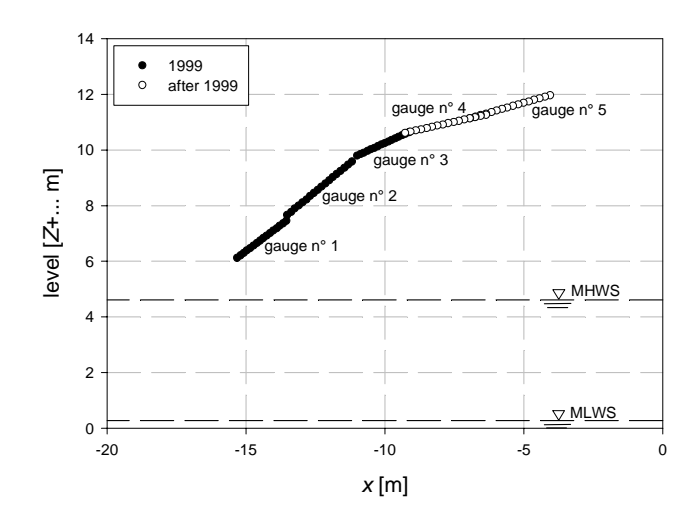


Figure 4.17: Position of the electrodes of the run-up gauge on the Zeebrugge breakwater.

## 4.4.4.3 Performance SP and RU

The 'spiderweb system' and the run-up gauge are prone to the same errors. An increase in output voltage not necessarily means that two neighbouring electrodes are submerged. The same output voltage could also be measured for two electrodes at larger distance. An electrode which is not functioning or which is not submerged while other adjacent electrodes are submerged cannot be detected. Thus, a lower wave run-up level than the actual level is registrated. In the opposite case, a malfunctioning electrode constantly indicating an output voltage of 0.5 V yields a upward shift of the measured water surface level. These adverse occurrences have been taken into account in the design of a novel laboratory step gauge (see paragraph 5.2). The solution is to measure simultaneously the cumulative output voltage (the number of wet electrodes) and the highest 'wet' electrode.

The advantage of the 'spiderweb system' with respect to the wave run-up gauge is found within the fact that the water surface elevations are known (with an accuray of 200 mm) in seven discrete points on the slope of the breakwater. The instantaneous wave profile in front of the breakwater is approximated by a polygon connecting the water surface levels measured by the step gauges. By extrapolation, the wave run-up level is calculated.

The disadvantage of using the step gauges of the 'spiderweb system' is that wave run-up levels have to be determined through a complicated algorithm and thus these are measured in an indirect way. The big advantage of the run-up gauge is that wave run-up levels are measured in a direct way on the slope and without intervention of a computing algorithm.

#### 4.4.5 Anemometer

Several wind gauges are installed on the measuring jetty to measure wind speed  $v_s$  and wind direction  $\beta$  (figure 4.18). Data of the yellow encircled anemometer are used. The other two anemometers (seen on the left side of figure 4.18) are owned by the Administration Waterways and Marine Affairs and Flanders Marine Institute of the Government of the Flemish Community as a part of the Monitoring Network Flemish Banks



Figure 4.18: Anometers placed on the measuring jetty provide wind data (wind speed  $v_s$  and wind blowing direction  $\beta$ ).

The anemometer has been calibrated both for wind speed and wind blowing direction in such way that  $\beta = 0^{\circ}$  coincides with a wind blowing from the north. A positive wind blowing direction indicates a wind coming more from the west. The wind blowing direction is

negative when the wind is coming more from the east. The measuring jetty is directed perfectly NW ( $\beta = 45^{\circ}$ ).

#### 4.4.6 Video camera

A video camera, suspended by means of a lever system to the jetty and directed towards the breakwater, makes it possible to visualise wave run-up on and wave overtopping over the breakwater (figure 4.19). The camera is connected to a TV set (with video recorder) placed inside the measuring container and visualises wave run-up on the breakwater. By means of a lever, the camera can be brought on top of the jetty to clean the window of the housing of the camera regularly. This is necessary because of condensation, salt intrusion,... in the housing.



Figure 4.19: Video camera suspended on the measuring jetty and directed towards the armour layer units of the breakwater.

## 4.4.7 Wave overtopping and spray measurement devices

Wave overtopping is measured by means of an overtopping tank. The volume of the tank is about 28 m³ (2 m wide, 7.30 m long and approximately 2 m high) (figure 4.20(a)). The overtopping tank has been placed just behind the crest of the breakwater in order not to obstruct the access road of the breakwater. Green water is collected in the overtopping tank. The volume of water (the water height in the overtopping tank) is measured by water pressure measurements at the bottom of the overtopping tank. The water height measurements are

based on the principle of communicating barrels. To ensure a continuous measurement of wave overtopping, a V-shaped compound weir is an integral part of one of the side walls of the overtopping tank (figure 4.20(b)). The weir controls the continuous outflow of the water. The compound weir has been calibrated carefully both in laboratory and in the field. The discharges at full scale are a little bit lower than the discharges measured in the laboratory.





Figure 4.20: View (a) on the overtopping tank from the quay behind the crest of the Zeebrugge breakwater and (b) on the compound weir from inside the overtopping tank.

Four wave detectors have been placed on the crest of the breakwater in front of the overtopping tank (figure 4.21). The wave detectors allow the measurement of the number, the location and the extent of the overtopping waves. Each time an overtopping wave passes the crest of the breakwater, it submerges the wave detector(s) and the overtopping wave is registrated.

Spray measurements are carried out by means of six conventional rain gauges, placed at distinct distances (x = 0 m, x = 20 m, x = 60 m, x = 90 m, x = 150 m and x = 1000 m) behind the crest of the breakwater on a pedestal (figure 4.22). The most remoted rain gauge is the reference gauge. It is supposed to measure only rain intensity and no spray.



Figure 4.21: Wave detectors on the crest of the Zeebrugge breakwater.



Figure 4.22: Position of five of the six rain gauges in Zeebrugge (indicated by white circles).

## 4.5 Offline data processing.

The computer language LabView<sup>TM</sup> of National Instruments has been used to write the analysis programme. LabView<sup>TM</sup> is very user and data friendly programming language. It is a graphical programming language which makes use of icons and wires to connect icons in stead of text lines to create applications. LabView<sup>TM</sup> allows the creation of virtual interfaces ('panel') to show data and/or to display analysis results. A data analysis programme has been developing for several years. A description of the data processing method is given hereafter.

Firstly, the raw data are edited, i.e. the quality is checked. Therefore, an overview is made of the measured time series over a long period (several days/weeks). The important, valuable and useful storm events are selected by these overviews.

A flow chart of the data analysis programme has been given in figure 4.23. Before running the actual data analysis programme. data of the info file must be read in. The info file contains general information about the measured storm event, a.o. a time indication, the number of raw files, the number of channels, the instrumentation with their calibration factors and co-ordinates,... The analysis programme offers the opportunity to select the starting and ending point in time of the time series to be analysed. The measuring devices of which data has to be analysed also need to be selected. The possibility to apply moving (overlapping) data windows is offered. When the computer programme is run, data within the selected period of time and measured by the selected channels are read in from the respective RAW files. The raw data are subsequently transformed into the desired unit (mwc [m], level [m] or pressure [kPa]) and displayed on the monitor screen before analysis. The density of the salt water ( $\rho_{ws} = 1.026 \text{ kg/m}^3$ ) has been taken into account for this conversion. The data collected by each measuring device is treated in a different way. Pressure sensor or infrared meter data are used to calculate the SWL as the average of all data within the selected time series. The spiderweb data and the run-up gauge data are used to calculate the wave run-up levels. The wave rider data are used to calculate the wave characteristics both in time domain and in frequency domain. The data of the second wave rider have been used to determine the wave characteristics. When the second wave rider was absent, the data of the first wave rider have been used.

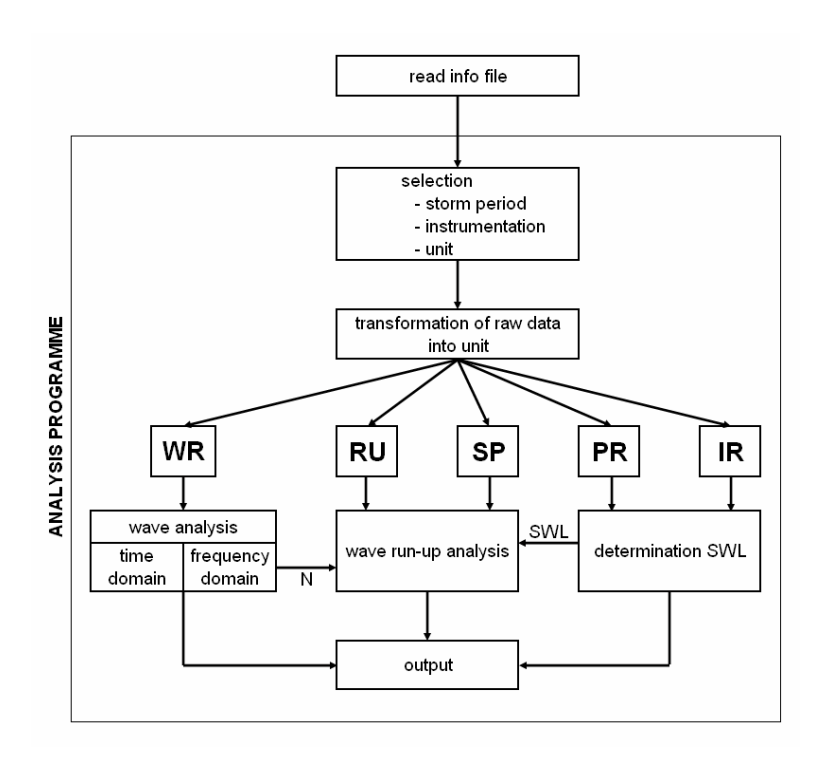


Figure 4.23: Flow chart of data analysis programme.

#### 4.5.1 Wave rider data

Wave data are analysed in both frequency domain and time domain.

# (i) Frequency domain analysis of wave data

In order to obtain the most reliable estimation for the spectrum, the recommendations given by Sand (1985) are followed. Firstly, the width  $\delta$  of the narrowest peak in the spectrum (which is in most cases  $6.10^{-2}$  to  $2.10^{-2}$  Hz) is estimated. If not already given, the length of the time series  $T_0$  is determined by  $T_0 \sim v/\delta$  where the number of degrees of freedom v is at least 30 to 40. The required record length  $T_0$  has to be at least 2000 s. The bandwidth b must lie in the interval  $0.5 \delta$  to  $\delta$  which gives the length of each subseries as  $M \sim 2/\delta$ . The smoothing occurs by application of a spectral window. It can be proved that, as far as it concerns the mean value, application of the Bartlett window corresponds to splitting up the actual time series into a number of subseries.

The Bartlett spectral window is a weighting figure with a base width of the order 2/M. Some years ago, the subseries had to have a length which was a power of 2. But since computational time needed to DFT in stead of FFT a time series does not make a big difference, this restriction can be omitted. One has to find a compromise between the variance and bias of each specific situation.

Input parameters of the computer programme are the number of samples in the data window (length of the time series), the number of samples over which the data window is shifted in case the data window is smaller than the total length of the time series, the number of samples in one subseries and the number of overlapping samples in the subseries. For wave data analysis, windows of  $1024 (= 2^{10})$  samples are used with 20% (204 samples) overlap (Schlütter and Frigaard (1999)). The selected time series is tapered with a cosine data window. A cosine data window is equivalent to a Hanning window over the first and the last 10% of the input sequence. By applying a cosine data window, the total energy content of the signal decreases. This decrease is compensated by multiplying time series by factor  $\sqrt{\sigma_{before\ taperling}^2/\sigma_{after\ taperling}^2}$  where  $\sigma^2$  is the variance of the time series.

Further, the Fourier transform of the time series is calculated, as well as the number of degrees of freedom and the 90% confidence bands for the mean value of the several estimates of the spectrum. Using windows of 1024 samples with 20% overlap results in a 90% confidence interval for the spectrum S(f) of  $[0.846\ S(f),\ 1.203\ S(f)]$  and a frequency resolution of  $\Delta f = 0.012\ Hz$ . The number of degrees of freedom depends on the length of the selected time series. The mathematical mean value of the several estimates of the same spectrum is the most reliable spectrum. The spectrum is drawn and shown on the screen.

Various wave periods have been calculated:  $T_{-1,0}$  [s],  $T_{01}$  [s] and  $T_{02}$  [s] according to (2.5).

# (ii) Time domain analysis of wave data The significant wave height H. [m] is define

The significant wave height  $H_s$  [m] is defined as the average of the highest one-third of the individual wave heights found

by the zero down crossing method. This method is described in a document supplementary to PIANC bulletin n° 52. The average wave period  $T_m$  [s] is the average of all individual wave periods found by applying the zero down crossing method to the time series.  $T_m$  equals the ratio of the length in time of the analysed time series  $T_0$  over the number of waves N.

Other calculated wave characteristics are  $H_{max}$ ,  $T_{max}$ ,  $H_{mean}$ ,  $T_{mean}$ ,  $H_{rms}$  and  $T_{rms}$ .  $T_{max}$  is the maximal wave period encountered in the wave train. All these parameters are calculated by a module in the LabVIEW<sup>TM</sup> environment.

All wave characteristics are written to an ASCII file and can be opened in any worksheet (EXCEL, Wordpad,...) for further processing.

# 4.5.2 Spiderweb system data

The algorithm to calculate the wave run-up levels out of the spiderweb data is as follows. Every 0.1 s, each step gauge measures the instantaneous water surface elevation. Each step gauge is awarded a code according to its immersion:

- step gauge is completely dry  $\rightarrow$  code 0
- step gauge is partly submerged → code 1
- step gauge is completely submerged  $\rightarrow$  code 2

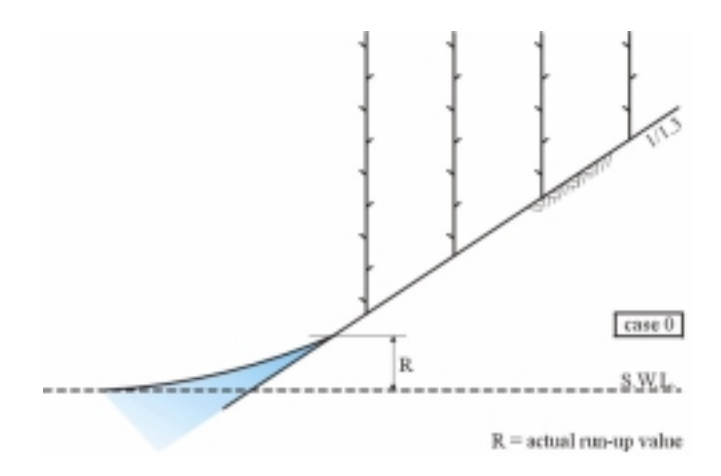


Figure 4.24: Case 0 (all step gauges are dry).

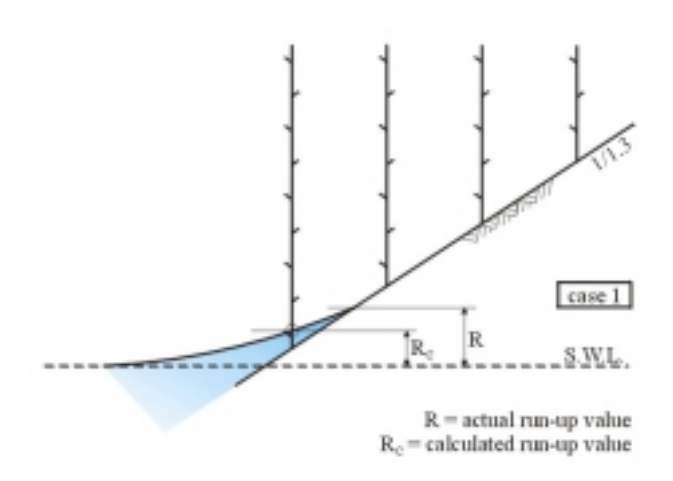


Figure 4.25: Case 1 (only one step gauge is (partly) submerged).

On the basis of these codes, a number is calculated. This number characterises the state of all step gauges at that particular moment. These numbers are tested to a criterium and are divided into three cases:

- case 0: all step gauges are dry (figure 4.24)
- case 1: only one step gauge detects the water surface (figure 4.25)
- case 2: more than one step gauge is (partly) submerged (figure 4.26)

In case 0, the wave run-up level is set to  $Ru = -\infty$ . In case 1, the level of the water surface detected by the only wet step gauge is taken as the wave run-up level. In case 2, the two most landward step gauges which have been awarded code 1 are detected. The x position of these two step gauges  $(x_{SP1}, x_{SP2})$  as well as the level of the water surface detected by each of these two gauges  $(z_{SP1}, z_{SP2})$  are registered. The intersection point of the straight line determined by  $(x_{SP1}, z_{SP1})$  and  $(x_{SP2}, z_{SP2})$  and the best fitting line through all mounting points of the step gauges of the spiderweb system is calculated. The level of the calculated intersection point is subjected to the check whether this 'calculated wave run-up level' is higher than the base of a more landward dry step gauge or not. In case the answer to this test is positive, the base of the more landward placed dry step gauge is taken as wave run-up

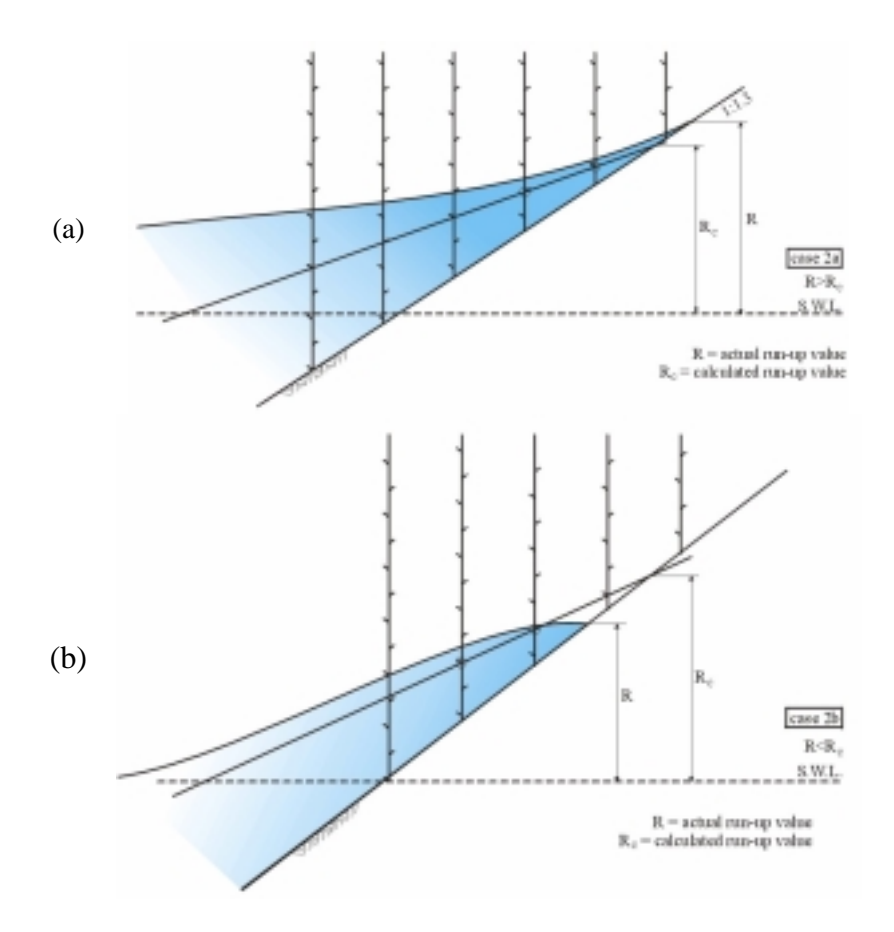


Figure 4.26: Case 2 (more than one step gauge is (partly) submerged).

level. When the answer is negative, the level of the intersection point is taken as the wave run-up level. When this method is followed for every single sample, a wave run-up time series is obtained. The peaks in the wave run-up signal to  $-\infty$  are eliminated by creating a smooth change between adjacent points which have a value different from  $-\infty$ . The signal of the wave run-up level is deduced with the SWL as wave run-up is the run-up height relative to the SWL. By a simple zero down crossing method, wave run-up and wave run-down are detected. Placing these values in descending order allows a statistical analysis and the determination of  $Ru_{x\%}$  values, wave run-up distributions,...

The slope of the breakwater has been taken equal to 1/1.3 = 0.769. This value is based on the data of the measuring campaign carried out by Eurosense on September  $17^{th}$ , 1992 and the calculations found in Versluys (1999). The co-ordinates of the middle of the upper surfaces of each single armour unit have been measured (figure 4.27). When all armour units within the zone [-5 m left of the axis of the measuring jetty, +5 m right of the measuring jetty] are taken into account, the regression line through all the centres of the upper surfaces of these armour units has the equation:

$$Z = -0.78x + 16.16 \tag{4.1}$$

So, the use of  $\tan \alpha = 1/1.3 \cong 0.769$  for the breakwater slope is justified. Equation (4.1) has been used to calculate the wave runup level with the SP measurement data. When a regression line is drawn through the toes of all step gauges of which the coordinates are given in table 4.2, the slopes of the regression lines are:

• 1999/2000 set-up:  $\tan \alpha = 0.746$ • 1998 set-up:  $\tan \alpha = 0.900$ • 1995 set-up:  $\tan \alpha = 0.907$ 

The location of the toe of the step gauges approached the measured slope of 1/1.3 the best during the storm events measured in 1999 and 2000.

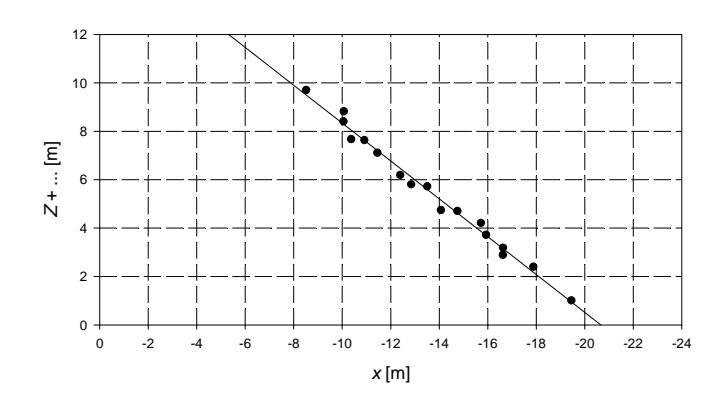


Figure 4.27: Position of the centres of the upper surface of all armour units within the zone [-5 m left of the axis of the measuring jetty, +5 m right of the measuring jetty].

# 4.5.3 Run-up gauge data

An example of a wave run-up signal obtained by the run-up gauge is displayed in figure 4.28. Whenever the level of the water surface on the breakwater slope is lower than Z+6.12 m (dashed line in figure 4.28), the run-up gauge detects no wave run-up (Ru level equals 0). The computer programme detects all peak values. These are reduced with the SWL to obtain the run-up values. Statistics are performed on these run-up values.

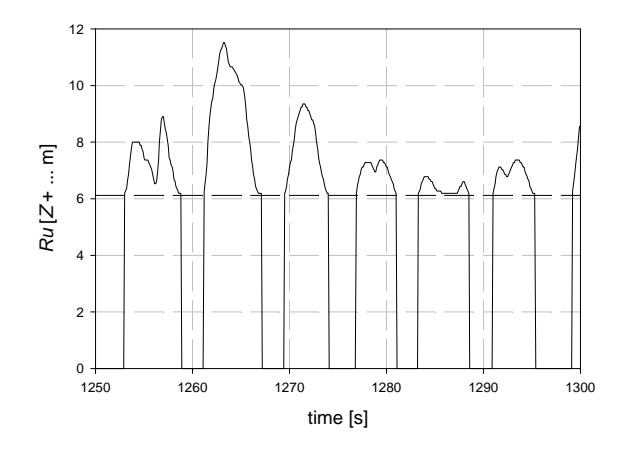


Figure 4.28: Example of wave run-up signal obtained by the run-up gauge (storm event of November 6<sup>th</sup>, 1999 (11h30 to 13h30)).

### 4.6 Analysis of data

For the storms taken place in 1995 and 1998 (storm events n° 1a, 2a, 3a and 4), the infrared meter measurements are not available because of a broken power supply of the infrared meter. For the storms n° 2a, 3a, 4 and 5, the *SWL* has been calculated using the data obtained by the pressure sensor 383 (at the pile). For all storms which have been observed in 1999 or in 2000 (i.e. storm events n° 5 to 13), the infrared meter measurements have been used to calculate the mean water level. During all storms wave run-up has been measured by the spiderweb system (SP). All storms of 1999 (i.e. storm events n° 5, 6 and 7) have additional to the spiderweb system three run-up gauges placed on the armour units parallel to the breakwater slope (five run-up gauges for storms n° 8, 9, 10, 11, 12 and 13). Data measured by the second step gauge of the spiderweb system have not been used when

analysing the data of the 1999 storms and later storms. The sixth step gauge of the spiderweb system was not available during the 1995 storms (i.e. storm events  $n^{\circ}$  1a and 2a). The second wave rider (WRII) was not present in 1999 and 2000, so the first wave rider (WRI) measurement data have been used for wave analysis for storm events  $n^{\circ}$  8 to 13. In table 4.3, the operational measuring devices per storm event are listed.

**Table 4.3: Instrumentation.** 

storm event n°	WRI	WRII	∝	A R	SP1	SP2	SP3	SP4	SP5	SP6	RU <sup>(*)</sup>	RU <sup>(**)</sup>
1 <sup>a</sup>	(x)	Х		Х	Х	Х	Х	Х	Х			
<b>2</b> <sup>a</sup>	(x)	Х		Х	Х	Х	Х	Х	Х			
3 <sup>a</sup>	(x)	Х		Х	Х	Х	Х	Х	Х	Х		
4	(x)	Х		Х	Х	Х	Х	Х	Х	Х		
5	(x)	Х	Х		Х		Х	Х	Х	Х	Х	
6	(x)	Х	Х		Х		Х	Х	Х	Х	Х	
7	(x)	Х	Х		Х		Х	Х	Х	Х	Х	
8	Х		Х		Х		Х	Х	Х	Х	Х	Х
9	Х		Х		Х		Х	Х	Х	Х	Х	Х
10	Х		Χ		Χ		Χ	Х	Χ	Х	Х	Х
11	Х		Χ		Χ		Χ	Х	Χ	Х	Х	Х
12	Х		Х		Х		Х	Х	X	Х	Х	Х
13	Х		Х		Х		Х	Х	Х	Х	Х	Х

<sup>(\*)</sup> lower 3 parts

When wind is blowing parallel to the axis of the bridge and landwards, the output value of the wind direction channel of the anemometer equals zero. A wind blowing from the south has a positive value, whereas a northern wind results in a negative value.

The moment in time of high water is noted as  $t_{HW}$ . The  $i^{th}$  hour before and the  $i^{th}$  hour after this moment  $t_{HW}$  are respectively  $t_{HW}$ -i and  $t_{HW}$ +i. Only during a period of time of two hours symmetric

<sup>(\*\*)</sup> upper 2 parts

<sup>(</sup>x) has not been used for analysis purposes

<sup>&</sup>lt;sup>a</sup>: time series slightly different from these in chapter 5

around the moment in time of high water [ $t_{HW}$ -1,  $t_{HW}$ +1], the SWL (i.e. the water level without wave action) in front of the Zeebrugge breakwater is almost constant. Because of the changing water depth (SWL) in front of the structure, the length of the time series is important when half a tide cycle is analysed as the wave run-up value is calculated relative to a constant water level. Thirty minutes time series have been analysed in the study of wave run-up within half a tide cycle (symmetric in time with regard to  $t_{HW}$ ). The  $Ru_{x\%}/H_{m0}$  values for the periods  $[t_{HW}-3,t_{HW}-2)]$ ,  $[t_{HW}-2,t_{HW}-1)], [t_{HW}+1,t_{HW}+2)], [t_{HW}+2,t_{HW}+3)]$  are the average values of the two values found analysing the successive 30 minutes time series within the one hour period. The  $Ru_{x}/H_{m0}$ value for the period  $[t_{HW}-1, t_{HW}+1]$  is the average value of the four successive 30 minutes time series within the two hour period. Wave run-up always has been referred to the SWL within the analysed 30 minutes period.

# 4.7 Analysis results

## 4.7.1 Wave characteristics

The Pearson  $\chi^2$  test and the test of Kolgomorov-Smirnov (see Annex F) have been performed on wave height data measured during storm event n° 8. The null hypothesis  $H_0$  reads: 'Wave heights are Rayleigh distributed'. For the Pearson  $\chi^2$  test, the test variable  $D_I$  equals 21.65, which is larger than the critical value  $\chi^2_{10,0.95} = 18.307$ , so the null hypothesis is not accepted. The test variable of the test of Kolgomorov-Smirnov  $D_2$  equals 0.0286 which is smaller than the critical value  $c_{0.95} = 0.0382$ . The null hypothesis is accepted. The test of Kolgomorov-Smirnov has a greater power than the Pearson  $\chi^2$  test (Taerwe (1996)). It is concluded that wave heights in Zeebrugge are Rayleigh distributed.

The waves in Zeebrugge are characterised as mainly non-breaking. According to (2.19), a wave with a significant wave height  $H_s$  of 3 m breaks in shallow water when  $d < H_s/0.40 = 7.50$  m. According to (2.22), a wave with a significant wave height  $H_{m0}$  of 3.5 m breaks when d < 5.83 m. This water depth is available most of the time (certainly at high water!).

Additional wave data analysis resulted in table 4.4. For WRI and WRII, the data of storm events n° 3 to 7 have been taken into account, for the IR measurements the data of storms events n° 5

to 13 and for the PR measurements only the data of storm events  $n^{\circ}$  1 and 2.

Table 4.4: Ratio of the measured wave characteristics with the different measuring devices.

	the united the intensating devices.											
	$H_s$ [m]	$H_{mo}$ [m]	$T_{\rho}$ [s]	$T_{01}[s]$	$T_{mean}$ [s]							
WRI/WRII	0.97	0.98	0.97	0.99	0.99							
IR/WRI	0.78	0.74	0.73	0.80	0.78							
IR/WRII	0.78	0.74	0.62	0.80	0.81							
PR/WRI	0.60	0.60	0.83	1.05	1.17							
PR/WRII	0.58	0.58	0.83	1.03	1.13							

Following conclusions can be drawn from table 4.4:

- •WRI and WRII measure almost the same waves (wave height and wave periods)
- •the infra red meter measures smaller wave heights  $(0.74 H_{s,WR})$  than the wave riders and measures smaller wave periods than the wave riders
- •the pressure sensor at the pile supporting the measuring jetty measures smaller pressure variations than expected by the wave rider measurements ( $H_{s,PR} \cong 0.6 \ H_{s,WR}$ !), a larger mean wave period than the wave riders and a shorter peak wave period than the wave riders. This longer period is probably due to an attenuation of the wave action by molluscs and other dirt obstructing the opening in the tube by which the PR sensor is protected.

The consequences of the findings above force not to use the PR or the IR measurements for wave analysis. Indeed, these instruments have been used only to determine the *SWL* (tidal waves).

The spectral sea state parameters are calculated using data windows of 1024 data points with 20% overlap ( $\cong$  204 samples).

Table 4.5 gives an overview of the most important wave characteristics measured during all 13 storms. The values of the significant wave height  $H_s$  and the mean wave period  $T_m$  in time domain, the significant wave height  $H_{mo}$ , the peak period  $T_p$ , the mean wave period  $T_{01}$ , the spectral width parameter  $\varepsilon$  and the

peakedness parameter  $Q_p$  in frequency domain are listed. All sea state parameters are measured at wave rider II (215 m from breakwater slope). Only for the last 6 storm sessions (that is to say storm n° 8, 9, 10, 11, 12 and 13), the recorded data of wave rider I ( $\pm$  150 m from the structure) are used, due to the absence state parameters, a time series with a duration of  $\Delta t = 3600$  s is used. I and II is very small (less than 5%). For the calculation of the sea of wave rider II. The difference between the results of wave rider

Table 4.5: Wave characteristics

storm n°	$H_s$ [m]	$T_m[s]$	$H_{m0}$ [m]	$T_{p}[s]$	$T_{01}[s]$	$\varepsilon$ [-]	$Q_{\rho}$ [-]	$\xi_{om}$ [-]	$\xi_{op}$ [-]	
1 <sup>a</sup>	2.65	5.69	2.73	7.31	6.16	0.5832	2.156	3.58	4.25	
2 <sup>a</sup>	2.55	5.75	2.68	7.88	6.31	0.5826	1.747	3.70	4.62	
3 <sup>a</sup>	2.77	5.95	2.89	8.53	6.68	0.6103	1.704	3.77	4.82	abi
4	2.87	6.02	3.00	8.53	6.61	0.6010	1.688	3.67	4.73	e 4:
5	3.00	5.89	3.12	8.53	6.57	0.5884	1.985	3.57	4.64	:: <b>₹</b>
6	2.41	5.56	2.52	7.88	6.26	0.6006	1.621	3.79	4.77	ave
7	2.78	5.62	2.90	8.53	6.32	0.5664	2.077	3.57	4.82	cnar
8	2.89	5.69	3.04	7.31	6.29	0.6166	2.591	3.47	4.03	acte
9	2.44	5.36	2.54	9.31	6.31	0.5642	1.725	3.81		
10	2.71	5.54	2.85	7.31	6.07	0.6126	2.431	3.46	4.17	S
11	2.48	5.37	2.58	7.31	5.87	0.5829	2.480	3.51	4.37	
12	2.35	5.34	2.43	7.88	5.87	0.5407	2.265	3.62	4.86	
13	2.28	5.64	2.39	7.88	6.16	0.5641	2.115	3.83	4.90	

## 4.7.2 Wave run-up

In paragraph 3.3, two methods have been presented to derive a characteristic value  $Ru_{x\%}$  from a measured wave run-up distribution. The **first method** is a direct method. The wave run-up level for which p/(N+1) equals 0.02 when wave run-up levels are put in descending order, is  $Ru_{2\%}$ . The **second method** approximates the wave run-up distribution by a theoretical distribution (Weibull, Rayleigh,...). The distributions are fit to the measurement data and characteristic wave run-up values are derived from these.

Both methods enable to derive a  $Ru_{2\%}$  value from the measured wave run-up distribution curves have been applied on the field measurement data of storm event n° 8 (November 6<sup>th</sup>, 1999 (11h30 to 13h30)). Figures 4.29 to figure 4.32 show the wave run-up distributions for time series with a length of two hours, resp. one hour, thirty minutes and fifteen minutes. The  $Ru_{2\%}$  values corresponding to the first method for the four different lengths of the time series are given in table 4.6.

Using the maximum likelihood method (see Annex A), the Weibull distribution (3.7) has been fit to the measurement data (figures 4.29 to 4.32). Also the Rayleigh distribution has been fit to the measurement data (figures 4.29 to 4.32) by means of the method of moments and/or the likelihood method (see Annex A). Not much difference is seen between the fit Weibull distribution and the fit Rayleigh distribution. The estimations of  $a_t$  and  $b_t$ ,  $\hat{a}$ and  $\hat{b}$  for the Weibull distribution are given in table 4.7. Using the values of  $\hat{a}$  and  $\hat{b}$  in (3.7), the  $Ru_{2\%}$  values mentioned in the last column of table 4.7 are obtained. These values are on average 9% lower than the  $Ru_{2\%}$  values obtained by the first method. The 95% confidence intervals of  $\hat{a}$  and  $\hat{b}$  are given in table 4.8. These have been calculated assuming the log normal distribution of a and b:  $P[|a - a_t| > k.\sigma_a] = 5\%$  with k = 1.95996. The probability that a and b are both in these intervals is  $0.95^2 =$ 0.9025. Thus, the (approximately) 90% confidence intervals of  $Ru_{2\%}$  are calculated combining the boundary values of the confidence intervals of  $\hat{a}$  and  $\hat{b}$  are also given in table 4.8. For the Rayleigh distribution, the estimation of  $a_t$  is  $\hat{a}$  and is given in table 4.9, together with the  $Ru_{2\%}$  value calculated by (3.16) and the estimated value  $\hat{a}$ , as well as the 95% confidence interval of  $\hat{a}$ . This confidence interval has been calculated assuming the log

normal distribution of a:  $P[|a - a_t| > k.\sigma_a] = 10\%$  with k = 1.645. The two boundary values of the confidence interval of  $\hat{a}$  has been used to calculate the 90% confidence interval of  $Ru_{2\%}$ , given in table 4.9.

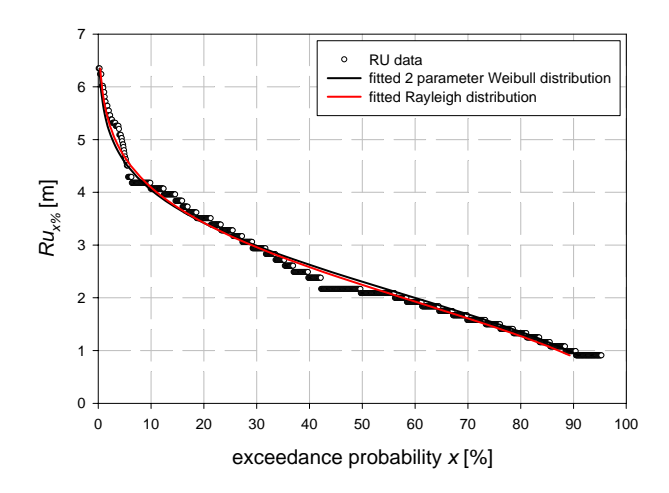


Figure 4.29: Weibull distribution and Rayleigh distribution fitted to wave run-up data (RU) gathered during the storm event n°8 (length of time series: 2 hours).

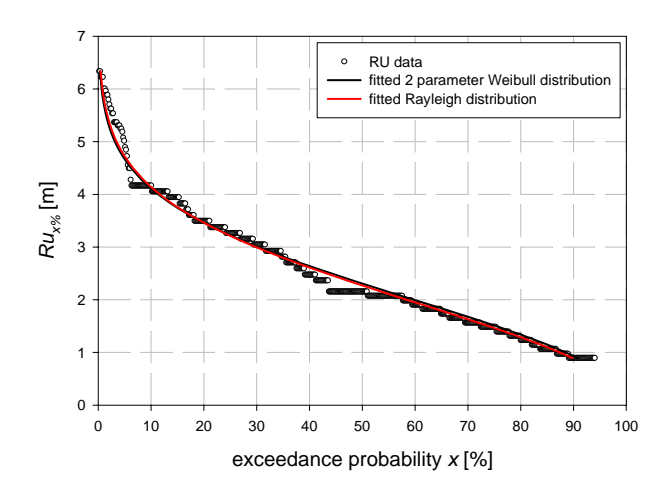


Figure 4.30: Weibull distribution and Rayleigh distribution fitted to wave run-up data (RU) gathered during the storm event  $n^{\circ}$  8 (length of time series: 1 hour).

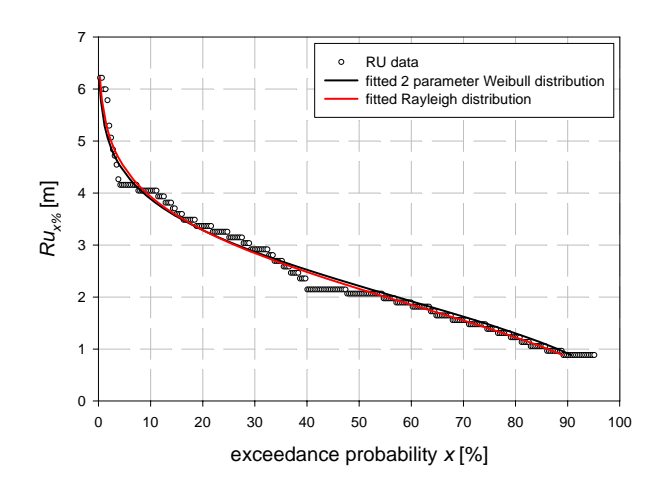


Figure 4.31: Weibull distribution and Rayleigh distribution fitted to wave run-up data (RU) gathered during the storm event  $n^{\circ}$  8 (length of time series: 30 minutes).

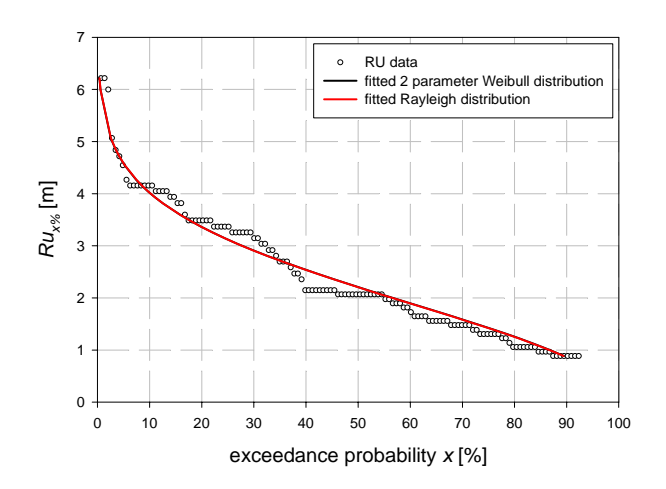


Figure 4.32: Weibull distribution and Rayleigh distribution fitted to wave run-up data (RU) gathered during the storm event  $n^{\circ}$  8 (length of time series: 15 minutes).

Table 4.6: Wave run-up value according to the first method p/(N+1) = 0.02.

storm event	$\Delta t$	<i>Ru</i> <sub>2%</sub> [m]
November 6 <sup>th</sup> , 1999 (11h30 to 13h30)	2h	5.55
November 6 <sup>th</sup> , 1999 (12h30 to 13h30)	1h	5.76
November 6 <sup>th</sup> , 1999 (12h30 to 13h00)	30min	6.03
November 6 <sup>th</sup> , 1999 (12h30 to 12h45)	15min	5.42

Equations (3.8), (3.9) and (3.22) indicate the dependency of the confidence intervals of a and b on the number of wave run-up events:  $\sigma_a$  and  $\sigma_b$  are inversely proportional to the square root of N. As a consequence, the confidence intervals of  $Ru_{2\%}$  will also be approximately inversely proportional to the number of wave run-up events. Indeed, for the investigated storm event, the confidence for a time series of 15 minutes is 1.16 m wide. For a thirty minutes time series, the confidence interval is 0.96 m wide. For a time series of one hour and a time series of two hours, the confidence intervals are approximately 0.56 m, resp. 0.42 m wide. The more wave run-up events are taken into account and thus, the longer the considered time series, the smaller the confidence interval of the Ru<sub>2%</sub> value and thus, with the more confidence the Ru2% value can be determined. Comparing the  $\Delta Ru_{2\%}$  values in table 4.8 and table 4.9, it can be concluded that the Rayleigh distribution yield smaller 90% confidence intervals than the two parameter Weibull distribution.

Table 4.7: Values of parameters a and b of the fitted Weibull distribution and the Ru<sub>2%</sub> value for different lengths of time

Series.								
	а	b	<i>Ru</i> <sub>2%</sub> [m]					
15min <sup>(1)</sup>	2.005	2.651	5.23					
30min <sup>(2)</sup>	2.133	2.628	4.98					
1h <sup>(3)</sup>	2.080	2.753	5.30					
2h <sup>(4)</sup>	2.135	2.737	5.18					

<sup>(1):</sup> November 6<sup>th</sup>, 1999 (12h30 to 12h45) (2): November 6<sup>th</sup>, 1999 (12h30 to 13h00) (3): November 6<sup>th</sup>, 1999 (12h30 to 13h30) (4): November 6<sup>th</sup>, 1999 (11h30 to 13h30)

Table 4.8: Confidence intervals of fitted Weibull distribution for different lengths of time series.

	confidence intervals							
	ć	Э		b	Ru <sub>2</sub>	<sub>%</sub> [m]	∆ <i>Ru</i> ₂% [m]	
15min <sup>(1)</sup>	1.903	2.109	2.450	2.852	4.68	5.84	1.16	
30min <sup>(2)</sup>	2.042	2.224	2.448	2.808	4.52	5.48	0.96	
1h <sup>(3)</sup>	2.029	2.131	2.652	2.854	5.03	5.59	0.56	
2h <sup>(4)</sup>	2.095	2.175	2.657	2.817	4.98	5.40	0.42	

Table 4.9: Values of parameter a of the *Rayleigh distribution*, the  $Ru_{2\%}$  value and the confidence intervals of a and  $Ru_{2\%}$ .

	a	<i>Ru</i> <sub>2%</sub> [m]	confidence intervals					
		[]		a	Ru <sub>29</sub>	<i>∆Ru</i> <sub>2</sub> <sub>%</sub> [m]		
15min <sup>(1)</sup>	1.873	5.24	1.687	2.059	4.72	5.76	1.04	
30min <sup>(2)</sup>	1.832	5.12	1.701	1.963	4.76	5.49	0.73	
1h <sup>(3)</sup>	1.929	5.40	1.833	2.026	5.13	5.67	0.54	
2h <sup>(4)</sup>	1.907	5.34	1.840	1.975	5.15	5.53	0.38	

A fifteen minutes time series only contains a limited number of wave run-up events, leading to a rather inaccurate estimation of  $Ru_{2\%}$ . This result pleads in favour of using a longer period of time for the estimation of the 2% wave run-up level. The errors introduced by considering the sea state to be constant during a longer time period (maximum  $0.5\Delta SWL$ ) will be rather small compared to the statistical inferences, especially for a time period symmetric around high tide or low tide.

The change in *SWL* during the period of approximately 2 hours at high tide as well as the variation in *SWL* using five minutes time series, the maximum and the minimum value of the *SWL* during the two hour period is indicated in table 4.10 for all considered storm events. During this period of two hours, the water level is esteemed to be constant at *SWL*. For all analysed storm events, the maximum error is  $(0.5\Delta SWL_{max}) = 0.35$  m, i.e. 12.6% of the

(average) significant wave height. The variation of *SWL* is assumed to be negligible.

Table 4.10: \( \Delta SWL \) for all storm events during the two hours period at high water during which the water level is assumed to be constant.

	to be constant.										
storm n°	SWL	$SWL_{max}^{(*)}$	$SWL_{min}^{(*)}$	$\Delta SWL$							
Storm	[ <i>Z</i> + m]	[ <i>Z</i> + m]	[Z+ m]	[Z+ m]							
1 <sup>a</sup>	5.45	5.62	5.30	0.32							
$2^{a}$	5.20	5.33	4.96	0.37							
$3^{a}$	4.84	4.91	4.69	0.22							
4	4.35	4.46	4.19	0.27							
5	5.07	5.21	4.95	0.26							
6	5.38	5.56	5.01	0.54							
7	5.19	5.40	4.72	0.69							
8	5.28	5.37	5.09	0.28							
9	5.11	5.26	4.82	0.44							
10	5.30	5.40	5.10	0.30							
11	4.65	4.74	4.52	0.22							
12	5.34	5.52	5.15	0.37							
13	5.04	5.21	4.73	0.48							

<sup>(\*)</sup> calculated using 5 minutes time series

Further on, the first method (direct method) for determining the  $Ru_{2\%}$  value will be used because this value will be the closest to the measurement data without having already introduced an error by fitting a standard distribution (Weibull, Rayleigh) to the data. This way of working is justified when a large time series is used so that the error on determining the  $Ru_{2\%}$  value is small. Also the (easy to apply) Rayleigh distribution will be used further on instead of the more complex Weibull distribution (two or more parameters). Not much difference is seen between both distributions when long time series are considered.

From the wave run-up distributions (Annex B), it is seen that no wave overtopping occurred at the location of the wave run-up measuring devices during the measured storm events. In the wave run-up distributions, the feet of the step gauges of the spiderweb system have been indicated as well as the crest level situated at Z + 12.39.

All wave run-up distributions obtained by analysing 'spiderweb system' (SP) data show large 'platforms' at distinct levels (see Annex B). The levels correspond to the levels of the bases of the step gauges of the spiderweb system relative to SWL. The origin of these "platforms" is found within the analysis algorithm. Once more than two step gauges of the spiderweb system are (partly) submerged, the intersection point of the line, determined by the upper electrode of each of the two most landward wet step gauges and the line representing the slope of the breakwater (tan  $\alpha$  = 1/1.3) is calculated. When the level of this intersection point is lower than the level of the lowest electrode of a more landward completely dry step gauge, the level of the calculated intersection point is taken as the wave run-up level. In case the intersection point is higher than the level of the lowest electrode of a more landward placed dry step gauge, the base of this sensor is taken as wave run-up level in stead of the intersection point. When latter case occurs (which happens quite frequently) the by the computer programme determined wave run-up level overestimates the real wave run-up level. This method can have some repercussions on the determination of the  $Ru_{2\%}$  value. It is possible that the  $Ru_{2\%}$ value has its representing point in such a platform. However, when low exceedance probabilities x are considered at large water depths, the  $Ru_{2\%}$  value is located outside the area in which platforms show up (e.g. figure B.3 ( $Ru_{2\%}$  value outside the platform area) in contrast to figure B.13 ( $Ru_{2\%}$  inside the platform area)).

In the run-up distribution, obtained by analysis of the wave runup gauge (RU) data, two smaller 'platforms' can be noticed (see Annex B). In contrast with the earlier mentioned platforms in the run-up distribution of the spiderweb system measurement data analysis, these platforms are not the result of the analysis algorithm, but these are the consequence of the particular placing of the armour units (i.e. gap between 2 elements (at approximately Z + 9.35), one block jumping out a little bit (at approximately Z + 7.45) (figure 4.33) These two small platforms occur in all wave run-up distributions at exact the same level with regard to Z 0.00. The lowest platform is due to the jump in electrodes between the second and the third part of the run-up gauge. When an uprushing wave has too little momentum, it cannot reach on top of the armour unit on which the third part of the run-up gauge is attached to. When the water mass reaching higher levels is too little it cannot overbridge the gaps between the upper armour units and disappears in the hole. Only when the

uprushing water mass is big enough to fill the gap completely with water, another amount of water can slide up the slope and is detected.

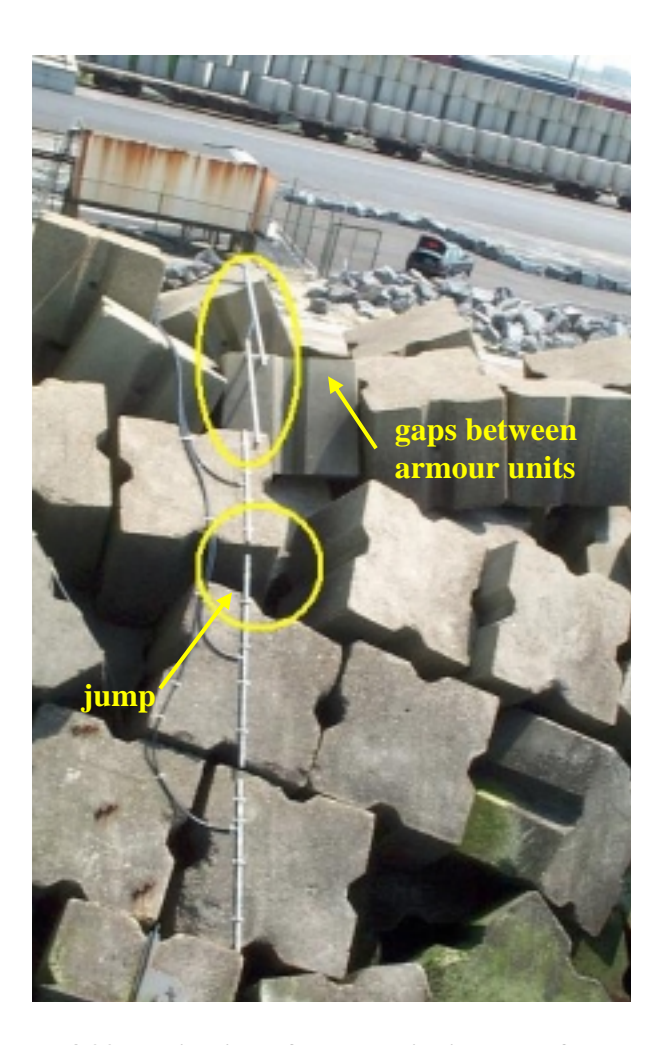


Figure 4.33: Indication of blocks sticking out of the mean slope and gaps between two neighbouring armour units.

The assumptions 'wave run-up is Weibull distributed' or 'wave run-up is Rayleigh distributed' have been tested. Two goodness-of-fit tests have been performed: the Pearson  $\chi^2$  test and the test of Kolgomorov-Smirnov (see Taerwe (1996) and Annex F). The null hypothesis reads:  $H_0$ :  $F_{Ru}(Ru_{x\%}) = F_{Ru,0}(Ru_{x\%})$ .

For the Pearson  $\chi^2$  test, the values of the test variable  $D_I$  based on wave run-up data collected during the storm of November  $6^{th}$ , 1999 has been given in table 4.11.

Table 4.11:  $D_1$  values (Pearson  $\chi^2$  test).

1 · · · · · · · · · · · · · · · · · · ·								
length time series	Weibull	Rayleigh						
2 hours	137	135						
1 hour	83	83						
30 minutes	37	36						
15 minutes	33	33						

The critical  $\chi^2$  value has been calculated based on k-r-1=13-0-1=12 degrees of freedom. k is the number of classes. r is put equal to zero because  $F_{Ru,0}(Ru_{x\%})$  has been fully (shape and parameters) prescribed (single hypothesis). The critical zone is  $D_I > \chi^2_{12,1-\alpha}$ .  $\alpha$  has been chosen 5%, so  $\chi^2_{12,0.95} = 21.026$ . The null hypothesis cannot be accepted, nor for the Weibull distribution, nor for the Rayleigh distribution. For  $\alpha = 0.01$ ,  $\chi^2_{12,0.99} = 26.217$ . Even with  $\alpha = 0.01$ , the null hypothesis is rejected, which means that wave run-up is not Rayleigh or Weibull distributed.

For the test of Kolgomorov-Smirnov, the null hypothesis is formulated as  $H_0$ :  $D_2 \le c_{1-\alpha}$ . The values  $c_{1-\alpha}$  are approximated by

$$c_{0.95} = \frac{1.3581}{\sqrt{n}} \tag{4.2}$$

$$c_{0.99} = \frac{1.6276}{\sqrt{n}} \tag{4.3}$$

with n = number of wave run-up events. The values of the test variable  $D_2$  based on wave run-up data collected during the storm of November  $6^{th}$ , 1999 have been given in table 4.12.

Only for time series of 15 minutes under the test of Kolgomorov-Smirnov, the null hypothesis is accepted as  $D_2 < c_{0.95}$  for both the Weibull and Rayleigh assumption.

Table 4.12:  $D_2$  values (test of Kolgomorov-Smirnov).

length time series	n	D <sub>2,Weibull</sub>	$D_{2,Rayleigh}$	<b>C</b> <sub>0.95</sub>	C <sub>0.99</sub>
2 hours	1092	0.1021	0.1063	0.041	0.049
1 hour	536	0.0904	0.1004	0.059	0.070
30 minutes	273	0.1346	0.1219	0.082	0.099
15 minutes	132	0.0973	0.0980	0.118	0.142

Based on statistical tests, it is concluded that wave run-up on the Zeebrugge rubble mound breakwater is not exactly Weibull or Rayleigh distributed. Wave run-up is approximated by a Weibull or a Rayleigh distribution. The rejection of the null hypothesis is probably due to the geometry of the breakwater. The difference between the Weibull distribution and the Rayleigh distribution is very small. Further on, the Rayleigh distribution has been used.

Table 4.13: Full scale wave run-up measurement results (run-up gauge, 9 storms, from  $t_{HW}$ -1 to  $t_{HW}$ +1, 2 hours time series)

			5	eries).				
storm event n°	$Ru_{max}/H_{mo}$ [-]	Ru1%/H <sub>m0</sub> [-]	Ru <sub>2%</sub> /H <sub>mo</sub> [-]	Ru <sub>5%</sub> /H <sub>mo</sub> [-]	$Ru_{10\%}/H_{mo}$ [-]	$Ru_s/H_{mo}$ [-]	$Ru_{25\%}/H_{mo}$ [-]	$Ru_{50}/H_{m0}$ [-]
5	1.77	1.75	1.74	1.74	1.37	1.34	1.08	0.68
6	2.05	1.63	1.57	1.48	1.26	1.17	0.82	0.65
7	1.84	1.82	1.80	1.43	1.40	1.28	1.01	0.69
8	2.09	1.95	1.82	1.55	1.34	1.30	1.08	0.69
9	2.53	2.14	1.89	1.67	1.45	1.32	1.00	0.76
10	2.19	1.86	1.60	1.46	1.39	1.27	0.99	0.70
11	2.66	2.09	1.86	1.73	1.43	1.29	1.05	0.73
12	2.33	1.70	1.65	1.47	1.28	1.14	0.87	0.70
13	2.38	2.07	1.85	1.54	1.24	1.10	0.94	0.59
μ	2.20	1.89	1.76	1.56	1.35	1.25	0.98	0.69
$\delta$	0.136	0.097	0.068	0.077	0.056	0.069	0.092	0.070

Even with omitting the values at the levels of the platforms, it cannot be concluded that wave run-up is Rayleigh or Weibull distributed.

When time series with a duration of two hours situated at high tide are analysed as a single wave record, the values of table 4.13 for the RU data and table 4.14 for the SP measurements are obtained. The average values  $\mu$  and the variation coefficients  $\delta$  have been given.

Tabel 4.14: Full scale wave run-up measurement results (spiderweb system, 13 storms, from  $t_{HW}$ -1 to  $t_{HW}$ +1, 2 hours time series).

-			ume	series).				
storm event n°	$Ru_{max}/H_{m0}$ [-]	Ru1%/ Hmo [-]	$Ru_{2\%}/H_{m0}$ [-]	Ru <sub>5%</sub> H <sub>mo</sub> [-]	$Ru_{10\%}/H_{mo}$ [-]	$Ru_s/H_{mo}$ [-]	$Ru_{25\%}/H_{m0}$ [-]	$Ru_{5o}/H_{mo}$ [-]
1 <sup>a</sup>	2.07	1.71	1.56	1.51	1.51	1.51	1.51	0.65
<b>2</b> <sup>a</sup>	2.34	1.63	1.63	1.63	1.63	1.63	1.00	0.75
3 <sup>a</sup>	2.19	1.93	1.75	1.64	1.64	1.64	1.64	0.82
4	2.12	1.87	1.79	1.74	1.74	1.74	1.40	0.96
5	2.05	1.92	1.71	1.63	1.42	1.42	1.42	0.72
6	2.43	1.89	1.74	1.63	1.63	1.63	1.63	0.76
7	2.14	1.83	1.71	1.58	1.49	1.49	1.49	0.73
8	2.11	2.01	1.90	1.60	1.39	1.39	1.39	0.97
9	2.48	1.98	1.95	1.73	1.73	1.73	1.73	0.86
10	2.22	1.75	1.70	1.48	1.48	1.48	1.48	0.70
11	2.58	2.08	1.88	1.88	1.88	1.88	1.03	1.03
12	2.49	1.97	1.71	1.71	1.71	1.71	1.71	0.81
13	2.13	1.87	1.87	1.87	1.87	1.87	0.95	0.95
μ	2.26	1.88	1.76	1.66	1.62	1.62	1.41	0.82
δ	0.081	0.067	0.064	0.072	0.098	0.098	0.187	0.146

An average  $Ru_{2\%}/H_{m0}$  value of 1.76 is obtained when the run-up gauge data (9 storms) are processed. The analysis of the SP data (13 storms) also yields an average  $Ru_{2\%}/H_{m0}$  value of 1.76. The average Iribarren number  $\xi_{om}$  is 3.63 (variation coefficient  $\delta = 0.006$ ), resp. 3.64 (variation coefficient  $\delta = 0.0046$ ). The Iribarren

number  $\xi_{om}$  in Zeebrugge varies only between 3.46 and 3.83 for the measured storm events. However, these results are not the correct results. A number of adverse occurrences, intrinsic to the measuring devices disturbed the wave run-up measurements. An important conclusion that is drawn from all wave run-up distribution curves (see Annex B) is that wave run-up on the Zeebrugge breakwater is Rayleigh distributed. This finding helps to determine the correct wave run-up values in cases in which the wave run-up could not be determined correctly.

The determination of the  $Ru_{2\%}$  level in case of wave run-up measurements by means of the spiderweb system does not always yield good results. In the wave run-up distribution curves (see Annex B), a lot of platforms at the level of the fixing points of the lower ends of the step gauges to the armour units are seen. These are the result of the calculation algorithm used to derive wave run-up levels from the spiderweb system measurements. Often, the  $Ru_{2\%}$  value is found within such a platform, which means that the  $Ru_{2\%}$  value in reality is lower than indicated by the algorithm.

Another remark has to be made concerning the results of the storms of February 1999. During three storms (Feb. 7, Feb. 17 and Feb. 22) only the three lowest parts of the five-part run-up gauge were available. Consequently, a truncation is seen in the wave run-up distribution curves of the respective storm events (see Annex B). This is not the case for the other storm events. The  $Ru_x N H_{m0}$  values for low exceedance probabilities x cannot be determined because the highest wave run-up levels reach higher than the upper electrode of the upper part of the run-up gauge. In table 4.13, this is seen by almost equal values of  $Ru_x N H_{m0}$  for low values of x.

A method to determine  $Ru_{2\%}$  in cases where wave run-up measurements 'failed' is by fitting a straight line through the measurements data indicated with red dots in the wave run-up distribution curves (see Annex B). Indeed, a straight line is fitted to the measurement data because wave run-up is assumed to be Rayleigh distributed and the exceedance probability axis is Rayleigh scaled. Once the slope of the straight line a is determined, the  $Ru_{x\%}$  value is calculated by

$$Ru_{x\%} = a\sqrt{-2\ln(x)} \tag{4.4}$$

A method to avoid the fitting procedure is to assume wave run-up to be Rayleigh distributed and to calculate  $Ru_{2\%}$  (or more general  $Ru_{x\%}$ ) directly from the significant wave run-up  $Ru_s$  by means of

$$P[Ru > Ru_{x\%}]_{Ru_s} = \frac{x}{100} = \exp\left(-2\left(\frac{Ru_{x\%}}{Ru_s}\right)^2\right)$$
 (4.5)

or

$$Ru_{x\%} = Ru_{s} \sqrt{-\frac{1}{2} \ln \left(\frac{x}{100}\right)}$$
 (4.6)

with x = 2.

Table 4.15: Full scale *equivalent wave run-up* measurement results (run-up gauge, 9 storms, from  $t_{HW}$ -1 to  $t_{HW}$ +1, 2 hours time series).

			ره	crics).				
storm event n°	Ru <sub>max</sub> /H <sub>mo</sub> [-]	Ru1%/H <sub>m0</sub> [-]	$Ru_{2\%}/H_{mo}$ [-]	$Ru_{5\%}/H_{mo}$ [-]	$Ru_{10\%}/H_{mo}$ [-]	$Ru_{s}/H_{mo}$ [-]	$Ru_{25\%}/H_{mo}$ [-]	$Ru_{50}/H_{m0}$ [-]
5	2.41	1.97	1.81	1.59	1.39	1.30	1.08	0.75
6	2.24	1.83	1.69	1.48	1.30	1.21	1.01	0.70
7	2.34	1.91	1.76	1.54	1.35	1.26	1.05	0.73
8	2.39	1.96	1.80	1.58	1.38	1.29	1.07	0.75
9	2.52	2.06	1.90	1.66	1.45	1.36	1.13	0.79
10	2.26	1.85	1.70	1.49	1.31	1.22	1.01	0.71
11	2.55	2.08	1.92	1.68	1.47	1.37	1.14	0.80
12	2.27	1.85	1.71	1.49	1.31	1.22	1.02	0.71
13	2.38	1.95	1.79	1.57	1.38	1.28	1.07	0.74
μ	2.37	1.94	1.79	1.56	1.37	1.28	1.06	0.74
δ	0.046	0.046	0.046	0.046	0.044	0.046	0.045	0.047

But one has to be very careful when the  $Ru_{2\%}$  level is determined starting from the  $Ru_s$  value and assuming a Rayleigh distribution

for wave run-up (thus leading to 'equivalent' wave run-up). If the  $Ru_s$  value is found in a 'platform' or when the  $Ru_s$  value is already ridden with an error, this method can give rise to a wrong determination of the  $Ru_{2\%}$  level. In such a case, this alternative solution is of no use. Therefore, the first method (by means of fitting a straight line through the measurement data by adjusting the parameter a) is used further on. To maximal wave run-up value Rumax has been approximated by  $Ru_{0.1\%}$  in the case the analysed time series lasted for two hours (about 1000 waves) and  $Ru_{0.4\%}$  in the case thirty minutes time series (about 250 waves) have been used.

The thus calculated wave run-up levels, either by means of the  $Ru_s$  value or by means of a fitted straight line through the wave run-up data are further on called ' $Rayleigh\ equivalent$ ' wave run-up values  $Ru_{x\%,eq}$ . The  $Ru_{x\%,eq}$  values get priority to the  $Ru_{2\%}$  values in the relevant cases.

For the spiderweb system measurements and for the wave run-up measurements, following storm events need an adjusted ('Rayleigh equivalent')  $Ru_{2\%}$  value: n° 2, 6, 7, 9, 10, 11, 12 and 13, resp. 5, 6 and 7.

By merging table 4.13 and table 4.15, resp. table 4.14 and table 4.16 wisely, i.e. be substituting the measured wave run-up values by their so-called 'Rayleigh equivalent wave run-up value' in the relevant cases, the values given in table 4.17 for the run-up gauge (RU) and in table 4.18 for the spiderweb system (SP) are obtained. The italic values in both tables are the 'Rayleigh equivalent' wave run-up values.

An average  $Ru_{2\%}/H_{m0}$  value of 1.77 for an average Iribarren number  $\xi_{om} = 3.63$  (variation coefficient  $\delta = 0.006$ ) is obtained when the RU data (9 storms) are processed. The analysis of the SP data (13 storms) yields an average  $Ru_{2\%}/H_{m0}$  value of 1.73 for an average Iribarren  $\xi_{om} = 3.64$  (variation coefficient  $\delta = 0.0046$ ). As wave run-up measurements by the run-up gauge are more reliable and are obtained in a direct way, only the data of table 4.17 will be taken into account further on. Moreover, most results of table 4.18 are 'equivalent wave run-up' values. The value  $Ru_{2\%}/H_{m0} = 1.77$  is considered as the final overall full scale wave run-up value valid for  $\xi_{om} = 3.63$ .

Tabel 4.16: Full scale *equivalent wave run-up* measurement results

(SP, 13 storms, from  $t_{HW}$ -1 to  $t_{HW}$ +1, 2 hours time series).

storm event n°	Ru <sub>max</sub> /H <sub>m0</sub> [-]	Ru1%/Hmo [-]	$Ru_{2\%}/H_{mo}$ [-]	$Ru_{5\%}/H_{mo}$ [-]	Ru <sub>10%</sub> /H <sub>mo</sub> [-]	$Ru_{s}/H_{mo}$ [-]	$Ru_{25\%}/H_{mo}$ [-]	$Ru_{50}/H_{m0}$ [-]
1 <sup>a</sup>	2.09	1.70	1.57	1.37	1.20	1.12	0.93	0.66
<b>2</b> <sup>a</sup>	2.04	1.67	1.54	1.35	1.18	1.10	0.92	0.65
3 <sup>a</sup>	2.35	1.92	1.77	1.55	1.36	1.27	1.05	0.75
4	2.33	1.90	1.76	1.54	1.35	1.26	1.04	0.74
5	2.28	1.86	1.72	1.50	1.32	1.23	1.02	0.72
6	2.41	1.97	1.82	1.59	1.39	1.30	1.08	0.76
7	2.24	1.83	1.69	1.48	1.30	1.21	1.01	0.71
8	2.42	1.98	1.82	1.59	1.40	1.30	1.08	0.77
9	2.41	1.97	1.81	1.59	1.39	1.30	1.08	0.76
10	2.23	1.82	1.68	1.47	1.29	1.20	1.00	0.71
11	2.39	1.96	1.80	1.58	1.38	1.29	1.07	0.76
12	2.32	1.89	1.74	1.53	1.34	1.25	1.04	0.73
13	2.16	1.76	1.63	1.42	1.25	1.16	0.97	0.68
μ	2.28	1.86	1.72	1.50	1.32	1.23	1.02	0.72
δ	0.055	0.056	0.054	0.055	0.055	0.056	0.054	0.055

As already mentioned afore, wave run-down could only be measured by the first (most seaward) step gauge of the spiderweb system. The level of wave run-down could also only be detected at high water because the level of the base of this first step gauge is Z+2.75 (MLWS=Z+0.27). The lowest sensor of the run-up gauge is situated at Z+6.12. Table 4.19 gives the  $Rd_{2\%}/H_{m0}$  values for the thirteen measured storm events. During the period of time of 2 hours at high tide, the average  $Rd_{2\%}/H_{m0}$  value equals -0.87 for  $\xi_{om}=3.64$  (variation coefficient  $\delta=0.0046$ ).

The  $Ru_{2\%}/H_{m0}$  values mentioned in table 4.17, table 4.18 and table 4.19 are shown in figure 4.35.

Table 4.17: Corrected full scale wave run-up measurement results (run-up gauge, 9 storms, from  $t_{HW}$ -1 to  $t_{HW}$ +1, 2 hours time series).

storm event n°	$Ru_{max}/H_{mo}$ [-]	$Ru_{1\%}/H_{mo}$ [-]	$Ru_{2\%}/H_{mo}$ [-]	$Ru_{5\%}/H_{mo}$ [-]	$Ru_{10\%}/H_{mo}$ [-]	$Ru_{s}/H_{mo}$ [-]	$Ru_{25\%}/H_{m0}$ [-]	$Ru_{5o}/H_{mo}$ [-]
5	2.41	1.97	1.81	1.59	1.39	1.34	1.08	0.68
6	2.24	1.83	1.69	1.48	1.30	1.17	0.82	0.65
7	2.34	1.91	1.76	1.54	1.35	1.28	1.01	0.69
8	2.09	1.95	1.82	1.55	1.34	1.30	1.08	0.69
9	2.53	2.14	1.89	1.67	1.45	1.32	1.00	0.76
10	2.19	1.86	1.60	1.46	1.39	1.27	0.99	0.70
11	2.66	2.09	1.86	1.73	1.43	1.29	1.05	0.73
12	2.33	1.70	1.65	1.47	1.28	1.14	0.87	0.70
13	2.38	2.07	1.85	1.54	1.24	1.10	0.94	0.59
μ	2.35	1.95	1.77	1.56	1.35	1.25	0.98	0.69
δ	0.073	0.072	0.058	0.059	0.052	0.069	0.092	0.070

Although both wave run-up measuring devices (RU and SP) yield different and occasionally almost the same  $Ru_{2\%}/H_{m0}$  value for each of the storm events, both wave run-up measuring devices yield almost the same average results. Both measuring devices are placed in different cross sections of the breakwater. Thus, the influence of the armour unit pattern (yard placing) is suspected. Averaging the wave run-up results neutralises the random influence of the placement pattern of the armour units.

The obtained wave run-up results are plotted against the spectral width parameter  $\varepsilon$  and the peakedness parameter  $Q_p$  in figure 4.36. The average values are  $(Ru_2\%/H_{m0})_{RU}=1.77$  for  $\varepsilon=0.5800$  and  $Q_p=2.140$  and  $(Ru_2\%/H_{m0})_{SP}=1.73$  for  $\varepsilon=0.5857$  and  $Q_p=2.045$ .

Tabel 4.18: Corrected full scale wave run-up measurement results (SP, 13 storms, from  $t_{HW}$ -1 to  $t_{HW}$ +1, 2 hours time series).

			SC	ries).				
storm event n°	$Ru_{max}/H_{m0}$ [-]	Ru <sub>1%</sub> /H <sub>mo</sub> [-]	$Ru_{2\%}/H_{mo}$ [-]	Ru <sub>5%</sub> /H <sub>mo</sub> [-]	$Ru_{10\%}/H_{mo}$ [-]	$Ru_{s}/H_{mo}$ [-]	$Ru_{25\%}/H_{mo}$ [-]	$Ru_{50}/H_{m0}$ [-]
1 <sup>a</sup>	2.07	1.71	1.56	1.37	1.20	1.12	0.93	0.66
2 <sup>a</sup>	2.34	1.67	1.54	1.35	1.18	1.10	0.92	0.65
3 <sup>a</sup>	2.19	1.93	1.75	1.55	1.36	1.27	1.05	0.75
4	2.12	1.87	1.79	1.54	1.35	1.26	1.04	0.74
5	2.05	1.92	1.71	1.50	1.32	1.23	1.02	0.72
6	2.43	1.97	1.82	1.59	1.39	1.30	1.08	0.76
7	2.14	1.83	1.69	1.48	1.30	1.21	1.01	0.71
8	2.11	2.01	1.90	1.59	1.40	1.30	1.08	0.77
9	2.48	1.97	1.81	1.59	1.39	1.30	1.08	0.76
10	2.22	1.82	1.68	1.47	1.29	1.20	1.00	0.71
11	2.58	1.96	1.80	1.58	1.38	1.29	1.07	0.76
12	2.49	1.89	1.74	1.53	1.34	1.25	1.04	0.73
13	2.13	1.76	1.63	1.42	1.25	1.16	0.97	0.68
μ	2.26	1.87	1.73	1.50	1.32	1.23	1.02	0.72
δ	0.081	0.057	0.061	0.055	0.055	0.056	0.054	0.055

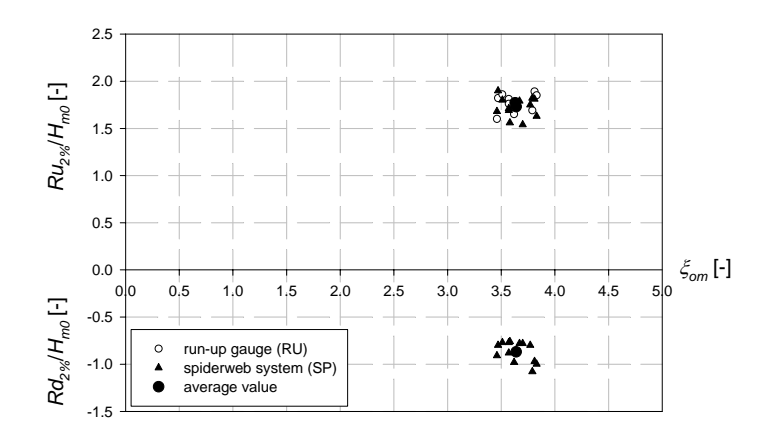


Figure 4.35:  $Ru_{2\%}/H_{m\theta}$  and  $Rd_{2\%}/H_{m\theta}$  vs. Iribarren number  $\xi_{om}$  (SP (13 storms) and RU (9 storms) from  $t_{HW}$ -1 to  $t_{HW}$ +1, 2 hours time series).

Tabel 4.19: Full scale wave run-down measurement results (SP, 13 storms, from  $t_{HW}$ -1 to  $t_{HW}$ +1, 2 hours time series).

storm event n°	$Rd_{ma\chi}/H_{mo}\left[ \cdot  ight]$	$Rd_{1\%}/H_{mo}$ [-]	$Rd_2\%/H_{mo}$ [-]	$Rd_{5\%}/H_{mo}$ [-]	$Rd_{10\%}/H_{m0}$ [-]	$Rd_{s}/H_{mo}$ [-]	$Rd_{25\%}/H_{m0}$ [-]	$Rd_{so}/H_{mo}$ [-]
1 <sup>a</sup>	-1.00	-0.85	-0.76	-0.66	-0.59	-0.54	-0.47	-0.33
2 <sup>a</sup>	-0.98	-0.81	-0.78	-0.67	-0.58	-0.54	-0.45	-0.32
3 <sup>a</sup>	-0.98	-0.85	-0.80	-0.71	-0.64	-0.60	-0.50	-0.36
4	-0.87	-0.79	-0.78	-0.72	-0.65	-0.60	-0.52	-0.34
5	-0.77	-0.77	-0.77	-0.77	-0.77	-0.77	-0.77	-0.67
6	-1.08	-1.08	-1.08	-1.02	-0.99	-0.96	-0.86	-0.61
7	-0.88	-0.88	-0.88	-0.88	-0.87	-0.85	-0.79	-0.66
8	-0.87	-0.80	-0.80	-0.78	-0.73	-0.72	-0.67	-0.58
9	-0.97	-0.97	-0.97	-0.95	-0.90	-0.89	-0.82	-0.64
10	-0.93	-0.93	-0.91	-0.86	-0.82	-0.80	-0.75	-0.58
11	-0.77	-0.77	-0.77	-0.77	-0.77	-0.77	-0.77	-0.69
12	-1.11	-1.02	-0.98	-0.93	-0.87	-0.86	-0.75	-0.57
13	-1.00	-1.00	-1.00	-1.00	-0.99	-0.96	-0.84	-0.58
μ	-0.94	-0.89	-0.87	-0.83	-0.78	-0.76	-0.69	-0.53
δ	0.111	0.117	0.126	0.150	0.179	0.196	0.218	0.265

The results of an analysis of the RU data of half a tide cycle (using time series of 30 minutes) are mentioned in table 4.20 and plotted in figure 4.37. SP measurement data have not been considered. The reasons for this are:

- on average, the SP data and the RU data yield comparable results.
  - wave run-up results are obtained in a direct way by analysing the RU data. Analysing the SP data is a very time consuming process. Moreover, wave run-up results are obtained in an indirect way.
  - the platforms disturb the determination of wave run-up values with exceedance probabilities x > 2%. These values become very unreliable because the wave run-up values are found within these platforms. Wave run-up values are thus overestimated.
  - too much approximations and assumptions have to be made to analyse the SP data.

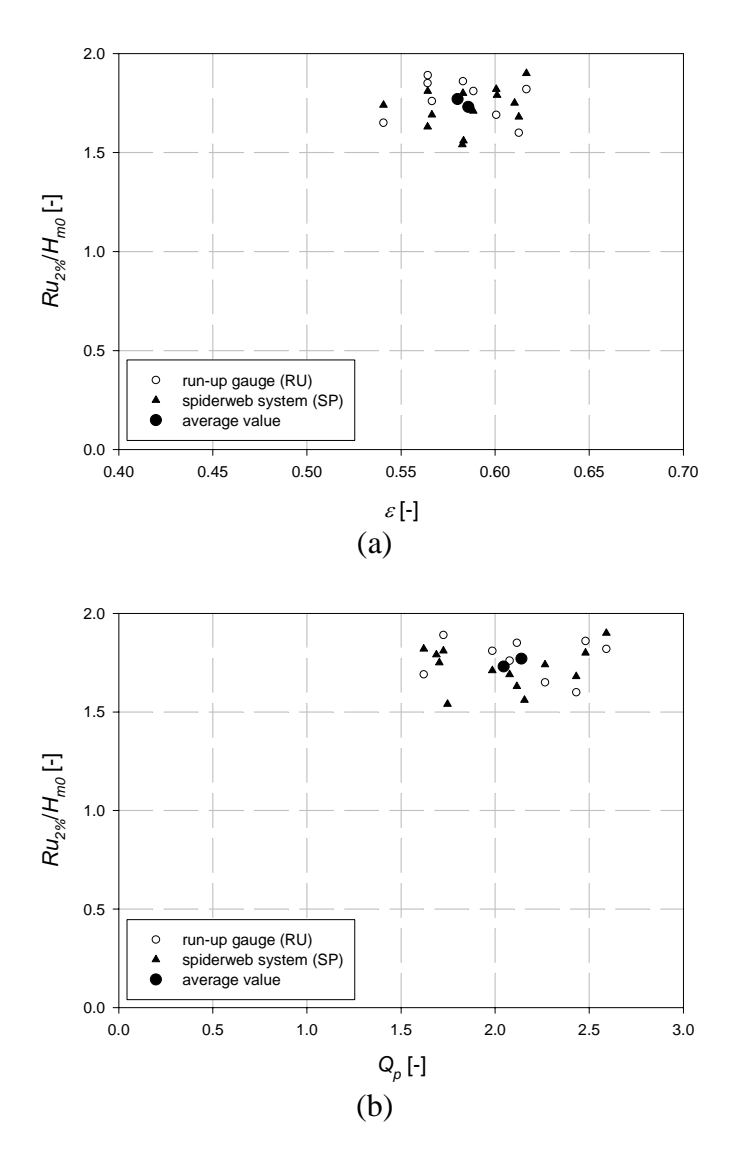


Figure 4.36: Wave run-up results  $Ru_{2\%}/H_{m\theta}$  plotted against (a) the spectral width parameter  $\varepsilon$  and (b) the peakedness parameter  $Q_p$  of Goda (1985) for both the run-up gauge (O) measurements and the spiderweb system ( $\triangle$ ) measurements.

Different values for the exceedance probability x ( $Ru_{max}/H_{m0}$ ,  $Ru_{1}\%/H_{m0}$ ,  $Ru_{2}\%/H_{m0}$ ,  $Ru_{5}\%/H_{m0}$ ,  $Ru_{10}\%/H_{m0}$ ,  $Ru_{s}/H_{m0}$  and  $Ru_{50}\%/H_{m0}$ ) have been considered.

Table 4.20: Dimensionless full scale wave run-up results  $Ru_{x\%}/H_{m0}$  (run-up gauge, 9 storms, 30 minutes time series)

$Ru_{x\%}/H_{m0}$ (run-up gauge, 9 storms, 30 minutes time series)										
	$Ru_{max}/H_{mo}$ [-]	Ru <sub>1%</sub> / H <sub>mo</sub> [-]	Ru <sub>2</sub> %/H <sub>mo</sub> [-]	Ru <sub>5%</sub> / H <sub>mo</sub> [-]	Ru <sub>10%</sub> /H <sub>mo</sub> [-]	$Ru_s/H_{m0}$ [-]	Ru <sub>25%</sub> /H <sub>mo</sub> [-]	Ru <sub>50%</sub> /H <sub>m0</sub> [-]		
	R	Œ	œ	Œ	Æ	Щ	Æ	R		
[t <sub>HW</sub> -3, t <sub>HW</sub> -2.5]	2.95	2.55	2.26	1.93	1.70	1.55	1.32	0.92		
$[t_{HW}$ -2.5, $t_{HW}$ -2]	2.70	2.44	2.22	1.89	1.59	1.46	1.21	0.90		
$[t_{HW}$ -2, $t_{HW}$ -1.5]	2.54	2.34	2.13	1.85	1.53	1.38	1.12	0.85		
$[t_{HW}$ -1.5, $t_{HW}$ -1]	2.39	2.14	1.97	1.71	1.47	1.33	1.03	0.74		
$[t_{HW}$ -1, $t_{HW}$ -0.5]	2.21	2.01	1.83	1.56	1.37	1.26	1.01	0.72		
$[t_{HW}$ -0.5, $t_{HW}]$	2.13	1.94	1.77	1.55	1.37	1.27	1.00	0.69		
$[t_{HW}, t_{HW} + 0.5]$	2.22	1.97	1.80	1.55	1.36	1.24	0.96	0.69		
$[t_{HW} + 0.5, t_{HW} + 1]$	2.23	1.98	1.78	1.62	1.39	1.28	1.02	0.71		
$[t_{HW} + 1, t_{HW} + 1.5]$	2.41	2.10	1.90	1.60	1.37	1.26	0.99	0.73		
$[t_{HW} + 1.5, t_{HW} + 2]$	2.41	2.11	1.96	1.70	1.47	1.32	1.05	0.76		
$[t_{HW} + 2, t_{HW} + 2.5]$	2.51	2.24	2.03	1.72	1.47	1.34	1.10	0.79		
$[t_{HW} + 2.5, t_{HW} + 3]$	2.80	2.42	2.17	1.77	1.53	1.42	1.18	0.85		

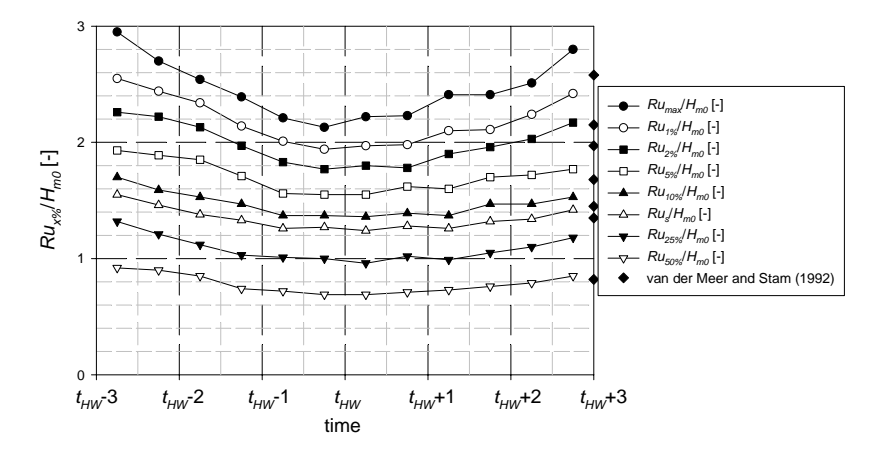


Figure 4.37: Dimensionless full scale wave run-up  $Ru_{xy}/H_{m0}$  vs. time (cf. data table 4.20).

Where necessary, 'Rayleigh equivalent' wave run-up values  $Ru_{x\%,eq}$  have been used. Especially  $Ru_{x\%}$  values with a high value of x at lower SWLs and  $Ru_{x\%}$  values with a small value of x at

high SWLs needed an adjusted wave run-up value. This was because in former case wave run-up only could be measured from the level of the lowest electrode of the lowest part of the wave run-up gauge on (Z+6.12) and in latter case because during the storm events  $n^{\circ}$  5, 6 and 7, only the three lowest parts of the wave run-up gauge were available for wave run-up measurements.

Following conclusions are drawn from the upper table and figure. When thirty minutes time series are used in the analysis of the data collected by the run-up gauge during a two hour period at high tide (from  $t_{HW}$ -1 to  $t_{HW}$ +1),  $Ru_{2\%}/H_{m0}$  equals  $\cong$  **1.80**. This value is the average of the four  $Ru_{2\%}/H_{m0}$  obtained within  $[t_{HW}$ -1,  $t_{HW}$ +1] and is compared to the result of the analysis of the entire two hours period as one time series  $((Ru_{2\%}/H_{m0})_{RU} = 1.77)$  and  $(Ru_{2\%}/H_{m0})_{SP} = 1.73)$  a little bit higher. One general remark has to be made: in the analysis of thirty minutes time series, the  $Ru_{2\%}$  value is based on a measurement of only about 200 waves whereas in the analysis of a two hours period the  $Ru_{2\%}$  value is based on a measurement of about 1000 waves, so the estimation of  $Ru_{2\%}$  in former is less accurate (see also confidence boundaries in table 4.9) than in latter case.

Wave run-up levels are slightly higher during rising tide than during receding tide. All considered exceedance probabilities x show the same trend.

It is clearly seen that the Ru/H values increase when water level decreases ( $t_{HW}$  is the moment in time of high water;  $t_{HW}$ -3 is approximately the moment in time of MWL). The lower the exceedence probability x, the more the dimensionless wave runup values increase (figure 4.37). A part of the explanation why dimensionless wave run-up values depend on the water level in front of the structure can be found within the fact that wave heights are lower when lower water depths are considered, so for constant wave run-up heights Ru the ratio  $Ru/H_{m0}$  becomes larger when  $H_{mo}$  decreases (at lower water levels). However, when looking at the Ru values, in general and filtering out the influence of wave period, these increase slightly when water depth decreases also. As an example to illustrate this, the significant wave height  $H_{m0}$ , the mean wave period  $T_{01}$ , the wave run-up characterised by  $Ru_{2\%}$  and the dimensionless wave run-up  $Ru_{2\%}/H_{m0}$  are displayed in figure 4.38 versus time (thus SWL) for storm event  $n^{\circ}$  9 (Nov. 6-7, 1999 (23h45 – 01h45)). The results of the last two periods of half an hour ( $[t_{HW}+2, t_{HW}+2.5]$ ) and  $[t_{HW}+2.5, t_{HW}+3]$ ) may not be taken into account because both wave period  $T_{0I}$  and wave height  $H_{m0}$  decrease so absolute and relative wave run-up decreases as well. Around  $t_{HW}$  the  $Ru_{2\%}$  value is clearly lower than the other  $Ru_{2\%}$  values. This phenomenon could be explained by the fact that at lower water levels wave run-up takes place at a lower part of the slope. The lower porosity of the armour layer at lower levels (due to the settlement of the armour units during the lifetime of the breakwater (built in 1983)) may cause larger wave run-up. Also the influence of the longshore currents is suspected, as well as the asymmetry of the tide curve.

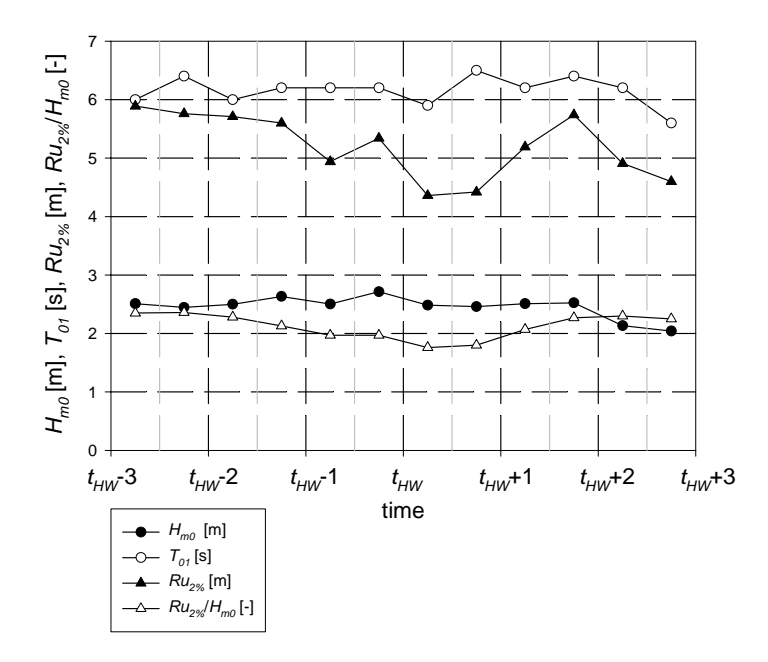


Figure 4.38: Significant wave height  $H_{m\theta}$ , mean wave period  $T_{\theta I}$ , wave run-up  $Ru_{2\%}$  and dimensionless wave run-up  $Ru_{2\%}/H_{m\theta}$  versus time for storm event n° 9 (Nov. 6-7, 1999 (23h45 – 01h45)).

For an exceedance probability x = 2, the results of the analysis of storm data of nine storm events collected by the run-up gauge during half a tide cycle and using 30 minutes time series are plotted in figure 4.39. The spreading on the results has been calculated. Table 4.21 gives the width of the 90% boundary

intervals of the average values given in table 4.20. The 90% confidence intervals of the average values are also indicated in the graphs. These are calculated by using the intervals

$$\left[\bar{x} - \frac{s}{\sqrt{n}} t_{n-1,0.95}, \bar{x} + \frac{s}{\sqrt{n}} t_{n-1,0.95}\right]$$
(4.7)

with  $\overline{x} =$ the average value given by  $\frac{1}{n} \sum_{i=1}^{n} x_i$ 

- $s^2$  = the variance, defined as  $\frac{1}{n-1} \sum_{i=1}^{n} (x_i \overline{x})^2$
- n = number of values
- $t_{n-1,0.95}$  = value for which the exceedance probability of the considered variable by  $t_{n-1,0.95}$  is 95% according to the t-distribution

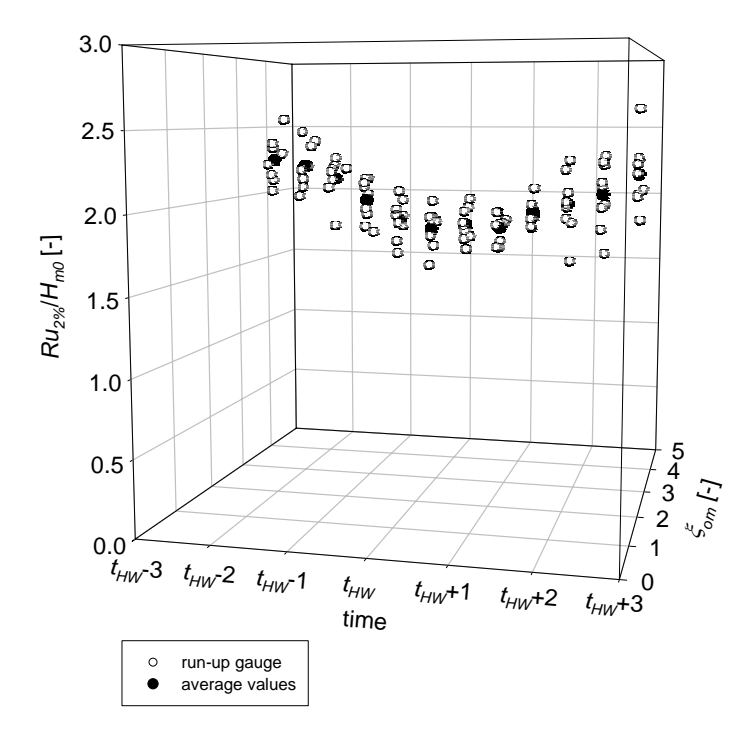


Figure 4.39:  $Ru_{2\%}/H_{m0}$  results (O: RU, 9 storms, 30 mniutes time series;  $\bullet$ : average of nine values) against time (from  $t_{HW}$ -3 to  $t_{HW}$ +3 per 30 minutes) and the Iribarren number  $\xi_{om}$  [-].

The lower the SWL, the more spreading is seen on the analysis results. The spreading is the smallest during the two hour period at high water during which the SWL is considered to have a constant value. The higher the value of the exceedance probability x, with the more confidence the  $Ru_{x\%}$  value can be estimated.

Table 4.21: Width of the 90% confidence intervals of the mean wave run-up values  $Ru_{x\%}/H_{m\theta}$  [-] of table 4.20 (run-up gauge, 9 storms, 30 minutes time series).

(Tun-up gauge, 9 storms, 30 minutes time series).										
	$Ru_{max}/H_{m0}$ [-]	Ru1%/H <sub>m0</sub> [-]	$Ru_{2\%}/H_{m0}$ [-]	Ru <sub>5%</sub> /H <sub>mo</sub> [-]	Ru <sub>10%</sub> /H <sub>mo</sub> [-]	$Ru_{s}/H_{mo}$ [-]	Ru <sub>25%</sub> /H <sub>mo</sub> [-]	Ru <sub>50%</sub> /H <sub>mo</sub> [-]		
$[t_{HW}$ -3, $t_{HW}$ -2.5]	0.55	0.33	0.20	0.22	0.15	0.17	0.13	0.11		
$[t_{HW}$ -2.5, $t_{HW}$ -2]	0.41	0.27	0.20	0.29	0.20	0.18	0.14	0.09		
$[t_{HW}$ -2, $t_{HW}$ -1.5]	0.15	0.28	0.18	0.25	0.16	0.12	0.10	0.06		
$[t_{HW}$ -1.5, $t_{HW}$ -1]	0.17	0.16	0.19	0.21	0.18	0.17	0.15	0.05		
$[t_{HW}$ -1, $t_{HW}$ -0.5]	0.22	0.24	0.17	0.19	0.18	0.19	0.10	0.08		
$[t_{HW}$ -0.5, $t_{HW}]$	0.18	0.17	0.17	0.12	0.10	0.09	0.11	0.05		
$[t_{HW}, t_{HW} + 0.5]$	0.29	0.14	0.15	0.15	0.10	0.11	0.13	0.06		
$[t_{HW} + 0.5, t_{HW} + 1]$	0.18	0.13	0.12	0.14	0.13	0.13	0.10	0.07		
$[t_{HW} + 1, t_{HW} + 1.5]$	0.24	0.12	0.11	0.21	0.18	0.12	0.11	0.05		
$[t_{HW} + 1.5, t_{HW} + 2]$	0.23	0.27	0.27	0.23	0.20	0.16	0.10	0.08		
$[t_{HW} + 2, t_{HW} + 2.5]$	0.27	0.24	0.29	0.15	0.14	0.07	0.05	0.08		
$[t_{HW} + 2.5, t_{HW} + 3]$	0.36	0.35	0.29	0.21	0.11	0.10	0.09	0.10		

### 4.8 Conclusions

Full scale measurements have been performed on the Zeebrugge rubble mound breakwater. Wave characteristics, wave run-up and wave run-down have been measured during thirteen storm events. Following main conclusions are drawn:

(1) The average dimensionless wave run-up value exceeded by 2% of the waves  $Ru_{2\%}/H_{m0}$  equals **1.77** for an Iribarren number  $\xi_{om} = 3.63$ . This value is obtained by analysing the RU data collected during 9 storm events. Time series of two hours (from  $t_{HW}$ -1 to  $t_{HW}$ +1) have been analysed. During three storms only the three lowest parts of the five part run-

up gauge were present. In these cases, a 'Rayleigh equivalent' wave run-up value  $Ru_{2\%,eq}$  has been calculated. Analysing the SP data collected during 13 storm events with time series of two hours (from  $t_{HW}$ -1 to  $t_{HW}$ +1) yields an average relative wave run-up value of 1.73 (valid for  $\xi_{om} = 3.64$ ). Due to the measuring principle of the spiderweb system, in a lot of cases, the 'Rayleigh equivalent' wave run-up value needs to be determined.

- (2) Average wave run-down, characterised by  $Rd_{2\%}/H_{m0}$  equals **0.87.** Data collected by the most seaward step gauge of the spiderweb system during a period of time of two hours at high water have been analysed. The Iribarren number  $\xi_{om}$  equals 3.64.
- (3) Wave run-up measurements on a rubble mound breakwater are very scarce and are the only data to validate and to calibrate small scale models. Therefore, these data have to be as reliable as possible. Per storm event, considerable differences are seen between the  $Ru_{2\%}$  values obtained by both measuring devices. The irregular pattern of the armour units (yard placing) and the ratio  $D_{n50}/H_{m0}$  are suspected to be the responsible parameters for these discrepancies. Two different wave run-up measuring devices (spiderweb system and run-up gauge), placed in different cross sections of the breakwater yield comparable average results for low exceedance probabilities. The influence of the random placed armour units is neutralised by averaging the wave run-up results.
- (4) When 30 minutes time series are used in the analysis of the RU data collected during 9 storms and during half a tide cycle (from  $t_{HW}$ -3 to  $t_{HW}$ +3), during a two hour lasting period around the moment in time of high water, the average dimensionless wave run-up value equals  $Ru_{2\%}/H_{m0} = 1.80$ . This value is slightly higher than the value obtained by analysing this two hour lasting time series as a whole. The length of the used time series does not affect the results significantly, but the confidence intervals are smaller when longer time series are considered.
- (5) Dimensionless wave run-up values are dependent on the water level:  $Ru_{2\%}/H_{m0}$  values increase when the SWL decreases. The wave run-up value Ru is less dependent on

the water level than the  $Ru_{2\%}/H_{m0}$  values, but wave run-up also increases when the water level decreases. This increase is thought to be the consequence of the settlement of the breakwater by which locally the lower part of the armour layer has become less prous than the upper part. A less porous slope is smoother and implies higher wave run-up. The dimensionless wave run-up values are also larger during rising tide than during receding tide by which an influence of currents and/or the asymetric tide is suspected.

(6) The lower the exceedance probability *x*, the more dimensionless wave run-up values vary with changing water levels.

# **Chapter 5: Scale model testing**

### 5.1 Introduction

A lot of laboratory investigation has been carried out. In the frame of the OPTICREST project, the Zeebrugge rubble mound breakwater has been modelled in three selected laboratories spread over Europe:

- Ministry of the Flemish Community, Flanders Hydraulics (Belgium) *FCFH*
- Universidad Politécnica de Valencia (Spain) *UPV*
- Aalborg University (Denmark) AAU

In FCFH and UPV, the breakwater has been modelled twodimensionally on a scale 1:30. A three dimensional model was built in AAU on a scale 1:40. Both reproductions of storm events measured on site at Zeebrugge and parametric tests have been carried out. The two dimensional model has been built twice at the same scale because:

- the costs of wave flume tests are a lot lower than the costs of 3D small scale model tests
- by carrying out the same tests in two different laboratories, test results are double checked.

Three-dimensional model tests have been performed in order to investigate the influence of wave obliqueness, directional spreading, foreshore bathymetry (refraction), longshore currents and other 3D effects.

To investigate the influence of important parameters on wave run-up (namely the spectral shape and the combined action the *SWL*, the armour unit pattern and the position of the comb of the run-up gauge relative to the armour unit pattern), additional laboratory tests have been carried out in the laboratories of Flanders Hydraulics (FCFH) and Ghent University (UGent).

Large scale wave run-up test have been carried out in the Large Wave Channel (GWK). By these tests the influence of the parameter  $D_{n50}/H_{m0}$  has been investigated and very valuable large scale data has been gathered.

In this chapter, all laboratory investigations are discussed and the obtained results are given. The digital run-up gauge used for wave run-up measurements is discussed in paragraph 5.2. Paragraph 5.3 deals with all laboratory experiments which have been carried out

during the OPTICREST project. Additional tests performed at Flanders Hydraulics are subject of paragraph 5.4. Paragraph 5.5 describes small scale model tests carried out at UGent. Paragraph 5.6 deals with large scale tests carried out at GWK. The conclusions are found in paragraph 5.7.

In order not to loose feeling with the full scale breakwater in Zeebrugge, the results of the small scale model tests described in paragraphs 5.3 and 5.4 have been rescaled to their full scale values, unless mentioned otherwise. Whenever needed so as to leave no doubt, full scale values are indicated by subscript 'f' and model values by subscript 'm'. Throughout paragraph 5.5, laboratory values have been used.

# 5.2 Digital laboratory run-up gauge

At the Civil Engineering Department of Ghent University, a novel digital run-up gauge has been developed in the frame of this Ph.D. by Tom Versluys. The run-up gauge consists of a comb, the 'master' box and the 'slave' box. The comb is connected to the slave box which is on its turn connected to the master box by a cable. The master box is connected to the data acquisition computer. The comb (figure 5.1) consists of a number of (a plural of eight) needles made of INOX welding rods held at a constant distance in a PVC frame. The lower ends of the needles have been sharpened to avoid droplets sticking to the end of the needles and giving rise to false wave run-up measurements. The PVC frame is suspended on a structure built above the model. The needles of the comb can be adjusted to the slope profile of the breakwater. The electrodes of the comb are numbered: the electrode with the lowest elevation gets number 1 and other electrodes have an increasing number with increasing elevation. It is recommended to rub the PVC frame with silicones in order to avoid an electrical contact between two neighbouring needles through water sticking to the comb.

The presence of the run-up gauge in the water does not induce diffraction of the incident waves. The dimension of the gauges measured parallel to the wave crests is very small (7 mm). Compared to the wave length L and the wave amplitude, only viscous forces are acted on the step gauge and diffraction is of no importance at all (Van Torre (2000)).



Figure 5.1: The novel digital step gauge installed in the flume of Flanders Hydraulics.

The 'master' is a hardware box with an LCD screen and a little keyboard which is connected to the data acquisition computer. The 'slave' is another hardware box which is placed close to the measuring spot. Both the master and the slave box contain a microcontroller which communicate continuously with each other by means of a shielded twisted pair cable.

An alternating current (AC of 2 to 3 kHz) of approximately 2 Volt is placed on each of the electrodes. This current is rectified to a direct current (DC), i.e. the envelope of the quickly oscillating AC amplitude is detected. When an electrical contact is made between the mass electrode and one of the electrodes of the gauge, the amplitude of the direct current is decreased due to the increased conductivity by the water. When this amplitude decreases below a certain threshold value (the amplitude is 'compared' to the threshold value), which can be adjusted by a little potentiometer, the comparator circuit detects a 'wet' electrode. Each electrode is connected to an input of an eight channel multiplexer. The microcontroller of the slave steers x multiplexers. x equals the number of electrodes divided by 8. The microcontroller of the slave checks every 0.008 s the status of each electrode. The slave scans all electrodes and searches for wet electrodes. At regular intervals ( $f_s = 100 \text{ Hz}$ ), the microcontroller of the master updates its output with the most recent status of all electrodes which it receives from the microcontroller of the slave. An example of the answer which the slave gives to the master is 'WWWWWWWWDDDDDD', with W = wet and D = dry. This is for a comb with 16 electrodes, excluding the mass electrode. The

master microcontroller has two analogue outputs. The first output gives a voltage which corresponds to the position of the electrode with the highest level that still makes contact with the water. The second output gives a voltage which corresponds to the number of electrodes which make contact with the water. The number of wet electrodes is called the 'sum' output and the highest number amongst all wet electrodes is called the 'max' output. By comparing these 2 signals it is possible to check the performance of the run-up gauge. The 'sum' output signal of the step gauges is mostly used to be analysed. In the aforementioned example is the 'sum' output 9 and the 'max' output is 10. A measurement of both outputs results in two digital signals. These digital 'sum' and 'max' output signals are converted to an analogue output signal between 0 and 10 Volt by DA convertion. Occasionally, an analogue low pass filter may be placed between the master box and the computer to eliminate high frequent noise. This filter is realised by an RC circuit (figure 5.2). The cut off frequency is determined by  $f_{cutoff} = 1/(2\pi RC)$  with  $R = 10 \text{ k}\Omega$  and C = 220 nF, resulting in  $f_{cut\ off} = 3.6$  Hz. Both filtered signals are sent to the data acquisition computer.

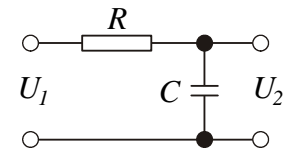


Figure 5.2: RC circuit.

The distance between the lower end of the needles and the slope surface is very important. On the one hand, this distance may not be too small as little droplets hanging on the sharp lower ends of the needles may touch the wettened armour units and thus giving contact with the water. On the other hand, this distance may not be too large either as the use of this novel run-up gauge would have no longer benefits in comparison to a traditional wire gauge. A good choice for the distance between the lower end of the needles and the slope surface is 2 mm. In the case of a traditional run-up gauge this distance can mount to much higher values because of the craggy slope surface. The accuracy of a traditional wire gauge has been estimated. Figure 5.3 shows a theoretical drawing of a wave running op the slope of a smooth slope at the moment in time of maximal wave run-up.

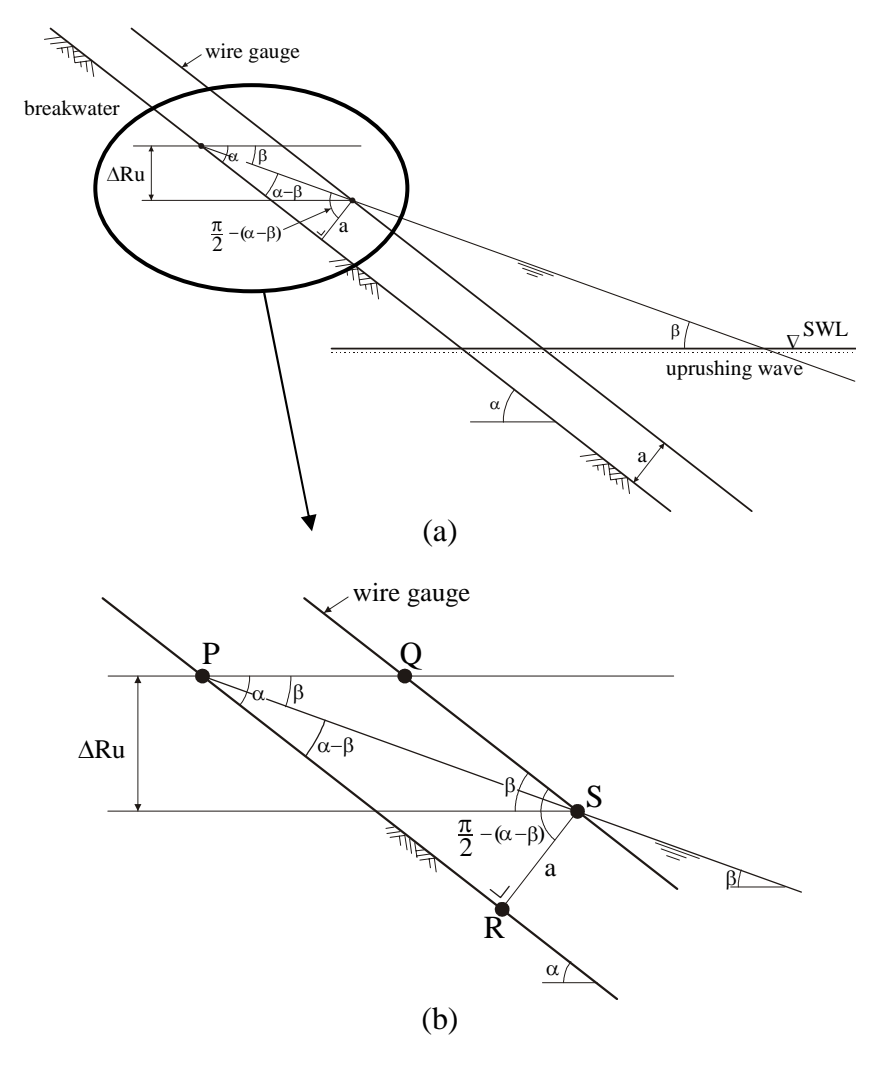


Figure 5.3: Sketch of wire gauge stretched above the structure slope at a distance *a*.

The error on the wave run-up measurements made by a traditional wire gauge, i.e. the difference between the measured wave run-up level and the actual wave run-up level is  $\Delta Ru$ :

$$\Delta Ru = |PS| \cdot \sin \beta \tag{5.1}$$

In triangle PRS is

$$a = |PS| \cdot \sin(\alpha - \beta) \tag{5.2}$$

so that

$$|PS| = \frac{a}{\sin(\alpha - \beta)} \tag{5.3}$$

Thus,

$$\Delta Ru = a. \frac{\sin \beta}{\sin(\alpha - \beta)} \tag{5.4}$$

The angle  $\beta$  between the water surface elevation at the moment in time of maximal wave run-up and the slope has been investigated for the Zeebrugge breakwater by De Rouck (1991) (based on earlier investigations of Brandtzaeg (1962)):

$$\beta = \alpha - 5\frac{H}{L} \tag{5.5}$$

with s = H/L is the steepness of the wave, so that (5.4) yields:

$$\frac{\Delta Ru}{a} = \frac{\sin(\alpha - 5s)}{\sin(5s)} \tag{5.6}$$

From figure 5.4 it is seen that steep waves (high s values) give rise to small ratios  $\Delta Rw/a$  between the difference in measured wave run-up level and actual wave run-up level and the distance between the wire gauge and the slope of the structure, whereas non steep waves give rise to very large  $\Delta Rw/a$  values. A long wave will flow under the gauge. The larger the distance a between the gauge and the slope, the larger the difference  $\Delta Ru$  for the same incident wave conditions. The ratio  $\Delta Rw/a = 1$  corresponds to s = 0.061 (in open seas, the wave steepness s varies between 0.02 and 0.03 and along coasts s increases up to 0.05 to 0.07 with a maximum of 1/7 (=0.143) (De Rouck (1998))). So, for waves with a steepness s < 0.06 the difference  $\Delta Ru$  becomes larger than the distance between the wire gauge and the

slope. For waves with a wave steepness s < 0.02, the error on wave run-up measurements equals at least five times the distance between the gauge and the slope! For non steep waves (long waves with a small wave height), the distance a has to be as small as possible in order not to increase the error  $\Delta Ru$  on wave run-up measurements.

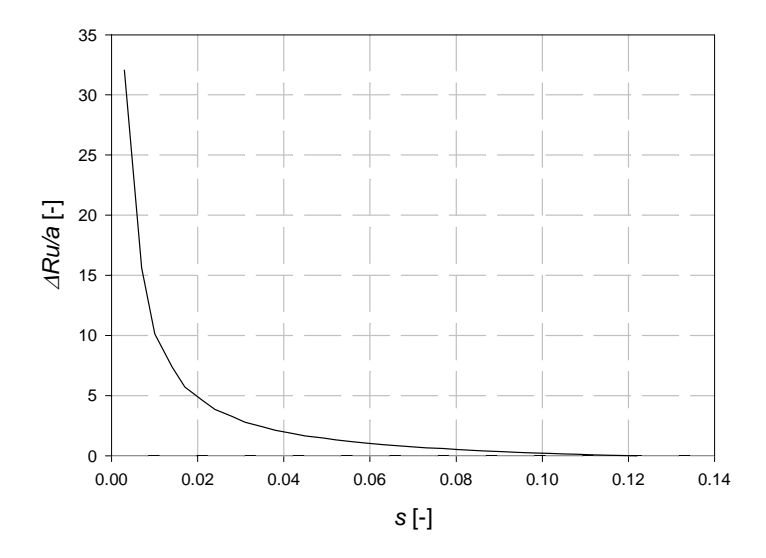


Figure 5.4: The difference between measured and actual wave run-up  $\Delta Ru$  for different wave steepnesses (s = H/L) and for different distances a between the gauge and the slope surface.

Concluding, attention must be paid to the distance between the gauge and the slope surface especially when low frequency waves (small s values) are present.

The digital step gauge as described in this paragraph has been used in all laboratories.

Calibrating the run-up gauge is very easy. Only one action needs to be undertaken before (or after) each series of tests: the exact elevation of each single electrode has to be measured. Each wet electrode counts for 100 mV. For example, an output voltage of 3.6 V corresponds with 36 electrodes. In the analysis programme, the level of the electrode with number 36 is than taken as the wave run-up level.

The 'sum' output is the most obvious output for analysis purposes.

#### **5.3 Small scale model tests – OPTICREST**

The objective of the small scale model tests performed during the OPTICREST project was to reproduce several storm events measured at full scale and to compare test results with full scale results. Much attention has been paid to the correct reproduction of the wave spectrum. This was done by tuning the significant wave height  $H_{m0}$ and the spectral mean wave period  $T_{0l}$  of the laboratory spectra to the full scale spectra. The data of the recorded full scale time series of a wave rider buoy (WRII for storms 1 to 5 and WRI for storms 6 and 7) and the SWL of the concerning storm events have been sent to the laboratories. Each laboratory analysed these data. A wave signal was generated and transformed by the Biésel transfer function to the paddle stroke signal. This paddle stroke signal was assigned to the wave generator and waves were measured. Several tests have been run, each time with a slightly modified wave spectrum until a satisfying agreement was seen between the parameters characterising the spectrum measured at the location of the wave rider buoy from which the water surface elevation time series was taken and the parameters characterising the (full scale) target spectrum. This was not an easy task as

- the spectrum measured by a wave rider close to the breakwater had to be reproduced. At FCFH, the wave paddle and the location of the wave rider were separated by a sand bar which transformed the wave spectrum.
- wave characteristics at the location of the second wave rider buoy (WRII) have been compared. At full scale no reflection analysis has been carried out. So, total waves (i.e. the sum of incident and reflected waves) have been considered which makes reproduction of a total spectrum more complicated.

As Schlütter et al. (2000) already mentioned, this method of reproducing waves in the laboratory does not ensure that the laboratory spectra and the full scale (target) spectra are completely the same as an ideal copy is very hard to obtain.

The overall geometrical scale of the scale models was 1:30 for the two 2D models built at FCFH and UPV and 1:40 for the 3D model built at AAU. Gravity forces are the most important for wave reproduction. Therefore, the breakwater has been scaled according to Froude's law. Similitude according to Froude implies a scale factor for the velocity

 $\alpha_v$  and for time  $\alpha_t$  for which holds the equation  $\alpha_v = \alpha_t = \sqrt{\alpha_s}$  with  $\alpha_s$ = scale of the model. In order to model the flow in the core of the breakwater properly, a special scaling method as presented by Burcharth et al. (1999) has been applied to scale the core material. This method yields a coarser material by which viscous scale effects in the core are avoided and the hydraulic gradients in the core are reproduced properly. More specific, this procedure aims for a Froude scaling for a characteristic pore velocity in the core. Scaling the model and keeping the Froude number constant (thus, scaling the core material by 1:30) would have resulted in an incorrect modelling of pore pressure distribution through the breakwater and as a consequence, incorrect wave run-up simulations. For the Zeebrugge breakwater, figure 5.5(a), resp. figure 5.5(b) present the ratio between the characteristic dimension of the model material and the characteristic dimension of the same material at full scale  $d_{n50}^{m} / d_{n50}^{p}$  for  $H_{s} = 3$  m, resp.  $H_{s} = 7$  m and  $T_{p} = 8$  s, resp.  $T_{p} = 12$ s. As figure 5.5(a) is relevant for the investigated storm events, the distorted scale of the core was 1:20 for the 2D models (on scale 1:30) and 1:24 for the 3D model (on scale 1:40).

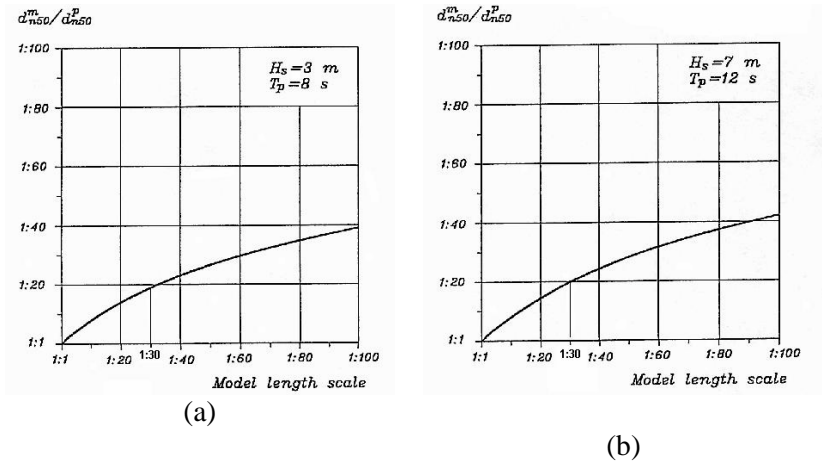


Figure 5.5: Core scaling (according to Burcharth et al. (1999)).

In all laboratories, the same methodology has been followed. To calculate the dimensionless wave run-up value  $Ru_{2\%}H_{m0}$ , the 'sum' output of the digital run-up gauge has been used to determine Ru2%.

In the denominator of  $Ru_{2\%}/H_{m0}$ , the total significant wave height has been used at the position of the second wave rider. To make comparison of full scale measurement results with laboratory results easier, in this paragraph, all laboratory values have been scaled to their full scale values. The storm events reproduced in the laboratories are mentioned in table 5.1. The hour and the date on which these occurred are also mentioned. In order to be able to compare full scale results with small scale model test results, the same length of a storm event time series has been applied in all laboratories. Only the time series of the storm events indicated with an asterix (\*\*) were different from the time series of the storm events analysed in chapter 4. A cross in the last three columns of table 5.1 indicates which storm has been reproduced in which laboratory.

Table 5.1: Overview of storm events reproduced in small scale model tests during the OPTICREST project at the involved laboratories.

storm event n°	Date [dd/mm/yyyy]	Hour	Time span	FCFH	AAU	UPV
1 <sup>b</sup>	28/08/1995 <sup>(*)</sup>	03h30 - 04h45	1h15min	Х	Х	
2 <sup>b</sup>	28/081995 <sup>(*)</sup>	14h45 – 17h00	2h15min	Χ	Χ	
3 <sup>b</sup>	19/01/1998 <sup>(*)</sup>	15h45 – 18h15	2h30min	Χ	Χ	
4	20/01/1998	04h15 - 06h15	2h	Χ	Χ	
5	07/02/1999	16h00 – 18h00	2h	Χ	Χ	
8	06/11/1999	09h30 - 15h30	6h	Х	Х	Х
9	06-07/11/1999	21h45 - 03h45	6h	Χ	Χ	Х

x: storm has been reproduced

Seven storm events have been reproduced in the laboratories of FCFH and AAU. Two of these storms events (n° 8 and 9) covered half a tide cycle (i.e. from  $t_{HW}$ -3 to  $t_{HW}$ +3) and have been reproduced at UPV as well. Each storm event was divided into five sub-events: (1)  $t_{HW}$ -3 to  $t_{HW}$ -2, (2)  $t_{HW}$ -2 to  $t_{HW}$ -1, (3)  $t_{HW}$ -1 to  $t_{HW}$ +1, (4)  $t_{HW}$ +1 to  $t_{HW}$ +2 and (5)  $t_{HW}$ +2 to  $t_{HW}$ +3 (figure 5.6). Not all sub events had the same duration: sub events (1), (2), (4) and (5) lasted for one hour (full scale value!) and sub event (3) lasted for two hours. Each sub event was reproduced

b: time series slightly different than these of chapter 4

separately. The change in *SWL* during the sub events at full scale was not simulated in the laboratory. Table 5.2 and table 5.3 give the water level rise per investigated time period for storm events n° 8 and 9. During rising tide the *SWL* rises much quicker than during receding tide. In the laboratory, the *SWL* during each of these sub events has been kept constant The *SWL* during the reproduction of each of the five sub events was taken equal to the *MWL* of the considered time series at full scale. The influence of the *SWL* on wave run-up results is less for sub event (3) than for the other sub events. The other five reproduced storm events covered only a period of time of approximately 2 hours around high water.

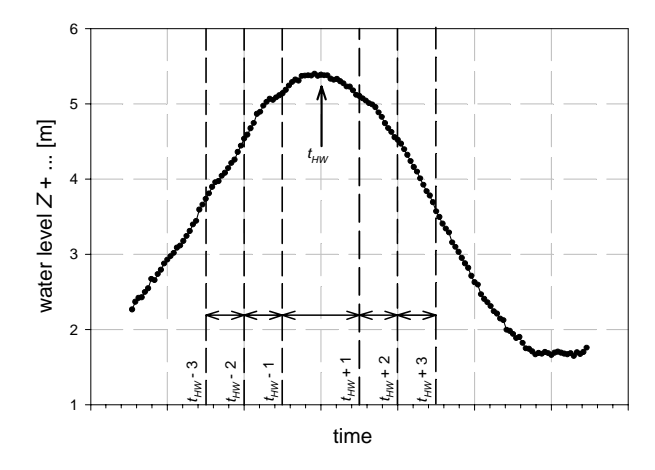


Figure 5.6: Definition sketch of storm event subseries.

The Antifer cubes of the scale models have been placed according to their position at the Zeebrugge rubble mound breakwater. This reconstruction has been done by means of photographical material. The first layer (the lower layer) of armour units is placed with a regular pattern. A recording of the actual location of the cubes in the second layer (the upper layer) is seen in figure 5.7.

Table 5.2: SWL and water level rise  $\triangle SWL$  during the investigated periods of the storm sessions of storm  $n^{\circ}$  8.

time period	SWL	$SWL_{max}^{(*)}$	$SWL_{min}^{(*)}$	$\Delta SWL$
unie period	[ <i>Z</i> + m]	[ <i>Z</i> + m]	[ <i>Z</i> + m]	[Z+ m]
$t_{HW}$ -3 to $t_{HW}$ -2	3.45	3.89	3.01	0.89
$t_{HW}$ -2 to $t_{HW}$ -1	4.53	5.02	3.98	1.04
$t_{HW}$ -1 to $t_{HW}$ +1	5.28	5.37	5.09	0.28
$t_{HW}+1$ to $t_{HW}+2$	5.01	5.22	4.70	0.52
$t_{HW}+2$ to $t_{HW}+3$	4.28	4.65	3.89	0.76

<sup>(\*)</sup> calculated using 5 minutes time series

Table 5.3: SWL and water level rise  $\Delta SWL$  during the investigated periods of the storm sessions of storm  $n^{\circ}$  9.

periods of the storm sessions of storm in 5.								
time period	SWL	$SWL_{max}^{(*)}$	$SWL_{min}^{(*)}$	∆SWL				
time period	[ <i>Z</i> + m]	[ <i>Z</i> + m]	[ <i>Z</i> + m]	[Z+ m]				
$t_{HW}$ -3 to $t_{HW}$ -2	3.26	3.54	3.04	0.50				
$t_{HW}$ -2 to $t_{HW}$ -1	4.16	4.72	3.64	1.08				
$t_{HW}$ -1 to $t_{HW}$ +1	5.11	5.26	4.82	0.44				
$t_{HW}+1$ to $t_{HW}+2$	4.71	4.95	4.38	0.57				
$t_{HW}+2$ to $t_{HW}+3$	3.89	4.34	3.42	0.92				

<sup>(\*)</sup> calculated using 5 minutes time series

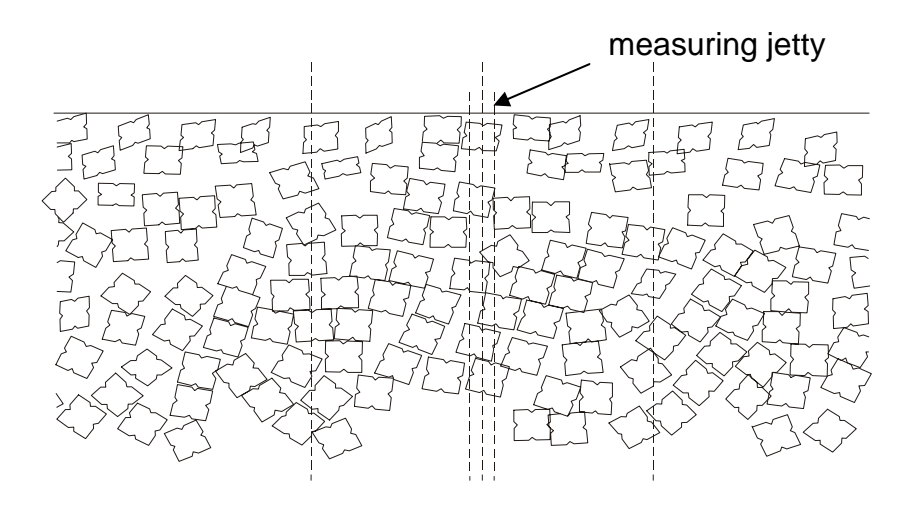


Figure 5.7: Second armour layer (upper layer) pattern at full scale.

#### 5.3.1 Small scale model tests – FCFH

## **5.3.1.1 Introduction**

Flanders Hydraulics and the Hydrological Research Division are part of the Waterways and Marine Affairs Administration within the Environment and Infrastructure Department of the Ministry of the Flemish Community (Belgium – http://www.watlab.lin.vlaanderen.be), abbreviated FCFH. The utilised wave flume has a length of 41 m, a width of 0.70 m and a depth of 0.85 m (figure 5.8(a)). The wave flume is equipped with a piston type wave paddle for generating regular and irregular waves (figure 5.8(b)). Active wave absorption has been implemented in the wave generation programme in order to avoid re-reflection of waves at the paddle.

## 5.3.1.2 Model setup

A cross section of the model setup is given in figure 5.9. The foreshore up to 600 m in front of the Zeebrugge breakwater has also been modelled in the wave flume. The used materials of the breakwater are presented in table 5.4. In order to obtain the right grading, several kinds of gravel have been riddled and recombined. The crest element is made of concrete. The willow mattress has been modelled as permeable and had a total length of 3.5 m (scale value).

Table 5.4: Materials used in the FCFH model.

	full scale	model scale			
	D <sub>50</sub> [mm]	<i>D</i> <sub>50</sub> [mm]	n [%]	$D_{85}/D_{15}$ [-]	V [dm³]
core (2-300 kg)	230	11.8	46.4	3.2	85
filter (1-3 ton)	950	32.6	49.4	1.3	110
sea gravel (backfilling)	12.5	0.42			100
sea sand (foundation)	0.2	0.1			2830
toe (3-6 ton)	1200	43.9	47.9	1.2	70
quarry run (2-80 kg)		6.3	45.9	2.4	21
quarry run (80-300 kg)	380	14.6	48.6	1.4	49
sand infiltration in core	0.2	0.1			140
berm (1-3 ton)	950	32.6	49.4	1.3	60

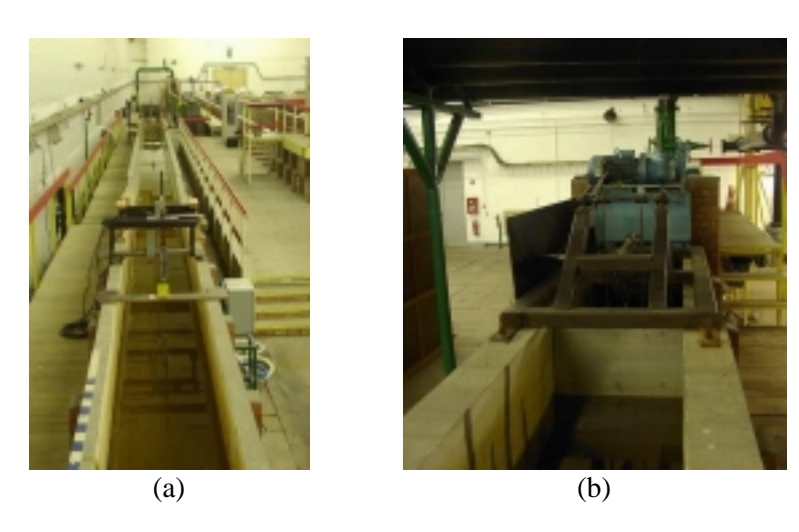


Figure 5.8: (a) View on the wave flume at FCFH and (b) piston type wave paddle installed at FCFH.

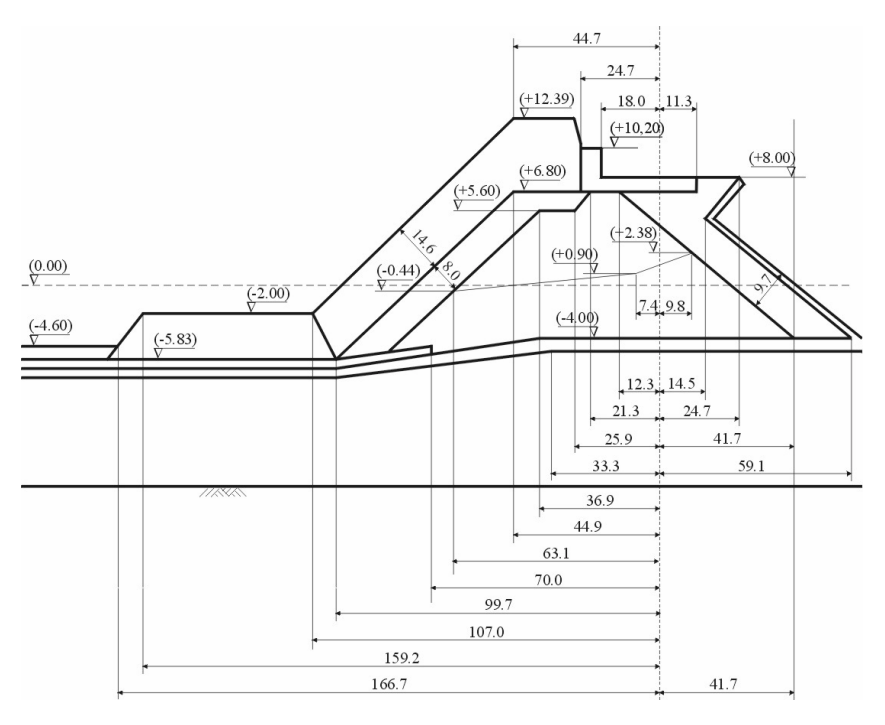


Figure 5.9: Cross section of the model setup in the wave flume of FCFH (dimensions in [cm] and levels in [Z + ... m]).

## **5.3.1.3 Instrumentation**

## **5.3.1.3.1** Wave height meters

Five resistance type wave height meters have been used to measure the incident and reflected waves: AWA1, AWA2, ZE1, ZE4 and ZE7. AWA1 and AWA2 are located near the wave paddle (figure 5.10(a)) and are used for active wave absorption. In order to be able to compare small scale model test results with full scale measurement results, wave gauges have been placed according to the position of wave measuring devices at full scale. Wave height meter ZE1 is located at the position of WRII in full scale. ZE4 is located at the position of WRI in full scale. The position of ZE7 is identical to the position of the infrared meter at full scale (figure 5.10(b)). Wave data have been band pass filtered with a low cut-off frequency of 0.05 Hz and a high cut-off frequency of 0.5 Hz. The number of data points in the applied data windows is 1028. Thus, a bandwidth of b = 0.002 Hz is obtained.





Figure 5.10: Wave height meters (a) AWA1 and AWA2 and (b) ZE7 in the wave flume at FCFH.

Table 5.5 mentions the channels and the corresponding full scale measuring devices.

Table 5.5: Naming of wave gauges and corresponding full scale measuring instrumentation.

	measurm	g msti umentatioi	L•
name wave height meter	distance to model axis [m]	corresponding full scale measuring device	distance to breakwater axis [m]
ZE1	7.99		
ZE2	7.79	WRII	239.7
ZE3	7.51		
ZE4	6.32		-
ZE5	6.12	WRI	189.7
ZE6	5.84		
ZE7	1.41	IR	42.3

## 5.3.1.3.2 Wave run-up gauge

Wave run-up has been measured by means of a traditional wire gauge (RU1). To improve the accuracy of the wave run-up measurements the digital run-up gauge step gauge (as described in paragraph 5.2) has been used to measure wave run-up. The run-up gauge was installed in the middle of the flume in the corresponding cross section at full scale in which the measuring jetty has been built (figure 5.1). The position of the comb of the run-up gauge in the model did not correspond with the position of the run-up gauge on the full scale Zeebrugge breakwater. Data of the 'sum' output of the run-up gauge has been used for wave run-up analysis. Simultaneously also the lowest sloping run-up gauge has measured wave run-up.

#### **5.3.1.4 Results**

The significant wave height  $H_{m0}$ , the mean wave period  $T_{01}$ , the peak wave period  $T_p$ , the spectral width parameter  $\varepsilon$ , the Iribarren number  $\xi_{om}$  and the absolute and relative wave run-up values  $Ru_{2\%}$ , resp.  $Ru_{2\%}/H_{m0}$  of all storm events reproduced in the laboratory of FCFH (cfr. table 5.1) are presented in table 5.6. The spectra of the storm event reproductions are found in Annex D.

The relative wave run-up height has been plotted versus the Iribarren number in figure 5.11. The average dimensionless wave run-up value which is exceeded by 2% of the waves is 1.46. The variation coefficient c of  $Ru_{2\%}/H_{m0}$  is 0.047. The average Iribarren number  $\xi_{om}$  equals 3.89.

Table 5.6: FCFH small scale model test results.

storm event n°	H <sub>m0</sub> [m]	T <sub>01</sub> [s]	$T_p$ [s]	€[-]	ξ <sub>om</sub> [-]	Ru <sub>2%</sub> [m]	Ru <sub>2%</sub> /H <sub>m0</sub> [-]
1 <sup>b</sup>	2.54	6.7	8.5	0.53	4.01	3.76	1.48
2 <sup>b</sup>	2.64	7.0	8.0	0.59	4.12	3.76	1.42
3 <sup>b</sup>	2.98	7.4	8.1	0.61	4.11	4.57	1.53
4	3.17	6.9	9.0	0.54	3.74	4.46	1.4
5	3.34	7.1	8.1	0.56	3.73	4.63	1.39
8a	2.74	5.9	7.2	0.50	3.45		1.26
8b	3.00	6.4	7.9	0.47	3.57		1.46
8c	3.08	6.8	7.8	0.49	3.71	4.42	1.44
8d	2.98	6.6	7.9	0.48	3.68		1.47
8e	2.62	6.2	7.1	0.52	3.65		1.57
9a	2.80	6.0	7.1	0.50	3.44		1.37
9b	3.01	6.2	7.0	0.51	3.46		1.5
9с	2.56	6.3	6.3	0.54	3.79	4.02	1.57
9d	2.80	6.3	7.6	0.48	3.61		1.46
9e	2.49	5.7	6.5	0.51	3.44		1.34

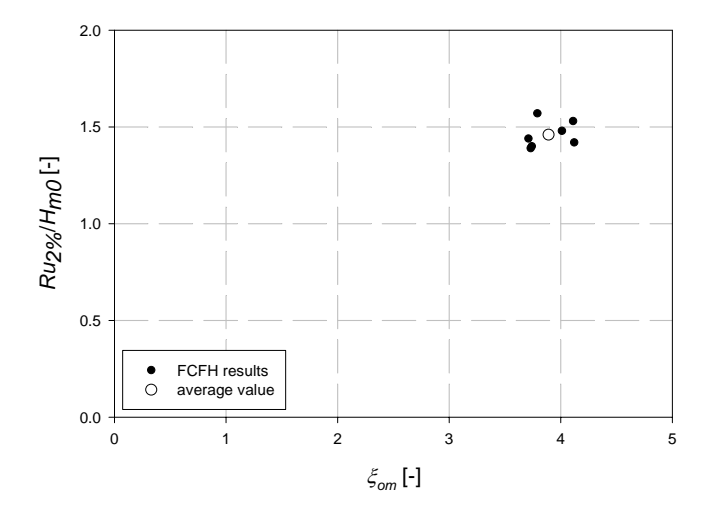


Figure 5.11: Results of storm event reproductions at FCFH.

Table 5.7: Comparison of absolute and relative wave run-up values of original (target) storm events and the storm events reproduced at FCFH.

	full scale me	asurements	laboratory ir	nvestigation
storm n°	<i>Ru</i> <sub>2%</sub> [m]	Ru <sub>2%</sub> /H <sub>m0</sub> [-]	<i>Ru</i> <sub>2%</sub> [m]	Ru <sub>2%</sub> /H <sub>m0</sub> [-]
1 <sup>b</sup>	4.38	1.54	3.76	1.48
2 <sup>b</sup>	4.20	1.58	3.76	1.42
$3_p$	5.09	1.74	4.57	1.53
4	5.38	1.79	4.46	1.40
5	5.66	1.81	4.63	1.39
8c	5.55	1.82	4.42	1.44
9c	4.81	1.89	4.02	1.57

Table 5.8: FCFH storm event reproduction (half a tide storms).

		$H_{m0}$ [m]	$T_{01}$ [s]	ξ <sub>om</sub> [-]	<i>Ru</i> 2% [m]	Ru <sub>2%</sub> /H <sub>m0</sub> [-]
	$t_{HW}$ -3 $t_{HW}$ -2	2.74	5.93	3.45	3.46	1.26
8	$t_{HW}$ -2 $t_{HW}$ -1	3.00	6.43	3.57	4.39	1.46
storm	$t_{HW}$ -1 $t_{HW}$ +1	3.08	6.77	3.71	4.42	1.44
st	$t_{HW}$ +1 $t_{HW}$ +2	2.98	6.61	3.68	4.39	1.47
	$t_{HW}$ +2 $t_{HW}$ +3	2.62	6.15	3.65	4.12	1.57
	$t_{HW}$ -3 $t_{HW}$ -2	2.80	5.99	3.44	3.84	1.37
6	$t_{HW}$ -2 $t_{HW}$ -1	3.01	6.24	3.46	4.51	1.50
storm	$t_{HW}$ -1 $t_{HW}$ +1	2.56	6.32	3.79	4.02	1.57
stc	$t_{HW}$ +1 $t_{HW}$ +2	2.80	6.29	3.61	4.11	1.46
	$t_{HW}$ +2 $t_{HW}$ +3	2.49	5.65	3.44	3.34	1.34

Both the absolute and relative wave run-up values  $Ru_{2\%}$ , resp.  $Ru_{2\%}/H_{m0}$  are a lot smaller than the full scale values (table 5.7). The average difference (i.e. the average of the absolute values of  $(Ru_{2\%,small} scale - Ru_{2\%,full scale})/Ru_{2\%,full scale})$  on the wave run-up  $Ru_{2\%}$  is 15.3%. The average difference on the dimensionless wave run-up value  $Ru_{2\%}/H_{m0}$  is 15.6%. Comparing the  $Ru_{2\%}/H_{m0}$  columns of table 5.7, it can be concluded that for the reproductions of the storm events at high water in the wave flume of FCFH, dimensionless wave run-up  $Ru_{2\%}/H_{m0}$  is smaller than dimensionless wave run-up values measured on site.

Table 5.8 gives the results of the reproduction of the storm events which covered almost half a tide cycle (storm events  $n^{\circ}$  8 and 9). From the results in table 5.8 it is seen that only for storm  $n^{\circ}$  9 an influence of the *SWL* is seen. Dimensionless wave run-up values are higher during rising tide than during receding tide. These findings contradict with the results of the reproduction of storm  $n^{\circ}$  8. In latter, dimensionless wave run-up increases with increasing elapsed time. On average, wave run-up seems not to be influenced by the *SWL*, this in contradiction to the full scale measurements.



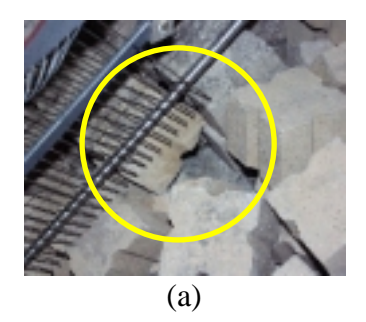
Figure 5.12: Indication of a hole underneath the upper 10 electrodes of the run-up gauge.

Wave run-up has been measured both by wire gauge (RU1) and by the novel wave run-up gauge. The wave run-up gauge measures higher wave run-up levels (on average 9% with a maximum of 29%) than the traditional wire gauge.

The influence of the specific pattern of the cubes underneath the electrodes of the run-up gauge has been investigated shortly. Underneath the 10 most upper electrodes of the run-up gauge, a hole between the cubes is noticed (figure 5.12). When the leading edge of the wave rushing up the slope reaches the level of this hole and the water does not have enough momentum and mass, the water tongue disappears in the hole without being detected by the run-up gauge. The porosity of the upper part of the armour layer has been changed by filling up the hole between the cubes (figure 5.13). The same time series of two tests have been sent to the wave paddle twice and wave

run-up has been measured. During the (a) tests there was a hole underneath the upper electrodes and during the (b) tests this hole was filled up.

Remarkable is the increase in dimensionless wave run-up: 25.7%, resp. 29.7% (table 5.9). This increase also has to do with the decrease in significant wave height between the original tests and the repeated tests with the filled hole. However, the decrease in significant wave heights (-6.6%, resp. -8.7%) only implies an increase in dimensionless wave run-up of 7.1%, resp. 9.5% with constant wave run-up. As only very little difference is seen between the wave periods of the (a) and (b) tests, the remaining increase in dimensionless wave run-up must be the consequence of an increased wave run-up level (15.5%, resp. 18.1%). The porosity of the armour layer has an influence on the wave run-up value. This has also been noticed at full scale: the dependency of wave run-up on the water depth is believed to be the consequence of the decreased porosity in the lower part of the armour layer, rather than the influence of the water depth itself.



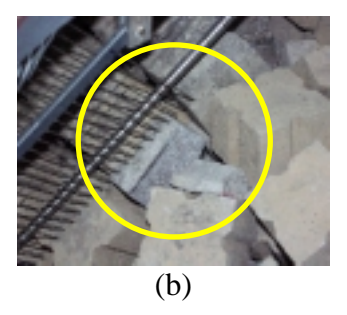


Figure 5.13: Detail of (a) a hole and (b) partly filled up hole underneath the upper electrodes of the run-up gauge.

Table 5.9: Results of tests with (a) an open hole and (b) a partly filled hole.

inica noic.								
	$H_{m0}$ [m]	$T_{01}$ [s]	ξ <sub>om</sub> [-]	Ru <sub>2%</sub> [m]	$Ru_{2\%}/H_{m0}$ [-]			
(a)	3.17	6.94	3.74	4.46	1.40			
(b)	2.96	6.78	3.79	5.15	1.76			
(a)	2.54	6.65	4.01	3.76	1.48			
(b)	2.32	6.50	4.10	4.44	1.92			

For further information reference is made to Willems et al. (2001).

## 5.3.2 Small scale model tests – UPV

## **5.3.2.1 Introduction**

The Laboratory for Ports and Coasts (Laboratorio de Puertos y Costas) is part of the Department of Transport Infrastructure and Engineering Universidad Politécnica de Valencia http://www.lpc.upv.es), abbreviated UPV. Wave run-up tests have been carried out in the combined wind tunnel and wave flume of UPV (figure 5.14). The flume measures 30 m long, 1.20 m high and 1.20 m wide. Waves are generated by a piston type hydraulic controlled wave paddle. The wave generation system is able to generate regular and irregular waves. The maximum piston displacement is 80 cm. No active wave absorption system has been installed. The power of the wind blower is controlled manually to fix a specific wind speed for each test. Wind speeds are measured between the air intake and the model.



Figure 5.14: View on the UPV combined wind tunnel and wave flume test facility.

# 5.3.2.2 Model setup

The model set-up of the UPV model was an exact copy of the FCFH model, except for the foreshore. Because of the limited length of the wave flume, the foreshore could not be modelled at UPV up till a distance of 650 m in front of the breakwater.

## **5.3.2.3** Instrumentation

Waves and *SWL* have been measured using capacitance wave gauges (figure 5.15). Figure 5.16 shows the position of the capacitance wave gauges along the wave flume.



Figure 5.15: Capacitance wave gauges in the UPV wave flume.

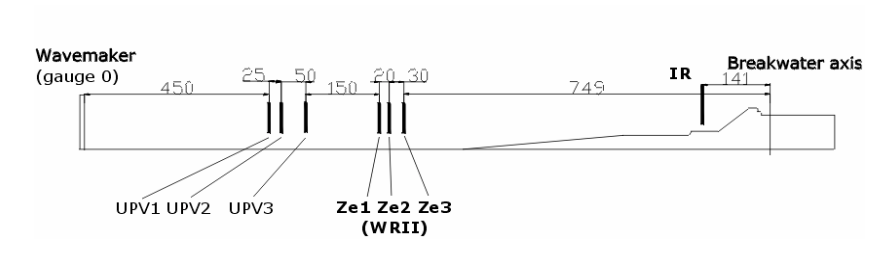


Figure 5.16: Position of wave gauges along the wave flume (dimensions in [cm]).

For tests without wind, wave run-up has been measured using the step gauge constructed at Ghent University. A modified version of the run-up gauge (identical to the run-up gauge discussed in paragraph 5.2 but with the comb inside the core of the breakwater) has been used for tests with wind. Wind speed has been measured by a pitot tube.

Wave run-down has also been measured by means of capacitance wave gauges. Two wave gauges have been placed parallel to the slope

at distances of 2 cm and 4 cm of the theoretical profile. These gauges have been placed 30 cm out of the middle of the wave flume.

Wave overtopping was measured using a channel and weighing box placed in the centre of the section. Though, wave overtopping measured at UPV has not been considered furtheron.

#### **5.3.2.4 Results**

Only a limited number of tests has been carried out. Storm events n° 8 and 9 have been reproduced. The significant wave height  $H_{m0}$ , the mean wave period  $T_{01}$ , the peak wave period  $T_p$ , the spectral width parameter  $\varepsilon$ , the Iribarren number  $\xi_{om}$  and the dimensionless wave runup value  $Ru_{2\%}/H_{m0}$  of the reproductions are given in table 5.10. At high water, the average  $Ru_{2\%}/H_{m0}$  value is 1.77. These results are discussed and compared to full scale measurement results and results of the same storm event reproductions carried out in other laboratories in paragraph 6.2.

Table 5.10: UPV small scale model test results.

storm event n°	<i>H</i> <sub>m0</sub> [m]	T <sub>01</sub> [s]	$T_{\rho}$ [s]	€[-]	ξ <sub>om</sub> [-]	Ru <sub>2%</sub> /H <sub>m0</sub> [-]
8a	2.58	6.4	9.5	0.60	3.81	2.13
8b	2.67	6.3	6.8	0.59	3.72	1.86
8c	2.69	6.4	9.4	0.62	3.72	1.72
8d	2.67	6.5	9.2	0.64	3.81	1.81
8e	2.24	6.1	7.6	0.65	3.89	1.53
9a	2.48	5.8	7.1	0.58	3.55	1.72
9b	2.98	6.2	7.5	0.58	3.45	1.97
9c	3.16	6.6	7.7	0.58	3.54	1.81
9d	2.99	6.5	7.8	0.59	3.62	1.91
9e	2.72	6.5	7.4	0.63	3.76	2.02

The influence of wind on wave run-up has been investigated through wave overtopping measurements. A quantitative estimation of the influence of wind on wave run-up was not possible as the wave run-up measuring device did not work properly during tests with wind. Increasing wave overtopping rates for increasing wind speeds  $v_s$  indicate increased wave run-up. Sixteen combinations of  $H_{m0}$ ,  $T_p$  and

SWL have been selected to generate spectra, resulting in JONSWAP spectra with a significant wave height between 4.43 m and 6.60 m and peak wave periods between 7.7 s and 11.6 s. The same wave paddle steering signals have been run four times using wind speeds  $v_s$  of 0 m/s, 3 m/s, 5 m/s and 7 m/s. The dependency of the dimensionless wave overtopping rate  $(q/\sqrt{gH_{m0}^3})$  on the dimensionless crest freeboard  $(R_c/H_{m0})$  as presented by de Waal et al. (1992) and others (cfr. Schüttrumpf (2001), Kofoed (2002)) has been selected to present the results. Figure 5.17 shows the observed wave overtopping rate in function of the dimensionless crest freeboard and the wind speed. Only a slight increase in dimensionless wave overtopping for increased wind speed has been observed.

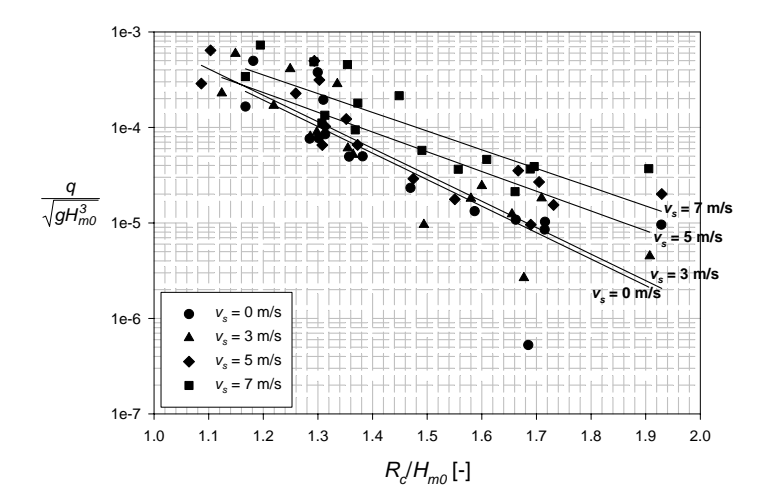


Figure 5.17: Wave overtopping  $q/\sqrt{gH_{m0}^3}$  [-] in function of the relative crest freeboard  $R_c/H_{m\theta}$  [-] for various wind speeds ( $v_s = 0$  m/s, 3 m/s, 5 m/s and 7 m/s).

Further detailed information on UPV testing is found in Medina et al. (2000a), Medina et al. (2000b), Medina et al. (2001a), Medina et al. (2001b) and Medina et al. (2001c).

#### 5.3.3 Small scale model tests – AAU

#### **5.3.3.1 Introduction**

Small scale model tests have been performed at the Hydraulics and Coastal Engineering Laboratory of Aalborg University (Denmark – http://www.civil.auc.dk/i5/engelsk/hyd/index.htm), abbreviated AAU. The model has been constructed in the 3D shallow water basin. The basin measures 12 m by 18 m. Waves can be generated in a water depth up to 60 cm. The wave maker has 25 paddles, each measuring 50 cm wide (figure 5.18). Waves have been generated by the PROFWACO software.



Figure 5.18: Wave maker in the 3D shallow water basin of AAU.

### 5.3.3.2 Model setup

The model scale was 1:40. The scale for the core material was 1:24 (cfr. scaling method of Burcharth et al. (1999)). Due to the limited length of the basin, the foreshore could not be modelled completely. The foreshore consisted of a platform of concrete slabs. To bridge the height between the bottom of the flume and the concrete slabs, a concrete slope leading up the platform was cast. The breakwater was constructed using different stone materials for the different parts of the breakwater (table 5.11). Finally, the armour layer was placed.

The co-ordinates of the middle point of the upper surface of each armour unit in situ has been measured. A detailed analysis of the measurement data pointed out that the breakwater is somewhat steeper at the location of the measuring jetty (figure 5.19). The design slope of the breakwater was 1/1.5. The average measured slope is 1/1.43. At the measuring jetty the slope is 1/1.3.

Table 5.11: Material characteristics for the 3D model.

material	range [mm]	$D_{n50}$ [mm]	$D_{n85}/D_{n15}$ [-]
core	2.3 - 12	5.8	3.0
core	3.8 - 20	9.6	3.0
filter	18 - 26	23.8	1.4
toe	26 - 33	30	1.2
berm	18 - 26	23.8	1.4
seabed	7.8 - 12	9.5	1.5

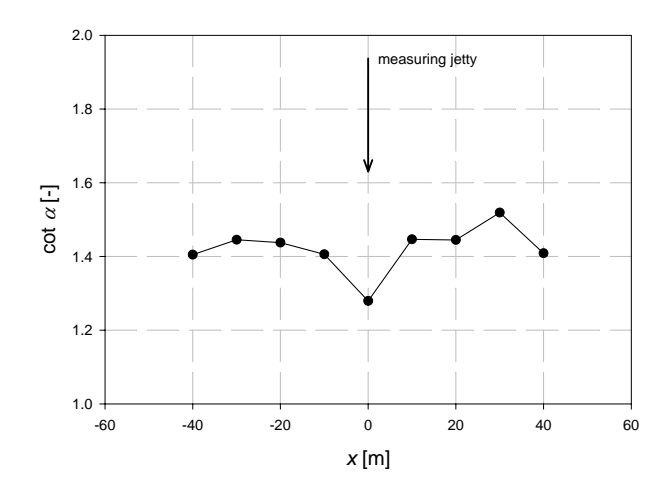


Figure 5.19: Slope angle (cot  $\alpha$ ) of the Zeebrugge breakwater (x = 0 corresponds with the position of the measuring jetty).

## 5.3.3.3 Instrumentation

The instrumentation consisted of six wave gauges, two wave run-up measuring devices (a traditional wire gauge and the novel digital wave run-up gauge) and an overtopping tank. Wave run-up has been measured in two different ways: using a traditional resistance wire gauge and the novel digital run-up gauge (figure 5.20 and figure 5.21).

At AAU problems occurred while measuring wave run-up. Measurements have been disturbed by water squirting out of the core of the breakwater from between the armour units. This water outrush had a very thin layer. This thin layer could be detected by the step gauge, but not by the wire gauge. The water layer made an electrical

contact between the needles and the mass and gave rise to false measurements at levels around *SWL*. Wave run-down measurements are disturbed by this effect. Nevertheless, the wave run-up height measurements did not encounter this problem.



Figure 5.20: The 3D model of the Zeebrugge breakwater at AAU.

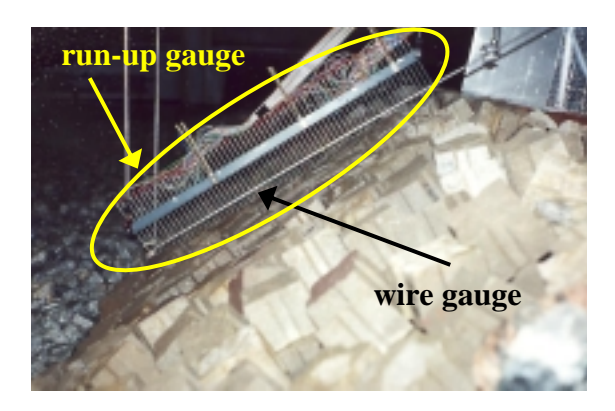


Figure 5.21: The wire gauge and the step gauge on the 3D model at Aalborg University.

## **5.3.3.4 Results**

The value of the significant wave height  $H_{m0}$ , the mean wave period  $T_{01}$ , the peak wave period  $T_p$ , the spectral width parameter  $\varepsilon$ , the Iribarren number  $\xi_{om}$  and the dimensionless wave run-up value  $Ru_{2\%}/H_{m0}$  of the reproduced storm events at AAU are given in table 5.12 and table 5.13. The wave run-up results are further discussed and compared to full scale measurement results and the results of the

reproduction of the same storm events in other laboratories in paragraph 6.2.

Table 5.12: AAU small scale model test results.

storm event n°	<i>H</i> <sub>m0</sub> [m]	T <sub>01</sub> [s]	$T_{\rho}$ [s]	€[-]	ξ <sub>om</sub> [-]	Ru <sub>2%</sub> /H <sub>m0</sub> [-]
1 <sup>b</sup>	2.90	6.3	7.4		3.53	1.52
2 <sup>b</sup>	2.69	6.9	9.0		4.02	1.91
3 <sup>b</sup>	2.96	7.2	8.3		4.03	1.76
4	3.00	7.2	9.1		4.01	1.89
5	3.12	6.9	9.0		3.78	1.71
8a	2.43	6.0	7.2	0.58	3.70	1.7
8b	2.76	6.1	7.2	0.54	3.53	1.5
8c	3.12	6.6	8.0	0.56	3.59	1.36
8d	2.88	6.7	7.2	0.65	3.79	1.44
8e	2.38	6.3	7.2	0.55	3.93	1.65
9a	2.42	6.2	7.2	0.58	3.83	1.70
9b	2.52	6.4	7.2	0.61	3.88	1.68
9с	2.61	6.4	8.9	0.52	3.81	1.28
9d	2.40	6.4	8.9	0.52	3.97	1.47
9e	2.08	5.9	8.0	0.53	3.93	1.68

Table 5.13: AAU wave run-up measurement results.

<b>L</b>							
	laboratory investigation						
storm n°	Ru <sub>2%</sub> (resistance	up gau	Ru <sub>2%</sub> (digital run- up gauge) [m]		Ru <sub>2%</sub> /H <sub>m0</sub> [-		
	gauge) [m]	'max'	'sum'	$H_{m0}$ [-]	]( )		
	gaage/ [m]	output	output				
1 <sup>b</sup>	3.04	4.72	4.40	2.90	1.52		
2 <sup>b</sup>	3.72	5.31	5.13	2.69	1.91		
$3^{b}$	4.08	5.40	5.21	2.96	1.76		
4	4.35	5.85	5.66	3.00	1.89		
5	4.21	5.70	5.33	3.12	1.71		

<sup>(\*)</sup> calculated using Ru<sub>2%,'sum'</sub> output

Wave run-up measurement results of storm events  $n^{\circ}$   $1^{b}$ ,  $2^{b}$ ,  $3^{b}$ , 4 and 5 are given in table 5.13. The resistance gauge clearly underestimates wave run-up (table 5.13). On average, the digital run-up gauge measures 33% higher wave run-up. A wire gauge is suited perfectly for wave run-down measurements, but yields unreliable results for wave run-up measurements as the distance between the gauge and the armour unit surface is too large to detect thin water layers.

Table 5.14 gives the absolute and relative wave run-up values of the reproduction of storm events n° 8 and 9 which covered half a tide cycle. The wave characteristics have been measured by the wave gauge at the position of wave rider I at full scale (because wave rider II was not present at full scale during these storm events). The reproduction of the storm spectra have been performed at the *MWL* of the considered subseries and tests have been repeated until an acceptable agreement between full scale spectra and model spectra was obtained. The dimensionless wave run-up values of table 5.14 have been plotted versus time (figure 5.22). The solid and dashed lines represent the results of storm event n° 8, resp. n° 9. It is seen that these values increase with decreasing *SWL*s.

Table 5.14: Absolute and relative wave run-up values of reproductions of storm events  $n^{\circ}8$  (Nov.  $6^{th}$ , 1999) and 9 (Nov.  $6^{th}$ , 1999).

storm n°	<i>Ru<sub>2%</sub></i> [m]	<i>Ru<sub>5%</sub></i> [m]	<i>Ru<sub>10%</sub></i> [m]	<i>Ru<sub>50%</sub></i> [m]	$Ru_{2\%}/H_{m0}$	Ru <sub>5%</sub> /H <sub>m0</sub> [-]	Ru <sub>10%</sub> /H <sub>mo</sub> [-]	Ru <sub>50%</sub> /H <sub>mo</sub> [-]
8a	4.13	3.75	3.68	1.59	1.70	1.54	1.51	0.65
8b	4.14	3.75	3.52	2.53	1.50	1.36	1.28	0.92
8c	4.24	3.78	3.39	2.50	1.36	1.21	1.09	0.80
8d	4.15	3.76	3.51	2.08	1.44	1.31	1.22	0.72
8e	3.93	3.69	3.02	2.04	1.65	1.55	1.27	0.86
9a	4.11	3.92	3.54	1.46	1.70	1.62	1.46	0.60
9b	4.23	3.95	3.28	2.21	1.68	1.57	1.30	0.88
9c	3.34	3.17	2.98	1.86	1.28	1.21	1.14	0.71
9d	3.53	3.34	3.06	2.11	1.47	1.39	1.28	0.88
9e	3.49	3.37	3.26	1.89	1.68	1.62	1.57	0.91

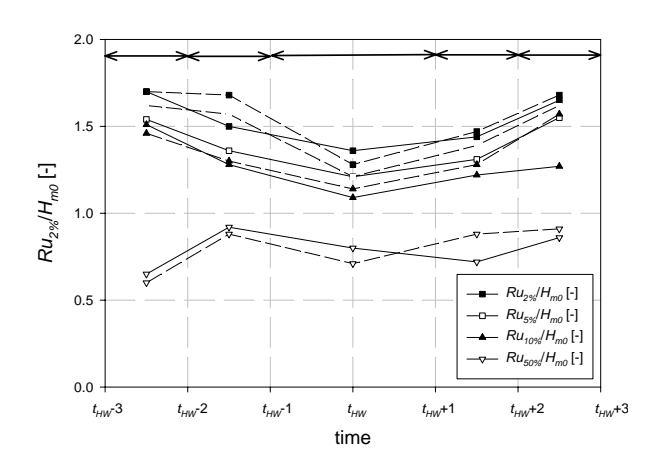


Figure 5.22: Dimensionless AAU laboratory values  $Ru_{x\%}/H_{m\theta}$  (x = 2, 5, 10 and 50) versus time (cfr. table 5.16).

Table 5.15: Results of wave run-up tests on a rubble mound breakwater with an artificially adapted porosity of the armour

	iayer.						
	tost nº	$Ru_{2\%}/H_{m0}$ [-]					
	test n°	first test run	second test run				
	1	1.39	1.38				
	2	1.60	1.60				
	3	1.79	1.81				

The influence of the porosity of the outer armour layer has been demonstrated by tests carried out at AAU. Three types of tests have been performed. During test  $n^{\circ}$  1, the breakwater model had (almost) the same porosity as the full scale rubble mound breakwater. For tests  $n^{\circ}$  2, the gaps between the units underneath the needles of the comb of the run-up gauge had been filled up partly with smaller stones. For tests  $n^{\circ}$  3, all armour units have been replaced so no holes between the units were present. All tests have been performed twice with the same stored wave generation signal. The waves, measured at the position of WRI at full scale, were characteristed by  $H_{m0} = 2.35$  m,  $T_p = 8.00$  s and  $T_{01} = 6.15$  s (all full scale values). The target SWL was Z + 5.28. An increased dimensionless wave run-up value with decreasing porosity has been observed (table 5.15).

Next to long crested waves, short crested waves have been generated too, thus wave obliqueness has been investigated. The water surface elevations have been measured by seven wave gauges (figure 5.18), positioned in an array as depicted in figure 5.23. The recorded data have been analysed by a directional estimation method using a Bayesian approach which separates incident and reflected short crested waves (Hashimoto and Kobune (1988), Yokoki et al. (1992)).

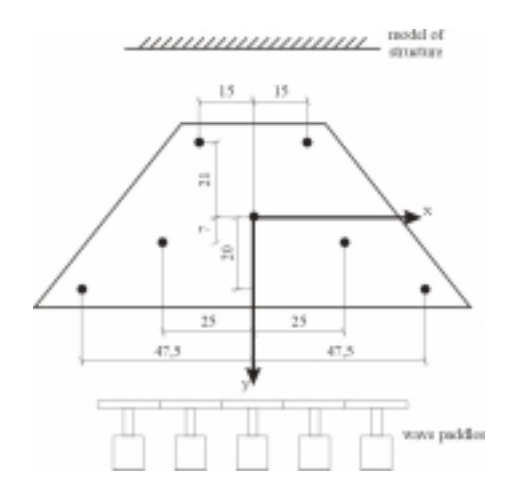


Figure 5.23: Array of wave probes.

From figure 5.24 it is shown that dimensionless wave run-up decreases with increasing incident wave angle  $\beta$ .  $\beta = 0^{\circ}$  corresponds with incident waves perpendicular to the breakwater axis. Not taking the lowest test results into account, a small decrease in relative wave run-up  $Ru_2\%H_{m0}$  has been noticed for increasing spreading angle  $\sigma$  (figure 5.25).

A longshore current was simulated in the laboratory. Therefore, a pumping system was installed in the wave flume which pumped water from one side of the basin to the other side. The current velocity has been measured by two propellers. Current velocity and wave obliqueness have been varied. A realistic current velocity profile over the water depth was realised by directing the flow of water through baskets filled with stones. The parameters of the JONSWAP spectrum were  $H_{m0} = 3$  m,  $T_p = 7$  s. The SWL was Z + 3.00 m (full scale value). Waves have been measured at the position of WRI at full scale.

Measurement results are given in table 5.16 and displayed in figure 5.26.

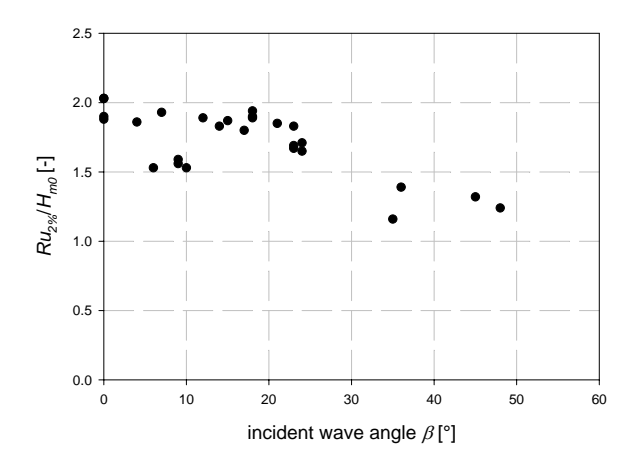


Figure 5.24: Influence of the incident wave angle  $\beta$  on wave runup.

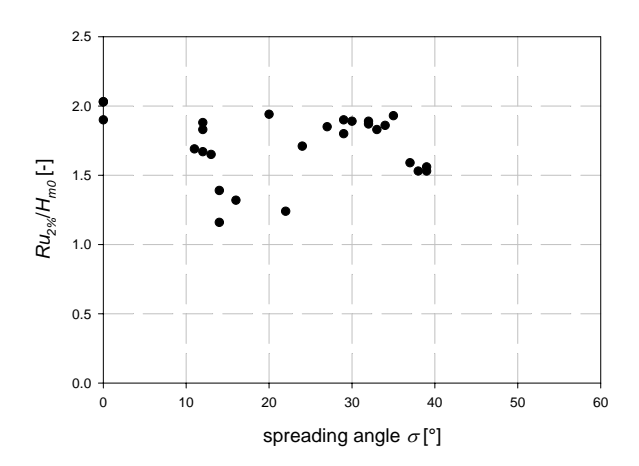


Figure 5.25: Influence of the energy spreading angle  $\sigma$  on wave run-up.

When only the results of the tests with a non-zero current velocity are looked into detail, one can state that increasing current velocity yields increasing dimensionless wave run-up. This increase is larger for head

on waves ( $\beta = 0^{\circ}$ ) than for oblique waves. This also has to do with the lower dimensionless wave run-up values for oblique waves whether a current is applied or not. Relative wave run-up is larger for zero current velocity ( $Ru_{2\%}/H_{m0} \cong 1.5$ ) than for  $v_c = 0.5$  m/s ( $Ru_{2\%}/H_{m0} \cong 1.2$ ) and approximately the same as the average wave run-up value for  $v_c = 1$  m/s.

Further detailed information on AAU testing is found in Schlütter et al. (2000), Jensen et al. (2000), Frigaard et al. (2000).

Table 5.16: Wave run-up results of tests with a longshore current.

direction [°]	current [m/s]	$H_{mo}$ [m]	Ru <sub>2%</sub> [-]	$Ru_{2\%}/H_{m0}$
0	1	2.9	4.73	1.63
0	1	2.98	4.68	1.57
0	0.5	2.92	3.44	1.18
0	0.5	2.97	3.48	1.17
0	0	2.96	4.44	1.50
0	0	2.95	4.3	1.46
15	0.5	2.9	3.44	1.19
15	0.5	2.9	3.46	1.19
15	1	3.24	4.31	1.33
15	1	3.34	4.74	1.42

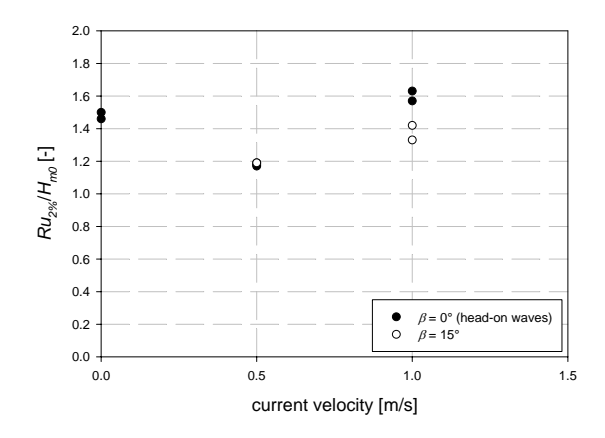


Figure 5.26: Results of wave run-up tests at AAU with a longshore current (cfr. table 5.16).

## 5.4 Small scale model tests – additional testing at FCFH

## **5.4.1** Objectives

Additional physical model tests on wave run-up have been performed in the small wave flume of Flanders Hydraulics in early 2002. The objectives of these extra tests were twofolded:

- to investigate the influence of the combined action of (1) the *SWL*, (2) the armour unit pattern and (3) the position of the comb of the run-up gauge and
- to investigate the influence of the spectral shape of the incident wave train.

During the storm reproduction tests framing within the OPTICREST project, armour units have been placed according to their actual position on the Zeebrugge breakwater. For the additional testing, armour units have been placed in a homogeneous pattern. The comb of the run-up gauge has been placed in three different positions relative to this regular pattern. The same test matrix has been run several times with the same stored wave paddle signals. The influence of the spectral shape has been investigated by means of the spectral width parameter  $\varepsilon$ .

## 5.4.2 Model set-up

For the materials, model geometry and instrumentation, reference is made to paragraph 5.3.1. In addition, the armour layer units have been placed successively in two different overall patterns.

Firstly, tests have been carried out with an irregular armour unit pattern. The armour units have been placed according to their position on the Zeebrugge breakwater (yard placing).

Secondly, another three series of tests have been carried out with a regular armour unit pattern in order to eliminate the influence of the irregularity of the armour unit pattern. The armour units of both the first (inner) and second (outer) armour layer have been placed in a regular pattern (i.e. 0.1255 blocks per  $m^2$  in each layer (the number taken into account in the breakwater design was 0.115)), yielding an overall porosity of 29% ( $k_{\Delta} = 1.05$ ), resp. 33% ( $k_{\Delta} = 1.10$ ). Figure 5.27 shows the regular armour layer of the model.

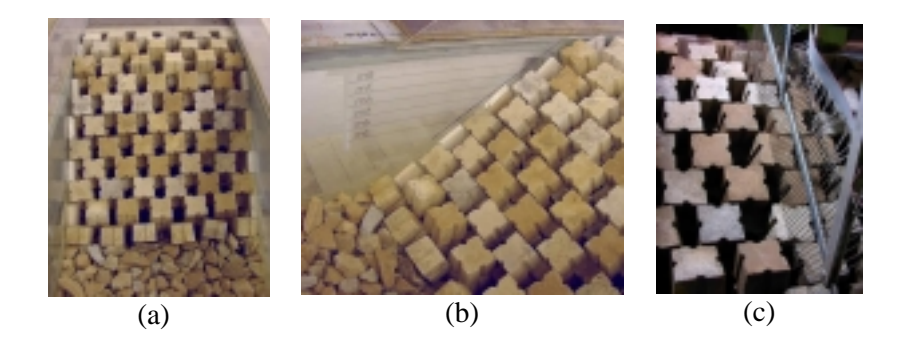


Figure 5.27: (a) & (b) Regular armour unit pattern with (c) the comb of the run-up gauge placed cfr. test series z3 or z4.

The wire gauge RU1 (see paragraph 5.3.1.3.2) has only been used during the z2 test series.

#### 5.4.3 Test matrix

Four different combinations of the position of the comb of the run-up gauge relative to the armour unit pattern have been tested. Tests series z2 contained tests on an irregular armour unit pattern (yard placing). For most tests, armour units have been placed in a regular pattern in order to avoid any influence of this pattern. Test series z3, z4 and z5 corresponded to a regular armour unit pattern (figure 5.27(a),(b)). The difference between the test series z3, z4 and z5 is found in the position of the comb of the run-up gauge relative to this regular armour unit pattern (figure 5.27(c)). The positions of the run-up gauge (z3, z4 and z5) correspond with the names of the test series. When the comb of the run-up gauge is placed in position z5, there are no holes underneath the comb. In positions z3 and z4, armour units and holes between two neighbouring armour units alternate under the needles of the comb of the run-up gauge (figure 5.28). Positions z3 and z4 are almost identical. Raising the SWL by  $D_{n50}$  and shifting the comb of the run-up gauge over  $2/3.D_{n50}$  does not change the slope configuration exposed to wave run-up (figure 5.29).

Four different water levels (*SWL*) have been considered: Z + 0.00, Z + 2.00, Z + 4.00, Z + 6.00, i.e. 50 cm, respectively 56.7 cm, 63.3 cm and 70 cm water depth in the wave flume. Standard JONSWAP spectra (with three parameters  $H_s$ ,  $T_p$  and  $\gamma$ ) have been generated. The peak enhancement factor in all tests was  $\gamma = 3.3$ . The full scale target wave

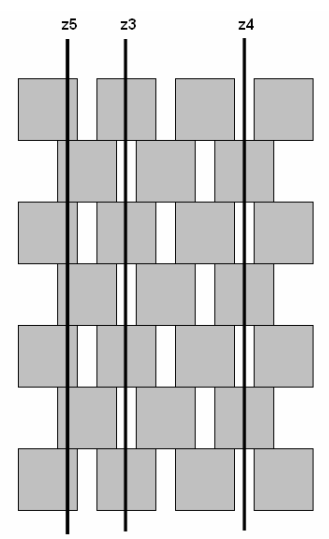


Figure 5.28: Different positions of the comb of the run-up gauge relative to the regular armour unit pattern in the outer armour layer.

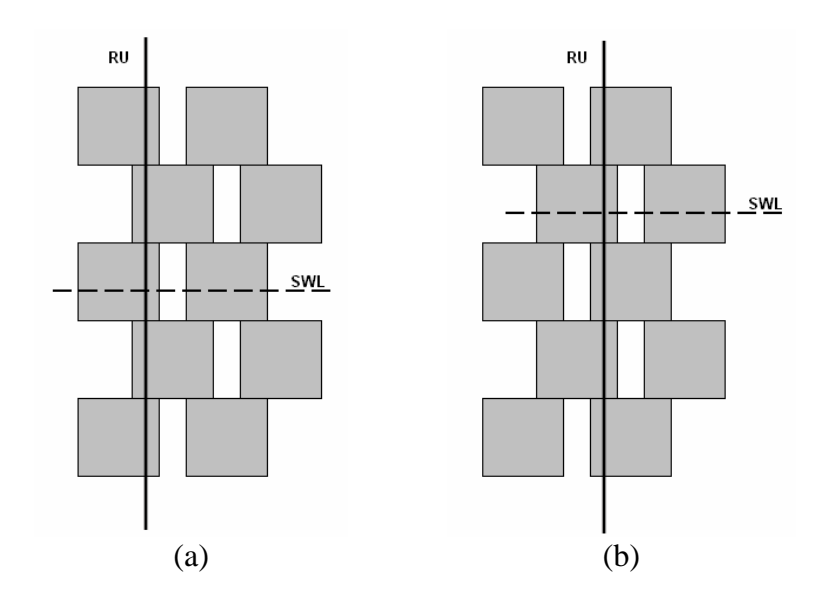


Figure 5.29: Shifting the comb of the run-up gauge over 2/3 of a block dimension and raising the SWL over one block dimension yields the same configuration for wave run-up.

height in all tests was  $H_{m0} = 3.00$  m. Thus, the influence of the wave height is minimised. Chosing  $H_{m0} = 3.00$  m sets the  $D_{n50}/H_{m0}$  ratio to 0.90. The target peak wave periods (full scale values) are  $T_{p1} = 7.6$  s ( $L_{op1} = 90$  m),  $T_{p2} = 9.8$  s ( $L_{op2} = 150$  m) and  $T_{p3} = 11.6$  s ( $L_{op3} = 210$  m). The scaled values in the laboratory are:  $T_{p1} = 1.39$  s ( $L_{op1} = 3.00$  m),  $T_{p2} = 1.79$  s ( $L_{op2} = 5.00$  m) and  $T_{p3} = 2.12$  s ( $L_{op3} = 7.00$  m). The test matrix is given in table 5.19. Tests are numbered according the considered test series: z3\*\*, resp. z4\*\* and z5\*\* in which the suffix '\*\*' indicates the test number within the concerning test series.

Table 5.19: Test matrix.

Test n°	<i>SWL</i> [Z+ m]	γ	$H_{mo}$	[m]	$T_{\rho}$ [s]	
			full scale	scale model	full scale	scale model
z*01	0.00	3.3	3.00	0.10	7.6	1.39
z*02	0.00	3.3	3.00	0.10	9.8	1.79
z*03	0.00	3.3	3.00	0.10	11.6	2.12
z*04	2.00	3.3	3.00	0.10	7.6	1.39
z*05	2.00	3.3	3.00	0.10	9.8	1.79
z*06	2.00	3.3	3.00	0.10	11.6	2.12
z*07	4.00	3.3	3.00	0.10	7.6	1.39
z*08	4.00	3.3	3.00	0.10	9.8	1.79
z*09	4.00	3.3	3.00	0.10	11.6	2.12
z*10	6.00	3.3	3.00	0.10	7.6	1.39
z*11	6.00	3.3	3.00	0.10	9.8	1.79
z*12	6.00	3.3	3.00	0.10	11.6	2.12

<sup>\* =</sup> number of test series (2, 3, 4 or 5)

Tests z\*07, z\*08 and z\*09 of the test series z2, z4 and z5 have been carried out twice. To make a distinction between the first run of a test and the second run, a prefix 'ra' (first run) or 'rb' (second run) has been added to the name of the test. The aim of repeating tests was to find out whether a test could be reproduced correctly or not. The same wave paddle steering signals have been used for the first run and for the second run. Therefore, before any test was carried out, the wave paddle displacement time series have been calculated and have been stored in a buffer. Running the tests, the steering signals were picked up from this buffer and were sent to the wave paddle.

#### **5.4.4 Results**

#### **5.4.4.1** Wave data

Only wave data measured by wave gauge ZE4 (i.e. at the location of WRI in the field) have been taken into account, unless mentioned otherwise. The sample frequency in the laboratory was set to  $f_{s,m}$  = 10.989 Hz ( $\Delta t_m = 0.091$  s). The corresponding full scale value is  $f_{s,f} =$ 2.006 Hz ( $\Delta t_f = 0.498$  s). Each laboratory test lasted for 1310 seconds (almost 22 minutes), which equals a testing period of approximately two hours at full scale. Waves have been analysed in frequency domain. To make sure the active wave absorption was already fully working before the actual measurements began, data of all tests have been analysed from  $t_0 = 60$  s on. The first minute of testing has been omitted in order to allow the waves to travel from the wave paddle to the structure, to reflect on the structure and to travel back to the wave paddle. Time series with a duration of  $T_0 = 1200 \text{ s}$  (laboratory value) have been selected. This duration corresponds with a duration at full scale of almost 110 minutes. The number of samples in a data window was 1024. The 90% confidence boundaries for the spectrum are found by multiplying the spectrum by [0.693, 1.594]. The spectral bandwidth is  $b = 2.10^{-3}$  Hz.

The wave height distribution (waves measured at ZE4) of test z209 is shown in figure 5.30 as an example. The waves at ZE4 are Rayleigh distributed except for the highest waves which deviate from this distribution.

In general, wave spectra are generated quite well. In some cases, double peaked spectra have been measured: a second peak appears in the spectrum (figure 5.31). Only small (compared to the peak values of the energy spectrum) subharmonic waves (the so-called 'long waves') are noticed in all tests.

The tests z\*07, z\*08 and z\*09 of the test series z2, z4 and z5 have all been repeated once. Figure 5.32 shows for both tests z207ra and z207rb the target wave paddle displacement and the actual wave paddle displacement measured by a potentiometer on the piston of the wave paddle during the first ten seconds of the test. The target wave paddle displacement is the calculated wave paddle displacement sent to the wave paddle during the test. In the beginning of the test, the target wave paddle displacement signals of both runs coincide. Also



Figure 5.30: Wave height distribution (waves measured at ZE4, i.e. the location of WR I in the field) of test z209.

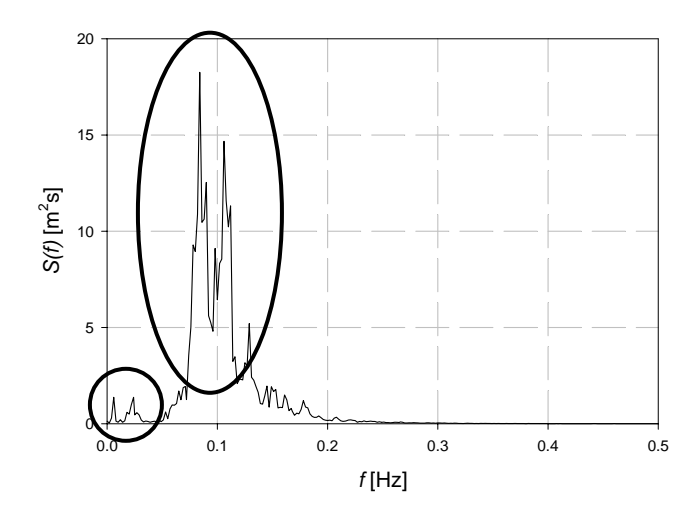


Figure 5.31: Double peaked wave spectrum of test z209ra measured by wave gauge ZE4 with indication of subharmonic waves.

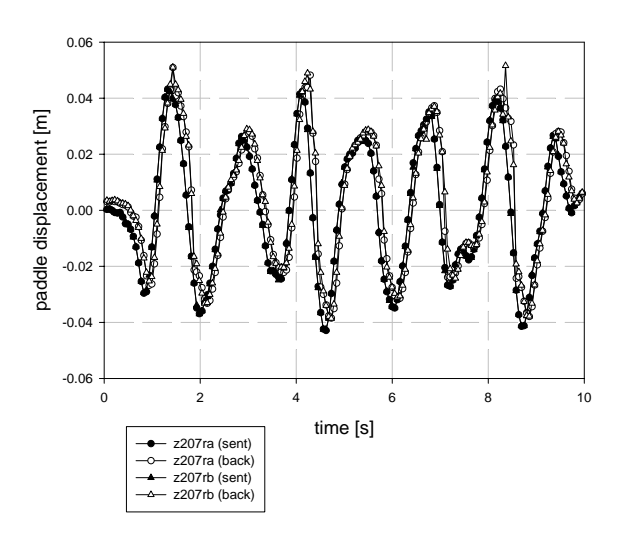


Figure 5.32: Comparison of steering signal sent to the wave paddle and the control wave paddle signal of tests z207ra and z207rb in the interval [0 s, 10 s].

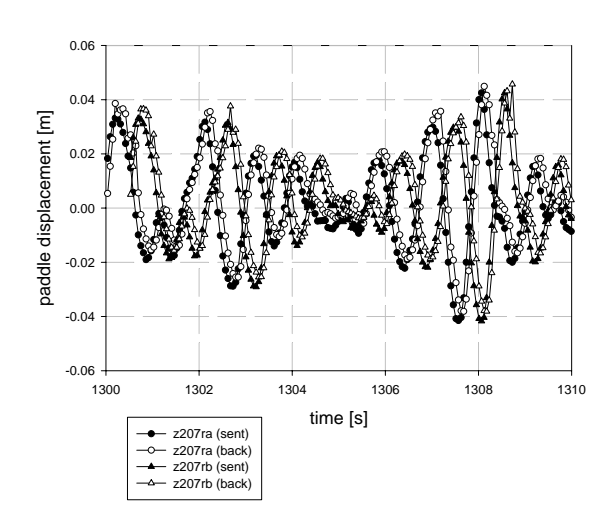


Figure 5.33: Comparison of steering signal sent to the wave paddle and the control wave paddle signal of test z207ra and z207rb in the interval [1300 s, 1310 s].

the measured wave paddle displacement signals coincide for both tests. The control signals run after the sent signals continuously only for a couple of milliseconds. At the end of the time series, the control signals still run after the sent signals for a couple of milliseconds for both runs, but a shift over about 0.5 s is seen on both the sent and the measured signals of the first run and the second run (figure 5.33). This difference is assumed due to an inaccuracy in the wave paddle steering computer programme.

In general, it is concluded that tests have been repeated quite accurately. The average deviation of the significant wave height  $H_{m0}$  of the repeated test to the first test is 1.4%. The maximum deviation is 3.9%. Peak wave periods are reproduced very well, except for test z507 ( $T_{p,z507ra} = 6.91$  s and  $T_{p,z507rb} = 7.85$  s). The average deviation on the mean wave period  $T_{01}$  is 0.2%. The maximal deviation is 0.8%. The average deviation of the wave periods  $T_{-1,0}$  is 0.2% and the average deviation on the spectral width parameters  $\varepsilon$  and  $Q_p$  are 1.0%, respectively 1.6%

Wave analysis results are given in Annex C. The spectral parameters  $H_{m0}$ ,  $T_{01}$ ,  $T_p$ ,  $\varepsilon$ ,  $Q_p$  and the Iribarren numbers  $\xi_{om}$  and  $\xi_{op}$  are listed.

The average value of the significant wave height  $H_{m0}$  measured by wave gauge ZE4 in all tests is 2.88 m. The variation coefficient  $c = s/\bar{x}$  equals 0.071. The spreading range of the significant wave height is w = 0.73 m (2.4 cm in model scale). The 90% confidence intervals of the average value of the significant wave height in all tests is [2.83, 2.94].

The average deviation on the target significant wave height ( $H_{m0} = 3$  m) is 5.4% and the average deviation of the target peak wave period  $T_p$  is 5.3%. The maximum deviation on the significant wave height  $H_{m0}$  and the peak wave period  $T_p$  are respectively 16% (test z203) and 17% (test z506).

### **5.4.4.2** Wave run-up

The 'sum' signal of the run-up gauge which has been used for analysis purposes does not look alike an ordinary wave signal (figure 5.34). The wave run-up measurements are disturbed by the water outflow during wave run-down. When a wave retains on the slope of the breakwater, a hydraulic gradient is created: the water surface level in the core of the breakwater is higher than the level of the wave trough.

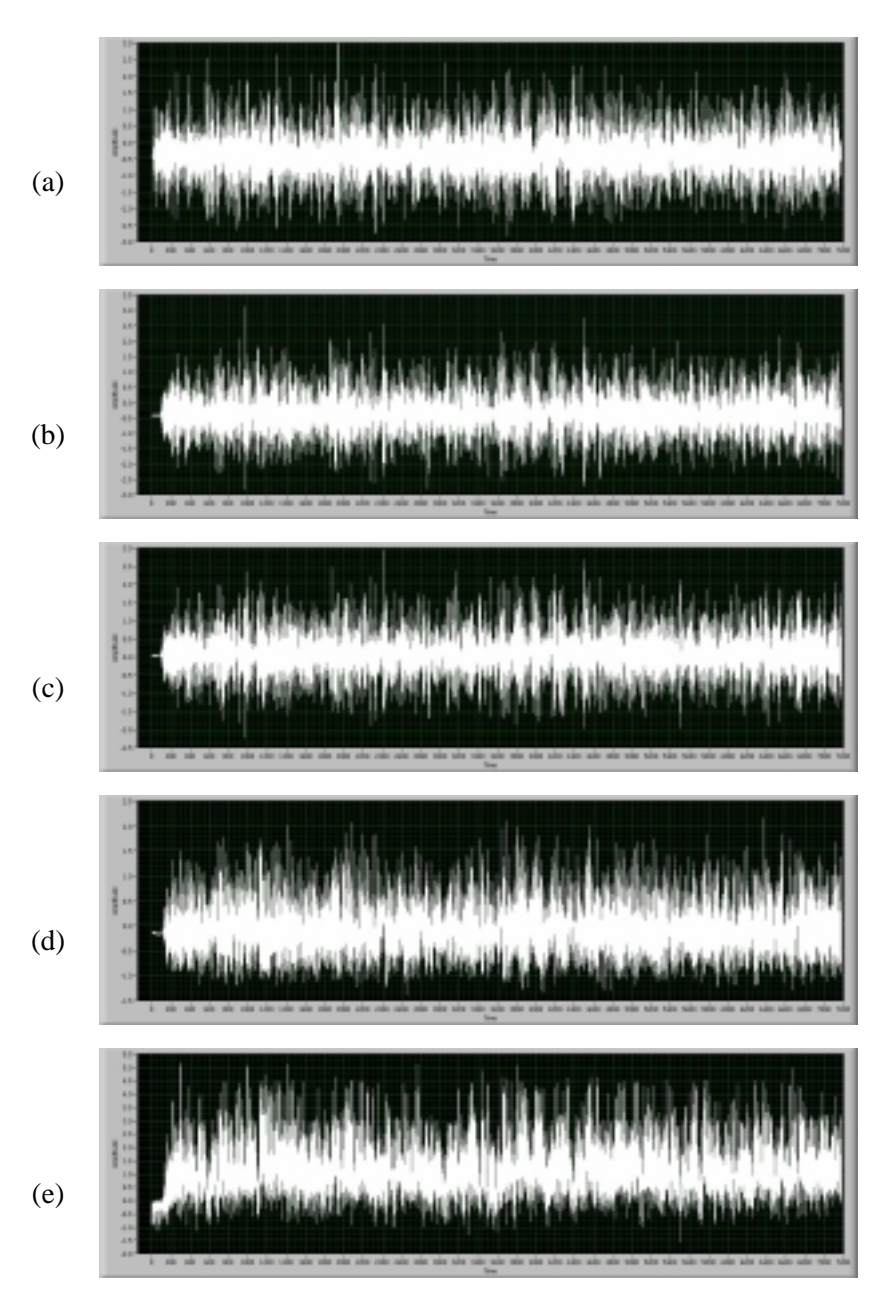


Figure 5.34: Example of (a) channel 07 (AWA1), (b) channel 01 (ZE1), (c) channel 02 (ZE4), (d) channel 03 (ZE7), (e) channel 05 (step gauge – sum output) of test z201ra.

By this hydraulic gradient, the water squirts out of the core through the armour layer. The water hits the needles of the comb of the run-up gauge, shortcircuiting some electrodes. Thus, wave run-down is wrongly detected. This squirting out of the water also has its repercussion on the determination of the wave run-up values Ru. A classical zero-down crossing (ZDC) method or zero-up crossing (ZUC) method as carried out for wave analysis in time domain cannot be performed as the wave run-up signal does not show many zero line (SWL) crossings. Consequently, the ZDC method has been adapted slightly to solve this problem. By virtually raising the still water level by 0.5  $H_s$ , a normal ZDC method could be applied relative to this artificial SWL. Afterwards, half a significant wave height has been added to all Ru values. This alternative method has however two adverse effects. Firstly, the smallest wave run-up values ( $Ru < 0.5 H_s$ ) cannot be detected by this method and the wave run-up distribution therefore shows a truncation at  $0.5 H_s$ . But, as only the highest wave run-up values are of importance ( $Ru_{x\%}$  with small values of the exceedance probability x), the alternative ZDC method yields reliable results. Secondly, the alternative method may also detect a wave runup event (figure 5.35 – dashed lines), although this wave run-up event is not detected by a normal zero down crossing method as it is part of a bigger wave run-up event (figure 5.35 - solid lines). Two wave runup events are detected in stead of one. However, the highest value of the two wave run-up events is not influenced and is also detected by the normal ZDC method. The lowest value of the two wave run-up events has a high exceedence probability x and is not considered furtheron. Also a lot more wave run-up events are detected than by performing a normal zero down crossing procedure. However, the exceedence probability x refers to the number of incident waves and not the number of run-up events which by consequence does not have to be calculated. The determination of the  $Ru_{2\%}$  value may disturbed in case two high wave run-up values are detected in stead of only one. It is however very unlikely that a high wave arriving at the toe of the breakwater is 'eaten' by its preceding (high) wave retaining on the slope of the structure. Wave heights are limited either by wave steepness ( $s_{max} = 0.142$  (cfr. De Rouck (1996)) or water depth (a rule of thumb is H/d = 0.4 to 0.5). The first restriction limits the wave height H to  $0.22 T^2$ . In case of the additional FCFH tests, the second restriction is more determining as for  $T_{p1} = 1.39$  s,  $H_{max}$  is 0.429 m. It is more likely that the second (smaller) wave run-up value is smaller than the first (larger) wave run-up value is found between other wave

run-up events which are also detected by the normal ZDC method but which have a high exceedence probability x.

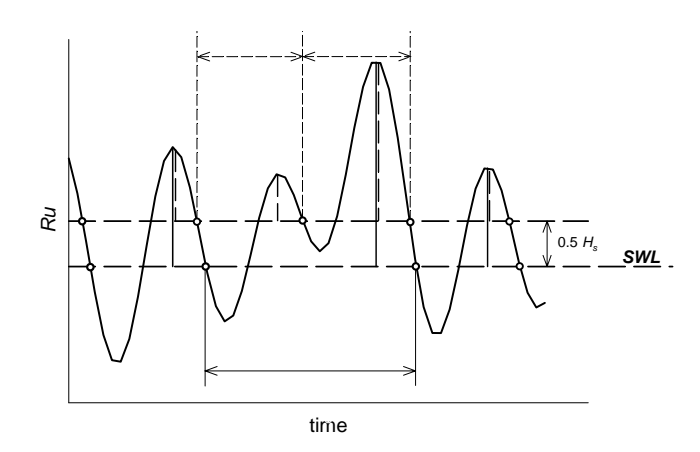


Figure 5.35: Difference between a normal ZDC and the adapted ZDC with an artificial SWL.

Wave run-up distributions have been evaluated into detail. The wave run-up distribution is not exactly Rayleigh distributed, but the deviations are rather small. These deviations have also been noticed in full scale wave run-up distribution curves. The deviations are due to the fact that the slope of the breakwater is categorised as 'very rough'  $(D_{n50}/H_{m0} \sim 0.90)$ . At certain levels of the slope, the water disappears in the gaps between different armour units. The water has not enough momentum to reach higher levels. Thus, a lot of wave run-up values have approximately the same value of the level of this 'gap' above SWL. The water can also be obstructed by armour units sticking out of the upper surface of the other armour units. The water is obstructed rushing up the breakwater slope. At other places, the uprush of water is facilitated due to the fact that an armour unit is sunken down in the slope with regard to the 'average' slope. Remarkable is that all run-up distributions of tests performed at one particular SWL (Z + 0.00, Z +2.00, Z + 4.00 or Z + 6.00) show bumps and dents at exactly the same levels. Even the curving at high levels in tests with a low SWL can be found again at low levels in tests with a higher SWL. It is concluded that the position of the armour units has an important influence on the wave run-up distribution and on the determination of the  $Ru_{2\%}$  value.

The  $Ru_{x\%}/H_{m0}$  values (with x=1, 2, 5, 10 as well as the maximal and significant dimensionless wave run-up  $Ru_{max}/H_{m0}$ , resp.  $Ru_{s}/H_{m0}$ ) have been plotted against the spectral width parameter  $\varepsilon$  in figures E.1. In case of x=2, the data are presented in figure 5.36. All graphs show dimensionless wave run-up values  $Ru_{x\%}/H_{m0}$  increasing with an increasing value of the spectral width parameter  $\varepsilon$ .

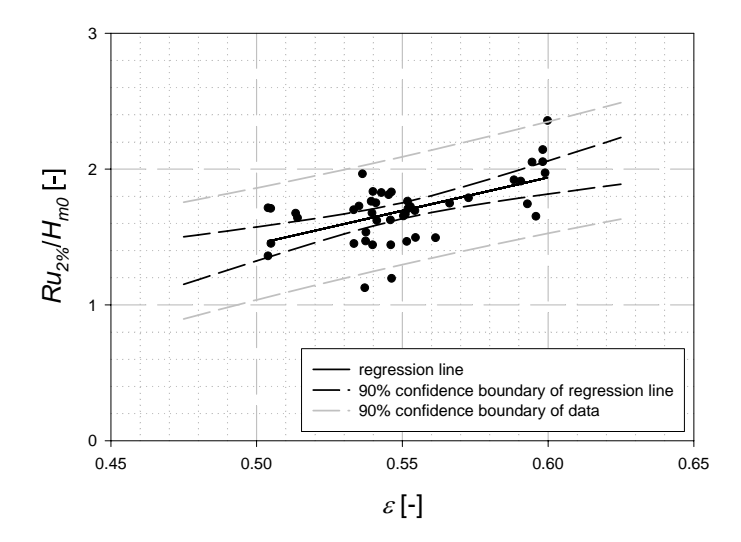


Figure 5.36: The dimensionless wave run-up values  $Ru_{2\%}/H_{m0}$  [-] versus the spectral width parameters  $\varepsilon$  [-] and the 90% confidence boundaries of the regression line and the data of all tests  $z^{***}$  excluding tests with SWL = Z + 6.00.

The 90% confidence boundaries of the regression line and the data have been determined (Taerwe (1996)) (figure 5.36).

$$b_0 + b_1 \varepsilon \pm t \int_{n-2, 1-\frac{\alpha}{2}} \cdot \hat{\sigma}_{E\left[\frac{Ru_{2\%}}{H_{m0}} \middle| \varepsilon\right]}$$
 (5.7)

$$b_0 + b_1 \varepsilon \pm t_{n-2,1-\frac{\alpha}{2}} \cdot \sigma_{\frac{Ru_{2\%}}{H_{m0}}|\varepsilon}$$

$$\tag{5.8}$$

with

$$\hat{\sigma}_{E\left[\frac{Ru_{2\%}}{H_{m0}}|\varepsilon\right]}^{2} = \frac{s^{2}}{n} \left(1 + \frac{\left(\varepsilon - \overline{\varepsilon}\right)^{2}}{s_{\varepsilon^{*}}^{2}}\right)$$
 (5.9)

$$\hat{\sigma}_{\frac{Ru_{2\%}}{H_{m0}}|\varepsilon}^{2} = s^{2} \left( 1 + \frac{1}{n} + \frac{\left(\varepsilon - \overline{\varepsilon}\right)^{2}}{ns_{\varepsilon^{*}}^{2}} \right)$$
 (5.10)

and

$$s_{\varepsilon^*}^2 = \frac{1}{n} \sum_{i=1}^n \left( \varepsilon_i - \overline{\varepsilon} \right)^2 \tag{5.11}$$

$$s^{2} = \frac{1}{n-1} \sum_{i=1}^{n} \left( \left( \frac{Ru_{2\%}}{H_{m0}} \right)_{i} - \frac{\overline{Ru_{2\%}}}{H_{m0}} \right)^{2}$$
 (5.12)

in which *n* is the number of data points. The  $t_{n-2,1-\alpha/2}$  value is  $t_{43,0.95} = 1.682$ .

Wave run-up results are shown in figure 5.37 to figure 5.40. Each graph is valid for one SWL: Z + 0.00 (figure 5.37), Z + 2.00 (figure 5.38), Z + 4.00 (figure 5.39) and Z + 6.00 (figure 5.40)). Within each graph, wave run-up results are grouped per position of the comb of the run-up gauge relative to the armour unit pattern (z2, z3, z4 and z5 – cfr. figure 5.28). The tables with the numerical values of  $Ru_{2\%}/H_{m0}$  are found in Annex C. The values of the Iribarren number  $\xi_{om}$  [-], the spectral width parameter  $\varepsilon$  [-] and the dimensionless wave run-up value exceeded by 2% of the waves  $Ru_{2\%}/H_{m0}$  [-] of the tests are given in table C.1 (for water level Z + 0.00), table C.2 (for water level Z + 2.00), table C.3 (for water level Z + 4.00) and table C.4 (for water level Z + 6.00).

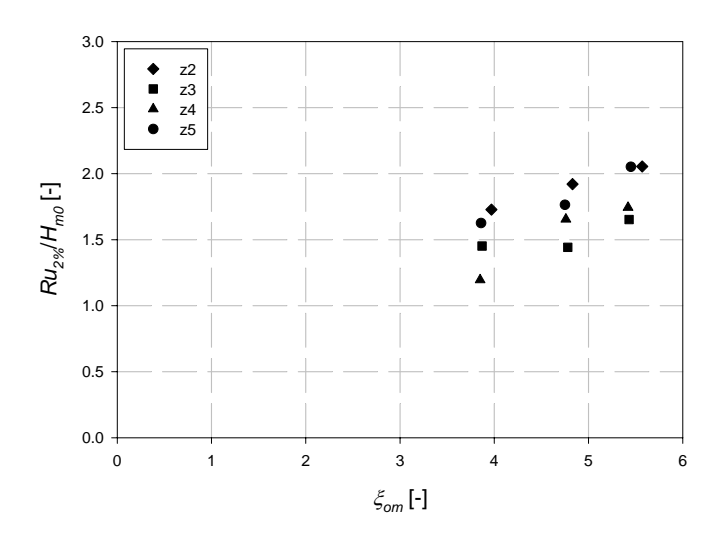


Figure 5.37: Dimensionless wave run-up  $Ru_{2\%}/H_{m0}$  [-] versus the Iribarren number  $\xi_{om}$  [-] for different positions of the comb of the run-up gauge relative to the armour layer for SWL = Z + 0.00.

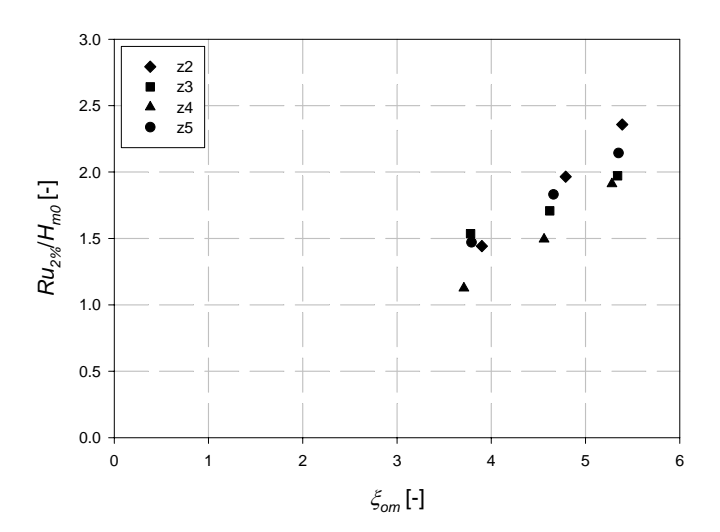


Figure 5.38: Dimensionless wave run-up  $Ru_{2\%}/H_{m0}$  [-] versus the Iribarren number  $\xi_{om}$  [-] for different positions of the comb of the run-up gauge relative to the armour layer for SWL = Z + 2.00.

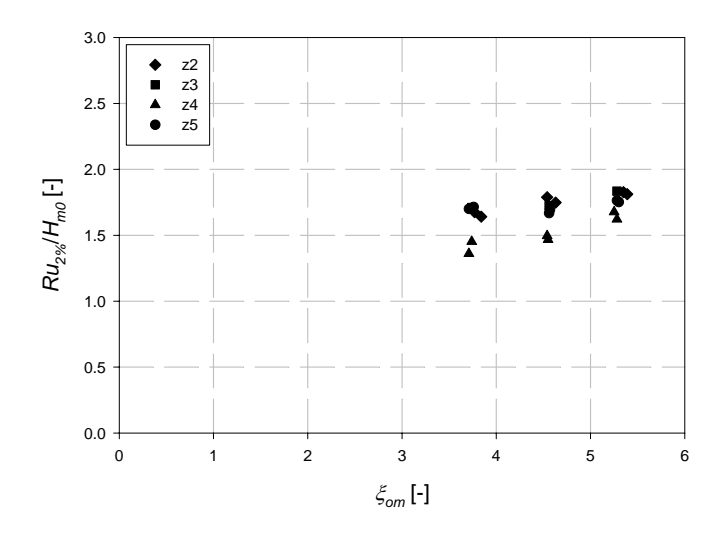


Figure 5.39: Dimensionless wave run-up  $Ru_2\%/H_{m0}$  [-] versus the Iribarren number  $\xi_{om}$  [-] for different positions of the comb of the run-up gauge relative to the armour layer for SWL = Z + 4.00.

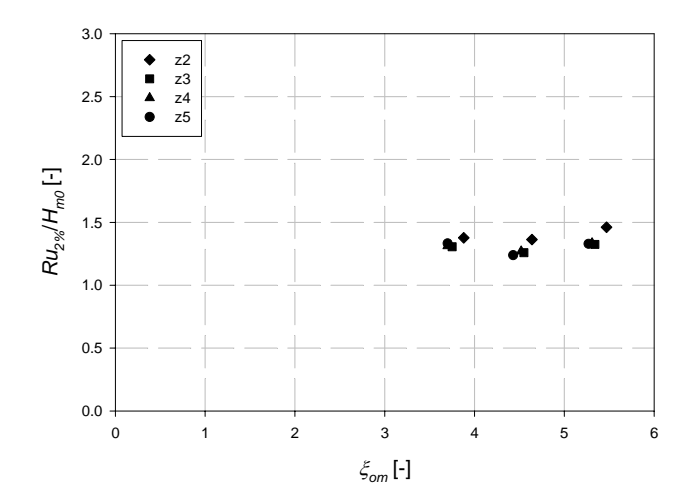


Figure 5.40: Dimensionless wave run-up  $Ru_{2\%}/H_{m0}$  [-] versus the Iribarren number  $\xi_{om}$  [-] for different positions of the comb of the run-up gauge relative to the armour layer for SWL = Z + 6.00.

In all graphs, three clouds of results are observed. Each cloud corresponds to one of the three target peak wave periods ( $T_p = 7.6 \text{ s}$ , 9.8 s and 11.6 s). Quite a large spreading is seen on the results. Dimensionless wave run-up values  $Ru_{2\%}/H_{m0}$  vary between 1.15 and 2.40. For the smallest value of the three tested target peak wave periods, the relative wave run-up exceeded by 2% of the waves is approximately  $Ru_{2\%}/H_{m0} = 1.5$ . The increase in dimensionless wave run-up value exceeded by 2% of the waves  $Ru_{2}$ // $H_{m0}$  with increasing Iribarren number  $\xi_{om}$  is larger for tests with SWL = Z + 2.00 than for tests with other water levels. Tests with SWL = Z + 0.00 show a larger increase in  $Ru_{2\%}/H_{m0}$  than tests with SWL = Z + 4.00. This increase in dimensionless wave run-up value is not seen at all at water level Z + 6.00: dimensionless 2% wave run-up values remain constant  $(Ru_{2\%}/H_{m0} = 1.3 \text{ to } 1.4)$  with increasing Iribarren numbers  $\xi_{om}$ . This is mainly due to the fact that for low SWLs, wave run-up takes place on the uniform 1:1.3 slope, whereas for high SWLs, wave run-up occurs on a more flattened and more porous armour layer (cfr. figure 5.27(b) - SWL levels are written mirrorwise on the side wall of the flume). The armour unit pattern in the upper part of the slope affects the highest wave run-up events. There are a lot more holes between the crest elements in which the water can disappear, not giving rise to wave run-up. Therefore, tests with SWL Z + 6.00 will no longer be taken into account. No firm conclusions concerning the influence of the water depth on wave run-up could be drawn. Remarkable is that the dots representing the results of the tests with an irregularly placed armour layer (test series z2 (♦)) are almost always found in the highest part of the clouds. The dots representing the results of the test series z4 (\( \) on the contrary are almost always found in the lower part of the clouds. The results of test series z5 (•) are only a little bit smaller than the results of test series z2.

The maximum differences in spectral width  $\Delta \varepsilon$ , Iribarren number  $\xi_{om}$  and dimensionless wave run-up  $Ru_{2\%}/H_{m0}$  between the four results within each cloud in figures 5.37 to 5.40 have been calculated in table 5.20. Within each cloud the  $Ru_{2\%}/H_{m0}$  values differ quite a lot. But, for each cloud of results, the ratio between  $\Delta \varepsilon$  and  $\Delta Ru_{2\%}/H_{m0}$  is much larger than for the slope of the regression line in figure 5.36. According to figure 5.36, a  $\Delta \varepsilon$  value as large as observed in figures 5.37 to 5.40 cannot yield differences (sometimes in negative!) between the  $Ru_{2\%}/H_{m0}$  values as large as observed in figures 5.37 to 5.40. A number of test results are discussed. Test z401 and test z501 are looked upon into detail. The spectral width measured in these tests

is  $\varepsilon = 0.5463$ , resp.  $\varepsilon = 0.5459$ . The Iribarren numbers are respectively  $\xi_{om} = 3.85$  and  $\xi_{om} = 3.86$ . The dimensionless wave run-up value exceeded by 2% of the waves is  $Ru_{2\%}/H_{m0} = 1.20$  in test z401 and is  $Ru_{2\%}/H_{m0} = 1.63$  in test z501. The Iribarren numbers and the spectral width parameters have almost the same values in both tests ( $\Delta \varepsilon$  = 0.0004 and  $\Delta \xi_{om} = 0.01$ ). Nevertheless, the dimensionless wave run-up value  $Ru_{2}$ // $H_{m0}$  differs 0.43! According to the regression line shown in figure 5.36, a difference in spectral width of  $\Delta \varepsilon = 0.0004$  yields only a difference of 0.002 in dimensionless wave run-up. The only varying parameter between both tests is the position of the comb relative to the armour unit pattern and the SWL. The spectral width parameter  $\varepsilon$  has the same value ( $\varepsilon = 0.5039$ ) for both tests z407ra and z407rb. The Iribarren numbers  $\xi_{om}$  in both tests are almost the same. For test z207ra is  $\xi_{om} = 3.71$  and for test z507rb is  $\xi_{om} = 3.76$ . The respective dimensionless wave run-up values are 1.36 and 1.72. The difference between both is  $\Delta Ru_{2\%}/H_{m0} = 0.36$ , nonetheless no difference has been measured in spectral width. Two other examples are tests z304 and z404 and tests z504 and z404. All examples show very little or no difference between Iribarren numbers  $\xi_{om}$  and between spectral width parameters  $\varepsilon$ , but a rather large difference in dimensionless wave runup value. In these cases, the difference in  $Ru_{2\%}/H_{m0}$  values is due to the combined action of the position of the comb of the run-up gauge, the SWL and the armour unit pattern. However, this influence is subjected to randomness. Despite the spreading (caused by the combined action of the three aforementioned items) on the results shown in figure 5.36, the influence of  $\varepsilon$  on  $Ru_{2\%}/H_{m0}$  is clear: increasing spectral width yields increasing wave run-up. The influence of the spectral shape has also been investigated upon the peakedness parameter  $Q_p$  of Goda (1985). Figure 5.41 shows the relationship between  $Q_p$  and the relative wave run-up value  $Ru_{2\%}/H_{m0}$ . Dimensionless wave run-up decreases with increasing peakedness parameter  $Q_p$ .

The combined action of the position of the comb of the run-up gauge, the SWL and the armour unit pattern introduce a kind of 'measuring error' on the  $Ru_2\%/H_{m0}$  measurements. Unfortunately the magnitude of this 'measuring error' is sometimes much larger than the influence of the spectral width by which latter is difficult to distinguish.

Table 5.20: Differences  $\Delta \varepsilon$ ,  $\Delta \xi_{om}$  and  $\Delta R u_{2\%}/H_{m0}$  for different SWLs.

		SWLS.		
		1 <sup>st</sup> cloud	2 <sup>nd</sup> cloud	3 <sup>rd</sup> cloud
		$(\xi_{om} \sim 3.79)$	$(\xi_{om} \sim 4.62)$	$(\xi_{om} \sim 5.36)$
	arDeltaarepsilon	0.0129	0.0423	0.0053
Z + 0.00	$arDelta \xi_{om}$	0.12	0.48	0.15
	$\Delta Ru_{2\%}/H_{m0}$	0.53	0.08	0.40
	arDeltaarepsilon	0.0027	0.0251	0.0092
Z + 2.00	$arDelta \xi_{om}$	0.19	0.23	0.11
	$\Delta Ru_{2\%}/H_{m0}$	0.41	0.48	0.45
	arDeltaarepsilon	0.0294	0.0217	0.0060
Z + 4.00	$arDelta \xi_{om}$	0.13	0.09	0.14
	$\Delta Ru_{2\%}/H_{m0}$	0.36	0.25	0.21
	$\Delta arepsilon$	0.0108	0.0201	0.0112
Z + 6.00	$arDelta \xi_{om}$	0.18	0.21	0.20
	$\Delta Ru_{2\%}/H_{m0}$	0.07	0.12	0.14

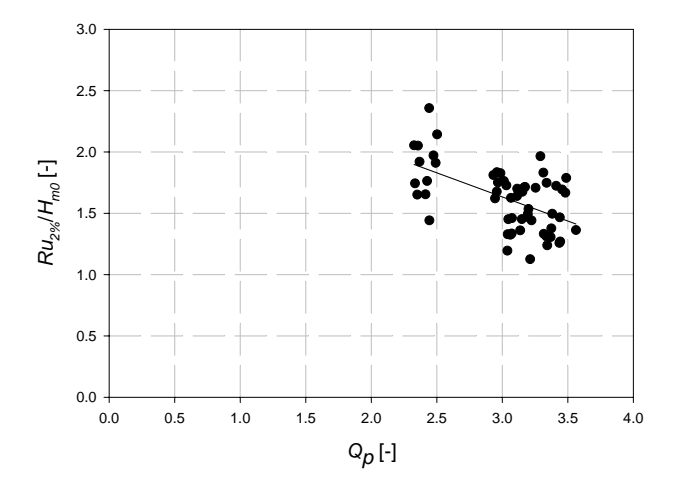


Figure 5.41: Influence of the spectral shape (characterised by the peakedness parameter  $Q_p$  of Goda (1985)) on the relative wave run-up value  $Ru_{2\%}/H_{m0}$ 

## 5.5 Small scale model tests – additional testing at UGent

## 5.5.1 Objectives

Additional small scale model tests have been performed on a simplified model of the Zeebrugge breakwater. The objectives of the additional small scale model tests at UGent were:

- to investigate the influence of the spectral shape (characterised by the spectral width parameter  $\varepsilon$  or the peakedness parameter  $Q_p$ )
- to investigate the influence of the combined action of the *SWL*, armour unit pattern and the position of the comb of the run-up gauge relative to the armour unit pattern
- to investigate the applied core scaling law

A lot of spreading was seen on the additional FCFH results (see paragraph 5.4). Differences were due to on the one hand the spectral width parameter  $\varepsilon$  and on the other hand the combined action of the SWL, armour unit pattern and the position of the comb of the run-up gauge relative to the armour unit pattern. Sometimes, a difference in dimensionless wave run-up was larger for a different combination of the three inextricably bound up parameters (armour unit pattern, SWL and position of the comb) for the same sea state than might be expected by the observed influence of the spectral width parameter  $\varepsilon$ . Also the comparison of full scale measurement results and small scale model test results of storm reproductions (see chapter 6) indicates the spectral shape as one of the suspected parameters. To short-circuit the discussion about the influence of  $D_{n50}/H_{m0}$  on wave run-up, tests have been carried out with wave heights  $H_s$  which were several times larger than  $D_{n50}$ . The Zeebrugge breakwater has been taken as starting point. The armour units have been removed and tests have been carried out with the filter material as armour layer. Wave run-up has been measured by means of two identical digital wave run-up gauges, installed on the model in two different cross sections. Thus, the influence of the parameter  $D_{n50}/H_{m0}$  was minimised.

## 5.5.2 Model set-up

A didactical example of a small scale rubble mound breakwater has been built in the small wave flume (15 m long, 0.60 m high and 0.35 m wide) of the Department of Civil Engineering of Ghent University (figure 5.42 and figure 5.43). Waves have been generated by means of a piston type wave maker. The model geometry is based on the geometry of the Zeebrugge breakwater. The dimensions of the materials of the different layers are given in table 5.21. The armour

layer of the model corresponds to the filter layer of the Zeebrugge breakwater and consists of rock material (1-3 ton). To investigate the influence of the core scaling law, two types of core material have been tested. A first series of tests has been carried out on a model with a distorted scale (scale 1:20) for the core material (cfr. Burcharth et al. (1999)) (further on called 'core 1'). The materials of the other layers have been scaled to 1:30. A second series of tests is performed on a model scaled to 1:30 (further on called 'core 2') and keeping the Froude number constant for all layers.

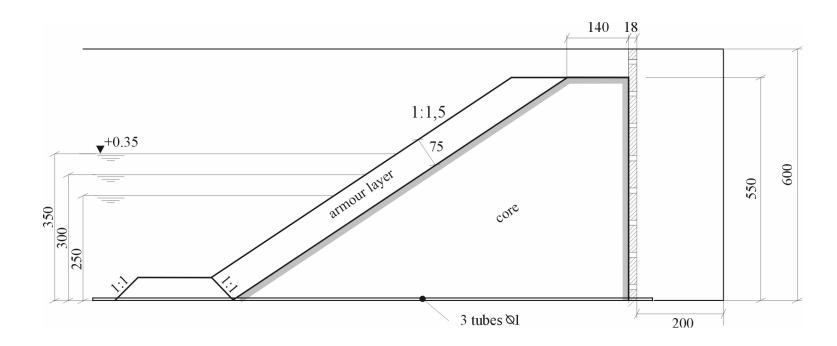


Figure 5.42: Model lay-out (dimensions in [mm], levels in [m]).



Figure 5.43: Scale model in the small wave flume of Ghent University.

A perforated paddle allows the evacuation of the water out of the core at the backside of the breakwater (figure 5.43). Water can flow back towards the berm of the breakwater through three plastic tubes of  $\phi =$ 

16 mm which have been placed on top of a geotextile underneath the breakwater. The seaward slope of the breakwater is 1:1.5. To exclude the effect of the crest level – as noticed in the additional FCFH tests, especially for tests with a high SWL – the slope has been extended high above the SWL so as to have a uniform slope.

Table 5.21: Dimensions of material of the UGent model.

	starting p	small scale	
	<i>W</i> [kg]	$W[kg]$ $D_n[m]$	
core	2 – 300 kg	0.094 m – 0.50 m	5 – 25 mm <sup>(*)</sup> 3 – 16 mm <sup>(**)</sup>
armour layer	1 – 3 ton	0.74 m – 1.03 m	25 – 36 mm
berm	3 – 6 ton	1.03 m – 1.36 m	36 – 45 mm

<sup>(\*\*)</sup> core scaled according to method of Burcharth et al. (1999) (1:20) – core 1

(\*\*) core scaled by Froude's law (1:30) – core 2

#### **5.5.3 Instrumentation**

The positions of the resistance type wave gauges along the wave flume have been determined according to paragraph 3.2. The two wave gauges closest to the wave paddle have been used for active wave absorption. Three wave gauges have been placed in the vicinity of the toe of the breakwater and have been used for reflection analysis (figure 5.44(a)) to determine the incident wave height at the toe of the structure. A sixth gauge was randomly placed between the before mentioned groups of gauges and has been used for simple wave analysis.

Wave run-up has been measured simultaneously by means of two identical run-up gauges RU1 and RU2 (figure 5.44(b)). Each run-up gauge has 64 active electrodes. The distance between the needles of the comb is 1 cm. The gauges have been placed in different cross sections of the breakwater. The simultaneous measurements of wave run-up not only allow to double check the wave run-up measurements and thus to exclude wrong measurements, but also to detect whether there is a significant difference in measured wave run-up due to the position of the comb of the step gauges with regard to the placement pattern of the armour layer.

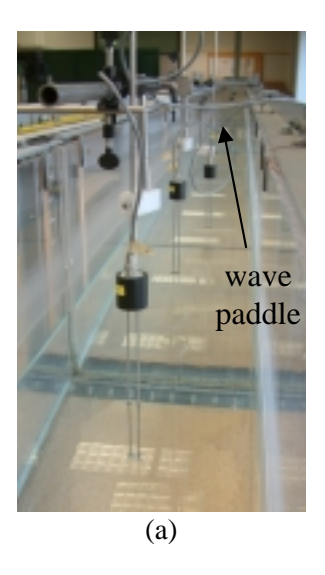




Figure 5.44: (a) A set of three wave gauges to measure the incident wave field at the toe of the structure and (b) two run-up gauges to measure wave run-up on the breakwater simultaneously.

The water height is measured by a ruler placed at the inner side of the flume in the vicinity of the wave paddle.

Data have been sampled at  $f_s = 40$  Hz. Wave data have been analysed by the ANASYS (Ghent University) computer programme.

#### 5.5.4 Test matrix

The wave height is not limited by the scale of the model, but rather by the breaker criterion (small wave periods) and the performance (stroke) of the paddle (for larger wave periods). Hudson's formula reads:

$$W_{50} = \frac{\rho g H_{des}^3}{K_D \Delta^3 \cot \alpha} \tag{5.13}$$

with  $\bullet$   $K_D$  is the damage factor

$$\bullet \ \Delta = \frac{\rho_s - \rho_w}{\rho_w} \ [-]$$

- $\rho_s = \text{rock density [kg/m}^3] (= 2650 \text{ kg/m}^3)$
- $\rho_w$  = density of water [kg/m<sup>3</sup>] (= 1000 kg/m<sup>3</sup>)
- $\cot \alpha = 1.5$  [-]
- $W_{50}$  = block weight for which 50% of the total sample weight is of lighter blocks [N]
- $H_{des}$  = allowed wave height for the no damage criterium [m],

The  $K_D$  factor for the no damage criterion (0% to 5% 'damage'), non breaking waves and rough angular rock is 4 (SPM (1977), SPM (1984), CEM (2001)). According to (5.13), wave heights are limited to 0.10 m for the no damage criterion.

Following van der Meer's stability formulae, the wave height is limited to

$$\frac{H_s}{\Delta D_{n50}} = 6.2P^{0.18} \left(\frac{S}{\sqrt{N}}\right)^{0.2} (\xi_m)^{-0.5}$$
 for plunging waves  $(\xi_m < \xi_{mc})$  (5.14)

$$\frac{H_s}{\Delta D_{n50}} = 1.0P^{-0.13} \left(\frac{S}{\sqrt{N}}\right)^{0.2} \left(\cot \alpha\right)^{0.5} \left(\xi_m\right)^P$$
for surging waves  $(\xi_m \ge \xi_{mc})$  (5.15)

in which the critical Iribarren number  $\xi_{mc}$  is determined by

$$\xi_{mc} = \left(6.2P^{0.31} \left(\tan \alpha\right)^{0.5}\right)^{\frac{1}{P+0.5}}$$
 (5.16)

S (i.e. the dimensionless damage level) is assumed to equal 2.5, the number of waves N is taken 1000 and the permeability factor P is 0.5 (cfr. figure 2.7). For the considered model,  $D_{n50}$  equals 28.9 mm. The density of the rock is  $\rho_r = 2650 \text{ kg/m}^3$  and the density of water is  $\rho_w = 1000 \text{ kg/m}^3$ , thus the relative rock density is  $\Delta = 1.65$ . The slope of the breakwater is  $\tan \alpha = 1/1.5$ . According to (5.16), the critical Iribarren number  $\xi_{mc}$  is 4.08. The equations (5.14) and (5.15) have been plotted in figure 5.45. The maximal significant wave height is plotted against the Iribarren number.

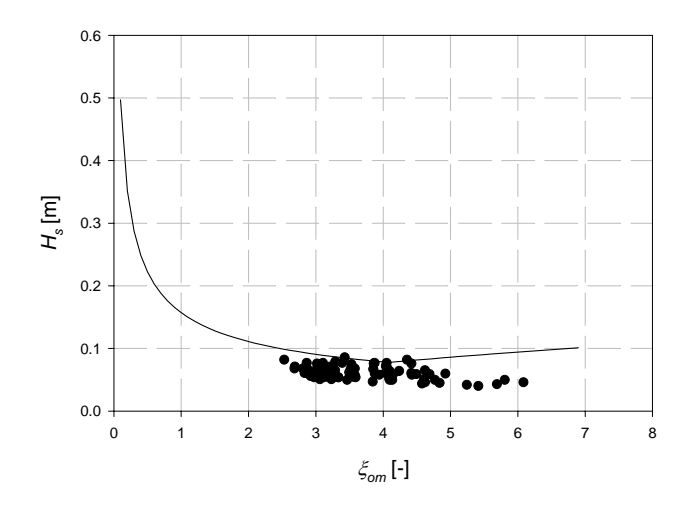


Figure 5.45: Maximal significant wave height  $H_s$  versus the Iribarren number  $\xi_{om}$  with indication of the test results.

The same test matrix has been run twice: one time for each type of core material. Irregular wave paddle displacement time series have been generated and stored on the hard disc of the computer in order to send identical steering signals to the wave paddle in both series of tests.

Three different water levels have been investigated: d = 0.25 m, d = 0.30 m and d = 0.35 m. Two parameter JONSWAP spectra (with the peakedness parameter  $\gamma = 3.3$ ) have been generated. Different combinations of  $H_s$  within the interval [0.06 m, 0.10 m] and  $T_p$  within the interval [0.8 s, 1.8 s] have been made. The test matrix has been given in Annex D. Each test has been run for approximately one thousand waves.

### **5.5.5 Results**

In a first step, all data has been checked for anomalies and errors visually. Next, all wave data have been analysed with the ANASYS programme. Wave run-up data have been analysed with a programme written in LabView<sup>TM</sup> in the framework of this Ph.D.

To investigate the influence of the plastic tubes underneath the breakwater, test n° 25 has been run another two times (test n° 25bis and test n° 25tris). The input parameters for the wave paddle were:

JONSWAP spectrum ( $H_s = 0.10$  m,  $T_p = 1.8$  s,  $\gamma = 3.3$ ), random phase method (RPM), d = 0.30 m. The same signal has been sent to the wave paddle in both repeated tests. A wave gauge has been placed behind the breakwater to measure the transmitted waves. During the first repeated test, the plastic tubes were open as during all other tests, whilst during the second repeated test, the plastic tubes have been closed by a textile plug.

The results of both repeated tests are almost the same (table 5.22). The presence of the plastic tubes does not affect the final results.

Table 5.22: Test results.

	test 25bis	test 25tris
$H_{s,i}$ [m]	0.079	0.078
$T_{m,i}$ [s]	1.31	1.31
$T_{ ho}$ [s]	1.77	1.77
$H_{s,t}[m]$	0.004	0.004
$T_{p,t}[s]$	15.61	15.61
$Ru_{2\%,RU1}/H_{s,i}$ [-]	1.57	1.59
$Ru_{2\%,RU2}/H_{s,i}$ [-]	1.46	1.48

Significant wave heights  $H_{m0}$  measured at the toe of the structure have been plotted against the Iribarren number  $\xi_{om}$  in figure 5.45. The curve of van der Meer indicates the maximum significant wave height for the no-damage criterion. A small amount of damage might have been expected in tests with large significant wave heights, but none has been observed. This conclusion was found by comparing photographs (of the armour layer of which several stones had been painted) taken after each test by which cumulative damage could be observed.

The results of the two series of tests (each corresponding with a different core material scale) are found in Annex E. The significant incident and reflected wave heights  $H_{m0,i}$ , resp.  $H_{m0,r}$ , the peak wave period  $T_p$  and the mean wave period  $T_{01}$ , measured at the toe of the structure and the reflection coefficient  $C_r$  of all tests are given. The spectral width parameter  $\varepsilon$  and the spectral peakedness parameter  $Q_p$  of the incident wave spectrum have been calculated. The Iribarren numbers  $\xi_{om}$  and  $\xi_{op}$  have been calculated using the aforementioned incident wave height  $H_{m0,i}$  and the mean wave period  $T_{01}$ , resp. the

peak wave period  $T_p$ . Wave run-up values  $Ru_{x\%}$  (with  $x = \sim 0.1$  (for  $Ru_{max}$ ), 1, 2, 5, 10,  $\sim 13.5$  (for  $Ru_s$ ), 25 and 50) measured by both run-up gauges as well as the  $Ru_{2\%}/H_{m0,i}$  values are listed. Finally, the number of waves is defined by (3.1) in which  $T_{01}$  is the mean wave period of the incident wave train.

Dimensionless wave run-up values exceeded by 2% of the waves have been plotted against various parameters such as the Iribarren numbers  $\xi_{om}$  (figure 5.46) and  $\xi_{op}$  (figure 5.47), the spectral width parameter  $\varepsilon$  (figure 5.48) and Goda's peakedness parameter  $Q_p$  (figure 5.49). Results of tests on the model with the 1:20 scaled core (core 1) are indicated with circles ( $\bullet$  or  $\bigcirc$ ). These of the 1:30 scaled core (core 2) are indicated with a triangle ( $\blacktriangle$  or  $\triangle$ ). The full, resp. open symbols represent the RU1, resp. RU2 measurements. The black symbols are valid for water depth d=0.25 m, the blue symbols are used for the results of the tests in which d=0.30 m. The red symbols represent the test results valid for a water depth d=0.35 m.

A number of interesting observations are made from figures 5.46 to 5.49. The influence of the Iribarren number  $\xi$  is clear. Test results confirm the trend in all formulae found in literature. The results presented in figure 5.46 and figure 5.47 show an upward tendency for increasing Iribarren numbers  $\xi_{om}$  and  $\xi_{op}$ . By means of a statistical ttest (see Annex F), the possible difference between the RU1 and the RU2 measurement results has been investigated. Linear regression has been applied to fit the measurement results. The reason for this is that most relationships between  $Ru_{2\%}/H_{m0}$  and  $\xi_{om}$  found in literature are approximately linear for surging waves. Distinction has been made between the two series of tests (core 1 (scale 1:20) and core 2 (scale 1:30)). It is seen in the last column of table 5.23 and table 5.24 that all levels of significance of the parameters c and d are larger than 0.05. Concluding, for  $\alpha = 0.05$ , no significant difference between the RU1 and the RU2 measurements could be demonstrated. Both step gauges measure the same wave run-up. The small differences in wave run-up value within the same test are due to the position of the step gauge with regard to the individual rocks. The suspicion of the big influence of the placement pattern of the armour units and the position of the comb of the run-up gauge relative to this armour unit pattern (as stipulated at the end of paragraph 5.4) is herewith taken off the edge.

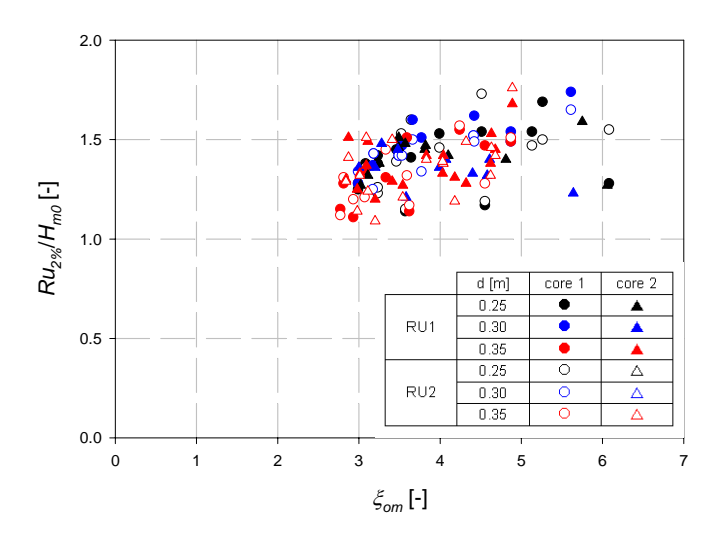


Figure 5.46: Dimensionless wave run-up values exceeded by 2% of the waves  $Ru_{2\%}/H_{m0}$  versus the Iribarren number  $\xi_{om}$ .

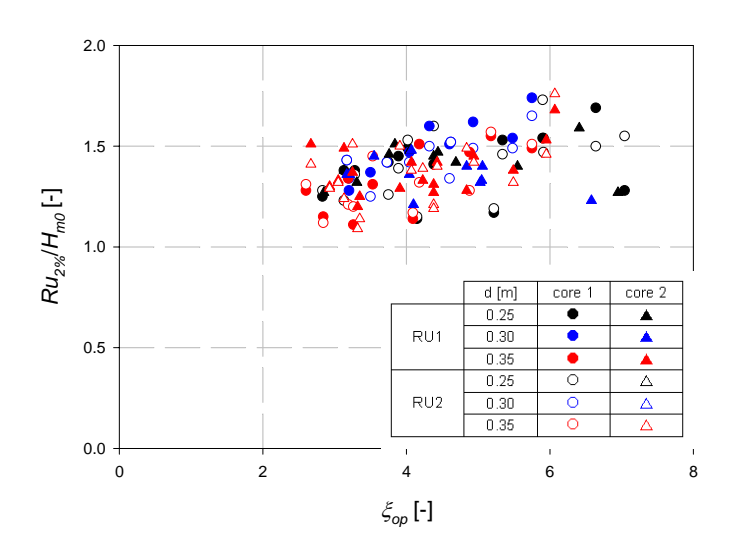


Figure 5.47: Dimensionless wave run-up values exceeded by 2% of the waves  $Ru_{2\%}/H_{m\theta}$  versus the Iribarren number  $\xi_{op}$ .

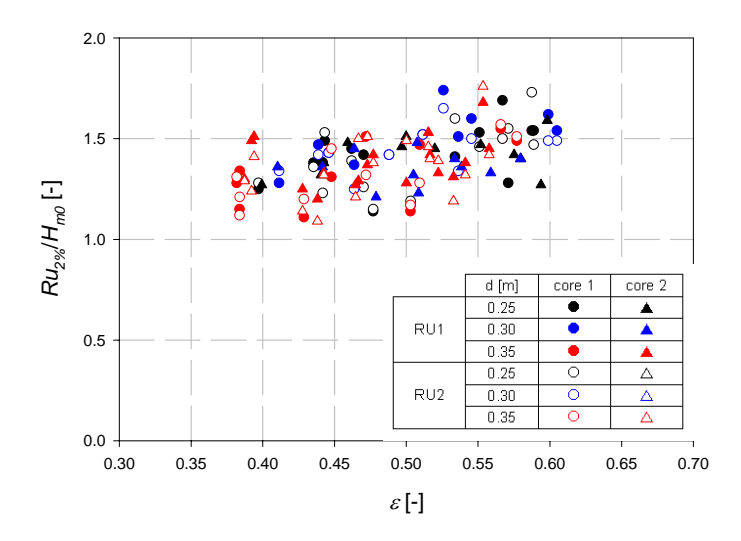


Figure 5.48: Dimensionless wave run-up values exceeded by 2% of the waves  $Ru_{2\%}/H_{m\theta}$  versus the spectral width parameter  $\varepsilon$ .

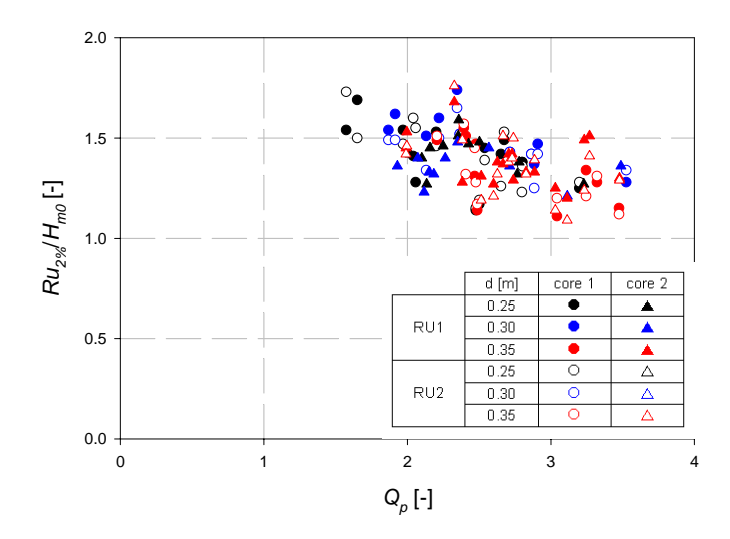


Figure 5.49 Dimensionless wave run-up values exceeded by 2% of the waves  $Ru_{2\%}/H_{m\theta}$  versus the peakedness parameter  $Q_p$ .

Table 5.23: SPSS output (RU1 and RU2 measurements for core 1).

variable	parameter estimate	$\sigma$	t value	significance
а	1.042	0.105	9.885	0.000
b	0.097	0.027	3.618	0.001
С	-5.58.10 <sup>-2</sup>	0.149	-0.375	0.709
d	8.21.10 <sup>-3</sup>	0.038	0.218	0.828

Table 5.24: SPSS output (RU1 and RU2 measurements for core 2).

variable	parameter estimate	$\sigma$	t value	significance
а	1.310	0.091	14.367	0.000
b	1.910.10 <sup>-2</sup>	0.023	0.832	0.409
С	-0.356	0.179	-1.983	0.052
d	9.001.10 <sup>-2</sup>	0.047	1.928	0.059

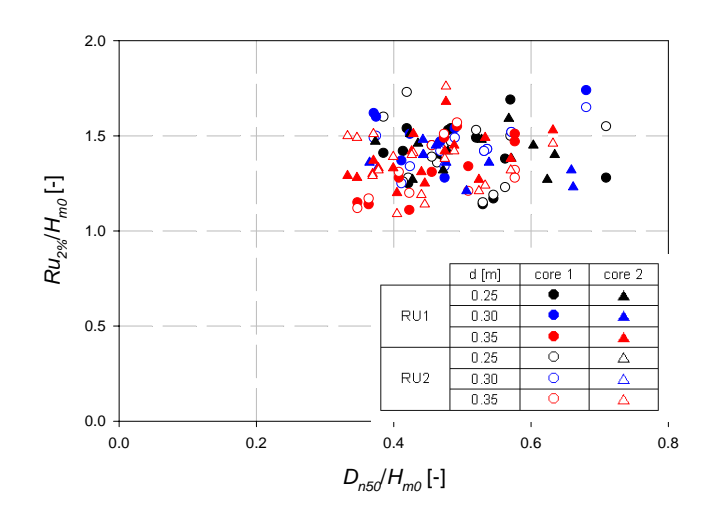


Figure 5.50: The dimensionless wave run-up values exceeded by 2% of the waves against the ratio  $D_{n50}/H_{m0}$ .

The dimensionless wave run-up values exceeded by 2% of the waves have been plotted against the ratio  $D_{n50}/H_{m0}$  in figure 5.50. Except for a lot of scatter, no influence of  $D_{n50}/H_{m0}$  has been noticed.

Table 5.25: SPSS output comparison  $Ru_{2\%}/H_{m0}$  values for different water depths for core 1 (scale 1:20 according to Burcharth et al. (1999)).

		value	$\sigma$	t	significance
	а	1.171	0.106	11.019	0.000
d = 0.25	b	5.826.10 <sup>-2</sup>	0.026	2.259	0.029
d = 0.30	С	-0.173	0.173	-0.999	0.323
	d	6.213.10 <sup>-2</sup>	0.043	1.453	0.153
	а	0.999	0.105	9.507	0.000
d = 0.30	b	0.120	0.026	4.574	0.000
d = 0.35	С	-1.850.10 <sup>-1</sup>	0.152	-1.215	0.232
	d	-2.242.10 <sup>-2</sup>	0.040	0.560	0.579
	а	1.171	0.119	9.836	0.000
d = 0.25	b	5.817.10 <sup>-2</sup>	0.029	2.013	0.050
d = 0.35	С	-0.357	0.120	-1.791	0.080
	d	$8.450.10^{-2}$	0.053	1.607	0.115

Table 5.26: SPSS output comparison  $Ru_{2\%}/H_{m0}$  values for different water depths for core 2 (scale 1:30 according to Froude's law).

		value	$\sigma$	t	significance
	а	1.371	0.112	12.277	0.000
d = 0.25	b	1.221.10 <sup>-2</sup>	0.027	0.452	0.656
d = 0.30	С	0.182	0.184	0.986	0.337
	d	-6.180.10 <sup>-2</sup>	0.045	-1.371	0.186
	а	1.552	0.192	8.097	0.000
d = 0.30	b	-4.959.10 <sup>-2</sup>	0.047	-1.049	0.300
d = 0.35	С	-0.526	0.220	-2.388	0.021
	d	0.080	0.055	2.566	0.014
	а	1.371	0.150	9.145	0.000
d = 0.25	b	1.221.10 <sup>-2</sup>	0.036	0.337	0.738
d = 0.35	С	-0.345	0.187	-1.846	0.072
	d	0.080	0.047	1.716	0.093

By means of a statistical t test (see Annex F), the influence of the SWL or the water depth d on wave run-up has been investigated (table 5.25 and table 5.26). It is concluded that there is no significant indication

( $\alpha$  < 0.05) that the water depth has an influence on wave run-up. This statement is valid for the tests on the model with core 1 (on scale 1:20). For the tests on the model with core 2, the results of the tests with d = 0.35 m deviate from the results of the tests with d = 0.30 m.

Remarkable is the influence of the shape of the spectrum: dimensionless wave run-up values  $Ru_{2\%}/H_{s,i}$  increase with increasing spectral width parameter  $\varepsilon$  (figure 5.48) and dimensionless wave run-up values decrease with increasing peakedness parameter  $Q_p$  (figure 5.49). The spectral parameters  $H_{m0}$ ,  $T_{01}$  or  $T_p$  do not describe the spectrum sufficiently. The spectral width parameter  $\varepsilon$  varies within the interval [0.40, 0.60]. Dimensionless wave run-up results are found within the interval [1.20, 1.60]. Goda's peakedness parameter varies within the interval [1.5, 3.5].

To proof statistically that the two different cores yield different results (figure 5.51), the method explained in Annex F has been applied. Table 5.27 shows the output of the SPSS programme. The dimensionless wave run-up values  $(Ru_2\%/H_{m0})_{RU1}$  and  $(Ru_2\%/H_{m0})_{RU2}$  of the tests with a 1:20 core have been compared to the  $(Ru_2\%/H_{m0})_{RU1}$  and  $(Ru_2\%/H_{m0})_{RU2}$  values of the 1:30 core.

Table 5.27: SPSS output (different size of core material).

variable		parameter estimate	standard error	t value	Significance
	а	1.014	0.071	14.259	0.000
	b	0.101	0.018	5.591	0.000
	С	0.203	0.109	1.858	0.066
	d	-5.888.10 <sup>-2</sup>	0.028	-2.115	0.036

The null hypothesis  $H_0$  sounds: 'the two regression lines are the same', or c=0 and d=0. The alternative hypothesis  $H_a$  is  $c \ne 0$  and  $d \ne 0$ . The critical value of  $t_{\alpha 2}$  is based on (n-(k+1)) degrees of freedom. n is the number of observations (in this case is n=70+59=129) and k is the number of independent variables in the model (in this case is k=4). For the critical value of t, the number of t0 has been taken equal to 120 instead of 124. For an error Type I t1 and t2 is rejected if the calculated value of t3 for the parameters t4 and t5 is rejected if the calculated value of t5 for the parameters t6 and t7 is found

outside the interval [-1.980, 1.980]. According to the SPSS output (table 5.27), the null hypothesis is accepted for parameter c, but is rejected for parameter d. The alternative hypothesis is accepted for parameter d.

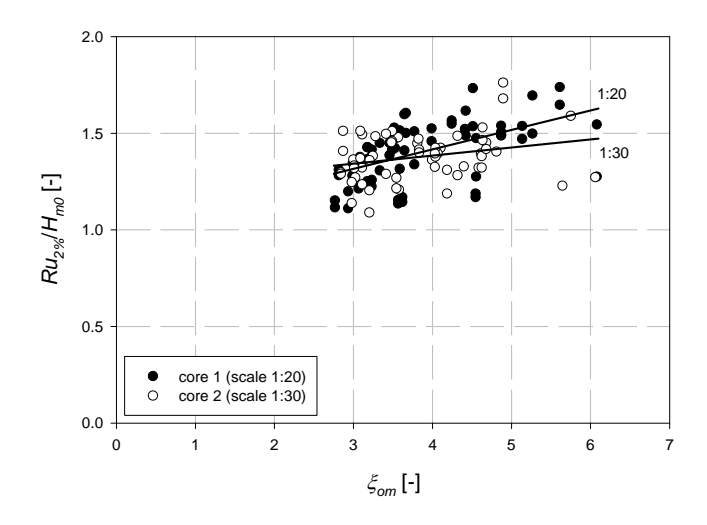


Figure 5.51: Comparison of results of tests on a model of a rubble mound breakwater with core material scaled to 1:20 and these of tests on the same model but with core material scaled to 1:30.

Hence, it is concluded that there is evidence that the model with the 'Burcharth core' yield other results than the model with the 'Froude' core. Whether the 1:20 core yields higher or lower results than the 1:30 core at all times is not clear (see figure 5.51). For  $\xi_{om} > 3.16$ , the model with the 1:20 core yields higher values than the model with the 1:30 core and vice versa for  $\xi_{om} < 3.45$ . However, differences are small.

The reflection coefficient has been plotted against the peak wave period  $T_p$  measured at the toe of the structure in figure 5.52. It is seen that the reflection coefficient increases with increasing spectral mean wave period  $T_{0l}$ . For a mean wave period of  $T_{0l} = 0.8$  s is  $C_r$  about 20%. For a spectrum with much longer waves,  $C_r$  increases to about 40% for  $T_{0l} = 1.5$  s.

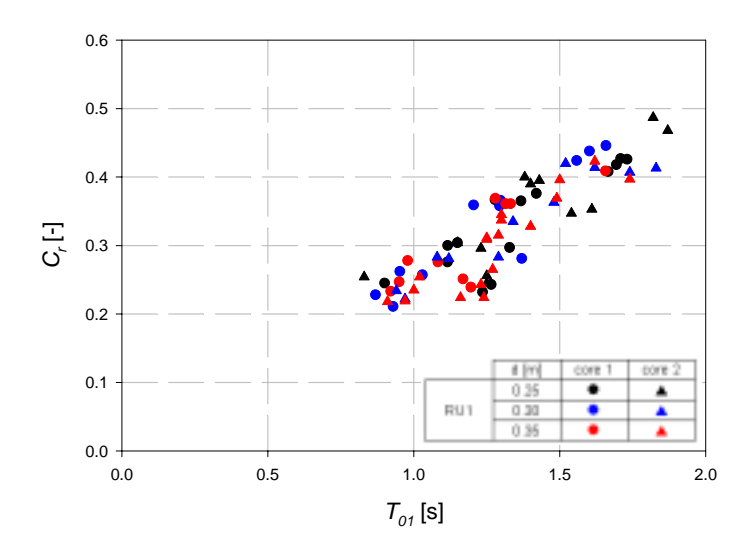


Figure 5.52: Reflection coefficient  $C_r$  versus the mean wave period  $T_{01}$ .

## 5.6 Large scale tests at GWK

#### 5.6.1 Introduction

The LARGE WAVE CHANNEL (GWK) is the most important facility for basic and applied research on Coastal Engineering phenomena at the Coastal Research Centre (FZK). Waves up to a height of 2.00 m under quasi full scale conditions can be simulated in the 307 m long, 7 m deep and 5 m wide flume. Both regular and irregular waves (JONSWAP wave spectra) have been generated. The installed power of the piston type wave generator combined with an upper flap is about 900 kW. The gearwheel driven carrier gives a maximum stroke of  $\pm$  2.10 m to the wave paddle. The stroke can be superimposed by upper flap movements of  $\pm$  10° in order to simulate natural water wave kinematics more accurately. A large cylinder integrated in the carrier compensates the water force in front of the paddle (rear is free of water) (figure 5.53 and 5.54).

The large scale tests have been performed during the project 'Research on the use of heavy rock in rubble mound breakwaters and seawalls' in the LARGE WAVE CHANNEL (GWK) of the Coastal Research Center (FZK) have been supported by the European Community under the Access to Research Infrastructures action of the

Human Potential Programme (contract n° HPRI-CT-1999-00101). The participants of the project were Aalborg University (Denmark), Ghent University (Belgium), Havnecon Consulting ApS (Denmark) and NCC Industry (Norway). Aalborg University was the co-ordinator of the project. The main objectives of the project were firstly to investigate the influence of rock density on the armour layer stability (investigated by Helgason (2003)) and secondly to collect large scale data on wave run-up and wave overtopping.

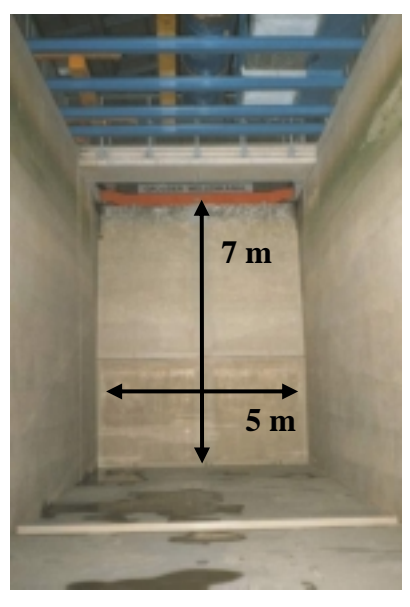




Figure 5.53 Wave paddle seen from inside the LARGE WAVE CHANNEL.

Figure 5.54: Wave generator of the LARGE WAVE CHANNEL.

The required rock weight (calculated by stability formulae like Hudson (see (5.17)), van der Meer ((5.14) and (5.15)),...) depends mainly on the wave characteristics. By using high density rock for coastal protection measures, the required size and volume of rock is reduced. The filter layer also benefits from this reduction and sections of a breakwater suffering severe wave attack are protected more effectively with high density rock without changing the rock size used in other sections. The disadvantage of using high density rock is the assumed higher wave run-up and increased wave overtopping

discharges. To obtain the same armour layer stability, the stones with a high density require smaller dimensions than the stones with a normal density. Small stones make the slope smoother than large stones. As already shown in paragraph 2.2.4, smooth(er) slopes induce higher wave run-up.

## 5.6.2 Model setup

A general overview of the flume and the location of the breakwater in the flume is given in figure 5.55. The structure is a didactical example of a conventional rubble mound breakwater (figure 5.56) consisting of a core, a filter layer and an armour layer (figure 5.57). The structure has been built on a two meter thick sand bed. A sloping foreshore (1:50) has been created. A geotextile has been placed between the sand bed and the breakwater.





Figure 5.56: View on (a) seaward slope and (b) landward slope of the breakwater.

For a first series of tests, the breakwater was protected with high density rock ( $\rho=3.05 \text{ t/m}^3$ ). Once the tests with the high density armour layer were finished, a part of the armour layer (between the toe and the crest of the landward slope) was removed and replaced by an armour layer consisting of normal density rock ( $\rho=2.65 \text{ t/m}^3$ ). Figures 5.58 and 5.59 show the cumulative mass distribution curves of the high density rock, resp. normal density rock. The numerical values are found in table 5.28. The characteristics of the core and filter material are given in table 5.28 as well.

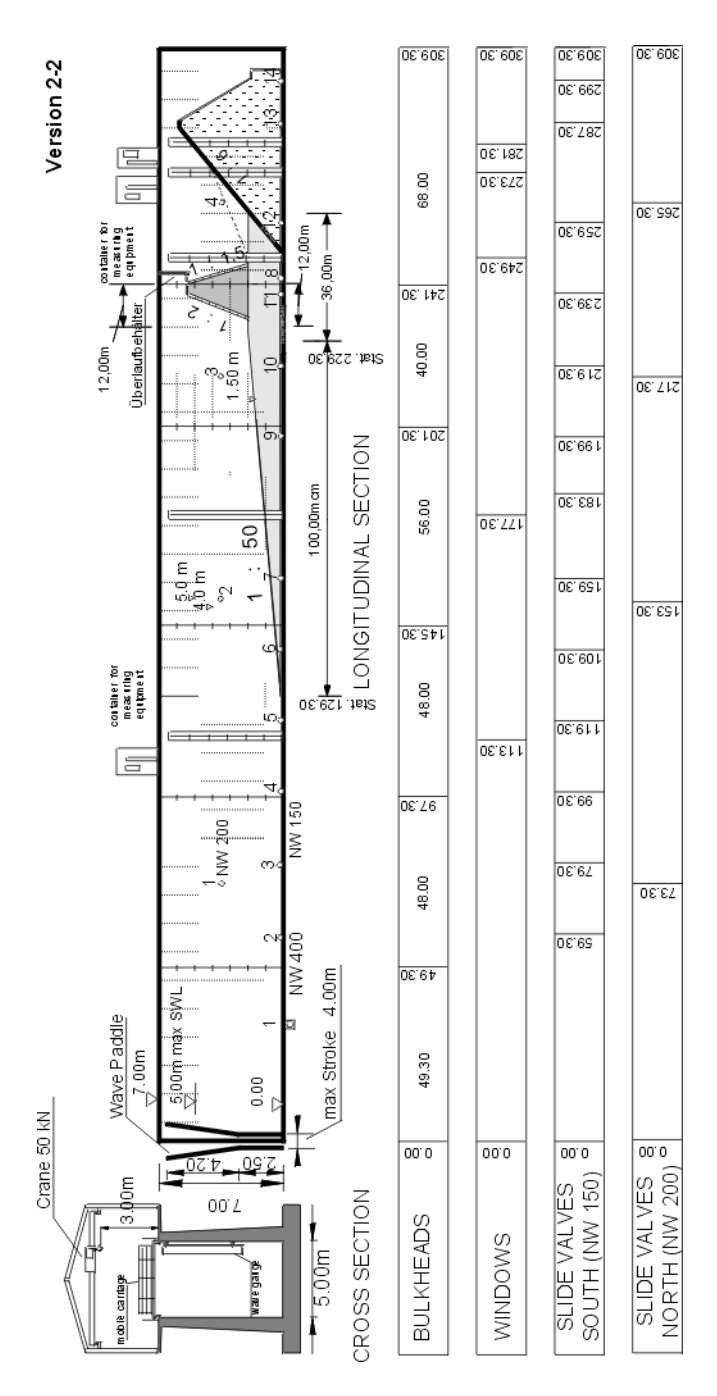


Figure 5.55: General view of the LARGE WAVE FLUME with indication of the position of the 1:50 slope and the breakwater.

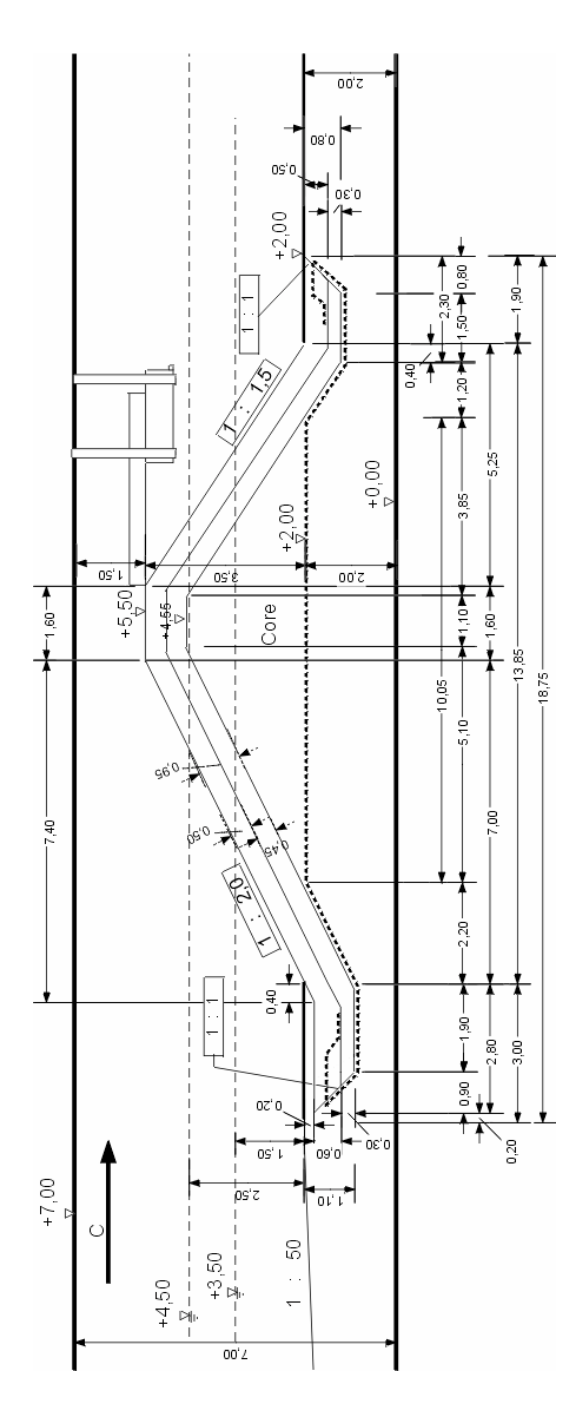


Figure 5.57: Geometry of the rubble mound breakwater.

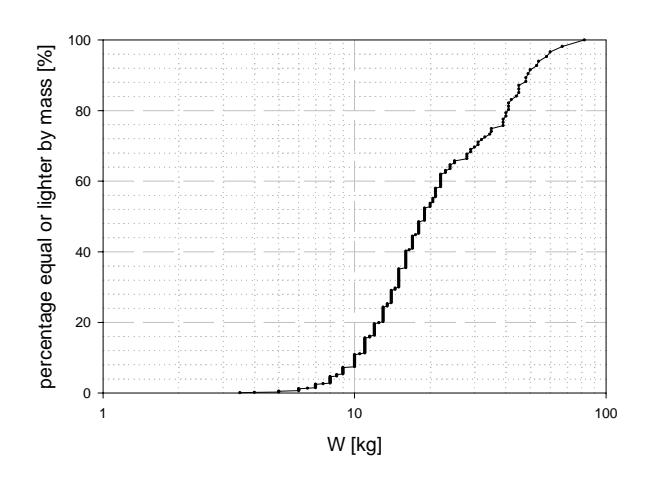


Figure 5.58: Cumulative rock mass distribution curve of the *high density rock* armour layer material of the rubble mound breakwater ( $W_{50} = 19 \text{ kg}$ ).

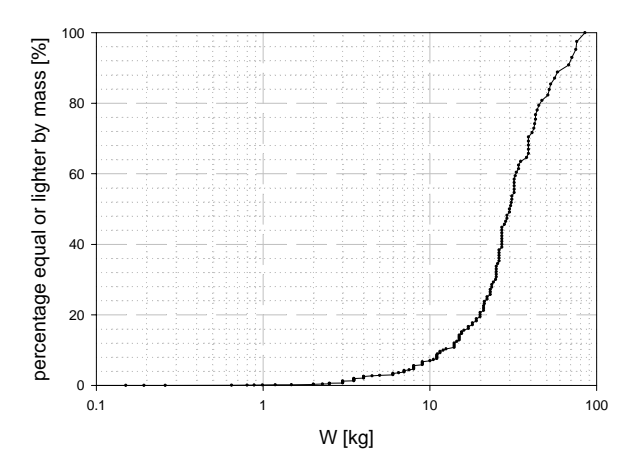


Figure 5.59: Cumulative rock mass distribution curve of the normal density rock armour layer material of the rubble mound breakwater ( $W_{50} = 30 \text{ kg}$ ).

Table 5.28: Characteristics of the materials of the GWK breakwater.

Di cakwatei.						
			armour layer			
characteristic	core f	filter	high density	normal		
			rock	density rock		
			$(\rho = 3.05 \text{ t/m}^3)$	$(\rho = 2.65 \text{ t/m}^3)$		
$D_{n10}$ [mm]	5	30	149	166		
$D_{n15}$ [mm] ( $W_{15}$ [kg])	6	32	153 (11)	180 (15.5)		
$D_{n50}$ [mm]	13	50	184 (19)	225 (30)		
$D_{n60}$ [mm] ( $W_{50}$ [kg])	15	57	193	231		
$D_{n85}$ [mm] ( $W_{85}$ [kg])	30.5	75	245 (45)	271 (53)		
D <sub>n85</sub> /D <sub>n15</sub> [-]	5.23	2.34	1.70	1.50		
$D_{n10}/D_{n60}$ [-]	0.31	0.53	0.77	0.72		
porosity [%]	35	45	40	42		

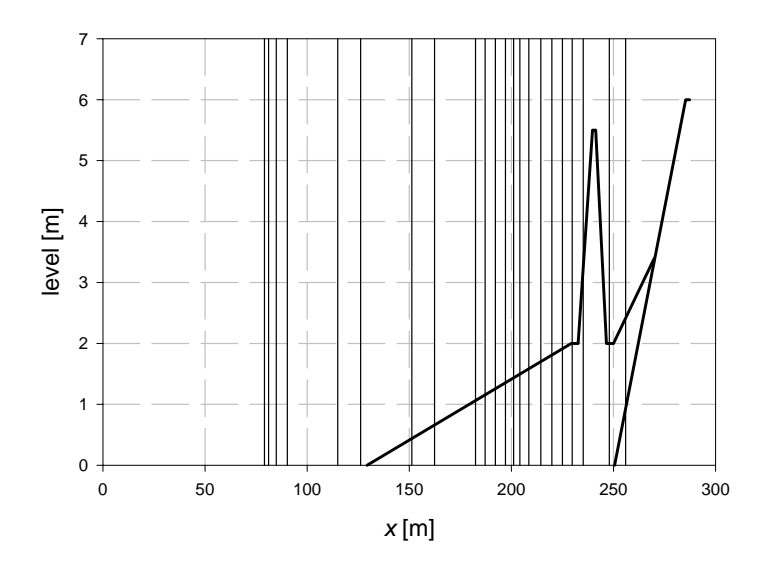


Figure 5.61: Wave gauge positioning along the wave flume with indication of the sand bed slope and the breakwater.

## **5.6.3** Measuring equipment

# 5.6.3.1 Wave gauges

Twenty two capacitance wave gauges (figure 5.60) have been placed along the wave flume (figure 5.61). The wave gauges are coated wires tensioned in aluminium frames which are fixed to one of the side walls of the wave flume. The exact location of each of the wave gauges is given in table 5.29.

Table 5.29: Position of wave gauges along the axis of the wave channel.

chamei.						
	x [m]	channel n°		x [m]	channel n°	
WG1	79.05	44	WG12	197.15	12	
WG2	81.15	45	WG13	201.15	13	
WG3	84.85	46	WG14	204.15	14	
WG4	90.29	47	WG15	208.60	15	
WG5	115.00	5	WG16	214.40	16	
WG6	126.22	6	WG17	219.80	17	
WG7	151.20	7	WG18	225.00	18	
WG8	162.40	8	WG19	229.80	19	
WG9	182.40	9	WG20	235.25	20	
WG10	187.15	10	WG21	248.00	21	
WG11	192.15	11	WG22	256.00	22	

## **5.6.5.2** Run-up gauge

Wave run-up has been measured by a three part run-up gauge mounted on the seaward slope of the breakwater (figure 5.56(a)). Each part of the run-up gauge (figure 5.62) measures 2.40 m long and has 24 electrodes. The distance between two electrodes is 10 cm. On a 1:2 slope, the gauge is able to detect wave run-up each 4.5 cm (vertical distance). The parts of the run-up gauge are attached to the armour layer by means of clamps and reinforcement bars with an equivalent diameter  $\phi = 20$  mm. The clamps are fixed to the run-up gauge by means of INOX tensioning strips (figure 5.63). The three parts are connected to each other by cables which are protected by a piece of garden hose (figure 5.64). During the second series of tests, a shield has been placed over the ends of the gauges in order to protect the

connection of the cables to the gauges (figure 5.65). The gauges are placed in such a way that the upper part of the electrodes are as good as possible in the upper surface of the armour layer (figure 5.66).



Figure 5.60: Capacitance type wave gauge.



Figure 5.62: Run-up gauges.





Figure 5.63: Clamps to fix the run-up gauges to steel bars driven into the outer layers of the breakwater.





Figure 5.64: Connection cable between run-up gauges protected by a piece of garden hose.



Figure 5.65: Shield protecting the connection of the cables to the gauges.

The run-up gauge has been calibrated together with all wave gauges, pressure sensors and pore pressure cells and load cells before each of the two series (each corresponding with a different type of armour layer rock) of tests. The digital step gauge did not have to be calibrated in the way all other sensors were calibrated. The step gauge detects the number of wet electrodes. By measuring the exact elevation of the top of the lowest and highest electrode of each gauge with a leveller and a levelling rod, the position of all intermediate electrodes can be calculated very easily. The position of all electrodes is given in figure 5.67 for the first series of tests (with the high density rock ( $\rho = 3.05 \text{ t/m}^3$ )) and in figure 5.68 for the second series of tests (with the normal density rock ( $\rho = 2.65 \text{ t/m}^3$ )). The slope of the gauges is indicated on the graphs. The (theoretical) slope of the gauges should be tan  $\alpha = 0.5$ . A good agreement is seen.





Figure 5.66: The run-up gauges are sunk down in and between the stones to have the upper part of the electrodes in the upper surface of the armour stones.

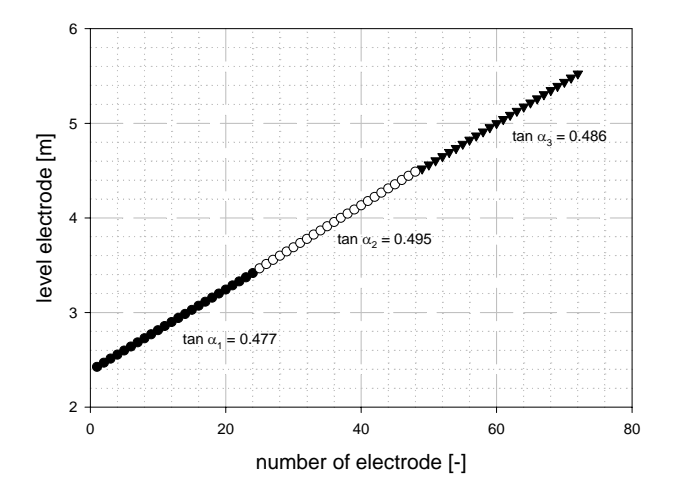


Figure 5.67: Position of the step gauges on the slope of the breakwater for the first series of tests (calibration on October  $22^{nd}$ , 2001).

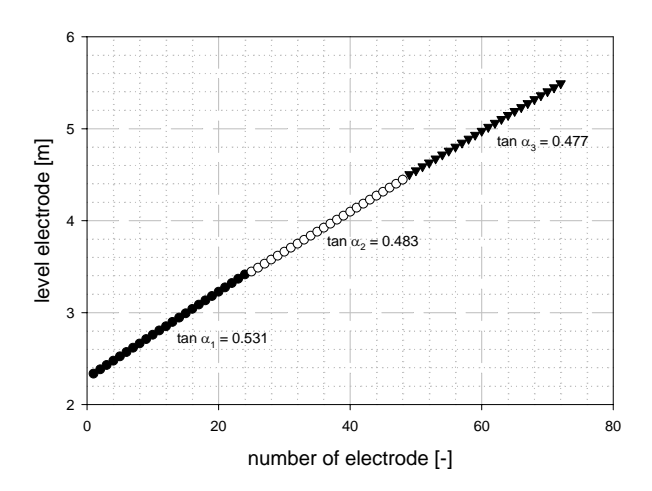


Figure 5.68: Position of the step gauges on the slope of the breakwater for the second series of tests (calibration on November  $19^{th}$ , 2001).

## 5.6.4 Test matrix

To study the influence of the water depth on wave run-up, tests have been carried out with three different water levels (water depths d = 3.50 m, d = 4.00 m and d = 4.50 m at the wave paddle and  $d_t = 1.50$  m, resp.  $d_t = 2.00$  m and  $d_t = 2.50$  m at the toe of the structure).

Non damage tests have been carried out before the tests in which wave heights exceeded the non-damage wave height calculated by Hudson's formula

$$W_{50} = \frac{\rho_s g H_{des}^3}{\Delta^3 K_{RR} \cot \alpha} \tag{5.17}$$

or

$$H_{des} = \sqrt[3]{\frac{\Delta^3 W_{50} K_{RR} \cot \alpha}{\rho_s g}}$$
 (5.18)

in which  $\Delta = \frac{\rho_s - \rho_w}{\rho_w}$  with  $\rho_s$  = density of rock and  $\rho_w$  = 979.63

kg/m<sup>3</sup> (density of water at 18°C, determined at Aalborg University) have been carried out.  $K_{RR}$  equals 2.2 (breaking waves) and  $W_{50} = 19$  kg for the high density rock and  $W_{50} = 30$  kg for the normal density rock (see table 5.28) have been taken into account. The critical wave heights are  $H_{s,l} = 0.64$  m, resp.  $H_{s,2} = 0.63$  m for the high density rock, resp. normal density rock.

Standard JONSWAP spectra (with peak enhancement factor  $\gamma=3.3$ ) have been generated. The parameters are the significant wave height  $H_s$  and the peak period  $T_p$ . Significant wave heights  $H_{m0}$  varied within the interval [0.30 m, 1 m] and peak wave periods  $T_p$  within [1.5 s, 6 s]. Thus, a broad range of Iribarren numbers has been investigated:  $\xi_{op}$  varies roughly between 2 and 5.5. The test matrix has been given in Annex G. Tests have been run as long as it took to have at least 1000 waves measured. The mean wave period  $T_m$  was calculated from the peak period  $T_p$  by a theoretical model of the JONSWAP spectrum. The ratio  $T_p/T_m$  for a JONSWAP spectrum is about 1.2. The time estimated to have one thousand waves  $(t_R)$  was 1000  $T_m$ . Only limited tests with regular waves have been carried out.

# **5.6.5 Results**

In the analysis, firstly, all original measurement data (sampled at  $f_s$  = 100 Hz) have been checked visually. Measuring errors and anomalies have been detected. This visual method allowed the omission of tests n° 10, 12, 28, 29, 33, 34 and 35 from the very beginning.

Subsequently, small anomaly errors in measurement data which had been overlooked by the first visual check such as shown in figure 5.69 have been minimised by a moving average filter (cfr. subsampling from 100 Hz to 10 Hz). Results of tests in which such errors showed up have been interpreted with care in order not to draw wrong conclusions.

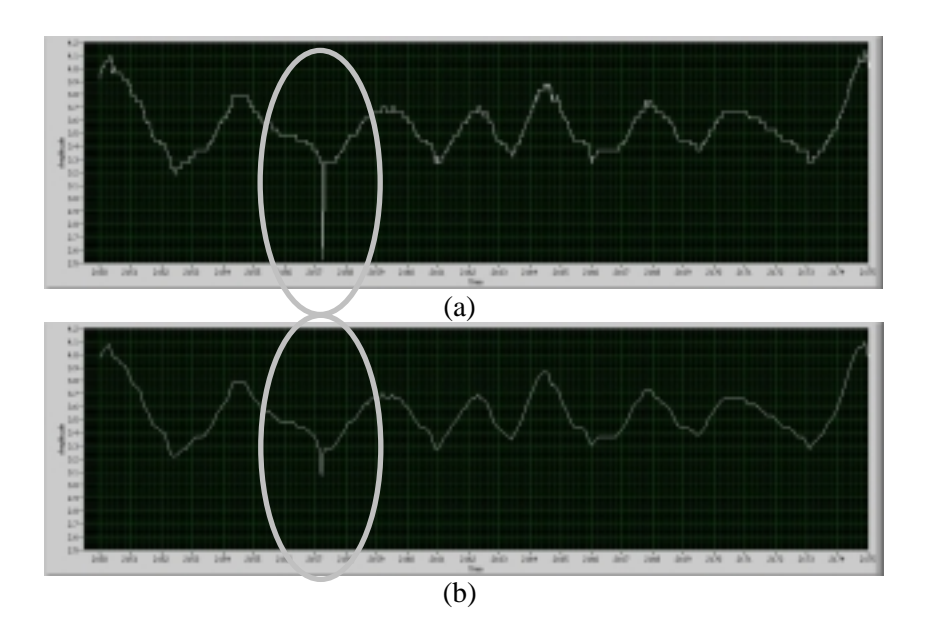


Figure 5.69: Sample of minimising anomaly errors in measurement data (a)  $f_s = 100$  Hz, (b)  $f_s = 10$  Hz (test 43, channel 43).

# 5.6.5.1 Waves

Wave data measured within the time interval  $[t_0, t_f]$  by the wave gauges connected to channels 44 (x = 79.05 m - close to the wave paddle but outside the 'near field' area), 05 (x = 115.00 m - just in front of the 1:50 slope) and 19 (x = 229.80 - at the toe of the breakwater) have been analysed both in time and in frequency domain. Data measurements started approximately when the wave paddle started generating waves. The time span the waves needed to reach the structure, to reflect and to travel back to the wave paddle, nor the die out of the wave action once the wave generator had been switched off have been taken into account in the analysis.  $t_0$  is calculated using the formula

$$t_0 = 2 \frac{x_{paddle-structure}}{c_w} \tag{5.19}$$

with

Table 5.30: Values of  $t_0$  and  $t_f$  for all tests with a standard JONSWAP spectrum.

JONSWAP spectrum.						
test nr.	$t_0$ [s]	$t_f[s]$	test n°	$t_0$ [s]	$t_f[s]$	
1	117	5000	37	117	5200	
2	105	3370	38	105	3500	
3	114	2750	39	114	2900	
4	107	4200	40	105	4400	
5	106	3100	41	106	3400	
6	108	3000	42	106	3200	
7	105	3300	43	105	3400	
8	104	3500	44	104	3700	
9	104	1850	45	104	2000	
10 <sup>(*)</sup>	-	-	46	104	2000	
11	105	1450	47	105	2150	
12 <sup>(*)</sup>	-	-	48	105	2150	
13	221	1300	49	221	1500	
14	98	4200	50	98	4400	
15	98	4200	51	98	4400	
16	105	5000	52	105	5200	
17	119	2560	53	119	2700	
18	140	2100	54	140	2300	
19	98	3500	55	98	3700	
20	96	5000	56	96	5200	
21	92	4400	57	92	4400	
22	110	2970	58	110	3000	
23	96	3500	59	96	3550	
24	172	1910	60 <sup>(**)</sup>	92	2300	
25	103	3100	61	103	3150	
26 <sup>(**)</sup>	98	3450	62 <sup>(**)</sup>	98	3400	
27 <sup>(**)</sup>	95	3700	63 <sup>(**)</sup>	95	3650	
28 <sup>(*)</sup>	-	-	64(**)	93	2800	
29 <sup>(*)</sup>	-	-				

$$c_{w} = \frac{L}{T} \tanh\left(\frac{2\pi d}{L}\right) \tag{5.20}$$

<sup>(\*)</sup> no wave run-up measurements available highest wave run-up levels exceed crest level

for the wave celerity in which L is given by (2.3) or (2.4), T = target peak wave period and d = water depth at the wave paddle. The distance between the wave paddle and the toe of the structure is  $x_{paddle-structure} = 232.70$  m.  $t_f$  has been chosen based on the recording time  $t_R$  and the time needed to have about one thousand waves. Table 5.30 gives the values of  $t_0$  and the values of  $t_f$ .

The number of data points per data window was 1028. So, the spectral band width was  $b = 1.21.10^{-2}$  Hz. The 90% confidence boundaries are found by multiplying the spectrum by [0.82, 1.26].

A comparison between the significant wave height measured by channels 05, 19 and 44 is given in figure 5.70. Only very small differences are seen between the significant wave height measured by channel 44 and channel 05 (on average, taking all (succeeded) tests into account, 2.6% difference). Wave heights at the toe of the breakwater differ from 'deep water' (at the wave paddle) wave heights more significantly (on average 9.0%).

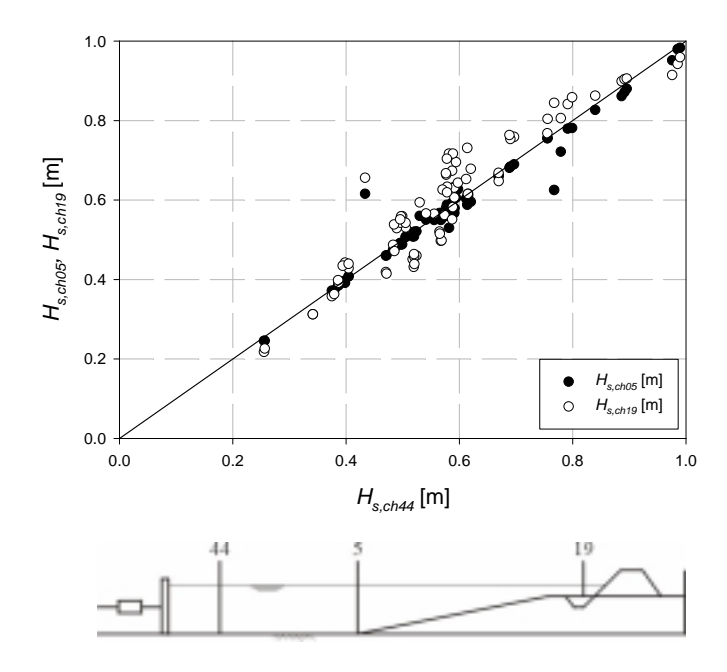


Figure 5.70: Comparison of significant wave heights of all tests measured by channels 05, 44 and 19.

In figure 5.71 the same comparison is presented, but data have been itemised per investigated water level. The average relative differences in significant wave height have been calculated for the three water levels (table 5.31).

Waves travel more undisturbed from the location of the wave gauge connected to channel 44 (i.e. close to the wave paddle) to the location of the wave gauge connected to channel 05 (i.e. just before the sand bed slope) than to the location of the wave gauge connected to channel 19 (i.e. at the toe of the structure). Between the locations of the wave gauges connected to channel 44 and channel 05, there is no change in water depth. Between the location of the wave gauge connected to channel 44 and the location of the wave gauge connected to channel 19, there is a change of 2 m in water depth due to the presence of the sand bed slope. A slight influence of the water depth on the transformation of the wave height towards the structure is noticed: the deeper the water, the less the wave heights measured at the toe of the structure deviate from the deep water wave height.

Table 5.31: Average deviations from the deep water wave height (measured by the wave gauge connected to channel 44) at the positions of the wave gauges connected to channels 05 and 19.

d	ch05/ch44	ch19/ch44
3.5	3.8%	9.7%
4.0	2.1%	9.4%
4.5	1.6%	8.1%

When waves are Rayleigh distributed, the ratio  $H_{mean}/H_s$  equals 0.626. The average relative difference to this value is 2.9% for the waves measured at the location of the wave gauge connected to channel 05 and 3.4% for the waves measured at the location of the wave gauge connected to channel 19. From these values and the figures above, it can be concluded that the change in water depth nor wave breaking had a significant influence on wave height distribution.

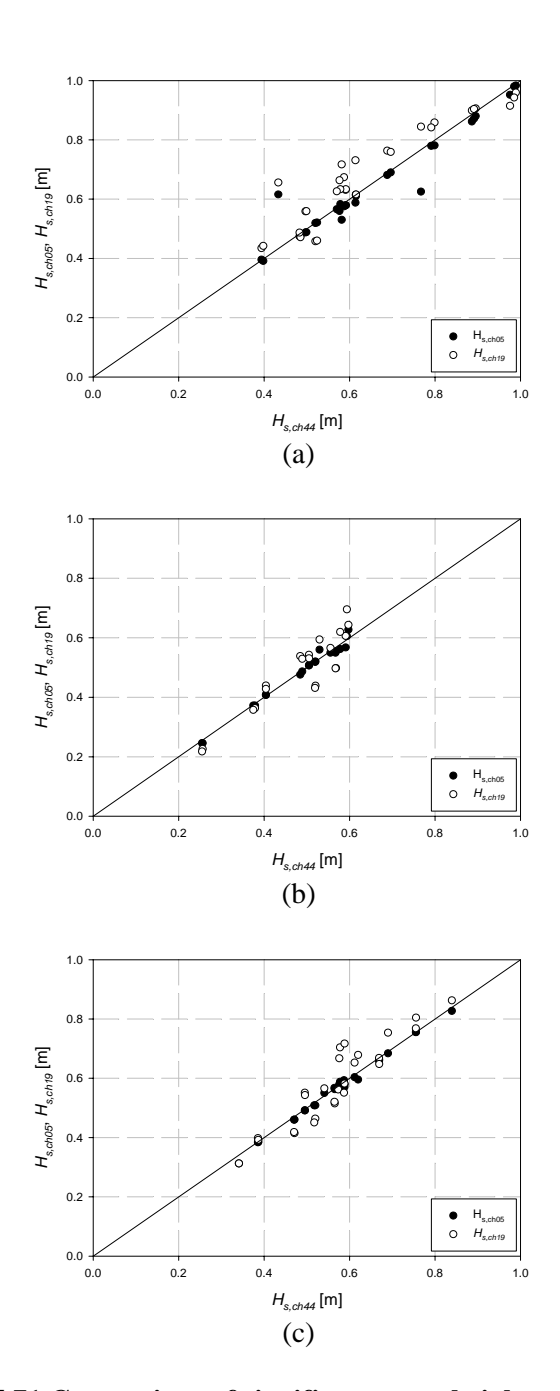


Figure 5.71 Comparison of significant wave height measured by channels 05, 44 and 19 for (a) d=3.50 m, (b) d=4.00 m and (c) d=4.50 m.

# **5.6.5.2** Wave run-up

Wave run-up time series have been analysed in time domain by a zero down crossing method. The number of wave run-up events has been determined according to the method explained in paragraph 3.1. Dimensionless wave run-up values have been referred to the significant wave height measured close to 'the toe of the structure'. Wave data measured by the wave gauge just before the slope of the sand bed (channel 05) have been used for this purpose. The wave gauge connected to channel 19 was located in the critical area in which the determination of the significant wave height by only one wave gauge is disturbed by the nodal and anti-nodal pattern of the wave field. According to paragraph 3.2, in case waves are measured by only one wave gauge, the minimum distance between the toe of the breakwater and the position of the wave gauge used for wave measurement purposes needs to be at least the double of the peak wave length. In case of a peak wave period of  $T_p = 6$  s is the peak wave length  $L_p = 56.20$  m and is the minimum distance between the wave gauge and the toe of the breakwater (x = 232.7) 112.40 m. The wave gauge connected to channel 05 is located at position x = 115 m. Also total waves have been considered because reflection analysis would require multiple wave gauges which are placed at distances which vary according the applied peak wave period. Peak wave periods  $T_p$  vary between 1.5 s and 6 s. Practical limitations did not allow flexible (transportable) wave gauges in the wave flume. Reflection analysis results would we worthless in some cases because of the encountered singularities. Also the number of wave run-up events (see paragraph 3.1 for the definition) has been related to the measurements made by the wave gauge connected to channel 05.

Tests indicated with one asterix  $^{(*)}$  in table 5.30 and the tables in Annex H have not been taken into account in further wave run-up presentations because wave run-up measurements failed. Tests indicated with a double asterix  $^{(**)}$  in table 5.30 and the tables in Annex H are tests in which the highest wave run-up levels exceeded the crest level of the breakwater. For these tests, the  $Ru_{2\%}$  has been determined by fitting a Rayleigh distribution through all wave run-up data with a wave run-up level lower than the crest level and thus, the 'equivalent' wave run-up value  $Ru_{2\%,eq}$  has been determined (according to paragraph 3.3).

Wave run-up levels exceeded by 2% of the wave run-up events  $Ru_{2\%}/H_{m0}$  results have been plotted versus the Iribarren numbers  $\xi_{om}$ 

and  $\xi_{op}$  in figure 5.72, resp. figure 5.73. Figure 5.74 and figure 5.75 show the  $Ru_{2\%}/H_{m0}$  values in function of the parameters  $\varepsilon$ , resp.  $Q_p$ . The full symbols (lacktriangle and lacktriangle) represent the results of the tests with the high density armour layer. The open symbols (lacktriangle armour layer. Following conclusions have been drawn from the presented graphs. Increasing Iribarren numbers (both  $\xi_{om}$  and  $\xi_{op}$ ) yield increasing dimensionless 2% wave run-up values. The majority of the tests had a spectral width parameters of  $\varepsilon \cong 0.6$ . Only a few tests indicated small spectral width values ( $\varepsilon \cong 0.50$ ). Latter tests all correspond with very small values of both the peak wave period  $T_p$  and the significant wave height  $H_{m0}$  in comparison to these in other tests. Quite a lot of spreading is seen on the results.

Wave run-up results of two series of tests, each corresponding to a type of armour rock, have been compared. Figure 5.72 shows the dimensionless wave run-up value  $Ru_{2\%}/H_{m0}$  versus the Iribarren number  $\xi_{om}$ . The regression lines of both series of results are also shown. A statistical test (see Annex F) has been performed on the two series of data. If the statistical test on both parameters c and d indicate that these do not differ significantly from 0 ( $H_0$ : c = 0 and d = 0;  $H_a$ :  $c \neq 0$  and  $d \neq 0$ ), one can conclude that both set of results are the same. The output of the statistical computer programme SPSS (table 5.32) gives the estimates of the parameters a, b, c and d in (I.1), as well as their t value and the level of significance.

Table 5.32: SPSS output (different type of armour rock).

	variable	parameter	standard	t value	Significance	
variable	estimate	error	t value	Significance		
	а	1.438	0.130	11.098	0.000	
	b	9.114.10 <sup>-2</sup>	0.042	2.181	0.034	
	С	8.742.10 <sup>-3</sup>	0.184	0.047	0.962	
	d	1.286.10 <sup>-2</sup>	0.059	0.217	0.829	

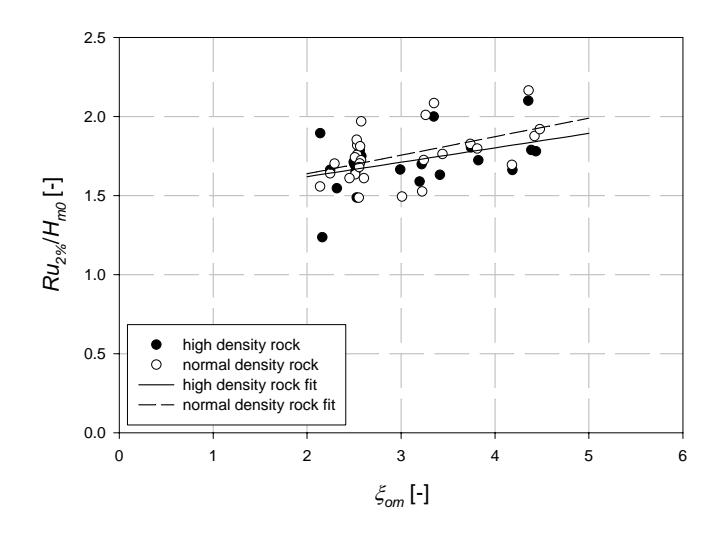


Figure 5.72: Comparison of wave run-up results of tests with a JONSWAP spectrum on a rubble mound breakwater armoured with either high density rock (●) or normal density rock (○).

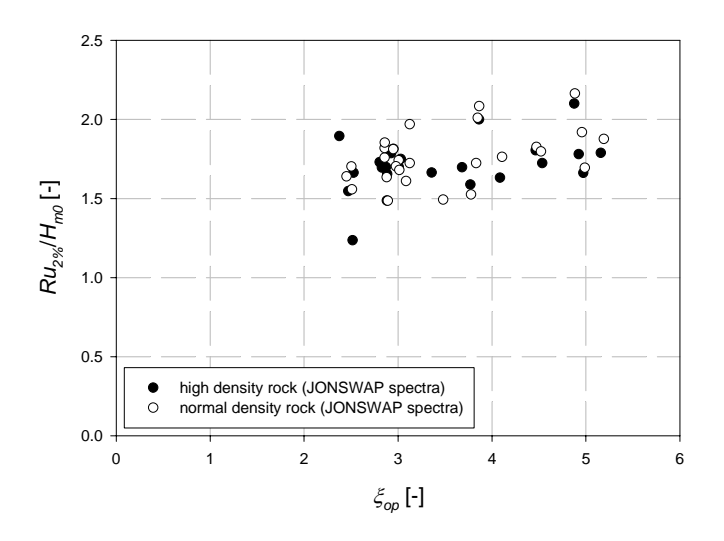


Figure 5.73: Dimensionless 2% wave run-up  $Ru_{2\%}/H_{m0}$  vs. Iribarren number  $\xi_{op}$  for both types of armour rock.

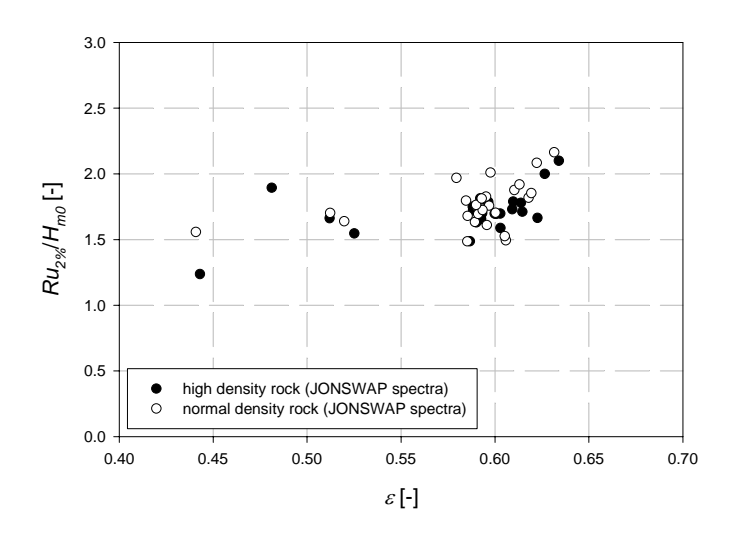


Figure 5.74: Dimensionless 2% wave run-up  $Ru_{2\%}/H_{m0}$  vs. spectral width parameter  $\varepsilon$  for both types of armour rock.

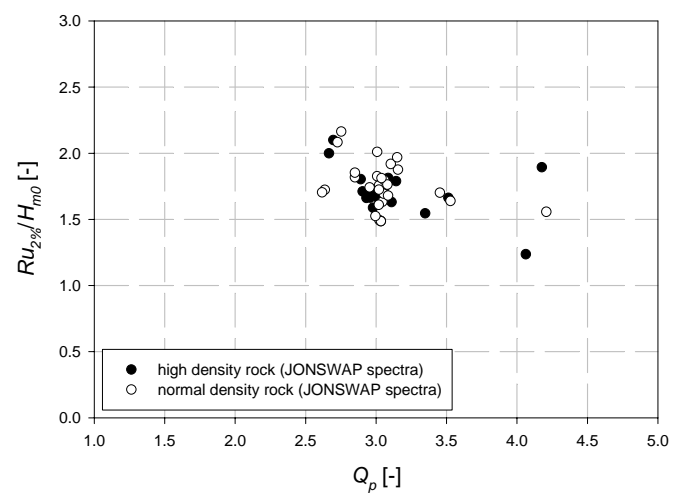


Figure 5.75: Dimensionless 2% wave run-up  $Ru_{2\%}/H_{m0}$  vs. peakedness parameter  $Q_p$  for both types of armour rock.

For this statistical problem,  $t_{\alpha 2}$  is based on (n - (k + 1)) = 25 + 28 - (4 + 1)) = 48 degrees of freedom. The critical value of t for  $\alpha = 0.05$  is  $t_{48,0.975} = 2.0123$  Therefore,  $H_0$  is rejected if t > 2.013 or t < -2.013. Since the observed value of t is outside the critical region for the parameters c and d, the null hypotheses are accepted. It is concluded that the results of both series of tests do not differ significantly from each other. However, these tests have indicated that wave run-up on slopes covered with high density rock is the same as wave run-up on a rubble mound slope covered with normal density rock. By this conclusion, the advantage of using high density rock for slope protection measurements is proven. For the remaining part of this discussion, no further distinction has been made between the results of the tests with either high density rock or normal density rock as armour layer rock.

A straight line has been fitted to the measurement results of all tests carried out with JONSWAP spectra. Following equation has been derived, valid for  $2.1 < \xi_{om} < 4.5$ :

$$\frac{Ru_{2\%}}{H_{m0}} = 0.1\xi_{om} + 1.42 \tag{5.21}$$

Two tests in which regular waves attacked the breakwater have been run at the very beginning of the project. The armour layer consisted of high density rock. The data comprised in the time interval [96,600] for test 83 and [104,600] for test 84 has been used. The average of all measured wave run-up levels has been calculated. The results are summarised in table 5.33. These are lower than the irregular test results.

Table 5.33: Regular wave run-up test results.

test n°	d <sub>paddle</sub> [m]	<i>H</i> [m]	<i>T</i> [s]	ξ [m]	N [-]	Ru/H [-]	Rd/H [-]
83	3.50	0.50	4	3.53	125	1.00	-0.38
84	3.50	0.70	3.5	2.61	141	0.97	-0.2

#### 5.6.6.3 Wave run-down

The wave run-up signals have been analysed for wave run-down as well. The results are shown in figure 5.76. Tests with a natural wave

spectrum (see Annex I and paragraph 6.3.2.1.1) have been taken into account as well. Increasing Iribarren numbers yield increasing (absolute) dimensionless 2% wave run-down values.

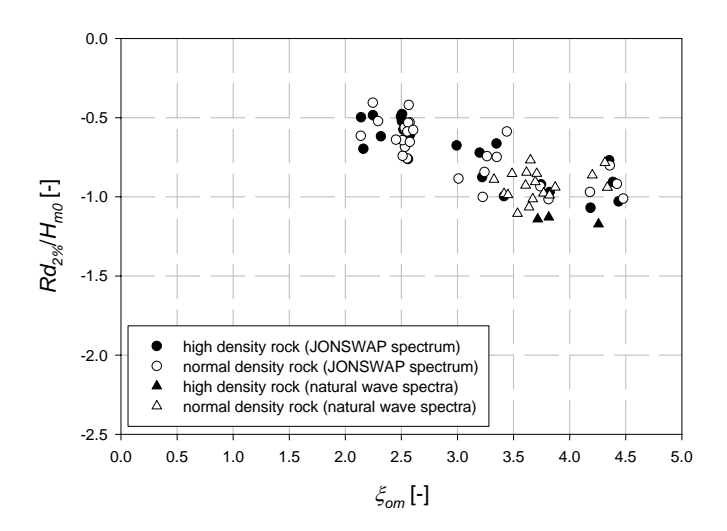


Figure 5.76: Dimensionless 2% wave run-down values versus the Iribarren number for all wave run-up tests.

A statistical test (see Annex F) has been performed to check whether wave run-down on the high density armour layer is different to wave run-down on the normal density armour layer or not. The critical t value is  $t_{n-(k+1),\omega/2} = t_{75-(4+1),0.025} = t_{70,0.025} = 1.997$ . The null hypothesis  $H_0$ : c = 0 and d = 0 is accepted as the t values of both the parameters c and d are found within the interval [-1.997, 1.997] (table 5.34). There is no significant difference ( $\alpha < 0.05$ ) between wave run-down measured on the high density armour layer and wave run-down measured on the normal density armour layer. Moreover, natural spectra yield the same value of wave run-down than the JONSWAP spectra do.

The equation of the regression line through all wave run-down results, valid for  $2.1 < \xi_{om} < 4.5$  reads:

$$\frac{Rd_{2\%}}{H_{m0}} = 0.24 \xi_{om} \tag{5.22}$$

Table 5.34: SPSS output (different type of armour rock).

variable	parameter estimate	standard error	t value	Significance
а	-1.007.10 <sup>-2</sup>	0.146	-0.069	0.945
b	-0.252	0.046	-5.522	0.000
С	-0.119	0.199	-0.596	0.553
d	4.935.10 <sup>-2</sup>	0.061	0.812	0.420

#### 5.7 Conclusions

Laboratory tests have been carried out in five selected laboratories spread over Europe:

- Aalborg University (Aalborg (Denmark)) AAU
- Flanders Hydraulics (Antwerp (Belgium)) FCFH
- Universidad Politécnica de Valencia (Valencia (Spain)) UPV
- Large Wave Channel (Hannover (Germany)) GWK
- Ghent University (Ghent (Belgium)) UGent

The tested structures were all permeable rubble mound breakwaters. Laboratory tests carried out in the framework of this thesis comprised tests on two different types of armour layer: rock  $(D_{n50}/H_{m0} \le 0.5)$  and grooved cubes  $(D_{n50}/H_{m0} \cong 1)$ . Small scale models of the Zeebrugge rubble mound breakwater have been built in the laboratories of FCFH, UPV and AAU. At FCFH and UPV a two-dimensional model has been built on scale 1:30. At AAU, a three-dimensional model has been constructed on scale 1:40. The Froude number in the scale models was the same as the Froude number at full scale. The core material has been scaled according to the method of Burcharth et al. (1999). The distorted scale of the core material was 1:20 for the models at FCFH and at UPV and 1:24 for the AAU model. The breakwater slope was 1/1.3. The armour units in the second (upper) armour layer of the small scale versions of the Zeebrugge breakwater have been placed in the same position (as good as practically possible) as these are positioned on the Zeebrugge breakwater. The armour units of the first layer have been placed in a regular pattern. The models have been subjected to small scale versions of storm events measured at full scale. Small scale versions of wave spectra measured in Zeebrugge have been reproduced in the wave flumes, resp. wave basin. Parametric tests have been carried out as well.

The tested structure for the additional small scale model tests at FCFH was the same model as used for the abovementioned tests. Two armour unit patterns have been investigated: a copy of the 'on site' (irregular) pattern and a regular (homogeneous) pattern of the outer armour layer. Fiftyseven parametric wave run-up tests have been performed. The tests have been divided over four test series. Each test series corresponded with a particular position of the comb of the run-up gauge relative to the (mainly regular) armour unit pattern. Within each test series, the water depth (four different water levels have been investigated) and peak wave period (three distinct peak periods have been used) have been varied. Standard JONSWAP spectra have been generated.

Small scale model tests have been performed at UGent on a simplified model of the Zeebrugge breakwater. Tests have been carried out with the filter layer (i.e. rock) of the Zeebrugge breakwater as the armour layer. The model has been built twice. The first time the distorted scale of the core material was 1:20 (according to the method of Burcharth et al. (1999)) whereas all other materials and dimensions had been scaled to 1:30. The second time, the overall scale factor of the model was 1:30. Wave run-up has been measured simultaneously by two run-up gauges placed in two different cross sections of the breakwater.

A conventional rubble mound breakwater has been built in the Large Wave Channel in Hannover. The total height of the structure was 5.5 m. The front slope of the breakwater was 1:2. The breakwater rested on a sand bed slope (1:50) of two meter thick. Two different types of armour layer rock have been tested successively: high density rock ( $\rho$  = 3.05 t/m³) and normal density rock ( $\rho$  = 2.65 t/m³). Tests have been carried out at three different water levels (water depth at the wave paddle: d = 3.50 m, d = 4.00 m and d = 4.50 m). Wave run-up tests and stability tests have been combined. Standard JONSWAP wave spectra have been generated. Fifteen pore pressure sensors and four pressure transducers have been installed in the core and in the interface between the different layers. Twenty two wave height meters spread over the entire flume measured the waves. A three part wave run-up gauge designed and constructed at UGent has been placed on the front slope of the breakwater.

In all laboratories, wave run-up has been measured by the novel digital wave run-up gauge developed at Ghent University in the

framework of this Ph.D. A comparison of the performance of this gauge with respect to a traditional wire gauge for wave run-up measurements has been made. For a traditional wire gauge, the difference between the measured wave run-up level and the real wave run-up level  $\Delta Ru$  is larger than the distance between the gauge and the slope surface when the wave steepness s is lower than 0.06. This difference  $\Delta Ru$  equals at least five times the distance between the gauge and the slope for s < 0.02! In case of the digital run-up gauge, the electrodes follow the craggy slope of the armour layer. The distance between the armour layer and the 'gauge' is everywhere less than 2 mm. The dimensionless wave run-up values  $Ru_2v_d/H_{m0}$  measured by the novel run-up gauge were 9% higher at FCFH and 33% higher at AAU than the dimensionless wave run-up value  $Ru_2v_d/H_{m0}$  measured by a traditional wire gauge.

The significant wave height during all additional FCFH tests was approximately 3.00 m (full scale value) by which the ratio  $D_{n50}/H_{m0}$  was fixed at ~0.90. The armour layer consisted of grooved cubes. Test results indicated rather big differences between test results obtained for almost the same input parameters (significant wave height  $H_{m0}$  and peak wave period  $T_p$ ) and output parameters (spectral width parameter  $\varepsilon$ , Iribarren number  $\xi$ ), but for different combinations of SWL, armour unit pattern and position of the comb of the run-up gauge relative to the armour unit pattern.

To minimise the influence of the abovementioned combination of parameters, additional tests have been carried out at UGent. The armour layer of the UGent model consisted of rock by which the ratio  $D_{n50}/H_{m0}$  was smaller than the FCFH value. During these tests, the influence of the position of the comb of the run-up gauge relative to the armour layer has also been investigated. Two run-up gauges measured wave run-up simultaneously in two different cross sections of the breakwater model.

Within one single test, the results of both run-up gauges differed from each other. This has also been noticed at full scale: the  $Ru_{2\%}$  value measured by the 'spiderweb system' and the  $Ru_{2\%}$  value measured by the run-up gauge during the same storm event differed from each other in many cases. But taking storm events into account, both measuring devices measure the same. This has also been noticed for the UGent laboratory experiments: no significant difference ( $\alpha$  < 0.05) has been found between the two series (each series corresponding with

one run-up gauge) of test results. The two run-up gauges measure the same wave run-up levels in different cross sections. The average difference between the measurements of the two run-up gauges was only 6.5%. The position of the run-up gauge relative to the armour layer and thus, the armour layer pattern has no influence on wave run-up.

Large scale tests have shown that wave run-up on two different gradations of rock (with different dimensions for the same level of stability, realised by using normal and high density rock) is the same ( $\alpha$ < 0.05). A large spreading on the results is introduced by the rough character of the armour layer. The effect of this spreading on wave run-up results is minimised by taking into account a large number of test results.

It is concluded that wave run-up on a rubble mound breakwater covered with artificial armour units is very sensitive to geometrical changes to the armour unit pattern from one test to another.

The porosity of the outer armour layer has been slightly modified at FCFH and AAU. By filling up a hole between the upper armour units underneath the needles of the comb of the run-up gauge, the armour layer became locally less porous. A remarkable increase in absolute wave run-up (up to 18%) has been noticed.

For the additional FCFH results, no firm conclusions concerning the influence of water depth on wave run-up could be made. The armour unit pattern at the crest of the breakwater had an influence on the results

Dimensionless wave run-up values  $Ru_{2\%}/H_{m0}$  increase with increasing Iribarren number  $\xi_{om}$ . This increase was larger at lower SWL. The increase in dimensionless wave run-up is mainly due to the influence of the wave period ( $\xi$  is proportional to the wave period), but also due to the armour layer pattern at the crest of the breakwater which was more porous than the lower part of the armour layer of the breakwater. Dimensionless wave run-up characterised by  $Ru_{2\%}/H_{m0}$  increases when the peak wave period  $T_p$  increases. The larger the peak period and thus, the larger the Iribarren number, the more spreading has been seen on the results.

There is evidence ( $\alpha = 0.05$ ) to proof that the results of the UGent tests with different cores (1:20 and 1:30) yield different results. It could not be stated with certainty whether the 1:20 core yield larger or smaller  $Ru_{2\%}$  values than the 1:30 core.

Model spectra have been tuned to full scale spectra for storm event reproductions. Even though a good agreement was seen between the frequency domain parameters  $H_{m0}$  and  $T_{01}$  in most tests, the spectral width parameter  $\varepsilon$  and the spectral peak period  $T_p$  in the models did not have necessarily the same value as the full scale values. Small scale model test results of storm event reproductions will be discussed further in detail in chapter 6.

The influence of wind on wave run-up has been investigated at UPV. Increasing wind speed yields increased wave run-up and wave overtopping. A linear relationship has been found between dimensionless wave overtopping  $log(q/\sqrt{gH_s^3})$  and the relative crest freeboard  $R_c/H_s$ . The influence of a.o. a longshore current, wave obliqueness and wave spreading angle have been investigated at AAU. Increasing wave obliqueness and wave spreading angle yield reduced dimensionless wave run-up. Increased current velocity  $v_c$  induced increased relative wave run-up.

The influence of the shape of the spectrum (characterised by the spectral width parameter  $\varepsilon$  and/or the peakedness parameter  $Q_p$  of Goda (1985)) is clear: in all tests it has been observed that an increasing value of the spectral width parameter  $\varepsilon$  and/or a decreasing value of the peakedness parameter  $Q_p$  yield an increasing relative wave run-up value  $Ru_2 \% H_{m0}$ .

The reflection coefficient for the UGent model (rubble mound breakwater with a rock armour layer) increases with increasing wave period from  $C_r = 0.20$  for  $T_{01} = 0.8$  s to  $C_r = 0.40$  for  $T_{01} = 1.5$  s.

The large scale tests at GWK indicated relative wave run-up values varying between  $Ru_{2\%}/H_{m0} = 1.64$  for  $\xi_{om} = 2.14$  and  $Ru_{2\%}/H_{m0} = 1.89$  for  $\xi_{om} = 4.48$ . Wave run-down has been measured at GWK and has been analysed. Increasing Iribarren numbers yield increasing (absolute) dimensionless 2% wave run-down values  $Rd_{2\%}/H_{m0}$ . Wave run-down is given by  $Rd_{2\%}/H_{m0} = -0.24 \xi_{om}$  for  $2.14 < \xi_{om} < 4.48$ .

## Chapter 6: Comparison and discussion of results.

#### 6.1 Introduction.

The full scale measurement results discussed in chapter 4, the results of the laboratory experiments discussed in chapter 5 (i.e. OPTICREST tests, additional small scale model tests at FCFH and UGent and large scale tests at GWK) and wave run-up data found in literature are compared.

Paragraph 6.2 deals with comparison and the discussion of the full scale measurement results and the results of the storm event reproductions in the laboratories of FCFH, UPV and AAU. Model effects and scale effects which may be held responsible for the observed discrepancies between full scale measurement and small scale model test results are treated in paragraph 6.3. Paragraph 6.4 compares the full scale measurement results with wave run-up data found in literature. A formula is derived from all obtained results in paragraph 6.5. The conclusions of this chapter are found in paragraph 6.6.

### **6.2 Comparison of OPTICREST results.**

To make comparison of full scale measurement results with laboratory results easier, in this paragraph, all laboratory values have been scaled to their full scale values. On behalf of the reproduction of the storm events in the laboratories, time series with slightly different length have been used than these analysed in chapter 4. It concerns storm events  $n^{\circ}$  1, 2 and 3 (here after called storm  $1^{b}$  (August  $28^{th}$ , 1995 (03h30 to 04h45)), storm  $2^{b}$  (August  $28^{th}$ , 1995 (14h45 to 17h00)) and storm  $3^{b}$  (January  $19^{th}$ , 1998 (15h45 to 18h15))) (see table 5.1). The results of the analysis of the full scale measurement data necessary for comparison with laboratory data are given in table 6.1. The wave characteristics of the storm event reproductions at FCFH, AAU and UPV are given in table 6.2 (for  $H_{m0}$ ), resp. table 6.3 (for  $T_{01}$ ) and table 6.4 (for  $T_p$ ).

The significant wave height  $H_{m0}$ , the mean wave period  $T_{0I}$  and the peak wave period  $T_p$  of the laboratory experiments have been plotted against their target (full scale) value in figure 6.1 (for  $H_{m0}$ ), figure 6.2 (for  $T_{0I}$ ) and figure 6.3 (for  $T_p$ ). To make a distinction between the results of the analysis of a time series with a duration of two hours at high water (from  $t_{HW}$ -1 to  $t_{HW}$  +1) and the results of the analysis of time series of one hour taken upon rising tide ([ $t_{HW}$ -3,  $t_{HW}$ -2], [ $t_{HW}$ -2,

 $t_{HW}$ -1]) or receding tide ([ $t_{HW}$ +1,  $t_{HW}$ +2], [ $t_{HW}$ +2,  $t_{HW}$ +3]), two hour results are represented by full symbols (full scale measurements:  $\bullet$ , FCFH:  $\blacktriangle$ , AAU:  $\diamond$ , UPV:  $\blacksquare$ ) and one hour results by open symbols (full scale measurements:  $\bigcirc$ , FCFH:  $\triangle$ , AAU:  $\diamondsuit$ , UPV:  $\square$ ). For full scale measurements, a one hour result is the average of the results of the two time series of half an hour within the considered hour. All values of table 6.1 have been plotted in the graphs. Some symbols are hidden behind others.

Table 6.1: Full scale measurement results of the storm events which have been reproduced in the laboratories.

storm event n°	<i>H</i> <sub>m0</sub> [m]	T <sub>01</sub> [s]	$T_p$ [s]	€[-]	ξ <sub>om</sub> [-]	Ru <sub>2%</sub> /H <sub>m0</sub> [-]
1 <sup>b</sup>	2.84	6.2	7.3	0.5893	3.54	1.54
2 <sup>b</sup>	2.66	6.4	9.4	0.5425	3.79	1.58
3 <sup>b</sup>	2.92	6.6	8.6	0.6015	3.73	1.74
4	3.00	6.6	8.5	0.6010	3.67	1.79
5	3.12	6.6	8.5	0.5884	3.57	1.81
8a	2.29	5.7	7.3	0.6016	3.61	2.42
8b	2.67	6.0	7.3	0.5956	3.51	2.15
8c	3.04	6.3	7.3	0.6166	3.47	1.82
8d	2.87	6.3	7.3	0.6385	3.57	1.89
8e	2.41	6.2	8.0	0.6286	3.86	2.45
9a	2.48	6.2	8.3	0.6024	3.77	2.36
9b	2.57	6.1	7.4	0.6377	3.66	2.21
9c	2.54	6.3	9.3	0.5642	3.81	1.89
9d	2.52	6.3	8.6	0.5991	3.82	2.17
9e	2.09	5.9	8.3	0.5952	3.92	2.28

The average values of the absolute values of the relative differences between laboratory and full scale values for  $H_{m0}$ ,  $T_{01}$  and  $T_p$  for all storm events reproductions are given in table 6.5. From figure 6.2 and table 6.5 it is seen that in all laboratories the mean wave periods  $T_{01}$  have been reproduced quite well. Wave heights reproduced in all laboratories were often higher than the full scale value. The largest spreading is seen on the values of the peak wave periods  $T_p$ . This is due to the fact that for storm reproduction, the significant wave height  $H_{m0}$  and the mean wave period  $T_{01}$  were the two parameters, next to

visual comparison of spectra, used for tuning the laboratory spectra to the full scale spectra. However, this way of working does not guarantee that also the peak wave period is reproduced accurately. Peak wave periods were not systematically higher in the models than at full scale. Wave spectra generated at FCFH and AAU are found in Annex J, resp. Annex K. The storm event reproductions have been less accurate at FCFH than at UPV and AAU.

Table 6.5: Average of absolute values of relative differences [%] between the laboratory values of the significant wave height  $H_{m0}$ , the mean wave period  $T_{01}$  and the peak wave period  $T_p$  and the full scale values compared to the full scale values for (a) all reproduced storm events and (b) storm events  $\mathbf{n}^{\circ}$  1b, 2b, 3b, 4, 5, 8c and 9c (i.e. the storm events with a duration of approximately two hours at high tide).

	two nours at mgn tide).					
	$H_{m0}$ [m]	$T_{01}[s]$	$T_p$ [s]			
FCFH	8.9	4.9	11.3			
AAU	2.0	4.0	4.9			
UPV	2.6	2.8	5.1			
	(	a)				
	$H_{m0}$ [m]	$T_{01}[s]$	$T_p$ [s]			
FCFH	4.0	7.1	12.4			
AAU	1.4	5.5	5.1			
UP\/	27	3.2	6.9			

In figure 6.4 and 6.5, the dimensionless wave run-up values  $Ru_{2\%}/H_{m0}$  have been plotted against the Iribarren number  $\xi_{om}$ . In figure 6.4, the test results of storm events n° 1, 2, 3, 4, 5, 8c and 9c are shown. In figure 6.5, the test results of storm events n° 8a, 8b, 8d, 8e, 9a, 9b, 9d and 9e are shown. All  $\xi_{om}$  values are found within the interval [3.44, 4.12]. The  $Ru_{2\%}/H_{m0}$  values vary between 1.26 and 2.45 when all analysed time series are taken into account and between 1.28 and 1.91 when only the time series at high water ([ $t_{HW}$ -1,  $t_{HW}$ +1]) are taken into account. The larger spreading on the  $Ru_{2\%}/H_{m0}$  values shown in figure 6.5 in comparison to these in figure 6.4 is due to the full scale measurement results which are found in the upper part of the cloud of results.

Table 6.2: Comparison of target (full scale) significant wave heights  $H_{m\theta}$  and significant wave heights measured in the laboratories.

storm event n°	full scale	FCFH	AAU	UPV
1 <sup>b</sup>	2.84	2.54	2.90	
2 <sup>b</sup>	2.66	2.64	2.69	
$3^{b}$	2.92	2.98	2.96	
4	3.00	3.17	3.00	
5	3.12	3.34	3.12	
8a	2.29	2.74	2.43	2.43
8b	2.67	3.00	2.76	2.76
8c	3.04	3.08	3.12	3.12
8d	2.87	2.98	2.88	2.88
8e	2.41	2.62	2.38	2.38
9a	2.48	2.80	2.42	2.42
9b	2.57	3.01	2.52	2.52
9c	2.54	2.56	2.61	2.61
9d	2.52	2.80	2.40	2.40
9e	2.09	2.49	2.08	2.08

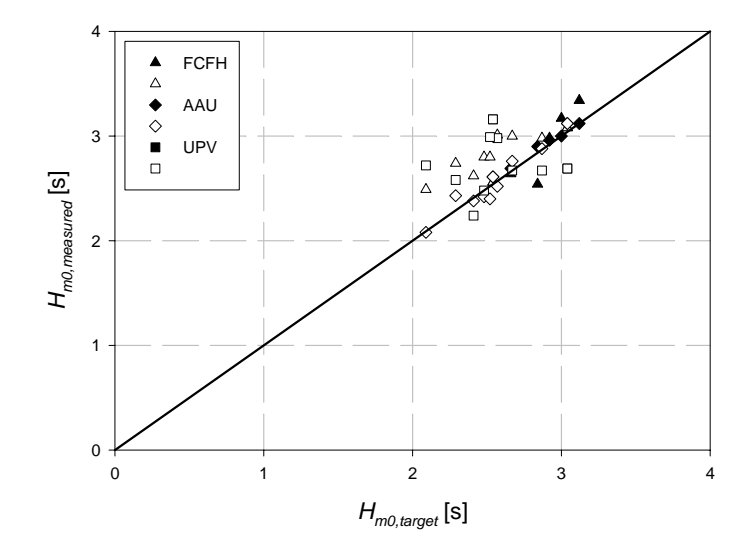


Figure 6.1: Comparison of target (full scale) significant wave heights  $H_{m\theta}$  and significant wave heights measured in the laboratories.

Table 6.3: Comparison of target (full scale) mean wave periods  $T_{01}$  and mean wave periods measured in the laboratories.

storm event n°	full scale	FCFH	AAU	UPV
1 <sup>b</sup>	6.2	6.7	6.3	
2 <sup>b</sup>	6.4	7.0	6.9	
3 <sup>b</sup>	6.6	7.4	7.2	
4	6.6	6.9	7.2	
5	6.6	7.1	6.9	
8a	5.7	5.9	6.0	6.0
8b	6.0	6.4	6.1	6.1
8c	6.3	6.8	6.6	6.6
8d	6.3	6.6	6.7	6.7
8e	6.2	6.2	6.3	6.3
9a	6.2	6.0	6.2	6.2
9b	6.1	6.2	6.4	6.4
9c	6.3	6.3	6.4	6.4
9d	6.3	6.3	6.4	6.4
9e	5.9	5.7	5.9	5.9

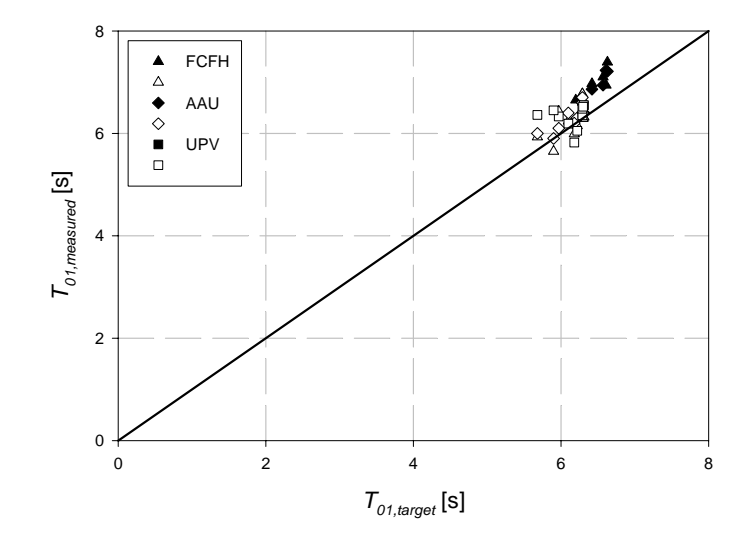


Figure 6.2: Comparison of target (full scale) mean wave periods  $T_{\theta I}$  and mean wave periods measured in the laboratories.

Table 6.4: Comparison of target (full scale) peak wave periods  $T_p$  and peak wave periods measured in the laboratories.

storm event n°	full scale	FCFH	AAU	UPV
1 <sup>b</sup>	7.3	8.5	7.4	
<b>2</b> <sup>b</sup>	9.4	8.0	9.0	
3 <sup>b</sup>	8.6	8.1	8.3	
4	8.5	9.0	9.1	
5	8.5	8.1	9.0	
8a	7.3	7.2	7.2	7.2
8b	7.3	7.9	7.2	7.2
8c	7.3	7.8	8.0	8.0
8d	7.3	7.9	7.2	7.2
8e	8.0	7.1	7.2	7.2
9a	8.3	7.1	7.2	7.2
9b	7.4	7.0	7.2	7.2
9c	9.3	6.3	8.9	8.9
9d	8.6	7.6	8.9	8.9
9e	8.3	6.5	8.0	8.0

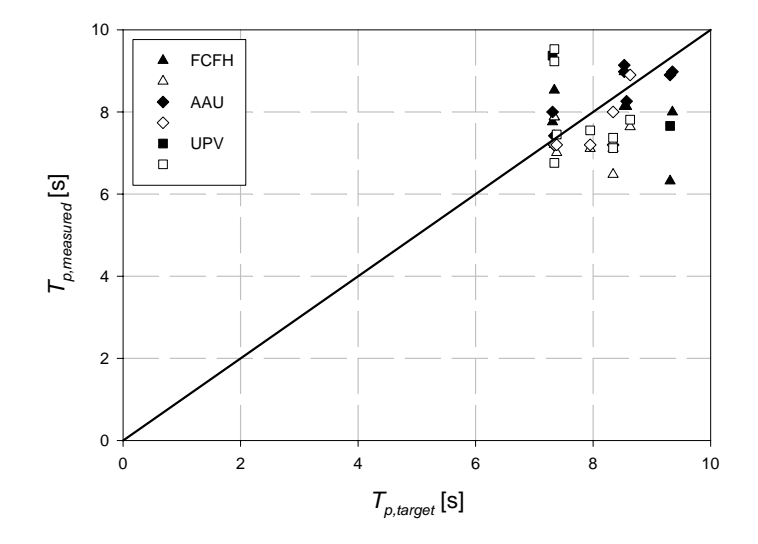


Figure 6.3: Comparison of the target (full scale) peak wave periods  $T_p$  and the peak wave periods measured in the laboratories.

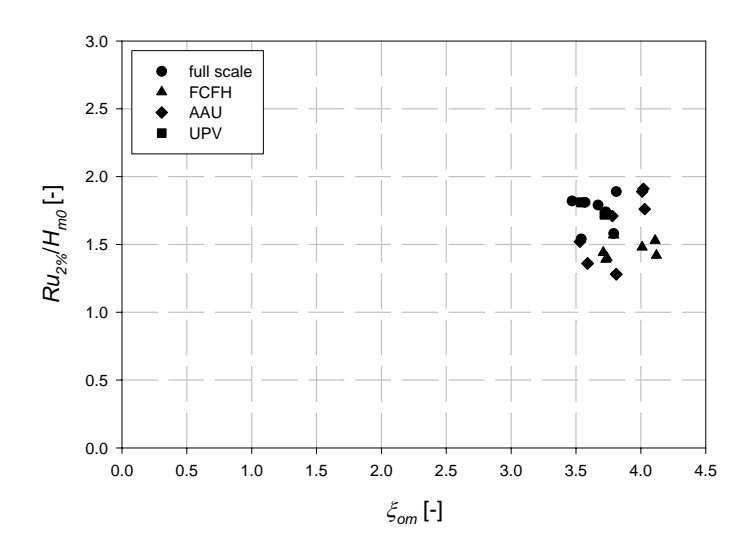


Figure 6.4:  $Ru_{2\%}/H_{m\theta}$  plotted against the Iribarren number  $\xi_{om}$  for full scale measurements and laboratory tests (two hour storm events at high water  $[t_{HW}$ -1,  $t_{HW}$ +1]).

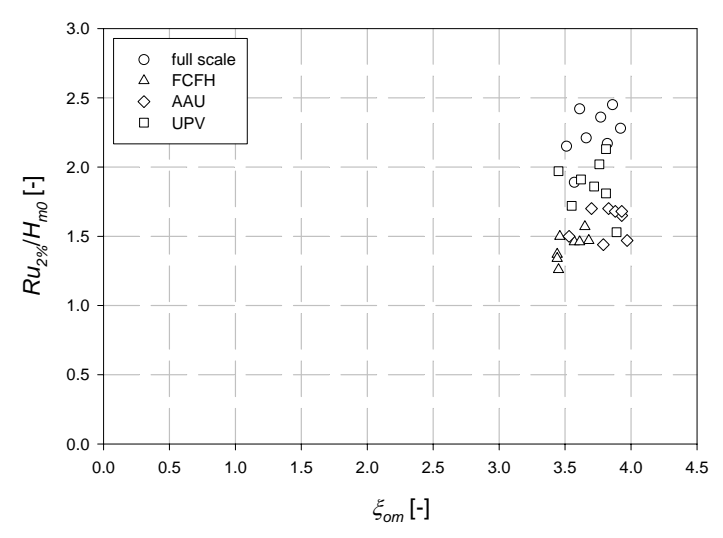


Figure 6.5:  $Ru_{2\%}/H_{m0}$  plotted against the Iribarren number  $\xi_{om}$  for full scale measurements and laboratory tests (storm events upon rising  $[t_{HW}$ -3,  $t_{HW}$ -2],  $[t_{HW}$  -2,  $t_{HW}$  -1] and receding tide  $[t_{HW}$ +1,  $t_{HW}$ +2],  $[t_{HW}$  +2,  $t_{HW}$  +3]).

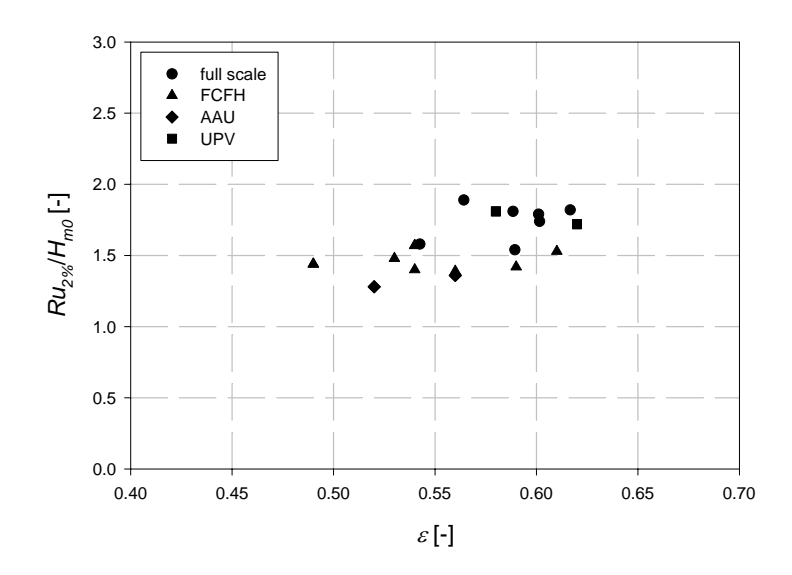


Figure 6.6:  $Ru_{2\%}/H_{m0}$  plotted against the spectral width parameter  $\varepsilon$  for full scale measurements and laboratory tests (two hour storm events at high water  $[t_{HW}$ -1,  $t_{HW}$ +1]).

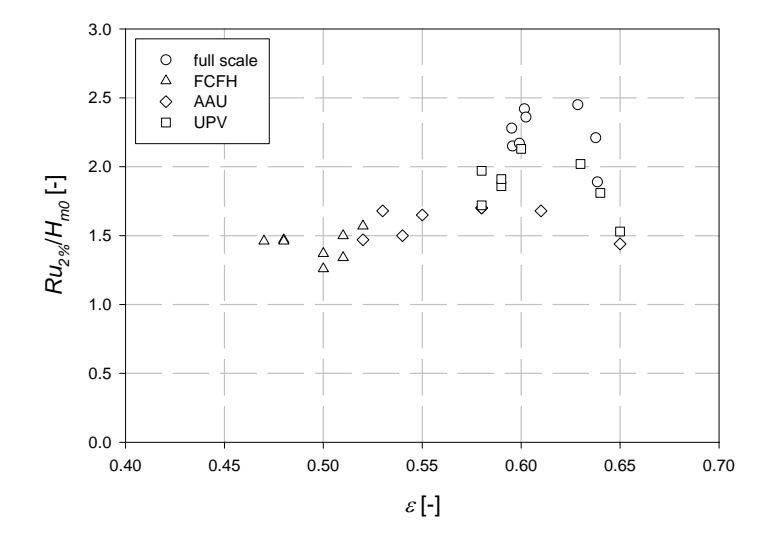


Figure 6.7:  $Ru_{2\%}/H_{m0}$  plotted against the spectral width parameter  $\varepsilon$  for full scale measurements and laboratory tests (storm events upon rising  $[t_{HW}$ -3,  $t_{HW}$ -2],  $[t_{HW}$ -2,  $t_{HW}$ -1] and receding tide  $[t_{HW}$ +1,  $t_{HW}$ +2],  $[t_{HW}$ +2,  $t_{HW}$ +3]).

Table 6.6:  $Ru_{2\%}/H_{m0}$  values of full scale measurement campaigns and small scale model tests at the laboratories of Flanders Hydraulics (FCFH), Universidad Politécnica de Valencia (UPV) and Aalborg University (AAU) for different storm events.

	full scale	scale model			
storm n°	measurements	FCFH	UPV	AAU	
		(2D, 1:30)	(2D, 1:30)	(3D, 1:40)	
1 <sup>b</sup>	1.54	1.48		1.52	
2 <sup>b</sup>	1.58	1.42		1.91	
$3^{b}$	1.74	1.53		1.76	
4	1.79	1.40		1.89	
5	1.81	1.39		1.71	
8c	1.69	1.44	1.72	1.36	
9c	1.76	1.57	1.81	1.28	
mean	1.70	1.46	1.77	1.63	
$s^2$	0.011	0.005	0.004	0.063	
С	0.0064	0.0032	0.0023	0.0385	

In figure 6.6 and 6.7, dimensionless wave run-up values  $Ru_{2\%}/H_{m0}$  have been plotted against the spectral width parameter  $\varepsilon$ . In figure 6.6, the test results of storm events n° 1, 2, 3, 4, 5, 8c and 9c are shown. In figure 6.7, the test results of storm events n° 8a, 8b, 8d, 8e, 9a, 9b, 9d and 9e are shown. Dimensionless wave run-up values increase when spectral width parameter values increase.

Full scale measurements revealed the overall mean prototype  $Ru_{2\%}/H_{m0}$  value of 1.77 (based on much more storms than the seven storm events which have been reproduced in the laboratories and all measured with the run-up gauge (RU)). This value has been found by small scale tests at UPV as well (table 6.6). A mean  $Ru_{2\%}/H_{m0}$  value for the seven storms at high water reproduced in the laboratories is 1.70 for full scale measurements.

The  $Ru_{2\%}/H_{m0}$  values of the storm event reproductions n° 8c and 9c at AAU are clearly lower than the results of storm events n° 1 to 5. These two storm events have a mean dimensionless 2% wave run-up value of 1.32. The average  $Ru_{2\%}/H_{m0}$  value for storm events n° 1 to 5 is 1.76, which is almost equal to the full scale value. Taking all

reproduced storm events into account, the mean value of  $Ru_{2\%}/H_{m0}$  is 1.63.

The results of the scale model tests performed at FCFH show a clear underestimation of the full scale values. The average  $Ru_{2\%}/H_{m0}$  value for FCFH is 1.46.

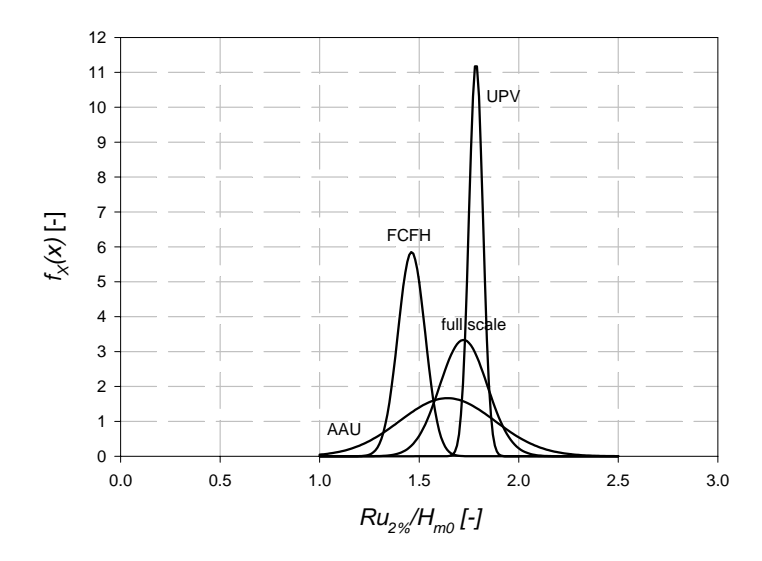


Figure 6.8: Probability distribution function of full scale measurements and laboratory testing.

To visualise the average values of the dimensionless wave run-up  $Ru_{2} \%/H_{m0}$  obtained at full scale and in the various laboratories, table 6.6 has been conversed to figure 6.8 in which the probability distribution of  $Ru_{2} \%/H_{m0}$  is depicted. As the obtained results are the results of a Gaussian process of which the realisations are independent from each other, a Gaussian distribution has been assumed (Van Torre (1997)). A lot of spreading is seen on the AAU results.

Not only the  $Ru_{2\%}/H_{m0}$  values, but also the  $Ru_{5\%}/H_{m0}$  and the  $Ru_{10\%}/H_{m0}$  values have been calculated and have been compared. The two storms covering half a tide cycle (storm events n° 8 and 9) have been focussed on. Each storm event was constituted of five subevents. The results have been summarised in table 6.7, 6.8 and 6.9 for

 $Ru_x H_{m0}$  with x = 2%, resp. 5% and 10% and are plotted in a graph showing the  $Ru_x H_{m0}$  values against the *SWL* (figures 6.9, 6.10 and 6.11).

From figure 6.9, 6.10 and 6.11 it is seen that full scale measurement results and AAU results show the same trend: dimensionless wave run-up values  $Ru_{x\%}/H_{m0}$  increase with decreasing water depth (SWL). AAU results are lower than full scale results at all time. At high water, UPV results have the same order of magnitude of full scale results, but diverge from full scale results when the water level becomes lower. A slight increase in  $Ru_{2\%}/H_{m0}$  and  $Ru_{5\%}/H_{m0}$  is noticed in the UPV results when the water depth is decreasing. A slight decrease in  $Ru_{10\%}/H_{m0}$ values is seen in the UPV results when the water depth is decreasing. At high water, FCFH are slightly higher than AAU results, but decrease when the SWL decreases. The difference between the results of all laboratories and full scale results become smaller and smaller when higher exceedence probabilities x are considered. All laboratory results become very similar when  $Ru_{10\%}$  is taken into account (figure 6.11). At higher water levels all values have almost the same value  $(Ru_{10\%}/H_{m0} \cong 1.28)$ . Full scale measurements are always higher than laboratory measurement results.

The influence of the water level on wave run-up may also be explained by the fact that for lower water levels wave run-up takes place on a lower part of the slope. The Zeebrugge breakwater has been built in 1983. In the meantime, some settlements of the armour units have occurred. Due to settlements the porosity in the lower part of the armour layer may have a higher value in the models than at full scale. This smaller porosity causes higher wave run-up.

Analysing the wave run-up distributions obtained by full scale measurement campaigns and all small scale storm event reproduction tests, it is seen that only the highest wave run-up levels (i.e. with an exceedance probability less than 1%) deviate from this theoretical distribution. The  $Ru_{2\%}$  value is always found within the theoretical curve of he Rayleigh distribution. It is concluded that  $Ru_{2\%}$  is a reliable parameter to describe wave run-up on a rubble mound breakwater.

Table 6.7:  $Ru_{2\%}/H_{m0}$  results.

Table 6.7. Ku 2%/11m0 Testites.					
Storm n°	full scale -	scale model			
Stormin	Tuli Scale -	FCFH	UPV	AAU	
8a	2.42	1.26	1.72	1.79	
8b	2.15	1.46	1.97	1.51	
8c	1.82	1.44	1.81	1.42	
8d	1.89	1.47	1.91	1.43	
8e	2.45	1.57	2.02	1.58	
9a	2.35	1.37	2.13	1.65	
9b	2.20	1.5	1.86	1.63	
9c	1.89	1.57	1.72	1.29	
9d	2.17	1.46	1.81	1.39	
9e	2.28	1.34	1.53	1.63	

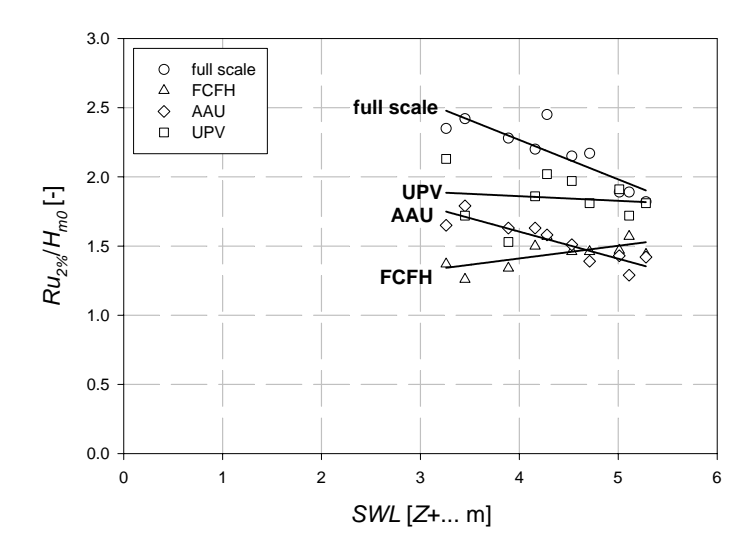


Figure 6.9: Comparison of the dimensionless wave run-up value  $Ru_{2\%}/H_{m\theta}$  exceeded by 2% of the waves for full scale measurements and laboratory results.

Table 6.8:  $Ru_{5\%}/H_{m0}$  results.

Tuble 0.0. Itas %/11m0 Testites.						
Storm n°	full scale -	scale model				
		FCFH	UPV	AAU		
8a	2.05	1.14	1.51	1.62		
8b	1.86	1.37	1.56	1.36		
8c	1.55	1.33	1.5	1.26		
8d	1.57	1.41	1.55	1.3		
8e	2.00	1.48	1.59	1.48		
9a	2.14	1.17	1.62	1.57		
9b	1.98	1.33	1.64	1.52		
9c	1.67	1.44	1.48	1.22		
9d	1.87	1.4	1.58	1.31		
9e	1.66	1.07	1.35	1.57		

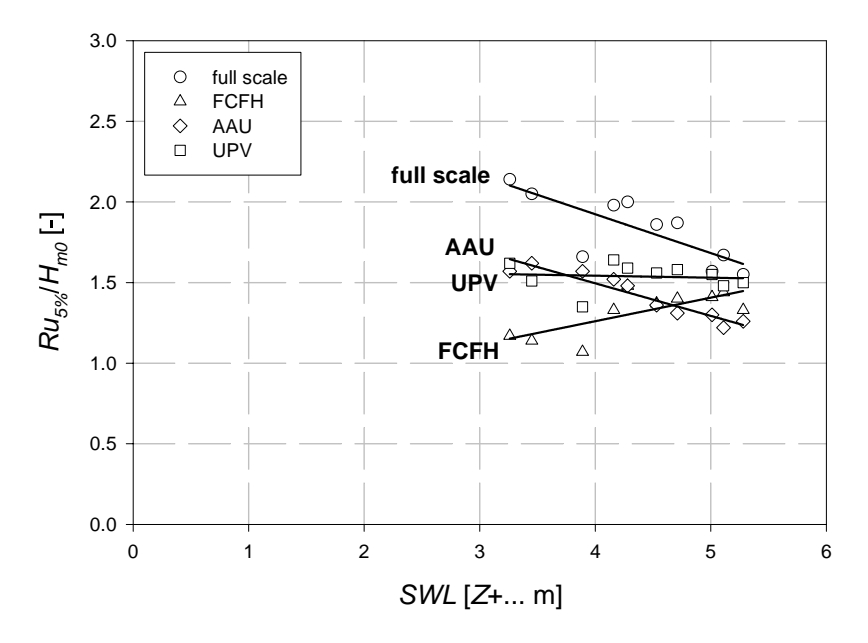


Figure 6.10: Comparison of the dimensionless wave run-up value  $Ru_{5\%}/H_{m0}$  exceeded by 5% of the waves for full scale measurements and laboratory results.

Table 6.9:  $Ru_{10\%}/H_{m0}$  results.

200210 000 1 200 10760 2 000 2						
Storm n°	full scale -	scale model				
		FCFH	UPV	AAU		
8a	1.65	1.07	1.23	1.59		
8b	1.64	1.27	1.33	1.28		
8c	1.34	1.22	1.28	1.13		
8d	1.49	1.3	1.36	1.21		
8e	1.62	1.3	1.36	1.21		
9a	1.67	1.08	1.26	1.42		
9b	1.65	1.08	1.28	1.26		
9c	1.45	1.35	1.35	1.15		
9d	1.54	1.33	1.26	1.2		
9e	1.50	0.97	1.02	1.52		

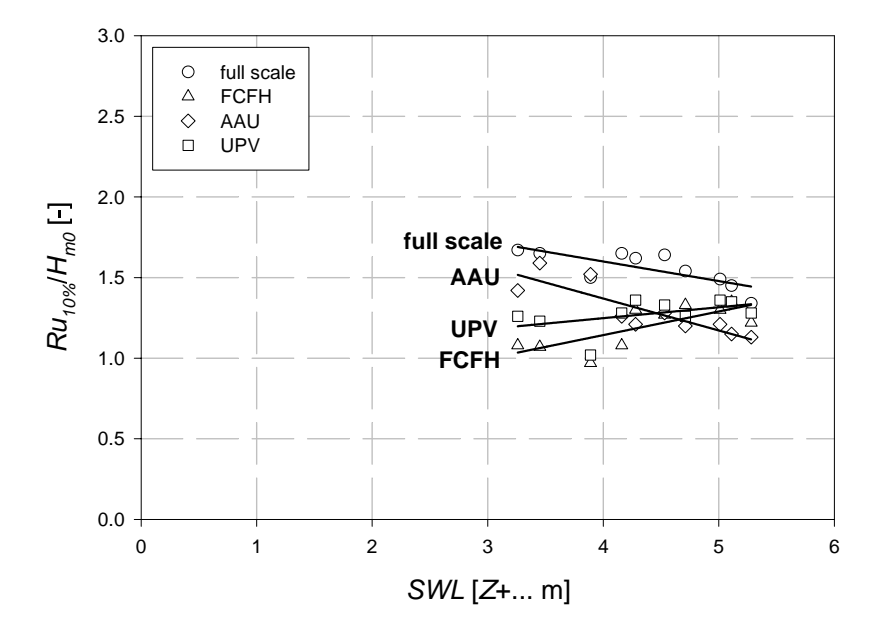


Figure 6.11: Comparison of the dimensionless wave run-up value  $Ru_{10\%}/H_{m0}$  exceeded by 10% of the waves for full scale measurements and laboratory results.

#### 6.3 Model effects and scale effects

In an attempt to explain the differences between laboratory results of storm event reproductions on a scale model of the Zeebrugge breakwater and full scale measurement results on the one hand and differences between the results obtained in the different laboratories on the other hand, next to the conclusions drawn at the end of chapter 5, scale effects and model effects have been highlighted:

- (i) scale effects
  - surface tension
  - viscosity
- (ii) model effects
  - hydraulical/meteorological
    - waves (spectral shape (cfr. paragraph 2.2.3.2), wave height)
    - wind (cfr. paragraph 5.3.2)
    - longshore currents
  - model geometry
    - armour layer
    - foreshore
    - sand filling in core

# **6.3.1 Scale effects**

Scale effects play an important role in scale model investigations. These effects are not likely to be quantified. Instead, a qualitative description has been made. Four types of scale effects have been considered:

- the influence of surface tension on wave run-up
- the influence of viscosity on wave propagation through the wave flume
- the influence of viscosity on wave run-up
- the influence of viscosity on internal flow regime (porosity and permeability)

The influence of these scale effects is estimated in the following paragraphs.

# **6.3.1.1 Definitions**

The Froude number is defined as

$$Fr = \frac{V}{\sqrt{gL}} \tag{6.1}$$

in which V is a characteristic velocity [m/s] and L a characteristic length [m]. g is the gravitational acceleration ( $g = 9.81 \text{ m/s}^2$ ). The Froude number is the ratio between inertia forces and gravity forces. The Reynolds number is defined as

$$Re = \frac{VD}{V} \tag{2.22}$$

in which V is a characteristic velocity [m/s], D is a characteristic length [m] and  $\nu$  is the kinematic viscosity of the fluid [m²/s] ( $\nu$  = 1.00 . 10<sup>-6</sup> m²/s at 20°C and  $\nu$  = 1.79 . 10<sup>-6</sup> m²/s at 0°C). The number of Weber, important when the surface tension becomes important, is defined as

$$We = \rho V^2 \left(\frac{L}{T}\right) \tag{6.2}$$

in which

- L is a characteristic length,
- V a characteristic velocity,
- T the surface tension which is the potential energy per unit of surface at the interface of two fluids,

The surface tension of the two fluids system water/air is  $T=74.9 \cdot 10^{-3}$  N/m at 5°C and 72.2 · 10<sup>-3</sup> N/m at 20°C. The density of water  $\rho_w$  equals 1000 kg/m<sup>3</sup>. The Weber number is the ratio between inertia forces and the forces caused by the surface tension.

In order that two systems (e.g. full scale on the one hand and a small scale model on the other hand) with a free water surface have an identical dynamic behaviour, two equations, namely  $Re = c^{te}$  and  $Fr = c^{te}$ , should be fulfilled. The Reynolds and the Froude number should have the same value in the scale model and at full scale. However, it is impossible to construct a perfect dynamic identical model. Not all compatibility conditions can be satisfied at the same time as viscosity and density of the water cannot be scaled. This shortcoming is

remedied by assuming an ideal fluid ( $\nu$  very small). This assumption is only appropriate when viscosity forces are small in comparison with inertia forces. This means that the value of the Reynolds number, inversely proportional to the kinematic viscosity, has to be large. So, to construct a reasonably good dynamic identical model, not only the equation  $Fr = c^{te}$  has to be fulfilled, but also the values of the other dimensionless numbers (Reynolds and other such as Weber, Cauchy,...) have to be taken into account and may not trespass a critical value (see next paragraphs). Otherwise, viscosity, elasticity, surface tension,... are not scaled properly and wave run-up is modelled incorrectly. For example, too small Reynolds numbers suggest too large viscous forces by which the flow in and through the core of the breakwater is slowed down. As a results, wave run-up values become smaller than large values of Re would imply.

# 6.3.1.2 Wave run-up velocity

Schüttrumpf et al. (2000) describe a method to determine wave run-up velocities. Schüttrumpf et al. (2000) consulted various sources in literature about the location of maximum front velocity. Some researchers found the maximum front velocity **above** SWL and other found the maximum front velocity **at** SWL. Schüttrumpf et al. (2000) applied their method to the full scale Zeebrugge breakwater data. Wave run-up and wave run-down velocities have been derived from the signal of the run-up gauge (RU). Because of the fact that the SWLs of the analysed time series were all lower than the level of the lowest electrode of the run-up gauge on the Zeebrugge breakwater (i.e. Z+6.12), it is believed that the maximum front velocity has not been measured on the Zeebrugge breakwater.

To draw up a general formula to describe wave run-up velocity, all researchers started from the theoretical energy equation:

$$\Delta E_{kin} - \Delta E_{pot} - \Delta E_{friction} = 0 \tag{6.3}$$

with

$$\Delta E_{kin} = \frac{m}{2} \left[ v_{\text{max}}^2 - (v(z))^2 \right] : \text{change in kinetic energy} \quad (6.4)$$

$$\Delta E_{pot} = mgz$$
: change in potential energy (6.5)

$$\Delta E_{friction} = \frac{\alpha m(v(z))^2}{2}$$
: change in friction energy (6.6)

and m = mass of control volume [N],  $\alpha = \text{constant [-]}$ , z = level [m], v(z) = velocity of water front at level z [m/s].

Substitution of (6.4), (6.5) and (6.6) in (6.3) yields:

$$v(z) - \sqrt{v_{\text{max}}^2 - 2gz - \Delta E_{\text{friction}}} = 0$$
 (6.7)

for z = Ru is v(Ru) = 0 so that

$$v_{\text{max}} = k\sqrt{2gRu} \tag{6.8}$$

with

$$k = \sqrt{\frac{1}{1 - \alpha}} \tag{6.9}$$

The change in friction energy  $\Delta E_{friction}$  is incorporated in (6.8) by means of the friction factor k. The friction factor k has the value 0.813 in case of the full scale Zeebrugge breakwater (Schüttrumpf et al. (2000)). In reality, the maximum front velocity is larger and thus, the k factor will have a larger value too.

The k factor has been calculated for all additional small scale model tests at FCFH and UGent. The same analysis method has been used to analyse the laboratory data and to derive the wave run-up velocities per wave run-up event. It is seen that the maximal wave run-up velocity is found just above SWL. As an example, the part of the time series between t = 295 s and t = 305 s of the run-up height and the run-up velocity are shown in figure 6.12 for test d24 of the additional UGent tests.

At FCFH, a value k = 0.6201 has been found for a small scale model of the Zeebrugge breakwater with mixed regular and irregular armour layer patterns. For the additional UGent tests, k equals 0.5799 for the tests with the 1:20 scaled core material and 0.5829 for the tests with the 1:30 scaled core material. Only data of RU1 have been analysed.

For all additional tests, k equals approximately 0.60. This is a much lower value than the value Schüttrumpf et al. (2000) found on the full scale Zeebrugge breakwater ( $k \ge 0.81$ ). It is concluded that wave runup velocities in small scale models are lower than in reality due to scale effects. The friction forces are stronger in small scale models than at full scale.

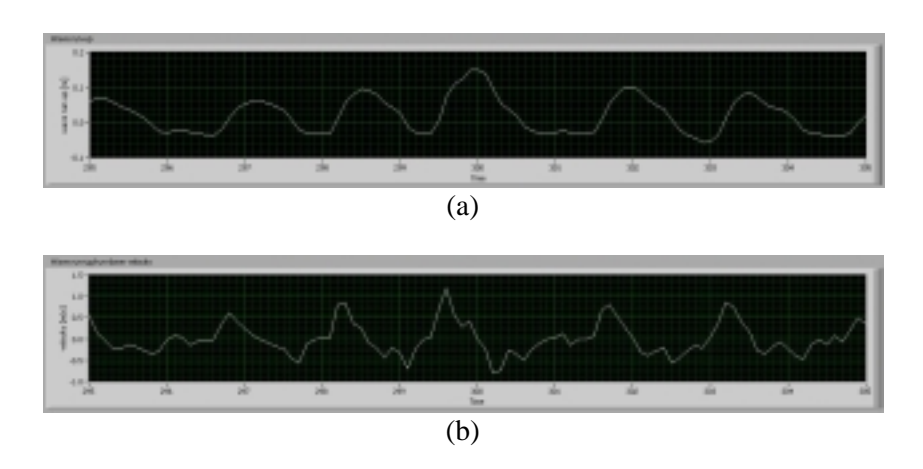


Figure 6.12: (a) Wave run-up signal and (b) wave run-up velocity signal of test d24 in the time interval [295, 305].

# **6.3.1.3** Estimation of influence of scale effects

# 6.3.1.3.1 Influence of surface tension on wave run-up

The influence of the surface tension on wave run-up is investigated through the investigation of the wave run-up velocities.

Assuming

$$v = k_{\gamma} \sqrt{2g \left(Ru + \frac{T}{\rho_w gh}\right)} \tag{6.10}$$

(an extra wave run-up height due to the surface tension is added to the wave run-up height Ru (Schüttrumpf et al. (2000)), the relation between the Froude number and the Weber number is expressed as

$$\frac{1}{2} = \frac{1}{c_2^* F r^2} + \frac{1}{We} \tag{6.11}$$

$$We = \frac{2c_2^* F r^2}{c_2^* F r^2 - 2} \tag{6.12}$$

with

$$c_2^* = \frac{h}{Ru_{2\%}} \tag{6.13}$$

(Schüttrumpf (2001)). h is the layer thickness at *SWL*. By model testing, Schüttrumpf (2001) succeeded in determining the value of  $c_2^*$ . Although this value is valid only for smooth dikes, the value of  $c_2^*$  ( $c_2^* = 0.216$ ) is assumed to be valid for rough slopes as well. A lack of information has been detected.

In this case, the Froude number and the Weber number have been calculated as

$$Fr = \frac{v}{\sqrt{gh}} \tag{6.14}$$

$$We = \frac{v^2 h \rho_w}{T} \tag{6.15}$$

in which v is the wave run-up velocity at *SWL*. (6.12) has been plotted in figure 6.13. The critical Weber number  $We_{critical}$  is 10 and is not likely to be underspent.

The critical layer thickness  $h_{critical}$  is found by transforming (6.15) into

$$h_{critical} = \frac{We_{critical}T}{\rho_{w}v^{2}}$$
 (6.16)

or

$$h_{critical} = \frac{0.00074}{v^2} \tag{6.17}$$

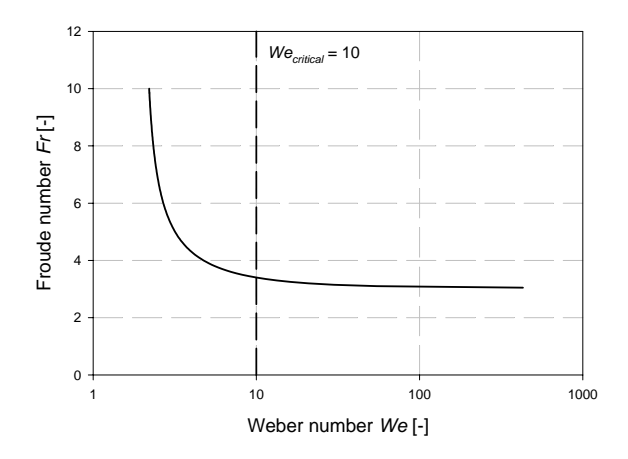


Figure 6.13: Influence of the surface tension on wave run-up velocity: Fr versus We.

The wave run-up velocity is written as  $v=k\sqrt{2gRu}$  , so with  $k\sim 0.60$  (cfr. paragraph 6.3.1.2) is

$$h_{critical} = \frac{0.00074}{k^2 2gRu} \approx \frac{10^{-4}}{Ru}$$
 (6.18)

The influence of the surface tension on wave run-up is negligible if

$$h > h_{critical}$$
 (6.19)

Combining equations (6.13) and (6.17), equation (6.19) becomes

$$Ru^2 > \frac{10^{-4}}{c_2^*} \tag{6.20}$$

so that Ru > 2.2 cm. If Ru > 2.2 cm, the influence of surface tension on wave run-up is negligible. Little influence of the surface tension on wave run-up is suspected for Ru < 2.2 cm. Assuming that the layer thickness h for wave run-up on rough permeable slopes is the same as for wave run-up on smooth dikes, according to (6.13),  $c_2^* \ge 0.216$  as  $Ru_{smooth} \ge Ru_{rough}$ . A larger value of  $c_2^*$  implies a smaller value of the critical run-up height cfr. (6.20).

## 6.3.1..3.2 Influence of surface tension on wave propagation

Schüttrumpf (2001) found in literature that the influence of the surface tension can be neglected when the water depth d > 2.0 cm and the wave period T > 0.35 s. Stam (1989) states the surface tension has no influence on the wave celerity as long as the wave length is larger than 0.1 m to 0.2 m. These conditions are fulfilled in all cases.

## 6.3.1.3.3 Influence of viscosity on wave propagation

In this case, the Froude number and the Reynolds number have been calculated by

$$Fr = \frac{c}{\sqrt{gd}} \tag{6.21}$$

$$Re = \frac{cd}{v} \tag{6.22}$$

The Reynolds number is calculated using the water depth d as characteristics length. The wave celerity c given by

$$c = \sqrt{\frac{gL}{2\pi}} \tanh\left(\frac{2\pi d}{L}\right) \tag{6.23}$$

as characteristic velocity.

Following expression has been given by Biesel (1949) (cfr. Schüttrumpf et al. (2000)) to estimate the influence of kinematic viscosity on wave celerity:

$$c = \left(1 - \frac{1}{\sinh\left(\frac{4\pi d}{L}\right)^{4}\sqrt{\frac{gL^{3}}{2\pi^{3}v^{2}}\tanh\left(\frac{2\pi d}{L}\right)}}\right)\sqrt{\frac{gL}{2\pi}\tanh\left(\frac{2\pi d}{L}\right)}$$
(6.24)

(6.24) is transformed into

$$Fr^2 = \left(1 - \frac{1}{2\sqrt{Rekd}}\right)^2 \tag{6.25}$$

Equation (6.25) has been plotted in figure 6.14 for various ratios d/L. The critical Reynolds number in this case is about  $10^4$ . Sakakiyama et al. (1998) estimated the critical Reynolds number over which scale effects in wave overtopping tests become negligible:  $Re_{critical} = 10^5$ . Scale effects had been noticed by comparison of small scale model test data on wave overtopping over a seawall covered with armour units.

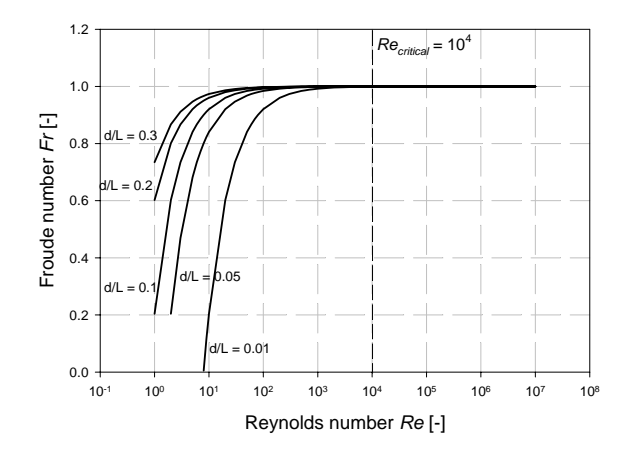


Figure 6.14: Influence of the viscosity on wave propagation: *Fr* versus *Re*.

All additional small scale model tests carried out at UGent had a Reynolds number Re in the order of magnitude of  $3.10^4$  to  $10^5$ . The

additional tests carried out at FCFH showed a Reynolds number Re between  $10^5$  and  $3.10^5$ .

## 6.3.1.3.4 Influence of viscosity on wave run-up

Schüttrumpf (2001) indicates the Froude number to be used:

$$Fr = \sqrt{\frac{1}{1 - \frac{f}{c_2}}} \tag{6.26}$$

where f is substituted by the Darcy-Weissbach formula (assuming laminar flow as only the influence of viscosity on wave run-up is envisaged)

$$f = \frac{16}{Re} \tag{6.27}$$

and

$$c_2 = \frac{c_2^*}{n} \text{ in which } n = \cot \alpha$$
 (6.28)

(6.26) has been plotted in figure 6.15 for various values of n. The critical Reynolds number in this case is  $Re_{critical} = 10^4$ .

In analogy to Schüttrumpf (2001) who developed a Reynolds number for wave overtopping, a Reynolds number for wave run-up is needed. The Reynolds number is therefore defined as:

$$Re = \frac{v_{Ru_{2\%}}Ru_{2\%}}{v} \tag{6.29}$$

The curves in figure 6.15 have to be compared to the results of the model tests where Reynolds numbers are calculated according to (6.29). The Froude number has been calculated as

$$Fr = \frac{v_{Ru_{2\%}}}{\sqrt{gRu_{2\%}}} \tag{6.30}$$

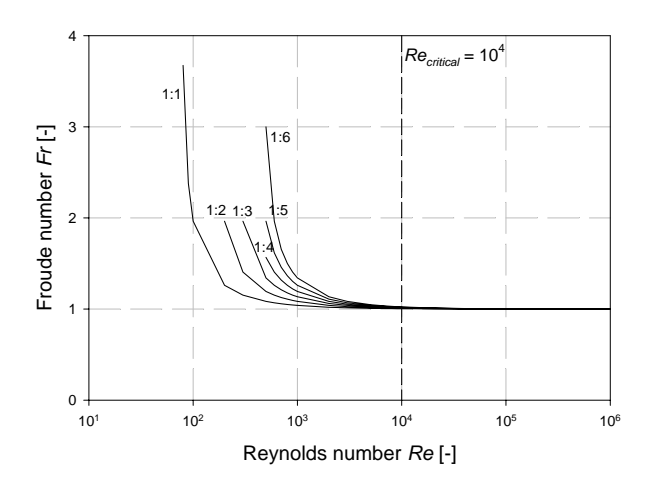


Figure 6.15: Influence of the viscosity on wave run-up: Fr versus Re.

For the additional UGent tests:

$$Re = \frac{k\sqrt{2gRu_{2\%}}Ru_{2\%}}{v}$$
 (6.31)

is valid. Reynolds values of all additional tests vary between  $6.10^4$  and  $2.10^5$ , i.e. larger than the critical Reynolds number  $Re_{critical} = 10^4$ .

# **6.3.1.3.4** Influence of viscosity on internal flow regime (porosity and permeability)

To meet the fourth type of scale effect, additional small scale model tests have been carried out at UGent. A scale model of a conventional rubble mound breakwater has been built twice. The cores of the respective models have been scaled according to Burcharth et al. (1999), resp. Froude's law (see chapter 5.3 and 5.5). The method proposed by Burcharth et al. (1999) scales the core material diameter in such a way that the Froude scale law holds for a characteristic pore velocity in order to model the flow in the core of the breakwater properly. This scaling method results into coarser core material than the overall scale would yield. Both methods yield different results ( $\alpha$  < 0.05).

#### **6.3.2 Model effects**

## 6.3.2.1 Hydraulical/meteorological

## **6.3.2.1.1** Spectral shape

Although some researchers did not find any dependency of relative wave run-up on the spectral shape (Kamphuis et al. (1958), Stam (1989), van der Meer and Stam (1992), Ward et al. (1997),...), the results of the tests carried out in the frame of this thesis indicate the opposite.

In the following graphs, the results of the analysis of time series with a duration of two hours at high water (from  $t_{HW}$ -1 to  $t_{HW}$  +1) are represented by full symbols. The results of the analysis of time series of one hour taken upon rising tide ([ $t_{HW}$ -3,  $t_{HW}$ -2], [ $t_{HW}$ -2,  $t_{HW}$ -1]) or receding tide ( $[t_{HW}+1, t_{HW}+2], [t_{HW}+2, t_{HW}+3]$ ) are represented by open symbols. The full scale measurements carried out on the Zeebrugge breakwater are indicated by circles (● and ○). The results of storm event simulations in the various laboratories are indicated by triangles ( $\triangle$  and  $\triangle$ ) for FCFH results, diamonds ( $\blacklozenge$  and  $\diamondsuit$ ) for AAU results and squares (■ and □) for UPV results. Red triangles represent the results of additional tests carried out at FCFH. The results of the additional tests carried out at UGent are represented by blue triangles. Full blue triangles represent results of tests on a scale model with core material scaled according to Burcharth et al. (1999) (scale 1:20). Open blue triangles represent results of tests on a scale model with a Froude core (scale 1:30). Results of GWK tests are represented by upside down triangles  $(\nabla)$ .

The dimensionless wave run-up values  $Ru_{2\%}/H_{m0}$  of all tests carried out have been plotted against the Iribarren number  $\xi_{om}$  in figure 6.16. A large spreading is seen on the results. Wave run-up results have been plotted against the peakedness parameter (cfr. Goda (1985)) in figure 6.17. Despite the large spreading on the results, a trend has been been noticed:  $Ru_{2\%}/H_{m0}$  values decrease with increasing value of the peakedness parameter  $Q_p$ .

The wave run-up results of the UGent tests have been plotted against the spectral parameter  $\kappa$  (cfr. Stam (1989)) in figure 6.18. Incident wave spectra have been used to calculate the spectral parameters. Figure 6.18 shows increasing  $Ru_{2\%}H_{m0,i}$  values for decreasing  $\kappa$  values.

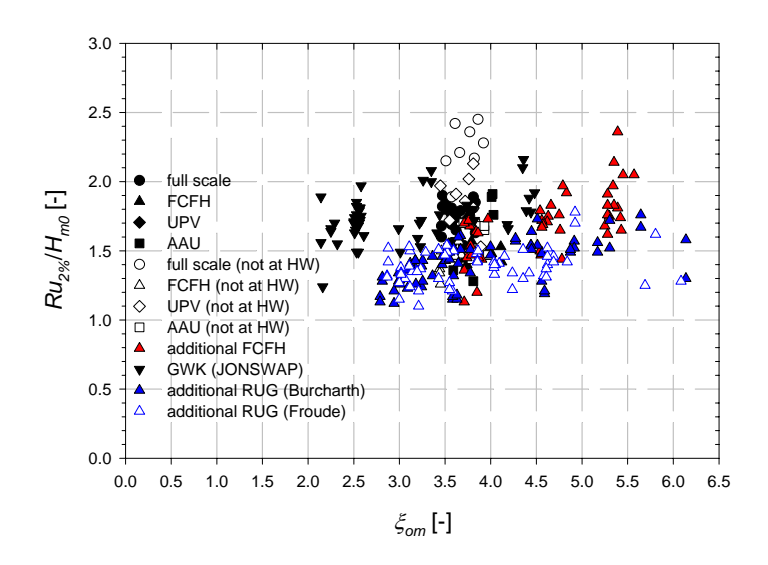


Figure 6.16:  $Ru_{2\%}/H_{m0}$  versus the Iribarren number  $\xi_{om}$  for all tests

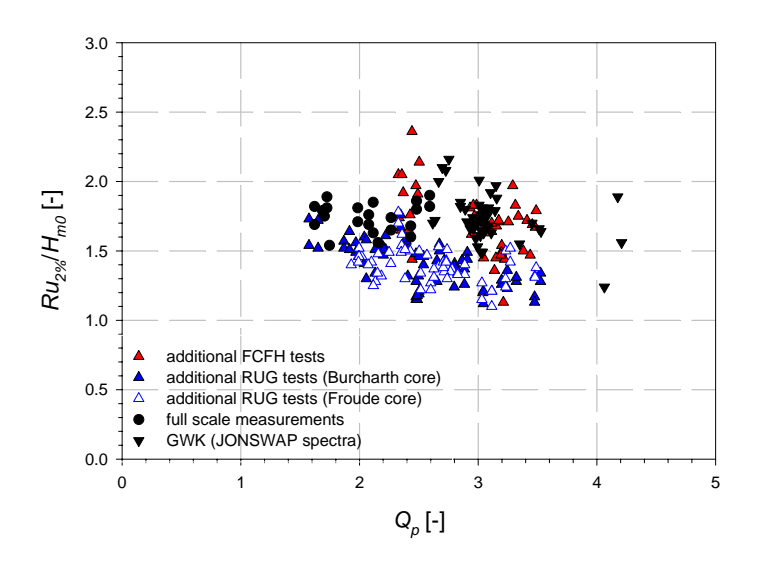


Figure 6.17:  $Ru_{2\%}/H_{m0}$  versus the peakedness parameter  $Q_p$  (cfr. Goda (1985))for all tests.

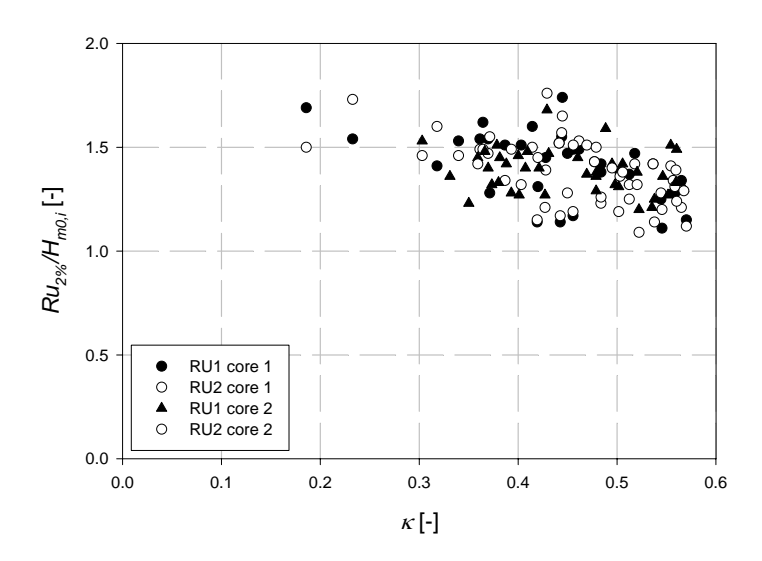


Figure 6.18:  $Ru_{2\%}/H_{m0,i}$  results vs. the spectral parameter  $\kappa$  (cfr. Stam (1989) for the UGent results.

The most important figure of this thesis is figure 6.19. Wave run-up results have been plotted against the spectral width parameter  $\varepsilon$ . Figure 6.19 summarises the results of the full scale measuring campaigns, all full scale storm reproduction results (obtained in three different laboratories, all with an irregular placement pattern of the armour units (as at full scale)), the additional small scale model test results (mixed regular and irregular armour unit patterns) performed at FCFH (the tests with SWL = Z + 6.00 excluded), the additional UGent small scale model test results (two different cores) and the large scale tests performed at GWK (JONSWAP wave spectra).

The trend noticed in figure 6.6 (full scale measurements in Zeebrugge and storm event reproductions in the laboratories) is confirmed by the data in figure 6.19. An overall tendency has been noticed in all investigations: dimensionless wave run-up values  $Ru_{2\%}/H_{m0}$  increase with increasing spectral width parameter value  $\varepsilon$ . One series of test results stand out, namely the full scale wave run-up measurement results upon rising and receding tide.

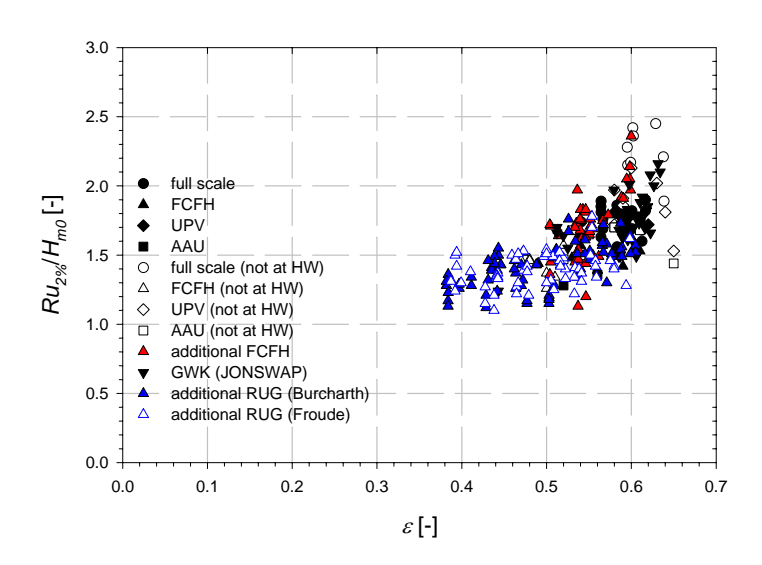


Figure 6.19:  $Ru_{2\%}/H_{m\theta}$  versus spectral width parameter  $\varepsilon$  for all tests.

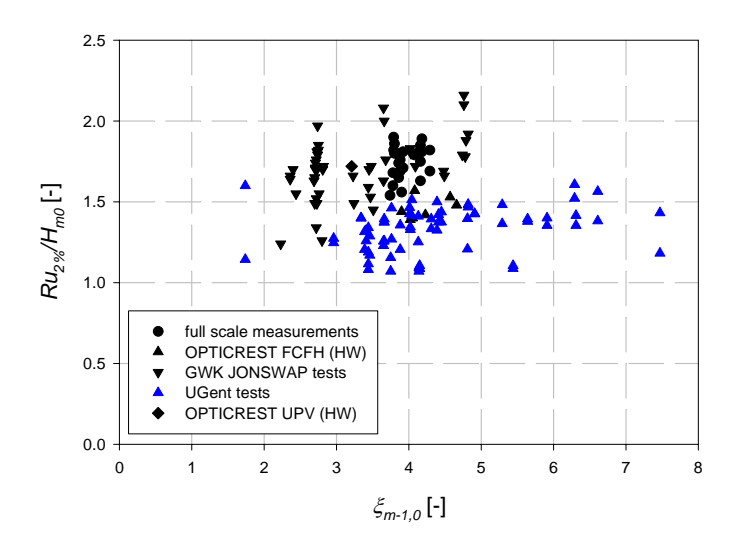


Figure 6.20:  $Ru_{2\%}/H_{m0}$  versus the Iribarren number  $\xi_{m-10}$  (calculated using the spectral wave period  $T_{m-10}$ ).

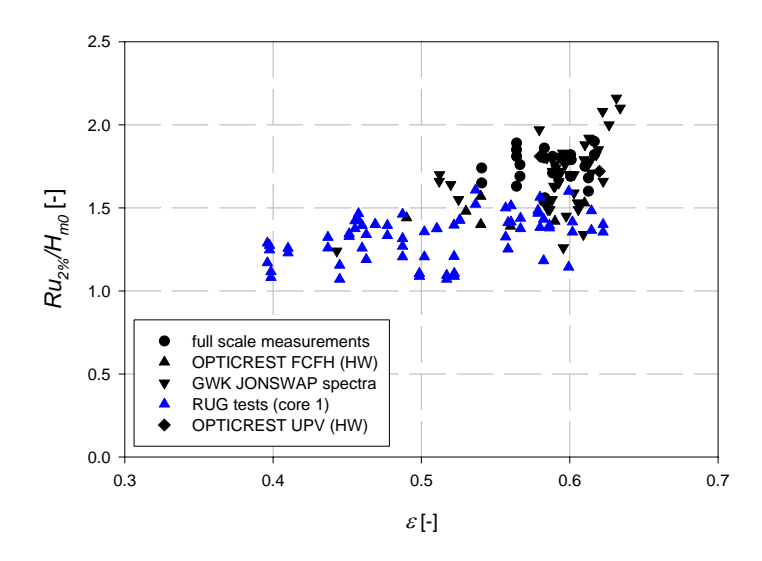


Figure 6.21:  $Ru_{2\%}/H_{m0}$  versus the spectral width parameter  $\varepsilon$  (cfr. data of figure 6.20).

TAW (2002) and van Gent (1999) advise to use the spectral wave period  $T_{m-10}$  instead of  $T_p$  or  $T_{01}$ . Figure 6.20 shows the wave run-up results against the Iribarren number  $\xi_{m-10}$  (calculated with the wave period  $T_{m-10}$ ) for the full scale measurements ( $\bullet$ ), the FCFH ( $\triangle$ ) and UPV ( $\diamond$ ) storm event reproductions, the GWK JONSWAP spectra tests ( $\nabla$ ) and the UGent tests with core 1 ( $\triangle$ ). These results are plotted against the spectral width parameter  $\varepsilon$  as well in figure 6.21.

The spreading on the test results in figure 6.21 is smaller than the spreading on the test results in figure 6.20. The UGent test results (core 1) are (on average) lower than the GWK JONSWAP test results. The difference between the UGent results and the GWK JONSWAP test results in figure 6.20 is explained by the influence of the spectral width parameter  $\varepsilon$  (cfr. figure 6.21). The value of  $\varepsilon$  for the GWK JONSWAP test results is quite large ( $\varepsilon \approx 0.60$ ) by which a large value of  $Ru_{2\%}/H_{m0}$  is expected. The UGent test results vary between 0.4 and 0.6 and show increasing wave run-up results for increasing values of the spectral width parameter  $\varepsilon$ . For single peaked JONSWAP type wave spectra, the spectral width parameter  $\varepsilon$  is a more suitable parameter to describe wave run-up than the Iribarren number  $\xi_{m-1,0}$ 

(calculated using the spectral wave period  $T_{m-10}$  (cfr. TAW (2002) and van Gent (1999)).

Table 6.10: Values of  $t_0$  and  $t_f$  for all tests with a natural spectrum.

test nr.	$t_0$ [s]	$t_f[s]$
30(**)	90	1200
31 <sup>(**)</sup>	100	950
32(**)	90	900
33 <sup>(*)</sup>	-	-
34 <sup>(*)</sup>	-	-
35 <sup>(*)</sup>	-	-
36 <sup>(**)</sup>	90	600
65	150	1139
66	150	844
67	150	625
68	150	482
69	150	596
70	150	516
71	150	1139
72	150	844
73	150	625
74	150	482
75	150	596
76	150	516
77 <sup>(**)</sup>	150	1139
78 <sup>(**)</sup>	150	844
79 <sup>(**)</sup>	150	625
80 <sup>(**)</sup>	150	482
81 <sup>(**)</sup>	150	596
82 <sup>(**)</sup>	150	516

<sup>(\*)</sup> no wave run-up measurements available highest wave run-up levels exceed crest level

Even though a good agreement was seen between the frequency domain parameters ( $H_{m0}$  and  $T_{01}$ ) of storm events measured at full scale and the respective storm events which have been reproduced in the laboratory, the spectral width parameter  $\varepsilon$  did not have necessarily the same value. The influence of the shape of the spectrum in general and the influence of the spectral width parameter  $\varepsilon$  in particular is clear. Wave run-up is affected by small changes in spectral shape (characterised by any parameter  $\varepsilon$ ,  $Q_p$ ,  $\kappa$  or GF,...). Out of all spectral parameters describing the spectral shape, the spectral width parameter  $\varepsilon$  has been chosen for further description of wave run-up. Whereas dimensionless wave run-up values  $Ru_{2\%}/H_{m0}$  vary within the interval [1.07, 2.16], spectral width values vary within a much smaller interval [0.40, 0.63] (see figure 6.21). This demonstrates sensitivity of  $Ru_{2\%}/H_{m0}$  on the spectral width parameter  $\varepsilon$ .

Next to parameterised standard JONSWAP spectra, also sea states measured at the German coast and at the coasts of the Wadden Sea (natural spectra) have been reproduced in the LARGE WAVE CHANNEL. The wave spectra of these particular tests have been plotted in Annex I. It is seen that these natural spectra are no standard wave spectra. For some tests, analysis in frequency domain yielded no reliable results. Results of the analysis in time domain of the wave data have been used instead ( $T_m$  instead of  $T_{01}$ , the number of waves N,  $H_s$  instead of  $H_{m0}$ ). This was the case for tests  $n^{\circ}$  63, 68, 74, 76, 80 and 82. These tests are indicated with  $f_s$  in the tables of Annex H. Table 6.10 gives the values of  $f_s$  and  $f_s$ . The analysis results are shown in figure 6.22. The circles indicate the tests with a JONSWAP spectrum and the triangles the tests with a natural spectrum.

The tests with a natural spectrum have another outcome than the tests with a standard JONSWAP spectrum. Remarkable is the dependency of  $Ru_{2\%}/H_{m0}$  on the SWL for tests on the second armour layer (high density rock). Tests with the lowest water depth (d=3.50 m) yielded the largest values of  $Ru_{2\%}/H_{m0}$  (on average  $Ru_{2\%}/H_{m0}=2.47$  for  $\xi_{om}=3.74$ ). Tests with the highest SWL (d=4.50 m) yielded the smallest  $Ru_{2\%}/H_{m0}$  values (on average  $Ru_{2\%}/H_{m0}=1.75$  for  $\xi_{om}=3.86$ ). Latter tests yielded results comparable to results of tests with a standard spectrum. For the first armour layer, the  $Ru_{2\%}/H_{m0}$  values are approximately the same as results of tests with a standard spectrum (on average  $Ru_{2\%}/H_{m0}=1.60$  for  $\xi_{om}=3.74$ ). These tests have been carried out with water depths of d=4.50 m for the first three tests and d=4.80 m for the fourth test.

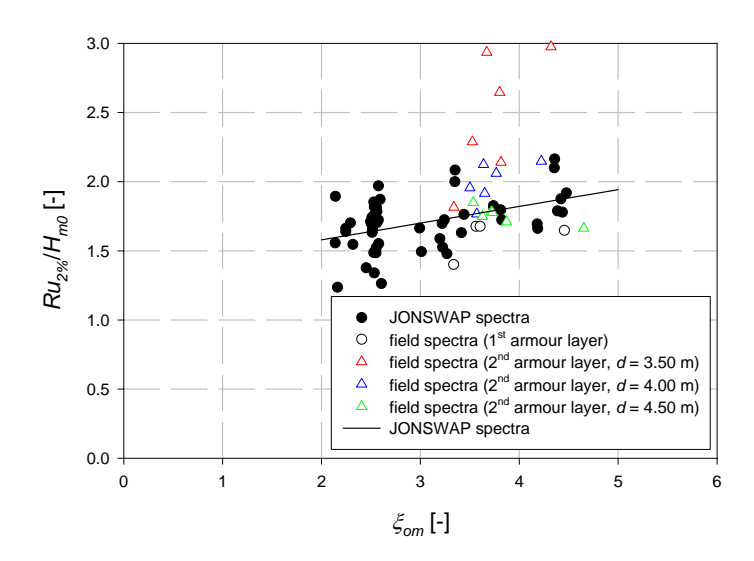


Figure 6.22: Dimensionless 2% wave run-up  $Ru_{2\%}/H_{m0}$  vs. Iribarren number  $\xi_{om}$  for wave run-up tests with JONSWAP spectra ( $\bullet$ ) and tests with natural spectra ( $\bigcirc$ ) for both types of armour layer.

An influence of the water depth on the wave run-up results of tests, in which a natural spectrum has been applied, has been noticed at GWK. Tests with a natural spectrum yield higher values than tests with a standard JONSWAP spectrum for low water depths. For high water levels, results are comparable to or even lower than results of tests with a standard JONSWAP spectrum. The influence of the *SWL* is believed to be through the transformation of wave characteristics over the foreshore as waves travel from deep water towards the structure. On average, tests with a reproduced natural spectrum did not yield higher wave run-up results than tests with a standard JONSWAP spectrum. However, when the results of the natural spectrum tests are studied into detail one by one, it is concluded that tests with a natural spectrum yield wave run-up results which cannot be predicted by means of the trend noticed in all JONSWAP spectrum tests.

The results of the GWK tests with natural wave spectra have been plotted against the spectral width parameter  $\varepsilon$  in figure 6.23 and against the Iribarren number  $\xi_{m-10}$  in figure 6.24. In the graphs, the

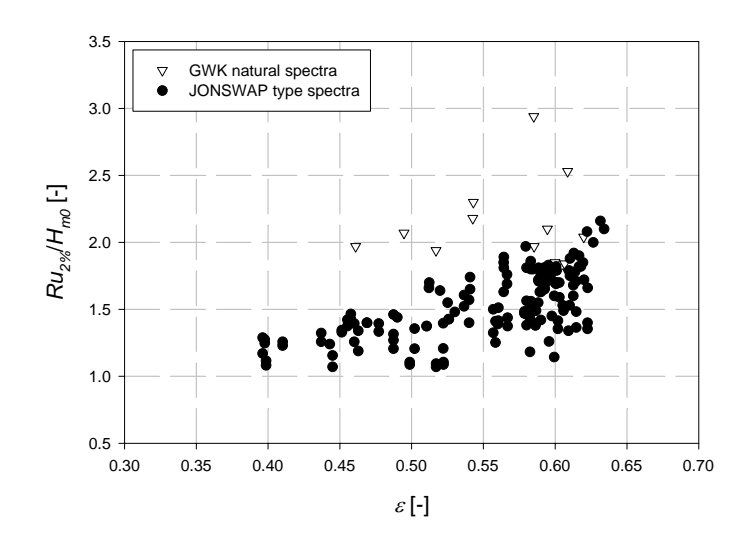


Figure 6.23:  $Ru_{2\%}/H_{m0}$  results of GWK tests with a natural spectrum against the spectral width parameter  $\varepsilon$ .

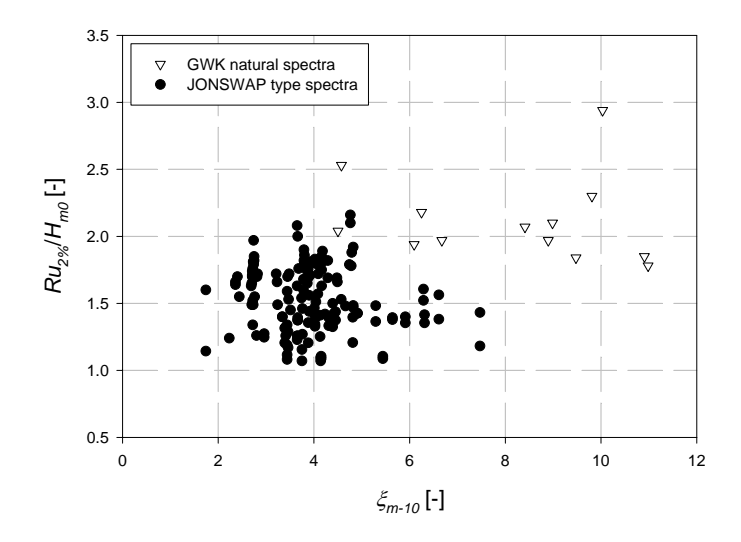


Figure 6.24:  $Ru_{2\%}/H_{m0}$  results of GWK tests with a natural spectrum against the Iribarren number  $\xi_{m-10}$ .

results of tests (full scale measurements, storm event reproductions, additional FCFH tests, UGent tests, GWK JONSWAP tests) have

been plotted as well. For the tests with a natural spectrum, the spreading on the results is large both for  $\xi_{m-10}$  and  $\varepsilon$ . Taking the natural wave spectra test results into account, it is concluded that neither  $T_{m-10}$ , nor  $\varepsilon$  are satisfactory parameters to describe wave run-up on the investigated structures.

The influence of the spectral shape is one of the missing links to explain why full scale measurements yield a much higher dimensionless wave run-up value  $Ru_2\%/H_{m0}$  than small scale model tests do and why laboratory results differ from each other. Tuning only the significant wave height and the mean wave period (or peak period) is insufficient for correct reproduction of wave kinematics. It is indispensable to built small scale models and to perform extensive testing to obtain the correct wave run-up results whenever natural spectra are considered.

## **6.3.2.1.2** Wave height

The wave height in the denominator of the ratio  $Ru_{2\%}/H_{m0}$  may also be cursed with errors. The higher the value of  $H_{m0}$ , the smaller the value of the dimensionless wave run-up. When only the incident wave height is considered in the ratio  $Ru_{2\%}/H_{m0}$ , this value will be higher (the difference is dependent on the reflection coefficient) than when the total wave height is used in the denominator. In Zeebrugge, total waves have been measured. Consequently, the total significant wave height has been measured in the scale models as well.

At full scale, a 3D effect takes place when waves reflect on the breakwater. Due to the curved shape of the breakwater in plan view, inciding energy which is comprised between two wave rays reflects on the structure and is scattered. This scattered reflected energy is also measured at the position of the wave buoy. In contradiction to the full scale situation, in two dimensional small scale model tests, all reflected energy is measured by a wave gauge. By this, dimensionless wave run-up could be higher for full scale measurements than measured in small scale models, because the total (full scale) wave height is smaller than the wave height measured in laboratory tests.

Although the radius of the curved breakwater (R = 500 m) is much larger than the wave length and the distance between the wave rider and the breakwater is only twice the peak wave length, in Annex L, a theoretical estimation of the total energy (inciding energy + scattered reflected energy) has been derived. The wave height measured at a

location where incident and scattered reflected energy is measured is maximal (for large wave obliqueness angles) 4% lower than the wave height measured at a location where normal reflected waves are measured together with the inciding waves. A decrease of 4% in wave height only yields an increase in dimensionless wave run-up of 4.2% (see figure 6.25). Dimensionless wave run-up values obtained by laboratory testing at FCFH differ a lot more from full scale measurement results than these 4.2%!

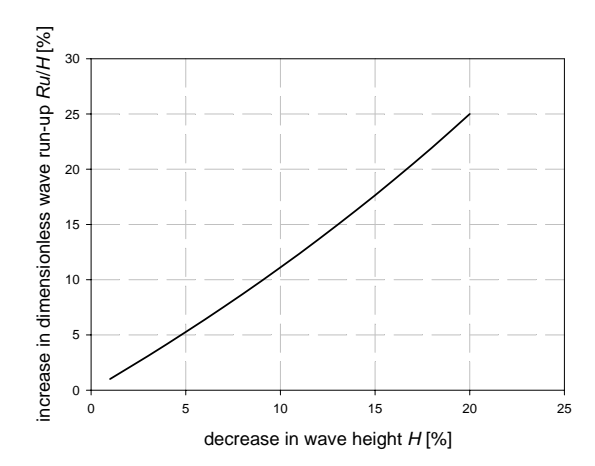


Figure 6.25: Increase in dimensionless wave run-up Ru/H in terms of percentage as a consequence of the decrease in wave height H in terms of percentage.

It has been noticed that the wave height distributions measured in the laboratories at the positions of WRI (or WRII) did not correspond with the full scale wave height distributions. Figure 6.26 shows the wave height distributions of the storm event  $n^{\circ}$  6 (November  $6^{th}$ , 1999 (11h30 – 13h30)) measured in Zeebrugge and the storm event reproduction at FCFH. The significant wave height is determined by  $H_{m0} = 4\sqrt{m_0}$  with  $m_0 = \sigma^2$ . The individual wave heights measured 'offshore', i.e. at the location of the first wave rider buoy, are slightly higher at full scale than these measured in the scale model. The significant wave heights differ only 1 cm (model scale). Wave heights measured 'nearshore', i.e. at the location of the infrared meter, are lower at full scale than these measured in the scale model. The

significant wave heights differ 2.9 cm (model scale)! Although the  $H_{m0}$  and  $T_{01}$  values correspond quite well at the location of the wave rider buoys, waves (and the corresponding wave parameters) do not correspond well at the toe of the breakwater. Either the significant wave height has not been measured correctly by the IR at full scale (cfr. paragraph 4.7.1:  $H_{m0,IR}/H_{m0,WRII} = 0.74$ ) or the wave heights are transformed to the extent that by shoaling other wave heights are measured at the toe of the structure at small scale than at full scale. Latter influence is not very likely. The higher significant wave height at the toe of the breakwater in the scale model may explain the lower dimensionless wave run-up values  $Ru_{2\%}/H_{m0}$  of the laboratories.

## 6.3.2.1.3 Wind

Small scale model tests have been performed without wind. Ward et al. (1994, 1996, 1997) concluded that the influence of wind on wave run-up is mainly found within the transfer of energy by which the incident wave spectrum changes. In Zeebrugge, waves have been measured close to the toe of the structure so little energy transfer could have occurred in the area between the wave rider buoy and the breakwater before waves arrive at the structure. Relying on the UPV investigation results (cfr. paragraph 5.3.2), wave run-up in small scale models would have been higher when full scale wind speeds (at least 7 Beaufort ( $v_s = 15.5 \text{ m/s}$ )) would have been applied in small scale model tests. Equating the wave overtopping results obtained in the combined wave flume/wind tunnel facility at UPV with the formula of de Waal and van der Meer (1992):

$$\frac{q}{\sqrt{gH_s^3}} = 8.10^5 \exp\left(3.1 \frac{Ru_{2\%} - R_c}{H_s}\right)$$
 (6.32)

the increase in  $Ru_{2\%}/H_{m0}$  value for tests with wind  $(v_s \ge 7 \text{ m/s})$  relative to the  $Ru_{2\%}/H_{m0}$  value for tests without wind has been estimated. The increase varies between 1% (for small values of the dimensionless crest freeboard  $R_c/H_s$ ) and 10% (for large values of  $R_c/H_s$ ).

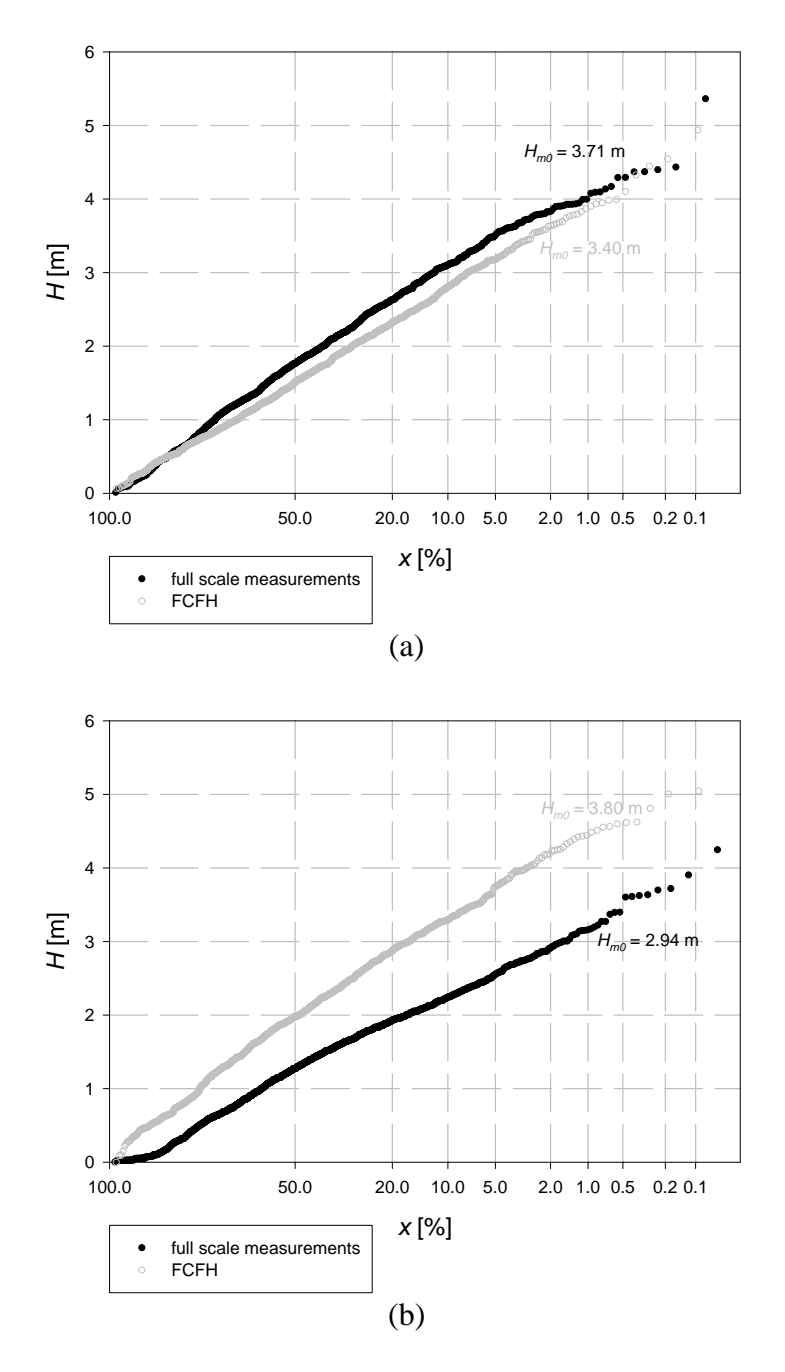


Figure 6.26: Comparison of wave height distribution (a) offshore (WRII) and (b) nearshore (IR).

## **6.3.2.1.4** Tidal currents parallel to the breakwater axis

At Zeebrugge, the mean spring tidal range is 4.34 m. The mean tidal range is 3.67 m. Tidal currents can reach speeds of 1.8 m/s or more along the Western Breakwater (Kerckaert (1985)). In Zeebrugge, the maximum current velocity occurs approximately 30 minutes before the moment in time of high water  $t_{HW}$  (figure 6.27). Positive current velocities are directed NE. Negative values are directed SW. The current velocity is the velocity at the water surface for mean tide. At MSL, the current velocity is almost zero. At high water, the current direction is NE. At low water, the current direction is SW.

Hedges et al. (1997) and Kingston (1994) concluded that currents have a strong influence on wave conditions in front of the structure and may not be neglected. Currents produce changes in wave properties such as water particle motions, the relationship between the wave length and the observed wave period, wave speed, wave refraction, wave height,... The currents cause difficulties both in wave measurement and in the subsequent interpretation of data.

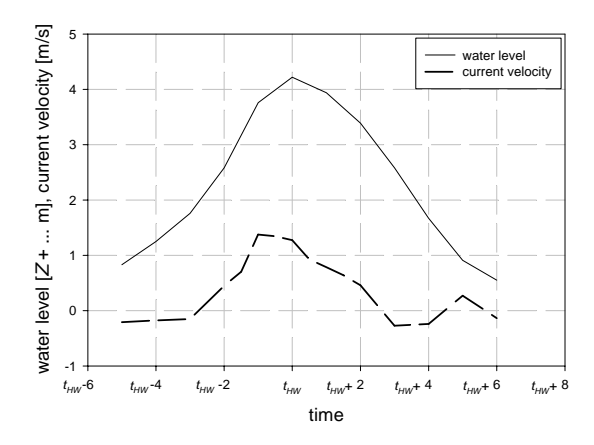


Figure 6.27: Water level (astronomical tide – Ministry of the Flemish Community (2000)) and current velocity (physical model – Ministry of the Flemish Community (1985)) at the Zeebrugge breakwater (at the location of the wave rider buoys).

In currents, buoy moorings will be relatively taut even before the buoys are displaced by wave action. Allender et al. (1989) found that the wave rider type and other buoys with similar moorings could

underrecord the highest waves, either by being dragged through the crests or by dodging around these. Strong currents will strengthen this phenomenon. Measuring a lower wave height yields higher dimensionless wave run-up values  $Ru_{2^{n}}/H_{m0}$ .

Kingston (1994) reports that no particular concentration of energy dissipation is observed at Zeebrugge. Storm energy is distributed equally along the whole Belgian coastline. When a current is present, it has a strong influence on wave refraction, whether vorticity is taken into account or not. Vorticity has an influence on wave refraction, but to a lesser extent than the presence of the current itself. The shorter the period of the waves, the more refraction the waves will experience upon entering a region where a current exists.

Hedges et al. (1996) applied a numerical model to investigate the influence of currents in front of the Zeebrugge breakwater on the wave height. The model has shown that the presence of strong currents has a significant effect on the observed wave heights. The wave heights measured at the Akkaert buoy (figure 4.3) have been taken as input for the model. The output of the model has been compared to the waves measured by the wave rider buoy in front of the Zeebrugge breakwater. When a current is applied, the numerical model predicts a decrease in significant wave height of approximately 25% in comparison with a no current case. The level of the sea bottom seems to have no significant influence.

Comparing the waves measured at the Akkaert buoy and at the Zeebrugge breakwater, a remarkable reduction in wave height (34%) is noticed. The numerical model also predicts this decrease in wave height, but this only holds for a current flow towards NE during rising tide. During receding tide, the model predictions are poor. The model gives an estimate of the effect of current on waves, but does not wholly explain the measured changes between the wave heights measured at the Akkaert buoy and these measured by the wave rider buoy in Zeebrugge. Building the model, a number of simplifying assumptions had to be made. These simplifications and assumptions are mainly the reason for the still remaining discrepancies.

In two dimensional small scale tests, no currents have been applied. Hence, wave heights are not influenced. AAU performed tests with and without currents. By creation of a current parallel to the breakwater axis, dimensionless wave run-up increased with increasing

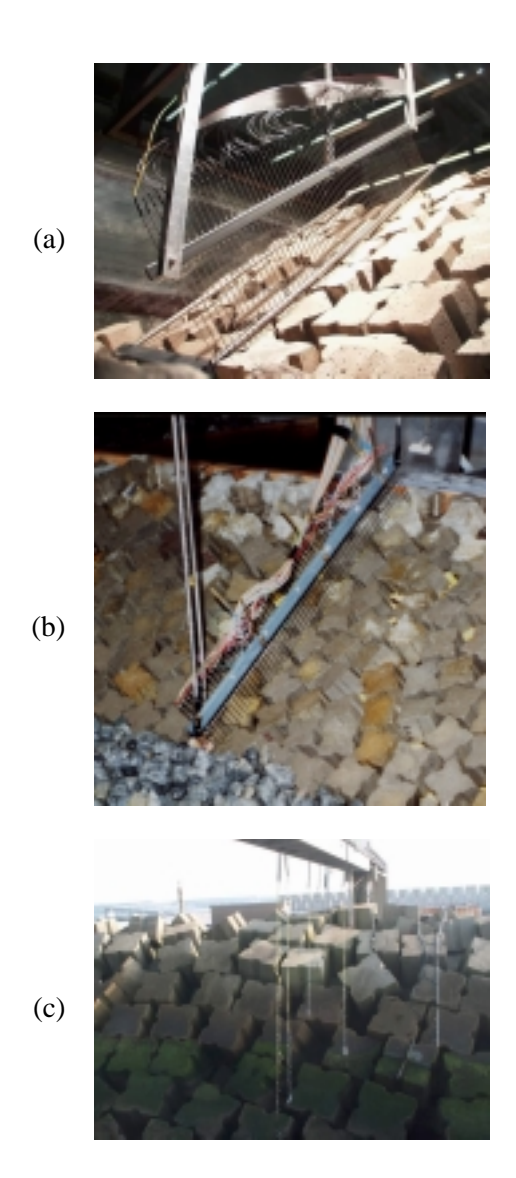
current velocity. Relying on the AAU results  $(Ru_{2\%}/H_{m0} \cong 1.5 \text{ for } v_c = 0 \text{ m/s over } Ru_{2\%}/H_{m0} \cong 1.2 \text{ for } v_c = 0.5 \text{ m/s to } Ru_{2\%}/H_{m0} \cong 1.6 \text{ for } v_c = 0.5 \text{ m/s})$ , the highest wave run-up should occur at high tide. As this finding is in contradiction with the observed phenomenon at full scale, wave run-up increases with decreasing *SWL*, so with decreasing current velocity, it is concluded that the effect of the lower porosity of the armour layer of the Zeebrugge breakwater at lower levels is stronger than the effect of the currents.

#### **6.3.2.2 Geometry**

#### **6.3.2.2.1 Armour layer**

In addition to the conlusions of the laboratory investigation about the armour layer (paragraph 5.7), results of the laboratory investigation are compared to the full scale measurement results and observations. Within one storm event, the wave run-up value  $Ru_{2\%,SP}$  obtained by the 'spiderweb system' measurements, and the wave run-up value  $Ru_{2\%,RU}$ , obtained by the run-up gauge measurements, may differ from each other. This is because both measuring devices have been installed in different cross sections of the Zeebrugge breakwater. The distance between both measuring devices is 2 to 3 armour units. Taking all analysed storm events into account, the average wave run-up values of both wave run-up measuring devices are approximately the same. The 'errors' (which are assumed to be normally distributed) on the wave run-up measurements introduced by the armour unit pattern are thus minimised.

Although much attention has been paid to copy the outer armour layer in the scale models (as good as practically possible), looking at figure 6.28, it is seen that the armour unit patterns underneath the lower end of the needles of the comb in the laboratories of FCFH and AAU are not exactly the same as at full scale. Also only seven reproductions of storm events with a duration of approximately two hours (full scale) around  $t_{HW}$  and eighth reproductions of storm events with a duration of one hour upon rising and receding tide have been run, which is too few number of storm event reproductions to draw firm conclusions.



The additional tests performed at FCFH indicated big differences in wave run-up results of two tests in which only the combination of the *SWL*, the armour unit pattern and the position of the comb of the run-

up gauge relative to the armour unit pattern was different. All other parameters and characteristics were approximately the same.

These findings have been confirmed by the additional small scale model tests performed at UGent. Two run-up gauges measured simultaneously wave run-up in two different cross sections of a breakwater model. Although differences have been found between the wave run-up values measured by the two wave gauges during the same test, no significant ( $\alpha$  < 0.05) difference has been found between the 'average' results of both run-up gauges. It is recommended not to base conclusions on the outcome of one or just a few number of tests, but to take into account a large number of tests. Alternatively, two run-up gauges may be installed in two different cross sections of the breakwater or if only one run-up gauge is available, tests should be repeated with the same wave paddle steering signal but with the wave run-up measuring device installed in different cross sections.

The influence of the water depth on wave run-up may not be confused with the influence of the armour layer pattern on wave run-up. Various authors stated that water depth has no influence on wave runup. No direct influence is seen, but there is an indirect influence through wave characteristics. Indeed, during laboratory experiments, little influence on wave characteristics has been seen by a changing water depth. The increase in wave run-up at lower water levels, and thus, the influence of the water depth has been investigated in different laboratory tests. No significant influence has been noticed. It is concluded that the lower porosity of the lower part of the armour layer of the Zeebrugge breakwater at low levels is responsible for the differences between dimensionless wave run-up at high tide and dimensionless wave run-up at mean tide at full scale. The lesser porosity of the armour layer at lower levels induced higher wave runup than at higher levels where waves are running up a more porous slope.

### **6.3.2.2.2** Foreshore

Due to the limited length of the wave basin, AAU did not model the foreshore. The foreshores at FCFH and UPV are slightly different. Only FCFH modelled the sand bar in front of the breakwater. FCFH modelled the Zeebrugge site up to 600 m in front of the breakwater to include the bar at approximately 550 m (figure 4.5). UPV did not model the bar (of which the crest is situated at Z - 9.5 m) and used a flat bottom at level Z - 13.3 m to model the foreshore for distances

larger than 210 meters from breakwater axis. According to the breaker criterium (see paragraph 2.2.3.4), no wave breaking is expected. Waves generated at the paddle at FCFH may have been transformed slightly by the presence of the sand bar. The presence of the bar made the reproductions of the storm spectra at the position of the wave rider buoys more complicated. Waves could propagate undisturbedly towards the breakwater model at UPV and AAU.

#### 6.3.2.2.3 Sand filling in core

Since the construction of the breakwater in the eighties, the core of the Zeebrugge breakwater has been partially filled up with sea sand. The level of the sand has been measured several years ago in four boreholes in which pressure sensors have been placed (table 6.11).

Initially, this sand was also present in the scale models but was unstable and has been washed out partially during testing. The core of the scale model became more permeable than the full scale version. However, it is not clear if the sand in the core of the breakwater is at present still there to the same extent in the Zeebrugge breakwater.

Table 6.11: Level of sand infiltration in the core of the Zeebrugge breakwater (for the definition of the co-ordinates, see figure 4.3).

x [m]	level [Z+ m]
2.30	2.20
-2.23	0.90
-7.97	0.60
-12.22	0.10

Waves running up the slope of the breakwater do not 'feel' the sand layer in the core of the breakwater when the *SWL* is rather high. The lower the *SWL*, the more important the sandy core may become. In the core of the breakwater, the water level is higher than the *SWL* by the internal set-up. The sand layer in the core makes the internal set-up higher than the internal set-up would have been if the core would not have contained sand. The storage capacity of the breakwater decreases by the presence of the sand layer in the core. Water running up the slope percolates through the armour layer in the core of the breakwater. Less water can be stored in comparison to a sandless core. The excess of water has to run-up higher to reach higher levels of the

armour layer where it gets the opportunity to percolate into the underlying layers. The crest of the sand layer in the core is found approximately at *MLWS*. This can also be one of the explanations why wave run-up at full scale is higher for lower water levels than for higher water levels as no exact knowledge exists on the level of the sand layer in the core of the breakwater.

## 6.4 Comparison with literature data

## 6.4.1 Wave run-up

Full scale wave run-up measurement results have been compared to formulae found by literature research.

The formula of Losada and Giménez-Curto (1982) is given by equation (2.44):

$$\frac{Ru}{H} = A(1 - \exp(B\xi)) \tag{2.44}$$

Allsop et al. (1985) reported A = 1.52 and B = -0.34, based on small scale model tests on a 1:1.5 Antifer cube slope with irregular waves (geometry very alike the Zeebrugge breakwater). Kingston and Murphy (1996) reported A = 1.76 and B = -0.28 for small scale model tests on a model of the Zeebrugge rubble mound breakwater.

Three remarks have to be made:

- (1) equation (2.44) results from tests with regular waves. It is not clear which parameters have to be used to calculate the Iribarren number and to link this to the  $Ru_{2\%}$  value;
- (2) the results reported by Allsop et al. (1985) relate to structures with highly permeable mounds. The porosity of the core was 1. The filter layer and the armour units had been placed on a perforated plate. Intuitively one knows that wave run-up will be lower than when a core would be present;
- (3) because all different investigations use different parameters, all surf similarity parameters had to be rescaled using the surf similarity parameter (calculated using  $H_{mo}$ ,  $T_{01}$  and tan  $\alpha = 1/1.3$  (for the Zeebrugge breakwater)). For the sea state in front of the Zeebrugge breakwater, following relationships between the different wave periods have been used:  $T_p/T_{01} = 1.26$  and  $T_{02}/T_{01} = 0.93$  (De Rouck et al. (1996)). These values are confirmed by full scale measurements carried out in the framework of this thesis:  $T_p/T_{01} = 1.28$  and  $T_{02}/T_{01} = 0.95$ .

The formulae of van der Meer and Stam (1992) (2.49a) to (2.49c) are valid for relatively deep water in front of the structure where the wave height distribution is close to the Rayleigh distribution and for rock armoured slopes attacked by long crested head on waves. This formula is obtained by tests on rip-rap slopes with rock dimensions which are much smaller than the wave height. In the tests was  $D_{n50} = 0.036$  m and the ratio  $D_{n50}/H_s$  varied between 0.14 and 0.76. In Zeebrugge, wave heights are Rayleigh distributed but the dimensions of the armour units are of the same magnitude as the significant wave height.

Equation (2.44) for both Allsop et al. (1985) and Kingston and Murphy (1996) and equation (2.49) (for x=2) have been plotted together with the full scale measurement results at high tide (two hour time series data collected by both the run-up gauge and the spiderweb system within the period [ $t_{HW}$ -1,  $t_{HW}$ +1] in figure 6.29. The individual test results of van der Meer and Stam (1992) has also been indicated by a crosshair.

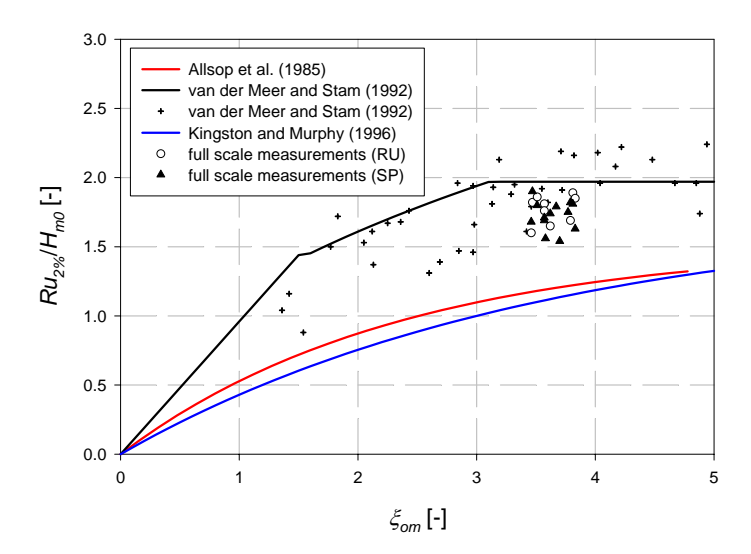


Figure 6.29: Comparison between dimensionless wave run-up values from full scale measurements (from  $t_{HW}$ -1 to  $t_{HW}$ +1, SP (13 storms) & RU (9 storms), 2 hours time series) and from literature.

For the full scale value  $\xi_{om} = 3.63$ , equation (2.44) yields  $Ru_{2\%}/H_{m0} = 1.08$  for the values of A and B found by Allsop et al. (1985) and  $Ru_{2\%}/H_{m0} = 1.12$  for the values of A and B found by Kingston and Murphy (1996). Both values are much smaller than the full scale values. During the period of two hours at high tide (from  $t_{HW}$ -1 to  $t_{HW}$ +1), equation (2.49) yields slightly higher values than the full scale values. The general trend given by van der Meer and Stam (1992) by equation (2.49) is situated in the upper part of the cloud of their test results. However, the cloud of dots representing the full scale measurements are found in the cloud of dots of the van der Meer and Stam (1992) investigation, at the lower side.

Equation (2.49) has also been compared to the full scale measurement results at the Zeebrugge site for other values of x. Thirty minutes time series have been used for this. From table 4.18 and figure 4.47 (the values of  $Ru_{max}/H_{m0}$ ,  $Ru_{1}$ %/ $H_{m0}$ ,  $Ru_{2}$ %/ $H_{m0}$ ,  $Ru_{5}$ %/ $H_{m0}$ ,  $Ru_{1}$ 0%/ $H_{m0}$ ,  $Ru_{2}$ %/ $H_{m0}$ ,  $Ru_{5}$ 9%/ $H_{m0}$ 0,  $Ru_{1}$ 9%/ $H_{m0}$ 9 of van der Meer et al. (1992) are indicated by ' $\bullet$ ' at the right side vertical axis) it is seen that equation (2.49) fits the full scale measurements remarkably very well during the time interval [ $t_{HW}$ -2,  $t_{HW}$ -1] and [ $t_{HW}$ +1.5,  $t_{HW}$ +2.5]. During all other time intervals, full scale measurements indicate lower dimensionless wave run-up values. However, the higher the exceedance probability x, the better the agreement between the formula of van der Meer and Stam (1992) and the measurement results.

Ahrens and Heimbaugh (1988) proposed another formula (2.51). Using the surf similarity parameter  $\xi_{op}$  (calculated using  $T_p$  instead of  $T_{01}$ ), the run-up coefficients a and b equal respectively 1.022 and 0.247. Figure 6.30 shows the comparison of equation (2.51) to the maximum measured wave run-up on site. The individual test results of Ahrens and Heimbaugh (1985) are also depicted in figure 6.30. A good agreement is seen, nonetheless equation (2.51) is also based on tests with irregular waves on riprap protected slopes. It has to be mentioned that the determination of  $Ru_{max}$  for full scale measurements is less accurate than the determination of  $Ru_{x\%}$  with  $x \ge 1$ .

It is concluded that wave run-up on a rubble mound breakwater armoured with grooved cubes may be evaluated by the formulae for rip rap slopes as investigated by van der Meer and Stam (1992) (equation (2.49) yields a small overestimation of  $Ru_{2\%}/H_{m0}$ ) and Ahrens and Heimbaugh (1985) (equation (2.51) yields a very small underestimation of  $Ru_{max}/H_{m0}$ ). However, the cloud of dots

representing the full scale data is found within the cloud of dots representing the test results of Ahrens and Heimbaugh (1988).

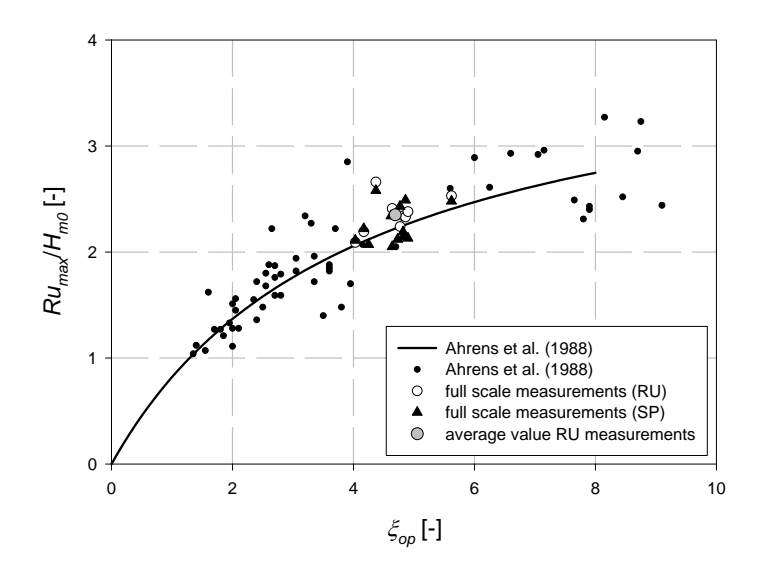


Figure 6.30: Comparison of full scale wave run-up data  $(Ru_{max}/H_{m\theta})$  to formula (2.51)  $([t_{HW}-1, t_{HW}+1], RU$  (9 storms) and SP (13 storms), 2 hours time series).

Dimensionless wave run-up values of the additional tests at UGent are a lot lower than expected by the formula of van der Meer and Stam (1992) for permeable rubble mound breakwaters. The UGent results are also lower than equation (5.25), i.e. the outcome of the GWK JONSWAP wave run-up tests, indicates. The formula (2.49) of van der Meer and Stam (1992) has been multiplied by one single reduction factor  $\gamma$ . The factor  $\gamma$  is determined by fitting the adapted formulae to the test results. The least square method indicate a factor  $\gamma = 0.73$  for core 1 (scale 1:20) and  $\gamma = 0.71$  for core 2 (scale 1:30). The formula of Losada and Giménez-Curto (1981) also has been fit to the results. The values of the parameters A and B are 1.67 and -0.51 for core 1 (scale 1:20) and 1.46 and -0.84 for core 2 (scale 1:30). The original formulae and the adapted formulae have been plotted in figure 6.31, together with the test results.

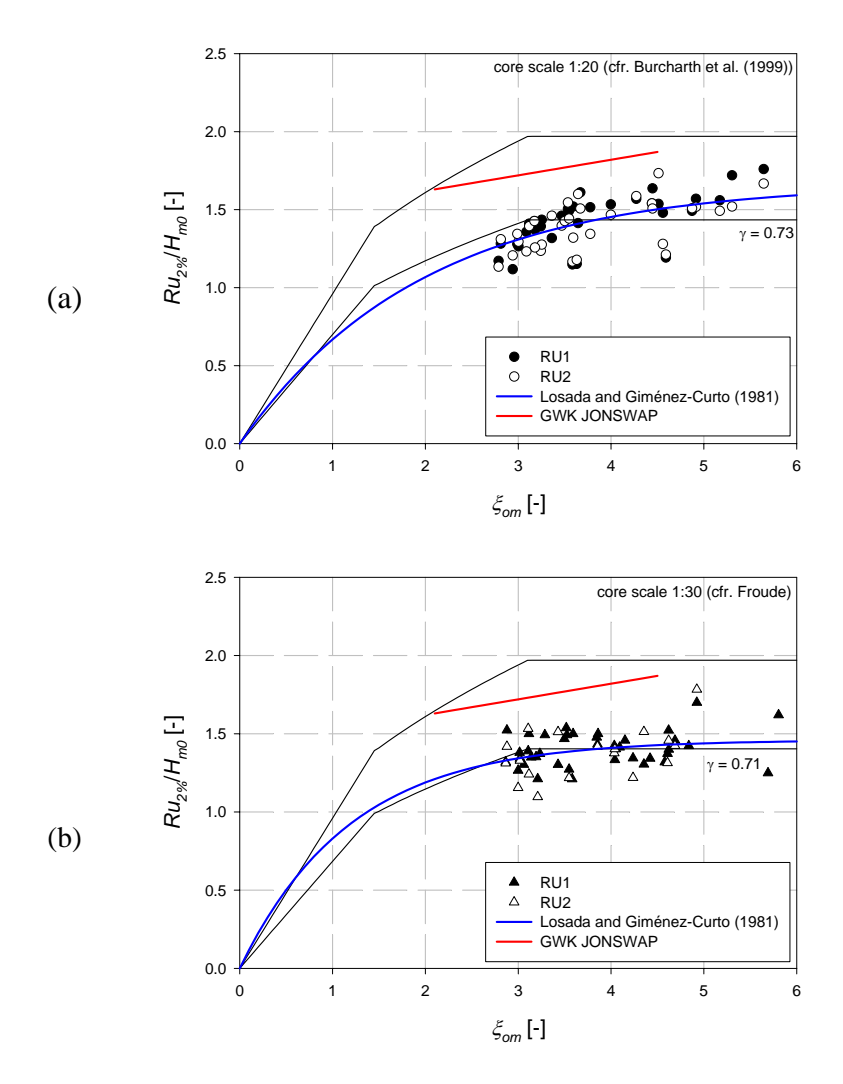


Figure 6.31: Comparison of laboratory results and the formulae of van der Meer and Stam (1992) for (a) core material scaled according to Burcharth et el. (1999) and (b) core material scaled according to Froude's law.

The explanation why the results of the additional tests at UGent are approximately 30% lower than the results of van der Meer and Stam (1992) is found within the type spectrum used to perform small scale model tests. For the additional UGent tests, JONSWAP spectra have

been generated. van der Meer and Stam (1992) generated Pierson Moskowitz spectra. A parameterised Pierson Moskowitz type spectrum is a two parameter spectrum and is defined by:

$$S(f) = \frac{5}{16} H_s^2 f_p^4 f^{-5} \exp\left(-\frac{5}{4} \left(\frac{f_p}{f}\right)^4\right)$$
 (6.33)

The spectral width parameter  $\varepsilon$  (cfr. equation (2.10)) has been calculated for both a Pierson Moskowitz spectrum and a JONSWAP spectrum. Varying the peak wave period  $T_p$  within the interval [0.1 s, 10 s], the value of the spectral width value of the theoretical spectra have been plotted against  $T_p$  in figure 6.32. The spectral width parameter  $\varepsilon$  is independent on the value of the wave height parameter. The difference between the values of the spectral width parameter of both types of spectra is the smallest for large peak wave periods. For small values of  $T_p$ , the difference becomes important. It is seen that the difference between the spectral width parameters of both types of spectra mounts up to 0.24 for  $T_p = 0.4$  s. A Pierson Moskowitz spectrum has a larger spectral width value than a JONSWAP spectrum. Relying on the type of generated spectrum and the findings of this thesis concerning the influence of the spectral shape, it could a priori be concluded that the results of van der Meer and Stam (1992) are higher than the results of the additional UGent tests.

Another explanation is found within the fact that the UGent test results make use of the total significant wave height and van der Meer and Stam (1992) make use of the incident significant wave height. As the total wave height  $H_{m0,t}$  is higher than the incident wave height  $H_{m0,t}$ , the ratio  $Ru_{2\%}/H_{m0,t}$  is smaller than the ratio  $Ru_{2\%}/H_{m0,t}$ .

#### 6.4.2 Wave run-down

Full scale wave run-down measurement results (both MAST II and OPTICREST measurement results) have been compared to wave run-down formulae found in literature (cfr. paragraph 2.4) and the wave run-down formula found by large scale tests at GWK (figure 6.33). The formulae of van der Meer (1993) (2.53) has been plotted with 1.2 in stead of 1.3

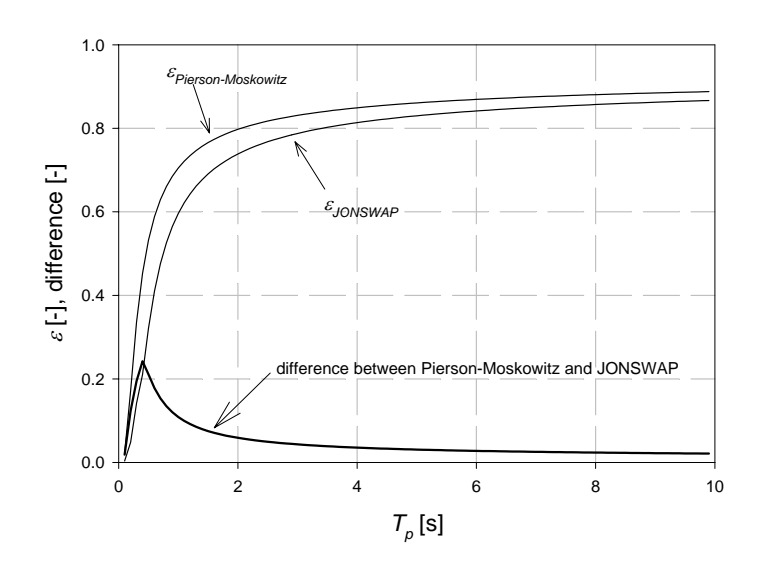


Figure 6.32: The spectral width parameter  $\varepsilon$  of a standard parameterised Pierson Moskowitz spectrum and JONSWAP spectrum and the difference between both.

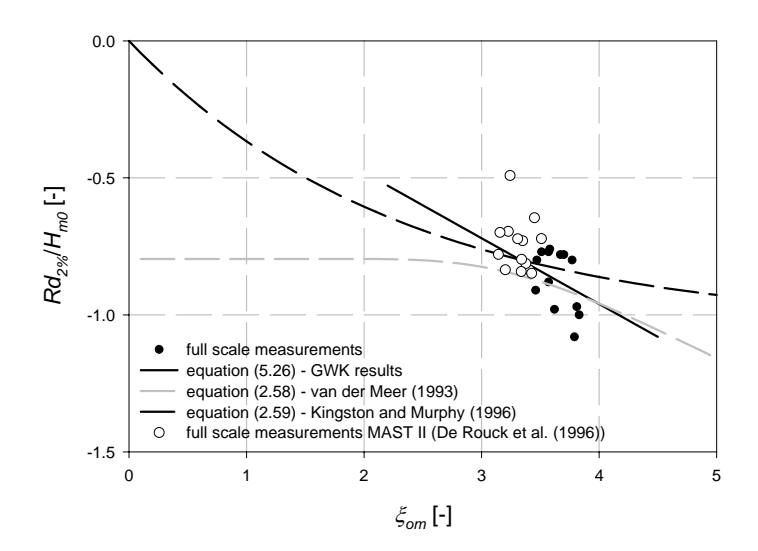


Figure 6.33: Comparion of wave run-down formula and large scale and full scale measurement results.

The most interesting result is found within the comparison of the outcome of the formula of Kingston and Murphy (1996) and the wave run-down formula (5.26) found by large scale tests at GWK and the full scale wave run-down measurement data of Zeebrugge breakwater: both formulae yield almost the same value of  $Rd_{2\%}/H_{m0}$ . The formula of van der Meer (1993) predicts higher (absolute) wave run-down values for  $\xi_{om} < 3$  and  $\xi_{om} > 4$ , but almost the same value of  $Rd_{2\%}/H_{m0}$  for  $3 \le \xi_{om} \le 4$ . Large scale test results agree very well with the formula of van der Meer (1993) for  $\xi_{om} > 3$ .

Wave run-down measured at full scale is very comparable to wave run-down values reported in literature and wave run-down values found by large scale model testing.

## 6.5 Wave run-up formula

Two different armour layer types have been investigated: (1) grooved cubes (by full scale measurements on the Zeebrugge rubble mound breakwater, the storm event reproductions in the laboratories of FCFH, AAU and UPV and the additional small scale model tests at FCFH) and (2) rock (by the additional small scale model tests performed at UGent and the large scale GWK tests). In the GWK tests, two different densities of rip rap have been examined: high density rock ( $\rho = 3.05 \text{ t/m}^3$ ) and normal density rock ( $\rho = 2.65 \text{ t/m}^3$ ).

The whole scale range covering full scale (Zeebrugge measurements), large scale (GWK) and small scale (storm event reproductions, additional FCFH tests, UGent tests) has been examined.

All wave run-up values have been referred to the total significant wave height measured at 'the toe of the breakwater'. For full scale measurements,  $H_{m0}$  has been measured by one of the wave riders (WRI or WRII). In the laboratories, during storm reproductions and additional testing, wave heights have been measured at exactly the same position as where waves have been measured at full scale. At UGent the total wave height has been measured by WG3 (i.e. 7.50 m from the toe of the structure). At GWK, wave heights have been measured at the position of the wave gauge connected to channel 5 (i.e. 117.70 m from the breakwater).

The slope of the investigated structures did not vary much. At the location of the measuring jetty, the Zeebrugge breakwater locally has a slope tan  $\alpha = 1/1.3$ . All models of the Zeebrugge breakwater also

had a slope 1/1.3. In the Large Wave Channel (GWK), the slope of the breakwater was 1/2. The additional small scale model tests performed at UGent have been carried out on a rubble mound breakwater with a slope tan  $\alpha=1/1.5$ . In comparison to literature in which a lot of investigations on gently sloping seawalls (cot  $\alpha>2$ ) have been found, the presented research has been focussed on quite steep slopes (tan  $\alpha \geq 0.5$ ). Assuming tan  $\alpha$  to have hardly any influence on wave run-up, equation (2.9) is read as

$$\frac{Ru}{H} = f(\xi) = f\left(\sqrt{\frac{m_0^{\frac{3}{2}}}{m_1^2}}\right) = f(m_0, m_1)$$
 (6.33)

Dimensionless wave run-up is only function of  $m_0$  and  $m_1$ . Kolodko et al. (1995) states that the applicability of the Iribarren number for wave run-up presentation is limited to breaking waves only, so for  $\xi < 3$ .

By assuming the spectral width parameter  $\varepsilon$  to contain more information about the wave spectrum than the Iribarren number  $\xi$ , for the tested range of  $\xi$  (i.e. surging waves), is:

$$\frac{Ru}{H} = f(\varepsilon) = f\left(\sqrt{1 - \frac{m_2^2}{m_0 m_4}}\right) = f(m_0, m_2, m_4) \tag{6.34}$$

For high Iribarren numbers (for most investigations  $\xi_{om}$  was larger than 3), higher order moments of the spectrum gain importance.

Multiregression analysis has been performed on the results of the various investigations. Based on equation (2.8), the limited range of tested slopes ( $tan \alpha$  is assumed to be constant) and the finding that  $\varepsilon$  has a clear influence on wave run-up), following model is proposed:

$$\frac{Ru_{2\%}}{H_{m0}} = a + b\varepsilon + cH_{m0} + dT_{m-10}$$
 (6.35)

Equation (6.35) has been fitted to the data of the full scale measurements, the storm event reproductions at FCFH and UPV, the additional tests carried out at FCFH, the UGent tests with core 1 and

the GWK tests with JONSWAP spectra. Following values have been found for the parameters a, b, c and d in (6.35):

- a = 0.546
- b = 1.623
- c = -0.120
- d = 0.072

The  $R^2$  value for the abovementioned combination of parameters equals 0.581.

#### **6.6 Conclusions**

In addition to the conclusions made in paragraph 5.7 about the laboratory investigation, following conclusions are drawn.

- (1) Results of full scale wave run-up data collected on the Zeebrugge breakwater and the results of storm event reproductions in the laboratories of FCFH, AAU and UPV have been compared. A clear difference is noticed between full scale measurement and small scale model test results: wave run-up is underestimated by small scale model tests. The storm event reproduction tests at FCFH and AAU showed that relative wave run-up values  $Ru_{2\%}/H_{m0}$  are underestimated by small scale model tests in comparison to full scale measurement results. The average  $Ru_{2\%}/H_{m0}$  value for the reproduction of storm events n° 1<sup>b</sup>, 2<sup>b</sup>, 3<sup>b</sup>, 4, 5, 8c and 9c for the FCFH tests is 1.46. The average  $Ru_{2\%}/H_{m0}$ value for the same storm event reproductions at AAU is 1.63. The full scale  $Ru_{2\%}/H_{m0}$  value is 1.77. UPV only reproduced the storm events which covered almost half a tide cycle (i.e. storm events n° 8 and 9). The average dimensionless wave run-up value obtained at UPV is the same as the average full scale value.
- (2) Full scale measurements have shown an influence of the water depth: dimensionless wave run-up increases for decreasing water depth. Large scale tests at GWK also indicated a dependency on the water level for tests with a reproduced natural spectrum: a low *SWL* gave rise to high dimensionless wave run-up values whereas a high *SWL* gave rise to low dimensionless wave run-up values. The influence of the water depth on wave run-up has not been observed in all laboratories. At FCFH dimensionless wave run-up values decreased with decreasing water depth. The difference between the results of all laboratories and full scale measurement

results become smaller and smaller when higher exceedance probabilities *x* are considered. It is concluded that water depth has no direct influence on wave run-up. Though, it has an indirect influence through the change of the wave parameters (shoaling, refraction) towards the structure and geometrical changes (armour layer pattern).

## (3) Scale effects and model effects have been identified

• scale effects due to viscosity and surface tension Both Reynolds number and Weber number are larger than their critical values  $Re_{critical} = 10^4$ , resp.  $We_{critical} = 10$ . Small scale modelling, only taking the requirement  $Fr = c^{te}$  into account is justified. Viscosity affects wave run-up by the internal flow regime in the core of the breakwater (P < 0.05). Wave run-up velocities are higher at full scale than at small scale. Scale effects are suspected. The surface tension may introduce a scale effect on wave run-up for values of Ru < 2.2 cm.

## spectral shape

The influence of the spectral shape has been investigated by means of the spectral width parameter  $\varepsilon$  and the peakedness parameter  $Q_p$ . The influence of the shape of the spectrum in general and the influence of the spectral width parameter  $\varepsilon$  in particular is clear: dimensionless wave run-up values increase with increasing spectral width parameter  $\varepsilon$  and decreasing peakedness parameter  $Q_p$ . Full scale spectral width parameters have quite large values by which the dimensionless wave run-up values are also quite large in comparison to small scale values.

For single peaked JONWAP type wave spectra, the spreading on the results is smaller when  $Ru_{2\%}/H_{m0}$  is expressed as a function of the spectral width parameter  $\varepsilon$  than when  $Ru_{2\%}/H_{m0}$  is expressed as a function of the Iribarren number  $\xi_{m-10}$  (calculated using  $T_{m-10}$ ). Neither  $T_{m-10}$ , nor  $\varepsilon$  yield a satisfactory explanation for differences in dimensionless wave run-up values for natural wave spectra.

The influence of the spectral shape on wave run-up is one of the explanations why full scale measurements yield a much higher dimensionless wave run-up value  $Ru_{2\%}/I_{m0}$  than small scale

model tests do and why laboratory results differ from each other. Tuning laboratory spectra to full scale spectra by comparing visually both spectra and mathematically their spectral parameters  $H_{m0}$  and  $T_{01}$  (and/or  $T_p$ ) is insufficient for correct reproduction of wave kinematics.

### • armour unit pattern

The armour unit pattern causes a large spreading on the waver run-up measurement results. The position of the run-up gauge relative to the armour unit pattern does not have an influence on wave run-up.

### wave run-up distribution

Wave run-up on the Zeebrugge breakwater obeys a theoretical Rayleigh distribution. The  $Ru_{2\%}$  value has shown to be a good parameter to describe wave run-up.

### · wave height

Total waves have been used in the denominator of the  $Ru_{2\%}/H_{m0}$  value. Total waves consist of incident waves and reflected waves. The reflected waves measured at full scale are only 4% lower than the reflected waves measured in a wave flume due to a scatter effect introduced by the curved breakwater.

# wind

Wave run-up is slightly increased by wind. The absence of wind in small scale model testing makes wave run-up results to have a smaller value than the full scale wave run-up results.

# • tidal currents parallel to the breakwater

Earlier investigations revealed decreasing wave heights for increasing current velocities. The influence of a tidal current parallel to the axis of the breakwater on wave run-up has been investigated in the wave basin at AAU. The model test results do not agree with the full scale measurement results. It is concluded that other parameters have a much larger influence on wave run-up than the tidal currents by which the influence of latter is not clear in the full scale measurement results.

### • foreshore

The foreshore of the Zeebrugge breakwater has been modelled at FCFH up to 600 m (full scale value) in front of the breakwater. The FCFH model included the sand bar. This bar

has not been modelled at UPV, neither at AAU. The presence of this bar was an extra difficulty to reproduce the target wave spectra at the location of the wave rider in the laboratory.

- sand filling in core
  - The core of the Zeebrugge breakwater is filled partially with sand. This sand filling might be a part of the explanation why wave run-up is higher at lower water levels. By creation of an internal setup of water, waves run-up higher.
- (4) Full scale wave run-up data have been compared with literature data. A lot of variation is seen on the wave run-up values found in literature. Wave run-down results of full scale measurements and large scale measurements equal wave run-down values found in literature.
- (5) The equation

$$\frac{Ru_{2\%}}{H_{m0}} = a + b\varepsilon + cH_{m0} + dT_{m-10}$$

has been fitted to the data of the full scale measurements, the storm event reproductions at FCFH and UPV, the additional tests carried out at FCFH, the UGent tests with core 1 and the GWK tests with JONSWAP spectra. Following values have been found for the parameters a, b, c and d:

- a = 0.546
- *b* = 1.623
- c = -0.120
- d = 0.072

The spectral width value  $\varepsilon$  is defined by (2.10), the spectral wave period  $T_{m-10}$  by (2.5). The formula is valid for permeable rubble mound breakwaters with a slope steeper than 1:2 and for surging waves.

In addition to these conclusions, following recommendations are given:

- For basic research purposes, small scale model tests should be performed in at least two different laboratories as to have a double check on the results of one laboratory. The methodology followed in both laboratories should be as similar as possible.
- With regard to wave run-up measurements on a rubble mound breakwater it is strongly advised to use the digital wave run-up gauge. It is recommended to use at least to wave run-up gauges placed in different cross sections for wave run-up measurements on an armour layer for which holds  $D_{n50}/H_{m0} \cong 1$ . A lot of spreading is seen on the individual test results. One has to be very careful with the interpretation of single wave run-up gauge test results, especially when a limited number of tests has been carried out. In case only one wave run-up gauge is available, tests should be run twice with the same wave paddle steering signal and the run-up gauge placed in another cross section. Alternatively, as many tests as possible should be carried out to minimise the influence of the armour unit pattern.
- Only tuning a spectrum generated in the laboratory to the target spectrum (measured at full scale) by comparing the spectral parameters  $H_{m0}$  and  $T_{01}$  (or  $T_p$ ) is not sufficient. Wave kinematics are not reproduced correctly. Also the value of the spectral width parameters of both spectra should be compared. The original wave train will never be reproduced in the laboratory. The phase spectrum should also be taken into account.

### **Chapter 7: Conclusions and areas for further research**

### 7.1 Final conclusions

The objectives mentioned in paragraph 1.6 have been met.

(1) to carry out a study of the existing literature to investigate the governing physical processes, influential parameters and points of special interest concerning wave run-up on coastal structures.

A literature overview has been made to identify the most influential parameters on wave run-up and the most important wave run-up investigations.

# (2) to collect full scale data on waves and wave run-up on a rubble mound breakwater.

Full scale measurements have been carried out on the Zeebrugge breakwater. Wave run-up has been measured by means of two different measuring systems based on different measuring principles: a so-called 'spiderweb system' (SP) and a five part wave run-up gauge (RU). The wave run-up values  $Ru_{2\%,SP}$  and  $Ru_{2\%,RU}$  which are the result of the analysis of the SP data, resp. the RU data collected during the same specific storm event vary slightly between both measuring devices, but on average, both instruments yield very similar results. Full scale measurements indicated  $Ru_{2\%}/H_{m0} = 1.77$  (for  $\xi_{om} = 3.63$ ) and  $Rd_{2\%}/H_{m0} = -0.87$  (for  $\xi_{om} = 3.64$ ).

# (3) to verify small scale models by comparison of full scale measurement results to results of small scale model testing in which storm events measured at full scale are reproduced.

A large number of small scale model tests have been carried out. The Zeebrugge breakwater has been modelled in three laboratories: Flanders Hydraulics (Belgium), Universidad Politécnica de Valencia (Spain) and Aalborg University (Denmark). Fifteen storm events measured at the full scale Zeebrugge breakwater have been reproduced. A clear difference in wave run-up results has been noticed between full scale measurement and small scale modelling results: full scale measurements yield larger  $Ru_2 \% H_{m0}$  values than the values obtained by laboratory testing.

Wave run-up has been measured by a novel digital wave run-up gauge in all laboratories. With this gauge, wave run-up has been measured more accurately than a traditional wire gauge. (4) to identify the driving forces behind the observed discrepancies in case results of full scale measurements do not agree with small scale model test results and to investigate the influencing parameters on wave run-up by small scale and large scale model testing.

The differences between full scale and small scale model test results have been studied. Scale and model effects have been investigated. It is concluded that scale effects are less important than model effects. Model effects are held responsible for the observed differences. The conclusions of chapter 6 are referred to.

Additional small scale model tests have been performed on a model of the Zeebrugge breakwater with a regular armour unit pattern instead of the irregular on-site armour unit pattern. A clear influence of the spectral shape (investigated by the spectral width parameter  $\varepsilon$  and the peakedness parameter  $Q_p$  of Goda (1985)) has been noticed. A lot of spreading is seen on the results. This spreading is introduced by the combined action of the *SWL*, the pattern of the armour units and the position of the comb of the run-up gauge relative to the armour unit pattern.

A rubble mound breakwater has been built in the Large Wave Channel (Hannover, Germany) and has been tested under a number of sea states. The aim of this research was to investigate the influence the density of the amour rock (and hence the dimensions of the rocks  $(D_{n50}/H_s)$ ). It is concluded that the  $Ru_{2\%}/H_{m0}$  value on both types of armour rock is the same.

A simplified version of the Zeebrugge breakwater has been built twice at UGent. Once with a core material scaled according to Burcharth et al. (1999) and a second time keeping the Froude number in the scale model the same as at full scale. A small difference between the results of the series of tests with a core scaled according to Burcharth et al. (1999) and the results of the series of tests with a core scaled according to Froude has been noticed (P < 0.05). In the additional small scale tests at UGent, two run-up gauges measured simultaneously wave run-up in two different cross sections of the breakwater. No difference has been noticed between the measurement results of the two run-up gauges (P < 0.05) within the same series of tests.

For storms with a return period of 1 to 10 years, the average dimensionless wave run-up value exceeded by 2% of the waves  $Ru_{2\%}/H_{m0}$  equals 1.77 for an Iribarren number  $\xi_{om} = 3.63$ . The full scale  $Ru_{2\%}/H_{m0}$  value is larger than the value found by laboratory testing. This value 1.77 is also clearly higher than values found in literature (which are based on small scale model test results). The slope, wave parameters,... (so, the Iribarren number  $\xi$ ) which have been considered in this study may be considered as very normal and thus, may occur very frequently. Consequently, wave overtopping over rubble mound breakwaters will occur more frequently than expected/assumed during the design of these structure. It is expected that wave overtopping amounts during design sea state conditions will be larger than the amounts measured by physical modelling.

# (5) to provide a formula to estimate wave run-up on a permeable rubble mound breakwater.

Wave run-up results have been combined in one single design formula valid for estimation of wave run-up on a permeable rubble mound breakwater with tan  $\alpha \geq 0.5$  and covered with either rock or grooved cubes:

$$\frac{Ru_{2\%}}{H_{m0}} = a + b\varepsilon + cH_{m0} + dT_{m-10}$$

with a = 0.546, b = 1.623, c = -0.120 and d = 0.072. Single peaked JONSWAP type wave spectra have been considered.

### 7.2 Further research areas

(1) Until now, the **water surface profile** at the moment of maximal wave run-up has only been investigated in small scale models (De Rouck (1991)). The knowledge of this profile is of major importance to calculate pore pressures in the soil underneath and in front of the breakwater for overall (macro) stability calculations of the breakwater against sliding and soil bearing resistance failure. Therefore, it would be very interesting to measure this profile at full scale or the carry out wave profile measurements in the laboratory, taking the knowledge gathered in this thesis into account (i.e. the influence of the spectral shape, the full scale value of  $Ru_{2y}/H_{m0}$ ).

- (2) A profound investigation of a problem makes full use of the triad (1) full scale measurements, (2) small scale measurements and (3) numerical modelling (Oumeraci (1999)). However, numerical modelling has never been a subject of this thesis, whereas full scale measurements and extensive laboratory testing are. Therefore, **numerical modelling** of wave run-up on a rubble mound breakwater is an interesting path for further research. Computational methods require parameters which have to be defined precisely, which diminishes the practical value of mathematical models. This is particularly true for rough permeable slopes (Pilarckzyk et al. (1996)). Moreover, numerical modelling needs full scale data and/or large scale data for calibration and verification purposes. Numerical modelling of wave run-up and wave overtopping on a permeable rubble mound breakwater is a possible path for further research.
- (3) As already mentioned in chapter 1, the crest height of a coastal structure is determined either by consideration of either wave run-up or wave overtopping. The first criterion (i.e. wave run-up by means of the parameter  $Ru_{2\%}$ ) has been dealt with in this thesis. The second criterion (i.e. wave overtopping) needs further elaboration. **Wave overtopping** is a very interesting parameter to investigate and is a logical continuation of the subject of this thesis. Not only the wave overtopping discharges, but also the individual wave overtopping volumes should be investigated. It is suspected that also wave overtopping is influenced by model and scale effects. A link between both criteria also needs to be made. Wave overtopping is the subject of the running CLASH project supported financially by the European Community (http://www.clash-eu.org, De Rouck et al. (2002)).
- (4) The method of storm event reproduction used during the OPTICREST project is insufficient. Because of the method of wave generation (i.e. random phase method (RPM),...) the reproduced wave train (in time domain) will never be the same as the original wave train from which the spectral parameters used for comparison are derived. Next to the amplitude spectrum, also the phase spectrum should be taken into account.
- (5) Up till now, the findings of Burcharth et al. (1999) concerning a distorted **core scale** are based only on theoretical considerations.

In this thesis a first initiative to verify theory with small scale model test data has been taken. Small difference has been noticed. More extensive laboratory research needs be carried out.

(6) The knowledge of wave run-up velocities/wave overtopping velocities, the layer thickness and the wave overtopping amounts are important parameters to estimate the loads on rubble mound breakwaters.

#### References

Ahrens J.P., Titus M.F., 1981. Lab data report: irregular wave run-up on plane, smooth slopes.

Ahrens J.P., Titus M.F., 1985. Wave run-up formulas for smooth slopes, Journal of Waterway, Port, Coastal and ocean Engineering, Vol. 111, No. 1.

Ahrens J.P., Heimbaugh M.S., 1988. Irregular wave run-up on riprap revetments, Journal of Waterway, Port, Coastal, and Ocean Engineering, Vol. 114,  $n^{\circ}$  4, pp. 524 - 530.

Allender J., Audunson T., Barstow S.F., Bjerkeen, S., Krogstad, H.E., Steinbakke P., Vartdal L; Borgman L.E., Graham C., 1989. The WADIC project: a comprehensive field evaluation of directional wave instrumentation, Ocean Engineering, 16, pp. 505-536.

Allsop N.W.H., Franco L., Hawkes P.J., 1985. Wave run-up on steep slopes – A literature review, Hydraulic Research Wallingford, Report SR1.

Allsop N.W.H., Hawkes P.J., Jackson F.A., Franco L., 1985. Wave run-up on steep slopes – Model tests under random waves, Hydraulic Research Wallingford, Report SR2.

Allsop N.W.H., Franco L., Hawkes P.J., 1985. Probability distributions and levels of wave run-up on armoured rubble slopes, Proceedings International Conference on Numerical and Hydraulic Modelling of Ports and Harbours, Birmingham, 23-25 April.

Andersen, Grønbech, Jensen, 1995. Refcross©, computer programme, Aalborg University.

Battjes J.A., 1974. Surf similarity, Proceedings ICCE 1974, Copenhagen (Denmark), pp. 466-480.

Battjes J.A., 1974. Computation of set-up, longshore currents, run-up and overtopping due to wind-generated waves, PhD thesis, Technishe Hogeschool Delft.

Brorsen M., Frigaard P., Experimental nd numerical wave generation and analysis, 1997. Lecture notes PhD Course, Aalborg University.

Burcharth H.F., 1998. Hydraulic responses – Wave runup, rundown and overtopping, OPTICREST Start-up workshop – note.

Burcharth H.F., Liu Z., Troch P., 1999. Scaling of core material in rubble mound breakwater model tests, Proceedings of 5<sup>th</sup> International Conference on Coastal and Port Engineering in Developing Countries (COPEDEC V), Cape Town, South Africa.

Carlson C.T., 1984. Field studies of run-up on dissipative beaches, Proceedings ICCE 1984, Houston (Texas), pp. 399-414.

Carter D., Draper L., 1988. Has the North-East Atlantic become rougher?, Nature, Vol. 332, 1988.

Cartwright, D.E., Longuet-Higgins M.S., 1956. The statistical distribution of the maxima of a random function, Proceedings of Royal Society of London, Series A (Mathematics and Physical Science), Vol. 237, pp. 212-232.

Chue S.H., 1980. Wave run-up formula of universal applicability, Proceedings Institution of Civil Engineers, part 2,  $n^{\circ}$  69, December, pp. 1035-1041.

CUR/CIRIA, 1991. Manual on the use of rock in coastal and shoreline engineering, CUR report 154.

CUR/CIRIA, 1995. Manual on the use of rock in hydraulic engineering, CUR/RWS report 169.

De Rouck J., 1991. De stabiliteit van stortsteengolfbrekers: Algemeen glijdingsevenwicht – Een nieuw deklaagelement, PhD thesis (in Dutch), Katholieke Universiteit Leuven.

De Rouck J., Troch P., 1996. MAST II – Full scale dynamic load monitoring of rubble mound breakwaters (MAS2-CT92-0023), Final report.

De Rouck J., 1996. OPTICREST – The optimisation of crest level design of sloping coastal structures through prototype monitoring and modelling (MAS3-CT97-0116), proposal.

De Rouck J., Troch P., Van Damme L., Eelen B., Schlütter F, 1998. Wave run-up: prototype versus scale models, Book of Abstracts, 26<sup>th</sup> I.C.C.E., Copenhagen, Denmark, June, 1998, pp. 632-633.

De Rouck J., 1998. Waterways and canals, syllabus RUG, academical year 1997-1998 (in Dutch).

De Rouck J., Troch P., Van de Walle B., Van Damme L., Bal J., 2000. The optimisation of crest level design of sloping coastal structures through prototype monitoring and modelling: OPTICREST, 2000, EurOCEAN 2000 Conference (Hamburg (Germany)), August  $29^{th}$  – September  $2^{nd}$ , 2000.

De Rouck J., Boone C., Van de Walle B., 2001. OPTICREST – The optimisation of crest level design of sloping coastal structures through prototype monitoring and modelling (MAS3-CT97-0116), Final report, Detailed scientific report – MAS03/1031.

De Rouck J., Troch P., Van de Walle B., Medina J.R., 2001. Análisis del remonte y rebase de diques en talud medidos a escala real, Jornadas Españolas de Ingeniera de Puertos y Costas (Mallorca), May  $17^{\rm th}-18^{\rm th}, 2001$ .

De Rouck J., Troch P., Van de Walle B., van Gent M.R.A., Van Damme L., De Ronde J., Frigaard P., Murphy J., 2001. Wave run-up on sloping coastal structures: prototype versus scale model results, Coastlines, Structures and Breakwaters 2001 Conference (London (United Kingdom)), September 26<sup>th</sup> – 28<sup>th</sup>.

De Rouck J., Van de Walle B., Troch P., Van Damme L., Willems M., Kofoed J.P., Frigaard P., Medina J.R., 2001. Wave run-up on a rubble mound breakwater, Medcoast Conference (Hammamet (Tunesia)), October  $23^{\rm rd}-27^{\rm th}, 2001$ .

De Rouck J., Van de Walle B., Van Damme L., Willems M., Frigaard P., Medina J.R., 2001. Prototype measurements of wave run-up on a rubble mound breakwater, International Conference on Port and

Maritime R&D and Technology (ICPMRDT) (Singapore), October  $29^{th} - 31^{st}$ .

De Rouck J., Allsop W., Franco L., van der Meer J., Verhaeghe H., 2002. Wave overtopping at coastal structures: development of a database towards up-graded prediction methods, Proceedings ICCE 2002, Cardiff, Wales (UK).

de Waal J.P., van der Meer J.W., 1992. Wave runup and overtopping on coastal structures, ICCE proceedings 1992, Venice (Italy), pp. 1758-1771.

Edge, Billy L., Baird, William F., Caldwell, Joseph M., Fairweather V., Magoon, Orville T., Treadwell Donald D., 1982, Failure of the breakwater at Port Sines, Portugal.

Frigaard P., Schlütter F., 1999. Laboratory investigation – Methodology, OPTICREST report.

Frigaard P., Schlütter F., 1999. Laboratory investigations – Progress report, OPTICREST report.

Führböter A., 1986. Model and prototype tests for wave impact and run-up on a uniform 1:4 slope, Coastal Engineering, No. 10, pp. 49-84.

Fürhböter A., Dette H.H., Töppe A., 1990. Recent changes in sea level rise, Jorunal of Coastal Research, Special issue nr. 9, Proceedings Skagen Symposium, Sept. 2-5, pp. 146 – 159.

Gadd P.E., Potter R.E., Safaie B., Resio D.,1984. Wave run-up and overtopping – A review and recommendations, Proceedings 16<sup>th</sup> Annual Offshore Technologie Conference, Houston (Texas).

Goda Y., 1985. Random seas and design of maritime structures, University of Tokyo.

Goda Y., Suzuki Y., Estimation of incident and reflected waves in random wave experiments, 1976. Proceedings 15<sup>th</sup> international conference on coastal engineering, Volume 1, pp. 828-845, Honolulu, Hawai.

Goda Y., 1998. An overview of coastal engineering with emphasis on random wave approach, Coastal Engineering, Vol. 40, No. 1, pp 1-21.

Gonzàlez-Escrivà J.A., Medina J.R., Garrido J., De Rouck J., 2002. Wind effects on run-up and overtopping: influence on breakwater crest design, Proceedings ICCE 2002, Cardiff (United Kingdom)).

Grüne J., 1982. Wave run-up caused by natural storm surge waves, Proceedings ICCE 1982, Cape Town, pp. 785-803.

Grüne J., Wang Z., 1999. The influence of wave climate on wave pressure and wave run-up, Proceedings of 5<sup>th</sup> International Conference on Coastal and Port Engineering in Developing Countries (COPEDEC V), Cape Town (South Africa).

Grüne J., Wang Z., 2000. Wave run-up on sloping seadikes and revetments, Proceedings ICCE 2000, Sydney (Australia).

Günbak A.R., 1979. Rubble mound breakwaters, Report n° 1, Division of Port and Ocean Engineering, University of Trondheim, Norwegian Institute of Technology, Trondheim (Norway).

Hardy T.A., Young I.R., Nelson R.C., Gourlay M.R., 1990. Wave attenuation on an offshore coral reef, Proceedings ICCE 1990, Delft, pp. 330-344.

Hashimoto N., Kobune K., 1988. Directional spectrum estimation from a Bayesian approach, Proceedings 21<sup>st</sup> ICCE, Spain, pp. 62-76.

Hedges T.S., Rogers J.R., 1996. Full scale dynamic load monitoring of rubble mound breakwaters – contract number MAS2-CT92-0023, Thematic Report A: Wave Climate, Final report, Liverpool University

Hosoi M., Shuto N., 1964. Run-up height on a single slope dike due to wave coming obliquely, Coastal Engineering, Japan, Volume 7, pp. 95-99.

Hunt, A., 1959. Design of seawalls and breakwaters, Journal of the Waterways and Harbors Division, Proceedings of the American Society of Civil Engineers, Vol. 85, No. WW2.

International association for hydraulic research, List of sea state parameters, 1996, Supplement to PIANC bulletin n° 52.

Jensen M.S., Frigaard P., 2000. Zeebrugge model: Wave run-up under simulated prototype storms (II) – The influence on wave run-up introducing a current, OPTICREST report.

Johnson R.R., Mansard E.P.D., Ploeg J., 1978. Effects of wave grouping on breakwater stability, Proceedings ICCE 1978, Hamburg (Germany), pp. 2228-2243.

Khattar M.D., Longest breakwater in India, 2001. Proceedings Ports '01 Conference, Norfolk (Virginia).

Kingston K., 1994. Refraction analysis, annual report (24 months), contract n° MAS2-CT92-0023, Full scale dynamic load monitoring of rubble mound breakwaters, University of Ghent.

Kingston K., Murphy J., 1996. Thematic report: Wave run-up / run-down, MAST II report.

Klopman G., van der Meer J., 1999. Random wave measurements in front of reflective structures, Journal of waterway, port, coastal and ocean engineering, Jan/Feb.

Kolodko J., Kapinski J., Szmytkiewicz M., Zeidler R.B., 1995. Wave run-up: recent IBW PAN investigations, Proceedings Coastal Dynamics, pp 197-208.

Kortenhaus A., Möller J., Oumeraci H., 2002. Work package 7: Methodology on quantification of measurement errors, model and scale effects, CLASH report.

Long Steven R., 1992. A self-zeroing capacitance probe for water wave measurements, NASA Reference publication 1278, June.

Losada M.A., Giménez-Curto L.A., 1981. Flow characteristics on rough, permeable slopes under wave action, Coastal Engineering,  $n^{\circ}$  4, pp. 187-206.

Losada M.A., Giménez-Curto L.A., 1981. Mound breakwaters under oblique wave attack – A working hypothesis, Coastal Engineering, n° 6, pp. 83-92.

Mansard E., Funke E., 1980. The measurement of incident and reflected spectra using a least square method, Proceedings, 17<sup>th</sup> International Conference on Coastal Engineering, Volume 1, pp. 154-172, Sydney, Australia.

Marchand K., 2002. Experimentele studie van de golfoploop bij stortsteengolfbrekers, scriptie, Universiteit Gent, academiejaar 2001-2002.

Mase H., 1988. Spectral characteristics of random wave run-up, Coastal Engineering, No. 12, pp. 175-189.

Mase H., Iwagaki Y., 1984. Run-up of random waves on gentle slopes, Proceedings ICCE 1984, Houston (Texas), pp. 593-609.

Medina J.R., Gonzàlez-Escrivà J.A., 2000. Laboratory results, OPTICREST report.

Medina J.R., Gonzàlez-Escrivà J.A., 2000. Zeebrugge 1:30 model – Laboratory investigations, OPTICREST report.

Medina J.R., Gonzàlez-Escrivà J.A., Garrido J., 2001. Subtask 3.3: Laboratory investigation two dimensional testing – Zeebrugge model tests performed at UPV, OPTICREST report.

Medina J.R., Gonzàlez-Escrivà J.A., Garrido J., 2001. OPTICREST MAST III Task 4 and subtask 3.3, CD-Rom.

Mendenhall W., Sincich T., 1992. Statistics for engineering and the sciences, 3rd edition, Dellen Publishing Company, Singapore.

Ministry of the Flemish Community, 2000. Getijtafels voor Oostende, Zeebrugge, Vlissingen, Prosperpolder en Antwerpen, Departement Leefmilieu en Infrastructuur, Administratie Waterwegen en Zeewezen, Afdeling Waterwegen Kust & Afdeling Maritieme Schelde.

Murphy J., 1998. OPTICREST report task 3.2, University College Cork.

Neter J., Kutner M.H., Nachtsheim C.J., 1996. Applied linear statistical models, 4<sup>th</sup> edition, McGraw Hill Interamericana Editores S.A de C.V.

Oumeraci H., 1999. Strengths and limitations of physical modelling in coastal engineering – Synergy with numerical modelling and field measurements, keynote lecture, proceedings of HYDRALAB workshop, Hannover, 17-19 February.

Pilarczyck K.W., 1999. Coastal Protection, A.A. Balkema, Rotterdam.

Pilarczyk, K.W., 1998. Dikes and revetments – Design, maintenance and safety assessment, A.A. Balkema, Rotterdam.

Pladys W., Zeebouw zeezand Zeebrugge, uitgave van 'Tijdelijke Vereniging Zeebouw-Zeezand'.

Rose G., 1991. Zakboekje elektronicaformules, Kluwer, 2e oplage.

Sakakiyama T., Kijama R., 1998. Scale effects on wave overtopping of seawall covered with armor units, extended abstract ICCE.

Sand S.E., 1985. Stochastic processes – pratical computation of spectra, Technical report Danish Hydraulic Institute (DHI), Horsholm (Denmark).

Savage R.P., 1958. Wave run-up on roughened and permeable slopes, Journal of the Waterways and Harbors Division, Vol. 84, No. WW3, paper 1640.

Saville T., 1956. Wave run-up on shore structures, Journal of the Waterways Division of the American Society of Civil Engineers, Vol. 82, No. WW2, paper 925.

Schijf J.B., 1974. Wave run-up and overtopping, Technical advisory committee on protection against inundation, Government publishing office, The Hague.

Schlütter F., Frigaard P., Liu Z., 2000. Zeebrugge model: wave run-up under simulated prototype storms, OPTICREST report.

Schüttrumpf H., 2001. Wellenüberlaufströmung bei Seedeichen – Experimentelle und theoretische Untersuchungen, PhD thesis (in German), Technischen Universität Braunschweig.

Schüttrumpf H., Troch P., Van de Walle B., De Rouck J., Oumeraci H., 2000. Prototype run-up velocities at Zeebrugge breakwater, proceedings ICCE 2000, Sydney.

Schüttrumpf H., Bergmann H., Dette H.-H., 1994. The concept of residence time for the description of wave run-up, wave set-up and wave run-down, Proceedings ICCE 1994, Kobe (Japan), Volume 1, pp. 553-564.

Silva R., Govaere G., Martin F., 1998. A statistical tool for breakwater design, Proceedings Coastal Engineering 1998, Vol. 2, pp. 1920-1933.

Smith J.M., 1999. Wave breaking on an opposing current, Coastal Engineering Technical Note CETN IV-17, U.S. Army Engineer Research and Development Center, Vicksburg, MS.

Sorensen R.M., 1997. Basic coastal engineering, Chapman & Hall.

Spiegel M.R., 1992. Mathematical handbook of formulas and tables, Schaum's outline series, McGraw-Hill, Inc.

Stam C.J.M., 1989. Taluds van losgestorte materialen – Golfoploop op statisch stabiele strotsteen taluds onder golfaanval, verslag modelonderzoek M1983, Waterloopkundig Laboratorium Delft.

Taerwe L., 1996. Waarschijnlijkheidsrekening en statistiek, syllabus, Ghent University, academical year 1995-1996 (in Dutch).

Tautenhain E., Kohlhase S., Partenscky H.W., 1982. Wave run-up at sea dikes under oblique wave approach, Coastal Engineering, pp. 804-810.

Technische Adviescommissie voor de Waterkeringen, 2002 Technisch Rapport Golfoploop en Golfoverslag bij Dijken, Delft.

Thornton E.B. and Guza R.T., 1982. Energy saturation and phase speeds measured on a natural beach, J. Geophys. Res., Vol. 87, No. C12, pp. 9499-9508.

- Troch P., De Somer M., De Rouck J., Van Damme L., Vermeir D., Martens J.P., Van Hove C., 1996. Full scale measurements of wave attenuation inside a rubble mound breakwater, proceedings ICCE, Vol. 2, pp. 1916-1929.
- Troch P., De Rouck J., Van Damme L., 1998. Instrumentation and prototype measurements at the Zeebrugge rubble mound breakwater, Coastal Engineering, n° 35, pp. 141-166.
- Troch P., 2000. Experimentele studie en numerieke modellering van golfinteractie met stortsteengolfbrekers, PhD Thesis (in Dutch), Universiteit Gent.
- U.S. Army Coastal Engineering Research Center, 1977. Shore Protection Manual, Department of the Army, Corps of Engineers.
- U.S. Army Coastal Engineering Research Center, 1984. Shore Protection Manual, Department of the Army, Corps of Engineers.
- U.S. Army Corps of Engineers. 2002. *Coastal Engineering Manual*. Engineer Manual 1110-2-1100, U.S. Army Corps of Engineers, Washington, D.C. (in 6 volumes).

Van Besien P., Wittebolle K., 1999. Ontwerp en kalibratie van een golfgoot, Master thesis, Universiteit Gent.

van der Meer J.W., 1988. Rock Slopes and Gravel Beaches under Wave Attack, PhD thesis, WL Delft Hydraulics.

van der Meer J.W., Stam C.J., 1992. Wave run-up on smooth and rock slopes of coastal structures, Journal of Waterway, Port, Coastal, and Ocean Engineering, Vol. 118, n° 5, September/October.

van der Meer J.W., Tönjes P. de Waal H., 1998. A code for dike height design and examination, Proceedings International Conference on Coastlines, Structures and Breakwaters, Institution of Civil Engineers, London (United Kingdom), March 19-20, 1998.

van der Meer J.W., Wouters J., 2000. Invloedsfactoren voor de ruwheid van toplagen bij golfoploop en golfoverslag, INFRAM.

Van de Walle B., Bal J., 2001, Prototype measurements Zeebrugge, final OPTICREST report MAS03/1115, final report task 2.2 'Prototype measurements (Zeebrugge)'.

Van de Walle B., De Rouck J., Van Damme L., Bal J., 2001. Wave run-up on and wave overtopping over a prototype rubble mound breakwater, Ports 2001 Conference (Norfolk (Virginia)), April  $29^{th}$  – May  $2^{nd}$ .

Van de Walle B., De Rouck J., Van Damme L., Frigaard P., Willems M., 2002. Parameters influencing wave run-up on a rubble mound breakwater, ICCE 2002, Cardiff (United Kingdom), July 7<sup>th</sup> – 12<sup>th</sup>.

van Gent M.R.A., 1999. Wave run-up and wave overtopping for double peaked wave energy spectra, WL Delft, H3351.

van Gent M.R.A., 2001. Wave run-up on dikes with shallow foreshores, Journal of Waterway, Port, Coastal and Ocean Engineering, Vol. 127, n° 5, Sept./Oct. 2001.

van Gent M.R.A, Wolf F.C.J., Murphy J., 2001. Synthesis of Petten measurements, OPTICREST report H3129.

Van Impe W.F., 1993. Grondmechanica – Fysische en mechanische eigenschappen van de grond, syllabus, Universiteit Gent, Academia Press.

Van Torre M, 2001. Wave forces on fixed and floating constructions, syllabus RUG, academical year 2000-2001.

Verdonck R., Troch P., De Rouck J., Burcharth H.F., 1998. Task 1 – Review of available information, OPTICREST report MAS03/545.

Verhoeven R., 1996. Stromingsleer I, syllabus RUG, academical year 1996-1997 (in Dutch).

Versluys T., 1999. Data for calculation of slope in Zeebrugge, OPTICREST report MAS03/790, Ghent University.

Vrijling J.K., Bruinsma J., 1980. Hydraulic boundary conditions related to the design of the Oosterschelde Storm Surge Barrier in the Netherlands – An example of a joint distribution of waves and surges,

reprint from the Proceedings on Hydraulic Aspects of Coastal Structures Part 1: Developments in Hydraulic engineering, Delft University Press, Delft, 1980 found in Pilarczyk K.W., 1990, Coastal protection, Balkema, Rotterdam.

Wang Z., Grüne J., 1995. Influence of berms on wave run-up on sloping seadykes, Proceedings, of 4<sup>th</sup> International Conference on Coastal and Port Engineering in Developing Countries (COPEDEC IV), Rio de Janeiro (Brazil).

Ward D.L., Wibner C.G., Zhang J., Edge B., 1994. Wind effects on runup and overtopping, Proceedings ICCE 1994, Kobe (Japan), Volume 2, pp. 1687-1699.

Ward D.L., Zhang J., Wibner C.G., Cinotto C.M., 1996. Wind effects on runup and overtopping of coastal structures, Proceedings ICCE 1996, Orlando (Florida), Volume 2, pp. 2206-2215.

Ward D.L., Zhang J., Cinotto C.M., Wibner C.G., 1997. Effects on runup of onshore winds and wave grouping, Proceedings Ocean wave measurement and analysis (Waves '97), Volume 2, pp. 1425 – 1439.

Yokoki H., Isobe M., Watanabe A., 1992. A method for estimating reflection coefficient in short crested random seas, Coastal Engineering, pp. 765-776.

Zhou L., Frigaard P., 2000. Zeebrugge model: 3D wave runup measurements and analysis, OPTICREST report.

### **World Wide Web**

http://bigfoot.wes.army.mil/6539.html

http://www.giss.nasa.gov/research/intro/gornitz\_01/

http://bigfoot.wes.army.mil/cem026.html

http://bigfoot.wes.army.mil/cetn.index.html, http://cirp.wes.army.mil/cirp/cetns/cetniv-17.pdf

http://www.kibron.com/Products/AquaPi/Aqua.html

# Maps

sounding map  $n^{\circ}$  202-01-eros-wdam-n-187-97, May 12<sup>th</sup>, 1997. sounding map  $n^{\circ}$  373-03-eros-wdam-b-643-98, November 23<sup>rd</sup>, 1998. sounding map  $n^{\circ}$  009dc-2002, July 4<sup>th</sup>, 2002.

Hessenatie N.V., 1996, file n° 96-07/17B 'Bouwen van auto-terminal (liggingsplan terminal Wielingendok)'.

Ministry of the Flemish Community, 1985. Stroomatlas – Werkgebied & Pas van het Zand, Ministerie van openbare werken, Bestuur der waterwegen, Dienst der kust, uitgave nr. 25.

Annex A: Rayleigh and Weibull distribution.
Annex A-1

# A.1 Rayleigh transformation

In most cases, when the cumulative distribution function (CDF)  $F_X(x)$  is plotted in function of x in a diagram with two linear axes, a typical S shaped curve is seen. For some applications, however, it is very useful to have a linear relationship in stead of an S shaped curve. Therefore, the scale of the vertical axis  $(F_X(x))$  is transformed in the following way.

The CDF  $F_X(x)$  is defined as

$$F_X(x) = P[X \le x] = g(x) \tag{A.1}$$

Assume a variable x which is Rayleigh distributed. The density function  $f_X(x)$  of the Rayleigh distribution is given by

$$f_X(x) = \frac{x}{a^2} e^{-\frac{x^2}{2a^2}}, x \ge 0$$
 (A.2)

De CDF  $F_X(x)$  is given by

$$F_X(x) = \int_{-\infty}^{x} f_X(x) dx = 1 - e^{-\frac{x^2}{2a^2}}, x \ge 0$$
 (A.3)

The inverse function of g(x) in (A.1) is

$$x = g^{-1}(F_X(x)) \tag{A.4}$$

or, with (A.3)

$$e^{-\frac{x^2}{2a^2}} = 1 - F_X(x) \tag{A.5}$$

so that

$$-\frac{x^2}{2a^2} = \ln(1 - F_X(x))$$
 (A.6)

Out of (A.6) follows that

$$x = \pm \sqrt{-2a^2 \ln(1 - F_X(x))}$$
 (A.7)

The negative solution in (A.7) is of no importance (see the definition of the Rayleigh distribution (A.2)).

The argument of the neperian logarithm in (A.7) is the exceedance probability  $1 - F_X(x)$ , so finally

$$x = g^{-1}(F_X(x)) = a\sqrt{-2\ln(1 - F_X(x))}$$
 (A.8)

The factor a in (A.8) may be taken equal to unity because the factor only causes a homothetical scaling of the transformed axis.

In the following, the exceedance probability is noted down as x and the wave run-up values as Ru.

The Rayleigh distribution function is given by expression (A.10) (Taerwe (1996)),

$$f_{Ru}(Ru) = \frac{Ru}{a^2} e^{-\frac{Ru^2}{2a^2}}$$
 (A.10)

whereas the cumulative Rayleigh distribution function can be read as

$$P[Ru \le Ru_{x\%}] = F_{Ru}(Ru_{x\%}) = 1 - e^{-\frac{Ru_{x\%}^2}{2a^2}}$$
(A.11)

The exceedance probability is

$$P[Ru > Ru_{x\%}] = 1 - F_{Ru}(Ru_{x\%}) = e^{-\frac{Ru_{x\%}}{2a^2}}$$
(A.12)

The parameter  $a^2$  can be estimated by several methods. Three different approaches are presented. The first method is the method of moments (Rice (1988), Taerwe (1996)) in which  $a^2$  can be solved from the equation

$$\mu_k = m_k \tag{A.13}$$

$$\int_{-\infty}^{+\infty} Ru^k f_{Ru}(Ru) dRu = \frac{1}{n} \sum_{i=1}^n Ru_i^k$$
 (A.14)

With k = 2 (and not with k = 1!)

$$\int_{0}^{+\infty} Ru^{2} \frac{Ru}{a^{2}} \exp\left(-\frac{Ru^{2}}{2a^{2}}\right) dRu = \frac{1}{n} \sum_{i=1}^{n} Ru_{i}^{2}$$
(A.15)

so that with the aid of the method of partial integration

$$2a^2 = \frac{1}{n} \sum_{i=1}^{n} Ru_i^2 \tag{A.16}$$

The second method is the method of maximum likelihood (Rice (1988), Taerwe (1996)). The likelihood function is given by

$$L(a|Ru_1, Ru_2, ..., Ru_n) = \prod_{i=1}^n f_{Ru}(Ru_i|a)$$
 (A.17)

so that

$$L = \prod_{i=1}^{n} \frac{Ru_i}{a^2} \exp\left(-\frac{Ru_i^2}{2a^2}\right)$$
 (A.18)

or

$$\ln L = \sum_{i=1}^{n} \ln \left( \frac{Ru_i}{a^2} \exp \left( -\frac{Ru_i^2}{2a^2} \right) \right)$$
 (A.19)

$$\ln L = \sum_{i=1}^{n} \left( \ln Ru_i - \ln a^2 - \frac{Ru_i^2}{2a^2} \right)$$
 (A.20)

The likelihood function reaches a maximum when dL/da = 0 or  $d(\ln L)/da = 0$ .

$$\frac{d \ln L}{da} = \sum_{i=1}^{n} \left( \frac{Ru_i^2}{a^3} - \frac{2}{a} \right) = 0$$
 (A.21)

which gives

$$a^2 = \frac{1}{2n} \sum_{i=1}^{n} Ru_i^2 \tag{A.22}$$

Thirdly, the parameter  $a^2$  can be assessed by linear regression (Mendenhall et al. (1992), Neter et al. (1996), Taerwe (1996)) when the cumulative distribution (A.11) is used and the exceedance probabilities are transformed by (A.8). Thus, the typical S-shaped curve is transformed into a straight line. The equations to be solved to determine the offset  $b_a$  and the slope  $b_l$  of the straight line are

$$b_{o} = \frac{\left(\sum_{i=1}^{n} x_{i}\right) \left(\sum_{i=1}^{n} Ru_{i}^{2}\right) - \left(\sum_{i=1}^{n} Ru_{i}\right) \left(\sum_{i=1}^{n} Ru_{i}x_{i}\right)}{n\left(\sum_{i=1}^{n} Ru_{i}^{2}\right) - \left(\sum_{i=1}^{n} Ru_{i}\right)^{2}}$$
(A.23)

$$b_{1} = \frac{n\left(\sum_{i=1}^{n} Ru_{i}x_{i}\right) - \left(\sum_{i=1}^{n} Ru_{i}\right)\left(\sum_{i=1}^{n} x_{i}\right)}{n\left(\sum_{i=1}^{n} Ru_{i}^{2}\right) - \left(\sum_{i=1}^{n} Ru_{i}\right)^{2}}$$
(A.24)

When wave run-up data are plotted versus the exceedance probability in a diagram with the exceedance probability axis scaled according to (A.8), the theoretical equation

$$Ru = b_0 + b_1 x \tag{A.25}$$

fits the experimental data.

When (A.8) and (A.11) are substituded in (A.25) is

$$Ru = b_o + b_1 \sqrt{-2\ln\left(\exp\left(-\frac{Ru^2}{2a^2}\right)\right)}$$
 (A.26)

so that

$$Ru = b_o + b_1 \frac{Ru}{a} \tag{A.27}$$

which yields the theoretical solution

$$\begin{cases}
b_0 = 0 \\
b_1 = a
\end{cases}$$
(A.28)

# A.2 Weibull distribution

The two parameter Weibull distribution is defined as

$$f_{Ru}(Ru) = \frac{a}{b^a} Ru^{a-1} \exp\left(-\left(\frac{Ru}{b}\right)^a\right)$$
 (A.29)

To estimate the parameters a and b, the method of the likelihood function has been applied. The likelihood function L of the Weibull distribution is read as

$$L = \prod_{i=1}^{n} \frac{a}{b^{a}} R u_i^{a-1} \exp\left(-\left(\frac{R u_i}{b}\right)^{a}\right)$$
 (A.30)

or

$$\ln L = \sum_{i=1}^{n} \frac{a}{b^a} R u_i^{a-1} \exp\left(-\left(\frac{R u_i}{b}\right)^a\right)$$
 (A.31)

The estimates of a and b are found by

$$\frac{\partial \ln L}{\partial a} = \sum_{i=1}^{n} \left[ \frac{1}{a} - \ln b + \ln R u_i - \left( \frac{R u_i}{b} \right)^a \ln \left( \frac{R u_i}{b} \right) \right] = 0 \quad (A.32)$$

$$\frac{\partial \ln L}{\partial b} = \sum_{i=1}^{n} \left[ -\frac{a}{b} + \frac{a}{b^{a+1}} R u_i^a \right] = 0 \tag{A.33}$$

Equation (A.33) yields

$$nb^a = \sum_{i=1}^n Ru_i^a \tag{A.34}$$

or

$$b = \left(\frac{1}{n} \sum_{i=1}^{n} R u_i^a\right)^{\frac{1}{a}}$$
 (A.35)

Equation (A.32) is

$$n\left(\frac{1}{a} - \ln b\right) = \sum_{i=1}^{n} \left[ \left(\frac{Ru_i}{b}\right)^a \ln \left(\frac{Ru_i}{b}\right) \right] - \sum_{i=1}^{n} \ln Ru_i$$
 (A.36)

Substituting (A.35) in (A.36) yields a non-linear equation.

Annex B: Wave run-up distributions.
Annex B-1

# SPIDERWEB SYSTEM

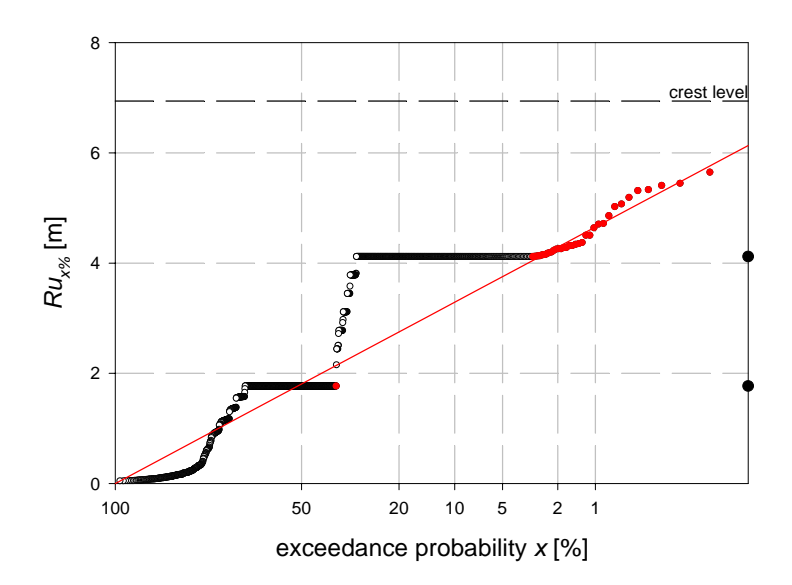


Figure B.1: Wave run-up distribution of August,  $28^{th}$ , 1995 (02h45-04h45).

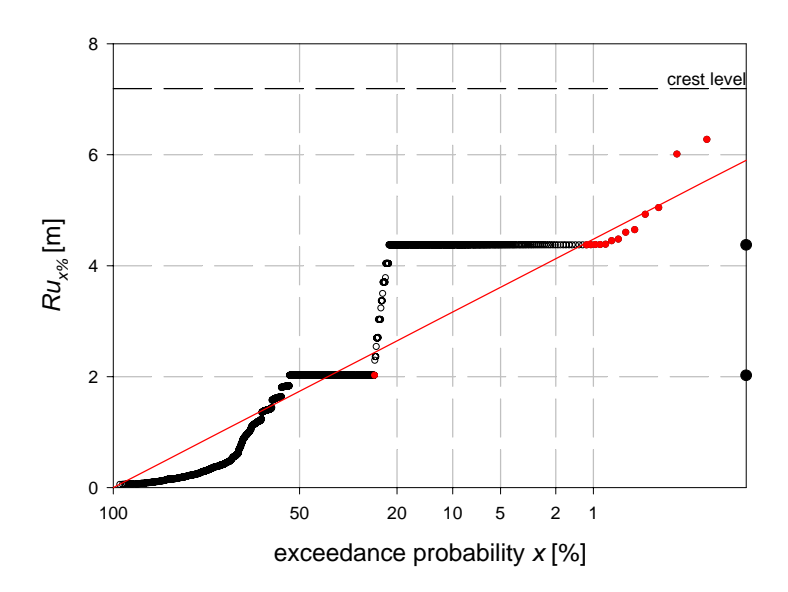


Figure B.2: Wave run-up distribution of August  $28^{th}$ , 1995 (15h00 - 17h00).

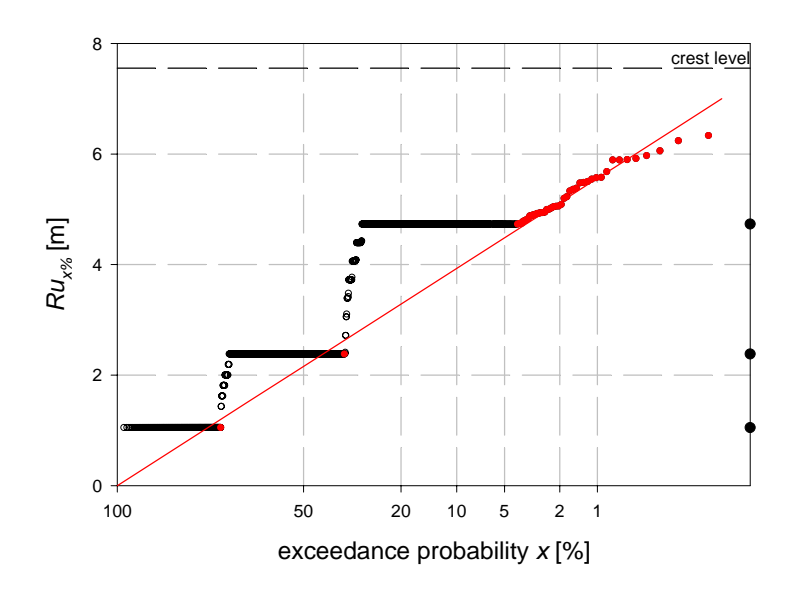


Figure B.3: Wave run-up distribution of January  $19^{th}$ , 1998 (16h00 - 18h00).

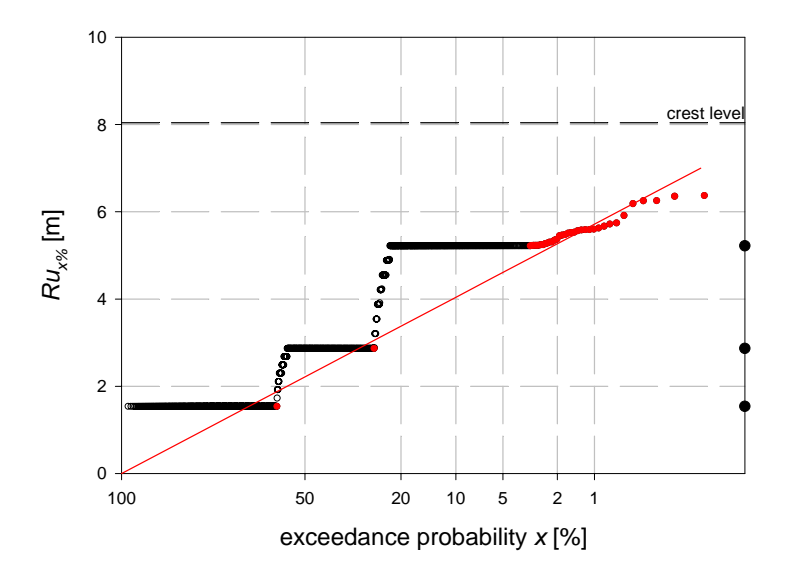


Figure B.4: Wave run-up distribution of January  $20^{th}$ , 1998 (04h15 - 06h15).

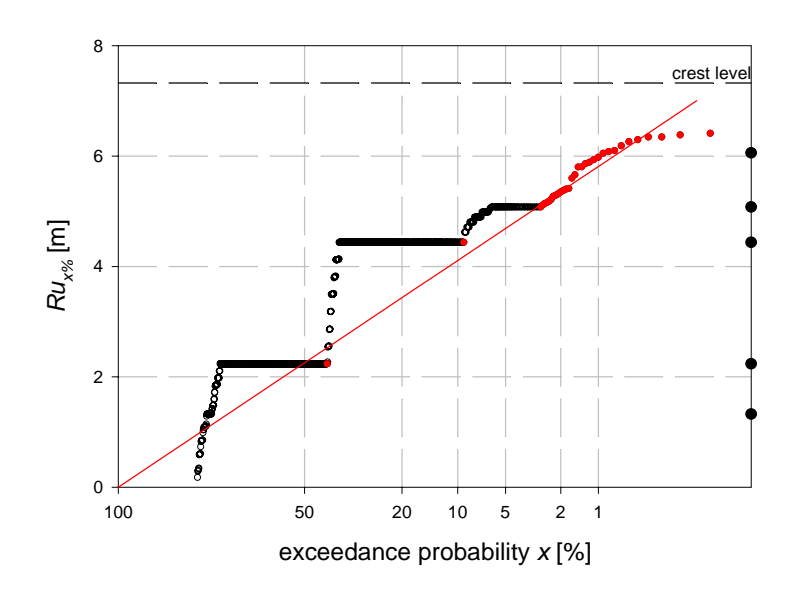


Figure B.5: Wave run-up distribution of February  $7^{th}$ , 1999 (16h00 – 18h00).

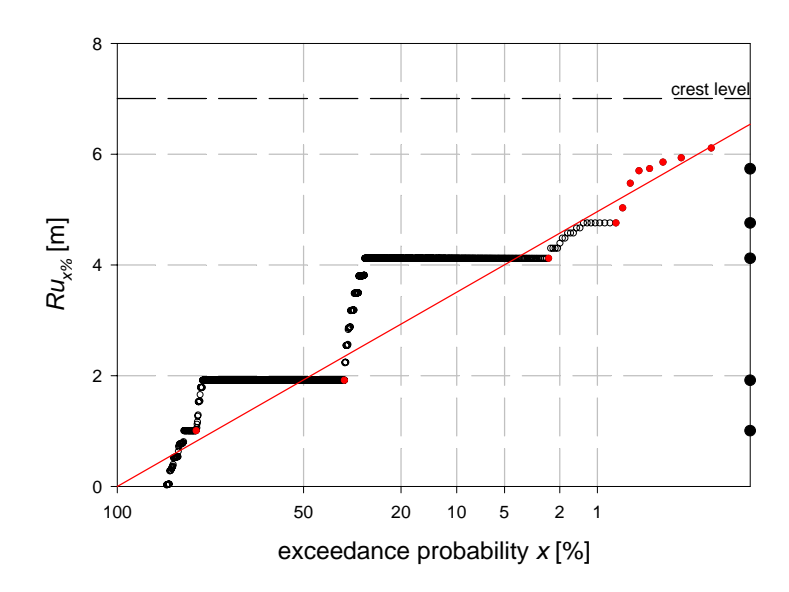


Figure B.6: Wave run-up distribution of February 17<sup>th</sup>, 1999 (12h45 – 14h45).

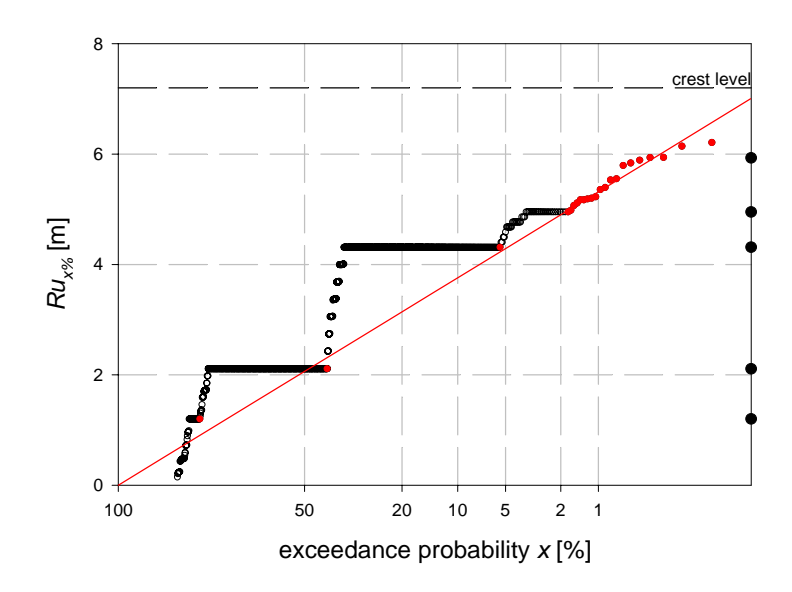


Figure B.7: Wave run-up distribution of February  $22^{nd}$ , 1999 (15h45 - 17h45).

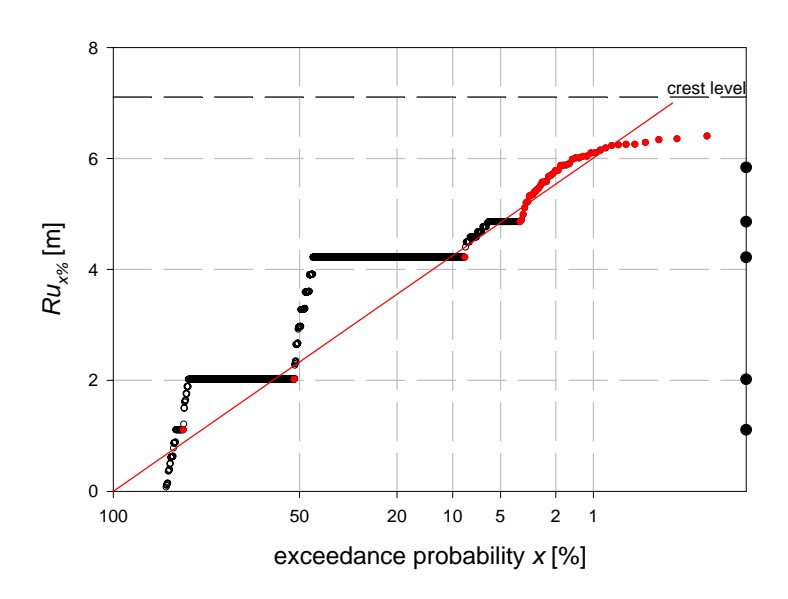


Figure B.8: Wave run-up distribution of November  $6^{th}$ , 1999 (11h30 – 13h30).

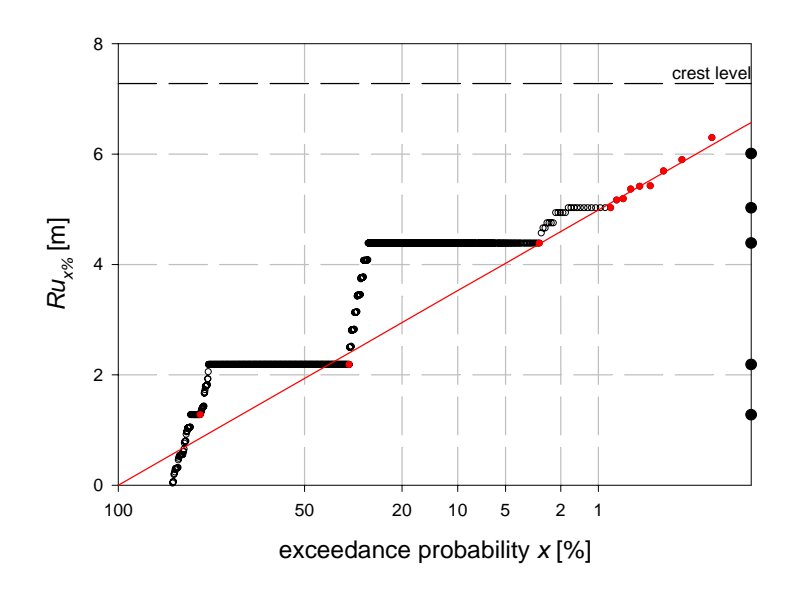


Figure B.9: Wave run-up distribution of November  $6^{th}$ - $7^{th}$ , 1999 (13h45 – 01h45).

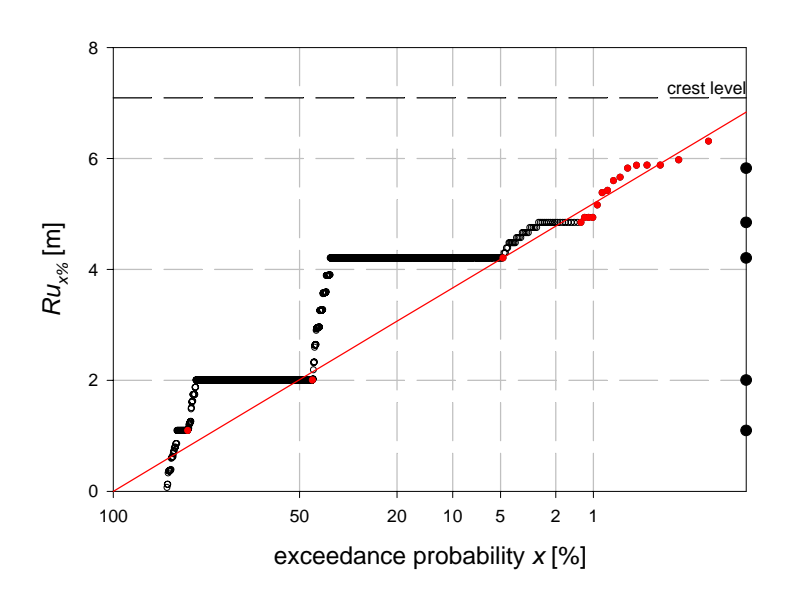


Figure B.10: Wave run-up distribution of December  $3^{rd}$ , 1999 (21h00 – 23h00).

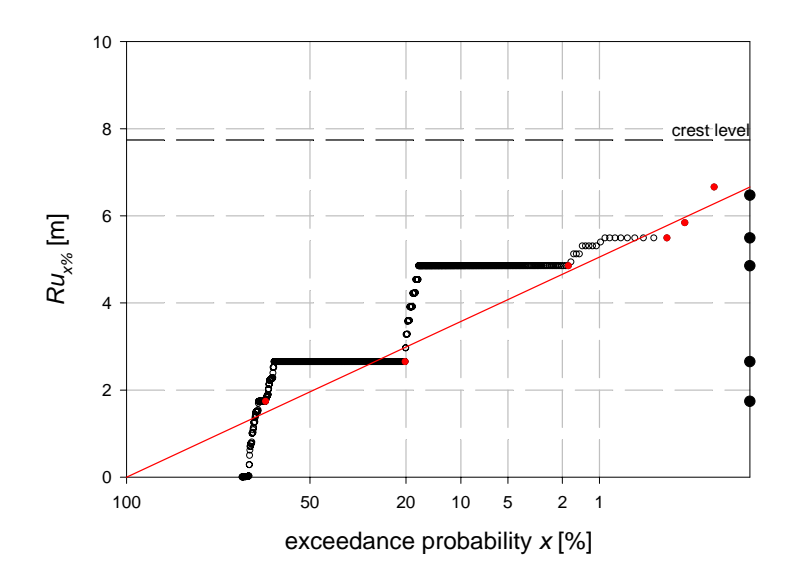


Figure B.11: Wave run-up distribution of December  $4^{th}$ , 1999 (22h00 – 0h00).

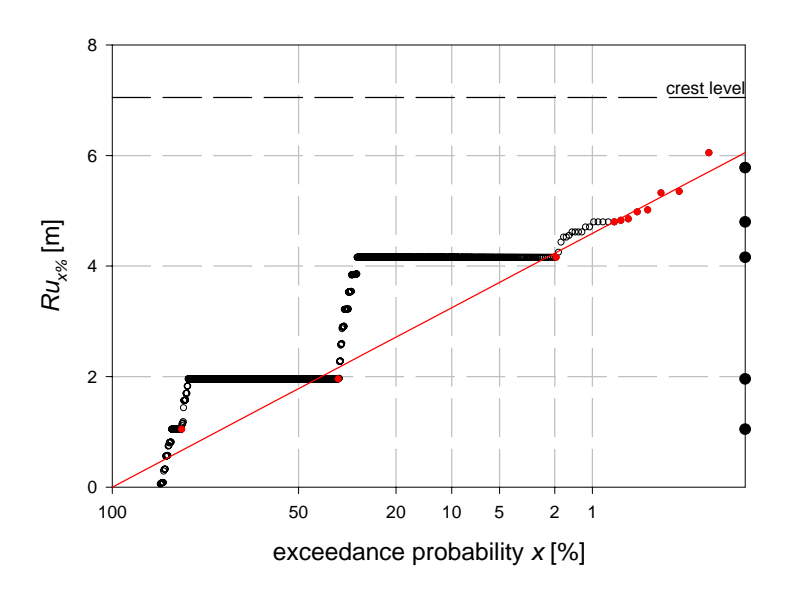


Figure B.12: Wave run-up distribution of January  $22^{nd}$ , 2000 (12h30-14h30).

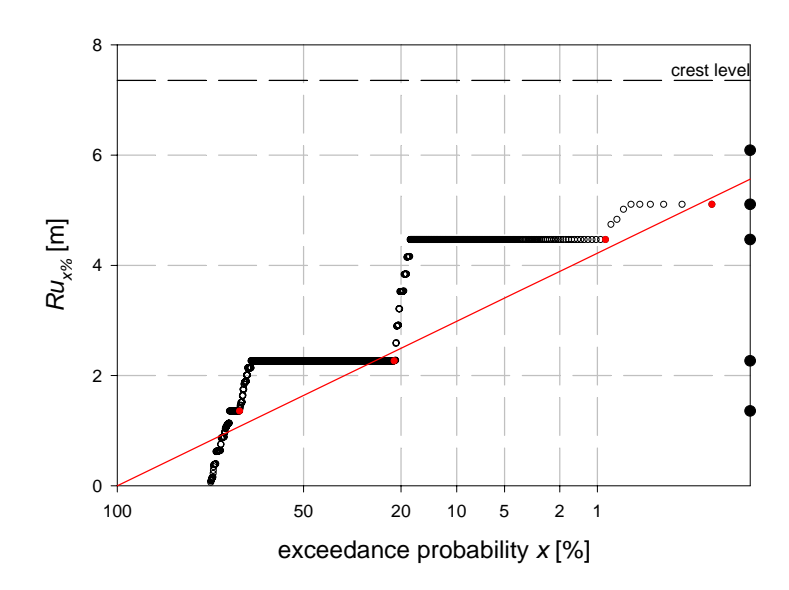


Figure B.13: Wave run-up distribution of January  $23^{rd}$ , 2000 (00h45 – 02h45).

## **RUN-UP GAUGE**

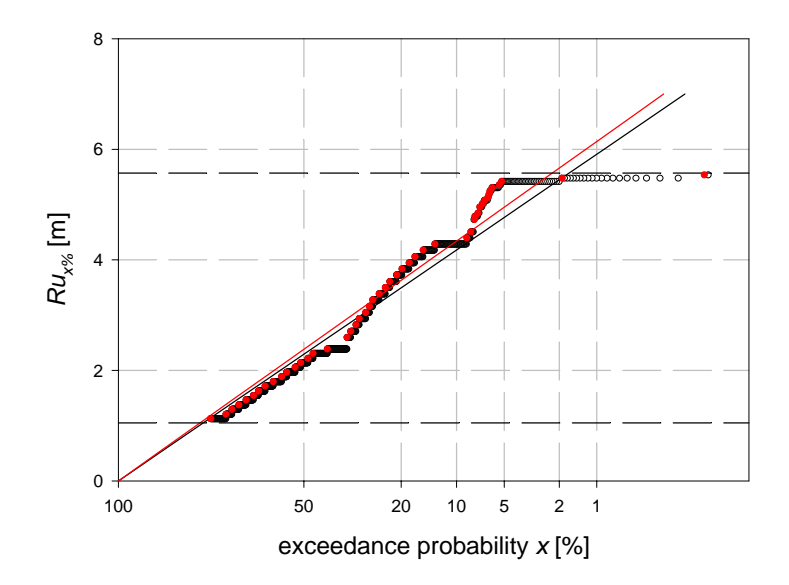


Figure B.14: Wave run-up distribution of February  $7^{th}$ , 1999 (16h00-18h00).

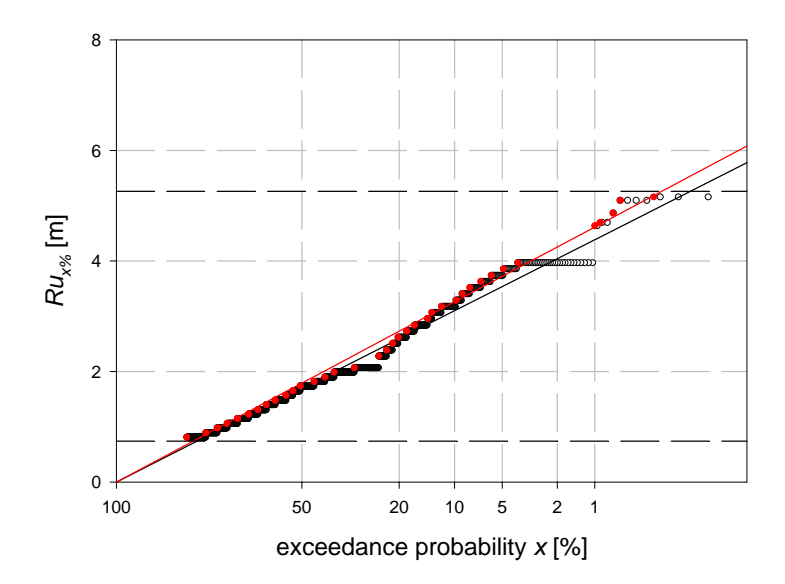


Figure B.15: Wave run-up distribution of February 17<sup>th</sup>, 1999 (12h45 – 14h45).

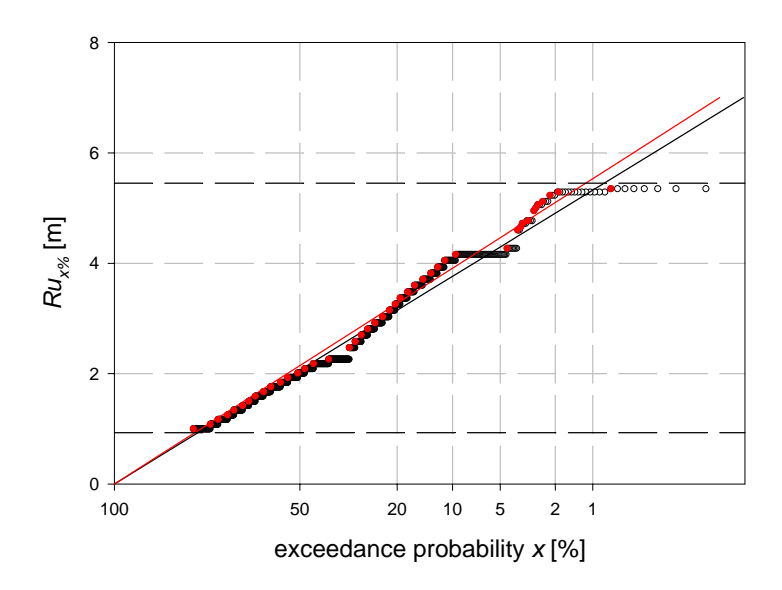


Figure B.16: Wave run-up distribution of February  $22^{nd}$ , 1999 (15h45 - 17h45).

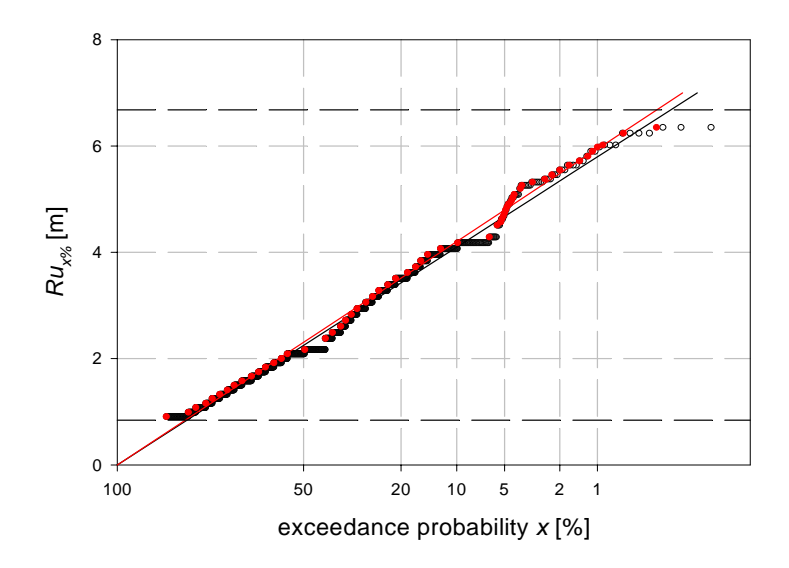


Figure B.17: Wave run-up distribution of November  $6^{th}$ , 1999 (11h30 – 13h30).

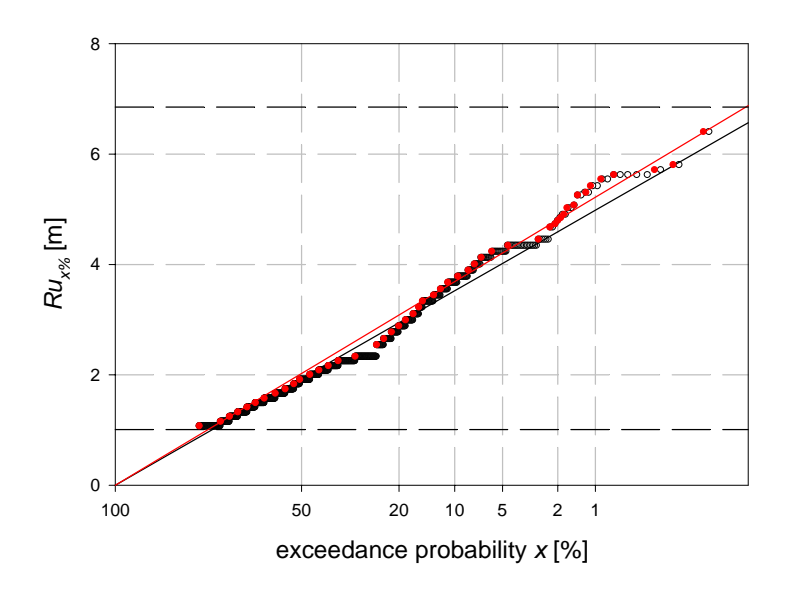


Figure B.18: Wave run-up distribution of November  $6^{th}$ - $7^{th}$ , 1999 (13h45 – 01h45).

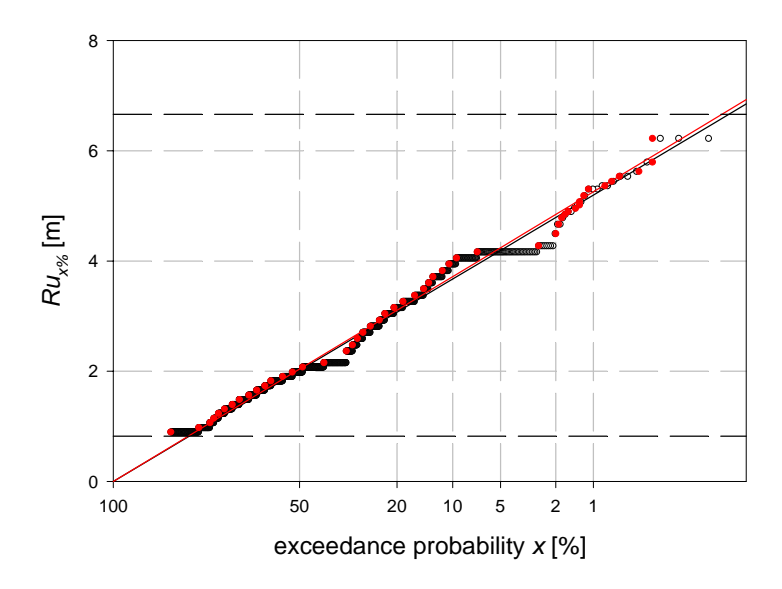


Figure B.19: Wave run-up distribution of December  $3^{rd}$ , 1999 (21h00 – 23h00).

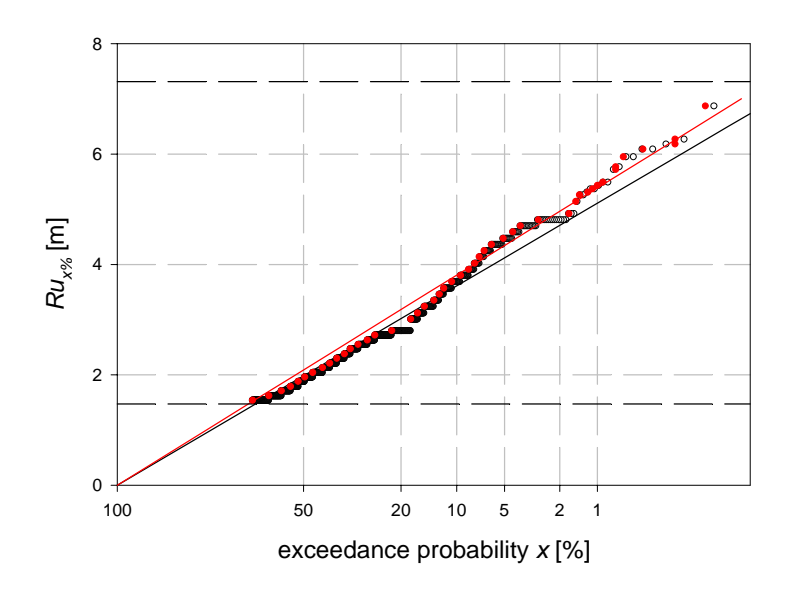


Figure B.20: Wave run-up distribution of December  $4^{th}$ , 1999 (22h00 – 0h00).

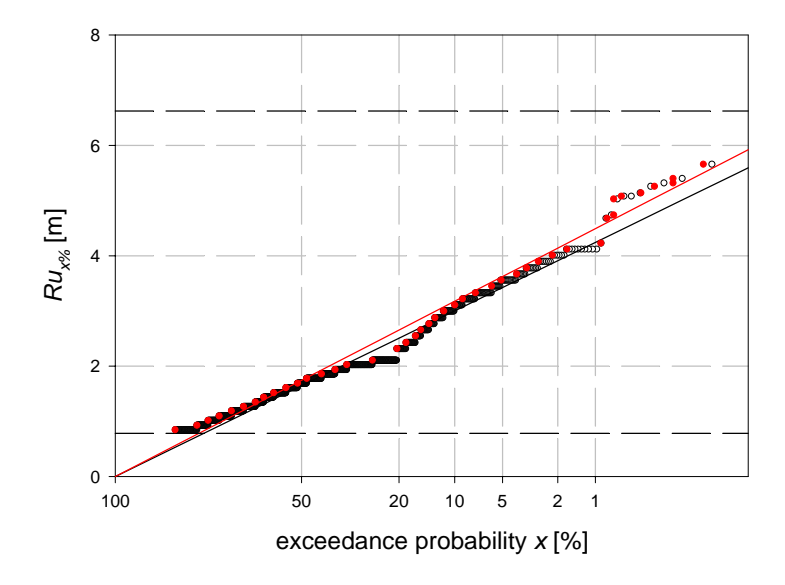


Figure B.21: Wave run-up distribution of January  $22^{nd}$ ,  $2000 \ (12h30-14h30)$ .

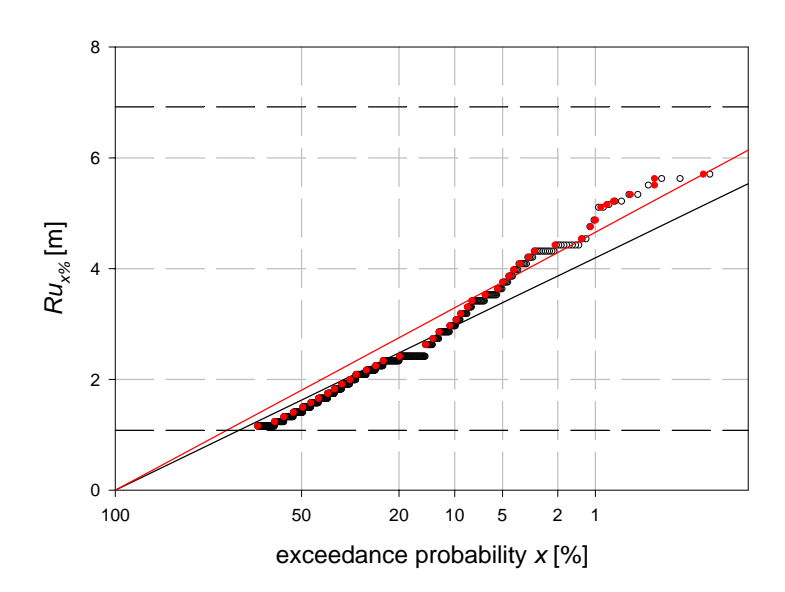


Figure B.22: Wave run-up distribution of January  $23^{rd}$ , 2000 (00h45 - 02h45).

Annex C: Results additional FCFH tests.	
Annex C-1	
Timox C I	

Table C.1: The Iribarren number  $\xi_{om}$  [-], the spectral width parameter  $\varepsilon$  [-] and the dimensionless wave run-up value exceeded by 2% of the waves  $Ru_{2\%}/H_{m0}$  [-] of the tests with water level Z + 0.00 (cfr. figure 5.33 and figure 5.22).

	0.00 (611.118	sur e e le e	una ngare e	·)·
	symbol	ξom	$Ru_{2\%}/H_{m0}$	${\cal E}$
z201		3.97	1.73	0.5351
z202	•	4.83	1.92	0.5883
z203		5.57	2.05	0.5982
z301		3.87	1.45	0.5334
z302	•	4.78	1.44	0.5460
z303		5.43	1.65	0.5958
z401		3.85	1.20	0.5463
z402	<b>A</b>	4.76	1.65	0.5504
z403		5.42	1.74	0.5929
z501		3.86	1.63	0.5459
z502	•	4.75	1.76	0.5518
z503		5.45	2.05	0.5945

Table C.2: The Iribarren number  $\xi_{om}$  [-], the spectral width parameter  $\varepsilon$  [-] and the dimensionless wave run-up value exceeded by 2% of the waves  $Ru_{2\%}/H_{m0}$  [-] of the tests with water level Z + 2.00 (cfr. figure 5.34 and figure 5.22).

	symbol	ξom	$Ru_{2\%}/H_{m0}$	${\cal E}$
z204		3.90	1.44	0.5398
z205	•	4.79	1.97	0.5363
z206		5.39	2.36	0.5998
z304		3.78	1.54	0.5375
z305	•	4.62	1.71	0.5519
z306		5.34	1.97	0.5990
z404		3.71	1.13	0.5371
z405	<b>A</b>	4.56	1.49	0.5614
z406		5.28	1.91	0.5906
z504		3.79	1.47	0.5374
z505	•	4.66	1.83	0.5462
z506		5.35	2.14	0.5982

Table C.3: The Iribarren number  $\xi_{om}$  [-], the spectral width parameter  $\varepsilon$  [-] and the dimensionless wave run-up value exceeded by 2% of the waves  $Ru_{2\%}/H_{m0}$  [-] of the tests with water level Z + 4.00 (cfr. figure 5.35 and figure 5.22).

	.00 (CII . IIg	gure 3.33	anu ngure s	•44)•
	symbol	ξom	$Ru_{2\%}/H_{m0}$	${\cal E}$
z207ra		3.84	1.64	0.5140
z207rb		3.77	1.68	0.5134
z208ra	•	4.63	1.75	0.5662
z208rb	•	4.54	1.79	0.5727
z209ra		5.39	1.81	0.5453
z209rb		5.35	1.83	0.5428
z307		3.74	1.71	0.5048
z308	•	4.56	1.72	0.5528
z309		5.28	1.83	0.5399
z407ra		3.71	1.36	0.5039
z407rb		3.74	1.45	0.5049
z408ra	•	4.54	1.50	0.5545
z408rb		4.55	1.47	0.5515
z409ra		5.25	1.68	0.5396
z409rb		5.28	1.62	0.5412
z507ra		3.71	1.70	0.5333
z507rb		3.76	1.72	0.5039
z508ra	•	4.57	1.69	0.5543
z508rb	•	4.56	1.67	0.5510
z509ra		5.30	1.75	0.5409
z509rb		5.28	1.76	0.5393

Table C.4: The Iribarren number  $\xi_{om}$  [-], the spectral width parameter  $\varepsilon$  [-] and the dimensionless wave run-up value exceeded by 2% of the waves  $Ru_{2\%}/H_{m0}$  [-] of the tests with water level Z + 6.00 (cfr. figure 5.36 and figure 5.22).

		oloo (ciii iig	ui e 2.20 t	ana ngare e	·)·
		symbol	ξom	$Ru_{2\%}/H_{m0}$	${\cal E}$
Z	210		3.88	1.38	0.5010
Z	211	•	4.64	1.36	0.5551
z	212		5.47	1.46	0.5669
Z	310		3.75	1.31	0.4961
Z	311		4.55	1.26	0.5523
z	312		5.34	1.32	0.5557
Z	410		3.70	1.31	0.5069
Z	411	<b>A</b>	4.52	1.27	0.5503
z	412		5.31	1.33	0.5577
Z	510		3.70	1.33	0.5037
Z	511	•	4.43	1.24	0.5704
z	512		5.27	1.33	0.5627

Table C.5: Results additional FCFH tests – wave characteristics test series z2.

				cha	ıracı	teris	tics	test	seri	es z	2.				
$\xi_{op}$ [-] number of waves [-]	286	816	715	663	786	713	1000	866	798	798	689	688	988	784	684
$\xi_{op}$ [-]	4.54	5.47	6.72	4.11	5.86	5.97	4.59	4.50	5.22	5.12	6.71	6.65	4.51	5.04	6.18
$\xi_{om}$ [-]	3.97	4.83	5.57	3.90	4.79	5.39	3.84	3.77	4.63	4.54	5.39	5.35	3.88	4.64	5.47
$Q_{\rho}$ [-]	3.031	2.368	2.327	3.223	3.291	2.442	3.113	3.153	3.338	3.488	2.931	2.986	3.374	3.562	3.074
$\varepsilon$ [-]	0.5351	0.5883	0.5982	0.5398	0.5363	0.5998	0.5140	0.5134	0.5662	0.5727	0.5453	0.5428	0.5010	0.5551	0.5669
$T_{01}\left[ \mathbf{s}\right]$	6.7	8.1	9.2	9.9	8.4	9.2	9.9	9.9	8.2	8.2	9.5	9.5	6.7	8.4	9.6
$\mathcal{T}_{ ho}\left[\mathrm{s}\right]$	7.6	9.1	1.1	7.0	10.2	10.2	7.9	7.9	9.3	9.3	11.9	11.9	7.7	9.1	10.9
$H_{m0}$ [m]	2.60	2.57	2.52	2.67	2.81	2.70	2.71	2.81	2.92	3.03	2.89	2.95	2.72	3.02	2.85
test n°	z201	z202	z203	z204	z205	z206	z207ra	z207rb	z208ra	z208rb	z209ra	z209rb	z210	z211	z212

Table C.6: Results additional FCFH tests – wave characteristics test series z3.

es [-]			CHAI	racu	erisi	ics (	est :	serie	es zo	<b>).</b>		
$\xi_{op}$ [-] number of waves [-]	066	805	714	962	792	402	994	791	289	986	783	681
$\xi_{op}$ [-]	4.45	6.23	6.55	4.00	5.46	5.55	4.44	5.10	6.54	4.35	4.85	6.01
ξom [-]	3.87	4.78	5.43	3.78	4.62	5.34	3.74	4.56	5.28	3.75	4.55	5.34
$Q_{\rho}$ [-]	3.046	2.443	2.351	3.199	3.254	2.475	3.167	3.411	2.959	3.369	3.435	3.062
[-]3	0.5334	0.5460	0.5958	0.5375	0.5519	0.5990	0.5048	0.5528	0.5399	0.4961	0.5523	0.5557
$\mathcal{T}_{O^{1}}[\mathbf{s}]$	9.9	8.2	9.2	9.9	8.3	9.3	9.9	8.3	9.6	6.7	8.4	9.6
$T_{ ho}\left[\mathrm{s}\right]$	9.7	10.6	1.	7.0	9.8	9.6	7.9	9.3	11.9	7.7	9.0	10.9
$H_{m0}$ [m] $T_{\rho}$ [s] $T_{01}$ [s]	2.71	2.69	2.65	2.82	2.98	2.78	2.89	3.06	3.04	2.92	3.15	3.01
test n°	z301	z302	z303	z304	z305	z306	z307	z308	z309	z310	z311	7312

Table C.7: Results additional FCFH tests – wave characteristics test series z4.

				cna	ıracı	teris	tics	test	seri	les z	4.				
number of waves [-]	992	807	715	866	797	711	866	994	793	791	688	289	066	782	682
ξ <sub>op</sub> [-]	4.18	6.22	69.9	3.94	5.42	5.83	4.43	4.44	5.08	5.08	6.53	6.55	4.31	4.82	5.99
ξ <sub>om</sub> [-]	3.85	4.76	5.42	3.71	4.56	5.28	3.71	3.74	4.54	4.55	5.25	5.28	3.70	4.52	5.31
۵ <sub></sub> [-]	3.039	2.414	2.334	3.212	3.195	2.491	3.137	3.149	3.381	3.438	2.958	2.944	3.336	3.442	3.071
[-] 3	0.5463	0.5504	0.5929	0.5371	0.5614	0.5906	0.5039	0.5049	0.5545	0.5515	0.5396	0.5412	0.5069	0.5503	0.5577
T <sub>01</sub> [s]	9.9	8.1	9.2	9.9	8.2	9.2	9.9	9.9	8.3	8.3	9.6	9.6	9.9	8.4	9.6
$\mathcal{T}_{\rho}\left[\mathbf{s}\right]$	7.2	10.6	11.3	7.0	9.8	10.2	7.9	7.9	9.3	9.3	11.9	11.9	7.7	9.0	10.9
<i>H</i> <sub>m0</sub> [m]	2.73	2.70	2.66	2.91	3.03	2.83	2.90	2.89	3.08	3.08	3.05	3.03	2.97	3.19	3.03
test n°	z401	z402	z403	z404	z405	z406	z407ra	z407rb	z408ra	z408rb	z409ra	z409rb	z410	z411	z412

Table C.8: Results additional FCFH tests – wave characteristics test series z5.

				cha	ıracı	teris	tics	test	seri	es z	5.					
$\xi_{op}$ [-] number of waves [-]	994	808	714	966	789	602	1001	663	791	791	989	989	992	792	683	
$\xi_{op}$ [-]	4.19	6.22	6.57	4.02	5.49	5.56	3.85	4.46	5.10	5.09	6.57	6.54	4.32	4.78	5.96	
ξom [-]	3.86	4.75	5.45	3.79	4.66	5.35	3.71	3.76	4.57	4.56	5.30	5.28	3.70	4.43	5.27	
$Q_{\rho}$ [-]	3.066	2.426	2.357	3.191	3.313	2.503	3.114	3.173	3.456	3.481	2.967	3.013	3.316	3.343	3.041	
[-]	0.5459	0.5518	0.5945	0.5374	0.5462	0.5982	0.5333	0.5039	0.5543	0.5510	0.5409	0.5393	0.5037	0.5704	0.5627	
$\mathcal{T}_{07}\left[\mathbf{s}\right]$	9.9	8.1	9.2	9.9	8.3	9.3	9.9	9.9	8.3	8.3	9.6	9.6	9.9	8.3	9.6	
$\mathcal{T}_{ ho}\left[\mathrm{s}\right]$	7.2	10.6	1.7	7.0	9.8	9.6	8.9	7.9	9.3	9.3	11.9	11.9	7.7	9.0	10.9	
$H_{mo}$ [m]	2.71	2.70	2.63	2.79	2.95	2.77	2.89	2.87	3.06	3.07	3.02	3.04	2.97	3.24	3.07	
test n°	z501	z502	z503	z504	z505	2506	z507ra	z507rb	z508ra	z508rb	z509ra	z509rb	z510	z511	z512	

Table C.9: Results additional FCFH tests – wave run-up test series z2.

	•					S	eries	s z2.							
$Ru_2\%H_{m0}$ [-]	1.73	1.92	2.05	1.44	1.97	2.36	1.64	1.68	1.75	1.79	1.81	1.83	1.38	1.36	1.46
<i>Ru<sub>50%</sub></i> [m]	2.430	2.790	3.030	2.230	2.380	2.440	1.520	1.520	1.700	1.910	1.670	1.940	1.830	1.950	1.980
<i>Ru</i> <sub>25%</sub> [m]	3.030	3.743	4.080	2.530	3.250	3.490	2.090	2.180	2.930	3.388	3.260	3.515	2.220	2.460	2.580
Ru <sub>s</sub> [m]	3.690	4.350	4.380	3.220	3.610	3.910	3.110	3.110	3.866	4.070	3.950	4.070	2.640	2.880	3.060
<i>Ru</i> <sub>10%</sub> [m]	4.080	4.440	4.440	3.370	3.760	4.363	3.392	3.512	4.040	4.331	4.160	4.310	2.730	2.979	3.381
<i>Ru</i> <sub>5%</sub> [m]	4.350	4.530	4.620	3.580	4.450	5.470	4.010	4.001	4.571	4.786	4.718	4.895	3.000	3.750	4.106
<i>Ru</i> <sub>2%</sub> [m]	4.500	4.930	5.175	3.846	5.518	6.370	4.444	4.714	5.104	5.424	5.240	5.384	3.745	4.110	4.170
<i>Ru</i> <sub>1%</sub> [m]	4.650	5.230	5.363	4.058	5.938	808.9	4.834	4.910	5.360	5.707	5.502	5.744	3.989	4.165	4.200
Ru <sub>max</sub> [m]	5.130	6.210	5.550	5.620	6.490	7.150	5.210	5.840	6.170	6.140	6.230	6.020	4.230	4.260	4.290
test n°	z201	z202	z203	z204	z205	z206	z207ra	z207rb	z208ra	z208rb	z209ra	z209rb	z210	z211	z212

Annex C-9

Table C.10: Results additional FCFH tests – wave run-up test series z3.

1	İ				Cot		UD ZIC	•				1
$Ru_{2\%}/H_{m0}$ [-]	1.45	1.44	1.65	1.54	1.71	1.97	1.71	1.72	1.83	1.31	1.26	1.32
<i>Ru<sub>50%</sub></i> [m]	2.040	2.325	2.730	1.500	1.510	1.690	2.090	2.270	2.000	1.800	2.550	2.550
<i>Ru</i> <sub>25%</sub> [m]	3.060	3.180	3.240	1.660	3.085	3.940	2.570	2.780	2.510	2.790	3.030	3.030
$Ru_{\rm s}$ [m]	3.300	3.444	3.510	2.470	4.210	4.510	2.840	3.170	3.350	3.090	3.270	3.240
<i>Ru<sub>10%</sub></i> [m]	3.420	3.510	3.690	3.142	4.420	4.726	2.930	3.614	4.220	3.150	3.450	3.420
<i>Ru</i> <sub>5%</sub> [m]	3.630	3.720	3.999	4.011	4.780	5.083	3.412	4.910	4.978	3.450	3.780	3.780
<i>Ru</i> <sub>2%</sub> [m]	3.935	3.883	4.380	4.330	5.097	5.489	4.940	5.270	5.576	3.808	3.960	3.990
<i>Ru</i> <sub>1%</sub> [m]	4.050	4.161	4.640	4.540	5.320	5.814	5.090	5.697	5.776	3.959	4.020	4.049
$Ru_{max}$ [m]	4.380	4.740	6.270	4.990	5.950	6.730	5.480	6.020	6.170	4.200	4.200	4.200
test n°	z301	z302	z303	z304	z305	z306	z307	z308	z309	z310	z311	z312

Table C.11: Results additional FCFH tests – wave run-up test series z4.

	1					test	ser	ies z	<b>4.</b>						
$Ru_{2\%}/H_{m0}$ [-]	1.20	1.65	1.74	1.13	1.49	1.91	1.36	1.45	1.50	1.47	1.68	1.62	1.31	1.27	1.33
<i>Ru<sub>50%</sub></i> [m]	1.680	1.710	1.770	1.840	2.170	2.230	1.500	1.500	1.500	1.500	1.550	1.610	1.530	1.620	1.620
<i>Ru</i> <sub>25%</sub> [m]	1.830	1.965	2.100	2.500	2.680	2.770	1.970	2.210	2.990	3.035	3.230	3.230	1.860	2.100	2.130
$Ru_{\rm s}$ [m]	2.070	2.400	2.848	2.740	3.040	3.154	3.050	3.110	3.558	3.500	3.560	3.590	2.130	2.595	3.010
<i>Ru<sub>10%</sub></i> [m]	2.190	2.766	3.324	2.890	3.190	3.400	3.350	3.350	3.650	3.620	3.710	3.770	2.292	3.384	3.690
<i>Ru<sub>5%</sub></i> [m]	2.580	3.810	4.182	3.123	3.651	4.210	3.620	3.680	4.088	3.941	4.310	4.400	2.940	3.960	3.990
<i>Ru</i> <sub>2%</sub> [m]	3.270	4.470	4.631	3.280	4.524	5.410	3.950	4.190	4.610	4.520	5.118	4.916	3.896	4.050	4.050
<i>Ru</i> <sub>1%</sub> [m]	3.782	4.579	4.880	3.580	5.019	5.930	4.182	4.408	5.095	4.970	5.240	5.174	3.990	4.080	4.080
Ru <sub>max</sub> [m]	4.590	5.340	5.490	4.600	6.040	6.940	5.390	5.120	5.990	2.600	5.990	5.960	4.200	4.200	4.290
test n°	z401	z402	z403	z404	z405	z406	z407ra	z407rb	z408ra	z408rb	z409ra	z409rb	z410	z411	z412

Table C.12: Results additional FCFH tests – wave run-up test series z5.

	test series z5.														
$Ru_{2\%}/H_{m0}$ [-]	1.63	1.76	2.05	1.47	1.83	2.14	1.70	1.72	1.69	1.67	1.75	1.76	1.33	1.24	1.33
<i>Ru<sub>50%</sub></i> [m]	2.280	2.520	2.700	1.900	2.200	2.320	1.820	1.790	2.030	2.030	2.120	2.090	1.830	1.830	2.160
<i>Ru</i> <sub>25%</sub> [m]	2.910	3.120	3.390	2.530	2.980	3.400	2.390	2.360	3.320	3.350	3.530	3.530	2.910	2.985	3.000
<i>Ru</i> <sub>s</sub> [m]	3.270	3.870	4.108	2.920	3.880	4.172	3.350	3.350	3.770	3.767	3.890	3.907	3.030	3.510	3.640
<i>Ru<sub>10%</sub></i> [m]	3.600	4.089	4.374	3.220	4.120	4.552	3.530	3.557	4.082	4.160	4.361	4.370	3.120	3.720	3.870
<i>Ru<sub>5%</sub></i> [m]	4.131	4.380	4.830	3.760	4.797	5.392	3.890	3.964	4.901	4.880	4.999	4.940	3.510	3.930	4.020
<i>Ru</i> <sub>2%</sub> [m]	4.410	4.770	5.402	4.107	5.410	5.933	4.910	4.921	5.180	5.120	5.287	5.364	3.952	4.020	4.080
<i>Ru</i> <sub>1%</sub> [m]	4.500	4.890	5.821	4.510	5.710	6.242	5.081	5.030	5.614	5.360	5.801	5.570	4.020	4.050	4.080
Ru <sub>max</sub> [m]	5.280	6.210	6.360	5.380	6.550	7.090	2.690	5.570	6.110	5.840	6.020	5.990	4.140	4.200	4.230
test n°	z501	z502	z503	z504	z505	z506	z507ra	z507rb	z508ra	z508rb	z509ra	z509rb	z510	z511	z512

Annex C-12

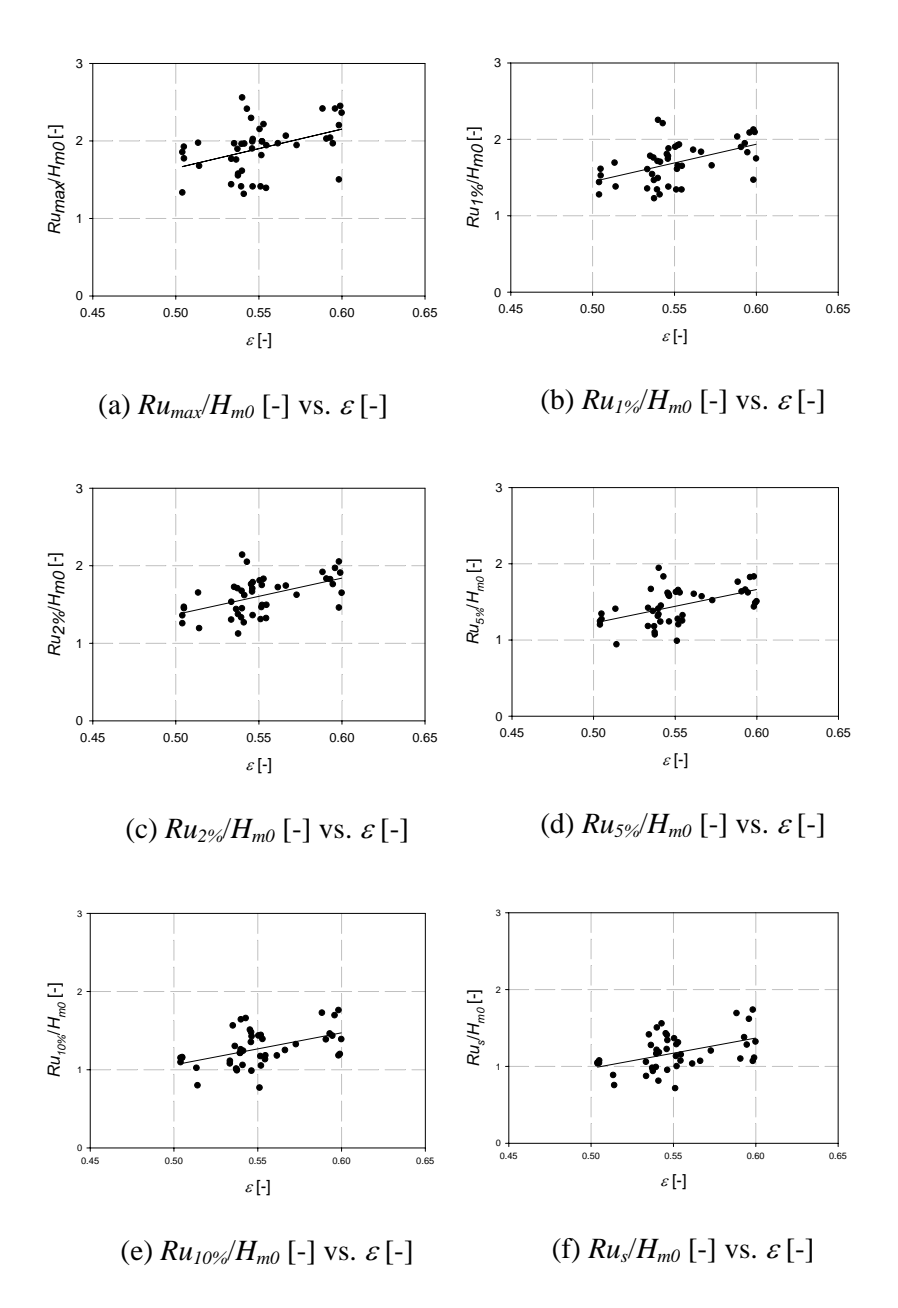


Figure C.1:  $Ru_{x\%}/H_{m\theta}$  versus the spectral width parameter  $\varepsilon$ .

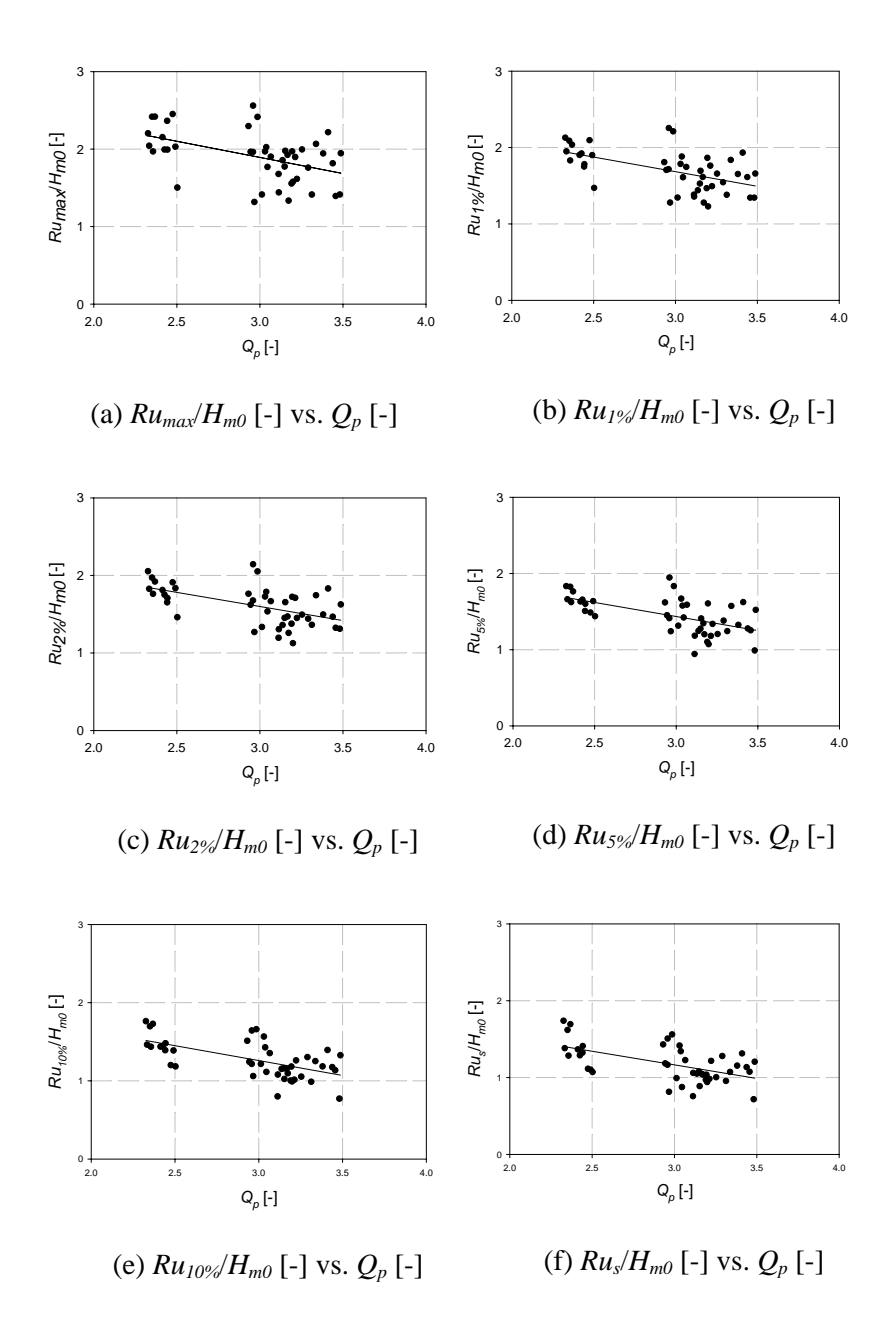


Figure C.2:  $Ru_{x\%}/H_{m0}$  versus the peakedness parameter  $Q_p$ .

Annex D: Test matrix additional UGent tests.											
Amour D 1											
Annex D-1											

Table D.1: Test matrix -d = 0.25 m.

test		$H_{\rm s}$ [m]	T [c]	$T_0$ [s]	$t_0$ [s]	<i>t</i> [c]
core 1 <sup>(*)</sup>	core 2 <sup>(*)</sup>	11 <sub>S</sub> [111]	$T_{\rho}$ [s]	10[8]	ι <sub>0</sub> [S]	$t_f[s]$
1	44	0.06	1.0	1100	115	960
2	45	0.08	1.0	1100	115	960
3	46	0.10	1.0	1100	115	960
4	47	0.06	1.2	1300	135	1140
5	48	0.07	1.2	1300	135	1140
6	49	0.08	1.2	1300	135	1140
7	50	0.09	1.2	1300	135	1140
8	51	0.06	1.5	1600	165	1410
9	52	0.08	1.5	1600	165	1410
10	53	0.10	1.5	1600	165	1410
11	54	0.06	1.8	2000	205	1770
12	55	0.07	1.8	2000	205	1770
13		0.08	1.8	2000	205	1770
14		0.10	1.8	2000	205	1770

Table D.2: Test matrix -d = 0.30 m.

		·	5	_	, O 1111	
test		<i>∐</i> [m]	T [c]	T [c]	<i>t</i> [c]	<i>t</i> [c]
core 1 <sup>(*)</sup>	core 2 <sup>(*)</sup>	$H_{\rm s}$ [m]	$T_p$ [s]	$T_0$ [s]	$t_0$ [s]	$t_f[s]$
15	56	0.06	1.0	1000	105	870
16	57	0.07	1.0	1000	105	870
17	58	0.06	1.2	1200	125	1050
18	59	0.07	1.2	1200	125	1050
19	60	0.08	1.2	1200	125	1050
20	61	0.06	1.5	1500	155	1320
21	62	0.08	1.5	1500	155	1320
22	63	0.10	1.5	1500	155	1320
23	64	0.06	1.8	1800	185	1590
24	65	0.08	1.8	1800	185	1590
25	66	0.10	1.8	1800	185	1590

Table D.3: Test matrix -d = 0.35 m.

tes		∐ [m]	T [c]	T [c]	<i>f</i> [c]	<i>t</i> [c]
core 1 <sup>(*)</sup>	core 2 <sup>(*)</sup>	$H_{\rm s}$ [m]	$T_p$ [s]	$T_0$ [s]	$t_0$ [s]	$t_f[s]$
26	67	0.06	1.0	1000	105	870
27	68	0.07	1.0	1000	105	870
28	69	0.08	1.0	1000	105	870
29	70	0.09	1.0	1000	105	870
30	71	0.06	1.2	1200	125	1050
31	72	0.07	1.2	1200	125	1050
32	73	0.08	1.2	1200	125	1050
33	74	0.09	1.2	1200	125	1050
34	75	0.06	1.5	1500	155	1320
35	76	0.06	1.5	1600	165	1410
36	77	0.07	1.5	1500	155	1320
37	78	0.07	1.5	1600	165	1410
38	79	0.08	1.5	1500	155	1320
39	80	0.08	1.5	1600	165	1410
40	81	0.10	1.5	1500	155	1320
41	82	0.08	1.8	1800	185	1590
42	83	0.09	1.8	1800	185	1590
43	84	0.10	1.8	1800	185	1590

Annex E: Results additional UGent tests.											
Annex E-1											
TIMON D I											

Table E.1: Results additional RUG tests – wave characteristics tests 1 to 14.

tests 1 to 14.														
number of waves	961	914	899	1005	1010	962	979	991	1059	1039	1062	1099	1038	1100
ξ <sub>op</sub> [-]	3.13	3.28	2.83	4.15	4.02	3.89	3.75	5.22	5.34	4.38	7.04	6.64	5.91	5.90
ξom [-]	3.23	3.08	2.99	3.57	3.52	3.46	3.23	4.55	3.99	3.64	80.9	5.26	5.13	4.51
Q <sub>p,i</sub> [-]	2.798	2.801	3.198	2.477	2.674	2.539	2.652	2.501	2.200	2.040	2.057	1.651	1.969	1.574
[-]	0.4418	0.4352	0.3969	0.4769	0.4431	0.4619	0.4702	0.5029	0.5509	0.5339	0.5710	0.5670	0.5887	0.5874
$\mathcal{T}_{\mathcal{O}_{\mathcal{I}}}$	6.0	6.0	6.0	1.0	1.0	1.0	1.0	1.3	1.2	1.2	1.5	4.1	1.5	1.4
$\mathcal{T}_{ ho}\left[\mathbf{s}\right]$	6.0	1.0	6.0	1.2	<u></u>	1.2	1.2	4.	1.6	4.	1.7	1.8	1.7	1.9
C, [-]	0.245	0.243	0.232	0.300	0.276	0.297	0.304	0.376	0.367	0.365	0.426	0.418	0.427	0.408
H <sub>mo,r</sub> [m]	0.013	0.015	0.016	0.016	0.015	0.019	0.021	0.020	0.022	0.027	0.017	0.021	0.026	0.028
H <sub>m0,i</sub> [m] H <sub>m0,r</sub> [m]	0.051	0.062	0.069	0.055	0.056	0.063	0.070	0.053	090.0	0.075	0.041	0.051	090.0	690.0
σ [m]	0.25	0.25	0.25	0.25	0.25	0.25	0.25	0.25	0.25	0.25	0.25	0.25	0.25	0.25
test n°	<del>-</del>	7	က	4	5	9	7	∞	တ	10	7	12	13	14

Table E.2: Results additional RUG tests – wave characteristics tests 15 to 25.

	tests 15 to 25.											
number of waves	864	863	947	879	916	978	986	953	1012	686	949	
ξ <sub>op</sub> [-]	3.17	3.20	3.73	4.04	3.50	4.62	4.60	4.32	5.75	5.48	4.93	
ξom [-]	3.18	2.99	3.49	3.53	3.17	4.41	3.77	3.66	5.61	4.87	4.42	
Q <sub>p,i</sub> [-]	2.715	3.525	2.864	2.908	2.884	2.365	2.131	2.220	2.346	1.868	1.915	
[-]	0.4459	0.4113	0.4879	0.4386	0.4636	0.5115	0.5362	0.5454	0.5259	0.6049	0.5988	
$\mathcal{T}_{O1}$	6.0	6.0	1.0	<del>.</del> .	1.0	1.2	1.2	1.2	4.	4.	1.5	
$T_{ ho}\left[\mathrm{s}\right]$	6.0	6.0	1.0	1.2	<u></u>	1.2	<b>4</b> .	<del>1</del> .	4.	1.6	1.7	
C, [-]	0.228	0.211	0.262	0.281	0.257	0.358	0.359	0.366	0.424	0.438	0.446	
H <sub>mo,r</sub> [m]	0.012	0.013	0.014	0.017	0.018	0.018	0.024	0.028	0.018	0.026	0.035	
$H_{m0,i}$ [m] $H_{m0,r}$ [m]	0.054	0.061	0.054	0.062	0.070	0.051	0.068	0.077	0.043	0.059	0.078	
σ [m] <i>ρ</i>	0:30	0.30	0.30	0.30	0.30	0.30	0.30	0.30	0.30	0.30	0.30	
test n°	15	16	17	18	19	20	21	22	23	24	25	

Table E.3: Results additional RUG tests – wave characteristics tests 26 to 41.

	tests 26 to 41.												
number of waves	872	831	850	798	626	913	1017	1008	1016	972			
ξ <sub>op</sub> [-]	3.19	3.26	2.60	2.84	4.18	3.53	4.88	5.18	4.09	5.75			
ξom [-]	3.07	2.93	2.81	2.77	3.59	3.33	4.55	4.24	3.62	4.87			
Q <sub>p,i</sub> [-]	3.245	3.043	3.321	3.475	2.407	2.497	2.476	2.393	2.487	2.206			
<i>G</i> <sup>[-]</sup>	0.3839	0.4286	0.3818	0.3838	0.4719	0.4311	0.5092	0.5658	0.5028	0.5769			
$\mathcal{T}_{O1}$	6.0	6.0	6.0	1.0	1.0	1.0	1.2	1.2	1.2	4.1			
$T_{ ho}\left[\mathrm{s}\right]$	6.0	1.0	0.8	1.0	<del></del>	<del></del>	1.3	1.5	<del>1</del> .	1.7			
C, [-]	0.247	0.251	0.233	0.239	0.278	0.276	0.369	0.361	0.361	0.409			
H <sub>mo,r</sub> [m]	0.014	0.017	0.017	0.020	0.014	0.018	0.019	0.021	0.029	0.025			
H <sub>m0,i</sub> [m] H <sub>m0,r</sub> [m]	0.057	0.068	0.071	0.083	0.050	0.063	0.050	0.059	0.080	0.061			
d [m]	0.35	0.35	0.35	0.35	0.35	0.35	0.35	0.35	0.35	0.35			
test n°	26	27	28	29	30	31	35	37	39	41			

Table E.4: Results additional RUG tests – wave characteristics tests 44 to 55.

	tests 44 to 55.											
number of waves	964	915	968	1004	1003	932	919	1010	1029	975	666	1004
ξορ [-]	3.13	3.31	2.85	4.38	4.05	3.76	3.84	5.55	4.69	4.44	6.95	6.41
ξom [-]	3.25	3.11	3.02	3.81	3.57	3.49	3.49	4.81	4.10	3.82	90.9	5.75
Q <sub>p,i</sub> [-]	2.779	2.766	3.230	2.158	2.503	2.249	2.355	2.100	2.019	2.427	2.135	2.358
<i>E</i> ; [-]	0.4425	0.4406	0.3992	0.5198	0.4591	0.4968	0.4998	0.5798	0.5751	0.5518	0.5938	0.5982
$\mathcal{T}_{01}$	6.0	6.0	6.0	1.0	1.0	7.	1.7	1.2	1.2	1.3	1.6	1.6
$T_{ ho}\left[\mathrm{s}\right]$	8.0	1.0	6.0	1.2	7.	1.2	1.2	1.4	4.1	1.5	1.8	1.7
C, [-]	0.254	0.256	0.245	0.304	0.296	0.353	0.347	0.390	0.395	0.400	0.487	0.468
<i>H</i> <sub>mo,r</sub> [m]	0.013	0.016	0.017	0.015	0.016	0.023	0.024	0.018	0.024	0.031	0.023	0.024
$H_{m0,i}$ [m] $H_{m0,r}$ [m]	0.051	0.061	0.068	0.048	0.055	990.0	0.068	0.046	090.0	0.077	0.046	0.051
<i>d</i> [m]	0.25	0.25	0.25	0.25	0.25	0.25	0.25	0.25	0.25	0.25	0.25	0.25
test n°	44	45	46	47	48	49	90	51	52	53	54	55

Table E.5: Results additional RUG tests – wave characteristics tests 56 to 66.

	tests 56 to 66.											
number of waves	859	863	901	885	919	1010	934	863	992	993	961	
ξ <sub>op</sub> [-]	3.17	3.21	4.10	3.55	4.07	5.03	4.84	4.04	6.58	5.06	5.05	
ξom [-]	3.20	3.00	3.58	3.48	3.28	4.58	4.07	3.99	5.64	4.61	4.40	
Q <sub>p,i</sub> [-]	2.713	3.488	3.115	2.568	2.351	2.184	2.264	1.930	2.116	2.073	2.151	
[-]	0.4415	0.4103	0.4789	0.4637	0.5075	0.5050	0.5336	0.5384	0.5085	0.5795	0.5588	
$\mathcal{T}_{O1}$	6.0	6.0	1.0	1.0	1.0	1.2	1.2	1.3	4.	4.	1.5	
$T_{ ho}\left[\mathrm{s}\right]$	6.0	6.0	1.2	<del>.</del> .	1.2	1.3	1.5	<del>1</del> .	1.7	1.6	1.7	
C, [-]	0.234	0.222	0.281	0.283	0.283	0.335	0.363	0.413	0.414	0.420	0.407	
H <sub>mo,r</sub> [m]	0.013	0.013	0.016	0.018	0.018	0.015	0.024	0.033	0.018	0.027	0.031	
$H_{m0,i}$ [m] $H_{m0,r}$ [m]	0.054	0.061	0.057	0.063	0.065	0.044	0.065	0.079	0.044	0.065	0.077	
d [m]	0:30	0.30	0.30	0.30	0.30	0.30	0.30	0.30	0.30	0.30	0:30	
test n°	99	25	28	29	09	61	62	63	64	65	99	

Table E.6: Results additional RUG tests – wave characteristics tests 67 to 75.

	tests 67 to 75.										
number of waves	880	840	855	802	926	901	926	894	979		
ξ <sub>op</sub> [-]	3.13	3.35	2.67	2.93	4.38	3.32	3.05	3.25	5.95		
ξom [-]	3.11	2.99	2.87	2.84	3.54	3.20	3.01	3.09	4.63		
Q <sub>p,i</sub> [-]	3.232	3.031	3.270	3.478	2.600	3.114	2.827	2.667	1.996		
<i>[-]</i>	0.3921	0.4276	0.3939	0.3872	0.4646	0.4380	0.4425	0.4728	0.5153		
$\mathcal{T}_{O1}$	6.0	6.0	6.0	1.0	1.0	1.0	1.0	1.0	1.2		
$T_{ ho}\left[\mathrm{s}\right]$	6.0	1.0	0.8	1.0	1.2	<del></del>	1.0	<del>[</del>	1.5		
C, [-]	0.219	0.224	0.218	0.224	0.235	0.243	0.254	0.265	0.328		
H <sub>mo,r</sub> [m]	0.012	0.015	0.015	0.018	0.013	0.017	0.019	0.021	0.015		
$d[m] H_{m0,i}[m] H_{m0,r}[m] C_r[-]$	0.054	0.065	0.067	0.078	0.055	0.071	0.077	0.078	0.046		
σ[m]	0.35	0.35	0.35	0.35	0.35	0.35	0.35	0.35	0.35		
test n°	29	89	69	20	71	72	73	74	75		

Table E.7: Results additional RUG tests – wave characteristics tests 76 to 84.

	1		te	sts 7	6 to	84.			ī
number of waves	266	902	1041	895	1039	965	1028	970	939
ξ <sub>op</sub> [-]	5.49	4.38	4.07	4.23	4.43	3.91	4.94	6.07	4.84
ξom [-]	4.62	4.18	4.04	4.03	3.83	3.41	4.68	4.89	4.32
Q <sub>p,i</sub> [-]	2.627	2.515	2.706	2.886	2.730	2.739	1.991	2.327	2.383
[-] '9	0.5411	0.5328	0.4770	0.5223	0.5164	0.4666	0.5577	0.5535	0.5000
T <sub>01</sub>	1.2	1.3	1.2	1.3	1.2	1.2	4.	4.	1.5
$T_{ ho}$ [s]	1.5	1.3	1.2	4.	4.	4.	4.	4.8	1.7
C, E	0.337	0.369	0.309	0.345	0.315	0.311	0.396	0.423	0.397
H <sub>mo,r</sub> [m]	0.017	0.024	0.019	0.025	0.021	0.027	0.023	0.026	0.033
$d[m] H_{mo,i}[m] H_{mo,r}[m] C_r[-]$	0.051	0.0666	0.061	0.072	0.068	0.087	0.059	0.061	0.083
σ [m]	0.35	0.35	0.35	0.35	0.35	0.35	0.35	0.35	0.35
test n°	9/	77	78	62	80	8	82	83	84

Table E.8: Results additional RUG tests – wave run-up tests 1 to  $14\ (RU1)$ .

						14	I (RU	J <b>I).</b>							
	$Ru_2\%/H_m$	1.38	1.38	1.25	1.14	1.49	1.45	1.42	1.17	1.53	1.41	1.28	1.69	1.54	1.54
	<i>Ru<sub>50%</sub></i> [m]	0.028	0.029	0.029	0.028	0.029	0.029	0.032	0.028	0.032	0.043	0.028	0.029	0.032	0.043
	<i>Ru<sub>25%</sub></i> [m]	0.029	0.043	0.043	0.032	0.043	0.043	0.052	0.029	0.044	0.071	0.032	0.041	0.044	0.071
Je 1	<i>Ru</i> s [m]	0.043	0.044	0.052	0.043	0.044	0.062	0.071	0.041	0.052	0.086	0.041	0.044	0.062	0.086
Run-up gauge	<i>Ru<sub>10%</sub></i> [m]	0.043	0.052	0.062	0.043	0.052	0.071	0.071	0.043	0.062	0.092	0.043	0.052	0.071	0.092
Run	<i>Ru<sub>5%</sub></i> [m]	0.044	0.071	0.071	0.052	0.071	0.086	0.086	0.044	0.071	0.099	0.044	0.067	0.086	0.099
	<i>Ru<sub>2%</sub></i> [m]	0.071	0.086	0.086	0.062	0.083	0.092	0.099	0.062	0.092	0.106	0.052	0.086	0.092	0.106
	Ru <sub>1%</sub> [m] Ru <sub>2%</sub> [m] Ru <sub>5%</sub> [m]	0.071	0.086	0.086	0.071	0.086	0.099	0.105	0.071	0.099	0.127	0.062	0.092	0.105	0.115
	$Ru_{max}$ [m]	0.086	0.099	0.099	0.092	0.105	0.127	0.129	0.086	0.115	0.146	0.071	0.115	0.183	0.174
-	test n	~	7	က	4	2	9	7	∞	တ	10	7	12	13	14

Table E.9: Results additional RUG tests – wave run-up tests 15 to 25 (RU1).

	ا ۽ ا				25	5 (RU	J <b>1).</b>					
	$Ru_2\%/H_m$ $_{oi}$ [-]	1.43	1.28	1.42	1.47	1.37	1.52	1.51	1.60	1.74	1.54	1.62
	<i>Ru<sub>50%</sub></i> [m]	0.021	0.021	0.021	0.036	0.042	0.021	0.036	0.049	0.021	0.036	0.055
	<i>Ru<sub>25%</sub></i> [m]	0.042	0.042	0.042	0.049	0.055	0.042	0.055	0.077	0.036	0.055	0.077
e 1	<i>Ru</i> s [m]	0.042	0.055	0.049	0.055	0.077	0.049	0.077	0.091	0.049	0.077	0.079
Run-up gauge	<i>Ru<sub>10%</sub></i> [m]	0.049	0.055	0.055	0.065	0.077	0.055	0.077	0.091	0.055	0.077	0.091
Run	Ru <sub>5%</sub> [m]	0.055	0.077	0.056	0.077	0.079	0.056	0.079	0.111	0.055	0.079	0.103
	Ru <sub>1%</sub> [m] Ru <sub>2%</sub> [m] Ru <sub>5%</sub> [m]	0.077	0.078	0.077	0.091	960.0	0.077	0.103	0.124	0.074	0.091	0.126
	Ru <sub>1%</sub> [m] <sub>'</sub>	0.077	0.083	0.078	0.103	0.110	0.077	0.112	0.133	0.077	0.097	0.130
	$Ru_{max}$ , [m]	0.091	0.117	0.103	0.125	0.126	960.0	0.133	0.141	0.091	0.133	0.184
0!	est n -	15	16	17	18	19	20	21	22	23	24	25

Table E.10: Results additional RUG tests – wave run-up tests 26 to 41 (RU1).

				t	o 41	(RU	1).				
	$Ru_2\%/H_m$	1.34	1.1	1.28	1.15	1.51	1.31	1.47	1.55	1.14	1.49
	<i>Ru<sub>50%</sub></i> [m]	0.027	0.028	0.028	0.029	0.028	0.028	0.028	0.029	0.041	0.029
	<i>Ru<sub>25%</sub></i> [m]	0.029	0.041	0.046	0.061	0.041	0.046	0.041	0.046	0.061	0.053
Je 1	$Ru_{\rm s}$ [m]	0.053	0.061	0.061	0.074	0.053	0.061	0.053	0.061	0.074	0.074
Run-up gauge	<i>Ru<sub>10%</sub></i> [m]	0.053	0.061	0.067	0.076	0.053	0.074	0.053	0.067	0.076	0.074
Run	Ru <sub>1%</sub> [m] Ru <sub>2%</sub> [m] Ru <sub>5%</sub> [m]	0.067	0.074	0.076	0.083	0.067	0.076	0.061	0.076	0.083	0.083
		0.076	0.076	0.091	960.0	0.076	0.083	0.074	0.091	0.091	0.091
	<i>Ru</i> <sub>1%</sub> [m]	0.083	0.083	960.0	960.0	0.076	0.091	0.076	960.0	960.0	960.0
	<i>Ru<sub>max</sub></i> [m]	0.096	0.134	0.134	0.131	0.102	0.131	0.102	0.134	0.134	0.131
0 !!	test n	56	27	28	59	30	31	35	37	39	41

Table E.11: Results additional RUG tests – wave run-up tests 44 to 55 (RU1).

					t	o 55	(RU	1).						
	$Ru_2\%/H_m$ $_{oi}$ [-]	1.38	1.32	1.27	1.45	1.48	1.46	1.51	1.40	1.42	1.47	1.27	1.59	
	<i>Ru<sub>50%</sub></i> [m]	0.009	0.009	0.026	0.009	0.015	0.026	0.031	0.018	0.037	0.048	0.015	0.026	
	<i>Ru<sub>25%</sub></i> [m]	0.020	0.037	0.048	0.026	0.037	0.053	0.064	0.037	0.053	0.070	0.037	0.042	
Je 1	$\it Ru_{\rm s}{ m [m]}$	0.037	0.059	0.064	0.042	0.059	0.064	0.070	0.042	0.064	0.081	0.042	0.053	
Run-up gauge	<i>Ru<sub>10%</sub></i> [m]	0.042	0.064	0.070	0.048	0.064	0.070	0.081	0.048	0.070	0.086	0.042	0.059	
Run	Ru <sub>1%</sub> [m] Ru <sub>2%</sub> [m] Ru <sub>5%</sub> [m]	0.053	0.070	0.075	0.064	0.070	0.081	0.086	0.059	0.081	0.097	0.053	0.070	
	<i>Ru</i> <sub>2%</sub> [m]	0.070	0.081	0.086	0.069	0.081	0.097	0.103	0.064	0.086	0.114	0.059	0.081	
	<i>Ru<sub>1%</sub></i> [m]	0.075	0.086	0.097	0.081	0.086	0.106	0.114	0.070	0.097	0.119	0.064	0.081	
	$Ru_{max}$ [m]	0.092	0.097	0.108	0.114	0.108	0.130	0.152	0.081	0.114	0.141	0.075	0.097	
	test nč	44	45	46	47	48	49	20	51	52	53	54	22	

Table E.12: Results additional RUG tests – wave run-up tests 56 to 66 (RU1).

					to 6	)6 (K	KU1).					
	$Ru_2\%/H_m$ $_{oi}$ [-]	1.36	1.36	1.21	1.45	1.48	1.32	1.40	1.36	1.23	1.40	1.33
	<i>Ru<sub>50%</sub></i> [m]	0.037	0.042	0.031	0.036	0.042	0.025	0.036	0.047	0.025	0.031	0.042
	<i>Ru<sub>25%</sub></i> [m]	0.053	0.058	0.036	0.047	0.058	0.036	0.047	0.069	0.031	0.047	0.058
Je 1	$Ru_{\rm s}{ m [m]}$	0.063	0.073	0.042	0.058	0.075	0.042	0.058	0.086	0.036	0.058	0.075
Run-up gauge	<i>Ru<sub>10%</sub></i> [m]	0.063	0.073	0.047	0.064	0.080	0.047	0.064	0.091	0.042	0.064	0.086
Run	<i>Ru<sub>5%</sub></i> [m]	0.073	0.073	0.058	0.079	0.086	0.053	0.080	0.097	0.047	0.075	0.097
	$Ru_{1\%}$ [m] $Ru_{2\%}$ [m] $Ru_{5\%}$ [m]	0.073	0.083	0.069	0.091	0.097	0.058	0.091	0.108	0.054	0.091	0.102
	<i>Ru<sub>1%</sub></i> [m]	0.079	0.086	0.080	0.102	0.102	0.068	0.097	0.108	0.064	0.097	0.108
	$Ru_{max}$ [m]	960.0	0.109	0.097	0.113	0.113	0.091	0.108	0.113	0.080	0.108	0.141
0 - 1 - 1	rest n	26	22	28	29	09	61	62	63	64	65	99

Table E.13: Results additional RUG tests – wave run-up tests 67 to 75 (RU1).

				to 7	75 (R	(U1).				
	$Ru_2\%/H_m$ $_{0i}$ [-]	1.49	1.25	1.51	1.30	1.27	1.20	1.33	1.37	1.53
	<i>Ru<sub>50%</sub></i> [m]	0.028	0.033	0.033	0.038	0.028	0.038	0.038	0.043	0.028
	<i>Ru<sub>25%</sub></i> [m]	0.038	0.049	0.049	0.059	0.043	0.049	0.054	0.059	0.038
le 1	$\it Ru_{\rm s}{ m [m]}$	0.054	0.059	0.059	0.070	0.054	0.059	0.065	0.074	0.049
Run-up gauge 1	<i>Ru<sub>10%</sub></i> [m]	0.059	0.059	0.065	0.070	0.054	0.065	0.070	0.081	0.054
Run	<i>Ru<sub>5%</sub></i> [m]	0.065	0.070	0.081	0.086	0.059	0.075	0.086	0.091	0.059
	Ru <sub>1%</sub> [m] Ru <sub>2%</sub> [m] Ru <sub>5%</sub> [m]	0.081	0.081	0.102	0.102	0.070	0.086	0.102	0.107	0.070
	<i>Ru</i> <sub>1%</sub> [m]	0.091	0.091	0.107	0.107	0.075	0.091	0.107	0.112	0.071
	$Ru_{max}$ [m]	0.102	0.118	0.128	0.112	0.118	0.112	0.134	0.144	960.0
0 9	lest n	29	89	69	20	71	72	73	74	75

Table E.14: Results additional RUG tests – wave run-up tests 76 to 84 (RU1).

i	. ~ .			to	54 (K	(UI).				i
	$Ru_2\%/H_m$ $o_i$ [-]	1.38	1.31	1.42	1.33	1.42	1.29	1.45	1.68	1.28
	<i>Ru<sub>50%</sub></i> [m]	0.033	0.038	0.038	0.043	0.043	0.054	0.038	0.049	0.054
	<i>Ru<sub>25%</sub></i> [m]	0.043	0.054	0.054	0.059	0.059	0.070	0.054	0.059	0.070
Je 1	<i>Ru</i> s [m]	0.054	0.059	0.059	0.070	0.070	0.086	0.065	0.070	0.081
Run-up gauge 1	<i>Ru<sub>10%</sub></i> [m]	0.054	0.065	0.065	0.075	0.075	0.091	0.065	0.075	0.086
Run	<i>Ru<sub>5%</sub></i> [m]	0.059	0.070	0.075	0.086	0.086	0.102	0.075	0.086	960.0
	Ru <sub>1%</sub> [m] Ru <sub>2%</sub> [m] Ru <sub>5%</sub> [m]	0.070	0.086	0.087	960.0	960.0	0.112	0.086	0.102	0.107
	<i>Ru<sub>1%</sub></i> [m]	0.070	0.091	0.094	0.102	0.102	0.123	960.0	0.107	0.112
	$Ru_{max}$ [m]	0.102	0.102	0.134	0.118	0.112	0.149	0.112	0.123	0.149
9	lest n	92	7.7	78	79	80	81	82	83	84

Table E.15: Results additional RUG tests – wave run-up tests 1 to 14 (RU2).

						14	l (RU	J <b>2).</b>							
	$Ru_2\%/H_m$ $_{oi}$ [-]	1.23	1.36	1.28	1.15	1.53	1.39	1.26	1.19	1.46	1.60	1.55	1.50	1.47	1.73
	<i>Ru<sub>50%</sub></i> [m]	0.021	0.027	0.027	0.021	0.027	0.027	0.039	0.021	0.035	0.039	0.015	0.021	0.039	0.039
	<i>Ru<sub>25%</sub></i> [m]	0.027	0.039	0.044	0.039	0.039	0.044	0.063	0.027	0.044	0.063	0.035	0.039	0.044	0.063
Je 2	$\it Ru_{\rm s}{ m [m]}$	0.039	0.061	0.063	0.039	0.054	0.063	0.063	0.039	0.063	0.085	0.039	0.044	0.063	0.076
Run-up gauge	<i>Ru<sub>10%</sub></i> [m]	0.039	0.063	0.063	0.044	0.063	0.063	0.076	0.039	0.063	0.085	0.039	0.054	0.063	0.085
Run	<i>Ru<sub>5%</sub></i> [m]	0.054	0.076	0.085	0.063	0.063	0.085	0.088	0.044	0.076	0.088	0.044	0.063	0.076	0.088
	<i>Ru<sub>1%</sub></i> [m] <i>Ru<sub>2%</sub></i> [m] <i>Ru<sub>5%</sub></i> [m]	0.063	0.085	0.088	0.063	0.085	0.088	0.088	0.063	0.088	0.120	0.063	0.076	0.088	0.120
	<i>Ru<sub>1%</sub></i> [m]	0.085	0.088	0.088	0.085	0.088	0.100	0.100	0.063	0.088	0.120	0.063	0.085	0.088	0.120
	$Ru_{max}$ [m]	0.088	0.100	0.100	0.100	0.088	0.120	0.138	0.085	0.120	0.132	0.063	0.088	0.193	0.160
-	test nč	_	7	က	4	2	9	7	80	တ	10	7	12	13	4

Table E.16: Results additional RUG tests – wave run-up tests 15 to 25 (RU2).

					to 2	25 (R	(U2).	,					
	$Ru_2\%/H_m$	1.43	1.34	1.42	1.42	1.25	1.52	1.34	1.50	1.65	1.49	1.49	
	<i>Ru<sub>50%</sub></i> [m]	0.026	0.035	0.035	0.035	0.038	0.026	0.038	0.038	0.013	0.038	0.038	
	<i>Ru<sub>25%</sub></i> [m]	0.038	0.038	0.038	0.038	0.038	0.038	0.038	0.077	0.038	0.038	0.077	
Je 2	$Ru_{\rm s}{ m [m]}$	0.038	0.050	0.038	0.050	0.070	0.038	0.070	0.088	0.038	0.070	0.088	
Run-up gauge	<i>Ru<sub>10%</sub></i> [m]	0.038	0.050	0.038	0.070	0.077	0.038	0.077	0.088	0.038	0.077	0.088	
Run	<i>Ru<sub>5%</sub></i> [m]	0.065	0.077	0.050	0.077	0.082	0.070	0.086	0.110	0.038	0.082	0.110	
	Ru <sub>1%</sub> [m] Ru <sub>2%</sub> [m] Ru <sub>5%</sub> [m]	0.077	0.082	0.077	0.088	0.088	0.077	0.091	0.116	0.070	0.088	0.116	
	<i>Ru<sub>1%</sub></i> [m]	0.077	0.088	0.082	0.101	0.101	0.077	0.111	0.132	0.077	0.101	0.142	
	$Ru_{max}$ [m]	0.088	0.115	0.101	0.119	0.114	0.088	0.119	0.143	0.088	0.143	0.161	
	test n°	15	16	17	18	19	20	21	22	23	24	25	

Table E.17: Results additional RUG tests – wave run-up tests 26 to 41 (RU2).

				t	0 41	(RU	2).				i
	$Ru_2\%/H_m$	1.21	1.20	1.31	1.12	1.32	1.45	1.28	1.57	1.17	1.51
	<i>Ru<sub>50%</sub></i> [m]	0.027	0.027	0.027	0.032	0.027	0.027	0.027	0.027	0.038	0.027
	<i>Ru<sub>25%</sub></i> [m]	0.032	0.038	0.038	090.0	0.038	0.038	0.038	0.038	090.0	0.051
je 2	$Ru_{\rm s}[{\rm m}]$	0.051	090.0	0.064	0.065	0.051	090.0	0.051	090.0	0.065	090.0
Run-up gauge 2	<i>Ru<sub>10%</sub></i> [m]	0.051	0.064	0.065	990.0	0.051	0.064	0.051	0.064	0.065	0.064
Run	<i>Ru<sub>5%</sub></i> [m]	0.064	990.0	0.069	0.092	0.064	990.0	090.0	990.0	0.071	990.0
	$Ru_{1\%}[{ m m}]Ru_{2\%}[{ m m}]Ru_{5\%}[{ m m}]$	0.069	0.082	0.093	0.093	0.066	0.092	0.064	0.092	0.093	0.092
	<i>Ru<sub>1%</sub></i> [m]	0.082	0.093	0.103	0.093	0.074	0.093	0.065	0.093	0.093	0.093
	<i>Ru<sub>max</sub></i> [m]	0.111	0.103	0.111	0.111	0.111	0.111	0.093	0.111	0.111	0.111
0 - 1 1	test n	26	27	28	29	30	31	35	37	39	41

Table E.18: Results additional RUG tests – wave run-up tests 67 to 75 (RU2).

				to 7	75 (R	(U2).	•			
	$Ru_2\%/H_m$ o:[-]	1.24	1.14	1.4	1.29	1.21	1.09	1.32	1.51	1.46
	<i>Ru<sub>50%</sub></i> [m]	0.027	0.033	0.033	0.038	0.027	0.033	0.038	0.044	0.027
	<i>Ru<sub>25%</sub></i> [m]	0.038	0.044	0.050	0.055	0.044	0.050	0.050	0.061	0.038
le 2	<i>Ru</i> s [m]	0.050	0.055	0.061	0.067	0.050	0.061	0.064	0.067	0.050
Run-up gauge 2	<i>Ru<sub>10%</sub></i> [m]	0.050	0.061	0.061	0.067	0.050	0.061	0.067	0.073	0.050
Run	Ru <sub>1%</sub> [m] Ru <sub>2%</sub> [m] Ru <sub>5%</sub> [m]	0.061	0.067	0.068	0.078	0.061	0.067	0.078	0.086	0.061
	<i>Ru</i> <sub>2%</sub> [m]	0.067	0.074	0.095	0.101	0.067	0.078	0.101	0.118	0.067
	<i>Ru</i> <sub>1%</sub> [m]	0.078	0.095	0.112	0.112	0.073	0.090	0.118	0.124	0.068
	<i>Ru<sub>max</sub></i> [m]	0.101	0.124	0.130	0.124	0.124	0.118	0.135	0.141	0.101
0 4 4	rest n	29	89	69	20	71	72	73	74	75

Table E.19: Results additional RUG tests - - wave run-up tests 76 to 84 (RU2).

				to 8	34 (R	(U2).					
	$Ru_2\%/H_m$ $oi$ [-]	1.32	1.19	1.38	1.39	1.40	1.50	1.42	1.76	1.49	
	<i>Ru<sub>50%</sub></i> [m]	0.033	0.038	0.038	0.044	0.038	0.050	0.038	0.044	0.050	
	<i>Ru<sub>25%</sub></i> [m]	0.044	0.050	0.050	0.055	0.055	0.067	0.050	0.061	0.067	
Je 2	$\it Ru_{\rm s}{ m [m]}$	0.050	0.061	0.061	0.067	0.067	0.084	0.061	0.067	0.078	
Run-up gauge 2	<i>Ru<sub>10%</sub></i> [m]	0.050	0.061	0.061	0.067	0.067	0.090	0.067	0.067	0.084	
Run	Ru <sub>1%</sub> [m] Ru <sub>2%</sub> [m] Ru <sub>5%</sub> [m]	0.061	0.067	0.067	0.084	0.078	0.116	0.070	0.084	0.107	
	<i>Ru</i> <sub>2%</sub> [m]	0.067	0.078	0.084	0.101	0.095	0.130	0.084	0.107	0.124	
	<i>Ru<sub>1%</sub></i> [m]	0.067	0.090	0.101	0.112	0.107	0.135	0.107	0.124	0.128	
	<i>Ru<sub>max</sub></i> [m]	0.112	0.112	0.141	0.130	0.130	0.141	0.130	0.141	0.141	
0: 11	test n°	92	77	78	62	80	8	82	83	84	

Annex F: Statistical tests.	
Annex F-1	

# F.1 Comparison of two data sets

The most elegant way to proof statistically that two sets of data which show a linear trend do not differ from each other significantly is to create a separate variable z. Linear regression has been used to fit the two sets of data. So, y = a + bx for the first set of data and

$$y = a + bx + cz + dzx (F.1)$$

for the second set of data. z equals 0 for the first regression line and 1 for the second regression line. Indeed, if z=0, (F.1) becomes y=a+bx, i.e. the first regression line. If z=1, the equation of the first regression line is as it was corrected to obtain the second regression line. The parameter c, resp. d indicates to what extent the intercept, resp. the slope of the first regression line has to be adjusted to arrive at the second regression line.

The value of the parameters a, b, c and d in (F.1) are estimated through the statistical computer programme SPSS. Therefore, the y values are put in the first column of the work sheet and the x, z and zx values in the second, resp. third and fourth column. Running the linear regression module, the values of a, b, c and d are given. At the same time, the t value (i.e. the ratio of the estimate of the parameter over the estimated standard error of this parameter) of all four parameters is calculated as well as the value of P. P is the probability of making a Type I error. A Type I error is rejecting the null hypothesis if it is true.

To test the null hypothesis  $H_0$ : c=0 (d=0) against the alternative hypothesis  $H_a$ :  $c \neq 0$  ( $d \neq 0$ ), a statistical two tailed t test has been performed. If the statistical test (by means of comparison of the t value of the parameters and a critical t value) on both parameters c and d indicate that these do not differ significantly from 0, one can conclude that both sets of data are the same. The null hypothesis  $H_0$  is accepted if  $t < t_{\alpha/2}$  or  $t > -t_{\alpha/2}$ . Or with other words, the rejection region is  $]-\infty$ ,  $-t_{\alpha/2}] \cup [t_{\alpha/2}, +\infty[$ .

The value of  $t_{\alpha/2}$  is based on (n - (k + 1)) degrees of freedom. n is the number of observations and k is the number of independent variables in the model. Using (F.1), k equals 4. The critical value of  $t_{n-(k+1), \alpha/2}$ , is found in standard tables in almost every book on statistics.

### F.2 Goodness-of-fit tests

These tests are used to test the hypothesis about a prescribed distribution model. The null hypothesis reads:

$$H_0: F_X(x) = F_{X,0}(x)$$
 (F.2)

with  $F_{X,0}(x)$  a prescribed distribution function. If  $F_{X,0}(x)$  is fully prescribed, a single hypothesis is tested. If only the shape of  $F_{X,0}(x)$  and not all parameters are specified, a compound hypothesis is tested. The Pearson  $\chi^2$  test and the test of Kolgomorov-Smirov are treated.

# 2.1 Pearson $\chi^2$ test

The differences between the empirical absolute frequencies and the frequencies according to the model are used. The absolute frequency of  $t_j$  (j = 1,...,k) is  $n_j$ . In case of a discrete variable is  $t_j$  one of the k possible values. In case of a continuous variable,  $t_j$  is the middle of one of the k data classes.

The theoretical relative frequency  $p_i$  is calculated as

$$p_j = p_{X,0}(t_j) \tag{F.3}$$

for a discrete variable and as

$$p_{j} = F_{X,0} \left( t_{j} + \frac{\Delta x}{2} \right) - F_{X,0} \left( t_{j} - \frac{\Delta x}{2} \right)$$
 (F.4)

for a continuous variable. The theoretical absolute frequency equals thus  $n.p_i$  with

$$n = \sum_{j=1}^{k} n_j \tag{F.5}$$

The variable

$$D_{1} = \sum_{j=1}^{k} \frac{\left(n_{j} - np_{j}\right)^{2}}{np_{j}}$$
 (F.6)

is distributed according to  $c_2$  with k-r-1 degrees of freedom. r is the number of estimated parameters. In case of a single hypothesis r equals zero. In case of a compound hypothesis, r > 0. The critical region is

$$D_1 > \chi^2_{k-r-1,1-\alpha} \tag{F.7}$$

# 2.2 Test of Kolgomorov-Smirnov

The test of Kolgomorov-Smirnov is based on the deviations between  $\hat{F}_X(x_{(i)})$  en  $F_{X,0(x_{(i)})}$  for the arranged values of  $x_{(i)}$ . The test variable

 $D_2$  is the largest absolute deviation between the cumulative relative frequency i/n and the hypothetical cumulative distribution function for the available random test values:

$$D_2 = \max_{i=1}^{n} \left| \frac{i}{n} - F_{X,0}(x_{(i)}) \right|$$
 (F.8)

In case of a single hypothesis, the distribution of  $D_2$  is independent on  $F_{X,0}$  and only dependent on the parameter n. The critical region is:

$$D_2 > c_{1-\alpha} \tag{F.9}$$

Approximately, for  $\alpha=0.05$  is  $c_{0.95}=\frac{1.3581}{\sqrt{n}}$  and for  $\alpha=0.01$  is

$$c_{0.99} = \frac{1.6276}{\sqrt{n}} \,.$$

Annex G: GWK test matrix.	
Annex G-1	
Ailles U-1	

Table G.1: Test matrix (armour layer 1, d = 3.50 m).

test n°	armour layer	<i>d</i> [m]	$H_s$ [m]	$T_p$ [s]	s <sub>op</sub> [-]	ξ <sub>ορ</sub> [-]
01	1	3.50	0.50	6.00	0.009	5.30
02	1	3.50	0.50	4.00	0.020	3.53
03	1	3.50	0.50	3.27	0.030	2.89
04	1	3.50	0.60	5.00	0.015	4.03
05	1	3.50	0.40	3.80	0.018	3.75
06	1	3.50	0.60	3.58	0.030	2.89
07	1	3.50	0.70	3.87	0.030	2.89
80	1	3.50	0.80	4.13	0.030	2.88
09	1	3.50	0.90	4.38	0.030	2.88
10	1	3.50	0.90	4.38	0.030	2.88
11	1	3.50	1.00	4.62	0.030	2.89
12	1	3.50	1.00	4.62	0.030	2.89

Table G.2: Test matrix (armour layer 1, d = 4.00 m).

test n°	armour layer	<i>d</i> [m]	$H_s$ [m]	$T_{\rho}$ [s]	s <sub>op</sub> [-]	ξ <sub>ορ</sub> [-]
13	1	4.00	0.30	1.50	0.085	1.71
14	1	4.00	0.40	5.00	0.010	4.94
15	1	4.00	0.50	5.00	0.013	4.42
16	1	4.00	0.50	6.00	0.009	5.30
17	1	4.00	0.60	3.00	0.043	2.42
18	1	4.00	0.40	2.50	0.041	2.47
19	1	4.00	0.50	4.20	0.018	3.71

Table G.3: Test matrix (armour layer 1, d = 4.50 m).

test n°	armour layer	<i>d</i> [m]	$H_{s}$ [m]	$T_{\rho}$ [s]	s <sub>op</sub> [-]	$\xi_{op}$ [-]
20	1	4.50	0.50	6.00	0.009	5.30
21	1	4.50	0.50	5.00	0.013	4.42
22	1	4.50	0.50	3.27	0.030	2.89
23	1	4.50	0.40	4.00	0.016	3.95
24	1	4.50	0.40	2.00	0.064	1.98
25	1	4.50	0.60	3.58	0.030	2.89
26	1	4.50	0.70	3.87	0.030	2.89
27	1	4.50	0.80	4.13	0.030	2.88
28	1	4.50	0.90	4.38	0.030	2.88
29	1	4.50	1.00	4.62	0.030	2.89

Table G.4: Test matrix (armour layer 1, field spectra).

test n°	armour layer	<i>d</i> [m]	H₅ [m]	$T_p$ [s]	s <sub>op</sub> [-]	ξ <sub>ορ</sub> [-]
30	1	4.50	0.60	5.27	0.014	4.25
31	1	4.50	0.60	4.63	0.018	3.73
32	1	4.50	0.60	5.44	0.013	4.39
33	1	4.50	0.60	4.24	0.021	3.42
34	1	4.50	0.60	3.85	0.026	3.11
35	1	4.80	0.80	5.28	0.018	3.69
36	1	4.80	0.80	3.85	0.035	2.69

Table G.5: Test matrix (armour layer 2, d = 3.50 m).

test n°	armour layer	<i>d</i> [m]	$H_{s}$ [m]	$T_p[s]$	s <sub>op</sub> [-]	ξ <sub>ορ</sub> [-]
37	2	3.50	0.50	6.00	0.009	5.30
38	2	3.50	0.50	4.00	0.020	3.53
39	2	3.50	0.50	3.27	0.030	2.89
40	2	3.50	0.60	4.00	0.024	3.23
41	2	3.50	0.40	3.80	0.018	3.75
42	2	3.50	0.60	3.85	0.026	3.11
43	2	3.50	0.70	3.87	0.030	2.89
44	2	3.50	0.80	4.13	0.030	2.88
45	2	3.50	0.90	4.38	0.030	2.88
46	2	3.50	0.90	4.38	0.030	2.88
47	2	3.50	1.00	4.62	0.030	2.89
48	2	3.50	1.00	4.62	0.030	2.89

Table G.6: Test matrix (armour layer 2, d = 4.00 m).

test n°	armour layer	<i>d</i> [m]	H₅ [m]	$T_{\rho}$ [s]	s <sub>op</sub> [-]	ор [-]
49	2	4.00	0.30	1.50	0.085	1.71
50	2	4.00	0.40	5.00	0.010	4.94
51	2	4.00	0.50	5.00	0.013	4.42
52	2	4.00	0.50	6.00	0.009	5.30
53	2	4.00	0.60	3.00	0.043	2.42
54	2	4.00	0.40	2.50	0.041	2.47
55	2	4.00	0.50	4.20	0.018	3.71

Table G.7: Test matrix (armour layer 2, d = 4.50 m).

test n°	armour layer	<i>d</i> [m]	H₅ [m]	$T_{\rho}$ [s]	s <sub>op</sub> [-]	ξορ [-]
56	2	4.50	0.50	6.00	0.009	5.30
57	2	4.50	0.50	5.00	0.013	4.42
58	2	4.50	0.50	3.27	0.030	2.89
59	2	4.50	0.40	4.00	0.016	3.95
60	2	4.50	0.70	5.00	0.018	3.73
61	2	4.50	0.60	3.58	0.030	2.89
62	2	4.50	0.70	3.87	0.030	2.89
63	2	4.50	0.80	4.13	0.030	2.88
64	2	4.50	0.90	4.38	0.030	2.88

Table G.8: Test matrix (armour layer 2, field spectra, d = 3.50 m).

test n°	armour layer	<i>d</i> [m]	H <sub>s</sub> [m]	$T_p$ [s]	s <sub>op</sub> [-]	ξ <sub>ορ</sub> [-]
65	2	3.50	0.60	5.29	0.014	4.27
66	2	3.50	0.60	4.62	0.018	3.73
67	2	3.50	0.60	4.24	0.021	3.42
68	2	3.50	0.60	3.46	0.032	2.79
69	2	3.50	0.60	3.80	0.027	3.06
70	2	3.50	0.60	3.89	0.025	3.14

Table G.9: Test matrix (armour layer 2, field spectra, d = 4.00 m).

test n°	armour layer	d [m]	$H_s$ [m]	$T_{\rho}$ [s]	s <sub>op</sub> [-]	$\xi_{op}$ [-]
71	2	4.00	0.60	5.29	0.014	4.27
72	2	4.00	0.40	2.50	0.041	2.47
73	2	4.00	0.60	4.24	0.021	3.42
74	2	4.00	0.60	3.46	0.032	2.79
75	2	4.00	0.60	3.80	0.027	3.06
76	2	4.00	0.60	3.85	0.026	3.11

Table G.10: Test matrix (armour layer 2, field spectra, d = 4.50

			111/0				
test n°	armour layer	<i>d</i> [m]	$H_s$ [m]	$T_p[s]$	s <sub>op</sub> [-]	ξ <sub>ορ</sub> [-]	
77	2	4.50	0.60	5.29	0.014	4.27	
78	2	4.50	0.60	4.62	0.018	3.73	
79	2	4.50	0.60	4.24	0.021	3.42	
80	2	4.50	0.60	3.46	0.032	2.79	
81	2	4.50	0.60	3.80	0.027	3.06	
82	2	4.50	0.60	3.89	0.025	3.14	

Table G.11: Test matrix (armour layer 1 & 2, additional tests).

test n°	armour layer	<i>d</i> [m]	$H_s$ [m]	$T_p$ [s]	s <sub>op</sub> [-]	$\xi_{op}$ [-]
83	1	3.50	0.50	4.00	0.020	3.53
84	1	3.50	0.70	3.50	0.037	2.61
85	1	4.00	0.50	4.00	0.020	3.53
86	1	4.00	0.50	4.00	0.020	3.53
87	1	4.00	0.50	3.50	0.026	3.09
88	1	3.95	0.50	4.00	0.020	3.53
89	1	3.95	0.50	3.50	0.026	3.09
90	1	4.50	0.50	5.00	0.013	4.42
91	2	4.50	0.60	3.00	0.043	2.42

Table G.12: Test matrix (armour layer 1, regular tests).

test n°	armour layer	<i>d</i> [m]	H₅ [m]	$T_p$ [s]	s <sub>op</sub> [-]	ξ <sub>ορ</sub> [-]
92	1	3.50	0.50	4	0.020	3.53
93	1	3.50	0.70	3.5	0.037	2.61

# Annex H: GWK test results. Annex H-1

Table H.1: GWK test results – wave characteristics tests 1 to 15.

l						1	Э.						ı
number of waves [-]	826	962	935	964	928	935	952	952	463	340	635	948	951
ξορ [-]	4.88	3.36	2.88	3.86	3.77	2.88	2.87	3.01	2.84	2.83	2.52	4.97	4.46
ξom [-]	4.35	2.99	2.53	3.35	3.20	2.52	2.53	2.50	2.50	2.51	2.16	4.19	3.75
Q <sub>p</sub> [-]	2.697	2.960	3.034	2.667	2.979	3.020	2.957	2.926	2.904	2.949	4.063	2.932	2.891
[-] 3	0.6340	0.6226	0.5866	0.6265	0.6029	0.5926	0.5998	0.5932	0.6146	0.6007	0.4430	0.5925	0.5940
T <sub>01</sub> [s]	5.1	3.4	2.8	4.2	3.2	3.1	3.4	3.6	3.8	4.0	1.7	4.3	4.3
$T_{\rho}$ [s]	2.7	3.8	3.2	4.9	3.8	3.5	3.8	4.3	4.3	4.5	2.0	5.1	5.1
$H_{mo}$ [m]	0.54	09.0	0.48	0.63	0.40	0.59	69.0	0.79	0.89	0.98	0.24	0.42	0.52
test n°	_	7	က	4	2	9	7	80	6	7	13	14	15

Table H.2: GWK test results – wave characteristics tests 16 to 27.

<b>⊢</b> I						to 2	/ <b>.</b>					
number of waves [-]	952	806	874	946	953	994	1018	991	882	926	966	1009
ξορ [-]	5.16	2.53	2.47	3.68	4.92	4.54	2.93	4.09	2.38	2.95	3.03	2.81
ξom [-]	4.39	2.25	2.32	3.22	4.44	3.82	2.56	3.41	2.14	2.56	2.58	2.53
Q <sub>p</sub> [-]	3.143	3.513	3.349	2.994	3.077	3.026	3.093	3.110	4.176	3.087	3.041	3.057
€[-]	0.6097	0.5120	0.5251	0.6028	0.6138	0.5883	0.5964	0.5901	0.4812	0.5922	0.5882	0.6092
T <sub>01</sub> [s]	5.1	2.7	2.2	3.6	5.1	4.3	2.8	3.4	2.0	3.1	3.4	3.6
$\mathcal{T}_{ ho}\left[\mathrm{s}\right]$	0.9	3.0	2.4	4.1	5.7	5.1	3.2	4.1	2.2	3.5	4.0	4.0
$H_{m0}$ [m]	0.54	0.56	0.37	0.49	0.53	0.50	0.47	0.40	0.33	0.56	0.67	0.78
test n°	16	17	18	19	20	21	22	23	24	25	26(**)	27(**)

Table H.3: GWK test results – wave characteristics tests 37 to 50.

ا سا							10 5	•						1
number of waves [-]	266	993	983	1012	1013	1000	926	1005	499	200	202	209	759	866
ξορ [-]	4.88	3.48	2.89	3.86	3.78	2.88	2.86	3.01	2.86	2.86	3.13	2.98	2.51	4.99
ξ <sub>om</sub> [-]	4.36	3.01	2.55	3.35	3.23	2.51	2.53	2.51	2.53	2.53	2.57	2.56	2.14	4.18
Q <sub>p</sub> [-]	2.753	3.023	3.035	2.727	2.995	3.046	3.022	2.954	2.850	2.851	2.636	2.617	4.208	3.053
[-] 3	0.6315	0.6058	0.5853	0.6222	0.6052	0.5893	0.5969	0.5907	0.6179	0.6193	0.5917	0.6003	0.4408	0.5911
T <sub>01</sub> [s]	5.1	3.4	2.8	4.2	3.3	3.1	3.4	3.6	3.8	3.8	4.0	4.0	1.7	4.3
$\mathcal{T}_{ ho}\left[\mathrm{s}\right]$	2.7	4.0	3.2	4.9	3.8	3.5	3.8	4.3	4.3	4.3	4.9	4.7	2.0	5.1
$H_{mo}$ [m]	0.53	09.0	0.48	0.63	0.40	0.59	69.0	0.79	0.88	0.88	96'0	96'0	0.24	0.41
test n°	37	38	39	40	41	42	43	44	45	46	47	48	49	20

Table H.4: GWK test results – wave characteristics tests 51 to 64.

l I							to o	т.						ĺ
number of waves [-]	1001	686	096	964	994	066	994	1023	1003	988	206	986	1041	717
ξ <sub>op</sub> [-]	4.47	5.19	2.45	2.50	3.83	4.96	4.52	3.13	4.11	2.95	3.85	3.01		3.09
ξom [-]	3.74	4.42	2.25	2.29	3.24	4.48	3.81	2.58	3.44	2.57	3.26	2.55	2.45	2.61
Q <sub>p</sub> [-]	3.007	3.156	3.529	3.453	3.020	3.104	3.059	3.150	3.081	3.039	3.008	3.085		3.020
[-] 3	0.5952	0.6103	0.5198	0.5123	0.5934	0.6130	0.5846	0.5795	0.5900	0.5929	0.5976	0.5854		0.5957
T <sub>01</sub> [s]	4.3	5.2	2.7	2.2	3.6	5.2	4.3	2.8	3.4	3.1	4.4	3.4	3.4	3.8
$\mathcal{T}_{ ho}\left[\mathrm{s}\right]$	5.1	6.0	2.9	2.4	4.3	2.7	5.1	3.4	4.1	3.5	5.1	4.0		4.5
<i>H</i> <sub>mo</sub> [m]	0.52	0.53	0.56	0.37	0.49	0.52	0.50	0.47	0.39	0.56	0.70	0.67	0.76	0.82
test n°	51	52	53	54	55	56	22	58	59	61	(**)09	62(**)	63(**)(°)	64(**)

Table H.5: GWK test results – wave characteristics tests 30 to 36 and 65 to 70.

h 1			ω	ou a	nu (	,5 w	, , 0.			
number of waves [-]	210	186	173	113	188	155	109	77	110	87
ξ <sub>op</sub> [-]	4.35	3.64	3.99	2.82	4.43	3.65	3.69		2.91	3.27
ξom [-]	4.26	3.72	3.81	3.22	4.31	3.65	3.61	3.67	3.33	3.49
Q <sub>p</sub> [-]	3.829	4.402	3.066	1.749	2.962	4.472	2.119		2.246	2.033
[-] 3	0.4777	0.4360	0.5719	0.6679	0.5851	0.5430	0.5999		0.6199	0.6087
<i>T</i> <sub>01</sub> [s]	5.3	4.6	4.7	4.5	5.3	4.5	4.4	4.3	4.0	4.2
$T_{\rho}$ [s]	5.4	4.5	4.9	4.0	5.4	4.5	4.5		3.5	4.0
$H_{mo}$ [m]	09'0	0.59	0.59	0.77	0.58	0.59	0.57	0.53	0.58	0.57
test n°	30(**)	31(**)	32(**)	36(**)	65	99	29	(°)89	69	70

Table H.6: GWK test results – wave characteristics tests 71 to 82.

<b>-</b> _						το δ.	<b>Z.</b>					
number of waves [-]	188	153	108	75	111	80	185	153	106	78	108	75
ξ <sub>op</sub> [-]	4.32	3.72	3.76		3.00		4.40	3.64	3.81		2.95	
ξom [-]	4.20	3.62	3.69	3.64	3.42	3.77	4.34	3.71	3.82	3.54	3.45	3.87
Q <sub>ρ</sub> [-]	3.330	2.000	2.078		2.214		3.595	5.014	2.004		2.205	
[-] 3	0.5426	0.5170	0.5853		0.6086		0.4947	0.4610	0.5946		0.6066	
T <sub>01</sub> [s]	5.3	4.5	4.4	4.4	4.0	4.5	5.3	4.5	4.5	4.2	4.1	4.8
$\mathcal{T}_{ ho}\left[\mathrm{s} ight]$	5.4	4.7	4.5		3.5		5.4	4.5	4.5		3.5	
$H_{mo}$ [m]	0.61	0.62	0.55	0.56	0.54	0.56	0.59	0.59	0.54	0.55	0.56	0.59
test n°	71	72	73	74(°)	75	(°)97	77(**)	78(**)	79(**)	80(**)(°)	81(**)	82(**)(°)

Table H.7: GWK test results – wave run-up tests 1 to 15.

Table	н./:	GV	VK	test	resu	lits -	- wa	ve r	un-ı	ıp te	ests	1 to	15.
$Ru_{2\%}/H_{m0}$ [-]	2.10	1.66	1.49	2.00	1.59	1.65	1.70	1.70	1.71	1.70	1.24	1.66	1.80
<i>Ru<sub>50%</sub></i> [m]	0.428	0.327	0.325	0.500	0.247	0.415	0.514	0.649	0.710	0.867	0.085	0.265	0.352
<i>Ru<sub>25%</sub></i> [m] <i>Ru<sub>50%</sub></i> [m]	0.695	0.460	0.435	0.735	0.380	0.571	0.714	0.871	1.011	1.110	0.165	0.398	0.531
$Ru_{ m s}$ [m]	0.828	0.571	0.505	0.868	0.460	0.679	0.847	1.066	1.179	1.286	0.205	0.515	0.662
Ru <sub>5%</sub> [m] Ru <sub>10%</sub> [m]	0.872	0.637	0.547	0.985	0.469	0.704	0.925	1.114	1.266	1.346	0.209	0.561	0.688
<i>Ru<sub>5%</sub></i> [m]	1.001	0.726	0.637	1.076	0.544	0.834	1.065	1.238	1.407	1.495	0.254	0.636	0.784
<i>Ru</i> <sub>2%</sub> [m]	1.124	0.835	0.721	1.254	0.632	0.975	1.164	1.346	1.524	1.653	0.298	0.693	0.933
<i>Ru<sub>max</sub></i> [m] <i>Ru</i> <sub>1%</sub> [m]	1.317	096.0	0.793	1.388	0.665	1.080	1.242	1.431	1.641	1.713	0.327	0.782	0.987
Ru <sub>max</sub> [m]	1.972	1.238	1.000	1.872	1.098	1.177	1.432	1.582	1.812	2.033	0.497	0.998	1.321
test n°	_	7	က	4	2	9	7	∞	6	1	13	14	15

Table H.8: GWK test results – wave run-up tests 16 to 27.

test n°	Ru <sub>max</sub> [m]	<i>Ru</i> <sub>1%</sub> [m]	<i>Ru</i> <sub>1%</sub> [m] <i>Ru</i> <sub>2%</sub> [m]		Ru <sub>5%</sub> [m] Ru <sub>10%</sub> [m]	Ru <sub>s</sub> [m]	Ru <sub>s</sub> [m] Ru <sub>25%</sub> [m] Ru <sub>50%</sub> [m]	<i>Ru<sub>50%</sub></i> [m]	$Ru_{2\%}/H_{m0}$ [-]
16	1.527	1.139	0.959	0.859	0.765	0.697	0.609	0.402	1.79
17	1.410	1.069	0.929	0.788	0.668	0.620	0.515	0.341	1.66
18	0.822	0.671	0.565	0.510	0.451	0.396	0.316	0.214	1.55
19	1.197	0.917	0.827	0.713	0.625	0.581	0.506	0.329	1.70
20	1.028	1.026	0.935	0.840	0.756	0.722	0.591	0.408	1.78
21	1.039	0.952	0.864	0.776	0.689	0.642	0.514	0.383	1.72
22	1.034	0.914	0.840	0.745	0.640	0.571	0.453	0.293	1.79
23	1.016	0.739	0.645	0.561	0.474	0.452	0.377	0.255	1.63
24	0.889	0.697	0.626	0.487	0.356	0.306	0.234	0.164	1.89
25	1.039	1.039	1.021	0.929	0.808	0.746	0.602	0.393	1.81
26(**)		1.265	1.166	1.001	0.922	0.857	0.695	0.483	1.75
27(**)		1.454	1.340	1.173	0.999	0.956	0.820	0.580	1.73

Table H.9: GWK test results – wave run-up tests 37 to 50.

rabie	C 11.	9. G		les	t res	ourts	— w	ave	ıun	-up	test	531	10 5	υ.
$Ru_2\%/H_{m0}$ [-]	2.16	1.49	1.49	2.08	1.53	1.63	1.76	1.74	1.82	1.85	1.72	1.70	1.56	1.69
<i>Ru<sub>50%</sub></i> [m]	0.429	0.351	0.330	0.490	0.257	0.401	0.519	0.621	0.747	0.736	0.879	0.844	0.103	0.316
<i>Ru<sub>25%</sub></i> [m]	0.635	0.481	0.447	0.686	0.366	0.575	0.660	0.904	1.096	1.097	1.222	1.158	0.146	0.425
<i>Ru</i> <sub>s</sub> [m]	0.781	0.568	0.534	0.916	0.444	0.640	0.846	1.118	1.272	1.288	1.347	1.308	0.181	0.513
Ru <sub>5%</sub> [m] Ru <sub>10%</sub> [m]	668.0	0.608	0.569	1.018	0.479	0.693	0.922	1.178	1.337	1.352	1.385	1.373	0.207	0.513
<i>Ru<sub>5%</sub></i> [m]	1.052	099'0	0.643	1.144	0.539	908.0	1.087	1.277	1.449	1.428	1.491	1.517	0.272	0.599
<i>Ru</i> 2% [m]	1.156	0.753	0.716	1.305	0.605	0.967	1.219	1.380	1.595	1.623	1.651	1.637	0.377	0.702
<i>Ru</i> 1% [m]	1.337	0.926	0.769	1.413	0.625	1.055	1.288	1.414	1.655	1.657	1.724	1.822	0.451	0.814
Ru <sub>max</sub> [m]	1.990	1.315	1.075	1.891	1.080	1.365	1.475	1.552	1.724	1.756	2.040	2.040	0.535	0.982
test n°	37	38	39	40	41	42	43	44	45	46	47	48	49	50

Table H.10: GWK test results - wave run-up tests 51 to 64.

Table	11.1	ιυ. (	3 44 1	x tes	st I e	Sult	5 – v	vave	iui	ւ-սբ	iesi	IS 31	w	)4.
$Ru_2\%/H_{m0}$ [-]	1.83	1.88	1.64	1.70	1.72	1.92	1.80	1.97	1.76	1.81	2.01	1.68	1.61	1.61
<i>Ru<sub>50%</sub></i> [m]	0.398	0.444	0.460	0.200	0.383	0.400	0.399	0.369	0.303	0.419	0.615	0.493	0.527	0.577
<i>Ru<sub>25%</sub></i> [m] <i>Ru<sub>50%</sub></i> [m]	0.534	0.571	0.613	0.364	0.526	0.637	0.571	0.528	0.389	0.616	0.836	0.678	0.727	0.801
$\it Ru_{\rm s}{ m [m]}$	0.620	0.816	069.0	0.470	0.603	0.701	0.657	0.627	0.475	0.742	0.988	0.803	0.889	0.947
Ru <sub>5%</sub> [m] Ru <sub>10%</sub> [m]	0.693	0.855	0.738	0.528	0.637	0.761	0.700	0.670	0.518	0.824	1.076	0.863	0.939	0.990
<i>Ru<sub>5%</sub></i> [m]	0.861	0.915	0.828	0.571	0.713	0.858	0.786	0.784	0.594	0.955	1.227	0.970	1.027	1.154
Ru <sub>max</sub> [m] Ru <sub>1%</sub> [m] Ru <sub>2%</sub> [m]	0.941	0.994	0.918	0.635	0.841	0.994	0.907	0.924	069.0	1.022	1.402	1.128	1.216	1.319
<i>Ru</i> <sub>1%</sub> [m]	0.977	1.126	1.025	0.686	906.0	1.003	1.002	0.970	0.808	1.031	1.521	1.224	1.319	1.431
Ru <sub>max</sub> [m]	1.299	1.518	1.249	0.876	1.248	1.003	1.002	1.015	0.992	1.031				
test n°	51	52	53	54	55	56	22	58	59	61	(**)09	62(**)	63(**)(°)	64(**)

Table H.11: GWK test results – wave run-up tests 30 to 36 and 65 to 70.

i	i		a	na c	<b>5</b> to	70.				
$Ru_{2\%}/H_{m0}$ [-]	1.87	1.76	1.66	1.75	2.94	2.30	1.85	2.94	2.04	2.53
<i>Ru<sub>50%</sub></i> [m]	0.422	0.418	0.406	0.329	0.583	0.555	0.482	0.310	0.387	0.359
<i>Ru<sub>25%</sub></i> [m] <i>Ru<sub>50%</sub></i> [m]	0.718	0.639	0.644	1.003	0.813	0.734	0.693	0.656	0.619	0.618
Ru <sub>s</sub> [m]	0.817	0.735	0.717	0.962	1.054	0.956	0.897	0.850	0.804	0.885
Ru <sub>2%</sub> [m] Ru <sub>5%</sub> [m] Ru <sub>10%</sub> [m]	0.849	0.771	0.763	1.032	1.131	1.078	0.960	0.933	0.882	1.076
<i>Ru<sub>5%</sub></i> [m]	0.988	0.862	0.917	1.177	1.310	1.193	1.028	1.203	1.013	1.185
<i>Ru<sub>2%</sub></i> [m]	1.129	1.039	0.972	1.345	1.714	1.346	1.059	1.555	1.176	1.442
<i>Ru<sub>1%</sub></i> [m]	1.225	1.127	1.103	1.460	1.935	1.565	1.112	1.346	1.300	1.432
Ru <sub>max</sub> [m]					1.993	1.582	1.117	1.726	1.312	1.630
test n°	30(**)	31(**)	32(**)	36(**)	65	99	29	(°)	69	20

Table H.12: GWK test results – wave run-up tests 71 to 82.

test n°	Ru <sub>max</sub> [m]	<i>Ru</i> <sub>1%</sub> [m]	<i>Ru</i> <sub>1%</sub> [m] <i>Ru</i> <sub>2%</sub> [m]		Ru <sub>5%</sub> [m] Ru <sub>10%</sub> [m]	Ru <sub>s</sub> [m]	Ru <sub>s</sub> [m] Ru <sub>25%</sub> [m] Ru <sub>50%</sub> [m]	<i>Ru<sub>50%</sub></i> [m]	$Ru_{2\%}/H_{m0}$ [-]
7.1	1.521	1.509	1.332	1.130	0.991	0.961	0.814	0.519	2.18
72	1.268	1.263	1.195	0.987	0.924	0.881	0.664	0.521	1.94
73	1.114	1.112	1.086	1.050	0.904	0.867	0.602	0.458	1.97
74(°)	1.271	0.966	1.193	1.014	0.861	0.793	0.605	0.459	2.12
75	0.980	0.979	0.970	0.932	0.867	0.825	0.625	0.414	1.78
76(°)	1.231	0.997	1.154	926.0	0.895	0.848	0.653	0.446	2.06
77(**)		1.324	1.220	1.068	0.917	0.894	0.745	0.521	2.07
78(**)		1.257	1.159	1.006	0.863	0.796	0.710	0.538	1.97
(**)62		1.225	1.129	0.971	0.856	0.795	0.706	0.455	2.10
80(**)(°)		1.127	1.039	1.009	0.841	0.785	0.635	0.369	1.89
81(**)		1.126	1.038	0.955	0.811	0.751	0.655	0.403	1.84
82(**)(°)		1.251	1.153	1.009	0.882	0.854	0.703	0.484	1.94

Table H.13: GWK test results – wave run-down tests 1 to 15.

test n°	$Rd_{max}$ [m]	<i>Rd</i> <sub>1%</sub> [m]	<i>Rd<sub>2%</sub></i> [m]	<i>Rd</i> <sub>5%</sub> [m]	<i>Rd</i> 10% [m]	Rd <sub>s</sub> [m]	<i>Rd<sub>25%</sub></i> [m]	<i>Rd<sub>50%</sub></i> [m]	$Rd_{2\%}/H_{mo}$ [-]
_	-0.455	-0.412	-0.412	-0.369	-0.326	-0.326	-0.283	-0.240	-0.77
7	-0.468	-0.348	-0.339	-0.296	-0.296	-0.283	-0.253	-0.210	-0.68
က	-0.337	-0.289	-0.259	-0.255	-0.255	-0.246	-0.212	-0.169	-0.53
4	-0.523	-0.416	-0.416	-0.373	-0.339	-0.330	-0.287	-0.244	99.0-
5	-0.382	-0.309	-0.287	-0.268	-0.244	-0.244	-0.244	-0.197	-0.72
9	-0.446	-0.359	-0.339	-0.317	-0.276	-0.274	-0.235	-0.209	-0.58
7	-0.436	-0.393	-0.380	-0.346	-0.319	-0.307	-0.264	-0.221	-0.55
∞	-0.503	-0.426	-0.413	-0.370	-0.340	-0.327	-0.288	-0.241	-0.52
<b>o</b>	-0.504	-0.450	-0.440	-0.400	-0.376	-0.354	-0.311	-0.225	-0.49
7	-0.537	-0.490	-0.466	-0.451	-0.429	-0.408	-0.343	-0.235	-0.48
13	-0.190	-0.190	-0.168	-0.146	-0.146	-0.137	-0.102	-0.102	-0.70
4	-0.545	-0.446	-0.446	-0.395	-0.314	-0.313	-0.268	-0.224	-1.07
15	-0.563	-0.481	-0.477	-0.433	-0.405	-0.388	-0.300	-0.255	-0.92

Table H.14: GWK test results – wave run-down tests 16 to

					2	7.						i
$Rd_{2\%}/H_{m0}$ [-]	-0.91	-0.48	-0.62	-0.88	-1.03	-0.97	-0.76	-1.00	-0.50	-0.63	-0.61	-0.64
<i>Rd<sub>50%</sub></i> [m]	-0.264	-0.227	-0.137	-0.204	-0.319	-0.264	-0.180	-0.216	-0.106	-0.175	-0.271	-0.339
<i>Rd</i> <sub>25%</sub> [m]	-0.326	-0.236	-0.181	-0.248	-0.408	-0.397	-0.256	-0.261	-0.106	-0.264	-0.315	-0.397
$Rd_{ m s}$ [m]	-0.402	-0.271	-0.222	-0.293	-0.452	-0.432	-0.269	-0.337	-0.146	-0.286	-0.360	-0.419
<i>Rd<sub>10%</sub></i> [m]	-0.442	-0.271	-0.226	-0.337	-0.466	-0.441	-0.300	-0.350	-0.150	-0.308	-0.360	-0.437
<i>Rd<sub>5%</sub></i> [m]	-0.477	-0.271	-0.226	-0.381	-0.497	-0.460	-0.340	-0.376	-0.150	-0.344	-0.379	-0.457
<i>Rd</i> <sub>2%</sub> [m]	-0.486	-0.271	-0.226	-0.427	-0.541	-0.486	-0.358	-0.394	-0.165	-0.353	-0.404	-0.495
<i>Rd</i> <sub>1%</sub> [m]	-0.515	-0.271	-0.257	-0.459	-0.577	-0.491	-0.358	-0.425	-0.181	-0.366	-0.422	-0.530
Rd <sub>max</sub> [m]	-0.531	-0.320	-0.270	-0.492	-0.706	-0.663	-0.402	-0.447	-0.194	-0.397	-0.448	-0.676
test n°	16	17	18	19	20	21	22	23	24	25	26(**)	27(**)

Table H.15: GWK test results – wave run-down tests 37 to 50.

	ı					3	U.							ı
$Rd_{2\%}/H_{m0}$ [-]	-0.80	-0.89	-0.76	-0.75	-1.00	-0.74	69:0-	-0.64	-0.58	-0.56	-0.53	-0.53	-0.62	-0.97
<i>Rd<sub>50%</sub></i> [m]	-0.249	-0.211	-0.163	-0.258	-0.180	-0.199	-0.231	-0.269	-0.265	-0.273	-0.282	-0.274	-0.071	-0.198
Rd <sub>25%</sub> [m] Rd <sub>50%</sub> [m]	-0.310	-0.298	-0.257	-0.347	-0.265	-0.298	-0.334	-0.368	-0.392	-0.395	-0.414	-0.401	-0.071	-0.241
$\it Rd_{\rm s} [m]$	-0.357	-0.347	-0.299	-0.399	-0.312	-0.340	-0.414	-0.415	-0.411	-0.429	-0.456	-0.439	-0.115	-0.285
<i>Rd</i> <sub>10%</sub> [m]	-0.357	-0.361	-0.304	-0.404	-0.312	-0.354	-0.419	-0.438	-0.449	-0.447	-0.461	-0.448	-0.115	-0.324
<i>Rd<sub>5%</sub></i> [m]	-0.404	-0.405	-0.336	-0.446	-0.350	-0.392	-0.457	-0.462	-0.496	-0.475	-0.508	-0.495	-0.115	-0.346
<i>Rd</i> <sub>2%</sub> [m]	-0.428	-0.446	-0.365	-0.469	-0.397	-0.439	-0.475	-0.509	-0.505	-0.494	-0.508	-0.512	-0.149	-0.402
<i>Rd</i> <sub>1%</sub> [m]	-0.451	-0.446	-0.389	-0.493	-0.425	-0.467	-0.509	-0.523	-0.552	-0.518	-0.550	-0.537	-0.158	-0.424
$Rd_{max}$ [m]	-0.498	-0.554	-0.440	-0.540	-0.476	-0.533	-0.541	-0.556	-0.561	-0.541	-0.602	-0.542	-0.158	-0.541
test n°	37	38	39	40	41	42	43	44	45	46	47	48	49	50

Table H.16: GWK test results – wave run-down tests 51 to 64.

1						U	4.							ĺ
$Rd_{2\%}H_{m0}$ [-]	-0.93	-0.92	-0.41	-0.52	-0.84	-1.01	-1.02	-0.65	-0.59	-0.42	-0.74	-0.59	-0.64	-0.58
<i>Rd<sub>50%</sub></i> [m]	-0.220	-0.226	-0.140	960'0-	-0.194	-0.306	-0.220	-0.164	-0.187	-0.148	-0.213	-0.199	-0.226	-0.275
<i>Rd<sub>25%</sub></i> [m] <i>Rd<sub>50%</sub></i> [m]	-0.303	-0.313	-0.184	-0.139	-0.238	-0.415	-0.385	-0.181	-0.230	-0.191	-0.387	-0.239	-0.335	-0.362
Rd <sub>s</sub> [m]	-0.351	-0.361	-0.227	-0.183	-0.303	-0.454	-0.438	-0.207	-0.230	-0.191	-0.445	-0.286	-0.413	-0.406
<i>Rd<sub>10%</sub></i> [m]	-0.376	-0.400	-0.227	-0.183	-0.324	-0.480	-0.438	-0.207	-0.230	-0.191	-0.470	-0.308	-0.439	-0.415
<i>Rd<sub>5%</sub></i> [m]	-0.438	-0.463	-0.227	-0.183	-0.368	-0.502	-0.481	-0.264	-0.230	-0.209	-0.496	-0.347	-0.465	-0.449
<i>Rd</i> <sub>2%</sub> [m]	-0.481	-0.487	-0.227	-0.195	-0.412	-0.524	-0.512	-0.307	-0.230	-0.237	-0.517	-0.395	-0.483	-0.474
<i>Rd</i> <sub>1%</sub> [m]	-0.490	-0.522	-0.258	-0.226	-0.443	-0.524	-0.525	-0.325	-0.248	-0.285	-0.527	-0.435	-0.487	-0.488
$Rd_{max}$ [m]	-0.524	-0.530	-0.271	-0.226	-0.498	-0.554	-0.551	-0.377	-0.326	-0.356	-0.557	-0.495	-0.517	-0.549
test n°	51	52	53	54	22	26	22	28	29	61	(**)09	62(**)	63(**)(° )	64(**)

Table H.17: GWK test results – wave run-down tests 30 to 36 and 65 to 70.

i i	Jo and 05 to 70.									
$Rd_2\%H_{mo}$ [-]	-1.17	-1.14	-1.13	-1.95	-0.78	-0.77	-0.93	-1.01	-0.89	-0.85
<i>Rd<sub>50%</sub></i> [m]	-0.411	-0.396	-0.418	-0.915	-0.250	-0.271	-0.258	-0.147	-0.229	-0.229
$Rd_{25\%}[{ m m}]\;\;Rd_{50\%}[{ m m}]$	-0.499	-0.459	-0.480	-1.265	-0.316	-0.351	-0.390	-0.349	-0.359	-0.346
$Rd_{ m s}$ [m]	-0.544	-0.506	-0.506	-1.355	-0.375	-0.389	-0.442	-0.396	-0.406	-0.405
<i>Rd<sub>5%</sub></i> [m] <i>Rd<sub>10%</sub></i> [m]	-0.579	-0.539	-0.543	-1.408	-0.410	-0.403	-0.446	-0.428	-0.450	-0.440
	-0.633	-0.583	-0.595	-1.483	-0.450	-0.437	-0.493	-0.507	-0.500	-0.482
<i>Rd<sub>2%</sub></i> [m]	-0.708	-0.672	-0.663	-1.502	-0.457	-0.450	-0.531	-0.537	-0.514	-0.487
<i>Rd</i> 1% [m]	-0.721	-0.695	-0.718	-1.525	-0.468	-0.486	-0.582	-0.419	-0.585	-0.428
Rd <sub>max</sub> [m]	-0.766	-0.761	-0.728	-1.529	-0.551	-0.497	-0.587	-0.537	-0.594	-0.487
test n°	30(**)	31(**)	32(**)	36(**)	9	99	29	(°)89	69	20

Table H.18: GWK test results – wave run-down tests 71 to 82.

<b>8</b> 2.												
$Rd_{2\%}/H_{m0}$ [-]	-0.86	-0.85	-0.91	-1.07	-0.98	-0.98	-0.94	-0.85	-0.99	1.1	-0.99	-0.94
<i>Rd<sub>50%</sub></i> [m]	-0.267	-0.261	-0.238	-0.222	-0.230	-0.242	-0.218	-0.210	-0.207	-0.169	-0.199	-0.208
<i>Rd</i> <sub>25%</sub> [m]	-0.354	-0.348	-0.346	-0.318	-0.317	-0.330	-0.425	-0.305	-0.339	-0.245	-0.278	-0.339
$Rd_{ m s}$ [m]	-0.441	-0.425	-0.417	-0.450	-0.412	-0.383	-0.486	-0.381	-0.410	-0.447	-0.434	-0.469
<i>Rd<sub>10%</sub></i> [m]	-0.459	-0.473	-0.452	-0.469	-0.448	-0.424	-0.507	-0.405	-0.430	-0.466	-0.452	-0.484
<i>Rd<sub>5%</sub></i> [m]	-0.527	-0.478	-0.499	-0.539	-0.508	-0.511	-0.523	-0.474	-0.503	-0.498	-0.521	-0.535
<i>Rd<sub>2%</sub></i> [m]	-0.527	-0.521	-0.499	-0.599	-0.534	-0.547	-0.555	-0.502	-0.532	-0.608	-0.557	-0.558
<i>Rd</i> <sub>1%</sub> [m]	-0.553	-0.521	-0.538	-0.504	-0.556	-0.474	-0.584	-0.508	-0.545	-0.540	-0.651	-0.442
Rd <sub>max</sub> [m]	-0.558	-0.521	-0.542	-0.663	-0.559	-0.585	-0.697	-0.511	-0.546	-0.684	-0.660	-0.582
test n°	71	72	73	74(°)	75	76(°)	77(**)	78(**)	79(**)	80(**)(°)	81(**)	82(**)(°)





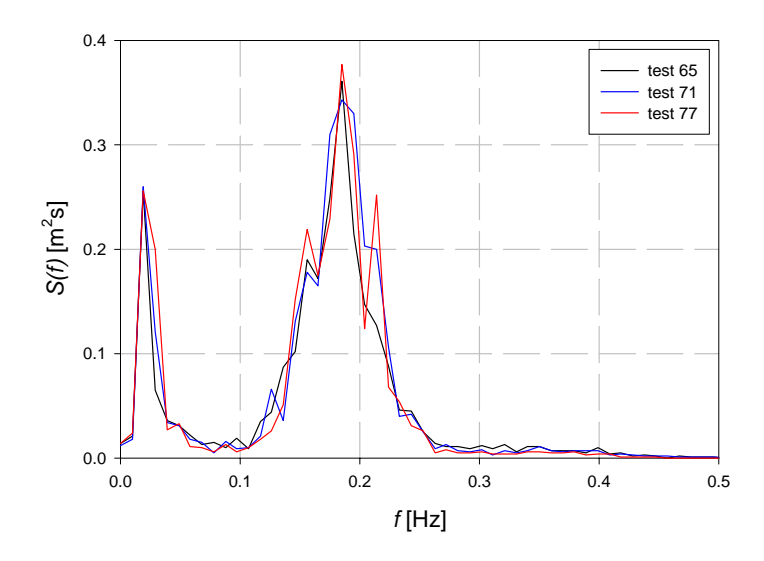


Figure I.1: Spectrum of tests  $n^{\circ}$  65, 71 and 77.

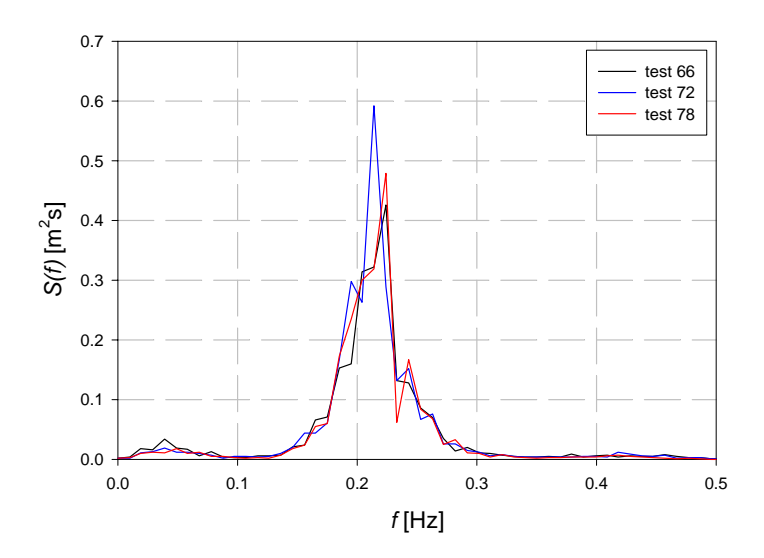


Figure I.2: Spectrum of tests  $n^{\circ}$  66, 72 and 78.

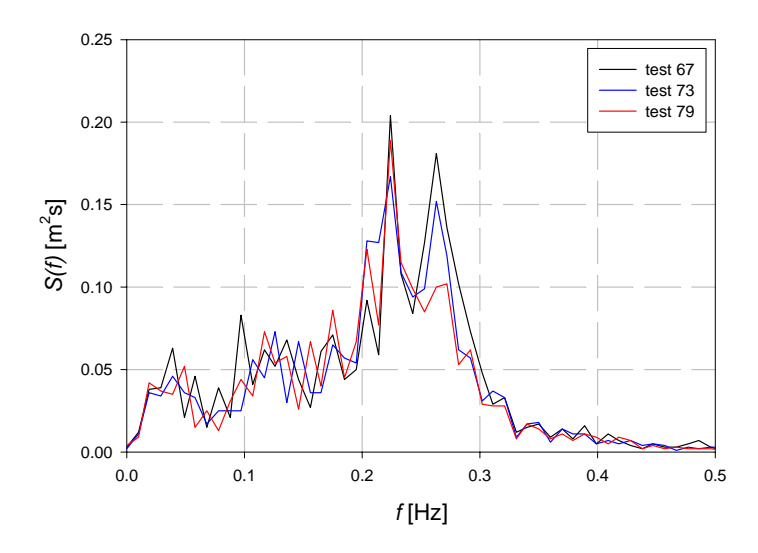


Figure I.3: Spectrum of tests  $n^{\circ}$  67, 73 and 79.

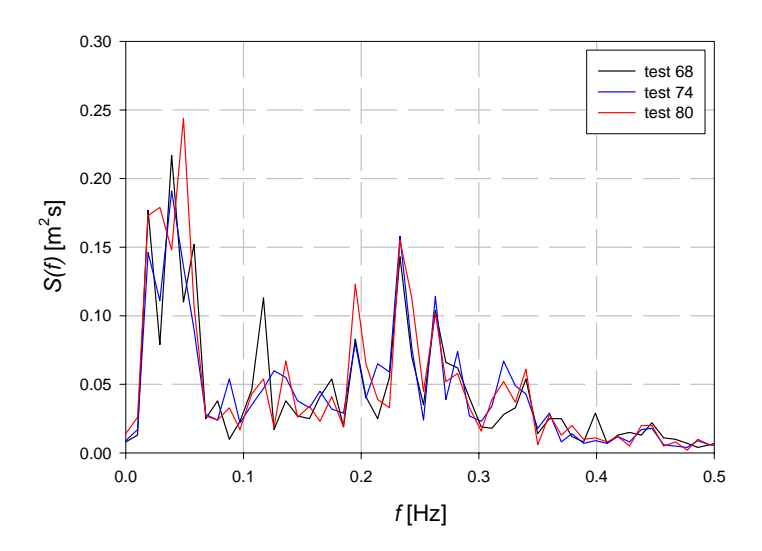


Figure I.4: Spectrum of tests  $n^{\circ}$  68, 74 and 80.

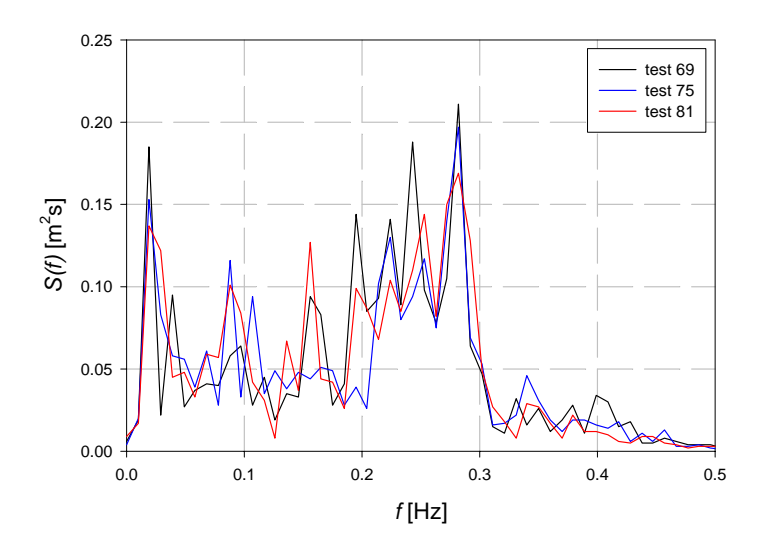


Figure I.5: Spectrum of tests  $n^{\circ}$  69, 75 and 81.

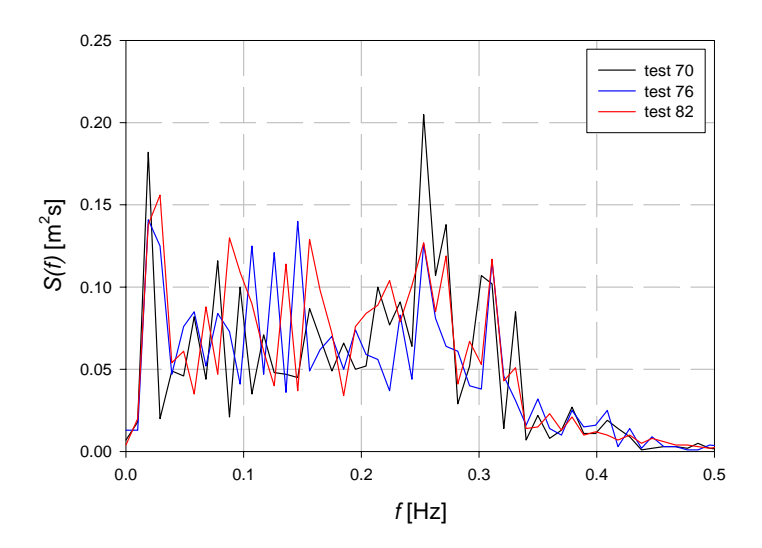


Figure I.6: Spectrum of tests  $n^{\circ}$  70, 76 and 82.

A	Annex J: FCFH wave spectra (OPTICREST tests).							
		Annex J-1						
		Almex J-1						

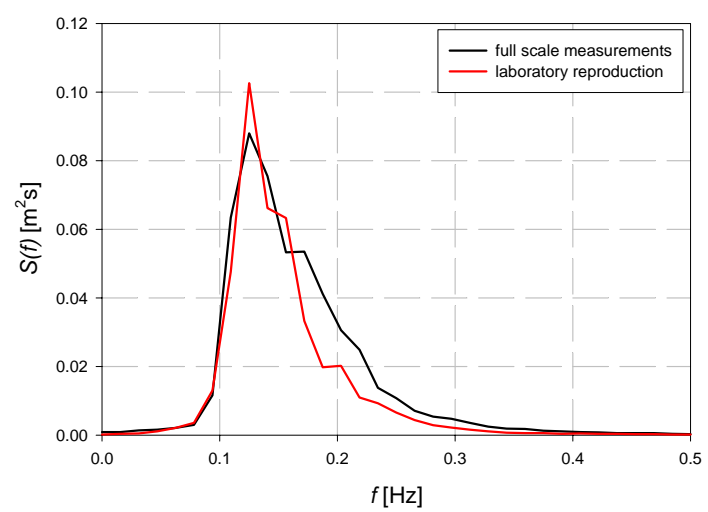


Figure J.1: Spectrum of reproduction of storm  $n^{\circ}$  1 (August  $28^{th}$ , 1995 (am)).

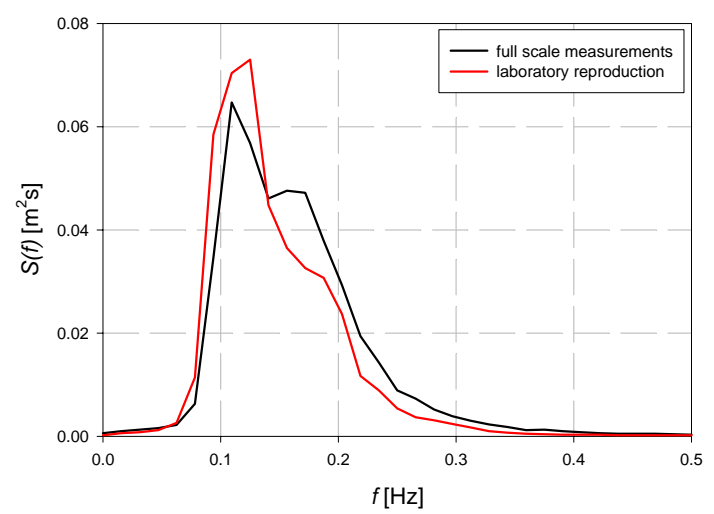
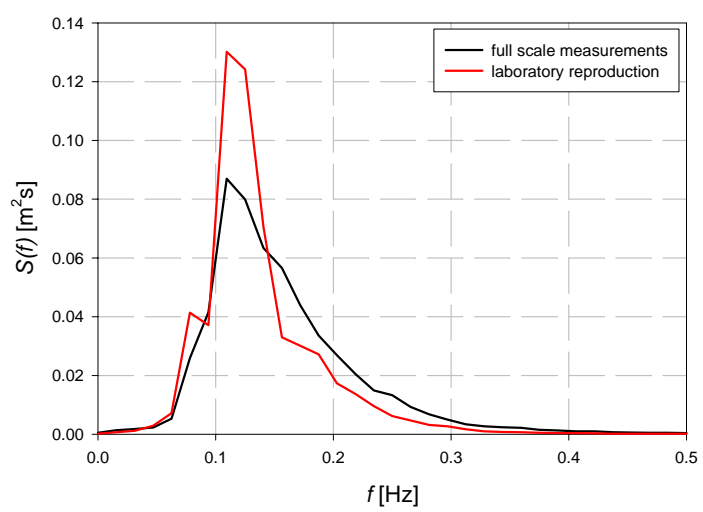


Figure J.2: Spectrum of reproduction of storm  $n^{\circ}$  2 (August 28<sup>th</sup>, 1995 (pm)).



 $\begin{array}{c} \textit{f}\,\text{[Hz]} \\ \textbf{Figure J.3: Spectrum of reproduction of storm } n^\circ\,3 \\ \textbf{(January 19}^\text{th}, 1998).} \end{array}$ 

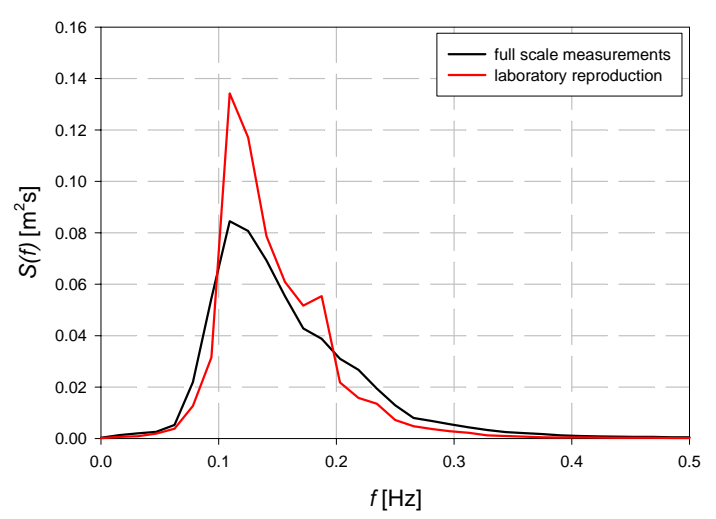
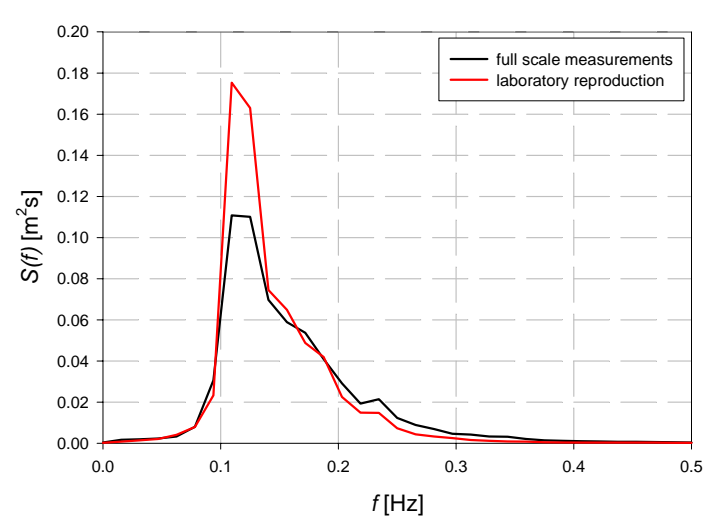
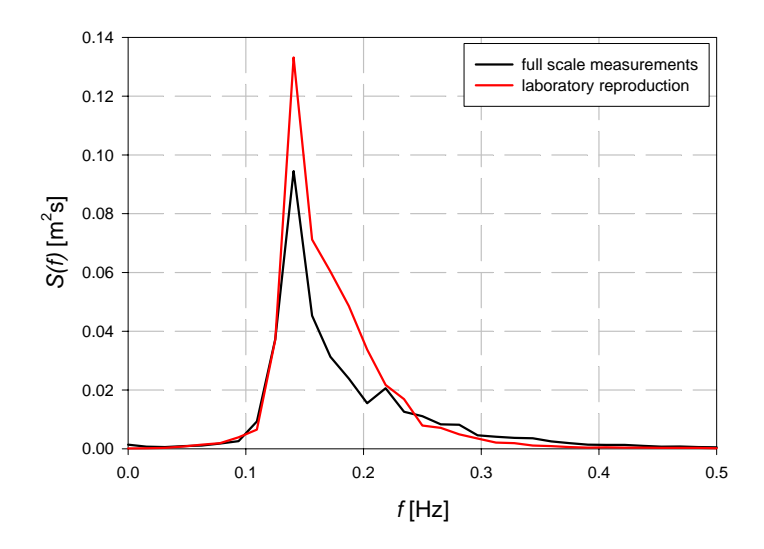


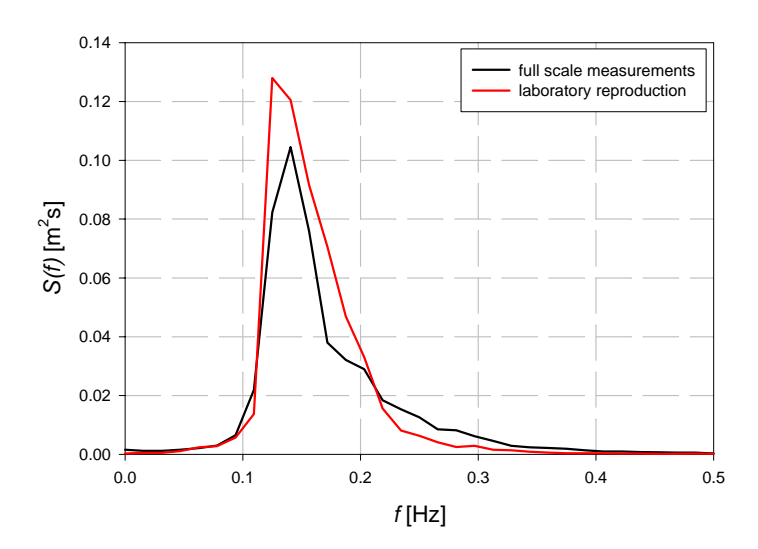
Figure J.4: Spectrum of reproduction of storm  $n^{\circ}$  4 (January  $20^{th}$ , 1998).



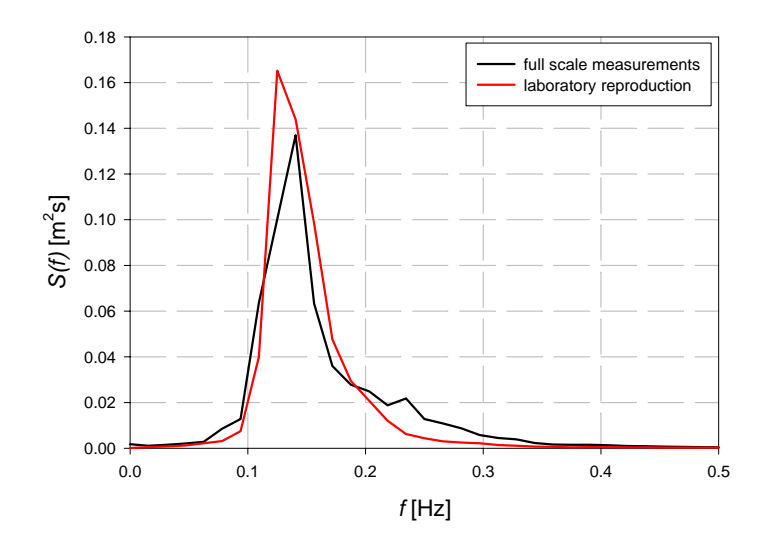
 $\begin{array}{c} \textit{f} \, [\text{Hz}] \\ \textbf{Figure J.5: Spectrum of reproduction of storm } n^{\circ} \, 5 \\ \textbf{(February 7}^{\text{th}}, 1999). \end{array}$ 



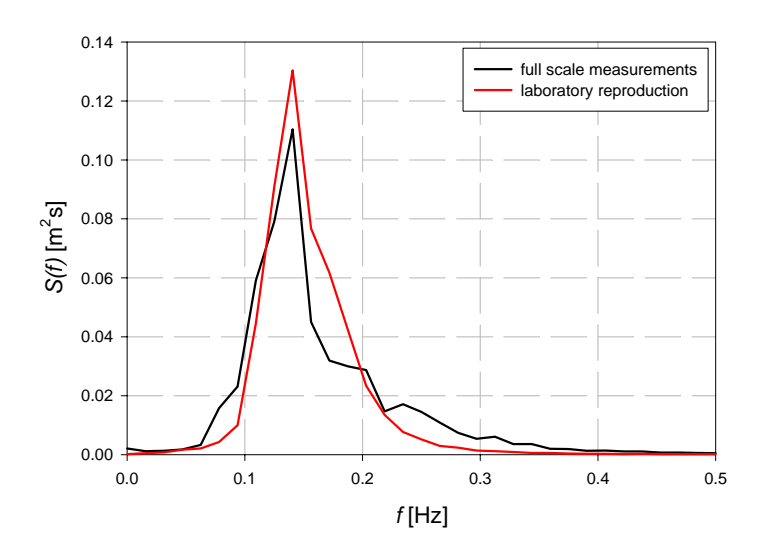
(a)  $t_{HW}$ -3  $t_{HW}$ -2



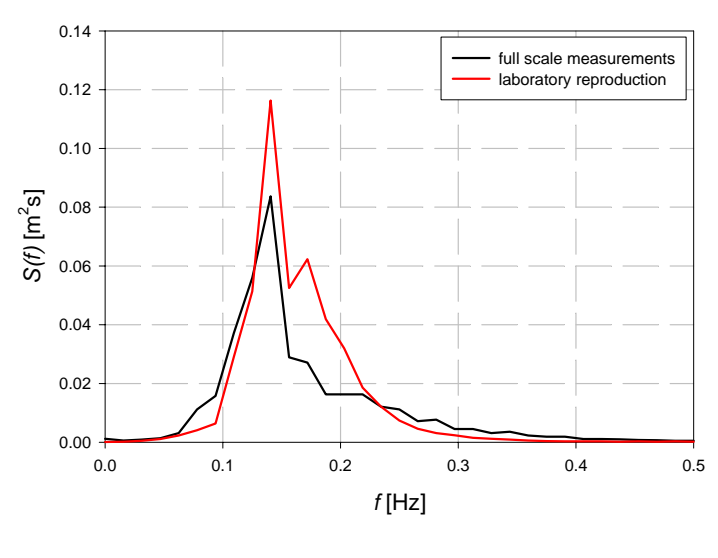
(b)  $t_{HW}$ -2  $t_{HW}$ -1



## (c) $t_{HW}$ -1 $t_{HW}$ +1



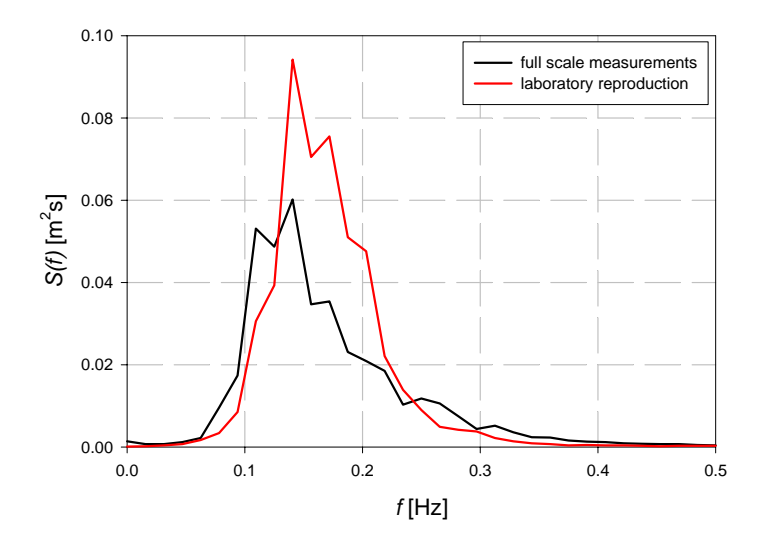
(d)  $t_{HW}$ +1  $t_{HW}$ +2



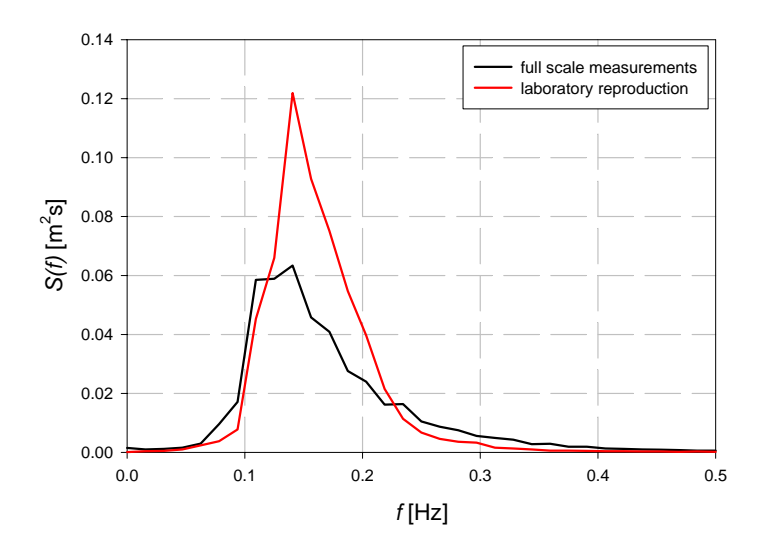
(e)  $t_{HW}$ +2  $t_{HW}$ +3

Figure J.6: Spectra of reproduction of storm  $n^{\circ}$  6 (November  $6^{th}$ , 1999).

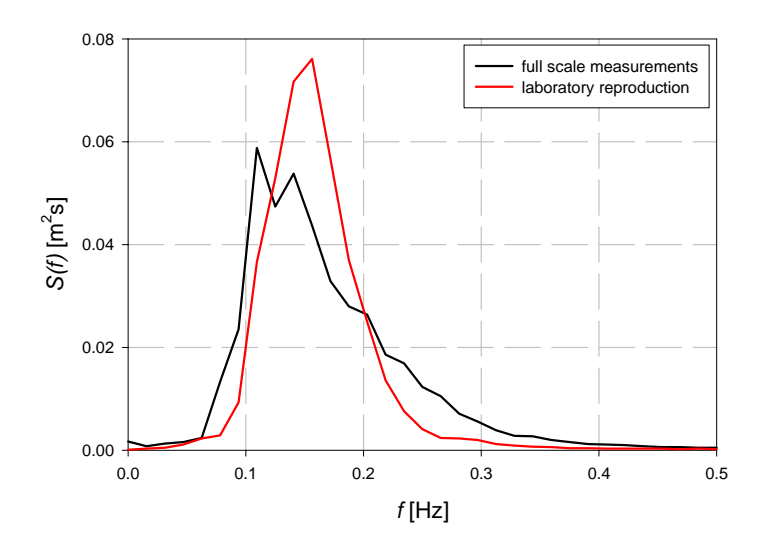
Annex J-7



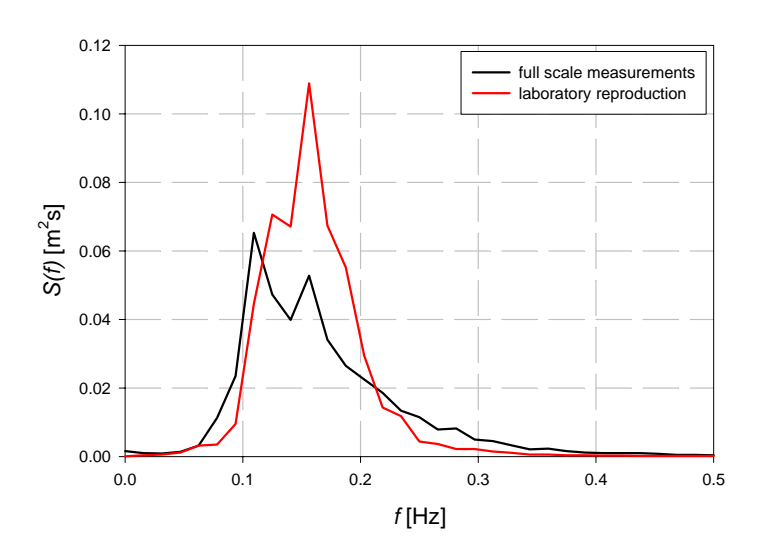
(a)  $t_{HW}$ -3  $t_{HW}$ -2



(b)  $t_{HW}$ -2  $t_{HW}$ -1



## (c) $t_{HW}$ -1 $t_{HW}$ +1



(d)  $t_{HW}$ +1  $t_{HW}$ +2

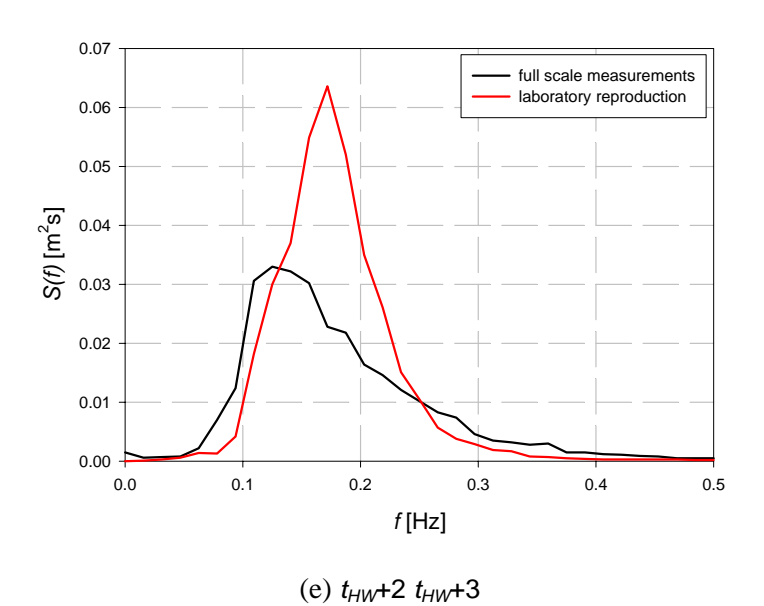


Figure J.7: Spectra of reproductions of storm  $n^{\circ}$  7 (November  $6^{th}$ - $7^{th}$ ,1999).

Annex K: AAU	wave spect	ra (OPTIC	CREST te	sts).
	Annex I	<b>ζ-1</b>		

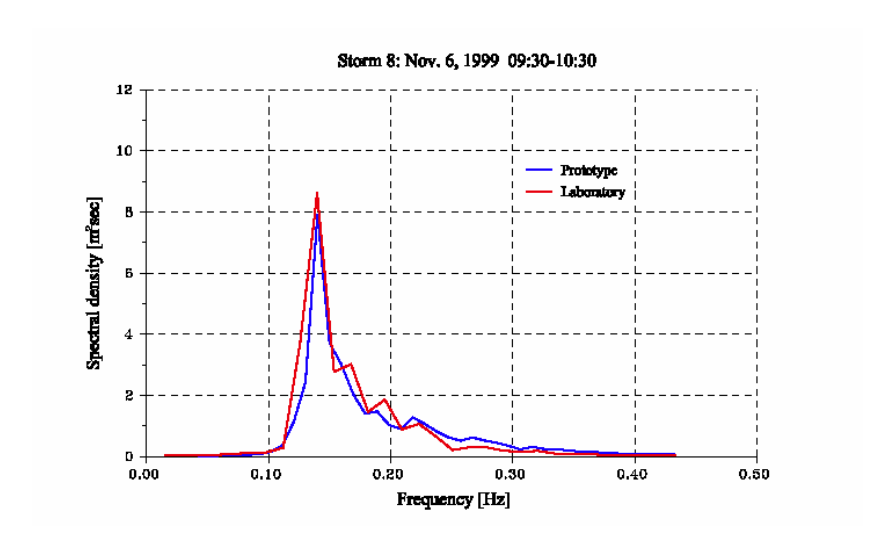


Figure K.1: Spectrum of November 6<sup>th</sup>, 1999 (09h30 to 10h30).

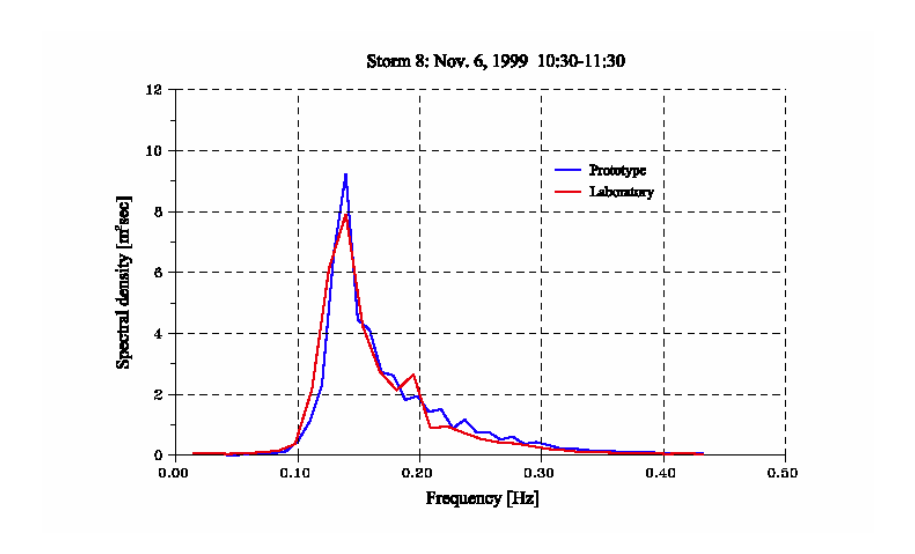


Figure K.2: Spectrum of November 6<sup>th</sup>, 1999 (10h30 to 11h30).

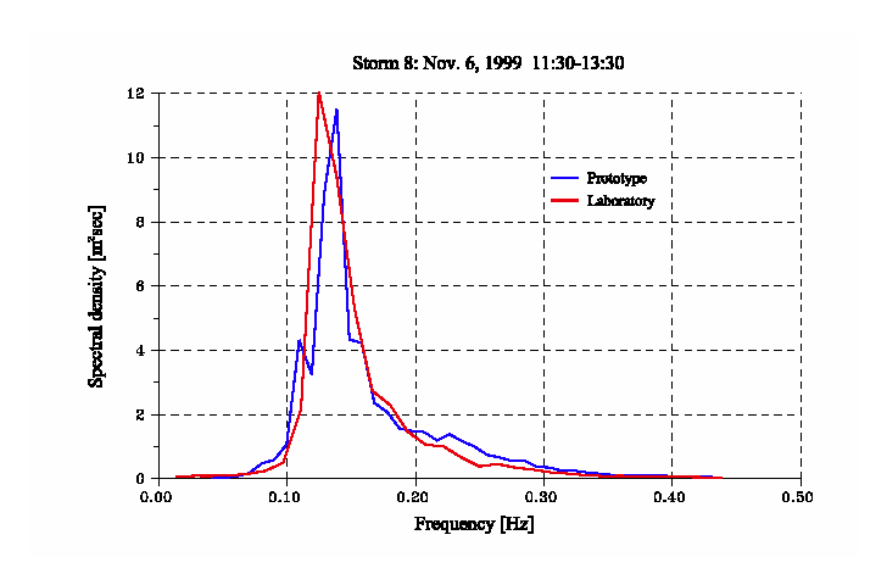


Figure K.3: Spectrum of November 6<sup>th</sup>, 1999 (11h30 to 13h30).

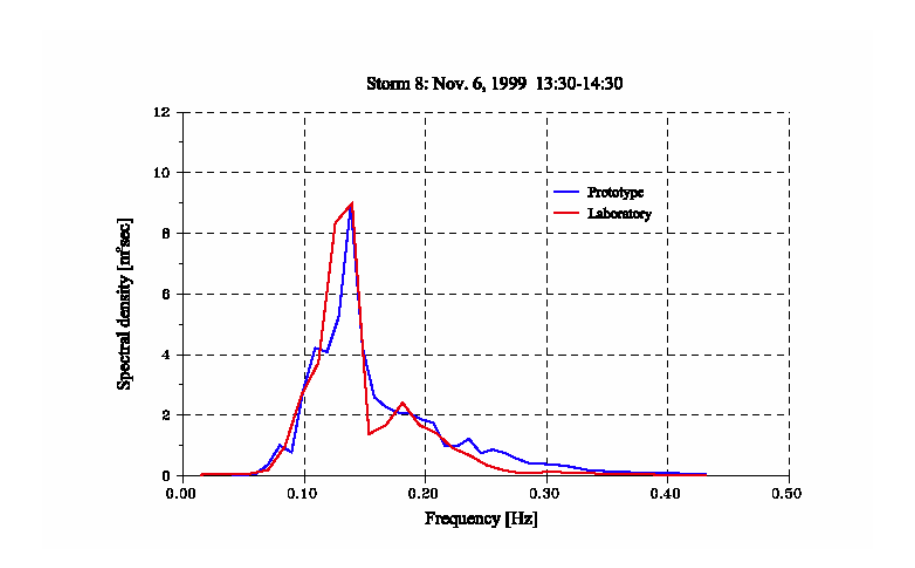


Figure K.4: Spectrum of November 6<sup>th</sup>, 1999 (13h30 to 14h30).

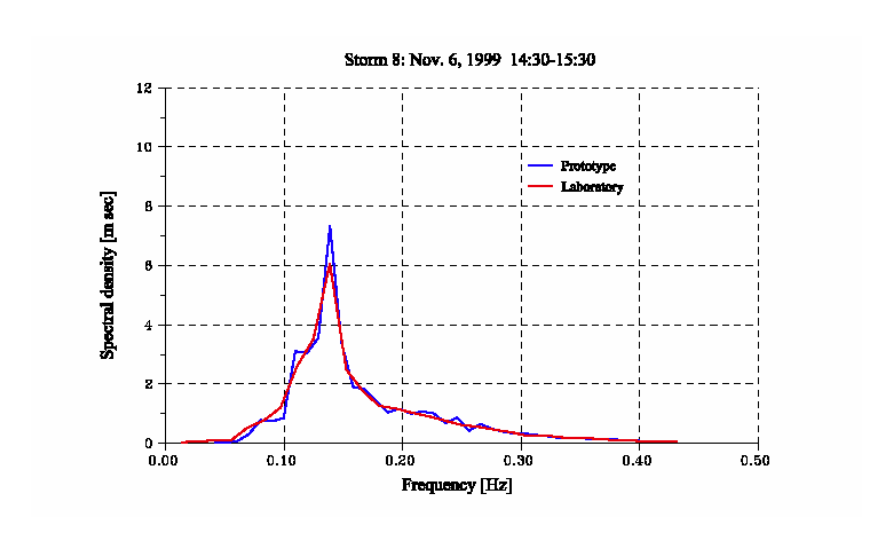


Figure K.5: Spectrum of November 6<sup>th</sup>, 1999 (14h30 to 15h30).

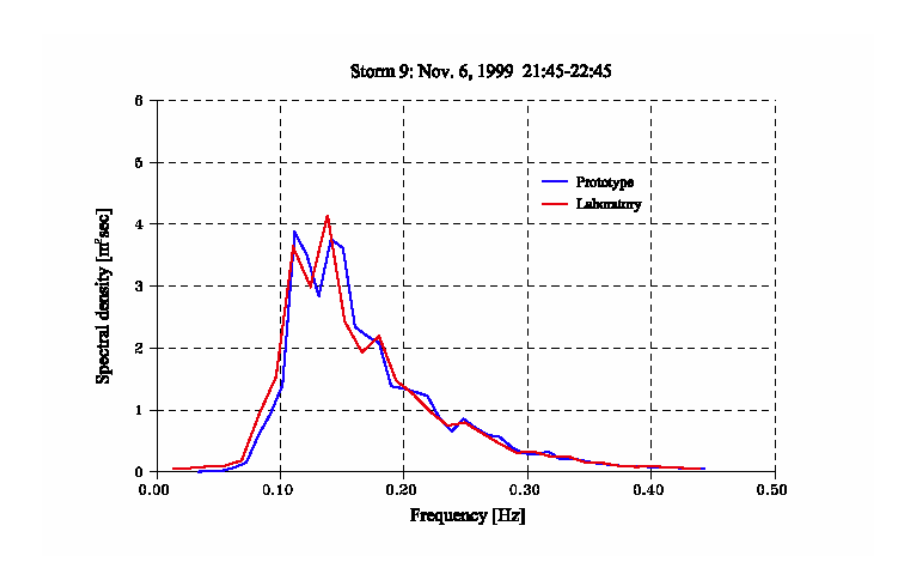


Figure K.6: Spectrum of November 6<sup>th</sup>-7<sup>th</sup>, 1999 (21h45 to 22h45).

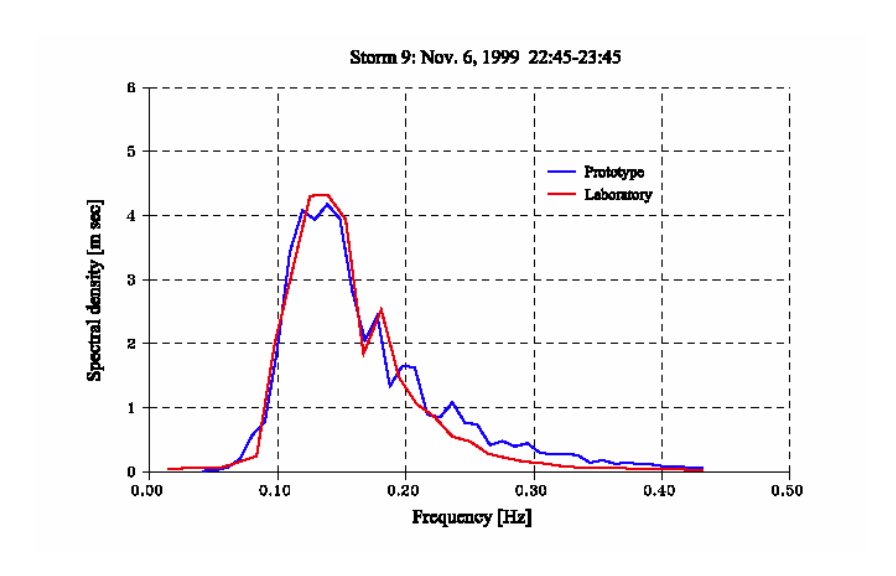


Figure K.7: Spectrum of November 6<sup>th</sup>-7<sup>th</sup>, 1999 (22h45 – 23h45).

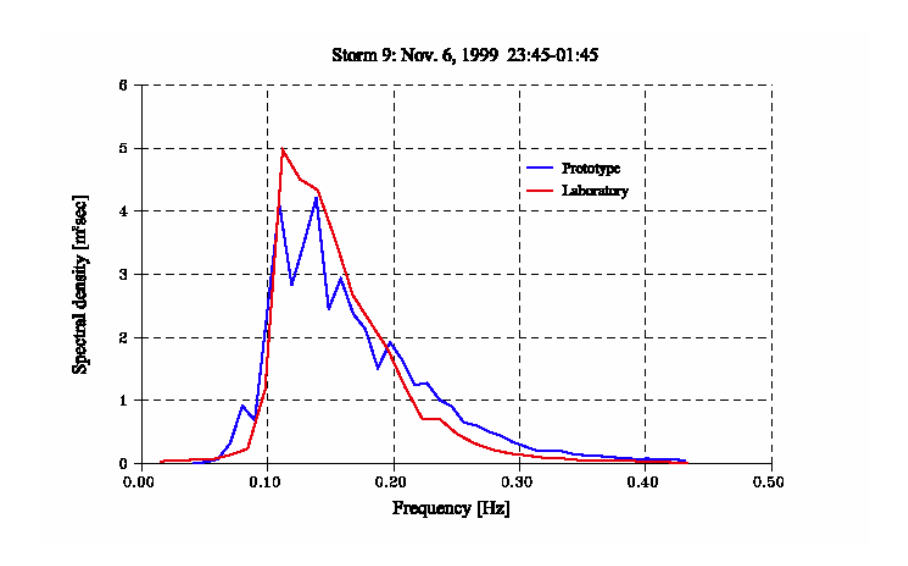


Figure K.8: Spectrum of November 6<sup>th</sup>-7<sup>th</sup>, 1999 (23h45 to 01h45).

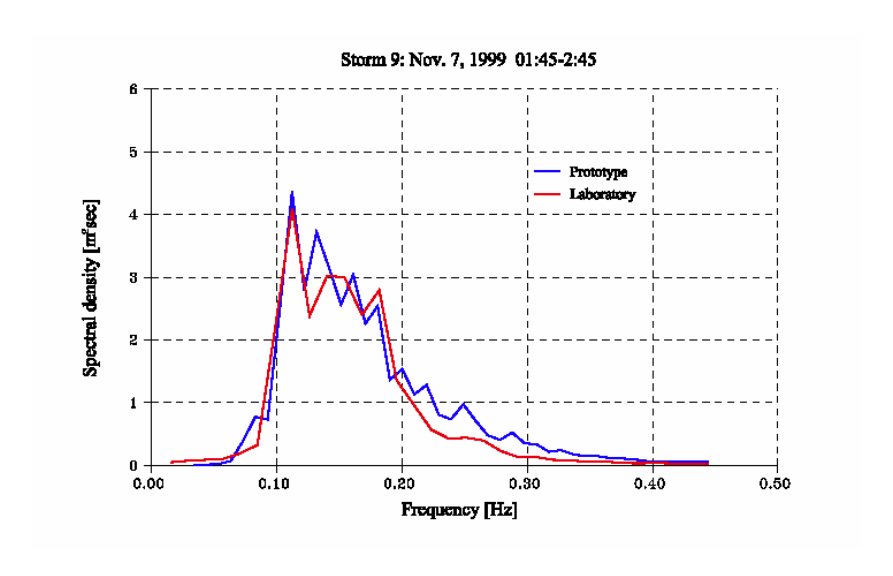


Figure K.9: Spectrum of November 6<sup>th</sup>-7<sup>th</sup>, 1999 (01h45 to 02h45).

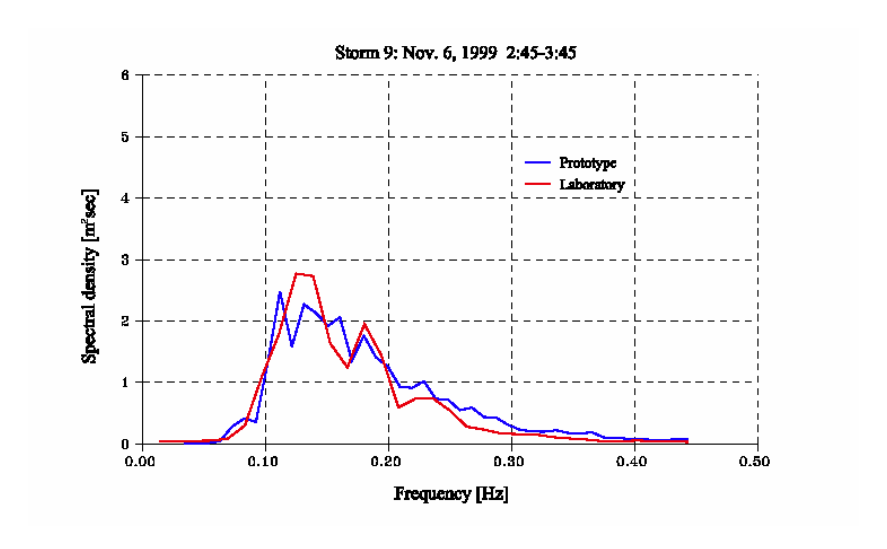


Figure K.10: Spectrum of November  $6^{th}$ - $7^{th}$ , 1999 (02h45 to 03h45).

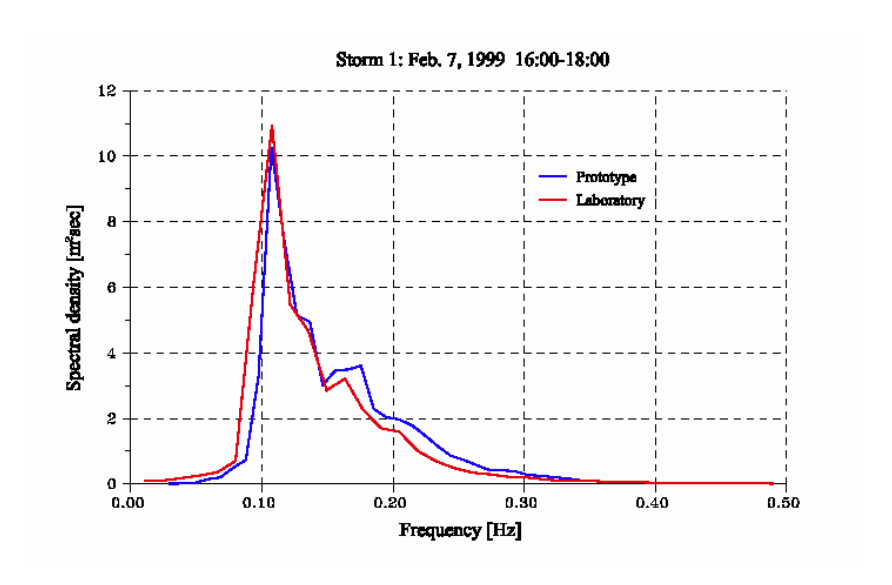


Figure K.11: Spectrum of February 7<sup>th</sup>, 1999 (16h00 to 18h00).

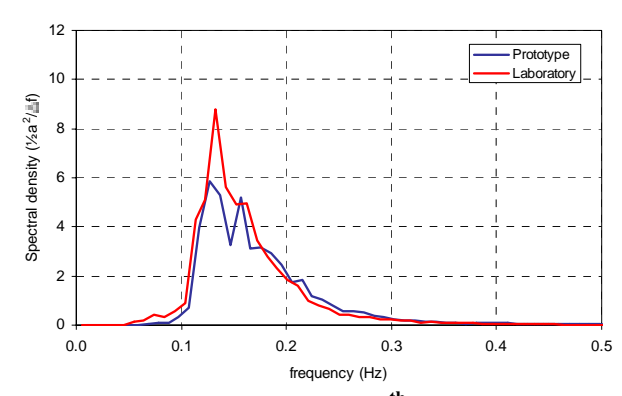


Figure K.12: Spectrum of August 28<sup>th</sup>, 1995 (03h30 to 04h45).

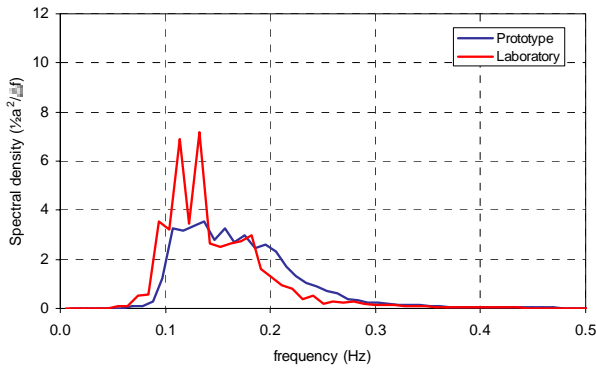


Figure K.13: Spectrum of August 28th, 1995 (14h45 to 17h00).

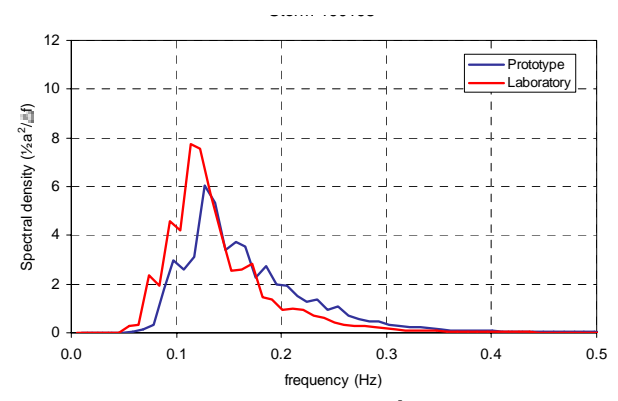


Figure K.14: Spectrum of January 19<sup>th</sup>, 1998 (15h45 to 18h15).

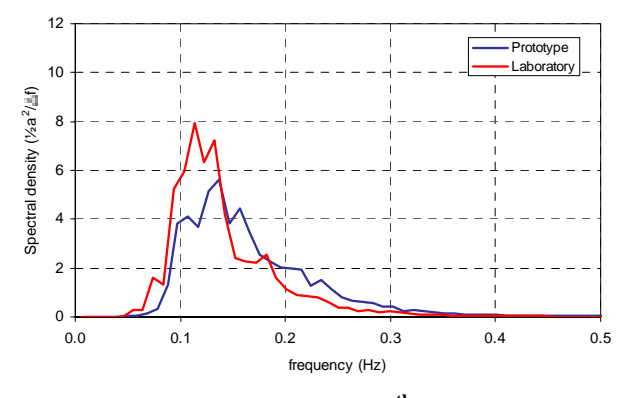
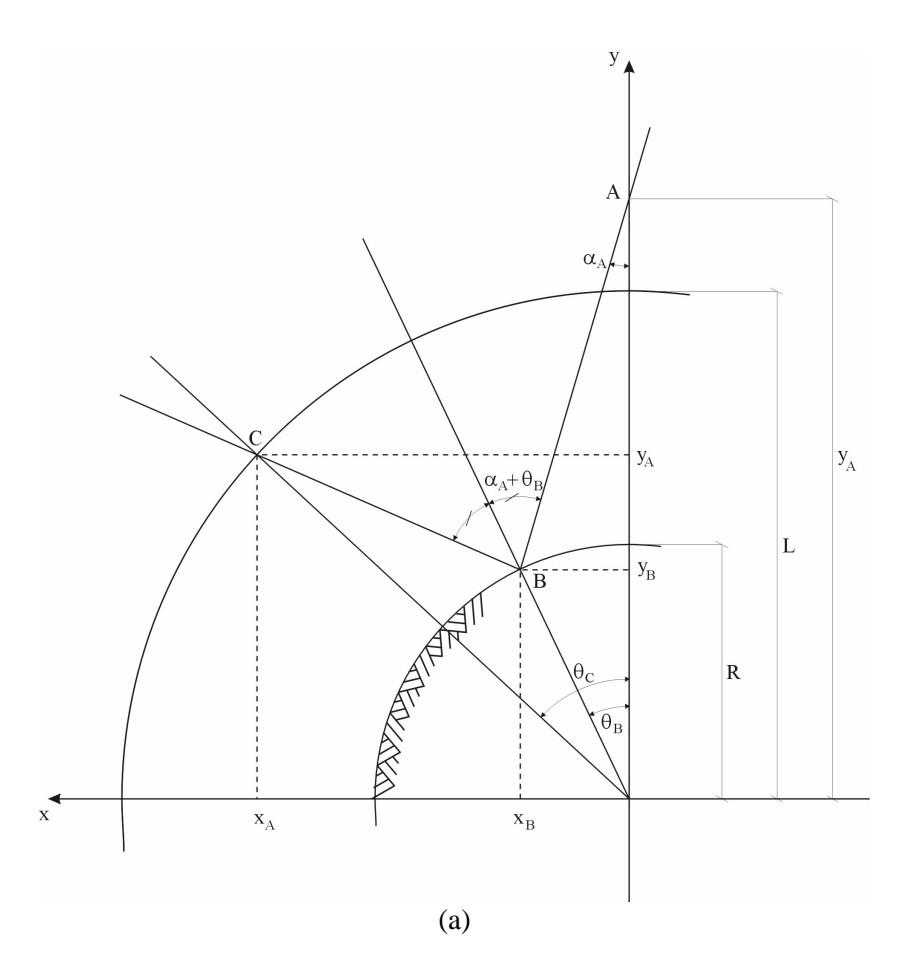


Figure K.15: Spectrum of January 20<sup>th</sup>, 1998 (04h15 to 06h15).

Annex L: Scatter effect.	
Annex L-1	

The energy inciding on a horizontal curved wall causes dispersion of energy. The reflected energy is added to the inciding energy, leading to an increase of the total measured energy (proportional to the square of the measured wave height). Assuming a wave rider buoy measures the total wave height (incident and reflected wave height), it can be theoretically shown that the reflected energy only contributes very little to the total (measured) energy.



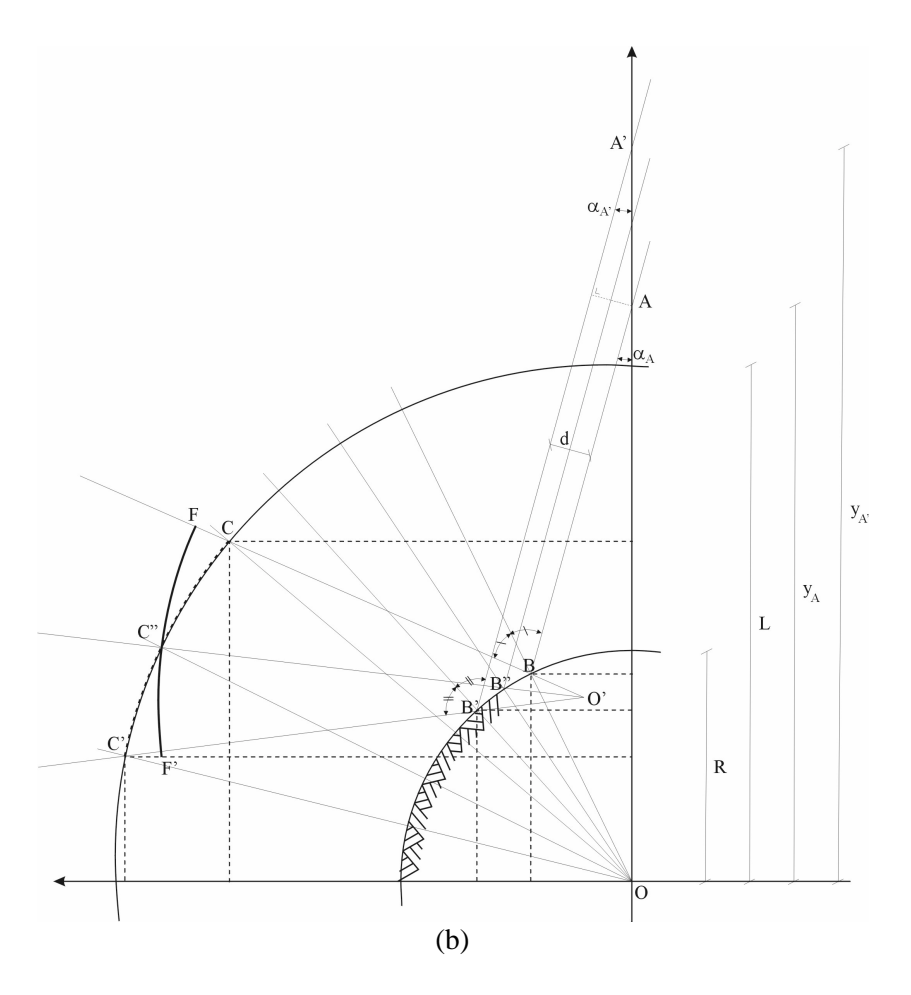


Figure L.1: Sketch of the calculation model.

There are five parameters:  $y_A$ ,  $\theta_A$ , R, L and d (see figure L.1(a) and (b)). The coordinates of point A are

$$\begin{cases} x_A = 0 \\ y_A \end{cases} \tag{L.1}$$

The coordinates of points B and C are

$$\begin{cases} x_B = R\sin\theta_B \\ y_B = R\cos\theta_B \end{cases}$$
 (L.2)

$$\begin{cases} x_C = L\sin\theta_C \\ y_C = L\cos\theta_C \end{cases}$$
 (L.3)

By means of the sine rule,  $\theta_B$  and  $\theta_C$  are calculated. From figure L.1(a):

$$\frac{R}{\sin \alpha_A} = \frac{y_A}{\sin(\pi - (\alpha_A + \theta_B))} \tag{L.4}$$

so that

$$\sin(\alpha_A + \theta_B) = \frac{y_A \sin \alpha_A}{R} \tag{L.5}$$

and

$$\theta_B = \arcsin\left(\frac{y_A \sin \alpha_A}{R}\right) - \alpha_A \tag{L.6}$$

From figure L.1(a),

$$\frac{L}{\sin(\pi - (\alpha_A + \theta_B))} = \frac{R}{\sin(\alpha_A + 2\theta_B - \theta_C)}$$
 (L.7)

so that

$$\sin(\alpha_A + 2\theta_B - \theta_C) = \frac{R\sin(\alpha_A + \theta_B)}{L}$$
 (L.8)

and

$$\theta_C = \alpha_A + 2\theta_B - \arcsin\left(\frac{R\sin(\alpha_A + \theta_B)}{L}\right)$$
 (L.9)

From figure L.1(b), the coordinates of A', B', C', A" and B" are

$$\begin{cases} x_{A'} = 0 \\ y_{A'} = y_A + \frac{d}{\sin \alpha_A} \end{cases}$$
 (L.10)

$$\begin{cases} x_{B'} = R \sin \theta_{B'} \\ y_{B'} = R \cos \theta_{B'} \end{cases}$$
 (L.11)

$$\begin{cases} x_{C'} = L\sin\theta_{C'} \\ y_{C'} = L\cos\theta_{C'} \end{cases}$$
 (L.12)

$$\begin{cases} x_{A''} = 0 \\ y_{A''} = y_A + \frac{d}{2\sin\alpha_A} \end{cases}$$
 (L.13)

$$\begin{cases} x_{B''} = R \sin \theta_{B''} \\ y_{B''} = R \cos \theta_{B''} \end{cases}$$
 (L.14)

$$\begin{cases} x_{C''} = L\sin\theta_{C''} \\ y_{C''} = L\cos\theta_{C''} \end{cases}$$
 (L.15)

The angles  $\theta_{B'}$ ,  $\theta_{C'}$  and  $\theta_{B''}$  are calculated in a similar way

$$\theta_{B'} = \arcsin\left(\frac{y_{A'}\sin\alpha_A}{R}\right) - \alpha_A$$
 (L.16)

$$\theta_{C'} = 2\theta_{B'} + \alpha_A - \arcsin\left(\frac{R\sin(\alpha_A + \theta_{B'})}{L}\right)$$
 (L.17)

$$\theta_{B''} = \arcsin\left(\frac{y_{A''}\sin\alpha_A}{R}\right) - \alpha_A \tag{L.18}$$

$$\theta_{C''} = 2\theta_{B''} + \alpha_A - \arcsin\left(\frac{R\sin(\alpha_A + \theta_{B''})}{L}\right)$$
 (L.19)

The length of the chords  $\overline{BB}'$  and  $\overline{CC}'$  are

$$\overline{BB'} = \sqrt{(x_B - x_{B'})^2 + (y_B - y_{B'})^2}$$
 (L.20)

$$\overline{CC'} = \sqrt{(x_C - x_{C'})^2 + (y_C - y_{C'})^2}$$
 (L.21)

The length of the arc segments  $\widehat{B}\widehat{B}'$  and  $\widehat{C}\widehat{C}'$ 

$$\widehat{B}\widehat{B}' = R(\theta_{B'} - \theta_B) \tag{L.22}$$

$$\widehat{C}\widehat{C}' = L(\theta_{C'} - \theta_{C}) \tag{L.23}$$

The theoretical equation of the straight lines BC and B'C' is

$$y = ax + b (L.24)$$

with

$$a = \frac{y_C - y_B}{x_C - x_B} \tag{L.25}$$

and

$$b = y_B - \frac{y_C - y_B}{x_C - x_B} x_B \tag{L.26}$$

and similar

$$\begin{cases} a' = \frac{y_{C'} - y_{B'}}{x_{C'} - x_{B'}} \\ b' = y_{B'} - \frac{y_{C'} - y_{B'}}{x_{C'} - x_{B'}} x_{B} \end{cases}$$
 (L.27)

The intersection point of BC and BC' are

$$\begin{cases} x_0 = -\frac{b - b'}{a - a'} \\ y_0 = \frac{a'b - ab'}{a' - a} \end{cases}$$
 (L.28)

*R*' is

$$R' = ||O'C''|| = \sqrt{(x_0 - x_{C''})^2 + (y_0 - y_{C''})^2}$$
 (L.29)

$$\theta = \arctan a - \arctan a' \tag{L.30}$$

$$FF' = R'\theta$$
 (L.31)

Consider

$$n_B = \frac{BB'}{d} \tag{L.32}$$

$$n_C = \frac{CC'}{d} \tag{L.33}$$

$$n = n_B . n_C (L.34)$$

Assume  $\chi = H_r/H_i$  to be the reflection coefficient of the breakwater. The incident wave energy per unit of width is  $E_{A,i}$ . The inciding energy  $E_{A,i}$ . d is incides on a distance d, so the energy is distributed over width d:

$$E_{B,i} = E_{A,i} \frac{d}{d'} = \frac{E_{A,i}}{n_P}$$
 (L.35)

The reflected energy is

$$E_{B,r} = \chi^2 E_{B,i} = \frac{\chi^2}{n_B} E_{A,i}$$
 (L.36)

$$E_{C,r} = E_{B,r} \frac{d}{d''} = \frac{E_{B,r}}{n_C} = \frac{\chi^2}{n_B n_C} E_{A,i} = \frac{\chi^2}{n} E_{A,i}$$
 (L.37)

The total energy measured at point C is

$$E_{C,t} = E_{C,i} + E_{C,r} = E_{A,i} + \frac{\chi^2}{n} E_{A,i} = \left(1 + \frac{\chi^2}{n}\right) E_{A,i}$$
 (L.38)

or

$$E_{C,t} = \chi^{"^2} E_{A,i} \tag{L.39}$$

Assuming point *A* is situated outside the scattering area, so  $E_{A,r} = \chi^2 E_{A,i}$ , the total energy measured at point *A* is

$$E_{A,t} = E_{A,i} + E_{A,r} = (1 + \chi^2)E_{A,i}$$
 (L.40)

so that

$$E_{A,i} = \frac{E_{A,t}}{1 + \chi^2} \tag{L.41}$$

Substituting (L.41) in (L.42) yields

$$E_{c,t} = \frac{1 + \frac{\chi^2}{n}}{1 + \chi^2} E_{A,t} = \chi^{2} E_{A,t}$$
 (L.42)

so that, as total wave energy is proportional to the square wave height,

$$H_C = \sqrt{\frac{1 + \frac{\chi^2}{n}}{1 + \chi^2}} H_A = \chi' H_A$$
 (L.43)

Applying (L.43) to the Zeebrugge breakwater

- $y_A = 550 \text{ m}$
- $\bullet$   $\alpha_A = 5^{\circ}$
- R = 500 m (taken from map n° 96-07/17B of the Hessenatie N.V. (1996))
- L = 715 m (= distance between center of circle with radius R and the position of the second wave rider)
- d = 1 m (distance between two inciding wave rays)
- $\chi = 0.30$  (average reflection coefficient of the Zeebrugge breakwater (based on the mean wave period) (see paragraph 5.5))

yields

$$n_B = 1.00$$

$$n_C = 1.87$$

$$n = 1.88$$

$$\chi' = 0.98$$

$$\chi$$
" = 1.02

From the upper results it is seen that the total measured wave height in point C (incident wave energy + scattered reflected wave energy) is 98% of the wave height measured in point A (incident wave energy + normal reflected wave energy). For other values of  $y_A$  and  $\alpha_A$ , the minimal value of  $\chi$ ' is 0.96.